

Medicinal Chemistry & Chemical Biology

Approaches to Investigate Prospective Treatments for CNS Diseases

Dopamine D₁ Receptor Positive Allosteric Modulators, Dopamine D₂ Receptor Positive & Negative Allosteric Modulators, Dopamine D₂ Receptor-Ligand Kinetics

A thesis submitted for the joint award degree of *Doctor of Philosophy* (2019)

Tim Fyfe

B.Sc. B.Pharm.Sc. (Hons)

Department of Medicinal Chemistry & Drug Discovery Biology

Faculty of Pharmacy & Pharmaceutical Sciences

Monash University

Division of Medicinal Chemistry & Biomolecular Science

Faculty of Science

The University of Nottingham



MONASH
University



The University of
Nottingham

Copyright notice

© Tim Fyfe (2019)

I certify that I have made all reasonable efforts to secure copyright permission for third-party content included in this thesis and have not knowingly added copyright content to my work without due recognition and the owner's permission.

Table of Contents

Statement of Originality	- 1 -
Declaration	- 2 -
Thesis Including Published Works Declaration	- 3 -
Acknowledgements	- 5 -
Abbreviations	- 6 -
Abstract	- 9 -
Chapter 1	- 12 -
Introduction	- 13 -
Thesis aims.....	- 51 -
Chapter 2	- 74 -
A Thieno[2,3- <i>d</i>]pyrimidine Scaffold is a Novel Negative Allosteric Modulator of the Dopamine D ₂ Receptor	- 75 -
Chapter 3	- 116 -
Subtle Modifications to a Thieno[2,3- <i>d</i>]pyrimidine Scaffold Yield Negative Allosteric Modulators and Agonists of the Dopamine D ₂ Receptor.....	- 117 -
Chapter 4	- 158 -
SAR Studies Toward the Synthesis of Irreversible and Fluorescent Analogues of a Dopamine D ₂ Receptor Positive Allosteric Modulator.....	- 159 -
Chapter 5	- 204 -
Declaration	- 205 -
Structure-Kinetic Profiling of Haloperidol Analogues at the Dopamine D ₂ Receptor	- 207 -
Chapter 6	- 308 -
Enantioenriched Positive Allosteric Modulators Display Distinct Pharmacology at the Dopamine D ₁ Receptor	- 309 -
Chapter 7	- 344 -
Thesis Outcomes & Future Prospects	- 345 -
Appendices	- 352 -

Statement of Originality

I hereby declare that this thesis contains no material which has been accepted for the award of any other degree or diploma at any university or equivalent institution and that, to the best of my knowledge and belief, contains no material previously published or written by another person, except where due reference has been made in the text of the thesis.

Tim Fyfe

Declaration

In accordance with Monash University Doctorate Regulation 17 Doctor of Philosophy and Research Master's regulations the following declarations are made:

I hereby declare that this thesis contains no material which has been accepted for the award of any other degree or diploma at any university or equivalent institution and that, to the best of my knowledge and belief, this thesis contains no material previously published or written by another individual, except where due reference is made in the text of the thesis.

Student Signature:

Date: 20/02/2019

Thesis Including Published Works Declaration

This thesis includes **2** original research articles published in a peer reviewed journal, and **1** original research article awaiting submission. This thesis explores the synthesis and pharmacological profiling of a variety of different small molecule allosteric modulators targeting both the dopamine D₁ and D₂ receptors (D₁R and D₂Rs, respectively). This thesis also details the chemical synthesis and *in vitro* kinetic profiling of an extensive library of structural analogues of the clinical antipsychotic haloperidol at the dopamine D₂R.

The ideas, development and writing up of all manuscripts/chapters in this thesis were the principal responsibility of myself, the candidate, working within both Monash University and The University of Nottingham, under the supervision of Dr Ben Capuano, Dr J. Robert Lane, Prof. Peter J. Scammells, Prof. Barrie Kellam, and Dr Shailesh N. Mistry.

The inclusion of co-authors reflects the fact that the work came from active collaboration between researchers and acknowledges input into team-based research.

In the case of chapters 2 and 3, my contribution to the work involved the following:

Thesis Chapter	Publication Title	Status	Nature and % of student contribution	Co-author name(s) Nature and % of Co-author's contribution*	Co-author(s), Monash student Y/N*
2	<i>A Thieno[2,3-d]pyrimidine Scaffold is a Novel Negative Allosteric Modulator of the Dopamine D₂ Receptor</i>	<i>Published</i>	<i>Synthesis, characterisation and pharmacological testing of all compounds. Primary author of manuscript. Preparation of figures and final manuscript. 80%.</i>	<ol style="list-style-type: none"> 1) <i>Barbara Zarzycka: conducted molecular docking, 1%</i> 2) <i>Herman D. Lim: co-author of manuscript, 1%</i> 3) <i>Barrie Kellam: co-author of manuscript, 1%</i> 4) <i>Shailesh N. Mistry: co-author of manuscript, 1%</i> 5) <i>Vsevolod Katrich: conducted molecular docking, 1%</i> 6) <i>Peter J. Scammells: co-author of manuscript, 5%</i> 7) <i>J. Robert Lane: co-author of manuscript, 5%</i> 8) <i>Ben Capuano: co-author of manuscript, 5%</i> 	<i>No</i>

3	<i>Subtle Modifications to the Thieno[2,3-d]pyrimidine Scaffold Yields Negative Allosteric Modulators and Agonists of the Dopamine D2 Receptor</i>	<i>Published</i>	<i>Synthesis, characterisation and pharmacological testing of all compounds.</i> <i>Primary author of manuscript. Preparation of figures and final manuscript. 80%.</i>	1) <i>Barrie Kellam: co-author of manuscript, 2.5%</i> 2) <i>Shailesh N. Mistry: co-author of manuscript, 2.5%</i> 3) <i>Peter J. Scammells: co-author of manuscript, 5%</i> 4) <i>J. Robert Lane: co-author of manuscript, 5%</i> 5) <i>Ben Capuano: co-author of manuscript, 5%</i>	<i>No</i>
---	--	------------------	--	---	-----------

I have not renumbered sections of published papers or unpublished manuscripts within this thesis. Every chapter stands on its own and therefore the numbering of the chemical structures, figures, schemes, tables and references commences in each chapter from 1.

Student Signature:

Date: 20/02/2019

Print Name: Tim Fyfe

The undersigned hereby certifies that the above declaration correctly reflects the nature and extent of the student's and co-authors' contributions to this work. In instances where I am not the responsible author I have consulted with the responsible author to agree on the respective contributions of the authors.

Main Supervisor signature:

Print Name: Dr Ben Capuano

Date: 20/02/2019

Acknowledgements

I would like to express sincere gratitude to my five supervisors, Dr Ben Capuano, Professor Peter Scammells, Dr Robert Lane, Professor Barrie Kellam, and Dr Shailesh Mistry. Ben, some years ago you originally took the risk of accepting me to undertake my honours degree in Medicinal Chemistry despite the fact I had minimal experience in this area, let alone in organic synthesis! I thank you for providing me with this opportunity, and for all your assistance over the years, whether it be troubleshooting the identity of reaction side-products, or with preparation of manuscripts - it has truly been a pleasure. Peter, many thanks for being happy for me to drop in for a quick chat to discuss whatever it may be, and for your mentorship over the years, particularly during our weekly group meetings. Rob, I've learnt much from you with regards to pharmacology - your tremendous insight, wealth of knowledge and critical thinking has been amazing to witness, and without you my PhD would certainly not have been what it is today. To both Barrie and Shailesh, thank you for allowing me to complete part of my PhD at the University of Nottingham under your mentorship. My year spent in England working with you both will certainly be a memorable one.

I would like to extend my thanks to Dr Chris Draper-Joyce and Dr Herman Lim. Your help in the set-up and analysis of the various biochemical and functional experiments at Monash has certainly enabled me to produce the large amount of data I have, and without you guys this simply would not have happened. In addition, I'd like to thank Dr David Sykes for your help in the set-up and analysis of the kinetic binding assay/data. You took time out of your busy schedule to give me a hand and get me started. Also, to Professor Steven Charlton, thanks for allowing me to work in your kinetics laboratory, and for our discussions regarding the robustness of our experimental data and assay optimisation – it was a pleasure.

I would also like to thank my panel members: Professor Meri Canals and Professor Jonathan Baell, for your advice and input regarding my projects over the course of my PhD.

To all of my family and friends, in particular my parents, thank you for your constant support during my studies over the years, I appreciate you all very much.

Finally, to my beautiful wife Maddy, you have been by my side from the very start. Your constant love, encouragement and support throughout my studies over these past eight years, and in particular my PhD, has enabled me to make it through this vast journey. I truly appreciate all that you have done and continue to do for me.

This research was supported by an Australian Government Research Training Program (RTP) Scholarship.

Abbreviations

7CN-THIQ	1,2,3,4-tetrahydroisoquinoline-7-carbonitrile
AC	adenylate cyclase
ACN	1,1'-azobis(cyclohexanecarbonitrile)
ADA	asymmetric Diels-Alder
AIBN	azobisisobutyronitrile
AP	allosteric potentiator
APD	antipsychotic drug
aq.	aqueous
BRET	bioluminescence resonance energy transfer
Boc	<i>tert</i> -butyloxycarbonyl
cAMP	cyclic adenosine monophosphate
CHO	Chinese hamster ovary
CNS	central nervous system
d	day
D ₁ R	dopamine D ₁ receptor
D ₂ R	dopamine D ₂ receptor
D ₃ R	dopamine D ₃ receptor
<i>d</i> ₆ -DMSO	deuterated dimethyl sulfoxide
DAR	dopamine receptor
1,2-DCE	1,2-dichloroethane
DCM	dichloromethane
DIPEA	<i>N,N</i> -diisopropylethylamine
DMEM	Dulbecco's modified eagle medium
DMF	<i>N,N</i> -dimethylformamide
Dopamine	DA
DMSO	dimethyl sulfoxide
EDC	<i>N</i> -(3-dimethylaminopropyl)- <i>N'</i> -ethylcarbodiimide hydrochloride
EDTA	ethylenediaminetetraacetic acid
EPS	extrapyramidal side effects
eq.	equivalent
Et ₂ O	diethyl ether
EtOAc	ethyl acetate
ERK1/2	extracellular signal-regulated kinase
FBS	foetal bovine serum

FCC	flash column chromatography
FGA	first-generation antipsychotic drug
FRET	Förster resonance energy transfer
FSK	forskolin
GDP	guanosine diphosphate
GPCR	G protein-coupled receptor
GTP	guanosine triphosphate
h	hour
HBSS	Hank's balanced salt solution
HTRF	homogeneous time-resolved fluorescence
HEPES	2-[4-(2-hydroxyethyl)piperazin-1-yl]ethanesulfonic acid
HPLC	high-performance liquid chromatography
IUPHAR	international union of basic and clinical pharmacology
K_B	equilibrium dissociation constant
K_i	inhibition constant
k_{off}	dissociation rate binding constant
k_{on}	association rate binding constant
LCMS	liquid chromatography-mass spectrometry
MAPK	mitogen-activated protein kinase
m/z	mass-to-charge ratio
min	minute
MsCl	methanesulfonyl chloride
NAM	negative allosteric modulator
NMR	nuclear magnetic resonance
PAM	positive allosteric modulator
PBS	phosphate-buffered saline
PD	Parkinson's disease
PDB	protein data bank
pERK	phosphorylated extracellular signal-regulated kinase
PFC	prefrontal cortex
PS	petroleum spirits
Rbf	round bottom flask
rt	room temperature
SAR	structure-activity relationship
sat.	saturated

SCZ	schizophrenia
SEM	standard error of the mean
SGA	second-generation antipsychotic drug
SKR	structure-kinetic relationship
S _N Ar	nucleophilic aromatic substitution
SNC	substantia nigra pars compacta
TBAF	tetra- <i>N</i> -butylammonium fluoride
TBS	<i>tert</i> -butyldimethylsilyl chloride
TEA	triethylamine
TFA	trifluoroacetic acid
TGA	third-generation antipsychotic drug
THF	tetrahydrofuran
TLC	thin layer chromatography
TM	transmembrane helix
<i>t_R</i>	retention time
UV	ultraviolet
VLS	virtual ligand screen
WT	wild-type
δ	chemical shift
λ	wavelength

Abstract

The dopamine (DA) D₁ and D₂ receptors (D₁R and D₂R, respectively) are G protein-coupled receptors (GPCRs) that are therapeutic targets for the symptomatic treatment of neurological disorders such as schizophrenia (SCZ) and Parkinson's disease (PD). Classical approaches to GPCR drug discovery have focused on developing orthosteric agents with the capacity to engage the endogenous ligand (dopamine) binding site. Allosteric modulators, molecules that act via a topographically distinct but spatially linked binding site, have been touted as the next generation of CNS therapeutics and may show promise towards the treatment of SCZ and PD. To facilitate an understanding of molecular drug-receptor interactions, such small-molecule allosteric compounds may also be developed and used as biochemical tools, enabling techniques such as rational structure-based drug design or advancement of knowledge regarding key residues responsible for emerging concepts such as functional selectivity. Alternatively, the molecular basis for antipsychotic drug-induced on-target toxicities are also of significant importance in order to facilitate the development of safer therapeutics, and receptor-ligand binding kinetics is a key area of interest. Accordingly, this thesis explores multiple medicinal chemistry and chemical biology approaches to investigate: i) structural drivers of small molecule allosteric pharmacology toward understanding structure-activity-relationships (SAR) for allosteric modulator optimisation and biochemical tool development; ii) the kinetic basis for the "on target" side effect profiles of clinical antipsychotic drugs (APDs) in order to develop novel scaffolds with enhanced efficacy/side-effect profiles.

Chapter 2 comprises work published in the *Journal of Medicinal Chemistry* and details the synthesis of a small molecule thieno[2,3-*d*]pyrimidine hit arising from a virtual ligand screen (VLS) performed using the crystal structure of an antagonist bound D₃R as a template. We validate the hit compound's allosteric mode of interaction at the D₂R using radioligand binding and functional assays. In addition, the synthesis and structure-activity-relationships (SARs) of a series of analogues are further explored. All compounds are evaluated via the use of an operational model of allosterism to determine values of functional affinity (K_B) and negative allosteric cooperativity (α , β). Moreover, molecular docking studies were conducted using the recently determined D₂R crystal structure (PDB code 6C38) to assist in elucidating a potential binding mode for these molecules, and provide rationale for the observed SAR. Promising analogues were identified that displayed differential attenuation of affinity/signalling efficacy, and/or increased functional binding affinity. Lastly, marked improvements in lipophilic ligand efficiency of key active analogues revealed a fragment-like starting point that can be elaborated through multiple vectors.

Chapter 3 comprises work published in the *European Journal of Medicinal Chemistry* and explores the synthesis and biological evaluation of an additional 36 compounds based on the core scaffold

identified in the chapter 2. We assess the influence of introducing various primary and secondary amino groups, both of aliphatic and aromatic nature (e.g. pyrrolidine, aniline, cyclohexylamine) to the 4-position of the thieno[2,3-*d*]pyrimidine core, whilst maintaining the fused cyclohexane moiety present within the parent VLS hit (Series 1). The functional analysis of this series of compounds identified three amines (cyclobutylamino, cyclopropylamino, *N,N*-diethylamino) that engendered higher affinities and robust allosteric properties relative to the parent ((3-trifluoromethyl)phenyl)amino substituent. Thus, in an effort to understand their utility, these amines were further employed in conjunction various 5,6-modifications (eg., aromatic/aliphatic carbocycles). This allowed us to further explore and establish the structural determinants of D₂R allosteric pharmacology and functional binding affinity. We describe the identification of analogues with a range of different functional pharmacologies, including two of the highest affinity derivatives to emerge from the investigation that maintain negative cooperativity, and surprisingly, agonists.

Chapter 4. A detailed structural understanding of allostery at the D₂R will enable the progression of allosteric modulators towards the potential treatment of the symptoms of PD. This chapter investigates the SARs of a novel D₂R positive allosteric modulator (PAM) as the basis for generating irreversible and fluorescent ligands to be used as biochemical tools, which may permit a better understanding of molecular allosteric interactions, and to guide rational structure-based drug design. In order to elucidate potential linking points from which we could append photoactivatable or fluorescent moieties, we designed and synthesised a focused library of analogues, initially re-synthesising the parent D₂R PAM using a slightly modified 11-step literature synthesis in order to further characterise its functional pharmacology, as well as making additional modifications to obtain two novel structural analogues. We also established a novel 7-step synthetic pathway to permit more efficient access to D₂R PAMs, resulting in the synthesis of a further 13 structural analogues. The compounds were evaluated via the use of an operational model of allostery to determine values of functional affinity (K_B), intrinsic agonism (τ_B) and positive allosteric cooperativity (α , β). These parameters allowed the elucidation of the molecular determinants of allostery so that this information may be used for the design of irreversible and fluorescent biochemical tool compounds that retain their parent pharmacological profile.

Chapter 5. This chapter explores the structure-kinetic-relationships of the butyrophenone APD haloperidol at the D₂R for which there currently exists minimal published literature. Extrapyramidal symptoms (EPS) and hyperprolactinemia are common debilitating side-effects of typical APDs, and binding kinetics (i.e. association and dissociation rate from their biological target) at the D₂R may play a role in determining these side-effect profiles. It has been suggested that a slow dissociation rate is associated with hyperprolactinemia, but that a fast association rate is associated with EPS. Our

investigation further examined the ligand kinetics of butyrophenone analogues at the D₂R, and how these might ultimately impact therapeutic and side-effect profiles. We assessed the ligand binding kinetics of 50 novel and literature structural analogues of the antipsychotic haloperidol using a time-resolved Förster resonance energy transfer (FRET) competition association kinetic binding assay. We determined association and dissociation rates (k_{on} , k_{off}), and equilibrium affinities (pK_d) and discovered that the kinetic profile of the butyrophenone scaffold can vary dramatically with subtle structural modifications. This may allow optimisation of ligand kinetic parameters to design new APDs with improved side-effect profiles.

Chapter 6. The D₁R has been implicated as useful target to ameliorate the cognitive deficits associated with key CNS disorders. This chapter focuses on the synthesis and pharmacological validation of D₁R PAMs “compound A” and “compound B”. We conducted various chemical syntheses to generate racemic PAMs, as well as investigated the use of chiral resolving techniques and alternative chiral auxiliaries for use in asymmetric Diels-Alder chemistry toward the synthesis of optically pure enantiomers of “compound B”. The compounds were evaluated at the D₁R via the use of an operational model of allosterism to yield estimates of functional affinity (K_B), intrinsic agonism (τ_B) and allosteric positive cooperativity (α , β). All compounds displayed allosteric pharmacology. These molecules were also assessed for their subtype selectivity over the D₂R (i.e. D₁R vs D₂R). Compound A was found to act as a competitive partial agonist, yet compound B in its racemic and enantioenriched forms, showed no activity. Compound B will now be used as a starting point to form the basis of an extensive SAR investigation into subtype selective PAMs of the D₁R.

Finally, **Chapter 7** provides a brief summary of the outcomes obtained from this thesis, as well as future prospects.

Chapter 1 – General Introduction & Thesis Aims

Introduction

1. G protein-coupled receptors as central nervous system drug targets

1.1 GPCR structure and function

GPCRs are a class of dynamic membrane-bound receptors that are encoded by more than 800 genes in the human genome,¹ and are the largest family of cell-surface signal transducers.² GPCRs form a superfamily that encompasses a large number of receptors embedded on the lipid bilayer of the plasma membrane of eukaryotic cells. These receptors share a common structural architecture of seven hydrophobic transmembrane (TM) spanning α helical domains, with an extracellular amino terminus and an intracellular carboxyl terminus (Figure 1).³

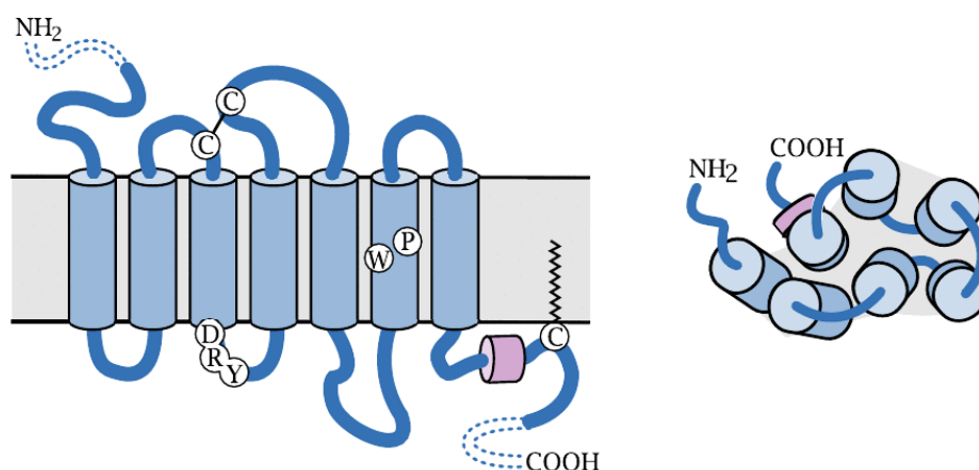


Figure 1. (Left) The simplified typical heptahelical architecture of a class A GPCR: the N-terminus is located extracellularly, and the C-terminus is located intracellularly. The location of several conserved amino acids among class A GPCRs, that play integral roles in receptor activation, are highlighted. These include the DRY motif located at the cytoplasmic end of helix 3, the proline and tryptophan residues located in helix 6, and the short, horizontally positioned C-terminal helix 8 resulting from palmitoylation. (Right) An extracellular view of a prototypical GPCR. The α -helices are arranged in an approximately circular fashion within the membrane plane. For many GPCRs, the extracellular accessible ligand binding site is located in a central crevice in the middle of the helices. Reproduced from Ramesh *et al.*⁴

Based on sequence similarity between the seven TM segments, GPCRs are classified into five distinct families/classes: rhodopsin-like (class A), secretin (class B), glutamate (class C), frizzled/taste family (class F), and adhesion family. The majority of transmembrane signal transduction in response to hormones and neurotransmitters is mediated by GPCRs, and these receptors are the principal signal transducers for the senses of light, odour, and taste.⁵ As such, they play an essential role in physiology

and disease, representing attractive therapeutic targets as exemplified by the fact that ~30% of clinically approved drugs currently target these receptors.⁶

GPCR activation occurs upon binding of a ligand (e.g. small molecule or peptide) which initiates signalling through canonical transducer proteins, called heterotrimeric guanine nucleotide-binding proteins (G proteins), as well as G protein independent pathways by G protein-coupled receptor kinase (GRK)-mediated phosphorylation, together with regulatory and scaffolding proteins such as arrestins, PDZ-domain-containing scaffold and non-PDZ scaffolds, such as A kinase anchor proteins (AKAPs) that initiate or control distinct patterns of signalling (Figure 2).⁷⁻¹⁰ Receptor-ligand activation initiates a major conformational change in the receptor, consequently exposing an intracellular pocket, allowing it to effectively promote dissociation of the heterotrimeric G proteins, as well as engage GRKs and arrestins, resulting in functional signalling complexes.¹¹ Heterotrimeric G proteins, composed of $G\alpha$, $G\beta$, and $G\gamma$ subunits, undergo a conformational change resulting in the release of guanosine diphosphate (GDP) and its exchange with guanosine triphosphate (GTP).¹² The $G\alpha$ and $G\beta\gamma$ subunits can then go to activate various effector molecules.¹³⁻¹⁹ In recent years, our mechanistic understanding of the complexity of GPCR function has seen a tremendous leap, and will pave the way for the identification and development of novel GPCR drugs.

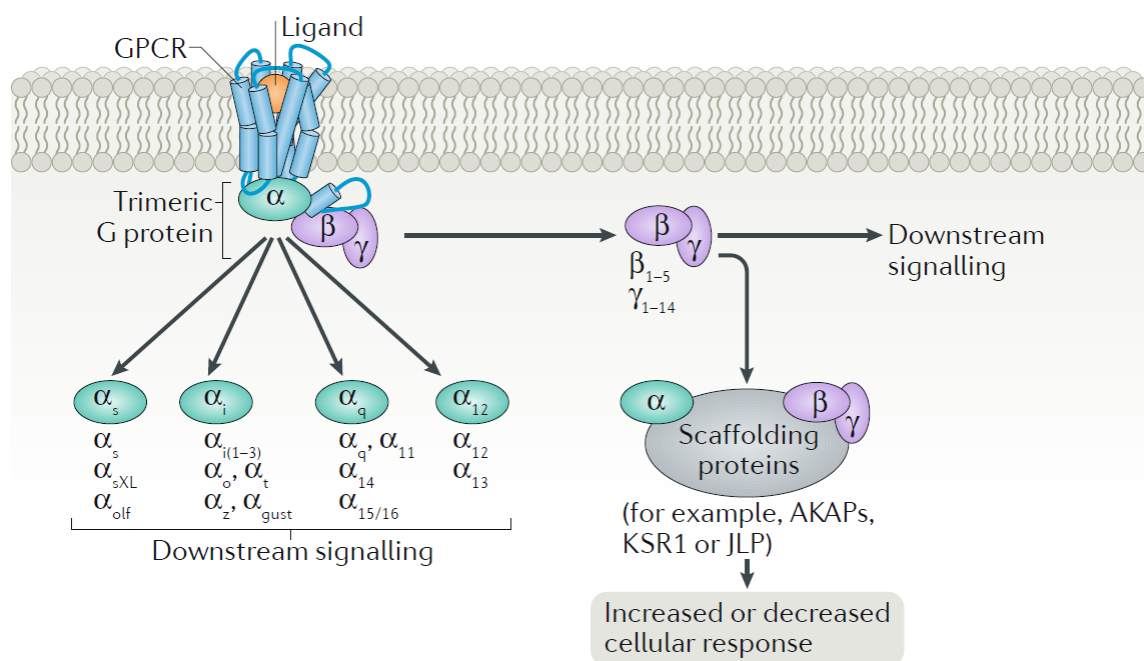


Figure 2. Schematic illustration of GPCR signalling. GPCR activation induces the dissociation of heterotrimeric G proteins ($G\alpha$, $G\beta\gamma$) which can each activate downstream signalling. There are multiple families of $G\alpha$ each with their unique signalling properties. There are also multiple $G\beta$ and $G\gamma$ subunits, increasing the complexity of signalling responses. Further, both $G\alpha$ and $G\beta\gamma$ subunits

may associate with scaffolding proteins that regulate distinct signalling profiles. Reproduced from Sexton *et al.*²⁰

1.2 Novel modes of GPCR targeting

1.2.1 Allosteric modulation

Traditional means of therapeutically targeting GPCRs have placed emphasis on identifying ligands that engage with the orthosteric binding site (OBS) (the binding site of the endogenous agonist/s), to either activate or inhibit the receptor. Ligands that bind to an allosteric site on a GPCR, termed allosteric modulators, can either act as positive allosteric modulators (PAMs) or negative allosteric modulators (NAMs) to potentiate or inhibit activation of the receptor by the endogenous agonist, respectively (Figure 3).²¹

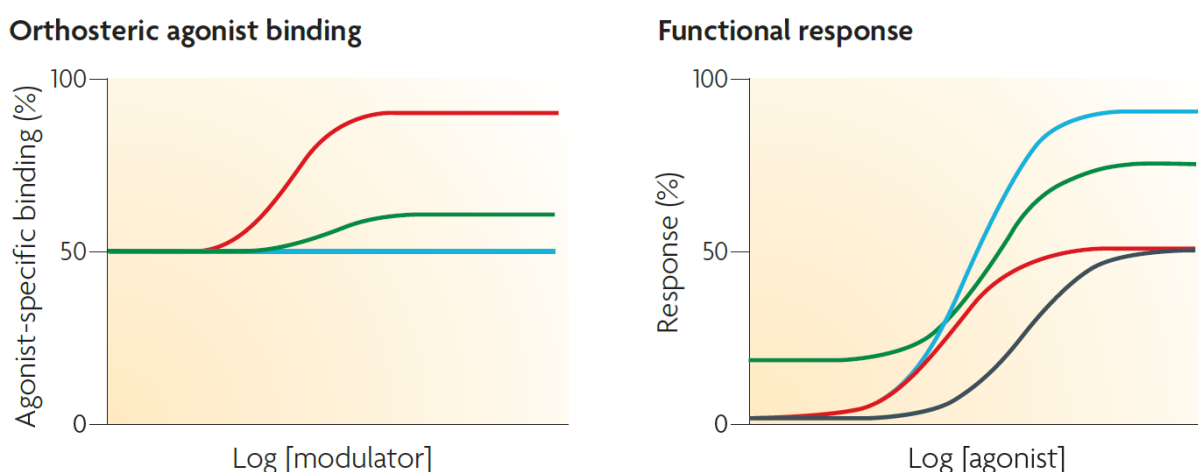


Figure 3. Simulations showing the effects on the binding (left) or function (right) of an orthosteric agonist (e.g. DA) mediated by allosteric potentiators with three different properties: (red) enhancement of DA affinity only; (blue) enhancement of DA efficacy only; (green) enhancement of DA affinity and efficacy in conjunction with direct receptor activation. The black line represents the unmodulated functional response of the agonist. Reproduced from Conn *et al.*²²

PAMs and NAMs are thought to stabilise receptors in specific conformational states that may act to increase or decrease the functional response to orthosteric agonists. These compounds have the ability to modulate the affinity of the orthosteric ligand for the OBS as well as modulate the intrinsic efficacy of an orthosteric agonist to engage downstream signalling mechanisms.²² As well as positive or negative modulation, the pharmacological effect of an allosteric modulator may also include inverse agonism, where the constitutive activity of a receptor is reduced. In addition to potentiating responses to orthosteric ligands, PAMs may also display intrinsic efficacy and thus activate the receptor in the absence of an orthosteric agonist (Figure 3). These compounds are often referred to as ago-PAMs.

Neutral allosteric ligands (NALs) can also bind to allosteric sites, but do not effect receptor responses to orthosteric ligands, instead competing for the allosteric binding site to block the actions of PAMs or NAMs.^{23,24} The types of allosteric modulators are officially described according to the IUPHAR Committee on Receptor Nomenclature and Drug Classification.²⁵

1.2.2 Allosteric modulator types and pharmacology

The effects of allosteric modulators on receptor pharmacology, and in particular orthosteric ligand binding, were originally described and quantified by ternary-complex mass-action models.^{26,27} However, more recently an operational model was introduced that not only incorporates the ability of a compound to modulate both affinity and efficacy, but also describes the ability of a compound to exert allosteric agonism.²⁸⁻³⁰ This model takes into account the interactions of orthosteric and allosteric ligands, and effector proteins to define the magnitude and direction of an allosteric effect. In the operational model, modulation of orthosteric binding affinity is governed by a cooperativity factor, denoted by α , and modulation of signalling efficacy is governed by the cooperativity factor β (Figure 4). Furthermore, allosteric compounds that exert an effect in their own right and in the absence of orthosteric ligand, can be quantified through a value of intrinsic efficacy (τ_B) (Figure 4).

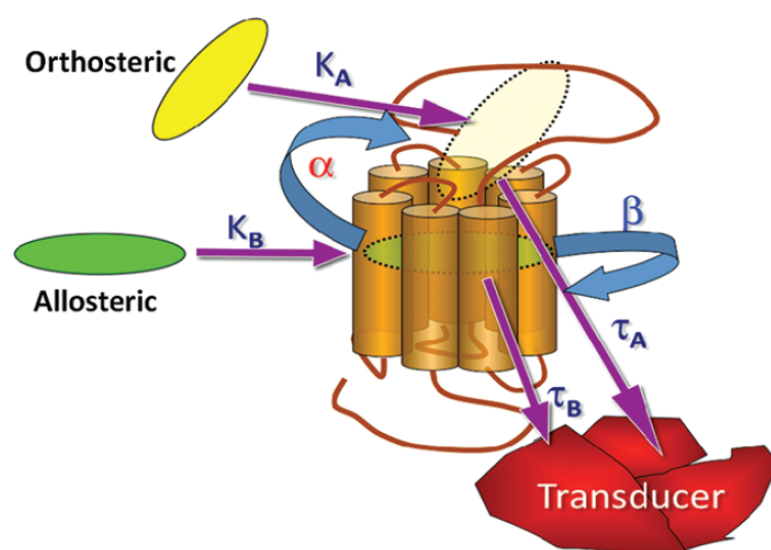


Figure 4. Schematic representation of the parameters underlying the operational model of allosterism and agonism. K_A and τ_A : Orthosteric ligand equilibrium association constant and intrinsic efficacy parameter, respectively. K_B and τ_B : Allosteric ligand equilibrium association constant and intrinsic efficacy parameter, respectively. Allosteric ligands may enhance or facilitate orthosteric-agonist induced receptor function through positive cooperativity (α , binding cooperativity constant), possibly impacting upon the orthosteric ligands intrinsic efficacy (β , modulation factor). Conversely, it may inhibit/diminish function through negative cooperativity. Reproduced from Melancon *et al.*³¹

1.2.3 Advantages of allosteric modulators

Exogenous synthetic ligands that bind to allosteric sites may offer a number of advantages over orthosteric ligands, and the existence of allosteric modulators of GPCRs has been known for over two decades.^{32,33} Inherent in their mechanism of action, they may alter the structure, dynamics and function of the receptor to achieve potential therapeutic advantages over orthosteric agents. For example, allosteric modulators have a ceiling level to their effect, as determined by the magnitude and nature of cooperativity between allosteric and orthosteric binding sites, resulting in a reduced potential for on-target overdose and/or toxicity.²⁵ Other advantages include the ability to obtain a higher degree of receptor subtype selectivity, as allosteric sites generally show greater sequence divergence among related GPCRs, and are less evolutionarily conserved.³⁴ Using the metabotropic glutamate receptors (mGluRs) as an example, only a few subtype-selective orthosteric mGluR ligands have been reported due to high sequence conservation.^{35,36} However, the allosteric binding domains of this receptor system have proved to be a tractable target, and hundreds of subtype-selective allosteric modulators have now been reported, primarily for mGlu₂,³⁷ mGlu₄,^{38,39} and mGlu₅Rs.^{40,41} In addition, further selectivity may also be achieved through selective cooperativity at a given receptor subtype with a given orthosteric ligand (probe dependence). Allosteric modulators may also display the potential to maintain physiological and spatiotemporal signalling patterns due to their ability to concurrently bind with the endogenous signalling molecule.⁴² Recent studies with subtype-selective mGlu₅Rs PAMs provide direct evidence that modulators for this receptor subtype maintain activity dependence in certain CNS circuits.⁴³ In addition, binding or functionally selective PAMs of the ligand-gated ion channel receptor GABA_A, such as benzodiazepines, have seen clinical validation. They provide advantages over traditional orthosteric agents as they only exert an effect following the synaptic release of γ -aminobutyric acid (GABA) and activation of the receptor by the endogenous agonist,⁴⁴ consequently conferring significantly better safety and tolerability profiles.⁴⁵

Finally, allosteric agents also have the potential to show differential effects on downstream signalling pathways, termed biased agonism. This concept reflects the fact that some drugs may have diverse functional effects on different signalling pathways mediated by a single receptor.^{46,47} This was demonstrated using mGlu₅Rs which, activates both intracellular Ca²⁺ mobilization and ERK signalling in rat cortical astrocytes. In the presence of two different PAMs, these downstream signalling pathways were differentially affected as both showed similar induced intracellular Ca²⁺ transients but their effects on ERK1/2 signalling differed.⁴⁸ Further, Cook *et al.* characterised the ligand-biased profile of novel calcimimetics in HEK293 cells stably expressing the calcium-sensing receptor, demonstrating molecules with differential bias towards allosteric modulation of Ca²⁺ immobilisation, IP₁ accumulation, and pERK1/2.⁴⁹ This behaviour suggests that allosteric ligands can possess multiple efficacies for the many behaviours that a receptor can exhibit.⁵⁰

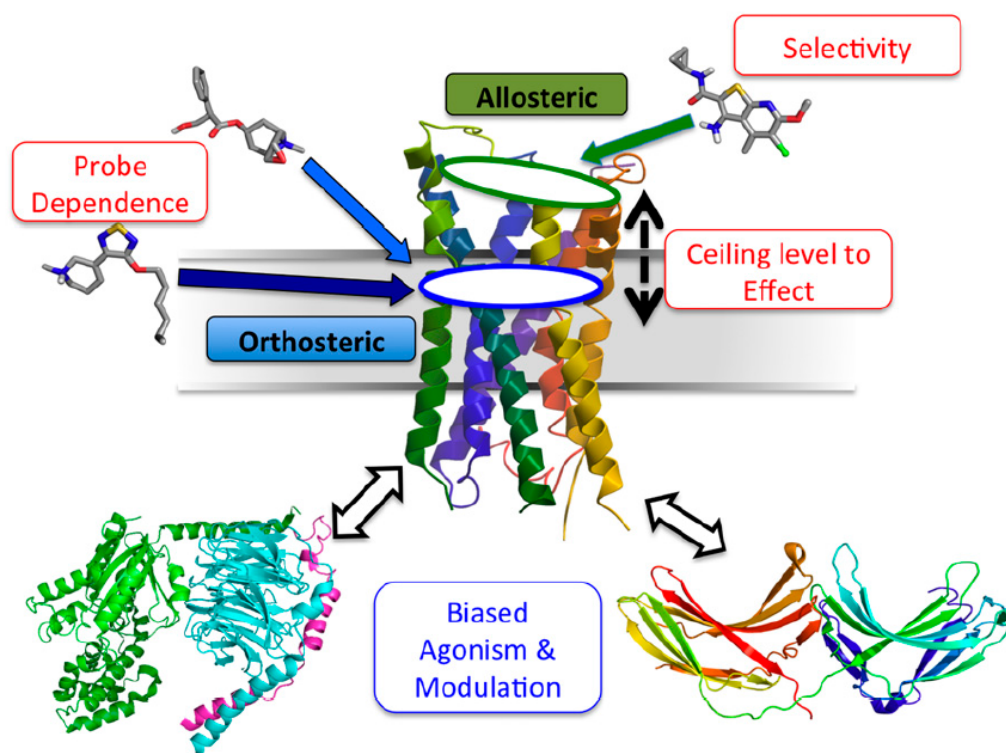


Figure 5. The various pharmacological characteristics and theoretical advantages of GPCR allostery. Reproduced from Christopoulos *et al.*⁵¹

2. The dopaminergic system

DA is the prevalent catecholamine neurotransmitter in the central nervous system (CNS). Its cognate receptors are members of the class A (rhodopsin-like) family of GPCRs, and can be divided into five subtypes, classified as D₁-like (D₁R and D₅R) and D₂-like (D₂R, D₃R, and D₄R). The D₁-like family receptors are coupled to the stimulatory G proteins (G α_s and G α_{olf}), which cause sequential activation of the effector adenylate cyclase (AC), an enzyme that converts adenosine triphosphate (ATP) to the second messenger cyclic adenosine monophosphate (cAMP), as well as cAMP-dependent protein kinase, and the protein phosphatase-1 inhibitor DARPP-32.⁵² D₂-like family receptor signalling is mediated by G α_i and G α_o , which inhibit AC, but also activate the mitogen-activated protein kinase (MAPK) pathway.⁵³ This receptor family also activates non-canonical arrestin-dependant signalling pathways.⁵³ The transmembrane domains of the DA receptors (DARs) are highly conserved,⁵⁴ with the D₁-like receptors sharing 78% homology, while D₃R and D₄R share 75% and 53% sequence conservation with the D₂R, respectively.⁵⁵ Variants also exist in the genes encoding the D₂R which can be split into two main types, the short form (D_{2s}) and the long form (D_{2L}), are generated as a result of differential splicing of exons. The D_{2s} variant is a presynaptic inhibitory auto receptor whilst the D_{2L} is a postsynaptic receptor.^{56,57} DA modulates activities in the brain regions that are innervated by nigrostriatal, mesocorticolimbic, and tuberoinfundibular dopaminergic pathways (Figure 6).⁵⁸

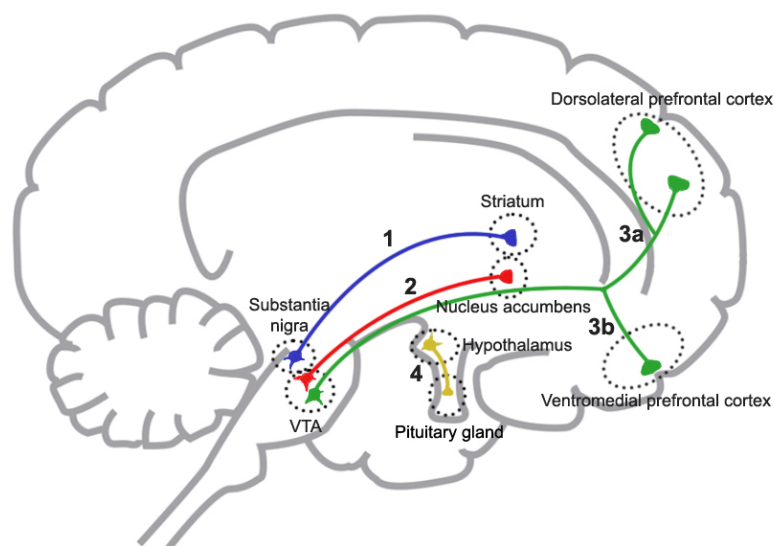


Figure 6. Four major dopaminergic pathways in the brain: nigrostriatal (1), mesolimbic (2), mesocortical (3a-b), and tuberoinfundibular (4). Figure adapted from Stahl's Essential Psychopharmacology (3rd edition).⁵⁹

2.1 Dopamine receptors: D₁R and D₂R subtypes

The D₁R and D₂R are involved in the control of numerous physiological functions such as cognition, emotion, motor behaviour, reward, sleep, memory, as well as neuroendocrine secretion.⁶⁰ D₁R are widely expressed in the CNS, with the D₁Rs being dominant neocortically, especially in the prefrontal cortex (PFC), and are also found in the striatum, whereas the D₂Rs have a high concentration in the striatum and lower presence in the PFC, hippocampal, entorhinal cortex, amygdaloid, and thalamic structures.⁶¹ The spatial expression patterns of the D₂R and D₃R are also distinct in certain areas of the brain. The D₂R is heavily expressed in regions responsible for motor and endocrine functions, whereas the brain regions within the mesolimbic circuitry, including the nucleus accumbens, islands of Calleja, and the ventral striatum, contain relatively localised expression of D₃R.^{58,62-64} D₁R are also expressed in the periphery, predominantly in the vasculature and kidneys, where they're involved in vascular tone, hormone secretion, sodium homeostasis, as well as hormone regulation and retinal processes.⁶⁵

Abnormal dopaminergic signalling has been suggested for a host of CNS pathologies, such as bipolar disorder, major depression, dyskinesias, and various somatic disorders, including hypertension and kidney dysfunction.⁶⁶⁻⁶⁸ Research in non-human primates also suggests an important role for the D₁R in the pathophysiology of schizophrenia (SCZ),^{69,70} and D₁R dysregulation has been linked to cognitive deficits in patients with this disease.⁷¹ Consequently, the D₁R has been hypothesised as a promising therapeutic target to instead ameliorate the negative and/or cognitive symptoms associated with SCZ that are not addressed by current APDs. Thus, there is a need for novel agents that can

better mimic endogenous levels of DA to improve cognitive function. Most notably, the D₂R is targeted for the symptomatic treatment of SCZ and Parkinson's disease (PD).⁷²⁻⁷⁸ In addition, brain regions with high levels of localised D₃R expression are associated with rewarding and motivational characteristics of addictive drugs, and thus the D₃R receptor has been implicated as an attractive target for the development of pharmacotherapies to treat substance abuse disorders such as cocaine and methamphetamine addiction.⁷⁹⁻⁸²

3. Structural elucidation of dopamine receptors

Class A GPCRs in the CNS are the most heavily investigated drug targets in the pharmaceutical industry.⁸³ As these receptors are involved in many different disease-related pathways, a molecular understanding of these drug targets is critical to enable the rational design of drugs with a specific pharmacological profile. Class A GPCRs are the most abundant GPCR superfamily, which is reflected by the number of unique receptor structures solved from this class.²⁰ The growing number of high-resolution three-dimensional structures of many GPCRs are being revealed through breakthroughs in techniques such as cryo-electron microscopy and X-ray free electron lasers as alternatives to standard X-ray diffraction. GPCR structure-based drug design has seen recent success in guiding the discovery of novel chemical probes and therapeutic leads.^{84,85} Crystal structures are now available for rhodopsin,⁸⁶ serotonin,⁸⁷⁻⁹⁰ adrenergic,⁹¹⁻⁹⁴ muscarinic,^{95,96} opioid,^{97,98} and adenosine^{99,100} receptors, in both inactive and activated forms, as well as for chemokine¹⁰¹ and histamine¹⁰² receptors in their inactive conformations. The crystal structures of the D₂R (Figure 7),¹⁰³ D₃R,¹⁰⁴ and D₄Rs¹⁰⁵ have also been solved in their inactive conformations. Despite this, ligand-bound GPCR complexes are notoriously difficult to elucidate due to their low receptor expression levels in native tissue, their inherent flexibility and instability upon their isolation from the lipid bilayer, and the low affinity of their endogenous ligands, in addition to small molecule allosteric modulators.¹⁰⁶

The D₃R structure was reported at a resolution of 3.2 Å,¹⁰⁴ and the D₄R at resolutions of 1.95 Å and 2.2 Å,¹⁰⁵ where these ligand complexes were obtained with the substituted benzamides eticlopride and nemonapride, respectively. However, the D₂R construct, determined at a resolution of 2.9 Å,¹⁰³ was purified and crystallised in complex with the atypical APD risperidone. It is hoped that the D₂R complexed with this non-benzamide ligand will aid in the clarification of specificity determinants of this receptor family, consequently expanding the understanding of how different structural classes interact with DARS to inform basic and translational neuroscience.¹⁰⁷ When comparing the orthosteric ligand binding pocket of the D₂R with structures of the D₃R and D₄R, marked differences, in addition to others, were found around residues Val/Phe^{2,61}, Trp^{EL1}, Phe/Leu^{3,28}, and Tyr/Val^{7,35}, which help to define an extended binding pocket (EBP) in the D₂R (superscript refers to the Ballesteros-Weinstein numbering system for GPCRs).¹⁰⁸ Indeed, previous studies on the D₃R¹⁰⁴ and D₄R¹⁰⁵ have also

revealed selective EBPs in each receptor, which has subsequently enabled the structure-based discovery of D₄R-selective agonists.¹⁰⁵ Interestingly, molecular docking studies of risperidone with homology models of the D₂R, based on either the D₃R or D₄R, have failed to reproduce the unique pose adopted by risperidone, nor do they predict a 90° rotation of its tetrahydropyridopyrimidine ring in the D₂R-complex.¹⁰³ These findings have implications toward our understanding of receptor-ligand recognition and the design of novel selective antipsychotic drugs. Furthermore, understanding the sequence divergence of EBPs located within the D₂-like receptors is crucial for the development of drugs with novel modes of action and unprecedented selectivity.

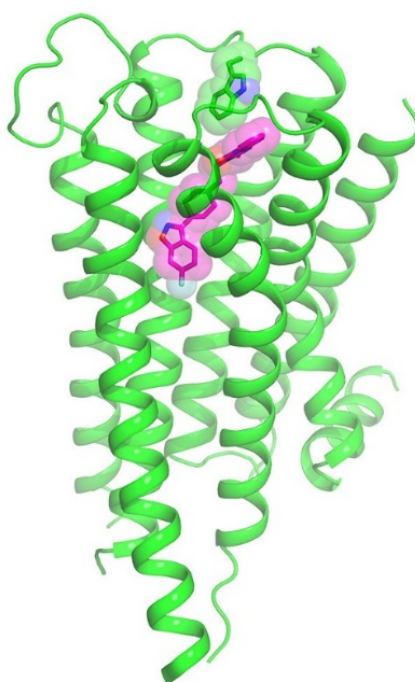


Figure 7. X-ray crystal structure of the dopamine D₂ receptor (green ribbons) in complex with the atypical antipsychotic drug risperidone (magenta) solved at a resolution of 2.9 Å. Figure adapted from Wang *et al.*¹⁰³

4. Schizophrenia: background & the dopamine hypothesis

SCZ is a chronic and debilitating neuropsychiatric illness that affects approximately 1% of the human population.¹⁰⁹ The disease is characterised into three distinct symptom domains, namely positive, negative, and cognitive symptoms, potentially arising from neurodegenerative and neurodevelopmental pathophysiologic processes (Figure 8).^{110,111} The positive symptoms refer to hallucinations, delusions, disordered thoughts and irrational behaviour, and are considered manifestations of psychosis. The negative symptoms are defined as a lack of motivation (avolition), lack of interest (apathy), poverty of speech (alogia) and absence of pleasure (anhedonia).¹¹² The cognitive deficits are now considered a central feature of SCZ, and refer to alterations in

neurocognition, including deficits in working memory, attention, learning, and executive functioning.^{113,114} The onset of SCZ is usually in the late teens and early twenties (16-25 years old), just prior to the commencement of adulthood.¹¹⁵ Recent genetic data from large-scale genome-wide association studies suggest that genes underlying the expression of the core symptoms of SCZ are associated with abnormalities in glutamatergic as well as dopaminergic neurotransmission,¹¹⁶ together with the overexpression of immune system genes, including those that regulate synaptic pruning, such as complement component 4 genes.¹¹⁷ However, the most widely known theory contributing to the cause of SCZ is currently the DA hypothesis.

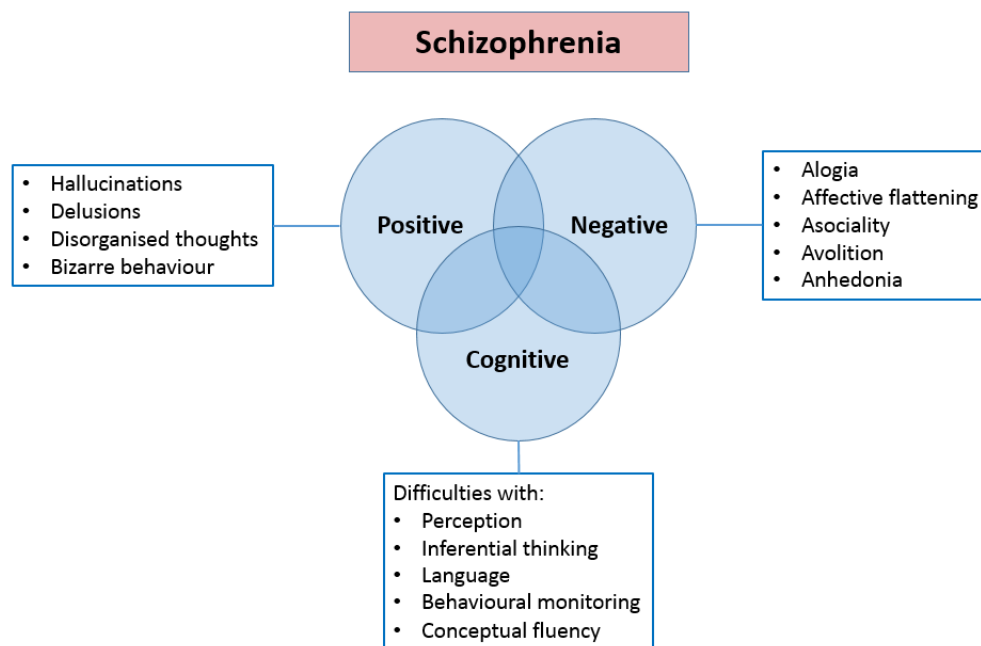


Figure 8. The interrelated set of symptoms that define schizophrenia.

This hypothesis states that SCZ is a result of hyperdopaminergic activity in the mesolimbic system (dopaminergic projections from the ventral tegmental area (VTA) to the limbic region). This hypothesis also suggests that disruption of the mesocortical system in patients with SCZ inhibits the negative feedback loop to the VTA. This leads to an increase in VTA firing and, consequently, an increase in DA activity in the mesolimbic system.^{118,119} The VTA is the origin of the dopaminergic mesolimbic pathway, which is known to be overactive in SCZ.^{120,121} In addition, post-mortem brain studies of schizophrenic patients show an increase in dopamine receptor sensitivity and concentration, also suggest the involvement of DA in SCZ.^{122,123} The proposal that SCZ is related to DA hyperactivity originally stemmed from early work revealing that superimposed X-ray crystal structures of chlorpromazine (the first SCZ treatment discovered in 1952) and DA, showed many molecular similarities.^{124,125} This suggested that chlorpromazine might in fact antagonize DARs, and therefore led to the proposal that SCZ is related to DA hyperactivity.¹²⁶ D₂R blockade in the brain is

a general pharmacodynamic property of all antipsychotic drugs,¹²⁷ and their clinical efficacy can be correlated with their D₂R affinity. D₂R antagonism is thought to ameliorate the positive symptoms of patients with SCZ by blocking the levels of excessive dopamine in the brain.¹²⁸⁻¹³¹ ¹³² Finally, DAR agonists produce psychosis that is indistinguishable from that of SCZ in healthy individuals, and also exacerbate positive symptoms of the disorder.^{133,134}

4.1 Antipsychotic drugs

Antipsychotic drugs (APDs) are mainstays in the treatment of SCZ and other related disorders, including but not limited to, schizoaffective disorder, delusional disorder, and bipolar affective disorder.¹³⁵ These drugs cover three main classes, namely typical and atypical, and DA system stabilisers. Typical APDs, such as chlorpromazine (**1**) and haloperidol (**2**) (Figure 9), are considered first generation antipsychotics (FGAs), acting in part through antagonism/inverse agonism of D₂Rs in the mesolimbic pathway.¹³⁶ FGAs are effective at decreasing the positive symptoms of SCZ, but are associated with various on-target-mediated side-effects, most notably extrapyramidal symptoms (EPS), tardive dyskinesia and hyperprolactinemia. EPS are detrimental to a person's motor control or function, and include akinesia, akathisia, acute dyskinesias and dystonic reactions, and Parkinsonism.^{137,138} EPS are thought to be mediated by D₂R signalling blockade in the nigrostriatal DA system, whereas hyperprolactinemia is associated with D₂R signalling blockade in the tuberoinfundibular pathway.¹³⁹⁻¹⁴⁵ Due to this reason, FGA's are less frequently used.¹⁴⁶

Second generation antipsychotics (SGAs), exemplified by clozapine (**3**) and risperidone (**4**) (Figure 9), display a wider therapeutic profile (improvement of positive and negative symptoms) with increased safety, and a diminished incidence of EPS and hyperprolactinemia.¹⁴⁷⁻¹⁴⁹ Their mechanism of action is believed to include more potent blockade of serotonin 5-HT_{2A} receptors than of DA D₂Rs,^{150,151} together with additional non-DA D₂R-mediated actions.¹⁵² Furthermore, most but not all atypical APDs share this particular feature, particularly modulation of serotonergic neurotransmission.¹⁵³ Blockade of 5-HT receptors has been demonstrated to be beneficial towards the improvement of negative symptoms associated with SCZ.¹⁵⁴⁻¹⁵⁶ Unfortunately, a lack of selectivity across aminergic receptors is associated with off-target side-effects, including sedation, metabolic issues including type II diabetes, weight gain, urinary incontinence and constipation.¹⁵⁷ Moreover, around 1-2% of clozapine-users will develop agranulocytosis, a potentially fatal blood disorder restricting its use and as such, it is now only prescribed for treatment-resistant SCZ.^{158,159}

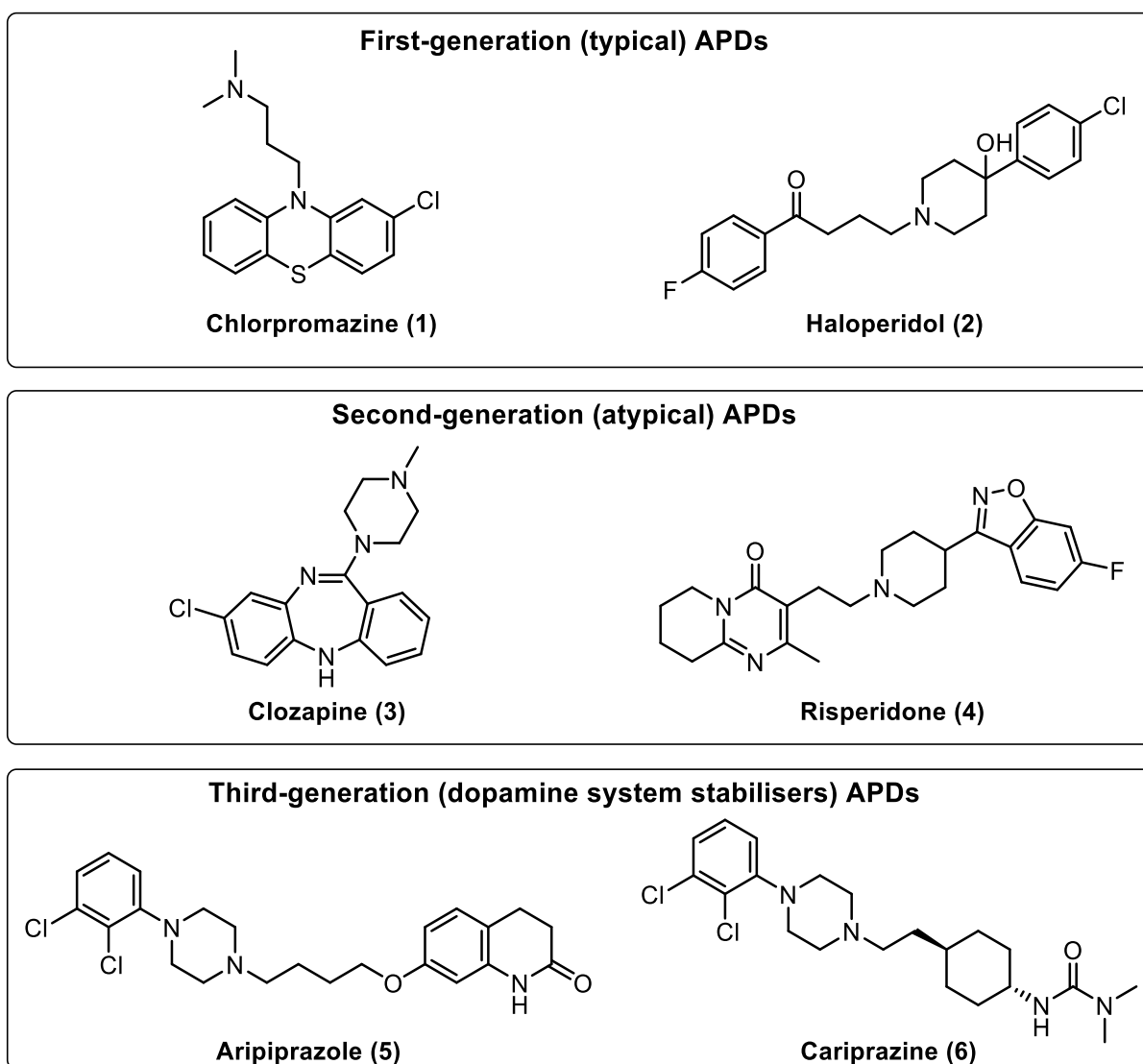


Figure 9. Antipsychotic drugs used for the treatment of SCZ, grouped according to their classifications.

The final class of APDs are classified as third-generation antipsychotics (TGAs), as exemplified by aripiprazole (5) and, more recently, cariprazine (6) and brexpiprazole, which were approved in the USA and Europe in 2015 for SCZ and bipolar disorder (Figure 9). Aripiprazole (5) displays a unique pharmacological profile in that it is a partial agonist at both presynaptic and postsynaptic D_2R s as well as the serotonin $5HT_{1A}$ receptor,¹⁶⁰⁻¹⁶³ and has antagonist activity at $5-HT_2$ receptors.¹⁶⁴ However, aripiprazole has recently been shown to display a unique functional profile for modulation of D_2R -stimulated G proteins.^{165,166} A D_2R partial agonist still activates the receptor upon binding, but displays only partial efficacy at the receptor relative to the endogenous agonist dopamine. This means aripiprazole possesses both agonistic and antagonistic effects. For example, depending on the receptor population and the concentration of the full agonist DA, a partial agonist can act as a functional antagonist, competing with the full agonist for receptor occupancy and producing a net decrease in the activation of the receptor as observed by DA alone.

In humans, this occurs at the postsynaptic receptors, where there are high concentrations of DA, consequently enabling aripiprazole to act as an antagonist. This means aripiprazole is able to reduce the overstimulation of receptors when excess amounts of DA are present as seen in patients with SCZ. Since dopaminergic neurons all contain autoreceptors responsive to agonists such as DA, activation of these autoreceptors may function to decrease DA synthesis, release, and neuronal firing pertaining to certain instances. Alternatively, DA concentrations can be reduced in some brain regions, therefore a partial agonist can consequently result in partial activation.¹⁶⁷ Due to their distinct pharmacology at the D₂R, partial agonists such as aripiprazole may display a reduced propensity to elicit side-effects still apparent in many SGAs by accommodating both hypo- and hyper-dopaminergic states in the brain. The clinical relevance of partial agonists for their treatment of SCZ and other related disorders is highlighted in reviews from Tamminga *et al.*^{168,169}

4.2 Antipsychotic drug discovery

While the field of APD discovery has seen significant advances over the last seven decades, historical issues still currently exist. Developing small molecule drugs that are subtype-selective is a major challenge. The non-selective nature of clinical APDs and their binding to several neurotransmitter receptors is responsible for a proportion of the side-effect profiles seen with these drugs. Typical and atypical APDs display complex pharmacological profiles, interacting with a number of dopaminergic (eg. D₂, D₃, and D₄),¹⁷⁰⁻¹⁷² serotonergic (e.g. 5-HT_{1A}, 5-HT_{2A}, 5-HT_{2C}, 5-HT₆, and 5HT₇),¹⁷³⁻¹⁷⁵ histaminergic (e.g. H₁ and H₄)^{176,177} adrenergic and muscarinic acetylcholine receptors.^{178,179} Other disadvantages associated with the use of FGAs, SGAs, and TGAs includes high receptor occupancy (75-80%) in the caudate/putamen, resulting from the administration of a high-affinity FGA generally causing the development of EPS. In order to sustain efficacy whilst reaching an appropriate point of receptor occupancy (60-80%) in brain areas such as the limbic system and cortex,¹⁸⁰⁻¹⁸² clinicians have to titrate the dosage of APDs to stay within this acceptable range, but this often leads to poor compliance.¹⁸³ Administration of SGAs also induces EPS, however the extent of which is dependent upon the type of SGA used.¹⁸⁴ Further, studies have shown a dependant relationship between the safety of SGAs and receptor occupancy, whereby increased dosage correlates to increased adverse effects.¹⁸⁵ Although TGAs such as aripiprazole display a lower propensity to induce dystonia, parkinsonism, and EPS, ~15-25% of patients still suffer from akathisia, one of aripiprazole's most frequent extra-pyramidal symptoms.¹⁸⁶⁻¹⁸⁸

5. Novel aspects of antipsychotic drug discovery

It is clearly evident that the way in which we design APDs requires a significant transformation, such that novel drugs can be both safe, efficacious, and devoid of on- and off-target side-effects. Despite more than a half-century of research being dedicated to building our molecular understanding of this disease state, there are many questions that still remain to be answered. Another significant limitation to current APDs are their inability to adequately address all three symptom domains of SCZ. They are generally effective against the positive symptoms^{189,190} but their effects on negative symptoms are limited.¹⁹¹⁻¹⁹³ Moreover, APD effects on neurocognitive deficits (e.g., executive functioning and working memory) have too been reported,¹⁹⁴⁻²⁰¹ albeit small.¹⁹⁰ Amelioration of these cognitive deficits is being increasingly recognised as the best predictor of effective long term prognoses, and thus development of APDs that address this symptom domain are a key target for the development of novel efficacious therapeutics.²⁰²⁻²⁰⁴ The negative symptoms and cognitive deficits are thought to be partly related to a deficit in cortical DA levels.²⁰⁵⁻²⁰⁷

5.1 The dopamine D₁ receptor as a therapeutic target

Impaired cognitive function is a common feature amongst patients with SCZ and other mental disorders, which inflicts an enormous emotional and social burden on the individual.²⁰⁸ Neuropsychological and neurophysiological studies have supported the importance of the PFC in cognition and cognitive deficits in SCZ.²⁰⁹⁻²¹⁴ The majority of DARs in the dorsolateral prefrontal cortex (dlPFC), a region critical for working memory performance, are of the D₁R subtype.²¹⁵ This region is especially underactive in schizophrenic patients, and this has been demonstrated as a critical liability region in SCZ.^{216,217} Further, increased D₁R expression in the PFC has been reported in patients with SCZ, potentially via compensatory upregulation due to reduced PFC-DA release. This increased expression has been directly associated with poor working memory performance.²¹⁸ Schizophrenic patients also perform poorly on PFC-mediated tasks that involve working memory.^{219,220} Unfortunately, there has been limited success in establishing effective treatments for normalising PFC cognitive abilities in humans. Early research conducted on rhesus monkeys, and later in marmosets, revealed that DA is essential for PFC spatial working memory functions, and that DA depletion from the dlPFC was as detrimental to cognition as removing the cortex itself.^{221,222} DA depletion from the dlPFC in marmosets was also shown to impair attentional set formation.^{223,224} Functional brain imaging studies showed alterations in SCZ correlated to poor performance on frontally mediated cognitive tasks.²²⁵ Following the advent of more selective pharmacological tools, additional studies showed that D₁R/D₅R blockade in the dlPFC impairs working memory function.^{226,227} Consistent with these findings, low systemic doses of the very first full D₁R/D₅R agonist, dihydrexidine (DHX) (**8**, Figure 10), were shown to improve working memory performance

in monkeys.²²⁸ Such observations have led to a reformulation of the classical DA hypothesis to now suggest that a deficit in DA transmission at D₁Rs in the PFC might be implicated in the cognitive impairments and negative symptoms.²²⁹ This is also supported by the fact that D₂R antagonism displays a lack of efficacy with respect to ameliorating negative and cognitive deficits.

Despite the support for clinical efficacy of D₁R agonists, and almost 25 years later, they have failed to successfully translate into clinical development. This failure is inherently due to the many challenges associated with the development of orthosteric D₁R agonists as therapeutics. Of particular concern is their propensity to display a narrow inverted U-shaped dose response. For example, high doses of D₁R/D₅R antagonist or agonist treatment after systemic or intra-PFC infusions, or very high levels of DA release in the PFC (as occurs during stress exposure), actually impairs cognition.²³⁰⁻²³⁴ Similar research in humans also suggests an inverted U-shaped dose response.^{235,236} Another major issue has been poor oral bioavailability, which can be attributed to a catechol moiety prevalent in all currently reported full D₁R agonists. In select cases where drugs have been shown to display moderate bioavailability, they also display high plasma protein binding and low free fraction, as well as high unbound clearance.²³⁷ Other D₁R agonists have been reported to induce seizures or lower seizure thresholds of which D₁R activation seems to be critical;²³⁸ however, this has been shown to be drug specific²³⁹ and the underlying mechanisms are at present poorly understood. An additional D₁R-related safety concern is hypotension, which was the reason for premature termination of the first human pilot trial of the full efficacy D₁R agonist DHX (**8**).²⁴⁰ These effects may be due to activation of peripheral D₁Rs, localised both in the cardiovascular system and renal tissues.²⁴¹ Finally, rapid acquisition of tolerance also has the potential to limit the use of D₁R agonists. Collectively, data from these studies support the hypothesis that subtype-selective D₁R full or partial agonists represent an attractive avenue for the treatment of cognitive dysfunction. Compounds of this description may also broaden the inverted U-shaped dose response subsequently expanding the dose range for therapeutic effects. Furthermore, selective PAMs of the D₁R may have a similar therapeutic profile, and provide the potential to explore novel chemical space and improve small molecule physicochemical properties. A more complete understanding of DA action at different receptor subtypes localised in the PFC will depend on the advent of highly subtype selective pharmacological tools to ultimately probe the role of the D₁R in neurocognitive dysfunction

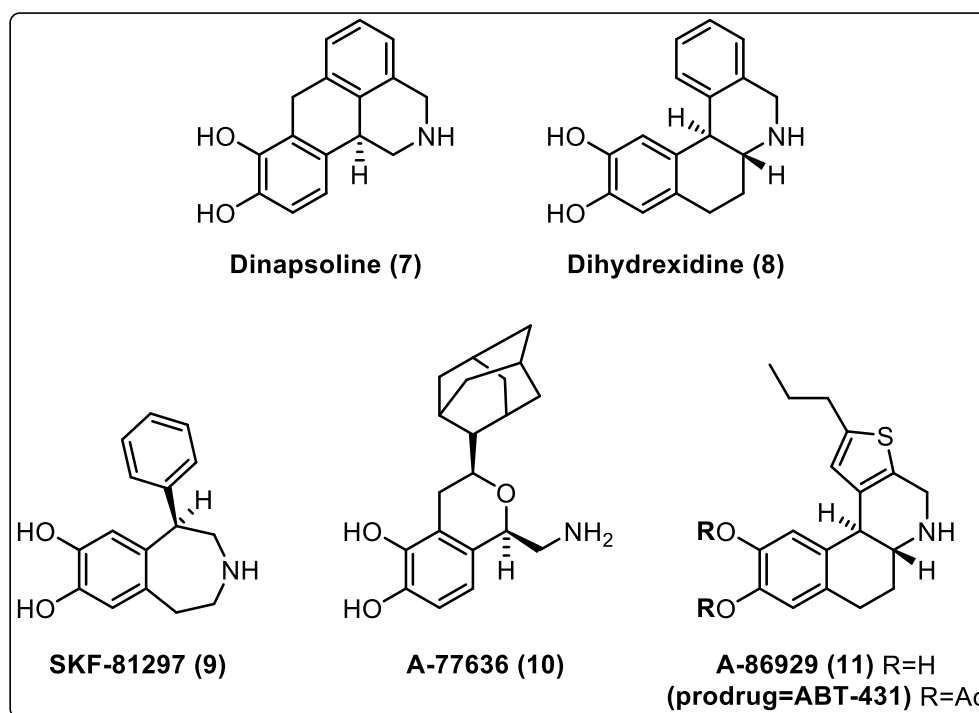


Figure 10. Examples of representative experimental D₁R agonists. (Top row) Full D₁R agonists dinapsoline (a D₁R/D₂R agonist with high intrinsic activity and significant functional selectivity at D₂Rs) and dihydraxidine (reported to improve working memory in monkeys but subsequent human studies hampered by poor pharmacokinetics). (Bottom row) The phenylbenzazapine SKF-81297, and full agonists A-77636 (selective D₁R agonist of the novel isochroman chemotype), and A-86829 (the active compound of the diacetyl prodrug ABT-431 shown to have antiparkinsonian effects but poor oral bioavailability).

5.2 Binding kinetics in the context of APD side-effect liabilities

Despite decades of research, the on-target side effects induced by administration of APDs remain a significant problem for the symptomatic treatment of SCZ, often resulting in poor drug adherence.^{242,243} Therefore, understanding the basis for these effects is critical towards enabling the design of better therapeutics.^{140,141} Central to most definitions of atypicality is the absence of EPS and the ability to avoid sustained hyperprolactinemia.²⁴⁴⁻²⁵¹ Various hypotheses have been put forward in an attempt to explain the basis of atypicality. The DA-serotonin theory suggests that antagonism of the 5-HT_{2A} receptor plays a role in efficacy as well as decreased risk of EPS development, as this is thought to “balance” striatal DA signalling.^{128,151,153,156,252} However, subsequent studies have suggested this theory cannot account for all examples of atypicality,^{253,254} and the role of DA receptor blockade and modulation remains dominant.

The concept of kinetic binding parameters, that is, the rate at which drugs bind to (association rate, k_{on}) and dissociate from (dissociation rate, k_{off}) their biological target, are being increasingly realised

as important parameters in drug discovery.^{255,256} Accordingly, another theory that has received widespread attention is based on the dissociation kinetics of APDs from the D₂R, a concept that originated from the observation that some atypical APDs have lower affinity for the D₂R than typical APDs.^{171,257,258} This was later proposed to be due to a faster dissociation rate.²⁵⁹⁻²⁶¹ Radiometric kinetic studies by Kapur *et al.*, determined the rate constants of a series of nine APDs in an attempt to relate them to their inhibition constants (K_i) and establish whether k_{on} , or k_{off} , or both, contribute to the differential affinity of APDs for the D₂R.²⁶¹ These data demonstrated that differences in APD affinity were correlated with their rate of dissociation as this parameter varied ~1000-fold, and differences in the k_{off} of these compounds could explain 99% of the variance in their affinity for the D₂R, whereas differences in their k_{on} did not meaningfully relate to differences in affinity. These observations formed the basis of the “fast dissociation hypothesis”, whereby faster rates of receptor dissociation are proposed to make an APD more accommodating to the rapid and transient nature of synaptic DA transmission through surmountable antagonism,²⁶² and thus less likely to give rise to on-target side effects such as EPS and prolactin elevation.²⁵⁴ This hypothesis was based on the widely held assumption that association rates are diffusion limited, thus all APDs exhibit similar D₂R association rates and consequently affinity is comparable and predominantly driven by differences in D₂R dissociation rate alone.^{128,263,264}

In order to further explore the kinetic basis for on-target side effects, Sykes *et al.* applied recently developed methodology to determine the binding kinetics of an extensive series of APDs at physiological temperature and Na⁺ concentration.²⁶⁵ These experiments used time-resolved Förster resonance energy transfer (TR-FRET) in a competition association kinetic binding assay, which significantly improved throughput relative to traditional radioligand binding assays, allowing a large number D₂R antagonists to be profiled under identical test conditions for the first time. Contrary to the historical link between APD D₂R affinity and dissociation rate (based on the assumption that APDs exhibit approximately the same k_{on} for D₂Rs),²⁶¹ Sykes *et al.* found that atypical APDs displayed an increased range of k_{on} values compared to a relatively small change in k_{off} values. In contrast, a much narrower variation in the value of k_{on} was found for typical APDs, whereby differences in affinity were instead driven by changes in k_{off} , highlighting the importance of directly measuring rate constants. They correlated their kinetic data with data from a recent and relatively comprehensive multi-treatment clinical meta-analysis that quantified the level of efficacy, EPS and hyperprolactinemia associated with a diverse group of APDs,²⁶⁶ as well as a summary of the primary literature of drug-naïve patients. To address a lack of information regarding EPS, they performed an additional exploratory analysis of studies in first episode or early psychosis drug-free patients. Intriguingly, they found that the incidence of hyperprolactinemia correlated with the kinetic k_{off} , data consistent with the “rapid dissociation hypothesis”,²⁵⁴ as ligands that were the slowest to dissociate

from the D₂R displayed the greatest liability for prolactin elevation in patients. In contrast, these authors found that k_{on} , but not k_{off} , correlated with the incidence of EPS. This demonstrated that APDs in which bind more rapidly have greater EPS liabilities, suggesting that k_{on} may be the predictor of a compounds liability to elicit this side effect. Interestingly, other studies to estimate APD-D₂R kinetics using D₂R-evoked potassium channel activation were unable to distinguish between typical and atypical APDs.^{267,268}

Based on these data, Sykes *et al.* proposed to expand the kinetic hypothesis for APD side-effects by considering not only the kinetic k_{off} (and therefore the propensity to display insurmountable antagonism), but also the kinetic k_{on} and the potential to for receptor rebinding, leading to increased competition with DA at the synapse. This was extended to incorporate three broad classes of APDs in an attempt to explain how different kinetic characteristics have the potential to influence on-target side effects in different tissues (Figure 11). This study suggested that the opposite profile of haloperidol, such as the slow k_{on} , fast k_{off} kinetics exhibited by clozapine, is optimal for APDs targeting D₂Rs, and that there is likely to be a “kinetic sweet spot”, whereby rebinding is sufficient for efficacy but not enough to cause EPS. Although these data are compelling and give tremendous insight into the potential role of kinetics in APD side-effect liabilities, it’s important to acknowledge that this study did not rule out alternative mechanisms that may contribute to such liabilities, including for example, 5HT_{1A} agonism.²⁶⁹ However, optimisation of APD kinetic parameters may permit the development of a newer generation of drugs devoid of debilitating on-target toxicities.

		Slow	Fast		
Association rate (k_{on})	Fast	e.g. Haloperidol ↑ Target rebinding ↑ Insurmountability = +++ EPS +++ prolactin	e.g. Chlorpromazine ↑ Target rebinding ↓ Insurmountability = ++ EPS + prolactin		
	Slow		e.g. Clozapine ↓ Target rebinding ↓ Insurmountability = +/- EPS - prolactin		
		Dissociation rate (k_{off})			

Figure 11. The three types of APDs identified from the study by Sykes *et al.* are represented in this box plot along with their relative potential for “on-target” toxic effects indicated by the following; (-) no evidence, (+) some evidence, moderate (++) and (+++) strong evidence. Reproduced from Sykes *et al.*²⁶⁵

6. Parkinson's disease

PD is the second most common progressive neurodegenerative disorder, with an average age of onset of ~60 years.²⁷⁰ The disease is characterised by a large number of motor and non-motor features. The four cardinal clinical manifestations generally used to describe PD can be grouped under the acronym TRAP: tremor at rest, rigidity, akinesia (or bradykinesia), and postural instability/gait disturbance.²⁷¹ Non-motor symptoms are both common and extensive, are present in all stages of the disease, and can be a major source of disability. These include neuropsychiatric problems such as impulse control disorder (ICD) amongst many others, as well as cognitive impairment and dementia.

PD is pathologically characterised by degeneration of dopaminergic neurons in the *substantia nigra pars compacta* (SNc) that project to the striatum (the nigrostriatal pathway), in addition to the manifestation of intracytoplasmic proteinaceous inclusions known as Lewy bodies (filamentous aggregates composed of the presynaptic protein α -synuclein).²⁷² These ultimately lead to dysfunction of the basal ganglia (a group of deep nuclei involved in the initiation and execution of movement), which in turn leads to an imbalance between the striato-pallidal and pallido-thalamic output pathways.^{273,274} However, it is also now appreciated that non-dopaminergic pathologies involving cholinergic, serotonergic, noradrenergic, as well as other neurons localised in the cerebral cortex, brainstem, and peripheral autonomic nervous system are associated with PD.²⁷⁵ Despite decades of research, the aetiology of PD still remains unknown but is believed to result from a complex interaction between environmental factors and genetic predisposition in individuals.²⁷⁶

6.1 Antiparkinsonian Drugs

There are currently no disease-modifying or neuroprotective/neurorestorative therapies to treat PD.²⁷⁷ Therefore the current goal of PD management is to address the symptomology of the disease (mainly motor function) as well as gain improvements in non-motor deficits. To achieve this, both pharmacotherapy and non-pharmacological measures (e.g. stereotaxic neurosurgery, deep-brain stimulation, and supportive therapies such as physio- and speech therapy) may be considered.

6.1.1 Oral levodopa therapy

The most effective pharmacotherapy currently available for the symptomatic treatment of PD motor symptoms is levodopa (**12**, L-DOPA, Figure 12), a biological precursor and prodrug of DA that acts to restore dopaminergic activity. This compound is still considered the 'gold standard' for the treatment of PD motor symptoms despite its US FDA approval almost 50 years ago. However, chronic L-DOPA use is associated with a range of side effects including: fluctuations of psychomotor state (on-off oscillations),²⁷⁸ nausea and vomiting,²⁷⁹ dyskinesia or hyperkinetic movement, and 'wearing

off², a form of tachyphylaxis whereby patients experience a re-emergence of PD symptoms prior to the next scheduled dose of L-DOPA.²⁸⁰ To circumvent various adverse and off-target effects associated with L-DOPA use it is often co-administered with other various agents. These include: DOPA decarboxylase inhibitors (e.g. carbidopa, **13**, Figure 12), which act to slow the peripheral degradation of L-DOPA prior to BBB penetration,²⁸¹ selective monoamine oxidase B (MAO-B) inhibitors (e.g. selegiline) which retard the metabolism of DA,²⁸² and catechol-*O*-methyltransferase (COMT) inhibitors (e.g. tolcapone) which improve the pharmacokinetics and pharmacodynamics of L-DOPA, thus increasing the half-life and enhancing CNS bioavailability.²⁸³⁻²⁸⁵ However, motor complications commonly develop in patients treated with L-DOPA after ~4-6 years.²⁸⁶ In the advanced phases of the disease, L-DOPA-induced dyskinesias have been proposed to be linked to the short half-life of the drug that causes non-physiological, pulsatile stimulation of supersensitive post-synaptic DARs in the striatum.²⁸⁷ Moreover, L-DOPA may be toxic to DA-containing neurons, further limiting the window of efficacy.²⁸⁸ Therefore, primary administration of L-DOPA is generally only considered if alternative therapies (such as D₂R agonists) demonstrate a lack of efficacy, or their side effect profiles begin to impede symptom control in younger patients. L-DOPA is, however, recommended as a first-line therapy for older patients in combination with other drugs.²⁸⁹

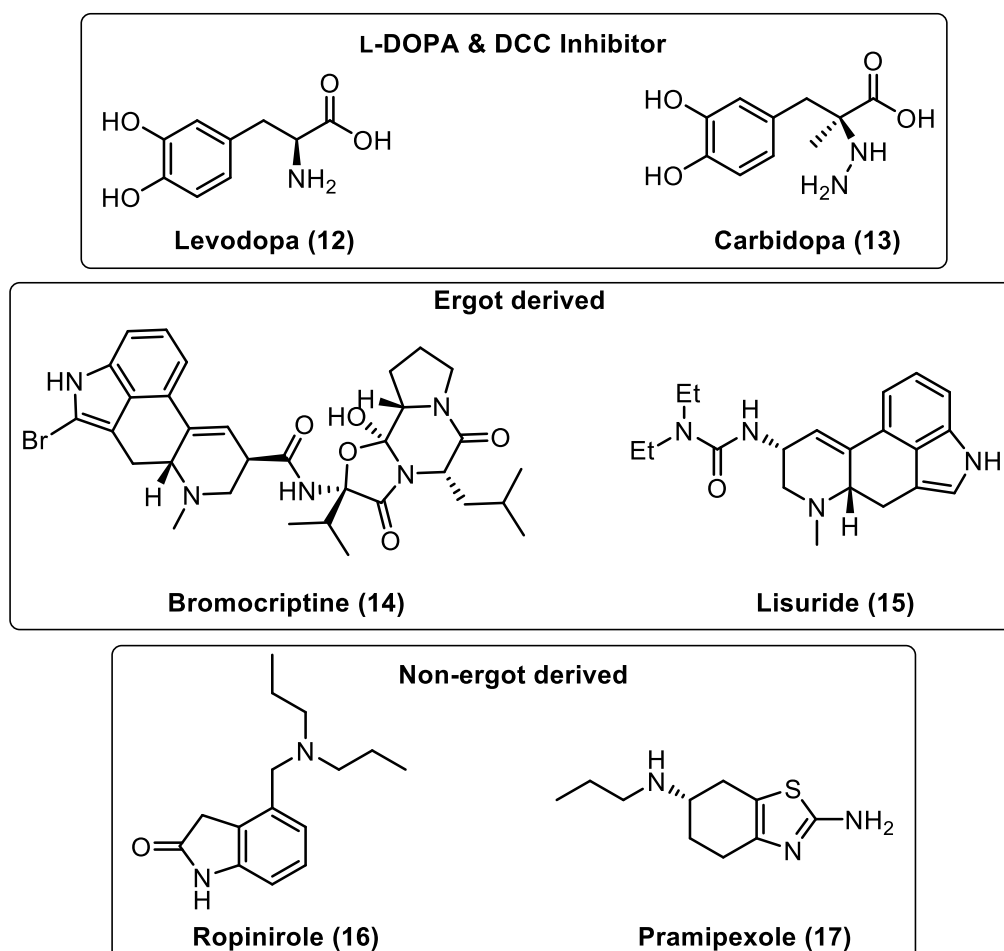


Figure 12. Chemical structures of L-DOPA, carbidopa, and common ergot- and non-ergot-derived D₂R agonists used for the symptomatic treatment of PD.

6.1.2 Dopamine receptor agonists

Agonists of the D₂R have been considered a viable alternative for the treatment of PD due to theoretical advantages over L-DOPA, including no requirement for enzymatic activation consequently bypassing presynaptic DA synthesis, increased duration of action, improved bioavailability, and fewer adverse effects.^{281,290,291} Despite their lower efficacies compared to L-DOPA, D₂R agonists are associated with a lower risk of dyskinesias and motor fluctuations, and may be used as an initial treatment to delay the need for L-DOPA, or as an add-on therapy in patients who develop motor complications with the aim to reduce L-DOPA usage. They can be divided into two classes based on their structural properties: ergot derived (e.g. bromocriptine (**14**), lisuride (**15**)) (Figure 12), and non-ergot derived (e.g. ropinirole (**16**), pramipexole (**17**)) (Figure 12). However D₂R agonists still possess extensive side-effect profiles, which include hallucinations, confusion, nausea, hypotension, somnolence and an increased incidence of ICDs such as pathological gambling, shopping, eating and hypersexuality.²⁹² These limiting side effects can be attributed to a lack of target specificity and/or the inability of orthosteric agonists to replicate the spatiotemporal pattern of endogenous DA brain signalling. Accordingly, there is clearly still an enormous unmet medical need for novel improved therapies for the treatment of PD. Thus, compounds that possess favourable selectivity profiles and the potential for ‘fine tuning’ of normal physiological signalling are of great interest. This is because they may offer distinct advantages over traditional agents due to their potential in reducing the propensity for desensitization and tachyphylaxis resulting from their theoretical prospective to maintain temporal, regional, and phasic potentiation of endogenous signalling. Thus, the identification and development of allosteric potentiators of the D₂R is an attractive avenue to explore novel treatments for PD.

7. Allosteric modulators of dopamine D₁ receptors

There are a number of potential advantages regarding the development of D₁R PAMs to combat cognitive dysfunction in SCZ pathologies. These include the potential for increased D₁R selectivity through targeting less homologous allosteric binding sites which can help to minimise off-target side-effects. In addition, compounds that can modulate endogenous dopaminergic tone by allowing DA to still bind the receptor may maintain the spatiotemporal patterns of neurohumoral signalling by amplifying physiologic control circuits.^{42,293} This may consequently enhance safety profiles providing they display no intrinsic agonism, but can also result in a reduced potential for receptor desensitization. Compounds of this description might also have advantages to be utilised as

pharmacological tools to further probe the role of the D₁R in neurocognitive deficits, and may circumvent other challenges associated with non-selective orthosteric D₁R agonists. A comprehensive review chronologically detailing the work of several companies and their efforts towards the identification of novel D₁R PAMs was very recently published in *J. Med. Chem.* by a Belgian research group from UCB Biopharmaceuticals. It revealed some interesting chemical structures and biological data contained within both patent applications and peer reviewed journals.²⁹⁴

7.1 First-in-class D₁R PAMs: compound A and compound B

Following a high-throughput screen of the Bristol-Myers Squibb (BMS) chemical library, in 2015 Lewis *et al.* reported two first-in-class D₁R PAM chemotypes represented by “compound A” [1-((*rel*-1*S*,3*R*,6*R*)-6-(benzo[*d*][1,3]dioxol-5-yl)bicyclo[4.1.0]heptan-3-yl)-4-(2-bromo-5-chlorobenzyl)piperazine] (piperazine series) (**18**, Figure 13), and “compound B” [*rel*-(9*R*,10*R*,12*S*)-*N*-(2,6-dichloro-3-methylphenyl)-12-methyl-9,10-dihydro-9,10-ethanoanthracene-12-carboxamide] (ethanoanthracene series) (**19**, Figure 13).²⁹⁵ Both compounds showed nanomolar PAM potency using both CHO and HEK cell backgrounds with no reported intrinsic agonism, whilst “compound B” was found to be D₁R-selective over the D₂R, D₄R, and D₅Rs. However, “compound A” was reported to display agonist activity at the D₂R thus it was consequently dropped as this profile would likely exacerbate positive symptoms of SCZ. “Compound B” was found to be inactive at D₁Rs expressed in rat primary neuronal cultures, which was then confirmed using HEK cells overexpressing the rat D₁R. Thus, as the human and rat D₁R sequence shares >90% sequence homology, Lewis *et al.* sought to determine the critical amino acid(s) that mediate this species selectivity. To achieve this, they used a parallel approach consisting of alanine mutagenesis in conjunction with D₁R human/rat chimera studies.

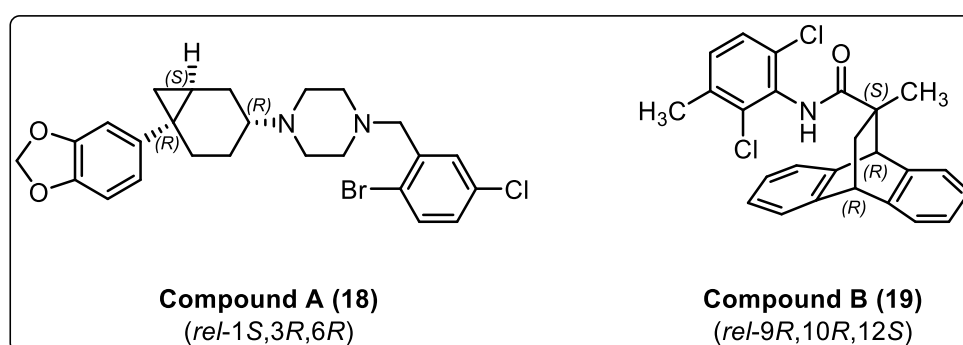


Figure 13. Chemical structures of two chemically distinct D₁R PAMs identified from a HTS of the Bristol-Myers Squibb chemical library.²⁹⁵

These data identified a critical amino acid, R130^{IC2.3}, as well as additional amino acids in intracellular loop 2 (ICL2) together with N- and C-terminal proximal regions of TM α -helix 2 and TM α -helix 3, suggesting an intracellular binding region for this PAM chemotype. To further rationalise these *in vitro* data, Lewis *et al.* employed a molecular dynamics-refined homology model of the D₁R/dinapsoline complex. This model was generated using the X-ray crystal structure of the nanobody-stabilised agonist-bound β_2 -adrenergic receptor as a template.²⁹⁶ In addition to R130, residues V58^{2.38}, V119^{3.48}, W123^{3.52}, and M135 were determined to likely comprise part of the Compound B D₁R binding site. Subsequent sequence alignment studies comparing the D₁R to the D₂R or D₃R revealed that none of the residues found to negatively impact binding are identical in these subtypes, whilst only arginine and valine were found to be present at the positions corresponding to R130 and V119^{3.48} in the D₄R. The lack of D₅R activity was less easily rationalised as these subtypes only differ at the position corresponding to V58^{2.38}. All residues mentioned previously, with the exception of R130, have hydrophobic side chains that could potentially make favourable interactions with the primarily hydrophobic/aromatic “compound B”. Furthermore, a side-chain of R130^{IC2.3} was proposed to make a key π -cation interaction with one of the aromatic rings of “compound B”. This study represented the initial steps toward the development of D₁R PAMs for the potential treatment of neurocognitive dysfunction in SCZ and other related disorders, and determined a key residue that determines species selectivity. BMS has since exited the neuroscience area, and no further reports have emerged from the BMS group.

7.2 UCB: isoindoline and tetrahydroisoquinolines

A Belgian research group at UCB Biopharmaceuticals has published a total of three patent applications disclosing novel D₁R PAMs, covering isoindoline and tetrahydroisoquinoline chemotypes. Pertinent examples from the isoindoline series include phenylacetamide (**20**) and urea (**21**) (Figure 14), where such compounds are reported to display EC₅₀ values of <100 nM in LMtk mouse fibroblast cells expressing the human D₁R.²⁹⁷ A simultaneous patent application disclosed representative tetrahydroisoquinoline examples **22** and **23** (Figure 14). As in the isoindoline patent, no specific SAR data were provided, but preferred examples are reported to show improved EC₅₀ values of < 10 nM in the same assay.²⁹⁸ The latest patent application, published in October 2017, described an optimized series of tetrahydroisoquinoline derivatives where the 2,6-dichlorophenyl ring of the acetamide has been replaced by bicyclic 3,5-dichloro-1*H*-indazol-4-yl and 3,5-dichloro-1*H*-pyrazolo[3,4-*b*]pyridin-4-yl moieties to give examples **24** and **25**, respectively (Figure 14).²⁹⁹ Such compounds are claimed to display D₁R PAM EC₅₀ values of < 30 nM in the same assay.

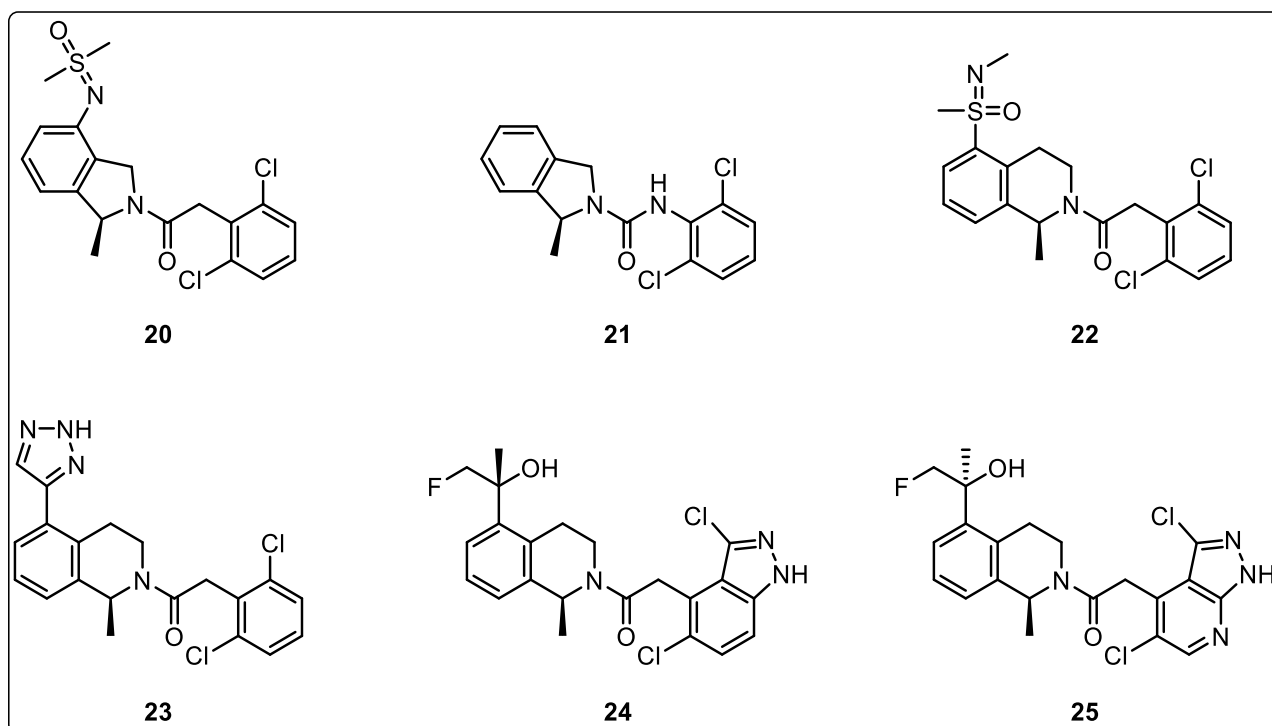


Figure 14. Representative D₁R positive allosteric modulators from three patent disclosures by UCB.

7.3 Astellas: Heterocyclic acetamides & imidazodiazepines

A Japanese research group at Astellas Pharmaceuticals have also published two patent families that describe D₁R PAMs for the treatment of cognitive impairment associated with SCZ, PD, Alzheimer's disease, and Huntington's disease. The first patent family outlines representative examples such as compounds **26** and **27** (Figure 15).^{300,301}

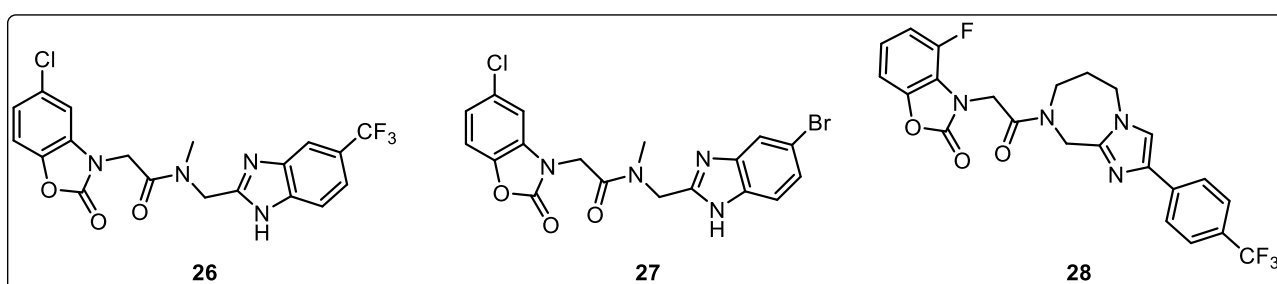


Figure 15. Representative D₁R positive allosteric modulators from two patent disclosures by Astellas.

Using a CHO cell line stably expressing the human D₁R, EC₅₀ values, defined as the concentration to elicit a 2-fold shift in the DA dose-response curve, were determined for compounds **26** and **27** to be 460 nM and 440 nM, respectively. The second patent disclosure details an optimized structure, wherein the benzimidazole moiety is replaced with a substituted phenylimidazole moiety and the imidazole nitrogen atom has been cyclised onto the amide nitrogen atom, giving representative compound **28** (Figure 15).³⁰² Despite no reports of an EC₅₀ value, two *in vivo* models, namely the Y-

maze test and acute phencyclidine (PCP) rat model were used to assess the efficacy of **27**. The Y-maze test measured improvements in spontaneous alteration behaviour following impairment mediated by an *N*-methyl-D-aspartate receptor antagonist, wherein a minimum effective dose (MED) was determined to be 0.3 mg/kg. The PCP rat model, however, determined the MED to be 0.03 mg/kg, although the reason for this 10-fold MED discrepancy between models is unclear, though differences in pharmacokinetic and/or CNS penetration differences and/or binding kinetics may offer a partial explanation.²⁹⁴ Astellas currently have a D₁R PAM in phase II clinical trials for cognitive impairment associated with SCZ; however, its chemical structure and mechanism of action are yet to be reported.

7.4 Eli Lilly: tetrahydroisoquinolines

An original 2014 patent application from a research group at Eli Lilly initially described *in vitro* and *in vivo* data for a series of *N*-acyl-tetrahydroisoquinolines, namely compounds **29** (also known as DETQ), **30** and **31** (Figure 16), and were reported to have originated from chemical modification of a HTS hit.³⁰³ As can be seen from the structures in Figure 16, DETQ (**29**), **30**, and **31** only differ by homologation of the methylene spacer between the tetrahydroisoquinoline phenyl ring and isopropyl alcohol moieties.

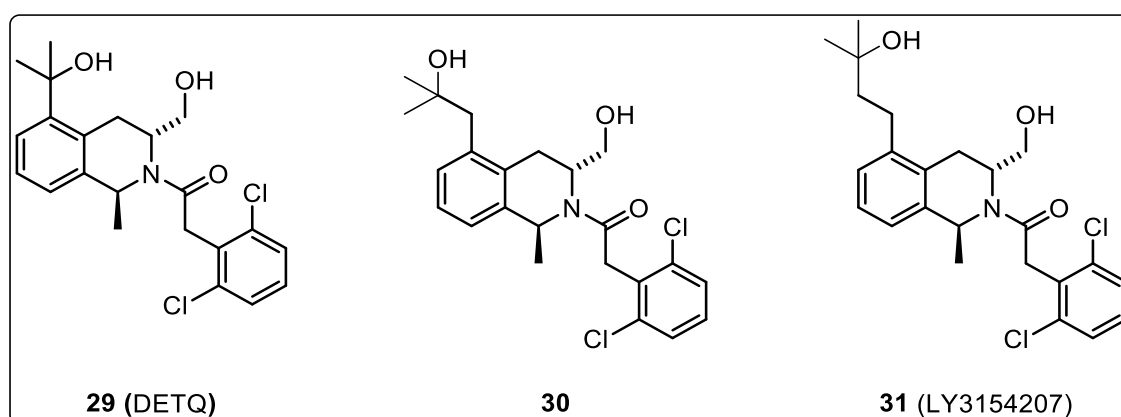


Figure 16. D₁R positive allosteric modulators disclosed in several patent applications by Eli Lilly.

D₁R PAM activity was determined using HEK293 cells overexpressing the human D₁R, and *in vivo* activity was assessed in two models of movement disorders using C57BI/6 mice with human knock-in (KI) D₁R due to the species difference between human and rodent receptors. The patent disclosed EC₅₀ values for compounds **29** (DETQ, EC₅₀ = 11.8 nM) and **31** (EC₅₀ = 3.66 nM), where the maximal effect is relative to the *E*_{max} elicited by DA. Despite no *in vitro* data being reported for compound **30**, it was shown to increase ACh levels in the PFC by approximately 2.6-fold after an intraperitoneal dose of 30 mg/kg to human D₁R KI mice, implying potential benefits on cognition. Again using D₁R KI mice, compound **31** was tested in a basal locomotor activity (LMA) assay and a reserpine

impairment model. The basal LMA model showed a dose-dependent response, with doses of 3 mg/kg displaying a statistically significant effect, whereas the reserpine-induced akinesia model demonstrated that a dose of 30 mg/kg of compound **31** was able to reverse the reduced LMA caused by a low dose of reserpine. Further work conducted on the *p*-hydroxybenzoic acid (PHBA) cocrystal of **31** showed a statistically significant effect at all doses and a dose-response up to 20 mg/kg. Further to this, a more recent patent application describes additional details on **31** and its PHBA cocrystal, with **31** reported to display a D₁R PAM EC₅₀ of 4.59 nM, while the PHBA cocrystal reported to display an EC₅₀ of 1.11 nM.³⁰⁴ No new additional *in vivo* data was disclosed. According to Eli Lilly's pipeline, compound **31** (Figure 16) (now named LY3154207) is currently in phase II trials for the treatment of dementia associated with PD.

7.5 Further studies on DETQ: a novel D₁R PAM chemotype

The novel, highly selective and potent D₁R PAM DETQ (**29**, Figure 16) has been the focus of subsequent publications providing extensive detail on its *in vitro* and *in vivo* pharmacological profile. In a study by Svensson and colleagues, the term “allosteric potentiator” (AP) was used in place of PAM to emphasise a specific focus on the consequences of amplifying DA-response.³⁰⁵ Despite the fact that APs have been widely hypothesised to provide many therapeutic advantages over their orthosteric counterparts, direct clinical or pre-clinical evidence still remained elusive. This compound is the prototype of a class of selective and brain penetrant D₁R potentiators reported to possess several interesting features that make it a useful biochemical tool for studying the D₁R. These include its >1000-fold D₁R/D₅R selectivity, in addition to high selectivity towards the D₁R compared to other related receptors (D₂R, 5HT₆R, β-AR₁₋₃). Furthermore, oral dosing of DETQ (**29**) achieves high free brain levels, implying sufficient headroom for dosing in animal studies, coupled with the absence of adverse behavioural effects, which is consistent with *in vitro* selectivity data. The level of allosteric agonism exerted by DETQ (**29**) was also quantified to be forty-three times less potent compared to it as an AP. This was further supported by *in vivo* studies observing the effect of DETQ (**29**) on hypokinesia in human D₁R-transgenic mice pre-treated with a high dose of the DA-depleting agent reserpine. These data indicated that DETQ (**29**) can be regarded as a pure PAM as it lacks direct-acting D₁R agonist effects *in vivo*, and demonstrate that the actions of DETQ (**29**) are dependent on dopaminergic tone. Furthermore, the increase in cAMP caused by DETQ (**29**) in HEK293 cells transfected with the hD₁R was dependent on the presence of DA.

More recently, the activity of DETQ (**29**) was further surveyed in a broad array of behavioural and neurochemical models thought to be predictive of therapeutic utility in neuropsychiatric disorders. In behavioural models to examine evidence for DETQ-mediated central potentiation of D₁Rs, DETQ (**29**) was shown to produce a dose-dependent activation in Y-maze locomotion, decreased immobility

in the forced-swim test, and increased wakefulness in sleep EEG. As previously reported for D₁R agonists,³⁰⁶ DETQ (**29**) was also shown to increase spontaneous eye-blink rate in the rhesus monkey, suggesting potential efficacy against attention deficits in PD. Collectively, these data revealed there may be several therapeutic opportunities for a D₁R potentiator. Specifically, it was hypothesised that compounds such as DETQ (**29**) may show utility as a symptomatic treatment for memory impairment, mood related symptoms, and daytime sleepiness in Alzheimer's disease. In early PD patients with partial DA depletion, D₁R APs may show utility as a monotherapy, possibly delaying the need to initiate L-DOPA treatment. Amplification of the D₁R signalling system may also have a beneficial effect in major depressive disorder. Finally, mounting evidence suggests a deficiency of DA release in the dlPFC of patients with SCZ.³⁰⁷ Moreover, the effect of current APDs to increase DA release through blocking D₂ autoreceptors on dopaminergic neurons indirectly increases postsynaptic D₁R tone, which may contribute to their therapeutic efficacy. Thus, these data also support the potential efficacy of D₁R PAMs for the treatment of negative symptoms and cognitive deficits in SCZ and related disorders.

7.6 MLS6585 and MLS1082: structurally distinct D₁R PAMs

The discovery and characterisation of two additional novel structurally distinct D₁R PAM scaffolds were recently reported from a HTS of the National Institutes of Health Molecular Libraries Program small molecule library.³⁰⁸ These compounds, MLS1082 (**32**) and MLS6585 (**33**) (Figure 17), were shown to potentiate both DA-stimulated G protein- and β -arrestin-mediated signalling, increase the affinity of DA for the D₁R and display no intrinsic agonist activity.

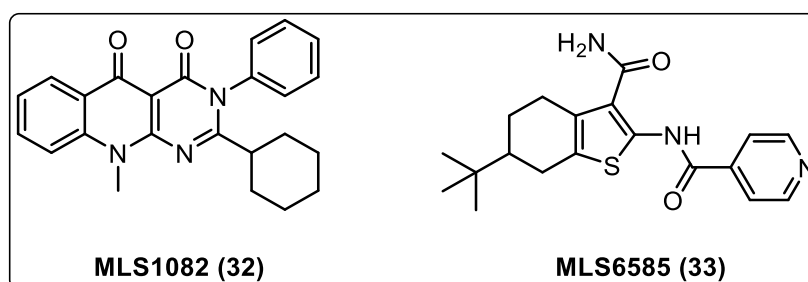


Figure 17. MLS1082 and MLS6585 are D₁-like receptor-selective PAMs discovered from a HTS as reported by Luderman *et al.*³⁰⁸

Receptor selectivity studies showed both compounds exhibited PAM activity at the D₅R, but both were completely devoid of any PAM activity at the D₂-like DAR family, or the β_2 AR, indicating selectivity for the D₁-like DAR family. Interestingly, both compounds functioned as NAMs of radiolabelled antagonist ([³H]-SCH23390) binding, but potentiated the affinity of both orthosteric

agonists DA and DHX, and partial agonists SKF82526 and apomorphine, demonstrating their activity is probe-dependant.

Due to the structural and activity differences seen with different classes of PAMs, Luderman *et al.* hypothesised they may be acting at different binding sites on the D₁R³⁰⁸ suggesting that MLS1082 (**32**) and “compound B” (**19**) share a common allosteric site on the D₁R, which is spatially distinct from the site that is modulated by MLS6585. Additionally, as Lewis *et al.* hypothesised that residue R130 is involved in “compound B” binding, this information was subsequently used by the authors to determine if residue R130 was involved in the activity of MLS1082 (**32**) or MLS6585 (**33**).²⁹⁵ Using mutagenesis, Luderman *et al.* changed R130 in the human D₁R to Q (R130Q) and used BRET assays to measure either β -arrestin recruitment or G α_s -stimulated potentiation of DA in the presence of the PAMs. Using the R130Q D₁R mutant, MLS6585 (**33**) but not MLS1082 (**32**) was able to potentiate DA’s potency for stimulating β -arrestin recruitment, identical to that of the wildtype D₁R. Furthermore, assessment of these compounds with respect to the G α_s BRET assays showed MLS1082 (**32**) was again inactive at potentiating DA, whereas MLS6585 (**33**) did. These data suggested that these novel PAMs (MLS6585 and MLS1082) are potentiating the D₁R via two distinct binding sites, and that residue R130 may be involved in the PAM activity of MLS1082 (**32**), but not MLS6585 (**33**). Interestingly, the structurally distinct PAM DETQ (**29**) was also reported by Bruns *et al.*³⁰⁹ to be inactive at rodent D₁Rs, but active in potentiating agonist stimulation at the human D₁R, suggesting that MLS1082 (**32**), “compound B” (**19**), and DETQ (**29**) may all function through the same intracellular binding site. A greater understanding of allosteric binding sites for which PAMs may engage the D₁R should facilitate the discovery of such compounds.

Using a combined mutagenesis and D₁R/D₅R chimera approach in conjunction with homology modelling and the small molecule allosteric potentiators DETQ and structurally distinct PAM CID2886111 (**34**) (Figure 18), Wang *et al.* recently described the further elucidation of distinct allosteric binding sites on the D₁R.³¹⁰ These results suggest that DETQ occupies a cleft in ICL2 as previously described for Compound B,²⁹⁵ and further confirm that PAMs comprising the 4,5,6,7-tetrahydrobenzo[*b*]thiophene moiety occupy a spatially distinct site of which is yet to be identified, implying a rich structural landscape for D₁R allosteric modulation. In agreement with studies conducted by Luderman *et al.*,³⁰⁸ Wang *et al.* also described a supra-additive response resulting from the combination of DA, DETQ (**29**) and CID2886111 (**34**), implying they bind to three distinct sites yet drive the same receptor conformation.³¹⁰ Interestingly, CID2886111 (**34**) was unaffected by any of the ICL2 mutations, and the general binding site location could not be definitively established with the D₁R/D₅R chimeras due to similar potencies at each subtype. However, these studies did indicate a tendency to favour a site in the C-terminal half of the D₁R, and a speculative binding site was

suggested to be located on the outward-facing parts of the cytoplasmic ends of TMs 5, 6, and 7 as observed for a glucagon-like peptide 1 receptor PAM.^{311,312}

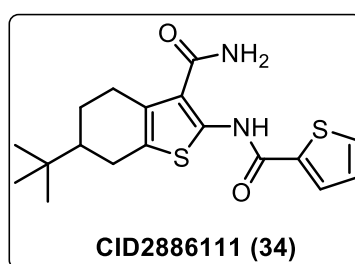


Figure 18. Chemical structure of 6-*tert*-butyl-2-(thiophene-2-carbonylamino)-4,5,6,7-tetrahydro-1-benzothiophene-3-carboxamide (CID2886111), a reference D₁R PAM.³¹³

8. Allosteric modulators of dopamine D₂ receptors

Allosteric sites have been described for D₂Rs, as well as endogenous allosteric ligands such as Na⁺ and Zn²⁺ ions that act to allosterically regulate the binding of agonists to aminergic GPCRs.³¹⁴ In addition, amiloride (**35**, Figure 19) and its *N*-substituted derivatives,³¹⁵ analogues of the tripeptide PLG^{316,317} (**36**, Figure 19), as well as (-)-OSU6162 (**37**, Figure 19)^{169,318} have been suggested to interact allosterically with DA D₂Rs.

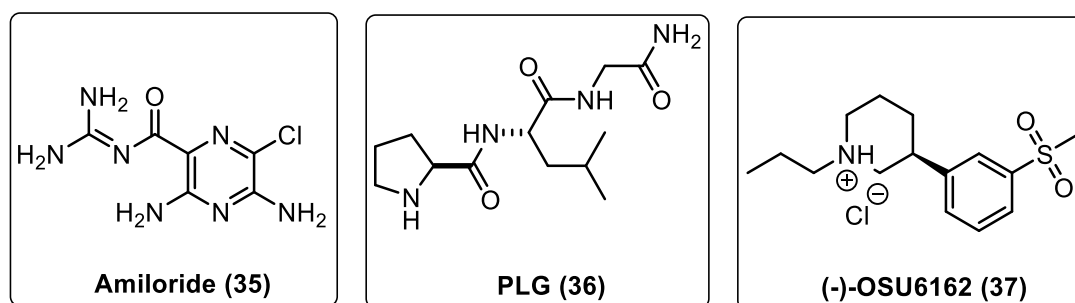


Figure 19. Chemical structures of D₂R allosteric modulators.

PLG (**36**) was shown to potentiate the induction of contralateral rotation by L-DOPA in unilateral 6-OHDA-lesioned rats without exacerbating the induction of dyskinesia,³¹⁹ and (-)-OSU6162 (**37**) was shown to display antipsychotic-like properties in rats with minimal dyskinesia induction and no EPS.^{169,320,321} Collectively, these data provided initial evidence to suggest that, in addition to orthosteric agents, PAMs and NAMs acting at DARs may be therapeutically useful agents.

8.1 SB269652: a NAM of the dopamine D₂ & D₃ receptors

The most extensively characterised NAM of the D₂R and D₃Rs, SB269652 (**38**, Figure 20), was reported by Silvano *et al.* in 2010.³²² SB269652 was originally synthesised by SmithKline Beecham in a bid to find novel selective orthosteric antagonists of the D₃R.^{323,324}

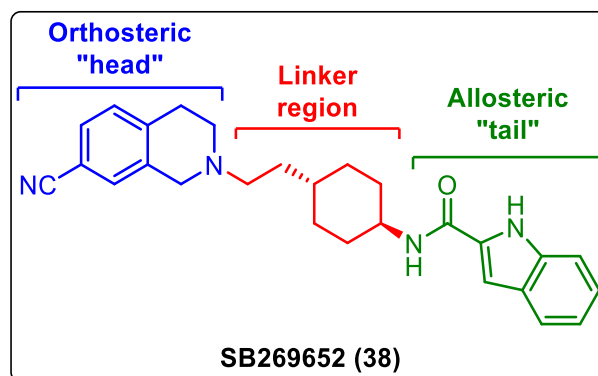


Figure 20. Chemical structure of the NAM SB269652, identified by Silvano *et al.*³²²

This molecule was shown to fully inhibit both [³H]spiperone and [³H]nemonapride binding at low concentrations at the D₂R or D₃R, but only sub-maximally inhibit their binding at high concentrations. Similarly, functional experiments conducted at the D₂R showed SB269652 could only submaximally suppress D₂R-mediated stimulation of G α_{i3} and G α_{q15} , and phosphorylation of ERK1/2 and Akt at high concentrations of DA. Thus, it was characterised as a NAM of the D₂R and D₃R.

8.1 SB269652 displays a unique mode of interaction

The unique pharmacology of SB269652 (**38**) at the D₂R relative to many other competitive ligands containing extended structures was hypothesised to be due to a bitopic binding pose that extends from the OBS into a secondary pocket between TMs 2 and 7 as reported by Lane *et al.*³²⁵ Bitopic molecules contain two pharmacophores, connected by an appropriately spaced linker, that can simultaneously engage both orthosteric and allosteric binding domains of a single receptor. The mechanism of SB269652 binding was extended to now suggest that its allosteric action is exerted across a D₂R dimer ($K_B = 776$ nM, $\alpha\beta = 0.06$).³²⁵ Using functional complementation assays, the authors showed that SB269652 behaved as a NAM in a dimeric wild-type D₂R system (i.e. it engages one protomer whereby it exerts negative cooperativity on the potency of DA bound to the adjacent protomer) (Figure 21). However, when using a heterodimeric system consisting of a wild-type D₂R and a D114A^{3.32} mutant (unable to facilitate key orthosteric binding interactions), SB269652 was observed to display competitive pharmacology. They further investigated this mode of interaction *via* the synthesis and pharmacological evaluation of the *cis*-cyclohexylene isomer of SB269652 (MIPS1217,

Figure 21), with the hypothesis that its 1*H*-indole-2-carboxamide moiety would have a different orientation relative to its 1,2,3,4-tetrahydroisoquinoline-7-carbonitrile (7CN-THIQ) orthosteric pharmacophore. This was supported by MD simulations showing that SB269652 remains in an extended conformation, with its cyclohexyl and 1*H*-indole-2-carboxamide moiety interacting with Val^{2.61} and Glu95^{2.65}, respectively (Figure 21). In contrast, the *cis*-isomer was shown to display a slightly different binding mode, with the 1*H*-indole-2-carboxamide moiety instead orientating toward TM6 and not TM2 (Figure 21). Functional experiments measuring pERK1/2 showed the *cis*-isomer to now antagonise DA in a purely competitive manner, confirming this hypothesis.

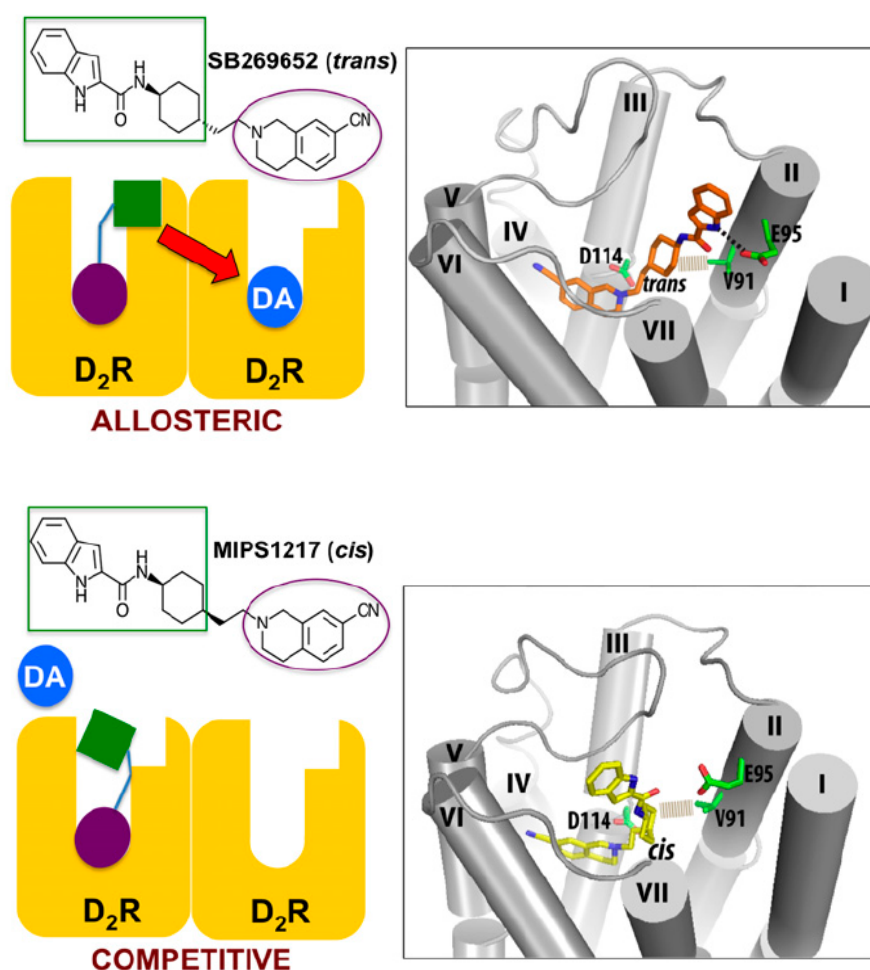


Figure 21. Allostery mediated by the bitopic ligand SB269652 across a GPCR dimer. The *trans*-isomer of SB269652 binds in a bitopic pose with one D₂R protomer to act as a NAM of DA binding and signalling via a second adjacent protomer. Key residues for engagement with the orthosteric site (D114) and allosteric site (E95 and V91) are indicated in the molecular model. In contrast, the indole moiety of the *cis*-isomer (MIPS1217) cannot engage the allosteric pocket to exert any negative cooperativity, instead acting in a competitive manner with DA. Figure adapted from Lane *et al.*³²⁵

To explore the interactions that might contribute to the allosteric effect of SB269652, mutagenesis experiments were performed. The authors firstly determined that the 7CN-THIQ moiety of SB269652, comprising a tertiary amine that is protonated at physiological pH, was required for making an

orthosteric interaction with the highly conserved aspartate residue (D114^{3.32}). In addition, key residues at the top of TM2 (Val91^{2.61} and Glu95^{2.65}) were identified, and the 1*H*-indole-2-carboxamide tail was predicted to extend into a secondary binding pocket between TM2 and TM7 of the D₂R whereby Glu95^{2.65} was predicted to hydrogen bond with the indolic NH. Accordingly, mutation of this residue to alanine caused a significant decrease in negative cooperativity exerted on DA binding and function. To summarise, these data identified key residues that govern allosteric cooperativity, and established a novel ligand binding mechanism for SB269652, whereby it engages the receptor via a bitopic mode of action to one GPCR protomer, which acts to allosterically modulate ligand binding to the OBS of a second adjacent protomer (Figure 22).³²⁵

The bitopic nature of SB269652 was further validated using a fragmentation process whereby progressively truncated fragments of the 7CN-THIQ moiety of SB269652 were synthesised and pharmacologically evaluated. Unlike SB269652, it was discovered that these fragments displayed competitive pharmacology.³²⁵ Conversely, further SAR studies of 1*H*-indole-2-carboxamide fragments by Mistry *et al.* yielded *N*-butyl-1*H*-indole-2-carboxamide (**40**) (Figure 22), which was subsequently shown to inhibit DA action in a non-competitive manner, displaying low μ M functional affinity and robust negative allosteric cooperativity.³²⁶ The authors went on to generate a novel bitopic ligand *via* the amalgamation of this allosteric fragment with the 7CN-THIQ (**39**) orthosteric head group of SB269652, finding that the resulting compound (**41**) now displayed a 10-fold improvement in affinity as compared to SB269652 whilst retaining negative cooperativity (Figure 22). Collectively, these data revealed the 1*H*-indole-2-carboxamide moiety as a novel pharmacophore for NAMs of the DA D₂R, and that the allosteric pocket between TMs 2 and 7 can be exploited for the design of novel NAMs and bitopic ligands acting at the DA D₂R.

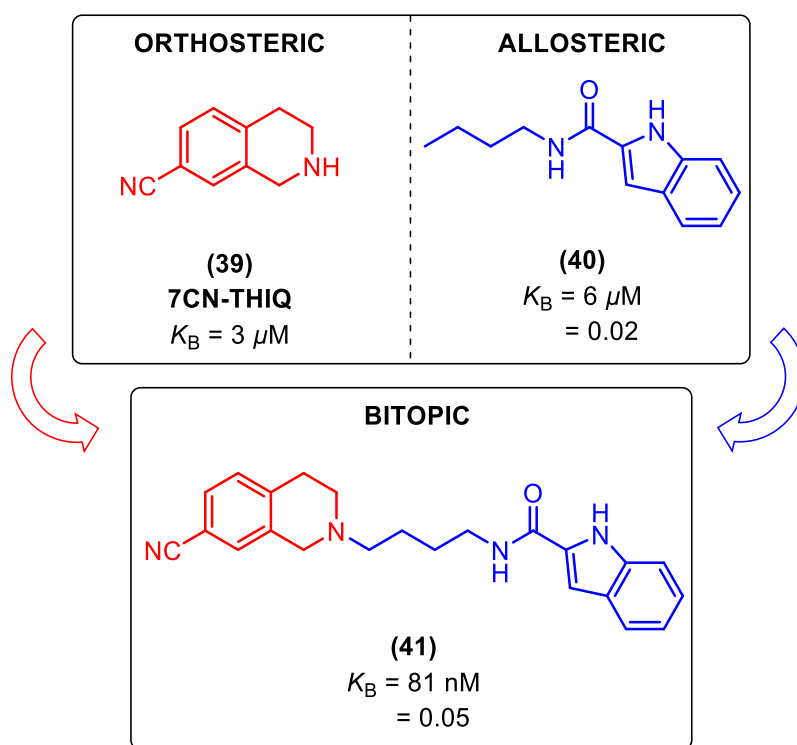


Figure 22. Using an approach combining fragments with orthosteric and allosteric pharmacology, Mistry *et al.* reported a novel derivative of SB269652 with a 10-fold improved affinity that retains robust negative cooperativity.³²⁶

Key ligand features required for the allosteric pharmacology of SB269652 were further determined by Shonberg *et al.*, subsequently extending the SAR.³²⁷ This study focused on synthetic analogues of three main portions of the molecule: the 7CN-THIQ head group; the *trans*-1,4-cyclohexylene spacer group; and the 1*H*-indole-2-carboxamide tail group. In agreement with previous studies, they found that the region most sensitive to chemical modification was the tail group, where any disturbance to the indolic NH hydrogen-bond donor ability, or size and lipophilicity, converted allosteric pharmacology to competitive. Replacing the 7CN-THIQ head group with higher affinity “privileged scaffolds” was also found to convert allosteric to competitive pharmacology. Thus it was established that the THIQ head group was also crucial for maintaining allostery, with the only requirement being a “small” substituent at the 7-position. Additionally, the authors discovered an intriguing relationship between polymethylene spacer length and allosteric pharmacology, and it was hypothesised that altering the length of this spacer, and consequently the flexibility, may change the orientation of the secondary pharmacophore causing a switch from allosteric to competitive pharmacology. Replacement with a linear 1,4-butylene, or 1,6-hexylene spacer conferred an increase in functional affinity whilst maintaining negative cooperativity, whilst the 1,5-pentylene spacer conferred competitive pharmacology. In agreement with these data, MD simulations of D₂R models in complex with the 1,4-butylene and 1,5-pentylene analogues of SB269652 show that the 4-carbon linker permits

a hydrogen-bond interaction between the indolic NH and E95^{2,65}, while this interaction was unable to form in simulations of the D₂R-bound with the 5-carbon linker analogue.³²⁸ Finally, replacing the 1*H*-2-indole-carboxamide moiety with a 1*H*-pyrrolo[2,3-*b*]pyridine-2-carboxamide moiety (7-azaindole, **42**) conferred a 30-fold increase in affinity whilst maintaining negative cooperativity (Figure 23).³²⁷

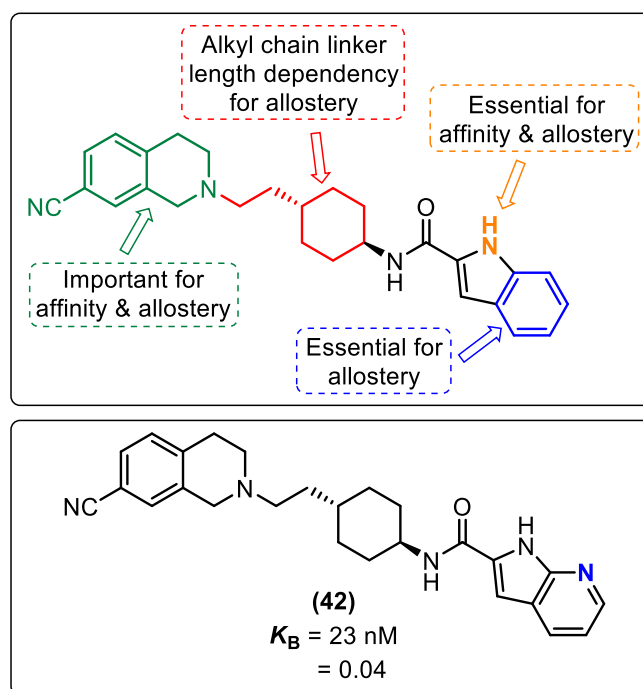


Figure 23. SAR summary for the SB269652 core (above); and the chemical structure of the 7-azaindole-2-carboxamide analogue of SB269652 that maintains affinity and negative cooperativity as reported by Shonberg *et al.*³²⁷

On the basis of these findings, Kopinathan *et al.* further extended the SAR of SB269652, paying particular attention to the influence of subtle structural modifications such as electronic effects, the positioning of the second nitrogen atom within the tail group, and the attachment point (2- or 3-position) of the bicyclic aryl moiety, upon allosteric cooperativity.³²⁹ Focusing on the benzo portion of the indole tail, a series of methoxy- and fluoro-substituted analogues were synthesised. Systematic incorporation of fluorine at positions 4–7 was shown to increase functional affinity, and modulated cooperativity based on its positioning. In contrast, electron-donating methoxy substituents increased functional affinity relative to the parent compound, but resulted in apparent competitive pharmacology with the exception of the 4-OMe analogue, which retained allosteric pharmacology. Incorporation of a second nitrogen on the 1*H*-indole-2-carboxamide moiety was observed to increase the functional affinity of all compounds as well as modulate the degree of negative cooperativity in a similar fashion to the fluoro-substituted analogues. Interestingly, repositioning of the indole-2-carboxamide tail attachment point from the 2-position to the 3-position increased affinity but

converted allosteric to competitive pharmacology. However, a similar scaffold-hop strategy was then employed to access analogues comprising a second nitrogen whilst being substituted at the 3-position, resulting in a range of properties from competitive to allosteric pharmacology. Most notably, they found that converting the 1*H*-2-indole-carboxamide moiety to the corresponding 1*H*-pyrrolo[3,2-*b*]pyridine-3-carboxamide (4-azaindole) not only yielded a compound with subnanomolar functional D₂R affinity (5,000-fold increase), but the ligand now acted to attenuate both orthosteric ligand potency and maximal response (100-fold increase) (**43**, Figure 24). This behaviour is in contrast to previous analogues of SB269652, which only attenuate agonist potency.

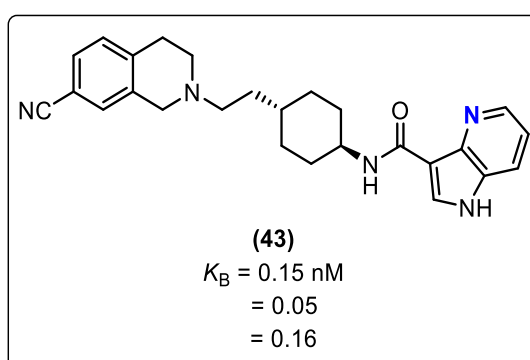


Figure 24. Chemical structure of the 4-azaindole-3-carboxamide analogue of SB269652 (**43**) that negatively modulate DA affinity and signalling efficacy with sub-nanomolar functional affinity.³²⁹

In conclusion, the indole motif of SB269652 was found to be particularly amenable to structural modification, causing changes in negative cooperativity without significant losses in affinity, thus providing an approach to generate novel derivatives with a spectrum of allosteric profiles. SB269652 has been the focus of intensive molecular pharmacology research efforts over the past eight years, with particular emphasis on understanding the structural determinants of bitopic NAM binding modes.^{328,330,331} Moreover, the potential of molecules such as SB269652 and their prospects as a new generation of APDs have been recently reviewed.³³²

8.2 Virtual ligand screening hit: “compound 7”

One of the ways to search for novel small molecules targeting orthosteric and allosteric pockets of GPCRs is to perform virtual ligand screening (VLS), either based on homology models or three-dimensional structures derived from X-ray crystallography or other structural biology techniques. VLS programs have previously demonstrated high efficiency in their ability to discover novel lead-like compounds.³³³⁻³³⁸ However, using these techniques to screen for allosteric compounds is known to be more challenging, with only limited examples currently describing allosteric hit compounds arising from VLS campaigns.³³⁹⁻³⁴² Using crystal structure and ligand-guided receptor optimised³⁴³ structural models of the D₃R, Lane *et al.* assessed their efficiency in prospective screening for ligands

targeting orthosteric and/or putative allosteric binding pockets.³⁴⁴ They performed a large-scale VLS campaign that used two optimised crystal-structure-based models: the receptor with an empty binding pocket and allosteric extension (D_3R^{APO}), and the receptor-complex with DA bound (D_3R^{Dopa}) (Figure 25). These optimised models were developed in order to expand large-scale VLS applications beyond orthosteric sites, and this study was the first to systematically search for and identify a number of chemically distinct allosteric modulators of the D_2R and D_3R .

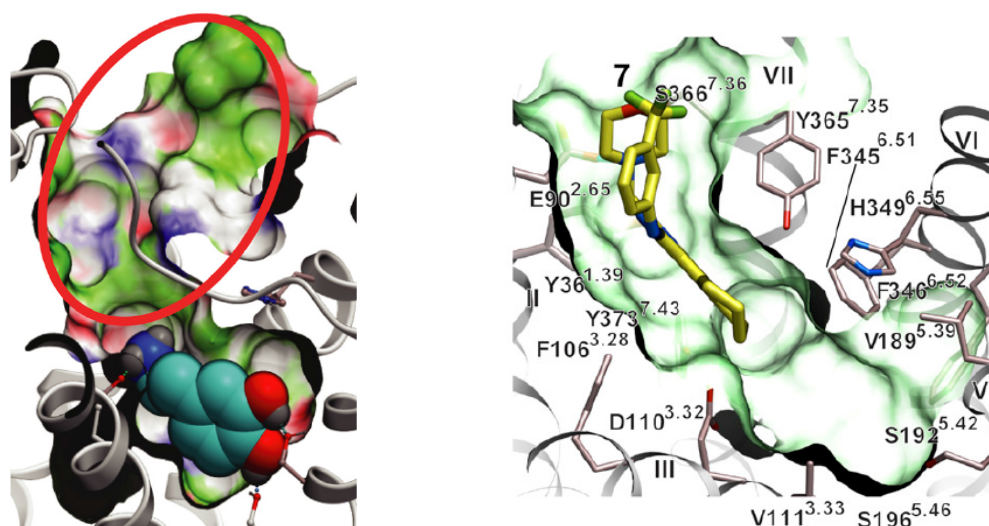


Figure 25. (Left) DA-bound model of the D_3R (D_3R^{Dopa}) designed for allosteric compound screening. DA is shown in a space filling representation with cyan carbons. The extended “allosteric” part of the pocket is highlighted by a red circle. (Right) Example of the binding pose obtained for compound **44** (Figure 26) as predicted by the ICM-VLS procedure with the D_3R^{APO} model. The ligand is shown as sticks with yellow carbons. The receptor is shown as a grey ribbon with the key side chains of the pocket shown as thin sticks; the binding pocket is illustrated as a green semitransparent surface. Reproduced from Lane *et al.*³⁴⁴

One of the most interesting non-orthosteric ligands to arise from the D_3R^{APO} set was “compound 7” (**44**, Figure 26). Interestingly, its structure comprises a thieno[2,3-*d*]pyrimidine scaffold which did not at the time feature in any known dopaminergic ligands. This compound was predicted to engage an extended binding pocket, with its amino group forming a salt-bridge with a non-conserved Glu90^{2.65} side chain instead of the conserved Asp110^{3.32} anchor. Other predicted contacts were hydrogen-bonding interactions with ECL2, particularly peptide-like polar interactions with the backbone amide groups of Cys181-Ile183, together with a range of polar and aromatic side chains on the extracellular side of the binding cavity. This compound proved to be the highest potency D_3R antagonist in their ERK1/2 phosphorylation assay ($IC_{50} = 7$ nM), and was also shown to cause a concentration-dependent inhibition of ERK1/2 phosphorylation consistent with its action as either an

antagonist or NAM of the DA effect. The same ERK1/2 phosphorylation assay was also performed using CHO cells expressing the D₂R, wherein it showed ~5-fold less potent effects compared with the D₃R. In conclusion, this study validated VLS campaigns as important tools for exploring orthosteric, allosteric and bitopic ligands with novel properties, and expanded on the success of recent structure-based VLS applications to class A GPCRs.

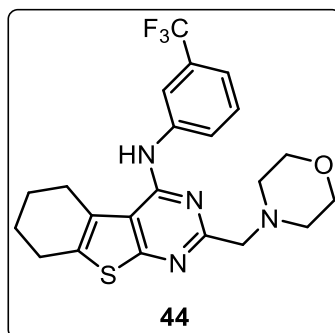


Figure 26. Chemical structure of VLS hit identified from a virtual ligand screen as reported by Lane *et al.*³⁴⁴

8.3 First-in-class PAMs of the dopamine D₂ & D₃ receptors

In an effort to develop novel pharmacotherapies for PD, Wood *et al.* recently reported the identification of racemic 1,3-benzothiazol-2-yl(2-methyl-2,3-dihydro-indol-1-yl)methanone (**45**) (Figure 27) from a HTS of 80,000 small molecules.³⁴⁵ The group went on to identify a more potent and efficacious PAM (**46**, Figure 27) suitable for *in vivo* experimentation. This compound lacked agonist effects on its own at the hD_{2L}R in a [³⁵S]-GTPγS binding assay, but potentiated the effects of a low concentration of DA. It also displayed no action at α_{2C}-adrenergic or histaminergic H₃ receptors. To further investigate the mechanism of the allosteric interaction, the group investigated the effect of the compound on the saturation binding of [³H]DA. In this assay, a 10 μM concentration failed to increase the affinity of [³H]DA for the D₂R, however markedly increased the number of high affinity binding sites. Selectivity studies observing the compounds ability to modulate the potency or efficacy of DA using functional cAMP assays at the hD₁R and hD₄R showed no response, but was able to potentiate DA at the hD₃R.

To demonstrate these robust allosteric effects are maintained under physiologic expression and signal transduction conditions, the effects of the *R*-isomer (**45**) on the D₂R-D₃R agonist quinpirole were assessed using dissociated rat striatal neurons. This compound potentiated the effect of quinpirole to induce decreases of *N*-methyl-D-aspartate currents in adult rat striatal neurons. In addition, it was shown to potentiate the effects of a threshold dose of L-dopa in a unilateral 6-hydroxydopamine (6-OHDA) lesion model in rats.³⁴⁶ Collectively, this study reported the first described PAMs of the

D₂R/D₃Rs, and demonstrated a stereoselective interaction for a novel allosteric scaffold, and that these PAMs maintain potentiation of DA in native tissue as well as *in vivo*.

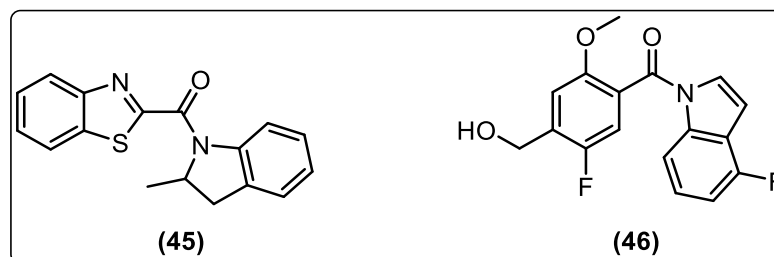


Figure 27. Novel PAMs identified by Wood *et al.*³⁴⁵ A chiral benzo[*d*]thiazol-2-yl(2-methylindolin-1-yl)methanone (45) and (4-fluoro-1*H*-indol-1-yl)(5-fluoro-4-(hydroxymethyl)-2-methoxyphenyl)methanone (46).

9. Summary

It is clearly evident that treatment options for CNS disease states such as SCZ and PD remain inadequate. However, emerging hypotheses regarding the design of novel drugs with different modes of action, improved side-effect profiles, and novel brain targets are revealing new opportunities. Furthermore, understanding the binding site location of small molecule allosteric modulators acting at the DRs may facilitate an improved drug discovery and design process. Using techniques in medicinal chemistry and chemical biology, this thesis further investigates the emerging concepts of allosterism at the D₁R and D₂Rs, in addition to APD binding kinetics as a way to potentially improve the treatment options for people living with SCZ. Finally, this thesis also explores the initial SAR of a novel D₂R PAM scaffold for photoactivatable or fluorescent derivatives that may be used as biochemical tools to supplement future investigations of the D₂R.

Thesis aims

Aim #1 – Validation of the allosteric pharmacology and SAR analysis of “compound 7”

Following a five step chemical synthesis of VLS hit “compound 7” (**44**), biochemical and functional *in vitro* pharmacological experiments were employed to confirm its allosteric mode of interaction at the D₂R. Observing the effects of **44** on the equilibrium binding of [³H]raclopride in FlpIn CHO cell membrane homogenates stably expressing the hD_{2L}R and hD₃R will validate target engagement, determine affinity, as well as quantify any allosteric effect **44** has on [³H]raclopride binding. The ability of a ligand to alter the rate of radioligand dissociation is consistent with it binding to a spatially distinct binding site whereby it induces a change in receptor conformation, subsequently altering the dissociation rate of the orthosterically-bound ligand. An isotopic dilution method will enable measurement of [³H]raclopride dissociation from the hD_{2L}R in the presence of the prospective modulator. Further, a cAMP accumulation functional assay will measure the prospective modulator’s ability to inhibit the action of DA at the hD_{2L}R and application of an operational model of allosterism to these data will yield estimates of affinity (K_B) and allosteric cooperativity ($\alpha\beta$). A comprehensive SAR study of **44** and analogues thereof will determine what structural features are essential for its activity. The proposed structural modifications are outlined in Figure 28 and will be achieved using various chemistry. The importance of the fused cyclohexane ring system will be assessed through increasing and decreasing the ring size, removing the fused ring, as well as substituting the 5- and 6-positions with aliphatic and aromatic carbocycles. The importance of the fused cyclohexane ring system will be assessed through increasing and decreasing the ring size, removing the fused ring, as well as substituting the 5- and 6-positions with aliphatic and aromatic carbocycles.

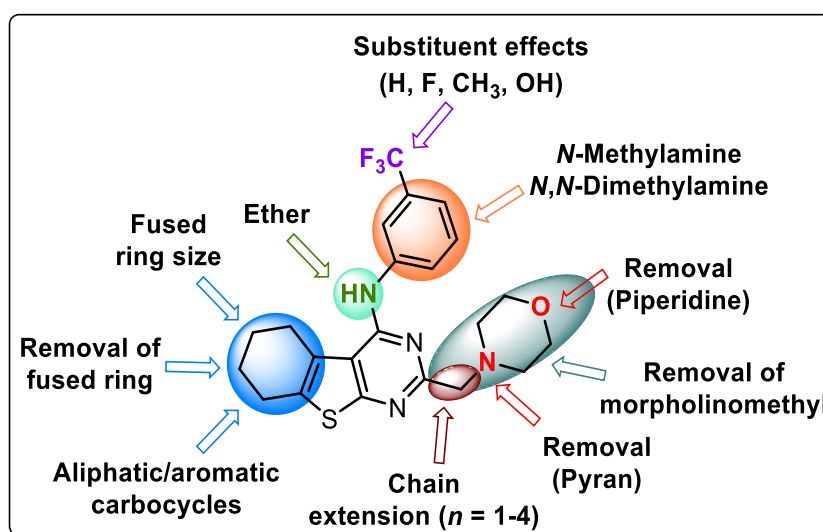


Figure 28. Initial structural diversification of compound **44**.

The importance of the secondary amino group will be assessed through replacement with an ether linkage. The *meta*-CF₃ substituent will be replaced with various electron withdrawing/donating substituents as well as being removed completely. The importance of this aromatic system will be further assessed through its removal and substitution with aliphatic secondary amines. The morpholinomethyl group will be removed to assess its importance, as well as observing the effect of incorporating piperidinomethyl and pyranomethyl substituents. Moreover, the effect of progressively increasing the polymethylene linker length from 1-4 carbons bearing the morpholinomethyl moiety will be assessed. Finally, various modifications will be employed in conjunction with one another (e.g. removal of the fused cyclohexane ring together with removal of the morpholinomethyl substituent) to assess additive effects and further refine the SAR. To determine their selectivity profiles, selected compounds will also be assessed using equilibrium binding experiments at the D₃R.

Aim #2 – Using initial SAR data to optimise the profile of “compound 7”

Using information obtained from the above SAR analyses of **44**, the initial aim was to expand the scope of analysis to further understand structural requirements for allosteric modulation at the D₂R, and to potentially optimise *in vitro* parameters (e.g. enhance affinity and cooperativity). As outlined in Figure 29, initial structural modifications for series #1 focused on functionalising the 4-position with various cyclic aliphatic amines as well as aniline. These data were then utilised to synthesise a second series of analogues to assess the effects of modification to the fused cyclohexane system in a similar fashion to Figure 28, but in conjunction with amines from series #1 that engendered favourable pharmacologic profiles. All compounds would be pharmacologically evaluated in a functional assay as described above.

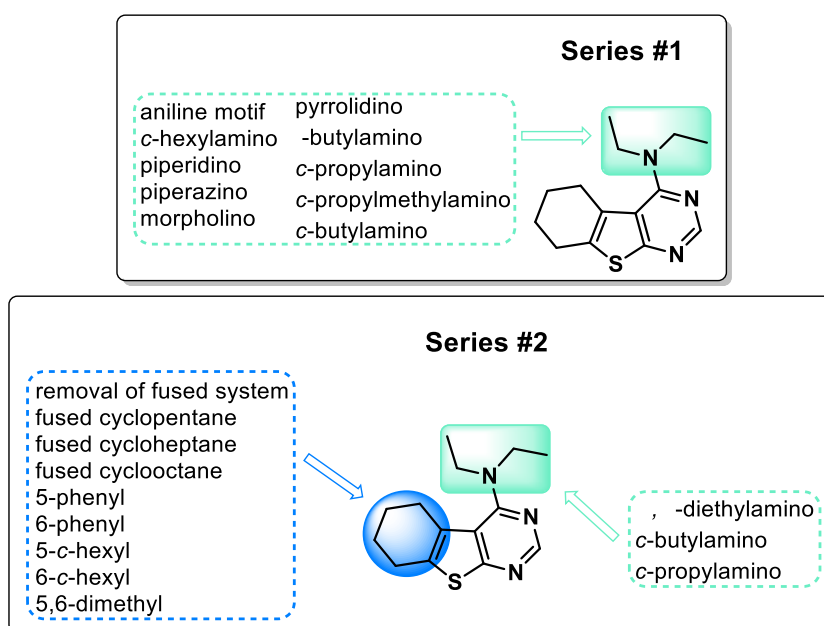


Figure 29. Further structural diversification of compound 7 (**44**).

Aim #3 – Understanding the structural limitations of a novel D₂R PAM scaffold

Using a small molecule allosteric modulator as a template for the development of biochemical tools will require a thorough analysis of the SAR to guide the rational design of such tools, particularly expensive fluorescent probes, and to lesser extent, irreversible photoactivatable ligands. The prospective chemical modifications conducted on this scaffold are highlighted in Figure 30, and all molecules were pharmacologically profiled using the functional cAMP assay described earlier. Accordingly, we aimed to initially employ a deletion strategy that will individually assess the requirement for existing substituents both on the benzene ring (A) as well as the indole moiety (B). In addition to this, the effect of simultaneous deletion of functionality will also be evaluated. Furthermore, additional structural changes will be conducted such as observing the effect of demethylating the aryl methyl ether, alkylating the hydroxy, replacing the hydroxymethyl substituent with a tolyl or methyl ether substituent, as well as conducting a ‘fluorine walk’ on various positions of the indole moiety. These modifications will ultimately enhance our understanding of allostery at the D₂R, as well as provide an indication of vectors that are amenable to functionalisation for the purpose of irreversible probe and fluorescent biochemical tool development.

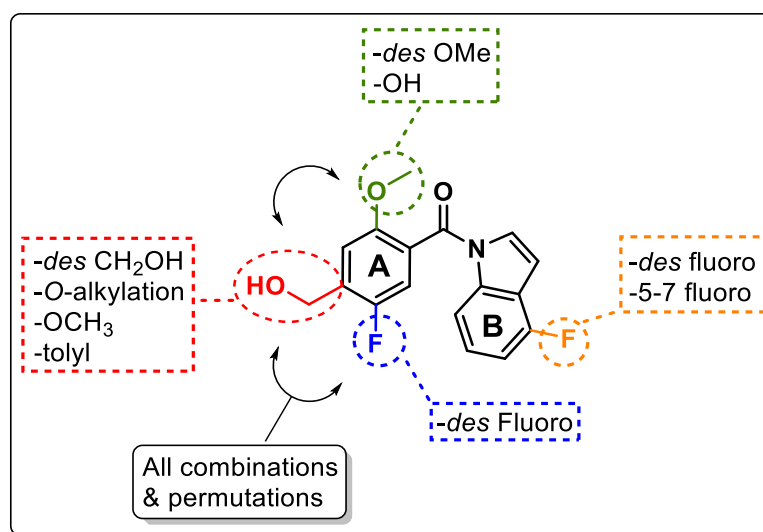


Figure 30. Proposed structural modifications to a D₂R PAM scaffold (46).

Aim #4 – Understanding how kinetic rate constants of haloperidol analogues are influenced through subtle structural modification

The role of ligand binding kinetics in producing the on-target side effects of APDs has long been a topic of intense interest. Recently, the kinetic hypothesis has been expanded to consider individual effects of both association and dissociation rates and their role in the propensity of an APD to cause hyperprolactinemia and EPS. Using haloperidol (**2**) as a model compound, we aim to conduct an extensive structure-kinetics relationship study to understand the role of structural modification on the ligand binding kinetics of a typical APD drug scaffold. To achieve this, a broad library of structurally similar analogues of haloperidol will be synthesised, and their kinetic profiles will be assessed using a competition association kinetic binding assay using homogeneous time-resolved fluorescence (HTRF) technology. All aspects of haloperidol's chemical structure will be investigated; the proposed structural changes are highlighted in Figure 31. These will include modifying substituents on the *para*-fluorophenyl moiety, reduction of the ketone to the corresponding secondary alcohol and replacement with an ether, thioether, *cis*- and *trans*-olefins, and *cis*- and *trans*-cyclopropanes. In addition, the effect of modifying linker length (to generate the corresponding propiophenones and valerophenones), and composition (to generate alkane and alkyne analogues) will be observed, as well as modification to the piperidinol moiety, and finally, modifying substituents on the *para*-chlorophenyl moiety.

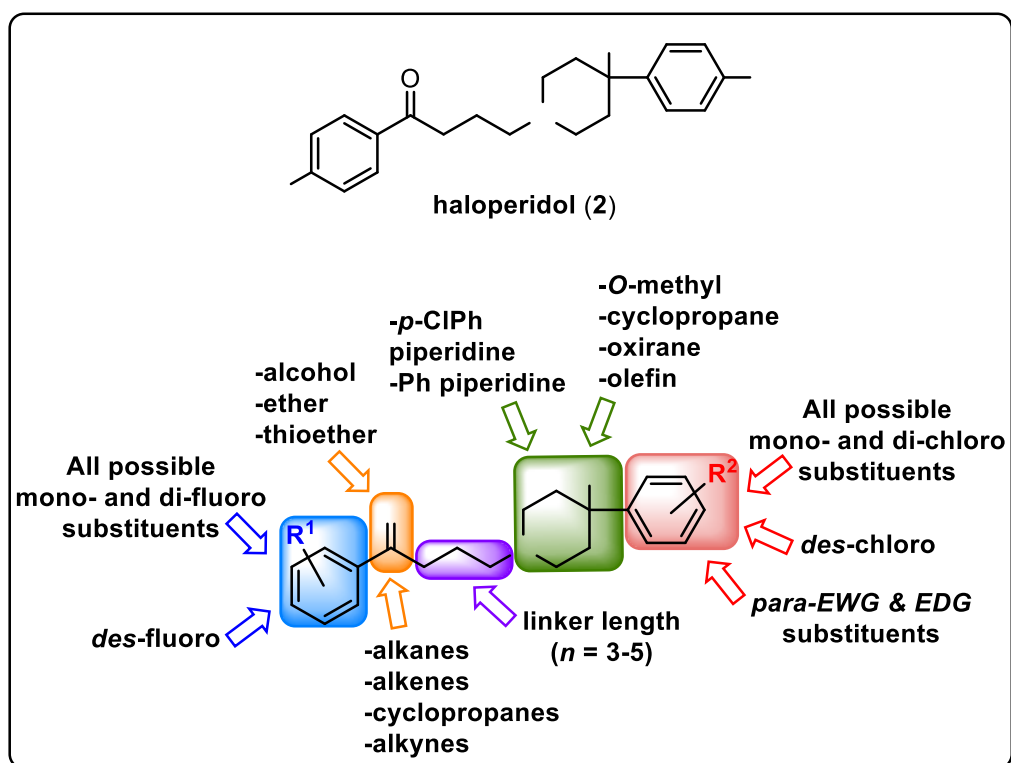


Figure 31. Chemical structure of typical APD haloperidol (**2**) and the structural modifications to be investigated during the proposed SKR study.

Aim #5 – Validation of D₁R PAM pharmacology and exploration of chemical methods to generate enantiopure allosteric modulators

PAMs of the DA D₁R may show promise as novel therapeutic agents for the symptomatic treatment of cognitive dysfunction associated with SCZ. Very few small molecule D₁R PAMs have been reported in the literature, of which minimal information regarding their SAR profiles is described. Accordingly, “compound A” (**18**) and “compound B” (**19**) are attractive starting points for the optimisation and development of novel D₁R PAMs. As such, we aim to synthesise these aforementioned small molecules as racemic mixtures to validate and quantify their allosteric pharmacology using functional measurements of D₁R activation. As the literature describes biological data for these compounds in their racemic form, chiral resolution and asymmetric synthesis will be used in an attempt to generate enantiomerically pure forms of “compound B” (Figure 32). This will provide insight for future SAR studies of D₁R PAMs, and in particular the relevance of absolute configuration and its influence on D₁R allosteric modulation.

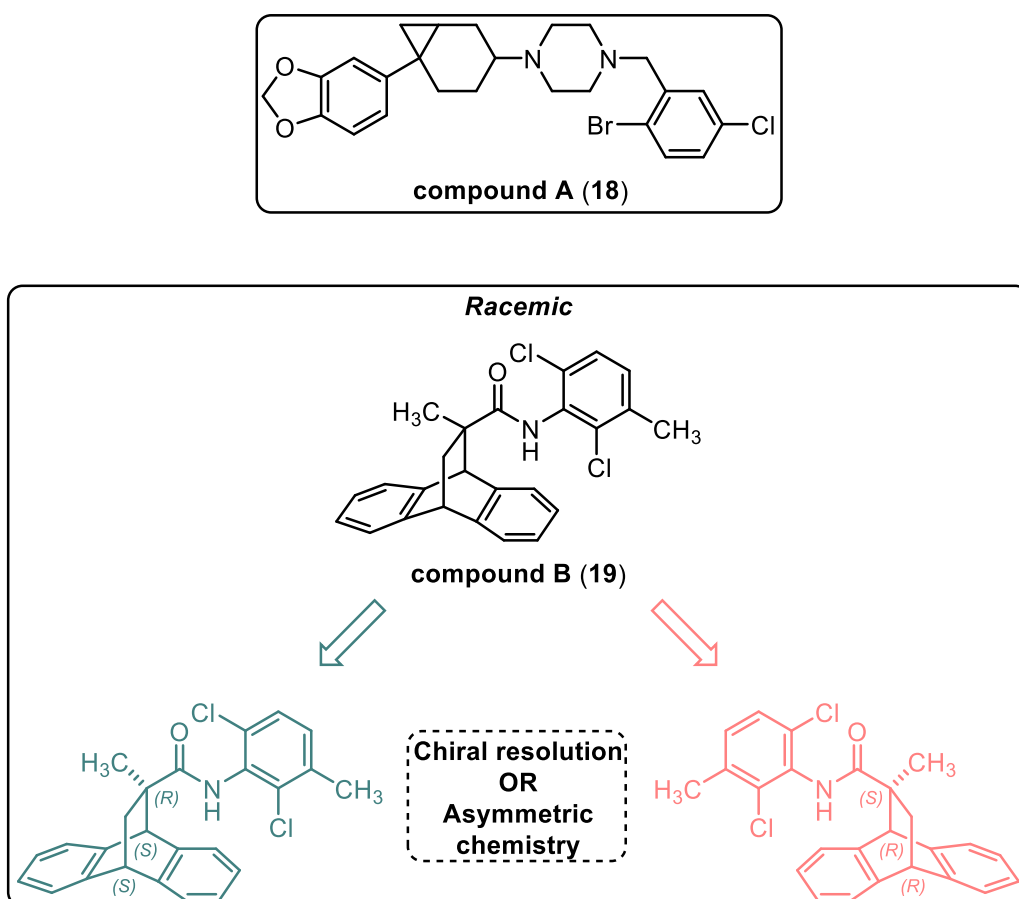


Figure 32. Chemical structure of reported D₁R PAMs, racemic “compound A” (**18**), and racemic “compound B” (**19**), together with its two enantiomers as defined by the distinct orientation of bridged methyl substituents.

References

1. Fredriksson, R.; Lagerstrom, M. C.; Lundin, L. G.; Schioth, H. B. The G-protein-coupled receptors in the human genome form five main families. Phylogenetic analysis, paralogon groups, and fingerprints. *Mol. Pharmacol.* **2003**, *63*, 1256-1272.
2. Santos, R.; Ursu, O.; Gaulton, A.; Bento, A. P.; Donadi, R. S.; Bologa, C. G.; Karlsson, A.; Al-Lazikani, B.; Hersey, A.; Oprea, T. I.; Overington, J. P. A comprehensive map of molecular drug targets. *Nat. Rev. Drug Discov.* **2017**, *16*, 19-34.
3. Kobilka, B. K. G protein-coupled receptor structure and activation. *Biochim. Biophys. Acta* **2007**, *1768*, 794-807.
4. Ramesh, M.; Soliman, M. E. G-protein coupled receptors (GPCRs): A comprehensive computational perspective. *Comb. Chem. High Throughput Screen* **2015**, *18*, 346-364.
5. Gether, U.; Kobilka, B. K. G Protein-coupled receptors: II. Mechanism of agonist activation. *J. Biol. Chem.* **1998**, *273*, 17979-17982.
6. Sriram, K.; Insel, P. A. G protein-coupled receptors as targets for approved drugs: How many targets and how many drugs? *Mol. Pharmacol.* **2018**, *93*, 251-258.
7. Dunn, H. A.; Ferguson, S. S. PDZ protein regulation of G protein-coupled receptor trafficking and signaling pathways. *Mol. Pharmacol.* **2015**, *88*, 624-639.
8. Ellisdon, A. M.; Halls, M. L. Compartmentalization of GPCR signalling controls unique cellular responses. *Biochem. Soc. Trans.* **2016**, *44*, 562-567.
9. Komolov, K. E.; Benovic, J. L. G protein-coupled receptor kinases: Past, present and future. *Cell Signal.* **2018**, *41*, 17-24.
10. Peterson, Y. K.; Luttrell, L. M. The diverse roles of arrestin scaffolds in G protein-coupled receptor signaling. *Pharmacol. Rev.* **2017**, *69*, 256-297.
11. Hilger, D.; Masureel, M.; Kobilka, B. K. Structure and dynamics of GPCR signaling complexes. *Nat. Struct. Mol. Biol.* **2018**, *25*, 4-12.
12. Dror, R. O.; Mildorf, T. J.; Hilger, D.; Manglik, A.; Borhani, D. W.; Arlow, D. H.; Philippsen, A.; Villanueva, N.; Yang, Z.; Lerch, M. T.; Hubbell, W. L.; Kobilka, B. K.; Sunahara, R. K.; Shaw, D. E. Structural basis for nucleotide exchange in heterotrimeric G proteins. *Science* **2015**, *348*, 1361-1365.
13. Oldham, W. M.; Van Eps, N.; Preininger, A. M.; Hubbell, W. L.; Hamm, H. E. Mechanism of the receptor-catalyzed activation of heterotrimeric G proteins. *Nat. Struct. Mol. Biol.* **2006**, *13*, 772-777.
14. Oldham, W. M.; Hamm, H. E. Structural basis of function in heterotrimeric G proteins. *Q. Rev. Biophys.* **2006**, *39*, 117-166.
15. Oldham, W. M.; Hamm, H. E. Heterotrimeric G protein activation by G-protein-coupled receptors. *Nat. Rev. Mol. Cell. Biol.* **2008**, *9*, 60-71.
16. Oldham, W. M.; Van Eps, N.; Preininger, A. M.; Hubbell, W. L.; Hamm, H. E. Mapping allosteric connections from the receptor to the nucleotide-binding pocket of heterotrimeric G proteins. *PNAS* **2007**, *104*, 7927-7932.
17. Rosenbaum, D. M.; Rasmussen, S. G.; Kobilka, B. K. The structure and function of G-protein-coupled receptors. *Nature* **2009**, *459*, 356-363.
18. Marinissen, M. J.; Gutkind, J. S. G-protein-coupled receptors and signaling networks: emerging paradigms. *Trends Pharmacol. Sci.* **2001**, *22*, 368-376.
19. Lohse, M. J.; Hein, P.; Hoffmann, C.; Nikolaev, V. O.; Vilardaga, J. P.; Bünemann, M. Kinetics of G-protein-coupled receptor signals in intact cells. *Br. J. Pharmacol.* **2008**, *153*, S125-S132.
20. Wootten, D.; Christopoulos, A.; Marti-Solano, M.; Babu, M. M.; Sexton, P. M. Mechanisms of signalling and biased agonism in G protein-coupled receptors. *Nat. Rev. Mol. Cell Biol.* **2018**.

21. Conn, P. J.; Lindsley, C. W.; Meiler, J.; Niswender, C. M. Opportunities and challenges in the discovery of allosteric modulators of GPCRs for treating CNS disorders. *Nat. Rev. Drug Discov.* **2014**, *13*, 692.
22. Conn, P. J.; Christopoulos, A.; Lindsley, C. W. Allosteric modulators of GPCRs: a novel approach for the treatment of CNS disorders. *Nat. Rev. Drug Discov.* **2009**, *8*, 41-54.
23. O'Brien, J. A.; Lemaire, W.; Chen, T. B.; Chang, R. S.; Jacobson, M. A.; Ha, S. N.; Lindsley, C. W.; Schaffhauser, H. J.; Sur, C.; Pettibone, D. J.; Conn, P. J.; Williams, D. L., Jr. A family of highly selective allosteric modulators of the metabotropic glutamate receptor subtype 5. *Mol. Pharmacol.* **2003**, *64*, 731-740.
24. Rodriguez, A. L.; Nong, Y.; Sekaran, N. K.; Alagille, D.; Tamagnan, G. D.; Conn, P. J. A close structural analog of 2-methyl-6-(phenylethynyl)-pyridine acts as a neutral allosteric site ligand on metabotropic glutamate receptor subtype 5 and blocks the effects of multiple allosteric modulators. *Mol. Pharmacol.* **2005**, *68*, 1793-1802.
25. Neubig, R. R.; Spedding, M.; Kenakin, T.; Christopoulos, A. International Union of Pharmacology Committee on Receptor Nomenclature and Drug Classification. XXXVIII. Update on terms and symbols in quantitative pharmacology. *Pharmacol. Rev.* **2003**, *55*, 597-606.
26. Wootten, D.; Christopoulos, A.; Sexton, P. M. Emerging paradigms in GPCR allostery: implications for drug discovery. *Nat. Rev. Drug Discov.* **2013**, *12*, 630-644.
27. Canals, M.; Sexton, P. M.; Christopoulos, A. Allostery in GPCRs: 'MWC' revisited. *Trends Biochem. Sci.* **2011**, *36*, 663-672.
28. Gregory, K. J.; Sexton, P. M.; Christopoulos, A. Overview of receptor allostery. *Curr. Protoc. Pharmacol.* **2010**, Chapter 1, Unit 1.21.
29. Leach, K.; Sexton, P. M.; Christopoulos, A. Allosteric GPCR modulators: taking advantage of permissive receptor pharmacology. *Trends Pharmacol. Sci.* **2007**, *28*, 382-389.
30. May, L. T.; Leach, K.; Sexton, P. M.; Christopoulos, A. Allosteric modulation of G protein-coupled receptors. *Annu. Rev. Pharmacol. Toxicol.* **2007**, *47*, 1-51.
31. Melancon, B. J.; Hopkins, C. R.; Wood, M. R.; Emmitte, K. A.; Niswender, C. M.; Christopoulos, A.; Conn, P. J.; Lindsley, C. W. Allosteric modulation of seven transmembrane spanning receptors: theory, practice, and opportunities for central nervous system drug discovery. *J. Med. Chem.* **2012**, *55*, 1445-1464.
32. Bruns, R. F.; Fergus, J. H. Allosteric enhancement of adenosine A1 receptor binding and function by 2-amino-3-benzoylthiophenes. *Mol. Pharmacol.* **1990**, *38*, 939-949.
33. Nemeth, E. F.; Steffey, M. E.; Hammerland, L. G.; Hung, B. C.; Van Wagenen, B. C.; DelMar, E. G.; Balandrin, M. F. Calcimimetics with potent and selective activity on the parathyroid calcium receptor. *Proc. Natl. Acad. Sci. U. S. A.* **1998**, *95*, 4040-4045.
34. Bridges, T. M.; Lindsley, C. W. G-protein-coupled receptors: from classical modes of modulation to allosteric mechanisms. *ACS Chem. Biol.* **2008**, *3*, 530-541.
35. Goudet, C.; Vilar, B.; Courtiol, T.; Deltheil, T.; Bessiron, T.; Brabet, I.; Oueslati, N.; Rigault, D.; Bertrand, H. O.; McLean, H.; Daniel, H.; Amalric, M.; Acher, F.; Pin, J. P. A novel selective metabotropic glutamate receptor 4 agonist reveals new possibilities for developing subtype selective ligands with therapeutic potential. *FASEB J.* **2012**, *26*, 1682-1693.
36. Ahmadian, H.; Nielsen, B.; Bräuner-Osborne, H.; Johansen, T. N.; Stensbøl, T. B.; Sløk, F. A.; Sekiyama, N.; Nakanishi, S.; Krosgaard-Larsen, P.; Madsen, U. (S)-Homo-AMPA, a specific agonist at the mGlu6 subtype of metabotropic glutamic acid receptors. *J. Med. Chem.* **1997**, *40*, 3700-3705.
37. Trabanco, A. A.; Cid, J. M. mGluR2 positive allosteric modulators: a patent review (2009 – present). *Expert Opin. Ther. Pat.* **2013**, *23*, 629-647.
38. Celanire, S.; Campo, B. Recent advances in the drug discovery of metabotropic glutamate receptor 4 (mGluR4) activators for the treatment of CNS and non-CNS disorders. *Expert Opin. Drug Discov.* **2012**, *7*, 261-280.
39. Lindsley, C. W.; Hopkins, C. R. Metabotropic glutamate receptor 4 (mGlu4)-positive allosteric modulators for the treatment of Parkinson's disease: historical perspective and review of the patent literature. *Expert Opin. Ther. Pat.* **2012**, *22*, 461-481.

40. Jaeschke, G.; Wettstein, J. G.; Nordquist, R. E.; Spooren, W. mGlu5 receptor antagonists and their therapeutic potential. *Expert Opin. Ther. Pat.* **2008**, *18*, 123-142.
41. Emmitte, K. A. mGlu5 negative allosteric modulators: a patent review (2010-2012). *Expert Opin. Ther. Pat.* **2013**, *23*, 393-408.
42. Kenakin, T.; Miller, L. J. Seven transmembrane receptors as shapeshifting proteins: the impact of allosteric modulation and functional selectivity on new drug discovery. *Pharmacol. Rev.* **2010**, *62*, 265-304.
43. Ayala, J. E.; Chen, Y.; Banko, J. L.; Sheffler, D. J.; Williams, R.; Telk, A. N.; Watson, N. L.; Xiang, Z.; Zhang, Y.; Jones, P. J.; Lindsley, C. W.; Olive, M. F.; Conn, P. J. mGluR5 positive allosteric modulators facilitate both hippocampal LTP and LTD and enhance spatial learning. *Neuropsychopharmacology* **2009**, *34*, 2057-2071.
44. Rudolph, U.; Knoflach, F. Beyond classical benzodiazepines: Novel therapeutic potential of GABA(A) receptor subtypes. *Nat. Rev. Drug Discov.* **2011**, *10*, 685-697.
45. Costa, E. The Di Mascio Lecture. The allosteric modulation of GABAA receptors. Seventeen years of research. *Neuropsychopharmacol.* **1991**, *4*, 225-235.
46. Urban, J. D.; Clarke, W. P.; von Zastrow, M.; Nichols, D. E.; Kobilka, B.; Weinstein, H.; Javitch, J. A.; Roth, B. L.; Christopoulos, A.; Sexton, P. M.; Miller, K. J.; Spedding, M.; Mailman, R. B. Functional selectivity and classical concepts of quantitative pharmacology. *J. Pharmacol. Exp. Ther.* **2007**, *320*, 1-13.
47. Mailman, R. B.; Murthy, V. Ligand functional selectivity advances our understanding of drug mechanisms and drug discovery. *Neuropsychopharmacology* **2010**, *35*, 345-346.
48. Zhang, C.; Marek, G. J. Group III metabotropic glutamate receptor agonists selectively suppress excitatory synaptic currents in the rat prefrontal cortex induced by 5-hydroxytryptamine_{2A} receptor activation. *J. Pharmacol. Exp. Ther.* **2007**, *320*, 437-447.
49. Cook, A. E.; Mistry, S. N.; Gregory, K. J.; Furness, S. G. B.; Sexton, P. M.; Scammells, P. J.; Conigrave, A. D.; Christopoulos, A.; Leach, K. Biased allosteric modulation at the CaS receptor engendered by structurally diverse calcimimetics. *Br. J. Pharmacol.* **2015**, *172*, 185-200.
50. Kenakin, T. Functional selectivity and biased receptor signaling. *J. Pharmacol. Exp. Ther.* **2011**, *336*, 296-302.
51. Christopoulos, A. Advances in G protein-coupled receptor allostery: From function to structure. *Mol. Pharmacol.* **2014**, *86*, 463-478.
52. Neve, K. A.; Seamans, J. K.; Trantham-Davidson, H. Dopamine receptor signaling. *J. Recept. Signal Transduct. Res.* **2004**, *24*, 165-205.
53. Sun, J.; Nan, G. The extracellular signal-regulated kinase 1/2 pathway in neurological diseases: A potential therapeutic target (Review). *Int. J. Mol. Med.* **2017**, *39*, 1338-1346.
54. McAllister, G.; Knowles, M. R.; Ward-Booth, S. M.; Sinclair, H. A.; Patel, S.; Marwood, R.; Emms, F.; Patel, S.; Smith, A.; Seabrook, G. R.; et al. Functional coupling of human D₂, D₃, and D₄ dopamine receptors in HEK293 cells. *J. Recept. Signal. Transduct. Res.* **1995**, *15*, 267-281.
55. Gingrich, J. A.; Caron, M. G. Recent advances in the molecular biology of dopamine receptors. *Annu. Rev. Neurosci.* **1993**, *16*, 299-321.
56. Usiello, A.; Baik, J. H.; Rouge-Pont, F.; Picetti, R.; Dierich, A.; LeMeur, M.; Piazza, P. V.; Borrelli, E. Distinct functions of the two isoforms of dopamine D₂ receptors. *Nature* **2000**, *408*, 199-203.
57. Wang, Y.; Xu, R.; Sasaoka, T.; Tonegawa, S.; Kung, M. P.; Sankoorikal, E. B. Dopamine D₂ long receptor-deficient mice display alterations in striatum-dependent functions. *J. Neurosci.* **2000**, *20*, 8305-8314.
58. Cho, D. I.; Zheng, M.; Kim, K. M. Current perspectives on the selective regulation of dopamine D(2) and D(3) receptors. *Arch. Pharm. Res.* **2010**, *33*, 1521-1538.
59. Stahl, S. M. *Stahl's essential psychopharmacology: neuroscientific basis and practical applications*. Third ed.; Cambridge University Press: 2008; p 1118.
60. Amato, D.; Vernon, A. C.; Papaleo, F. Dopamine, the antipsychotic molecule: A perspective on mechanisms underlying antipsychotic response variability. *Neurosci. Biobehav. Rev.* **2018**, *85*, 146-159.

61. Meisenzahl, E. M.; Schmitt, G. J.; Scheuerecker, J.; Moller, H. J. The role of dopamine for the pathophysiology of schizophrenia. *Int. Rev. Psychiatry* **2007**, *19*, 337-345.
62. Sokoloff, P.; Giros, B.; Martres, M. P.; Bouthenet, M. L.; Schwartz, J. C. Molecular cloning and characterization of a novel dopamine receptor (D3) as a target for neuroleptics. *Nature* **1990**, *347*, 146-151.
63. Searle, G.; Beaver, J. D.; Comley, R. A.; Bani, M.; Tziortzi, A.; Slifstein, M.; Mugnaini, M.; Griffante, C.; Wilson, A. A.; Merlo-Pich, E.; Houle, S.; Gunn, R.; Rabiner, E. A.; Laruelle, M. Imaging dopamine D3 receptors in the human brain with positron emission tomography, [¹¹C]PHNO, and a selective D3 receptor antagonist. *Biol. Psychiatry* **2010**, *68*, 392-399.
64. Gurevich, E. V.; Joyce, J. N. Distribution of dopamine D3 receptor expressing neurons in the human forebrain: comparison with D2 receptor expressing neurons. *Neuropsychopharmacology* **1999**, *20*, 60-80.
65. Emilien, G.; Maloteaux, J. M.; Geurts, M.; Hoogenberg, K.; Cragg, S. Dopamine receptors--physiological understanding to therapeutic intervention potential. *Pharmacol. Ther.* **1999**, *84*, 133-156.
66. Iversen, S. D.; Iversen, L. L. Dopamine: 50 years in perspective. *Trends Neurosci.* **2007**, *30*, 188-193.
67. Aperia, A. C. Intrarenal dopamine: a key signal in the interactive regulation of sodium metabolism. *Annu. Rev. Physiol.* **2000**, *62*, 621-647.
68. Missale, C.; Nash, S. R.; Robinson, S. W.; Jaber, M.; Caron, M. G. Dopamine receptors: from structure to function. *Physiol. Rev.* **1998**, *78*, 189-225.
69. Sedvall, G. C.; Karlsson, P. Pharmacological manipulation of D1-dopamine receptor function in schizophrenia. *Neuropsychopharmacology* **1999**, *21*, S181.
70. Goldman-Rakic, P. S. The relevance of the dopamine-D1 receptor in the cognitive symptoms of schizophrenia. *Neuropsychopharmacology* **1999**, *21*, S170.
71. Arnsten, A. F.; Wang, M.; Paspalas, C. D. Dopamine's actions in primate prefrontal cortex: Challenges for treating cognitive disorders. *Pharmacol Rev* **2015**, *67*, 681-696.
72. Rinne, U. K.; Lönnberg, P.; Koskinen, V. Dopamine receptors in the parkinsonian brain. *J. Neural Transm.* **1981**, *51*, 97-106.
73. Guttman, M.; Seeman, P. L-dopa reverses the elevated density of D2 dopamine receptors in Parkinson's diseased striatum. *J. Neural Transm.* **1985**, *64*, 93-103.
74. Wong, D. F.; Wagner, H. N., Jr.; Tune, L. E.; Dannals, R. F.; Pearlson, G. D.; Links, J. M.; Tamminga, C. A.; Broussolle, E. P.; Ravert, H. T.; Wilson, A. A.; Toung, J. K.; Malat, J.; Williams, J. A.; O'Tuama, L. A.; Snyder, S. H.; Kuhar, M. J.; Gjedde, A. Positron emission tomography reveals elevated D2 dopamine receptors in drug-naive schizophrenics. *Science* **1986**, *234*, 1558-1563.
75. German, D. C.; Manaye, K.; Smith, W. K.; Woodward, D. J.; Saper, C. B. Midbrain dopaminergic cell loss in Parkinson's disease: computer visualization. *Ann. Neurol.* **1989**, *26*, 507-514.
76. Tune, L. E.; Wong, D. F.; Pearlson, G.; Strauss, M.; Young, T.; Shaya, E. K.; Dannals, R. F.; Wilson, A. A.; Ravert, H. T.; Sapp, J.; Cooper, T.; Chase, G. A.; Wagner, H. N. Dopamine D2 receptor density estimates in schizophrenia: A positron emission tomography study with ¹¹C-N-methylspiperone. *Psychiatry Res.* **1993**, *49*, 219-237.
77. Hietala, J.; Syvalahti, E.; Vuorio, K.; Nagren, K.; Lehtikoinen, P.; Ruotsalainen, U.; Rakkolainen, V.; Lehtinen, V.; Wegelius, U. Striatal D2 dopamine receptor characteristics in neuroleptic-naive schizophrenic patients studied with positron emission tomography. *Arch. Gen. Psychiatry* **1994**, *51*, 116-123.
78. Goldsmith, S. K.; Shapiro, R. M.; Joyce, J. N. Disrupted pattern of D2 dopamine receptors in the temporal lobe in schizophrenia. A postmortem study. *Arch. Gen. Psychiatry* **1997**, *54*, 649-658.
79. Heidbreder, C. A.; Newman, A. H. Current perspectives on selective dopamine D(3) receptor antagonists as pharmacotherapeutics for addictions and related disorders. *Ann. N. Y. Acad. Sci.* **2010**, *1187*, 4-34.
80. Micheli, F. Recent advances in the development of dopamine D3 receptor antagonists: a medicinal chemistry perspective. *ChemMedChem* **2011**, *6*, 1152-1162.

81. Newman, A. H.; Blaylock, B. L.; Nader, M. A.; Bergman, J.; Sibley, D. R.; Skolnick, P. Medication discovery for addiction: translating the dopamine D3 receptor hypothesis. *Biochem. Pharmacol.* **2012**, *84*, 882-890.
82. Micheli, F.; Heidebreder, C. Dopamine D3 receptor antagonists: a patent review (2007 - 2012). *Expert Opin. Ther. Pat.* **2013**, *23*, 363-381.
83. Xiaojing, C.; Jeremie, T.; Jerome, G. Class A GPCRs: Structure, Function, Modeling and Structure-based Ligand Design. *Curr. Pharm. Des.* **2017**, *23*, 4390-4409.
84. Wacker, D.; Stevens, R. C.; Roth, B. L. How ligands illuminate GPCR molecular pharmacology. *Cell* **2017**, *170*, 414-427.
85. Manglik, A.; Lin, H.; Aryal, D. K.; McCorvy, J. D.; Dengler, D.; Corder, G.; Levit, A.; Kling, R. C.; Bernat, V.; Hubner, H.; Huang, X. P.; Sassano, M. F.; Giguere, P. M.; Lober, S.; Da, D.; Scherrer, G.; Kobilka, B. K.; Gmeiner, P.; Roth, B. L.; Shoichet, B. K. Structure-based discovery of opioid analgesics with reduced side effects. *Nature* **2016**, *537*, 185-190.
86. Palczewski, K.; Kumasaka, T.; Hori, T.; Behnke, C. A.; Motoshima, H.; Fox, B. A.; Le Trong, I.; Teller, D. C.; Okada, T.; Stenkamp, R. E.; Yamamoto, M.; Miyano, M. Crystal structure of rhodopsin: A G protein-coupled receptor. *Science* **2000**, *289*, 739-745.
87. Wacker, D.; Wang, C.; Katritch, V.; Han, G. W.; Huang, X.-P.; Vardy, E.; McCorvy, J. D.; Jiang, Y.; Chu, M.; Siu, F. Y.; Liu, W.; Xu, H. E.; Cherezov, V.; Roth, B. L.; Stevens, R. C. Structural features for functional selectivity at serotonin receptors. *Science* **2013**, *340*, 615-619.
88. Wacker, D.; Wang, S.; McCorvy, J. D.; Betz, R. M.; Venkatakrishnan, A. J.; Levit, A.; Lansu, K.; Schools, Z. L.; Che, T.; Nichols, D. E.; Shoichet, B. K.; Dror, R. O.; Roth, B. L. Crystal structure of an LSD-bound human serotonin receptor. *Cell* **2017**, *168*, 377-389.
89. Yin, W.; Zhou, X. E.; Yang, D.; de Waal, P. W.; Wang, M.; Dai, A.; Cai, X.; Huang, C.-Y.; Liu, P.; Wang, X.; Yin, Y.; Liu, B.; Zhou, Y.; Wang, J.; Liu, H.; Caffrey, M.; Melcher, K.; Xu, Y.; Wang, M.-W.; Xu, H. E.; Jiang, Y. Crystal structure of the human 5-HT1B serotonin receptor bound to an inverse agonist. *Cell Discov.* **2018**, *4*, 12.
90. Kimura, K. T.; Asada, H.; Inoue, A.; Kadji, F. M. N.; Im, D.; Mori, C.; Arakawa, T.; Hirata, K.; Nomura, Y.; Nomura, N.; Aoki, J.; Iwata, S.; Shimamura, T. Structures of the 5-HT2A receptor in complex with the antipsychotics risperidone and zotepine. *Nat. Struct. Mol. Biol.* **2019**, *26*, 121-128.
91. Cherezov, V.; Rosenbaum, D. M.; Hanson, M. A.; Rasmussen, S. G. F.; Thian, F. S.; Kobilka, T. S.; Choi, H.-J.; Kuhn, P.; Weis, W. I.; Kobilka, B. K.; Stevens, R. C. High-resolution crystal structure of an engineered human β 2-adrenergic G protein-coupled receptor. *Science* **2007**, *318*, 1258-1265.
92. Rasmussen, S. G. F.; Choi, H.-J.; Rosenbaum, D. M.; Kobilka, T. S.; Thian, F. S.; Edwards, P. C.; Burghammer, M.; Ratnala, V. R. P.; Sanishvili, R.; Fischetti, R. F.; Schertler, G. F. X.; Weis, W. I.; Kobilka, B. K. Crystal structure of the human β 2 adrenergic G-protein-coupled receptor. *Nature* **2007**, *450*, 383.
93. Rasmussen, S. G.; DeVree, B. T.; Zou, Y.; Kruse, A. C.; Chung, K. Y.; Kobilka, T. S.; Thian, F. S.; Chae, P. S.; Pardon, E.; Calinski, D.; Mathiesen, J. M.; Shah, S. T.; Lyons, J. A.; Caffrey, M.; Gellman, S. H.; Steyaert, J.; Skinotitis, G.; Weis, W. I.; Sunahara, R. K.; Kobilka, B. K. Crystal structure of the beta2 adrenergic receptor-Gs protein complex. *Nature* **2011**, *477*, 549-555.
94. Warne, T.; Edwards, P. C.; Leslie, A. G.; Tate, C. G. Crystal structures of a stabilized beta1-adrenoceptor bound to the biased agonists bucindolol and carvedilol. *Structure* **2012**, *20*, 841-849.
95. Thal, D. M.; Sun, B.; Feng, D.; Nawaratne, V.; Leach, K.; Felder, C. C.; Bures, M. G.; Evans, D. A.; Weis, W. I.; Bachhawat, P.; Kobilka, T. S.; Sexton, P. M.; Kobilka, B. K.; Christopoulos, A. Crystal structures of the M(1) and M(4) muscarinic acetylcholine receptors. *Nature* **2016**, *531*, 335-340.
96. Haga, K.; Kruse, A. C.; Asada, H.; Yurugi-Kobayashi, T.; Shiroishi, M.; Zhang, C.; Weis, W. I.; Okada, T.; Kobilka, B. K.; Haga, T.; Kobayashi, T. Structure of the human M2 muscarinic acetylcholine receptor bound to an antagonist. *Nature* **2012**, *482*, 547.

97. Manglik, A.; Kruse, A. C.; Kobilka, T. S.; Thian, F. S.; Mathiesen, J. M.; Sunahara, R. K.; Pardo, L.; Weis, W. I.; Kobilka, B. K.; Granier, S. Crystal structure of the μ -opioid receptor bound to a morphinan antagonist. *Nature* **2012**, *485*, 321-326.
98. Che, T.; Majumdar, S.; Zaidi, S. A.; Ondachi, P.; McCorvy, J. D.; Wang, S.; Mosier, P. D.; Uprety, R.; Vardy, E.; Krumm, B. E.; Han, G. W.; Lee, M. Y.; Pardon, E.; Steyaert, J.; Huang, X. P.; Strachan, R. T.; Tribo, A. R.; Pasternak, G. W.; Carroll, F. I.; Stevens, R. C.; Cherezov, V.; Katritch, V.; Wacker, D.; Roth, B. L. Structure of the nanobody-stabilized active state of the kappa opioid receptor. *Cell* **2018**, *172*, 55-67.e15.
99. Jaakola, V.-P.; Griffith, M. T.; Hanson, M. A.; Cherezov, V.; Chien, E. Y. T.; Lane, J. R.; Ijzerman, A. P.; Stevens, R. C. The 2.6 Å crystal structure of a human A(2A) adenosine receptor bound to an antagonist. *Science* **2008**, *322*, 1211-1217.
100. Sun, B.; Bachhawat, P.; Chu, M. L.-H.; Wood, M.; Ceska, T.; Sands, Z. A.; Mercier, J.; Lebon, F.; Kobilka, T. S.; Kobilka, B. K. Crystal structure of the adenosine A2A receptor bound to an antagonist reveals a potential allosteric pocket. *PNAS* **2017**, *114*, 2066-2071.
101. Qin, L.; Kufareva, I.; Holden, L. G.; Wang, C.; Zheng, Y.; Zhao, C.; Fenalti, G.; Wu, H.; Han, G. W.; Cherezov, V.; Abagyan, R.; Stevens, R. C.; Handel, T. M. Crystal structure of the chemokine receptor CXCR4 in complex with a viral chemokine. *Science* **2015**, *347*, 1117-1122.
102. Shimamura, T.; Shiroishi, M.; Weyand, S.; Tsujimoto, H.; Winter, G.; Katritch, V.; Abagyan, R.; Cherezov, V.; Liu, W.; Han, G. W.; Kobayashi, T.; Stevens, R. C.; Iwata, S. Structure of the human histamine H1 receptor complex with doxepin. *Nature* **2011**, *475*, 65-70.
103. Wang, S.; Che, T.; Levit, A.; Shoichet, B. K.; Wacker, D.; Roth, B. L. Structure of the D2 dopamine receptor bound to the atypical antipsychotic drug risperidone. *Nature* **2018**, *555*, 269-273.
104. Chien, E. Y.; Liu, W.; Zhao, Q.; Katritch, V.; Han, G. W.; Hanson, M. A.; Shi, L.; Newman, A. H.; Javitch, J. A.; Cherezov, V.; Stevens, R. C. Structure of the human dopamine D3 receptor in complex with a D2/D3 selective antagonist. *Science* **2010**, *330*, 1091-1095.
105. Wang, S.; Wacker, D.; Levit, A.; Che, T.; Betz, R. M.; McCorvy, J. D.; Venkatakrishnan, A. J.; Huang, X. P.; Dror, R. O.; Shoichet, B. K.; Roth, B. L. D4 dopamine receptor high-resolution structures enable the discovery of selective agonists. *Science* **2017**, *358*, 381-386.
106. Shonberg, J.; Kling, R. C.; Gmeiner, P.; Löber, S. GPCR crystal structures: Medicinal chemistry in the pocket. *Bioorg. Med. Chem.* **2015**, *23*, 3880-3906.
107. McCorvy, J. D.; Butler, K. V.; Kelly, B.; Rechsteiner, K.; Karpiak, J.; Betz, R. M.; Kormos, B. L.; Shoichet, B. K.; Dror, R. O.; Jin, J.; Roth, B. L. Structure-inspired design of β -arrestin-biased ligands for aminergic GPCRs. *Nat. Chem. Biol.* **2017**, *14*, 126.
108. Ballesteros, J. A.; Weinstein, H. Integrated methods for the construction of three-dimensional models and computational probing of structure-function relations in G protein-coupled receptors. In *Methods Neurosci.*, Sealfon, S. C., Ed. Academic Press: 1995; Vol. 25, pp 366-428.
109. Insel, T. R. Rethinking schizophrenia. *Nature* **2010**, *468*, 187-193.
110. Lieberman, J. A. Is schizophrenia a neurodegenerative disorder? A clinical and neurobiological perspective. *Biol. Psychiatry* **1999**, *46*, 729-739.
111. Kim, D. H.; Maneen, M. J.; Stahl, S. M. Building a better antipsychotic: receptor targets for the treatment of multiple symptom dimensions of schizophrenia. *Neurotherapeutics* **2009**, *6*, 78-85.
112. Rosen, W. G.; Mohs, R. C.; Johns, C. A.; Small, N. S.; Kendler, K. S.; Horvath, T. B.; Davis, K. L. Positive and negative symptoms in schizophrenia. *Psychiatry. Res.* **1984**, *13*, 277-284.
113. Bowie, C. R.; Harvey, P. D. Cognitive deficits and functional outcome in schizophrenia. *Neuropsychiatr. Dis. Treatment* **2006**, *2*, 531-536.
114. Mier, D.; Kirsch, P. Social-cognitive deficits in schizophrenia. *Curr. Top Behav. Neurosci.* **2017**, *30*, 397-409.
115. Andreasen, N. C. Symptoms, signs, and diagnosis of schizophrenia. *Lancet* **1995**, *346*, 477-481.
116. Biological insights from 108 schizophrenia-associated genetic loci. *Nature* **2014**, *511*, 421-427.
117. Sekar, A.; Bialas, A. R.; de Rivera, H.; Davis, A.; Hammond, T. R.; Kamitaki, N.; Tooley, K.; Presumey, J.; Baum, M.; Van Doren, V.; Genovese, G.; Rose, S. A.; Handsaker, R. E.; Schizophrenia

- Working Group of the Psychiatric Genomics, C.; Daly, M. J.; Carroll, M. C.; Stevens, B.; McCarroll, S. A. Schizophrenia risk from complex variation of complement component 4. *Nature* **2016**, *530*, 177-118.
118. Capuano, B.; Crosby, I. T.; Lloyd, E. J. Schizophrenia: genesis, receptorology and current therapeutics. *Curr. Med. Chem.* **2002**, *9*, 521-548.
119. Toda, M.; Abi-Dargham, A. Dopamine hypothesis of schizophrenia: making sense of it all. *Curr. Psychiatry Rep.* **2007**, *9*, 329-336.
120. Ena, S.; de Kerchove d'Exaerde, A.; Schiffmann, S. N. Unraveling the differential functions and regulation of striatal neuron sub-populations in motor control, reward, and motivational processes. *Front. Behav. Neurosci.* **2011**, *5*, 47.
121. Cacho, R.; Cheer, J. F. Local control of striatal dopamine release. *Front. Behav. Neurosci.* **2014**, *8*, 188.
122. Owen, F.; Cross, A. J.; Crow, T. J.; Longden, A.; Poulter, M.; Riley, G. J. Increased dopamine-receptor sensitivity in schizophrenia. *Lancet* **1978**, *2*, 223-226.
123. Cross, A. J.; Crow, T. J.; Longden, A.; Owen, F.; Poulter, M.; Riley, G. J. Evidence for increased dopamine receptor sensitivity in post mortem brains from patients with schizophrenia. *J. Physiol.* **1978**, *280*, 37p.
124. van Rossum, J. M. The significance of dopamine-receptor blockade for the mechanism of action of neuroleptic drugs. *Arch. Int. Pharmacodyn. Ther.* **1966**, *160*, 492-494.
125. Baumeister, A. A.; Francis, J. L. Historical development of the dopamine hypothesis of schizophrenia. *J. Hist. Neurosci.* **2002**, *11*, 265-277.
126. Seeman, P.; Lee, T.; Chau-Wong, M.; Wong, K. Antipsychotic drug doses and neuroleptic/dopamine receptors. *Nature* **1976**, *261*, 717-719.
127. Seeman, P. Atypical antipsychotics: mechanism of action. *Can J Psychiatry* **2002**, *47*, 27-38.
128. Horacek, J.; Bubenikova-Valesova, V.; Kopecek, M.; Palenicek, T.; Dockery, C.; Mohr, P.; Hoschl, C. Mechanism of action of atypical antipsychotic drugs and the neurobiology of schizophrenia. *CNS Drugs* **2006**, *20*, 389-409.
129. Creese, I.; Hess, E. J. Biochemical characteristics of D1 dopamine receptors: relationship to behavior and schizophrenia. *Clin. Neuropharmacol.* **1986**, *9 Suppl 4*, 14-16.
130. Seeman, P. Atypical antipsychotics: mechanism of action. *Can. J. Psychiatry* **2002**, *47*, 27-38.
131. Seeman, P. Dopamine receptors and the dopamine hypothesis of schizophrenia. *Synapse* **1987**, *1*, 133-152.
132. Seeman, P. Targeting the dopamine D2 receptor in schizophrenia. *Expert Opin. Ther. Targets* **2006**, *10*, 515-531.
133. Lieberman, J. A.; Kane, J. M.; Gadaleta, D.; Brenner, R.; Lesser, M. S.; Kinon, B. Methylphenidate challenge as a predictor of relapse in schizophrenia. *Am. J. Psychiatry* **1984**, *141*, 633-638.
134. Angrist, B.; Peselov, E.; Rubinstein, M.; Wolkin, A.; Rotrosen, J. Amphetamine response and relapse risk after depot neuroleptic discontinuation. *Psychopharmacology* **1985**, *85*, 277-283.
135. Lally, J.; MacCabe, J. H. Antipsychotic medication in schizophrenia: a review. *Br. Med. Bull.* **2015**, *114*, 169-179.
136. Seeman, P.; Lee, T.; Chau-Wong, M.; Wong, K. Antipsychotic drug doses and neuroleptic/dopamine receptors. *Nature* **1976**, *261*, 717-719.
137. Meltzer, H. Y. An atypical compound by any other name is still a. *Psychopharmacology* **2000**, *148*, 16-19.
138. Blair, D. T.; Dauner, A. Extrapyramidal symptoms are serious side-effects of antipsychotic and other drugs. *Nurse Pract.* **1992**, *17*, 56, 62-64, 67.
139. Ginovart, N.; Kapur, S. Role of dopamine D(2) receptors for antipsychotic activity. *Handb. Exp. Pharmacol.* **2012**, *212*, 27-52.
140. Miyamoto, S.; Miyake, N.; Jarskog, L. F.; Fleischhacker, W. W.; Lieberman, J. A. Pharmacological treatment of schizophrenia: a critical review of the pharmacology and clinical effects of current and future therapeutic agents. *Mol. Psychiatr.* **2012**, *17*, 1206-1227.

141. Meltzer, H. Y. Update on typical and atypical antipsychotic drugs. *Annu. Rev. Med.* **2013**, *64*, 393-406.
142. Leucht, S.; Corves, C.; Arbter, D.; Engel, R. R.; Li, C.; Davis, J. M. Second-generation versus first-generation antipsychotic drugs for schizophrenia: a meta-analysis. *Lancet* **2009**, *373*, 31-41.
143. Farde, L.; Nordstrom, A. L.; Wiesel, F. A.; Pauli, S.; Halldin, C.; Sedvall, G. Positron emission tomographic analysis of central D1 and D2 dopamine receptor occupancy in patients treated with classical neuroleptics and clozapine. Relation to extrapyramidal side effects. *Arch. Gen. Psychiat.* **1992**, *49*, 538-544.
144. Caron, M. G.; Beaulieu, M.; Raymond, V.; Gagne, B.; Drouin, J.; Lefkowitz, R. J.; Labrie, F. Dopaminergic receptors in the anterior pituitary gland. Correlation of [3H]dihydroergocryptine binding with the dopaminergic control of prolactin release. *J. Biol. Chem.* **1978**, *253*, 2244-2253.
145. Glazer, W. M. Extrapyramidal side effects, tardive dyskinesia, and the concept of atypicality. *J. Clin. Psychiatry* **2000**, *61*, 16-21.
146. Battaglia, J. Pharmacological management of acute agitation. *Drugs* **2005**, *65*, 1207-1222.
147. Leucht, S.; Pitschel-Walz, G.; Abraham, D.; Kissling, W. Efficacy and extrapyramidal side-effects of the new antipsychotics olanzapine, quetiapine, risperidone, and sertindole compared to conventional antipsychotics and placebo. A meta-analysis of randomized controlled trials. *Schizophr. Res.* **1999**, *35*, 51-68.
148. Halbreich, U.; Kinon, B. J.; Gilmore, J. A.; Kahn, L. S. Elevated prolactin levels in patients with schizophrenia: mechanisms and related adverse effects. *Psychoneuroendocrinology* **2003**, *28*, 53-67.
149. Mauri, M. C.; Paletta, S.; Maffini, M.; Colasanti, A.; Dragogna, F.; Di Pace, C.; Altamura, A. C. Clinical pharmacology of atypical antipsychotics: an update. *EXCLI J.* **2014**, *13*, 1163-1191.
150. Kapur, S.; Remington, G. Dopamine D(2) receptors and their role in atypical antipsychotic action: still necessary and may even be sufficient. *Biol. Psychiat.* **2001**, *50*, 873-883.
151. Meltzer, H. Y.; Matsubara, S.; Lee, J. C. Classification of typical and atypical antipsychotic drugs on the basis of dopamine D-1, D-2 and serotonin₂ pKi values. *J. Pharmacol. Exp. Ther.* **1989**, *251*, 238-246.
152. Marcus, M.; Wiker, C.; Frånberg, O.; Konradsson-Geuken, A.; Langlois, X.; Jardemark, K.; Svensson, T. Adjunctive alpha(2)-adrenoceptor blockade enhances the antipsychotic-like effect of risperidone and facilitates cortical dopaminergic and glutamatergic, NMDA receptor-mediated transmission. *Int. J. Neuropsychopharmacol.* **2009**, *13*, 891-903.
153. Roth, B. L.; Sheffler, D. J.; Kroeze, W. K. Magic shotguns versus magic bullets: selectively non-selective drugs for mood disorders and schizophrenia. *Nat. Rev. Drug Discov.* **2004**, *3*, 353.
154. Meltzer, H. Y. Role of serotonin in the action of atypical antipsychotic drugs. *Clin. Neurosci.* **1995**, *3*, 64-75.
155. Meltzer, H. Y. The role of serotonin in antipsychotic drug action. *Neuropsychopharmacology* **1999**, *21*, 106s-115s.
156. Meltzer, H. Y.; Massey, B. W. The role of serotonin receptors in the action of atypical antipsychotic drugs. *Curr. Opin. Pharmacol.* **2011**, *11*, 59-67.
157. Raja, M. Clozapine safety, 35 years later. *Curr. Drug. Saf.* **2011**, *6*, 164-184.
158. Iqbal, M. M.; Rahman, A.; Husain, Z.; Mahmud, S. Z.; Ryan, W. G.; Feldman, J. M. Clozapine: a clinical review of adverse effects and management. *Ann. Clin. Psychiatry* **2003**, *15*, 33-48.
159. Cohen, D.; Bogers, J. P.; van Dijk, D.; Bakker, B.; Schulte, P. F. Beyond white blood cell monitoring: screening in the initial phase of clozapine therapy. *J. Clin. Psychiatry* **2012**, *73*, 1307-1312.
160. Inoue, T.; Domae, M.; Yamada, K.; Furukawa, T. Effects of the novel antipsychotic agent 7-(4-[4-(2,3-dichlorophenyl)-1-piperazinyl]butyloxy)-3,4-dihydro -2(1H)-quinolinone (OPC-14597) on prolactin release from the rat anterior pituitary gland. *J. Pharmacol. Exp. Ther.* **1996**, *277*, 137-143.
161. Jordan, S.; Koprivica, V.; Chen, R.; Tottori, K.; Kikuchi, T.; Altar, C. A. The antipsychotic aripiprazole is a potent, partial agonist at the human 5-HT_{1A} receptor. *Eur. J. Pharmacol.* **2002**, *441*, 137-140.

162. Shapiro, D. A.; Renock, S.; Arrington, E.; Chiodo, L. A.; Liu, L. X.; Sibley, D. R.; Roth, B. L.; Mailman, R. Aripiprazole, a novel atypical antipsychotic drug with a unique and robust pharmacology. *Neuropsychopharmacology* **2003**, *28*, 1400-1411.
163. Hirose, T.; Kikuchi, T. Aripiprazole, a novel antipsychotic agent: dopamine D2 receptor partial agonist. *J. Med. Invest.* **2005**, *52*, 284-290.
164. Mamo, D.; Graff, A.; Mizrahi, R.; Shammi, C. M.; Romeyer, F.; Kapur, S. Differential effects of aripiprazole on D(2), 5-HT(2), and 5-HT(1A) receptor occupancy in patients with schizophrenia: a triple tracer PET study. *Am. J. Psychiatry* **2007**, *164*, 1411-1417.
165. Szabo, M.; Klein Herenbrink, C.; Christopoulos, A.; Lane, J. R.; Capuano, B. Structure-activity relationships of privileged structures lead to the discovery of novel biased ligands at the dopamine D(2) receptor. *J Med Chem* **2014**, *57*, 4924-4939.
166. Klein Herenbrink, C.; Sykes, D. A.; Donthamsetti, P.; Canals, M.; Coudrat, T.; Shonberg, J.; Scammells, P. J.; Capuano, B.; Sexton, P. M.; Charlton, S. J.; Javitch, J. A.; Christopoulos, A.; Lane, J. R. The role of kinetic context in apparent biased agonism at GPCRs. *Nat. Commun.* **2016**, *7*, 10842.
167. Mailman, R. B.; Murthy, V. Third generation antipsychotic drugs: partial agonism or receptor functional selectivity? *Curr. Pharm. Des.* **2010**, *16*, 488-501.
168. Tamminga, C. A. Partial dopamine agonists in the treatment of psychosis. *J. Neural. Transm.* **2002**, *109*, 411-420.
169. Tamminga, C. A.; Carlsson, A. Partial dopamine agonists and dopaminergic stabilizers, in the treatment of psychosis. *Curr. Drug Targets CNS Neurol. Disord.* **2002**, *1*, 141-147.
170. Seeman, P.; Lee, T. Antipsychotic drugs: Direct correlation between clinical potency and presynaptic action on dopamine neurons. *Science* **1975**, *188*, 1217-1219.
171. Seeman, P.; Corbett, R.; Van Tol, H. H. Atypical neuroleptics have low affinity for dopamine D2 receptors or are selective for D4 receptors. *Neuropsychopharmacology* **1997**, *16*, 93-110.
172. Van Tol, H. H.; Bunzow, J. R.; Guan, H. C.; Sunahara, R. K.; Seeman, P.; Niznik, H. B.; Civelli, O. Cloning of the gene for a human dopamine D4 receptor with high affinity for the antipsychotic clozapine. *Nature* **1991**, *350*, 610-614.
173. Roth, B. L.; Ciaranello, R. D.; Meltzer, H. Y. Binding of typical and atypical antipsychotic agents to transiently expressed 5-HT1C receptors. *J. Pharmacol. Exp. Ther.* **1992**, *260*, 1361-1365.
174. Roth, B. L.; Craigo, S. C.; Choudhary, M. S.; Uler, A.; Monsma, F. J., Jr.; Shen, Y.; Meltzer, H. Y.; Sibley, D. R. Binding of typical and atypical antipsychotic agents to 5-hydroxytryptamine-6 and 5-hydroxytryptamine-7 receptors. *J. Pharmacol. Exp. Ther.* **1994**, *268*, 1403-1410.
175. Roth, B. L.; Meltzer, H. Y.; Khan, N. Binding of typical and atypical antipsychotic drugs to multiple neurotransmitter receptors. In *Advances in Pharmacology*, Goldstein, D. S.; Eisenhofer, G.; McCarty, R., Eds. Academic Press: 1997; Vol. 42, pp 482-485.
176. Peroutka, S. J.; Synder, S. H. Relationship of neuroleptic drug effects at brain dopamine, serotonin, alpha-adrenergic, and histamine receptors to clinical potency. *Am. J. Psychiatry* **1980**, *137*, 1518-1522.
177. Nguyen, T.; Shapiro, D. A.; George, S. R.; Setola, V.; Lee, D. K.; Cheng, R.; Rauser, L.; Lee, S. P.; Lynch, K. R.; Roth, B. L.; O'Dowd, B. F. Discovery of a novel member of the histamine receptor family. *Mol. Pharmacol.* **2001**, *59*, 427-433.
178. Bolden, C.; Cusack, B.; Richelson, E. Antagonism by antimuscarinic and neuroleptic compounds at the five cloned human muscarinic cholinergic receptors expressed in Chinese hamster ovary cells. *J. Pharmacol. Exp. Ther.* **1992**, *260*, 576-580.
179. Zeng, X. P.; Le, F.; Richelson, E. Muscarinic m4 receptor activation by some atypical antipsychotic drugs. *Eur. J. Pharmacol.* **1997**, *321*, 349-354.
180. Kasper, S.; Tauscher, J.; Kufferle, B.; Barnas, C.; Pezawas, L.; Quiner, S. Dopamine- and serotonin-receptors in schizophrenia: results of imaging-studies and implications for pharmacotherapy in schizophrenia. *Eur. Arch. Psychiatry Clin. Neurosci.* **1999**, *249 Suppl 4*, 83-89.
181. Remington, G.; Kapur, S. D2 and 5-HT2 receptor effects of antipsychotics: bridging basic and clinical findings using PET. *J. Clin. Psychiatry* **1999**, *60 Suppl 10*, 15-19.
182. Kapur, S.; Zipursky, R.; Jones, C.; Shammi, C. S.; Remington, G.; Seeman, P. A positron emission tomography study of quetiapine in schizophrenia: a preliminary finding of an antipsychotic

- effect with only transiently high dopamine D2 receptor occupancy. *Arch. Gen. Psychiatry* **2000**, *57*, 553-559.
183. Haddad, P. M.; Brain, C.; Scott, J. Nonadherence with antipsychotic medication in schizophrenia: challenges and management strategies. *Patient Relat. Outcome Meas.* **2014**, *5*, 43-62.
184. Rummel-Kluge, C.; Komossa, K.; Schwarz, S.; Hunger, H.; Schmid, F.; Lobos, C. A.; Kissling, W.; Davis, J. M.; Leucht, S. Head-to-head comparisons of metabolic side effects of second generation antipsychotics in the treatment of schizophrenia: a systematic review and meta-analysis. *Schizophr. Res.* **2010**, *123*, 225-233.
185. Divac, N.; Prostran, M.; Jakovcevski, I.; Cerovac, N. Second-generation antipsychotics and extrapyramidal adverse effects. *Biomed. Res. Int.* **2014**, *2014*, 656370.
186. Fleischhacker, W. W. Aripiprazole. *Expert Opin. Pharmacother.* **2005**, *6*, 2091-2101.
187. Kinghorn, W. A.; McEvoy, J. P. Aripiprazole: pharmacology, efficacy, safety and tolerability. *Expert Rev. Neurother.* **2005**, *5*, 297-307.
188. Poyurovsky, M. Acute antipsychotic-induced akathisia revisited. *Br. J. Psychiatry* **2010**, *196*, 89-91.
189. Lehmann, H. E.; Ban, T. A. The history of the psychopharmacology of schizophrenia. *Can. J. Psychiatry* **1997**, *42*, 152-162.
190. Miyamoto, S.; Duncan, G. E.; Marx, C. E.; Lieberman, J. A. Treatments for schizophrenia: a critical review of pharmacology and mechanisms of action of antipsychotic drugs. *Mol. Psychiatry* **2005**, *10*, 79-104.
191. Marder, S. R.; Davis, J. M.; Chouinard, G. The effects of risperidone on the five dimensions of schizophrenia derived by factor analysis: combined results of the North American trials. *J. Clin. Psychiatry* **1997**, *58*, 538-546.
192. Breier, A.; Buchanan, R. W.; Kirkpatrick, B.; Davis, O. R.; Irish, D.; Summerfelt, A.; Carpenter, W. T., Jr. Effects of clozapine on positive and negative symptoms in outpatients with schizophrenia. *Am. J. Psychiatry* **1994**, *151*, 20-26.
193. Kasper, S.; Lerman, M. N.; McQuade, R. D.; Saha, A.; Carson, W. H.; Ali, M.; Archibald, D.; Ingenito, G.; Marcus, R.; Pigott, T. Efficacy and safety of aripiprazole vs. haloperidol for long-term maintenance treatment following acute relapse of schizophrenia. *Int. J. Neuropsychopharmacol* **2003**, *6*, 325-337.
194. Davidson, M.; Galderisi, S.; Weiser, M.; Werbeloff, N.; Fleischhacker, W. W.; Keefe, R. S.; Boter, H.; Keet, I. P.; Prelipceanu, D.; Rybakowski, J. K.; Libiger, J.; Hummer, M.; Dollfus, S.; Lopez-Ibor, J. J.; Hranov, L. G.; Gaebel, W.; Peuskens, J.; Lindfors, N.; Riecher-Rossler, A.; Kahn, R. S. Cognitive effects of antipsychotic drugs in first-episode schizophrenia and schizophreniform disorder: a randomized, open-label clinical trial (EUFEST). *Am. J. Psychiatry* **2009**, *166*, 675-682.
195. Keefe, R. S.; Silva, S. G.; Perkins, D. O.; Lieberman, J. A. The effects of atypical antipsychotic drugs on neurocognitive impairment in schizophrenia: a review and meta-analysis. *Schizophr. Bull.* **1999**, *25*, 201-222.
196. Green, M. F.; Marshall, B. D., Jr.; Wirshing, W. C.; Ames, D.; Marder, S. R.; McGurk, S.; Kern, R. S.; Mintz, J. Does risperidone improve verbal working memory in treatment-resistant schizophrenia? *Am. J. Psychiatry* **1997**, *154*, 799-804.
197. Kern, R. S.; Green, M. F.; Marshall, B. D., Jr.; Wirshing, W. C.; Wirshing, D.; McGurk, S.; Marder, S. R.; Mintz, J. Risperidone vs. haloperidol on reaction time, manual dexterity, and motor learning in treatment-resistant schizophrenia patients. *Biol. Psychiatry* **1998**, *44*, 726-732.
198. Green, M. F.; Marder, S. R.; Glynn, S. M.; McGurk, S. R.; Wirshing, W. C.; Wirshing, D. A.; Lieberman, R. P.; Mintz, J. The neurocognitive effects of low-dose haloperidol: a two-year comparison with risperidone. *Biol. Psychiatry* **2002**, *51*, 972-978.
199. Keefe, R. S.; Seidman, L. J.; Christensen, B. K.; Hamer, R. M.; Sharma, T.; Sitskoorn, M. M.; Lewine, R. R.; Yurgelun-Todd, D. A.; Gur, R. C.; Tohen, M.; Tollefson, G. D.; Sanger, T. M.; Lieberman, J. A. Comparative effect of atypical and conventional antipsychotic drugs on neurocognition in first-episode psychosis: a randomized, double-blind trial of olanzapine versus low doses of haloperidol. *Am. J. Psychiatry* **2004**, *161*, 985-995.

200. Keefe, R. S.; Seidman, L. J.; Christensen, B. K.; Hamer, R. M.; Sharma, T.; Sitskoorn, M. M.; Rock, S. L.; Woolson, S.; Tohen, M.; Tollefson, G. D.; Sanger, T. M.; Lieberman, J. A. Long-term neurocognitive effects of olanzapine or low-dose haloperidol in first-episode psychosis. *Biol. Psychiatry* **2006**, *59*, 97-105.
201. Keefe, R. S.; Bilder, R. M.; Davis, S. M.; Harvey, P. D.; Palmer, B. W.; Gold, J. M.; Meltzer, H. Y.; Green, M. F.; Capuano, G.; Stroup, T. S.; McEvoy, J. P.; Swartz, M. S.; Rosenheck, R. A.; Perkins, D. O.; Davis, C. E.; Hsiao, J. K.; Lieberman, J. A. Neurocognitive effects of antipsychotic medications in patients with chronic schizophrenia in the CATIE Trial. *Arch. Gen. Psychiatry* **2007**, *64*, 633-647.
202. Green, M. F. What are the functional consequences of neurocognitive deficits in schizophrenia? *Am. J. Psychiatry* **1996**, *153*, 321-330.
203. Green, M. F.; Kern, R. S.; Braff, D. L.; Mintz, J. Neurocognitive deficits and functional outcome in schizophrenia: are we measuring the "right stuff"? *Schizophr. Bull.* **2000**, *26*, 119-136.
204. Arnsten, A. F.; Girgis, R. R.; Gray, D. L.; Mailman, R. B. Novel Dopamine Therapeutics for Cognitive Deficits in Schizophrenia. *Biol. Psychiatry* **2017**, *81*, 67-77.
205. Pycocock, C. J.; Kerwin, R. W.; Carter, C. J. Effect of lesion of cortical dopamine terminals on subcortical dopamine receptors in rats. *Nature* **1980**, *286*, 74-76.
206. Weinberger, D. R. Implications of normal brain development for the pathogenesis of schizophrenia. *Arch. Gen. Psychiatry* **1987**, *44*, 660-669.
207. Davis, K. L.; Kahn, R. S.; Ko, G.; Davidson, M. Dopamine in schizophrenia: a review and reconceptualization. *Am. J. Psychiatry* **1991**, *148*, 1474-1486.
208. Green, M. F.; Harvey, P. D. Cognition in schizophrenia: Past, present, and future. *Schizophr. Res. Cogn.* **2014**, *1*, e1-e9.
209. Levin, S. Frontal lobe dysfunctions in schizophrenia--II. Impairments of psychological and brain functions. *J. Psychiatr. Res.* **1984**, *18*, 57-72.
210. Merriam, A. E.; Kay, S. R.; Opler, L. A.; Kushner, S. F.; van Praag, H. M. Neurological signs and the positive-negative dimension in schizophrenia. *Biol. Psychiatry* **1990**, *28*, 181-192.
211. Goldberg, T. E.; Torrey, E. F.; Gold, J. M.; Ragland, J. D.; Bigelow, L. B.; Weinberger, D. R. Learning and memory in monozygotic twins discordant for schizophrenia. *Psychol. Med.* **1993**, *23*, 71-85.
212. Morihisa, J. M.; Duffy, F. H.; Wyatt, R. J. Brain electrical activity mapping (BEAM) in schizophrenic patients. *Arch. Gen. Psychiatry* **1983**, *40*, 719-728.
213. Weinberger, D. R.; Berman, K. F.; Zec, R. F. Physiologic dysfunction of dorsolateral prefrontal cortex in schizophrenia. I. Regional cerebral blood flow evidence. *Arch. Gen. Psychiatry* **1986**, *43*, 114-124.
214. Wolkin, A.; Angrist, B.; Wolf, A.; Brodie, J. D.; Wolkin, B.; Jaeger, J.; Cancro, R.; Rotrosen, J. Low frontal glucose utilization in chronic schizophrenia: a replication study. *Am. J. Psychiatry* **1988**, *145*, 251-253.
215. Hall, H.; Sedvall, G.; Magnusson, O.; Kopp, J.; Halldin, C.; Farde, L. Distribution of D1- and D2-dopamine receptors, and dopamine and its metabolites in the human brain. *Neuropsychopharmacology* **1994**, *11*, 245-256.
216. Callicott, J. H.; Bertolino, A.; Mattay, V. S.; Langheim, F. J.; Duyn, J.; Coppola, R.; Goldberg, T. E.; Weinberger, D. R. Physiological dysfunction of the dorsolateral prefrontal cortex in schizophrenia revisited. *Cereb. Cortex* **2000**, *10*, 1078-1092.
217. Lett, T. A.; Voineskos, A. N.; Kennedy, J. L.; Levine, B.; Daskalakis, Z. J. Treating working memory deficits in schizophrenia: a review of the neurobiology. *Biol. Psychiatry* **2014**, *75*, 361-370.
218. Abi-Dargham, A.; Mawlawi, O.; Lombardo, I.; Gil, R.; Martinez, D.; Huang, Y.; Hwang, D. R.; Keilp, J.; Kochan, L.; Van Heertum, R.; Gorman, J. M.; Laruelle, M. Prefrontal dopamine D1 receptors and working memory in schizophrenia. *J. Neurosci.* **2002**, *22*, 3708-3719.
219. Park, S.; Holzman, P. S. Schizophrenics show spatial working memory deficits. *Arch. Gen. Psychiatry* **1992**, *49*, 975-982.
220. Wexler, B. E.; Stevens, A. A.; Bowers, A. A.; Sernyak, M. J.; Goldman-Rakic, P. S. Word and tone working memory deficits in schizophrenia. *Arch. Gen. Psychiatry* **1998**, *55*, 1093-1096.

221. Brozoski, T. J.; Brown, R. M.; Rosvold, H. E.; Goldman, P. S. Cognitive deficit caused by regional depletion of dopamine in prefrontal cortex of rhesus monkey. *Science* **1979**, *205*, 929-932.
222. Collins, P.; Roberts, A. C.; Dias, R.; Everitt, B. J.; Robbins, T. W. Perseveration and strategy in a novel spatial self-ordered sequencing task for nonhuman primates: effects of excitotoxic lesions and dopamine depletions of the prefrontal cortex. *J. Cogn. Neurosci.* **1998**, *10*, 332-354.
223. Roberts, A. C.; De Salvia, M. A.; Wilkinson, L. S.; Collins, P.; Muir, J. L.; Everitt, B. J.; Robbins, T. W. 6-Hydroxydopamine lesions of the prefrontal cortex in monkeys enhance performance on an analog of the Wisconsin Card Sort Test: possible interactions with subcortical dopamine. *J. Neurosci.* **1994**, *14*, 2531-2544.
224. Robbins, T. W.; Roberts, A. C. Differential regulation of fronto-executive function by the monoamines and acetylcholine. *Cereb Cortex* **2007**, *17 Suppl 1*, i151-160.
225. Knable, M. B.; Weinberger, D. R. Dopamine, the prefrontal cortex and schizophrenia. *J. Psychopharmacol.* **1997**, *11*, 123-131.
226. Sawaguchi, T.; Goldman-Rakic, P. S. D1 dopamine receptors in prefrontal cortex: involvement in working memory. *Science* **1991**, *251*, 947-950.
227. Sawaguchi, T.; Goldman-Rakic, P. S. The role of D1-dopamine receptor in working memory: local injections of dopamine antagonists into the prefrontal cortex of rhesus monkeys performing an oculomotor delayed-response task. *J. Neurophysiol.* **1994**, *71*, 515-528.
228. Arnsten, A. F.; Cai, J. X.; Murphy, B. L.; Goldman-Rakic, P. S. Dopamine D1 receptor mechanisms in the cognitive performance of young adult and aged monkeys. *Psychopharmacology* **1994**, *116*, 143-151.
229. Abi-Dargham, A. Probing cortical dopamine function in schizophrenia: what can D1 receptors tell us? *World Psychiatry* **2003**, *2*, 166-171.
230. Abi-Dargham, A.; Moore, H. Prefrontal DA transmission at D1 receptors and the pathology of schizophrenia. *Neuroscientist* **2003**, *9*, 404-416.
231. Vijayraghavan, S.; Wang, M.; Birnbaum, S. G.; Williams, G. V.; Arnsten, A. F. Inverted-U dopamine D1 receptor actions on prefrontal neurons engaged in working memory. *Nat. Neurosci.* **2007**, *10*, 376-384.
232. Murphy, B. L.; Arnsten, A. F.; Goldman-Rakic, P. S.; Roth, R. H. Increased dopamine turnover in the prefrontal cortex impairs spatial working memory performance in rats and monkeys. *PNAS* **1996**, *93*, 1325-1329.
233. Gamo, N. J.; Lur, G.; Higley, M. J.; Wang, M.; Paspalas, C. D.; Vijayraghavan, S.; Yang, Y.; Ramos, B. P.; Peng, K.; Kata, A.; Boven, L.; Lin, F.; Roman, L.; Lee, D.; Arnsten, A. F. Stress Impairs Prefrontal Cortical Function via D1 Dopamine Receptor Interactions With Hyperpolarization-Activated Cyclic Nucleotide-Gated Channels. *Biol. Psychiatry* **2015**, *78*, 860-870.
234. Zahrt, J.; Taylor, J. R.; Mathew, R. G.; Arnsten, A. F. Supranormal stimulation of D1 dopamine receptors in the rodent prefrontal cortex impairs spatial working memory performance. *J. Neurosci.* **1997**, *17*, 8528-8535.
235. Gibbs, S. E.; D'Esposito, M. A functional magnetic resonance imaging study of the effects of pergolide, a dopamine receptor agonist, on component processes of working memory. *Neurosci.* **2006**, *139*, 359-371.
236. Cools, R.; D'Esposito, M. Inverted-U-shaped dopamine actions on human working memory and cognitive control. *Biol. Psychiatry* **2011**, *69*, e113-125.
237. Gulwadi, A. G.; Korpinen, C. D.; Mailman, R. B.; Nichols, D. E.; Sit, S. Y.; Taber, M. T. Dinapsoline: characterization of a D1 dopamine receptor agonist in a rat model of Parkinson's disease. *J. Pharmacol. Exp. Ther.* **2001**, *296*, 338-344.
238. Starr, M. S.; Starr, B. S. Seizure promotion by D1 agonists does not correlate with other dopaminergic properties. *J. Neural. Transm. Park. Dis. Dement. Sect.* **1993**, *6*, 27-34.
239. DeNinno, M. P.; Schoenleber, R.; MacKenzie, R.; Britton, D. R.; Asin, K. E.; Briggs, C.; Trugman, J. M.; Ackerman, M.; Artman, L.; Bednarz, L.; Bhatt, R.; Curzon, P.; Gomez, E.; Chae Hee, K.; Stittsworth, J.; Keabian, J. W. A68930: a potent agonist selective for the dopamine D1 receptor. *Eur. J. Pharmacol.* **1991**, *199*, 209-219.

240. Blanchet, P. J.; Fang, J.; Gillespie, M.; Sabounjian, L.; Locke, K. W.; Gammans, R.; Mouradian, M. M.; Chase, T. N. Effects of the full dopamine D1 receptor agonist dihydroxidine in Parkinson's disease. *Clin. Neuropharmacol.* **1998**, *21*, 339-343.
241. Amenta, F.; Ferrante, F.; Ricci, A. Pharmacological characterisation and autoradiographic localisation of dopamine receptor subtypes in the cardiovascular system and in the kidney. *Hypertens. Res.* **1995**, *18*, S23-S27.
242. Perkins, D. O. Predictors of noncompliance in patients with schizophrenia. *J. Clin. Psychiatry* **2002**, *63*, 1121-1128.
243. Higashi, K.; Medic, G.; Littlewood, K. J.; Diez, T.; Granström, O.; De Hert, M. Medication adherence in schizophrenia: factors influencing adherence and consequences of nonadherence, a systematic literature review. *Ther. Adv. Psychopharmacol.* **2013**, *3*, 200-218.
244. Gerlach, J.; Peacock, L. New antipsychotics: the present status. *Int. Clin. Psychopharmacol.* **1995**, *10 Suppl 3*, 39-48.
245. Waddington, J. L.; O'Callaghan, E. What makes an antipsychotic 'atypical'? *CNS Drugs* **1997**, *7*, 341-346.
246. Copolov, D. New name for atypical antipsychotics? *Am. J. Psychiatry* **1997**, *154*, 439.
247. Hippus, H. The history of clozapine. *Psychopharmacology* **1989**, *99*, S3-5.
248. Deutch, A. Y.; Moghaddam, B.; Innis, R. B.; Krystal, J. H.; Aghajanian, G. K.; Bunney, B. S.; Charney, D. S. Mechanisms of action of atypical antipsychotic drugs. *Schizophr. Res.* **1991**, *4*, 121-156.
249. Kinon, B. J.; Lieberman, J. A. Mechanisms of action of atypical antipsychotic drugs: a critical analysis. *Psychopharmacology* **1996**, *124*, 2-34.
250. Lieberman, J. A. Understanding the mechanism of action of atypical antipsychotic drugs. A review of compounds in use and development. *Br. J. Psychiatry Suppl.* **1993**, 7-18.
251. Kerwin, R. W. The new atypical antipsychotics. A lack of extrapyramidal side-effects and new routes in schizophrenia research. *Br. J. Psychiatry* **1994**, *164*, 141-148.
252. Janssen, P. A.; Niemegeers, C. J.; Awouters, F.; Schellekens, K. H.; Megens, A. A.; Meert, T. F. Pharmacology of risperidone (R 64 766), a new antipsychotic with serotonin-S2 and dopamine-D2 antagonistic properties. *J. Pharmacol. Exp. Ther.* **1988**, *244*, 685-693.
253. Martinot, J. L.; Dao-Castellana, M. H.; Loc'h, C.; Maziere, B.; Poirier, M. F.; Paillere-Martinot, M. L. In vivo characteristics of dopamine D2 receptor occupancy by amisulpride in schizophrenia. *Psychopharmacology* **1996**, *124*, 154-158.
254. Kapur, S.; Seeman, P. Does fast dissociation from the dopamine d(2) receptor explain the action of atypical antipsychotics?: A new hypothesis. *Am. J. Psychiat.* **2001**, *158*, 360-369.
255. Copeland, R. A.; Pompliano, D. L.; Meek, T. D. Drug-target residence time and its implications for lead optimization. *Nat. Rev. Drug Discov.* **2006**, *5*, 730-739.
256. Copeland, R. A. The drug-target residence time model: a 10-year retrospective. *Nat. Rev. Drug Discov.* **2016**, *15*, 87-95.
257. Burki, H. R. Effects of fluperlapine on dopaminergic systems in rat brain. *Psychopharmacology* **1986**, *89*, 77-84.
258. Seeman, P.; Corbett, R.; Nam, D.; Van Tol, H. H. Dopamine and serotonin receptors: amino acid sequences, and clinical role in neuroleptic parkinsonism. *Jpn. J. Pharmacol.* **1996**, *71*, 187-204.
259. Seeman, P.; Tallerico, T. Antipsychotic drugs which elicit little or no parkinsonism bind more loosely than dopamine to brain D2 receptors, yet occupy high levels of these receptors. *Mol. Psychiatry* **1998**, *3*, 123-134.
260. Seeman, P.; Tallerico, T. Rapid release of antipsychotic drugs from dopamine D2 receptors: an explanation for low receptor occupancy and early clinical relapse upon withdrawal of clozapine or quetiapine. *Am. J. Psychiat.* **1999**, *156*, 876-884.
261. Kapur, S.; Seeman, P. Antipsychotic agents differ in how fast they come off the dopamine D2 receptors. Implications for atypical antipsychotic action. *J. Psychiatr. Neurosci.* **2000**, *25*, 161-166.
262. Charlton, S. J.; Vauquelin, G. Elusive equilibrium: the challenge of interpreting receptor pharmacology using calcium assays. *Br. J. Pharmacol.* **2010**, *161*, 1250-1265.

263. Seeman, P. An update of fast-off dopamine D2 atypical antipsychotics. *Am. J. Psychiatry* **2005**, *162*, 1984-1985.
264. Roth, B. L.; Sheffler, D.; Potkin, S. G. Atypical antipsychotic drug actions: unitary or multiple mechanisms for 'atypicality'? *Clin. Neurosci. Res.* **2003**, *3*, 108-117.
265. Sykes, D. A.; Moore, H.; Stott, L.; Holliday, N.; Javitch, J. A.; Lane, J. R.; Charlton, S. J. Extrapyramidal side effects of antipsychotics are linked to their association kinetics at dopamine D2 receptors. *Nat. Commun.* **2017**, *8*, 763.
266. Leucht, S.; Cipriani, A.; Spineli, L.; Mavridis, D.; Orey, D.; Richter, F.; Samara, M.; Barbui, C.; Engel, R. R.; Geddes, J. R.; Kissling, W.; Stapf, M. P.; Lassig, B.; Salanti, G.; Davis, J. M. Comparative efficacy and tolerability of 15 antipsychotic drugs in schizophrenia: a multiple-treatments meta-analysis. *Lancet* **2013**, *382*, 951-962.
267. Sahlholm, K.; Marcellino, D.; Nilsson, J.; Ogren, S. O.; Fuxe, K.; Arhem, P. Typical and atypical antipsychotics do not differ markedly in their reversibility of antagonism of the dopamine D2 receptor. *Int. J. Neuropsychopharmacol.* **2014**, *17*, 149-155.
268. Sahlholm, K.; Zeberg, H.; Nilsson, J.; Ogren, S. O.; Fuxe, K.; Arhem, P. The fast-off hypothesis revisited: A functional kinetic study of antipsychotic antagonism of the dopamine D2 receptor. *Eur. Neuropsychopharmacol.* **2016**, *26*, 467-476.
269. Newman-Tancredi, A.; Kleven, M. S. Comparative pharmacology of antipsychotics possessing combined dopamine D2 and serotonin 5-HT1A receptor properties. *Psychopharmacology* **2011**, *216*, 451-473.
270. Sveinbjornsdottir, S. The clinical symptoms of Parkinson's disease. *J. Neurochem.* **2016**, *139*, 318-324.
271. Jankovic, J. Parkinson's disease: clinical features and diagnosis. *J. Neurol. Neurosurg. Psychiatry* **2008**, *79*, 368-376.
272. Moore, D. J.; West, A. B.; Dawson, V. L.; Dawson, T. M. Molecular pathophysiology of Parkinson's disease. *Annu. Rev. Neurosci.* **2005**, *28*, 57-87.
273. Shulman, J. M.; De Jager, P. L.; Feany, M. B. Parkinson's disease: genetics and pathogenesis. *Annu. Rev. Pathol.* **2011**, *6*, 193-222.
274. Albin, R. L.; Young, A. B.; Penney, J. B. The functional anatomy of basal ganglia disorders. *Trends. Neurosci.* **1989**, *12*, 366-375.
275. Forno, L. S. Neuropathology of Parkinson's disease. *J. Neuropathol. Exp. Neurol.* **1996**, *55*, 259-272.
276. Dorsey, E. R.; Constantinescu, R.; Thompson, J. P.; Biglan, K. M.; Holloway, R. G.; Kieburtz, K.; Marshall, F. J.; Ravina, B. M.; Schifitto, G.; Siderowf, A.; Tanner, C. M. Projected number of people with Parkinson disease in the most populous nations, 2005 through 2030. *Neurology* **2007**, *68*, 384-386.
277. AlDakheel, A.; Kalia, L. V.; Lang, A. E. Pathogenesis-targeted, disease-modifying therapies in Parkinson disease. *Neurotherapeutics* **2014**, *11*, 6-23.
278. Lees, A. J. The on-off phenomenon. *J. Neurol. Neurosurg. Psychiatry* **1989**, *52*, 29-37.
279. Fahn, S. The history of dopamine and levodopa in the treatment of Parkinson's disease. *Mov. Disord.* **2008**, *23*, S497-508.
280. Stocchi, F. The levodopa wearing-off phenomenon in Parkinson's disease: pharmacokinetic considerations. *Expert Opin. Pharmacother.* **2006**, *7*, 1399-1407.
281. Jorg, M.; Scammells, P. J.; Capuano, B. The dopamine D2 and adenosine A2A receptors: past, present and future trends for the treatment of Parkinson's disease. *Curr. Med. Chem.* **2014**, *21*, 3188-3210.
282. Riederer, P.; Muller, T. Monoamine oxidase-B inhibitors in the treatment of Parkinson's disease: clinical-pharmacological aspects. *J. Neural Transm.* **2018**.
283. Kurth, M. C.; Adler, C. H.; Hilaire, M. S.; Singer, C.; Waters, C.; LeWitt, P.; Chernik, D. A.; Dorflinger, E. E.; Yoo, K. Tolcapone improves motor function and reduces levodopa requirement in patients with Parkinson's disease experiencing motor fluctuations: a multicenter, double-blind, randomized, placebo-controlled trial. Tolcapone Fluctuator Study Group I. *Neurology* **1997**, *48*, 81-87.

284. Nutt, J. G.; Woodward, W. R.; Beckner, R. M.; Stone, C. K.; Berggren, K.; Carter, J. H.; Gancher, S. T.; Hammerstad, J. P.; Gordin, A. Effect of peripheral catechol-O-methyltransferase inhibition on the pharmacokinetics and pharmacodynamics of levodopa in parkinsonian patients. *Neurology* **1994**, *44*, 913-919.
285. Khor, S. P.; Hsu, A. The pharmacokinetics and pharmacodynamics of levodopa in the treatment of Parkinson's disease. *Curr. Clin. Pharmacol.* **2007**, *2*, 234-243.
286. Fahn, S.; Oakes, D.; Shoulson, I.; Kieburtz, K.; Rudolph, A.; Lang, A.; Olanow, C. W.; Tanner, C.; Marek, K. Levodopa and the progression of Parkinson's disease. *N. Engl. J. Med.* **2004**, *351*, 2498-2508.
287. Obeso, J. A.; Olanow, C. W.; Nutt, J. G. Levodopa motor complications in Parkinson's disease. *Trends Neurosci.* **2000**, *23*, S2-7.
288. Fahn, S. Levodopa-induced neurotoxicity. *CNS Drugs* **1997**, *8*, 376-393.
289. Talati, R.; Baker, W. L.; Patel, A. A.; Reinhart, K.; Coleman, C. I. Adding a dopamine agonist to preexisting levodopa therapy vs. levodopa therapy alone in advanced Parkinson's disease: a meta analysis. *Int. J. Clin. Pract.* **2009**, *63*, 613-623.
290. Alonso Cánovas, A.; Luquin Piudo, R.; García Ruiz-Espiga, P.; Burguera, J. A.; Campos Arillo, V.; Castro, A.; Linazasoro, G.; López Del Val, J.; Vela, L.; Martínez Castrillo, J. C. Dopaminergic agonists in Parkinson's disease. *Neurología (English Edition)* **2014**, *29*, 230-241.
291. Stacy, M.; Galbreath, A. Optimizing long-term therapy for Parkinson disease: levodopa, dopamine agonists, and treatment-associated dyskinesia. *Clin. Neuropharmacol.* **2008**, *31*, 51-56.
292. Constantinescu, R. Update on the use of pramipexole in the treatment of Parkinson's disease. *Neuropsychiatr. Dis. Treatment* **2008**, *4*, 337-352.
293. May, L. T.; Christopoulos, A. Allosteric modulators of G-protein-coupled receptors. *Curr. Opin. Pharmacol.* **2003**, *3*, 551-556.
294. Hall, A.; Provins, L.; Valade, A. Novel strategies to activate the dopamine D1 receptor: recent advances in orthosteric agonism and positive allosteric modulation. *J. Med. Chem.* **2019**, *62*, 128-140.
295. Lewis, M. A.; Hunihan, L.; Watson, J.; Gentles, R. G.; Hu, S.; Huang, Y.; Bronson, J.; Macor, J. E.; Beno, B. R.; Ferrante, M.; Hendricson, A.; Knox, R. J.; Molski, T. F.; Kong, Y.; Cvijic, M. E.; Rockwell, K. L.; Weed, M. R.; Cacace, A. M.; Westphal, R. S.; Alt, A.; Brown, J. M. Discovery of D1 dopamine receptor positive allosteric modulators: characterization of pharmacology and identification of residues that regulate species selectivity. *J. Pharmacol. Exp. Ther.* **2015**, *354*, 340-349.
296. Rasmussen, S. G. F.; Choi, H.-J.; Fung, J. J.; Pardon, E.; Casarosa, P.; Chae, P. S.; DeVree, B. T.; Rosenbaum, D. M.; Thian, F. S.; Kobilka, T. S.; Schnapp, A.; Konetzki, I.; Sunahara, R. K.; Gellman, S. H.; Pautsch, A.; Steyaert, J.; Weis, W. I.; Kobilka, B. K. Structure of a nanobody-stabilized active state of the β_2 adrenoceptor. *Nature* **2011**, *469*, 175.
297. Skolc, D. A., A.; Jnoff, E.; Valade, A. Isoindoline derivatives. PCT Patent Application WO2016055482, April 14, 2016.
298. Valade, A. J., E.; Ates, A.; Burssens, P.; Skolc, D. Tetrahydroisoquinoline derivatives. PCT Patent Application WO2016055479, April 14, 2016.
299. Ates, A. J., E.; Provins, L.; Valade, A.; Hall, A. Tetrahydroisoquinoline derivative. PCT Patent Application WO2017178377, October 19, 2017.
300. Shiraki, R. T., T.; Kawakami, S.; Moritomo, H.; Ohmiya, M. Heterocyclic acetamide compounds. U.S. Patent 2014/0315963 A1, October 23, 2014.
301. Shiraki, R. T., T.; Kawakami, S.; Moritomo, H.; Ohmiya, M. Heterocyclic acetamide compound. U.S. Patent 2015/0045402, February 12, 2015.
302. Kawakami, S. I., T.; Masuda, N.; Kunikawa, S.; Morita, M.; Yarimizu, J. . Imidazodiazepine compound. U.S. Patent 2018/0185383, July 5, 2018.
303. Beadle, C. D. C., D. A.; Hao, J.; Krushinski, J. H., Jr.; Reinhard, M. R.; Schaus, J. M.; Wolfgangel, C. D. 3,4-Dihydroisoquinolin-2(1H)-yl compounds. PCT Patent Application WO2014193781, December 4, 2014.

304. Stephenson, G. A. Form of 2-(2,6-dichlorophenyl)-1-[(1*S*,3*R*)-3-(hydroxymethyl)-5-(3-hydroxy-3-methylbutyl)-1-methyl-3,4-dihydroisoquinolin-2(1*H*)-yl]ethanone for the treatment of Parkinson's Disease. PCT Patent Application WO2017070068, April 27, 2017.
305. Svensson, K. A.; Heinz, B. A.; Schaus, J. M.; Beck, J. P.; Hao, J.; Krushinski, J. H.; Reinhard, M. R.; Cohen, M. P.; Hellman, S. L.; Getman, B. G.; Wang, X.; Menezes, M. M.; Maren, D. L.; Falcone, J. F.; Anderson, W. H.; Wright, R. A.; Morin, S. M.; Knopp, K. L.; Adams, B. L.; Rogovoy, B.; Okun, I.; Suter, T. M.; Statnick, M. A.; Gehlert, D. R.; Nelson, D. L.; Lucaites, V. L.; Emkey, R.; DeLapp, N. W.; Wiernicki, T. R.; Cramer, J. W.; Yang, C. R.; Bruns, R. F. An allosteric potentiator of the dopamine D1 receptor increases locomotor activity in human D1 knock-in mice without causing stereotypy or tachyphylaxis. *J. Pharmacol. Exp. Ther.* **2017**, *360*, 117-128.
306. Jutkiewicz, E. M.; Bergman, J. Effects of dopamine D1 ligands on eye blinking in monkeys: efficacy, antagonism, and D1/D2 interactions. *J. Pharmacol. Exp. Ther.* **2004**, *311*, 1008-1015.
307. Slifstein, M.; van de Giessen, E.; Van Snellenberg, J.; et al. Deficits in prefrontal cortical and extrastriatal dopamine release in schizophrenia: A positron emission tomographic functional magnetic resonance imaging study. *JAMA Psychiatry* **2015**, *72*, 316-324.
308. Luderman, K. D.; Conroy, J. L.; Free, R. B.; Southall, N.; Ferrer, M.; Sanchez-Soto, M.; Moritz, A. E.; Willette, B. K. A.; Fyfe, T. J.; Jain, P.; Titus, S.; Hazelwood, L. A.; Aube, J.; Lane, J. R.; Frankowski, K. J.; Sibley, D. R. Identification of positive allosteric modulators of the D1 dopamine receptor that act at diverse binding sites. *Mol. Pharmacol.* **2018**.
309. Bruns, R. F.; Mitchell, S. N.; Wafford, K. A.; Harper, A. J.; Shanks, E. A.; Carter, G.; O'Neill, M. J.; Murray, T. K.; Eastwood, B. J.; Schaus, J. M.; Beck, J. P.; Hao, J.; Witkin, J. M.; Li, X.; Chernet, E.; Katner, J. S.; Wang, H.; Ryder, J. W.; Masquelin, M. E.; Thompson, L. K.; Love, P. L.; Maren, D. L.; Falcone, J. F.; Menezes, M. M.; Zhang, L.; Yang, C. R.; Svensson, K. A. Preclinical profile of a dopamine D1 potentiator suggests therapeutic utility in neurological and psychiatric disorders. *Neuropharmacology* **2018**, *128*, 351-365.
310. Wang, X.; Heinz, B. A.; Qian, Y. W.; Carter, J. H.; Gadski, R. A.; Beavers, L. S.; Little, S. P.; Yang, C. R.; Beck, J. P.; Hao, J.; Schaus, J. M.; Svensson, K. A.; Bruns, R. F. Intracellular binding site for a positive allosteric modulator of the dopamine D1 receptor. *Mol. Pharmacol.* **2018**, *94*, 1232-1245.
311. Nolte, W. M.; Fortin, J. P.; Stevens, B. D.; Aspnes, G. E.; Griffith, D. A.; Hoth, L. R.; Ruggeri, R. B.; Mathiowetz, A. M.; Limberakis, C.; Hepworth, D.; Carpino, P. A. A potentiator of orthosteric ligand activity at GLP-1R acts via covalent modification. *Nat. Chem. Biol.* **2014**, *10*, 629-631.
312. Bueno, A. B.; Showalter, A. D.; Wainscott, D. B.; Stutsman, C.; Marin, A.; Ficorilli, J.; Cabrera, O.; Willard, F. S.; Sloop, K. W. Positive allosteric modulation of the glucagon-like peptide-1 receptor by diverse electrophiles. *J. Biol. Chem.* **2016**, *291*, 10700-10715.
313. Luderman, K. D.; Conroy, J. L.; Free, R. B.; Southall, N. T.; Ferrer, M.; Aubé, J.; Frankowski, K. J.; Sibley, D. R. Structurally diverse positive allosteric modulators of the D1 dopamine receptor potentiate G-protein and β -arrestin-mediated signaling. *FASEB J.* **2016**, *30*, 931.
314. Schetz, J. A. Allosteric modulation of dopamine receptors. *Mini Rev. Med. Chem.* **2005**, *5*, 555-561.
315. Hoare, S. R.; Strange, P. G. Regulation of D2 dopamine receptors by amiloride and amiloride analogs. *Mol. Pharmacol.* **1996**, *50*, 1295-1308.
316. Verma, V.; Mann, A.; Costain, W.; Pontoriero, G.; Castellano, J. M.; Skoblenick, K.; Gupta, S. K.; Pristupa, Z.; Niznik, H. B.; Johnson, R. L.; Nair, V. D.; Mishra, R. K. Modulation of agonist binding to human dopamine receptor subtypes by L-prolyl-L-leucyl-glycinamide and a peptidomimetic analog. *J. Pharmacol. Exp. Ther.* **2005**, *315*, 1228-1236.
317. Fisher, A.; Mann, A.; Verma, V.; Thomas, N.; Mishra, R. K.; Johnson, R. L. Design and synthesis of photoaffinity labeling ligands of the L-Prolyl-L-leucyl-glycinamide binding site involved in the allosteric modulation of the dopamine receptor. *J. Med. Chem.* **2006**, *49*, 307-317.
318. Rung, J. P.; Rung, E.; Helgeson, L.; Johansson, A. M.; Svensson, K.; Carlsson, A.; Carlsson, M. L. Effects of (-)-OSU6162 and ACR16 on motor activity in rats, indicating a unique mechanism of dopaminergic stabilization. *J. Neural. Transm.* **2008**, *115*, 899-908.

319. Ott, M. C.; Mishra, R. K.; Johnson, R. L. Modulation of dopaminergic neurotransmission in the 6-hydroxydopamine lesioned rotational model by peptidomimetic analogues of L-prolyl-L-leucyl-glycinamide. *Brain. Res.* **1996**, *737*, 287-291.
320. Natesan, S.; Svensson, K. A.; Reckless, G. E.; Nobrega, J. N.; Barlow, K. B.; Johansson, A. M.; Kapur, S. The dopamine stabilizers (*S*)-(-)-(3-methanesulfonyl-phenyl)-1-propyl-piperidine [(-)-OSU6162] and 4-(3-methanesulfonylphenyl)-1-propyl-piperidine (ACR16) show high in vivo D2 receptor occupancy, antipsychotic-like efficacy, and low potential for motor side effects in the rat. *J. Pharmacol. Exp. Ther.* **2006**, *318*, 810-818.
321. Rung, J. P.; Rung, E.; Helgeson, L.; Johansson, A. M.; Svensson, K.; Carlsson, A.; Carlsson, M. L. Effects of (-)-OSU6162 and ACR16 on motor activity in rats, indicating a unique mechanism of dopaminergic stabilization. *J. Neural Transm.* **2008**, *115*, 899-908.
322. Silvano, E.; Millan, M. J.; Mannoury la Cour, C.; Han, Y.; Duan, L.; Griffin, S. A.; Luedtke, R. R.; Aloisi, G.; Rossi, M.; Zazzeroni, F.; Javitch, J. A.; Maggio, R. The tetrahydroisoquinoline derivative SB269,652 is an allosteric antagonist at dopamine D3 and D2 receptors. *Mol. Pharmacol.* **2010**, *78*, 925-934.
323. Reavill, C.; Taylor, S. G.; Wood, M. D.; Ashmeade, T.; Austin, N. E.; Avenell, K. Y.; Boyfield, I.; Branch, C. L.; Cilia, J.; Coldwell, M. C.; Hadley, M. S.; Hunter, A. J.; Jeffrey, P.; Jewitt, F.; Johnson, C. N.; Jones, D. N.; Medhurst, A. D.; Middlemiss, D. N.; Nash, D. J.; Riley, G. J.; Routledge, C.; Stemp, G.; Thewlis, K. M.; Trail, B.; Vong, A. K.; Hagan, J. J. Pharmacological actions of a novel, high-affinity, and selective human dopamine D(3) receptor antagonist, SB-277011-A. *J. Pharmacol. Exp. Ther.* **2000**, *294*, 1154-1165.
324. Stemp, G.; Ashmeade, T.; Branch, C. L.; Hadley, M. S.; Hunter, A. J.; Johnson, C. N.; Nash, D. J.; Thewlis, K. M.; Vong, A. K.; Austin, N. E.; Jeffrey, P.; Avenell, K. Y.; Boyfield, I.; Hagan, J. J.; Middlemiss, D. N.; Reavill, C.; Riley, G. J.; Routledge, C.; Wood, M. Design and synthesis of trans-*N*-[4-[2-(6-cyano-1,2,3,4-tetrahydroisoquinolin-2-yl)ethyl]cyclohexyl]-4-quinolinecarboxamide (SB-277011): A potent and selective dopamine D(3) receptor antagonist with high oral bioavailability and CNS penetration in the rat. *J. Med. Chem.* **2000**, *43*, 1878-1885.
325. Lane, J. R.; Donthamsetti, P.; Shonberg, J.; Draper-Joyce, C. J.; Dentry, S.; Michino, M.; Shi, L.; Lopez, L.; Scammells, P. J.; Capuano, B.; Sexton, P. M.; Javitch, J. A.; Christopoulos, A. A new mechanism of allostery in a G protein-coupled receptor dimer. *Nat. Chem. Biol.* **2014**, *10*, 745-752.
326. Mistry, S. N.; Shonberg, J.; Draper-Joyce, C. J.; Klein Herenbrink, C.; Michino, M.; Shi, L.; Christopoulos, A.; Capuano, B.; Scammells, P. J.; Lane, J. R. Discovery of a novel class of negative allosteric modulator of the dopamine D2 receptor through fragmentation of a bitopic ligand. *J. Med. Chem.* **2015**, *58*, 6819-6843.
327. Shonberg, J.; Draper-Joyce, C.; Mistry, S. N.; Christopoulos, A.; Scammells, P. J.; Lane, J. R.; Capuano, B. Structure-activity study of *N*-((trans)-4-(2-(7-cyano-3,4-dihydroisoquinolin-2(1*H*)-yl)ethyl)cyclohexyl)-1*H*-indole-2-carboxamide (SB269652), a bitopic ligand that acts as a negative allosteric modulator of the dopamine D2 receptor. *J. Med. Chem.* **2015**, *58*, 5287-5307.
328. Draper-Joyce, C. J.; Michino, M.; Verma, R. K.; Klein Herenbrink, C.; Shonberg, J.; Kopinathan, A.; Scammells, P. J.; Capuano, B.; Thal, D. M.; Javitch, J. A.; Christopoulos, A.; Shi, L.; Lane, J. R. The structural determinants of the bitopic binding mode of a negative allosteric modulator of the dopamine D2 receptor. *Biochem. Pharmacol.* **2018**, *148*, 315-328.
329. Kopinathan, A.; Draper-Joyce, C.; Szabo, M.; Christopoulos, A.; Scammells, P. J.; Lane, J. R.; Capuano, B. Subtle modifications to the indole-2-carboxamide motif of the negative allosteric modulator *N*-((trans)-4-(2-(7-cyano-3,4-dihydroisoquinolin-2(1*H*)-yl)ethyl)cyclohexyl)-1*H*-indole-2-carboxamide (SB269652) yield dramatic changes in pharmacological activity at the dopamine D2 receptor. *J. Med. Chem.* **2018**, *62*, 371-377.
330. Draper-Joyce, C. J.; Verma, R. K.; Michino, M.; Shonberg, J.; Kopinathan, A.; Klein Herenbrink, C.; Scammells, P. J.; Capuano, B.; Abramyan, A. M.; Thal, D. M.; Javitch, J. A.; Christopoulos, A.; Shi, L.; Lane, J. R. The action of a negative allosteric modulator at the dopamine D2 receptor is dependent upon sodium ions. *Sci. Rep.* **2018**, *8*, 1208.

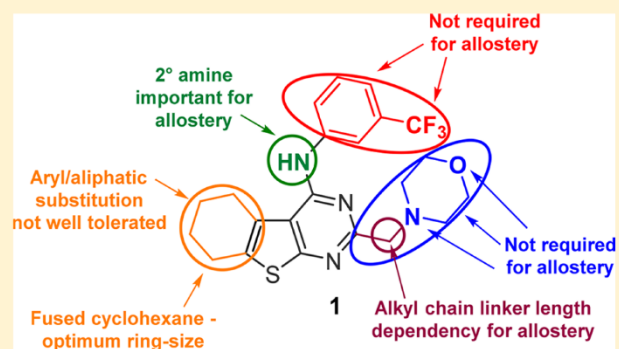
331. Verma, R. K.; Abramyan, A. M.; Michino, M.; Free, R. B.; Sibley, D. R.; Javitch, J. A.; Lane, J. R.; Shi, L. The E2.65A mutation disrupts dynamic binding poses of SB269652 at the dopamine D2 and D3 receptors. *PLoS Comput. Biol.* **2018**, *14*, 1005948.
332. Rossi, M.; Fasciani, I.; Marampon, F.; Maggio, R.; Scarselli, M. The first negative allosteric modulator for dopamine D2 and D3 Receptors, SB269652 may lead to a new generation of antipsychotic drugs. *Mol. Pharmacol.* **2017**, *91*, 586-594.
333. Kolb, P.; Rosenbaum, D. M.; Irwin, J. J.; Fung, J. J.; Kobilka, B. K.; Shoichet, B. K. Structure-based discovery of beta2-adrenergic receptor ligands. *Proc. Natl. Acad. Sci. U. S. A.* **2009**, *106*, 6843-6848.
334. Carlsson, J.; Yoo, L.; Gao, Z.-G.; Irwin, J. J.; Shoichet, B. K.; Jacobson, K. A. Structure-based discovery of A(2A) adenosine receptor ligands. *J. Med. Chem.* **2010**, *53*, 3748-3755.
335. Katritch, V.; Jaakola, V. P.; Lane, J. R.; Lin, J.; Ijzerman, A. P.; Yeager, M.; Kufareva, I.; Stevens, R. C.; Abagyan, R. Structure-based discovery of novel chemotypes for adenosine A(2A) receptor antagonists. *J. Med. Chem.* **2010**, *53*, 1799-1809.
336. de Graaf, C.; Kooistra, A. J.; Vischer, H. F.; Katritch, V.; Kuijter, M.; Shiroishi, M.; Iwata, S.; Shimamura, T.; Stevens, R. C.; de Esch, I. J.; Leurs, R. Crystal structure-based virtual screening for fragment-like ligands of the human histamine H(1) receptor. *J. Med. Chem.* **2011**, *54*, 8195-8206.
337. Mysinger, M. M.; Weiss, D. R.; Ziarek, J. J.; Gravel, S.; Doak, A. K.; Karpiak, J.; Heveker, N.; Shoichet, B. K.; Volkman, B. F. Structure-based ligand discovery for the protein-protein interface of chemokine receptor CXCR4. *Proc. Natl. Acad. Sci. U. S. A.* **2012**, *109*, 5517-5522.
338. Zheng, Z.; Huang, X. P.; Mangano, T. J.; Zou, R.; Chen, X.; Zaidi, S. A.; Roth, B. L.; Stevens, R. C.; Katritch, V. Structure-based discovery of new antagonist and biased agonist chemotypes for the kappa opioid receptor. *J. Med. Chem.* **2017**, *60*, 3070-3081.
339. de Graaf, C.; Rein, C.; Piwnicka, D.; Giordanetto, F.; Rognan, D. Structure-based discovery of allosteric modulators of two related class B G-protein-coupled receptors. *ChemMedChem* **2011**, *6*, 2159-2169.
340. Mysinger, M. M.; Weiss, D. R.; Ziarek, J. J.; Gravel, S.; Doak, A. K.; Karpiak, J.; Heveker, N.; Shoichet, B. K.; Volkman, B. F. Structure-based ligand discovery for the protein-protein interface of chemokine receptor CXCR4. *Proc Natl Acad Sci U S A* **2012**, *109*, 5517-5522.
341. Renner, S.; Noeske, T.; Parsons, C. G.; Schneider, P.; Weil, T.; Schneider, G. New allosteric modulators of metabotropic glutamate receptor 5 (mGluR5) found by ligand-based virtual screening. *ChemBioChem* **2005**, *6*, 620-625.
342. Feng, Z.; Hu, G.; Ma, S.; Xie, X.-Q. Computational advances for the development of allosteric modulators and bitopic ligands in G protein-coupled receptors. *AAPS J.* **2015**, *17*, 1080-1095.
343. Katritch, V.; Rueda, M.; Abagyan, R. Ligand-guided receptor optimization. *Methods Mol. Biol.* **2012**, *857*, 189-205.
344. Lane, J. R.; Chubukov, P.; Liu, W.; Canals, M.; Cherezov, V.; Abagyan, R.; Stevens, R. C.; Katritch, V. Structure-based ligand discovery targeting orthosteric and allosteric pockets of dopamine receptors. *Mol. Pharmacol.* **2013**, *84*, 794-807.
345. Wood, M.; Ates, A.; Andre, V. M.; Michel, A.; Barnaby, R.; Gillard, M. In vitro and in vivo identification of novel positive allosteric modulators of the human dopamine D2 and D3 receptor. *Mol. Pharmacol.* **2016**, *89*, 303-312.
346. Schwarting, R. K.; Huston, J. P. The unilateral 6-hydroxydopamine lesion model in behavioral brain research. Analysis of functional deficits, recovery and treatments. *Prog. Neurobiol.* **1996**, *50*, 275-331.

Chapter 2 – A Thieno[2,3-*d*]pyrimidine Scaffold is a Novel Negative Allosteric Modulator of the Dopamine D₂ Receptor

A Thieno[2,3-*d*]pyrimidine Scaffold Is a Novel Negative Allosteric Modulator of the Dopamine D₂ ReceptorTim J. Fyfe,^{†,‡,§} Barbara Zarzycka,^{||} Herman D. Lim,[‡] Barrie Kellam,[§] Shailesh N. Mistry,[§] Vsevolod Katrich,^{||,⊥} Peter J. Scammells,[†] J. Robert Lane,^{*,‡} and Ben Capuano^{*,†}[†]Medicinal Chemistry and [‡]Drug Discovery Biology, Monash Institute of Pharmaceutical Sciences, Monash University, Parkville, Victoria 3052, Australia[§]School of Pharmacy, Centre for Biomolecular Sciences, University of Nottingham, Nottingham NG7 2RD, U.K.^{||}Department of Biological Sciences, Bridge Institute, University of Southern California, Los Angeles, California 90089, United States[⊥]Department of Chemistry, Bridge Institute, University of Southern California, Los Angeles, California 90089, United States

Supporting Information

ABSTRACT: Recently, a novel negative allosteric modulator (NAM) of the D₂-like dopamine receptors **1** was identified through virtual ligand screening. This ligand comprises a thieno[2,3-*d*]pyrimidine scaffold that does not feature in known dopaminergic ligands. Herein, we provide pharmacological validation of an allosteric mode of action for **1**, revealing that it is a NAM of dopamine efficacy and identify the structural determinants of this allosterism. We find that key structural moieties are important for functional affinity and negative cooperativity, while functionalization of the thienopyrimidine at the 5- and 6-positions results in analogues with divergent cooperativity profiles. Successive compound iterations have yielded analogues exhibiting a 10-fold improvement in functional affinity, as well as enhanced negative cooperativity with dopamine affinity and efficacy. Furthermore, our study reveals a fragment-like core that maintains low μM affinity and robust negative cooperativity with markedly improved ligand efficiency.



INTRODUCTION

The dopamine D₂ receptor (D₂R), a class A G-protein-coupled receptor (GPCR), is a therapeutic target for central nervous system disorders such as schizophrenia and Parkinson's disease. Accordingly, it has been the subject of intensive drug discovery efforts for the past 60 years. Such efforts have focused on targeting the orthosteric binding site of the D₂R where dopamine (DA) binds.^{1,2} Clinically marketed drugs indicated for the treatment of schizophrenia display efficacy with respect to treating the positive symptoms of the disease. These drugs all act as either competitive antagonists or partial agonists at the D₂R. However, these drugs can cause deleterious side effects. First-generation antipsychotics (FGAs) are associated with a high frequency of extrapyramidal motor symptoms (EPS) caused by antagonism of D₂R signaling in the nigrostriatal system.³ Although second generation antipsychotic (SGAs) are thought to be associated with a lower risk of EPS, such drugs are associated with other limiting side effects such as metabolic side effects.⁴

In order to adequately address the unmet medical need associated with antipsychotic drug discovery, novel approaches are required. NAMs that display limited negative cooperativity with dopamine have been proposed as a safer therapeutic option

to treat the positive symptoms of schizophrenia, in particular for the onset of EPS, because they would cause only partial blockade of the D₂R.⁵ Indeed, targeting allosteric sites within GPCRs may be associated with a number of advantages over classical orthosteric drug discovery such as improved subtype selectivity and thus reduced off-target side effects, as well as maintenance of spatiotemporal patterns associated with endogenous neurohumoral signaling because they still allow the endogenous neurotransmitter to bind the receptor.^{6,7}

Virtual screening of orthosteric and putative allosteric sites within the human dopamine D₃ receptor (D₃R) recently identified an active thienopyrimidine compound (**1**, Figure 1).⁸ In this study, screening was undertaken using two optimized crystal-structure-based models (PDB code 3PBL):⁹ the receptor with an empty (unliganded) binding pocket (D₃R^{AP0}) and the receptor complex with DA (D₃R^{Dopa}). In particular, D₃R^{Dopa} was used to screen for allosteric compounds that can bind along with the endogenous ligand. Interestingly, **1**, although identified using D₃R^{AP0}, was predicted to bind in an allosteric pose and showed

Special Issue: Allosteric Modulators

Received: October 30, 2017

Published: April 23, 2018

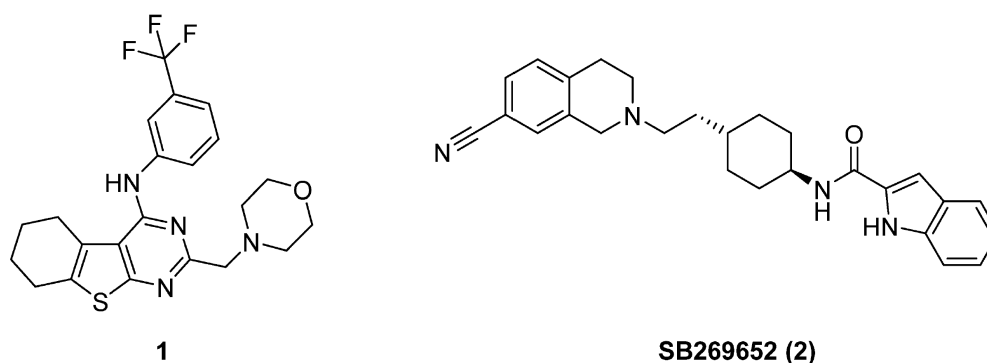


Figure 1. Compound **1** (2-(morpholinomethyl)-*N*-(3-(trifluoromethyl)phenyl)-5,6,7,8-tetrahydrobenzo[4,5]thieno[2,3-*d*]pyrimidin-4-amine) (left) was identified from a virtual ligand screen targeting orthosteric and allosteric pockets of the dopamine D₂-like receptors. SB269652 (**2**) (right) is the first drug-like NAM of the dopamine D₂ receptor.¹⁰

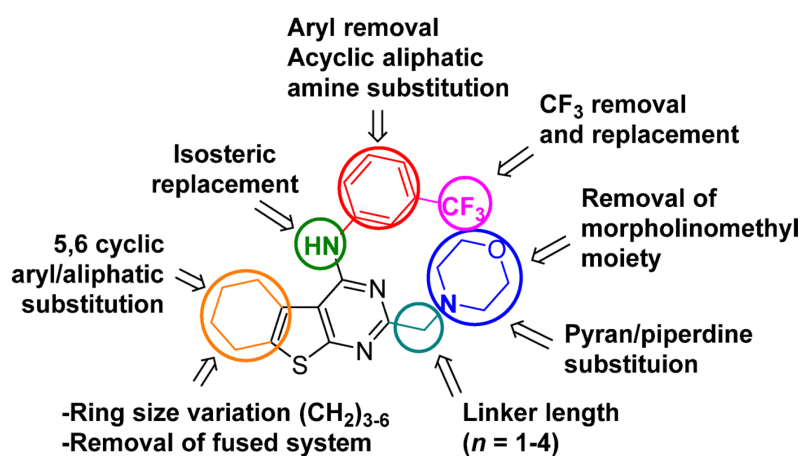


Figure 2. Areas of structural modification of **1** conducted during initial SAR investigation.

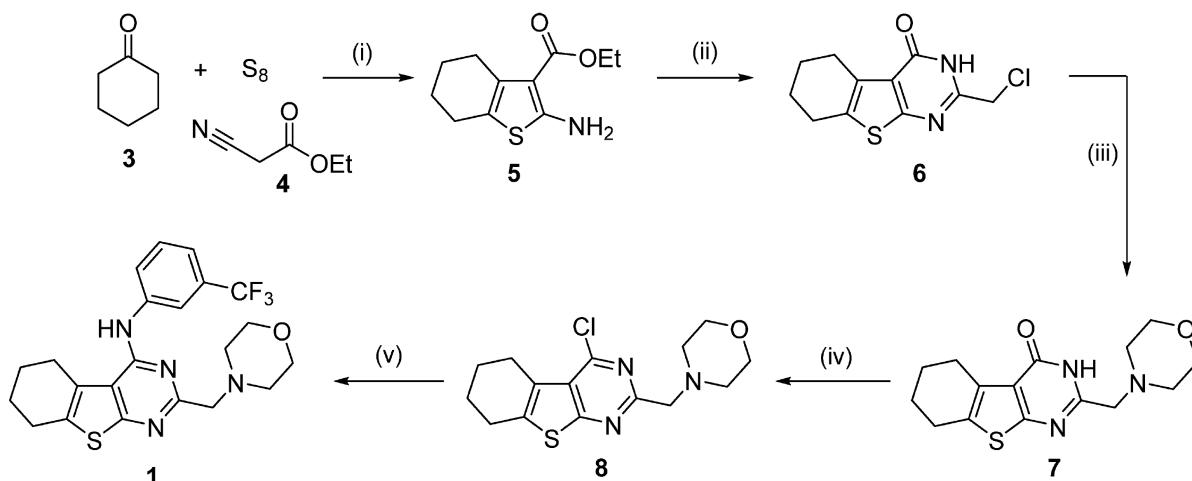
the highest potency of DA inhibition *in vitro*.⁸ Furthermore, this compound also displayed activity at the D₂R, and as such, may represent a novel allosteric scaffold for this receptor.

To date, very few ligands have been characterized as allosteric modulators of D₂-like dopamine receptors including the drug-like ligand SB269652 (Figure 1), which acts to negatively modulate dopamine affinity at the D₂R and D₃R.^{10–12} Structure-based virtual ligand screening (VLS) provides an attractive path for efficient discovery of allosteric ligands. However, it is important to validate this approach through optimization of initial VLS hits.^{13,14} Currently, there is no structure–activity relationship (SAR) data associated with **1**, but there is much scope for further structural interrogation. We therefore undertook a study to identify novel allosteric modulators for the D₂R, based on the structure of **1**. Through modifications to the scaffold of **1**, we aimed to identify key molecular features responsible for its allosteric action at the D₂R (Figure 2). We applied analytical pharmacological methods to allow us to supplement this SAR study with measures of allosteric ligand action to include not only allosteric ligand affinity (K_B) but also the magnitude of modulatory effects upon dopamine affinity (α) and efficacy (β). Such an approach may be useful as a starting point to understand the relationship between allosteric ligand behavior and the *in vivo* efficacy of such modulators. Indeed, to explore negative allosteric modulation as an approach to treat the positive symptoms of schizophrenia, it would be advantageous to have a set of D₂R NAMs that display a range of different allosteric

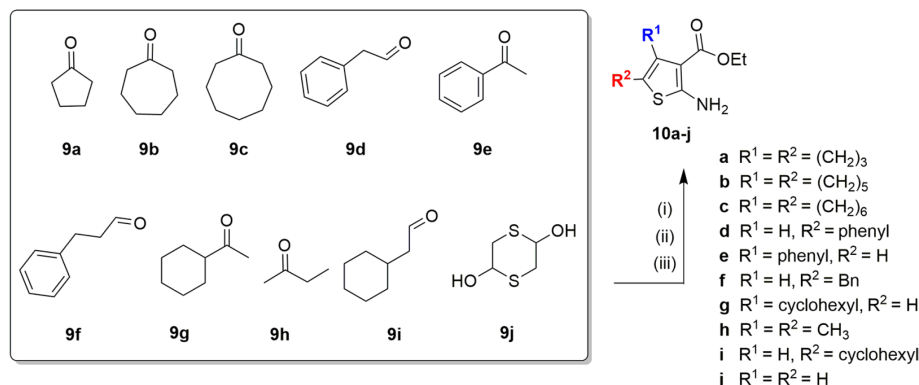
behaviors from modulation of dopamine affinity through to modulation of dopamine efficacy. Herein, we report the design, synthesis, and detailed pharmacological characterization of **1**, together with a library of structural analogues. We provide evidence that **1** does indeed act via an allosteric site at the D₂R and reveal that **1** exerts distinct pharmacology to that of SB269652, whereby it acts to modulate dopamine efficacy rather than dopamine affinity. Promising low molecular weight candidates with marketed improved lipophilic ligand efficiencies (LLE) have been identified and thus represent an attractive starting point for the development of novel D₂R NAMs that modulate dopamine efficacy, affinity, or both.

RESULTS AND DISCUSSION

Chemistry. In order to validate the pharmacological activity of lead compound **1**, it was resynthesized using a five step chemical synthesis outlined in Scheme 1.¹⁵ Gewald chemistry permitted the one-pot assembly of ethyl 2-amino-4,5,6,7-tetrahydrobenzo[*b*]thiophene-3-carboxylate **5** via commercially available cyclohexanone **2**, ethyl cyanoacetate **3**, and sulfur, catalyzed by diethylamine in absolute ethanol at 60 °C to afford the fused thiophene **5** as brilliant orange needles.¹⁵ Next, **5** was subjected to an acid catalyzed intermolecular cyclization in 1,4-dioxane at room temperature using chloroacetonitrile and hydrogen chloride gas generated *in situ* (Kipp's apparatus) to yield the 2-chloro substituted thieno[2,3-*d*]pyrimidin-4(3*H*)-one core scaffold **6** as a precipitated white solid.¹⁶ Subsequent N-alkylation with morpholine

Scheme 1. Chemical Synthesis of **1**^a

^aReagents and conditions: (i) morpholine, 0–45 °C, 80%; (ii) chloroacetonitrile, 1,4-dioxane, HCl_(g) (Kipp's apparatus), 50 °C, 2 h, 85%; (iii) DMF, morpholine, Et₃N, 100 °C, 2 h, 80%; (iv) POCl₃, toluene, 100 °C, 4 h, 75%; (v) *i*-PrOH, *m*-trifluoromethylaniline, MWI, 2 h, 70%.

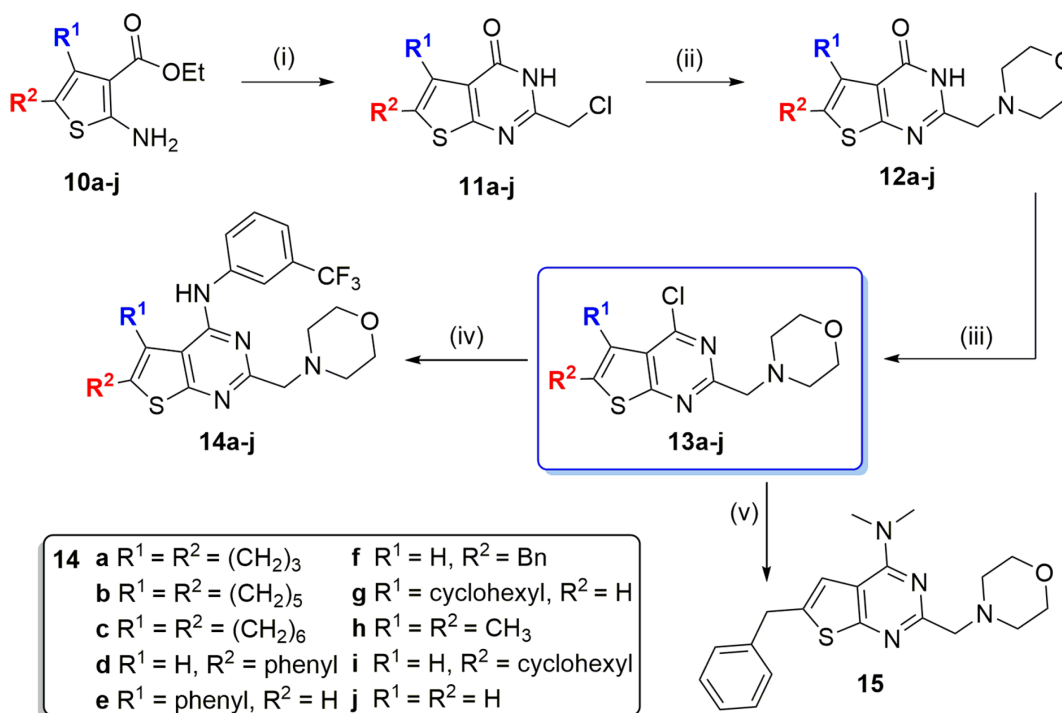
Scheme 2. Chemical Synthesis of 2-Amino-3-carbomethoxythiophenes^a

^aReagents and conditions: (i) sulfur, abs EtOH, ethyl cyanoacetate, 60 °C, 3–4 h, 50–80% (**10a–c**); (ii) sulfur, morpholine (neat), ethyl cyanoacetate, rt, ~18 h, 45–80% (**10d–i**); (iii) Et₃N, ethyl cyanoacetate, DMF, 45 °C, 0.5 h, 55% (**10j**).

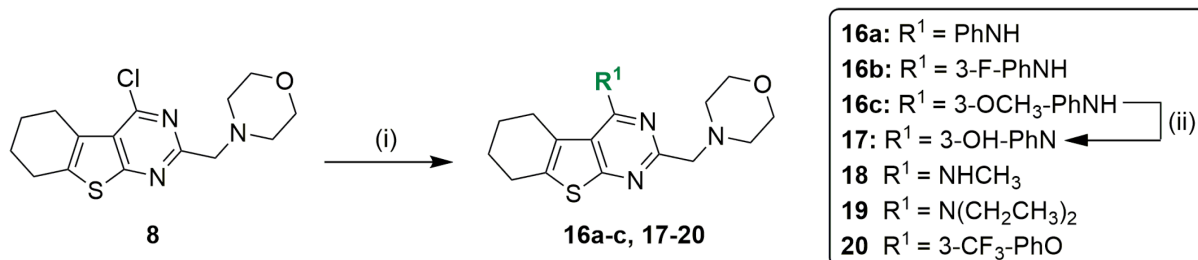
was achieved in DMF at 100 °C followed by cooling to room temperature to precipitate the desired product **7**. Activation of the pyrimidinone was accomplished with an adapted procedure using phosphorus oxychloride (POCl₃) and catalytic DMF in toluene to give the corresponding chloropyrimidine **8** as a brown oil in good yield. Finally, **8** was subjected to microwave assisted nucleophilic aromatic substitution with 3-(trifluoromethyl)aniline in *i*-PrOH to afford the target compound **1**, following chromatography and recrystallization from chloroform.

Single Modifications to Fused Cyclohexane Moiety, 2- and 4-Positions of 1. In addition to **1**, we generated a focused library of thieno[2,3-*d*]pyrimidine analogues bearing single structural modifications to examine the effect on functional binding affinity and allosteric pharmacology of the scaffold (Figure 2). This included modifying the fused ring system, initially observing the effect of differing ring size (fused cyclopentane **14a**, cycloheptane **14b**, and cyclooctane **14c**) (Schemes 2 and 3), as well as the effects of removing substitution at the 5- and 6-position of the thienopyrimidine **14j**. Moreover, we explored functionalization of both the 5- and 6-positions with various substituents (6-phenyl, **14d**; 5-phenyl, **14e**; 6-benzyl, **14f**; 5-cyclohexyl, **14g**; 5,6-dimethyl, **14h**; 6-cyclohexyl, **14i**) (Scheme 3) to provide an understanding

of the chemical space surrounding this moiety for further future elaboration. We investigated the effect of removing the CF₃ substituent on the aryl ring **16a** and the influence of incorporating additional substituents with different electronic effects (3-F, **16b**; 3-OCH₃, **16c**; 3-OH, **17**) (Scheme 4). In addition to this, we explored the role of the secondary aliphatic amine bridging the substituted aryl moiety in **1** through the synthesis of two analogues bearing *N*-methylamino (**18**) and *N,N*-diethylamino (**19**) substituents (Scheme 4). The role of this secondary amine was further probed through the removal of its hydrogen-bond donor property via isosteric replacement with an ether linkage (**20**) (Scheme 4). This would permit the assessment and influence of hydrogen bond donor removal and any subsequent functional effects on the allosteric pharmacology of **1**. The *N*-methylamino derivative (**18**) would test the importance of aromaticity while still maintaining hydrogen-bond characteristics of **1**, while the *N,N*-diethylamino analogue (**19**) investigates the impact of removing aromaticity and hydrogen-bond donor properties at the 4-position. Additionally, the ether derivative (**20**) assesses the importance of removing hydrogen-bond donor properties while maintaining aromaticity. We also focused on the 2-position of **1**, where we sought to evaluate the impact of

Scheme 3. Chemical Synthesis of Analogues of 1 with Modifications to Fused Cyclohexane System^a

^aReagents and conditions: (i) thiophene, chloroacetonitrile, HCl_(g), 50 °C to reflux, 4–24 h, 20–95%; (ii) DMF, Et₃N, 100 °C, 4–8 h, 50–90%; (iii) POCl₃, DMF_(cat.), toluene, 3–5 h, 70–90%; (iv) 3-(trifluoromethyl)aniline, Et₃N, *i*-PrOH, MWI, 1–3 h, 60–90%; (v) 15, DMF, 100 °C, 33%.

Scheme 4. Synthesis of Analogues Modified at the 4-Position^a

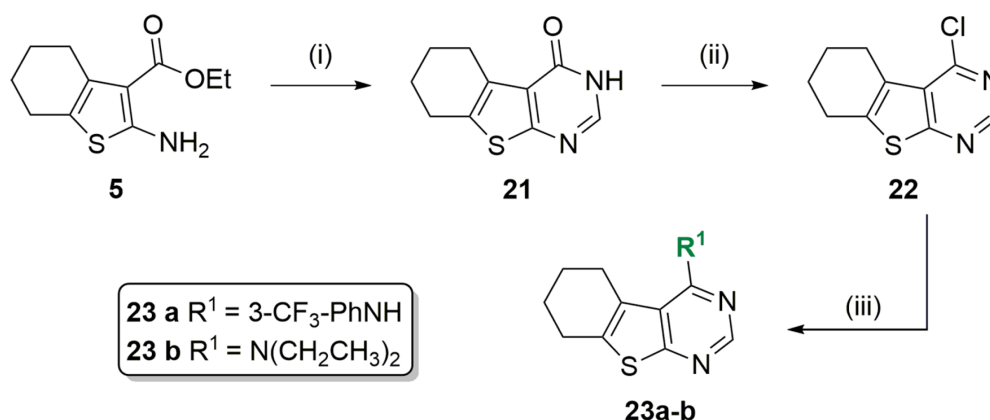
^aReagents and conditions: (i) substituted aniline, *i*-PrOH, MWI, 2 h, 65–90% (16a–c); (ii) BBr₃ (1 M in DCM), rt, overnight, 53% (17); (iii) *i*-PrOH, methylamine, MWI, 140 °C, 2.5 h, 85% (18); *i*-PrOH, *N,N*-diethylamine, MWI, 140 °C, 3 h, 91% (19); *i*-PrOH, 3-(trifluoromethyl)phenol, TRIDENT_(cat.), MWI, 6 h, 72% (20).

removing the 2-morpholinomethyl moiety entirely (23a, Scheme 5), subsequently conferring no substitution at the 2-position of the thienopyrimidine. In addition to this, we investigated isosteric replacement of the morpholino O for CH₂ to afford the piperidine analog 26 (Scheme 6), as well as a similar replacement of N for CH to furnish the tetrahydropyran analog 33a (Scheme 7). Moreover, we investigated the effects of increasing the methylene linker length bearing morpholine (ethylene, 39a; propylene, 39b; butylene, 39c) (Scheme 8).

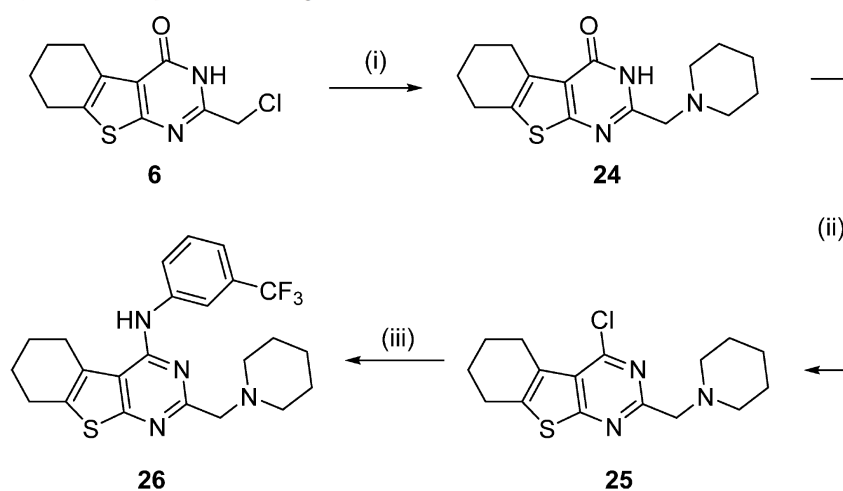
Hybrid Modification of 1. Several additional compounds were synthesized to further investigate the effects of the aforementioned structural modifications. These modifications included deletion of the fused cyclohexane system of the tricyclic scaffold, removal of the 2-morpholinomethyl pendant, isosteric replacement through substitution of the morpholine ring for tetrahydropyran, and the incorporation of a 1,4-butylene linker; all bearing the *N,N*-diethylamino functionality in place of the aryl *m*-CF₃

moiety. These subsequent analogues 23b (Scheme 5), 33b (Scheme 7), 40 (Scheme 9), 44 (Scheme 11) were synthesized as outlined previously by varying the nature of the nucleophile used in the final nucleophilic aromatic substitution. Finally, a further four analogues (43a,b, Scheme 10; 47a,b, Scheme 11) were synthesized to examine the effects of simultaneous deletion/instalment of functionality with respect to maintaining one of either *m*-CF₃-aryl or *N,N*-diethylamino substituents at the 4-position of 1.

The thieno[2,3-*d*]pyrimidine moiety (Figure 2) is prevalent in a variety of reported compounds; thus its synthesis is well established.^{17–23} Rapid access to a series of analogues substituted at the 5- and 6-positions was achieved using the appropriate aldehyde or ketone as a starting material, by means of Gewald-type chemistry (Scheme 2). An alternative method to traditional Gewald chemistry using solvent-free conditions for the preparation of substituted 2-aminothiophene derivatives from respective

Scheme 5. Chemical Synthesis of Analogues of 1 Devoid of Morpholinomethyl Moiety^a

^aReagents and conditions: (i) formamide, 170 °C, 12 h, 85%; (ii) POCl₃, DMF_(cat.), toluene, 100 °C, 3–5 h, 90%; (iii) *i*-PrOH, *m*-CF₃-aniline, DIPEA, MWI, 2 h, 75% (23a); (iv) *i*-PrOH, Et₃NH, DIPEA, MWI, 2 h, 90% (23b).

Scheme 6. Chemical Synthesis of Piperidine Analogue^a

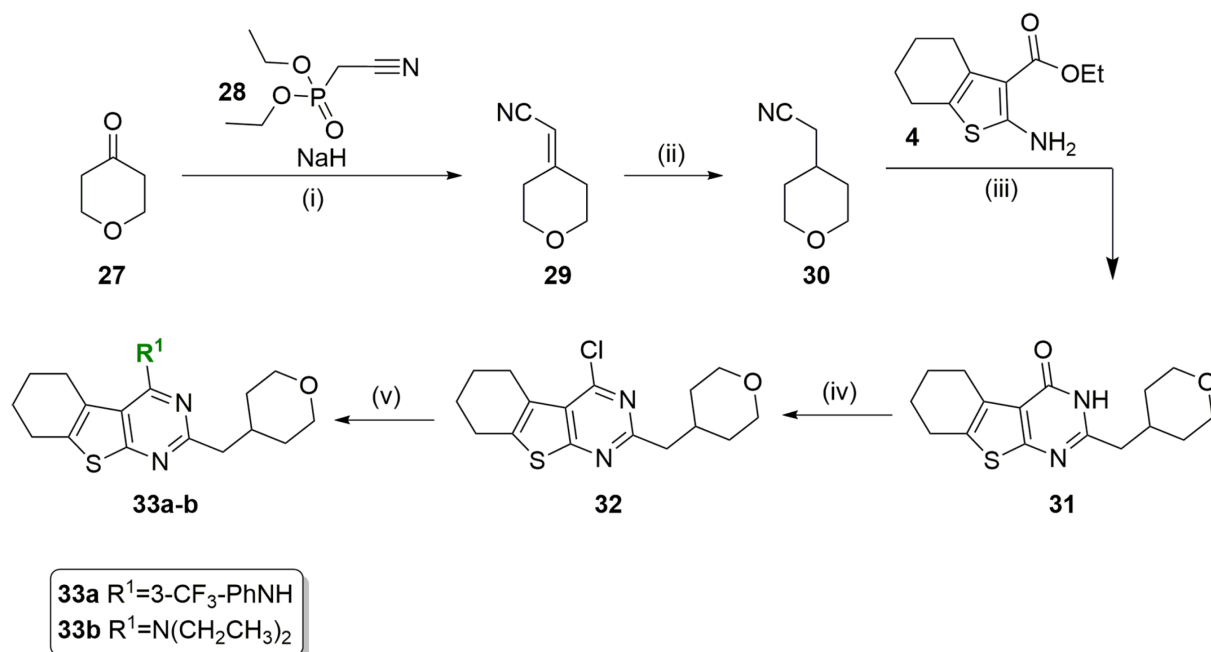
^aReagents and conditions: (i) piperidine, Et₃N, 100 °C, 2 h, 71%; (ii) toluene, 100 °C 4 h, 46%; (iii) *i*-PrOH, *m*-trifluoromethylaniline, MWI, 2 h, 70%.

ketones/aldehydes in the presence of morpholine as catalyst was used to furnish a parallel set of analogues (Scheme 2).²³ The commercial availability of aldehydes (9d, 9f, 9i) or ketones (9a–c, 9e, 9g, 9h) and their usefulness in Gewald-type chemistries or variations thereof permitted easy access to a variety of substituted thienocarboxylate precursors 10a–i bearing a primary amine and ethyl ester as functional handles. Ethyl 2-aminothiophene-3-carboxylate 10j was obtained in accordance with an adapted procedure²⁴ (Scheme 2) using the commercially available mercaptoacetaldehyde dimer 1,4-dithiane-2,5-diol (9j). This reagent was successfully used to afford 10j as a yellow crystalline solid in good yield.

To allow construction of the 2-chloromethyl-substituted pyrimidine bearing a functional handle for further elaboration, the appropriate thiophenes 10a–j were subjected to an intermolecular cyclization reaction under acidic conditions in the presence of chloroacetonitrile to afford the desired thieno[2,3-*d*]pyrimidine core which could be utilized for further derivatization (Scheme 3). Cyclization required dry HCl gas to be generated in situ (Kipp's apparatus) and to be passed through a solution containing the respective nitrile and thiophene,

furnishing the corresponding 2-haloalkyl pyrimidinones 11a–j in high yields.¹⁶

N-Alkylation of morpholine with 11a–j was conducted in DMF and typically proceeded smoothly to provide the corresponding morpholinomethyl analogues 12a–j. Products could often be precipitated with H₂O, washed with an appropriate solvent, and/or recrystallized. Carbonyl activation was achieved through the use of POCl₃ along with catalytic DMF in toluene to attain clean conversion to the corresponding chloropyrimidines (13a–j). Finally, the appropriate chloropyrimidine (13a–j) could be taken up in *i*-PrOH and subjected to microwave-assisted nucleophilic aromatic substitution in the presence of the appropriate nucleophile (primary aromatic or secondary acyclic aliphatic amine) and an excess of Hünig's base to furnish target analogues 14a–j in good yields. Initially, DMF was trialed as a potential reaction solvent for nucleophilic aromatic substitution but produced suboptimal yields and byproducts and thus was not used further. Compound 15 was isolated as a reaction byproduct during the attempted synthesis of 14f, due to the presence of *N,N*-dimethylamine existing as an impurity in DMF; thus it was characterized and tested for its *in vitro* activity.

Scheme 7. Synthesis of Tetrahydro-2H-pyran-4-yl Analogues of 1^a

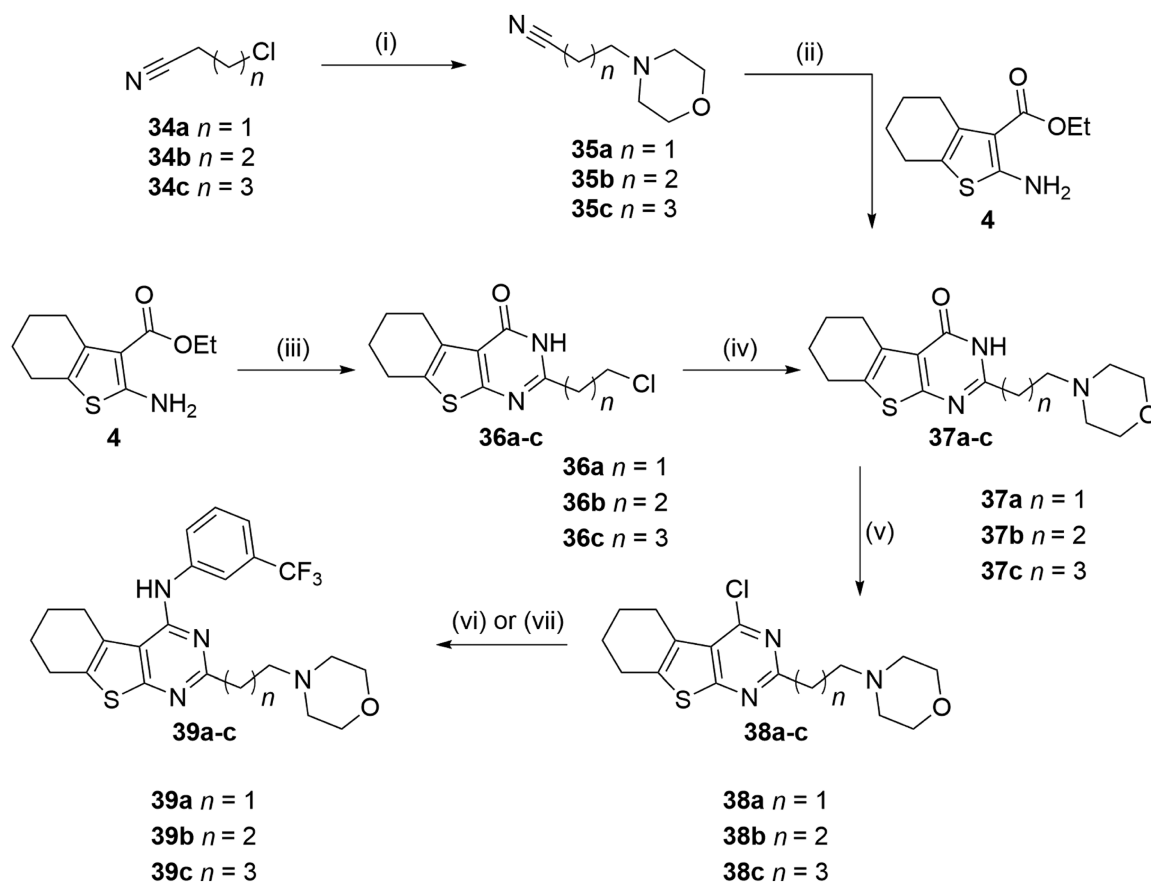
^aReagents and conditions: (i) Et₂O, 0 °C to rt, 24 h, 39%; (ii) 10% Pd/C, EtOAc, AcOH, 1 atm, rt, 5 h, 100%; (iii) 1,4-dioxane, HCl_(g), rt to reflux, 13 h, 93%; (iv) toluene, POCl₃, DMF_(cat.), 100 °C, 4 h, 24%; (v) amine, *i*-PrOH, MWI, 120 °C, 3 h, 48% (33a); (vi) *i*-PrOH, Et₂NH, MWI, 120 °C, 2 h, 85% (33b).

Substituents at the Thienopyrimidine 4-Position. Compounds 16a–c were similarly obtained as previously outlined, through the use of various substituted anilines via nucleophilic aromatic substitution with key chloropyrimidine intermediate 8 (Scheme 4). Compound 16c was used to access the phenolic analogue via O-demethylation employing boron tribromide in DCM at 0 °C to afford the corresponding phenol 17 in good yield. To assess the impact of removing aromaticity from the 4-position, several additional analogues of 1 were synthesized (Scheme 4). To do this, key intermediate 8 was again subjected to nucleophilic aromatic substitution using an excess of *N*-methyl or *N,N*-diethylamine under basic conditions in *i*-PrOH which furnished the corresponding *N*-methylamino and *N,N*-diethylamino analogues in good yields as light brown oils (18 and 19, respectively). To advance our understanding of the aniline's role within 1, we generated a compound deficient of a hydrogen-bond donor group through isosteric replacement with an ether linkage but still bearing the aryl-CF₃ substituent (20, Scheme 4). To achieve this, compound 8 was subjected to MWI in the presence of 3-(trifluoromethyl)phenol and a 10% molar equivalent of phase-transfer catalyst tris[2-(2-methoxyethoxy)ethyl]amine (TRIDENT). Subsequent chromatographic purification afforded the target ether derivative 20 as a transparent oil in 72% yield.

Substituents at the Thienopyrimidine 2-Position. To assess the effects of removing the 2-morpholinomethyl moiety (Scheme 5), 4,5,6,7-tetrahydrobenzothiophene 5 was refluxed for several hours in neat formamide to construct the corresponding pyrimidinone 21. This compound was similarly converted to 4-chloro analogue 22, followed by nucleophilic aromatic substitution with 3-(trifluoromethyl)aniline to yield compound 23a (Scheme 5). To further assess the effect of introducing an *N,N*-diethylamino substituent at the 4-position of 1, we synthesized an additional analogue that incorporated this amine in conjunction with removal

of the 2-morpholinomethyl substituent (23b, Scheme 5). This compound was accessed using key intermediate 22 via nucleophilic aromatic substitution, thereby permitting us to further probe the effect of incorporating an aliphatic 4-substituent but still bearing similar hydrogen-bonding capabilities.

Next, we focused on the morpholine moiety to probe the effect on the allosteric pharmacology of 1 by replacing the O or N heteroatoms with a methylene or methine group to give piperidine analogue 26 and tetrahydropyran analogue 33a, respectively. Compound 26 (Scheme 6) was accessed via the *N*-alkylation of piperidine with key intermediate 6, again followed by chlorination (25) and substitution to afford 26 in good yield. Compound 33a (Scheme 7) was furnished via a multistep synthesis that initially involved activation of diethyl cyanomethylphosphonate 28 with NaH, followed by dropwise addition of tetrahydro-4H-pyran-4-one 27 in diethyl ether. Vacuum distillation and recrystallization from petroleum ether afforded the corresponding nitrile 29 as a transparent crystalline solid in moderate yield. Catalytic hydrogenation employing Pd/C as catalyst in EtOAc and AcOH under atmospheric pressure gave the corresponding saturated nitrile 30 as a transparent oil in high purity. Intermolecular cyclization of thiophene 5 with 30 proceeded in 1,4-dioxane under standard acidic conditions (Kipp's apparatus) to afford the thienopyrimidinone 31, though requiring reflux temperatures to achieve full conversion. Subsequent DMF-catalyzed POCl₃ activation in toluene provided the chloropyrimidine 32, followed by nucleophilic aromatic substitution in *i*-PrOH to afford the target tetrahydropyran 33a as a white foam in moderate yield. To better assess the effects of *N,N*-diethylamino substitution of the 4-position in combination with the tetrahydropyran functionality, one additional analogue was synthesized (33b). This compound was readily accessed by reacting the appropriate starting material 32 under standard conditions to afford the target as a light gold oil in good yield (Scheme 7).

Scheme 8. Synthesis of Morpholino-Substituted Nitriles and Corresponding Alkyl Chain-Extended Analogues of **1**^a

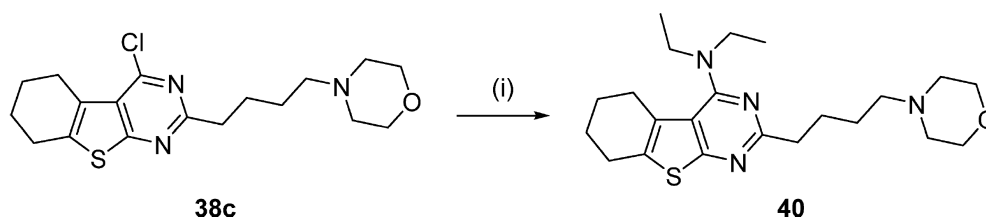
^aReagents and conditions: (i) morpholine, toluene, reflux, 7 h, 45–65% (**35a–c**); (ii) 1,4-dioxane, nitrile, HCl_(g), rt, 12 h, reflux 4 h, 57–80% (**37b,c**); (iii) **34a–c**, 1,4-dioxane, HCl_(g), rt 12 h to reflux 3 h, 60–83% (**36a–c**); (iv) DMF, 50 °C, 4 h, 56% (**37a**); (v) POCl₃, toluene, DMF_(cat.), 2–5 h, 67–88% (**38a–c**); (vi) NaH, 3-(trifluoromethyl)aniline, DMF, 100 °C, 6 h, 27% (**39a**); (vii) *i*-PrOH, MWI, 2–4 h, 56–59% (**39b,c**).

Chain-Extension of the 2-Substituent Linker of 1. To investigate the effects of increasing the methylene linker length on the allosteric pharmacology of **1**, we generated a series of analogues of differing methylene chain length (2–4) bridging the morpholine substituent to the pyrimidine core (Scheme 8). Commercially available primary chloroalkyl nitriles 3-chloropropionitrile **34a**, 4-chlorobutanenitrile **34b**, and 5-chloropentanenitrile **34c** were reacted in the presence of thienopyrimidinone **5** under standard acidic conditions in order to furnish the corresponding chain-extended pyrimidinones (**36a–c**). These nitriles were substantially less reactive than chloroacetonitrile and thus required reflux temperatures to complete the conversion of the amidinium species formed in situ to the corresponding 2-chloropyrimidinone.

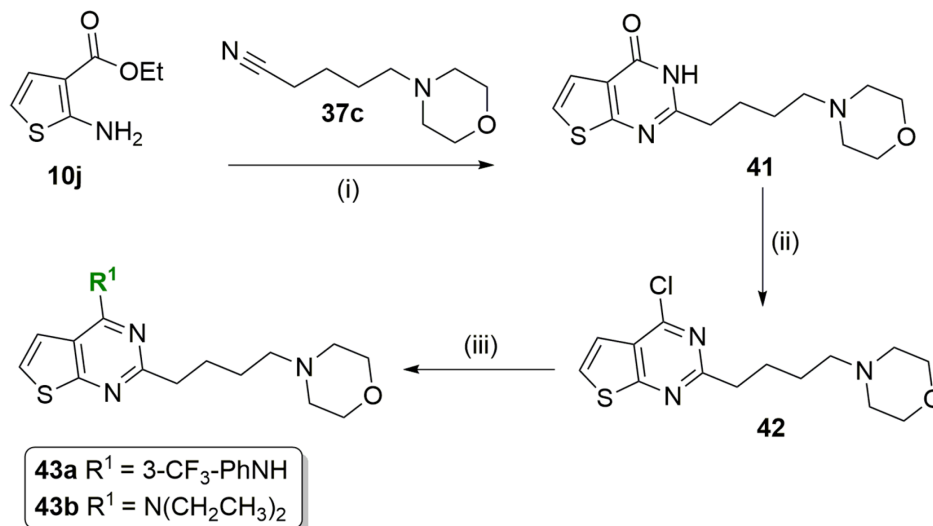
By use of standard conditions, alkylation of morpholine with the appropriate chain extended chloropyrimidinone was attempted to generate the corresponding morpholinoethyl, morpholinopropyl, and morpholinobutyl substituted intermediates **37a–c**. This methodology successfully afforded the morpholinoethyl pyrimidinone **37a** in good yield as a yellow crystalline solid (Scheme 8); however pyrimidinone derivatives bearing the longer chloroalkyl chains were suspected to be eliminating under basic conditions. ¹H NMR analysis provided confirmation of favored intramolecular cyclization under both ambient and reflux conditions, generating two tetracyclic regioisomers in a 1:1 ratio.²⁵ In light of this,

additional efforts focused on construction of the N-substituted nitrile moiety first (Scheme 8). This was accomplished by stirring the appropriate nitrile (**34a–c**) with an excess of morpholine in refluxing toluene for several hours to furnish the corresponding N-morpholino nitriles (**35a–c**) in good yields as transparent oils. These intermediates were reacted with **5** under acidic conditions to afford the target morpholinopropyl and morpholinobutyl pyrimidinones in good yields (**37b,c**) followed by chlorination (**38a–c**) and subsequent nucleophilic aromatic substitution to furnish the final chain extended analogues **39a–c**.

Hybrid Functionalization of 2- and 4-Positions of 1. The subsequent pharmacological effects of incorporating extended morpholinoalkyl substituents into analogues of **1** (**39a–c**) conveyed interesting changes in the functional properties of this scaffold. The 1,4-butylene linker was of particular interest. Thus, compound **40** was synthesized using intermediate **38c** (Scheme 9) via nucleophilic aromatic substitution to enhance our understanding of the SAR surrounding the 4-position of **1** with respect to *N,N*-dimethylamino substitution. In addition to further investigate the 1,4-butylene linker, removal of the fused functionality within **1** (**14j**) not only resulted in a loss of binding affinity but rendered this analogue functionally inactive. To this end, we sought to investigate the effect of removing the fused cyclohexane system while maintaining the morpholinobutyl functionality in conjunction with one of either 3-(trifluoromethyl)anilino or *N,N*-diethylamino substituents at the 4-position (Scheme 10).

Scheme 9. Synthesis of *N,N*-Diethylamino Analogue Bearing Morpholinobutyl Substituent and Fused Cyclohexane Moiety^a

^aReagents and conditions: (i) *i*-PrOH, Et₂NH, MWI, 120 °C, 3 h, 85%.

Scheme 10. Further Analogues of **1** Bearing the Morpholinobutyl Substituent^a

^aReagents and conditions: (i) 1,4-dioxane, HCl_(g), rt overnight, reflux 3–6 h, 57–65%; (ii) toluene, POCl₃, DMF_(cat.), 3 h, 60–88% (iii) *i*-PrOH, Et₂NH, MWI, 120 °C, 1.5 h, 80% (**43a**); *i*-PrOH, Et₂NH, MWI, 120 °C, 4 h, 90% (**43b**).

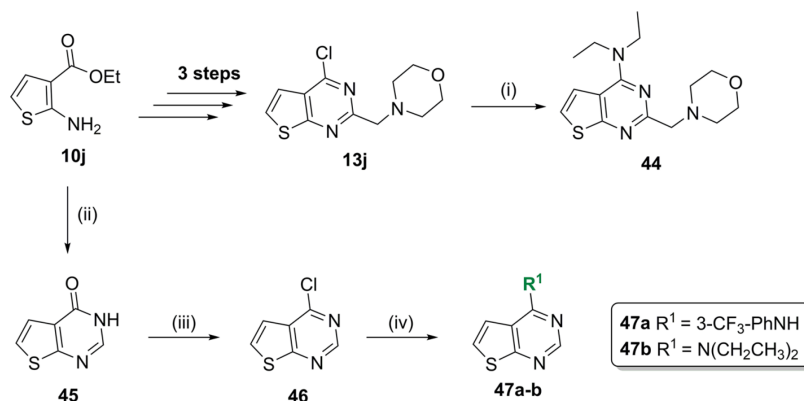
These two additional analogues were accessed by reacting the appropriate unsubstituted thiophene **10j** with **35c** under acidic conditions to provide cyclized product **41**, followed by chlorination **42** and nucleophilic aromatic substitution employing conditions as outlined previously to furnish **43a,b** in good yields (Scheme 10).

In addition to this, we wanted to observe the effects of *N,N*-diethylamino substitution of **14j** as a direct comparison with 3-(trifluoromethyl)aniline. Thus, **13j**, whose synthesis is depicted in Scheme 3, was reacted with *N,N*-diethylamine under microwave irradiation to afford **44** in good yield (Scheme 11). Moreover, we wanted to observe the effect of aromatic and aliphatic substituents at the 4-position of **1** in conjunction with concurrent removal of the fused cyclohexane and morpholinomethyl moieties. Removal of said functionalities on the structure of **1** effectively results in a low molecular weight fragment-like core. These compounds were readily accessed using chemistry as outlined previously (Scheme 11) to furnish the target analogues **47a,b** in high yields.

Pharmacology. Confirmation of an Allosteric Mode of Action for **1 at the D₂R.** Our previous study predicted that **1** can adopt an allosteric pose within the D₃R^{AP0} model and revealed that this compound also displayed activity at the D₂R, our primary target of interest.⁸ Prior to initiating an investigation into **1**, we wanted to confirm its activity at the D₂R and determine if it displays competitive or allosteric pharmacology. Equilibrium radioligand binding experiments were performed on **1** to monitor its effect upon orthosteric ligand ([³H]raclopride) binding in

membranes prepared from FlpIn CHO cells stably expressing the long isoform of the human D₂R (hD_{2L}R).²⁶ This assay may also provide indication of an allosteric versus competitive mode of action. If the compound displays incomplete or partial displacement of the radioligand, this is consistent with the saturable effect of an allosteric modulator whereby the degree of negative cooperativity with the radioligand determines the level of radioligand displacement. In cases where one observes only partial displacement, data may be fit using an allosteric ternary complex model to derive a value of affinity, denoted as *K_B*, and cooperativity with [³H]raclopride (α).²⁷ However, in our assay, **1** was able to completely displace [³H]raclopride. Therefore, this assay did not allow us to discriminate between high negative cooperativity with the [³H]raclopride or competition for the orthosteric binding site (Table 1). Thus, to determine evidence of an allosteric mode of action for this ligand, we extended our evaluation to measurements of [³H]raclopride dissociation from the D₂R (Figure 3A). Dissociation of the radioligand was measured following addition of a high concentration of cold orthosteric ligand (10 μ M haloperidol) to prevent [³H]raclopride rebinding in the absence or presence of **1**. In the presence of 100 μ M **1**, the dissociation rate of [³H]raclopride from the D₂R significantly increased (Table 2 and Figure 3A), consistent with **1** binding to an allosteric site within the D₂R.²⁸

Our pharmacological analysis using the above radioligand binding assay did not provide information regarding the modulatory effect of **1** upon the neurotransmitter dopamine. Therefore, we tested **1** in an assay measuring inhibition of

Scheme 11. Further Thieno[2,3-*d*]pyrimidin-4-amine Analogues of **1**^a

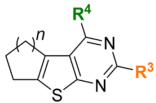
^aReagents and conditions: (i) Et₂NH, DIPEA, *i*-PrOH, MWI, 120 °C 1.5 h, 94% (**44**); (ii) formamide, 170 °C, 6 h, 76%; (iii) toluene, POCl₃, DMF_(cat.), 3 h, 88%; (iv) *m*-CF₃-aniline, DIPEA, *i*-PrOH, MWI, 120 °C 2.5 h, 80% (**47a**); Et₂NH, DIPEA, *i*-PrOH, MWI, 120 °C 1.5 h, 90% (**47b**).

forskolin-stimulated cyclic adenosine monophosphate (cAMP) accumulation through activation of the hD_{2L}R stably expressed in FlpIn CHO cells using a BRET biosensor.²⁹ The concentration-dependent response of dopamine was measured in the presence of increasing concentrations of **1** and 10 μM forskolin. Application of an operational model of allosterism to the concentration–response data yielded an estimate of affinity of **1** for the unoccupied receptor (K_B) and its cooperativity with dopamine where α is cooperativity exerted upon dopamine binding, and β denotes modulation of dopamine efficacy.³⁰ These data are reported in Table 4 and are presented as logarithms to base 10 to allow statistical comparison.³¹ Values of α or β of <1 signify negative cooperativity with dopamine. The lead compound **1** acted as a negative allosteric modulator at the D₂R, with low μM functional affinity ($K_B = 3.9$ μM). The depression in the maximal response upon the dopamine dose–response curve caused by increasing concentrations of **1** is characteristic of the action of a NAM of agonist efficacy (Figure 3B). In order to fit these data, the cooperativity of **1** with dopamine affinity (α) was constrained to be neutral, allowing us to estimate a value of modulatory action upon dopamine efficacy ($\beta = 0.28$) that equates to a maximal 3-fold decrease (Figure 3B, Table 4). This action is different from the action of the competitive antagonist haloperidol at the D₂R that acts to cause a dextral shift in the dopamine dose–response curve with no effect upon the maximal effect of dopamine (Figure 3C). Thus, by using complementary pharmacological approaches including equilibrium and dissociation kinetic binding analyses, together with experiments measuring D₂ receptor function, we have confirmed that **1** acts through a noncompetitive mechanism to modulate the activity of dopamine at the D₂R; i.e., it is NAM of the efficacy of dopamine. The thienopyrimidine scaffold of **1** is unique to known dopaminergic receptor ligands. Therefore, a novel allosteric scaffold for the D₂R has been identified and validated. Moreover, further validation has been provided for virtual allosteric ligand screening at the dopamine D₂-like receptors.

Radioligand Binding Analysis of Analogues of 1. To begin to explore the structural features of **1** that determine its allosteric activity, we employed the equilibrium [³H]raclopride binding assay described in our characterization of **1** above. For the majority of compounds, we observed complete displacement of the radioligand. Therefore, while this simple assay provides us with both confirmation of target activity and a value of affinity, for

these compounds, we cannot distinguish between a competitive mode of interaction or an allosteric interaction that exerts high negative cooperativity upon [³H]raclopride binding. We first examined modifications to the fused cyclohexane system of **1** (Table 1). Replacement of the six-membered saturated ring with a fused cyclopentane (**14a**) or cycloheptane (**14b**) system made no significant impact on binding affinity. However, replacement with the cyclooctane (**14c**) system caused a significant 6-fold decrease in affinity. No significant effect on affinity was seen when various other substituents were introduced to the 5- and 6-positions of the thienopyrimidinone (**14d–g,i**). Conversely, introduction of the 5-phenyl substituent (**14e**) did result in an apparent decrease in negative cooperativity manifested by an incomplete displacement of [³H]raclopride that allowed us to determine a value of cooperativity, $\alpha = 0.13$ (Table 1). 5,6-Dimethyl substitution (**14h**) and removal of the fused system (**14j**) both caused a significant 5- to 10-fold decrease in affinity ($K_B = 250$ and 120 μM, respectively). To further explore the role of the *N*-(3-(trifluoromethyl)phenyl) substituent of **1**, we generated a small series of analogues of **1** that incorporated changes to this functionality, including removal of the CF₃ substituent (**16a**), as well as substitution with various groups (3-F, **16b**; 3-OCH₃, **16c**; 3-OH, **17**). Removal of the CF₃ substituent caused a 6-fold decrease in affinity, whereas both the 3-OH and 3-OMe analogues displayed similar affinity to the parent compound (**1**). To investigate the effects of removing the *N*-(3-(trifluoromethyl)phenyl) substituent at the 4-position, we synthesized a series of analogues of **1** that included an *N,N*-dimethylamino group (**15**) that was isolated as a byproduct from the synthesis of **14f** as a result of trialing DMF as a reaction solvent, as well as analogues bearing *N*-methylamino (**18**) and *N,N*-diethylamino (**19**) moieties. In addition to this, we investigated the effect of removing the secondary amine bridging the aryl moiety to the pyrimidine moiety of **1** by isosteric replacement with an ether linkage (**20**). These analogues all saw no significant change in affinity as compared to **1**. Interestingly, however, **19** displayed only partial displacement of [³H]raclopride at the D₂R ($K_B = 6.0$ μM, $\alpha = 0.23$) (Table 1, Figure 4A). These data demonstrate that the secondary amine plays no role in the functional affinity of **1**, but modification of this feature can modulate the negative cooperativity with [³H]raclopride. Additional analogues were synthesized to examine the effect of increasing the methylene linker length bearing the morpholine substituent (**39a–c**), as well as

Table 1. Ability of 1 and Derivatives of 1 To Displace the Radiolabeled Antagonist [³H]Raclopride at the D_{2L}R Expressed in FlpIn CHO Cells



1, 14a-c, 16a-c, 17-20,
23a-b, 26, 33a-b, 39a-c, 40



14d-j, 15, 43a-b, 44, 47a-b

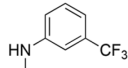
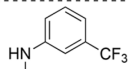
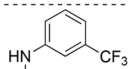
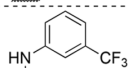
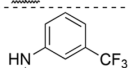
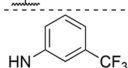
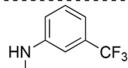
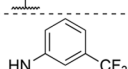
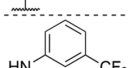
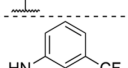
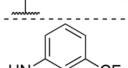
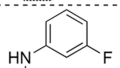
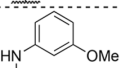
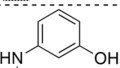
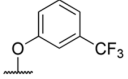
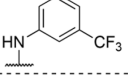
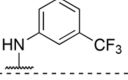
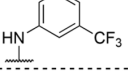
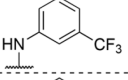
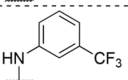
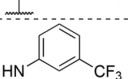
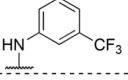
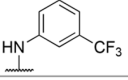
	<i>n</i>	R ¹	R ²	R ³	R ⁴	p <i>K</i> _B (<i>K</i> _B , μM) ^a	Log α (α) ^b
1	2	-	-			4.78 ± 0.11 (16.6)	-
14a	1	-	-			4.23 ± 0.12 (59)	-
14b	3	-	-			4.43 ± 0.21 (37)	-
14c	4	-	-			3.98 ± 0.17 (106)	-
14d	-	H				4.35 ± 0.13 (45)	-
14e	-		H			4.31 ± 0.11 (48.6)	-0.88 ± 0.10 (0.13)
14f	-	H				4.30 ± 0.18 (50)	-
14g	-		H			4.42 ± 0.20 (38)	-
14h	-	CH ₃	CH ₃			3.59 ± 0.15 (250)	-
14i	-	H				4.34 ± 0.18 (45.8)	-
14j	-	H	H			3.91 ± 0.20 (120)	-
15	-	H			N(CH ₃) ₂	4.51 ± 0.14 (30)	-
16a	2	-	-			4.00 ± 0.16 (99)	-
16b	2	-	-			nd	nd
16c	2	-	-			4.32 ± 0.14 (48)	-
17	2	-	-			4.45 ± 0.10 (35)	-
18	2	-	-		NHCH ₃	4.28 ± 0.11 (53)	-
19	2	-	-		N(CH ₂ CH ₃) ₂	5.22 ± 0.16 (6)	-0.64 ± 0.06 (0.23)

Table 1. continued

20	2	-	-			4.66 ± 0.12 (22)	-
23a	2	-	-	H		4.51 ± 0.13 (31)	-0.41 ± 0.04 (0.39)
23b	2	-	-	H	N(CH ₂ CH ₃) ₂	4.76 ± 0.07 (17)	-
26	2	-	-			4.41 ± 0.12 (39)	-
33a	2	-	-			3.99 ± 0.27 (100)	-0.41 ± 0.08 (0.39)
33b	2	-	-		N(CH ₂ CH ₃) ₂	4.45 ± 0.09 (35)	-
39a	2	-	-			4.16 ± 0.16 (70)	-
39b	2	-	-			4.89 ± 0.17 (13)	-
39c	2	-	-			5.48 ± 0.09 (3.31)	-1.03 ± 0.09 (0.09)
40c	2	-	-		N(CH ₂ CH ₃) ₂	4.79 ± 0.08 (16)	-
43a	-	H	H			4.71 ± 0.09 (19)	-
43b	-	H	H		N(CH ₂ CH ₃) ₂	5.51 ± 0.11 (3)	-
44	-	H	H		N(CH ₂ CH ₃) ₂	5.89 ± 0.09 (1.3)	-
47a	-	H	H	H	N(CH ₂ CH ₃) ₂	4.20 ± 0.09 (63)	-
47b	-	H	H	H		4.65 ± 0.12 (23)	-1.01 ± 0.14 (0.10)

^aEstimate of the negative logarithm of the equilibrium dissociation constant ± SEM determined by radioligand binding. ^bEstimate of the logarithm of the net cooperativity factor between the modulator and [³H]raclopride. Values represent the mean ± SEM from at least three experiments performed in duplicate.

the effect of replacing either the oxygen or nitrogen atoms within morpholine with CH₂ and CH (**26** and **33a**, respectively, Table 1). Of note, the addition of a morpholinobutyl substituent (**39c**) not only appeared to increase affinity 5-fold but also appeared to cause an apparent decrease in negative cooperativity such that this compound was only able to partially inhibit the binding of [³H]raclopride ($\alpha = 0.09$). Interestingly, while incorporation of piperidine **26** saw no changes in affinity, the tetrahydropyran analogue **33a** lost affinity and apparent negative cooperativity with [³H]raclopride as the highest concentration of **33a** only partially displaced the radioligand from the receptor ($K_B = 100 \mu\text{M}$, $\alpha = 0.39$) (Table 1, Figure 4A). Similarly, removal of the morpholinomethyl moiety **23a** did not affect binding affinity despite having effects on negative cooperativity with only partial displacement of the radioligand again observed ($K_B = 31 \mu\text{M}$, $\alpha = 0.39$) (Table 1, Figure 4A). In summary, the removal of the

morpholinomethyl moiety or incorporation of *N,N*-diethylamino, tetrahydropyranomethyl, and morpholinobutyl functionalities yielded ligands that exhibited incomplete displacement of [³H]raclopride, suggesting that these functionalities were important determinants of cooperativity (compounds **23a**, **19**, **33a**, and **39c**, respectively). Accordingly, analogues were synthesized integrating these changes with additional structural changes (Table 1). We synthesized four analogues combining the incorporation of the *N,N*-diethylamino moiety into these novel analogues of **1**, including **23b** (morpholinomethyl deletion), **33b** (tetrahydropyranomethyl), **40** (morpholinobutyl), and (**44**) (fused cyclohexane deletion). In addition to these modifications, we wanted to examine the effects of bis-functionalization with respect to incorporating *m*-trifluoromethylaniline or *N,N*-diethylamine. We synthesized two compounds devoid of the fused cyclohexane system and morpholinomethyl moieties but maintained substitution with

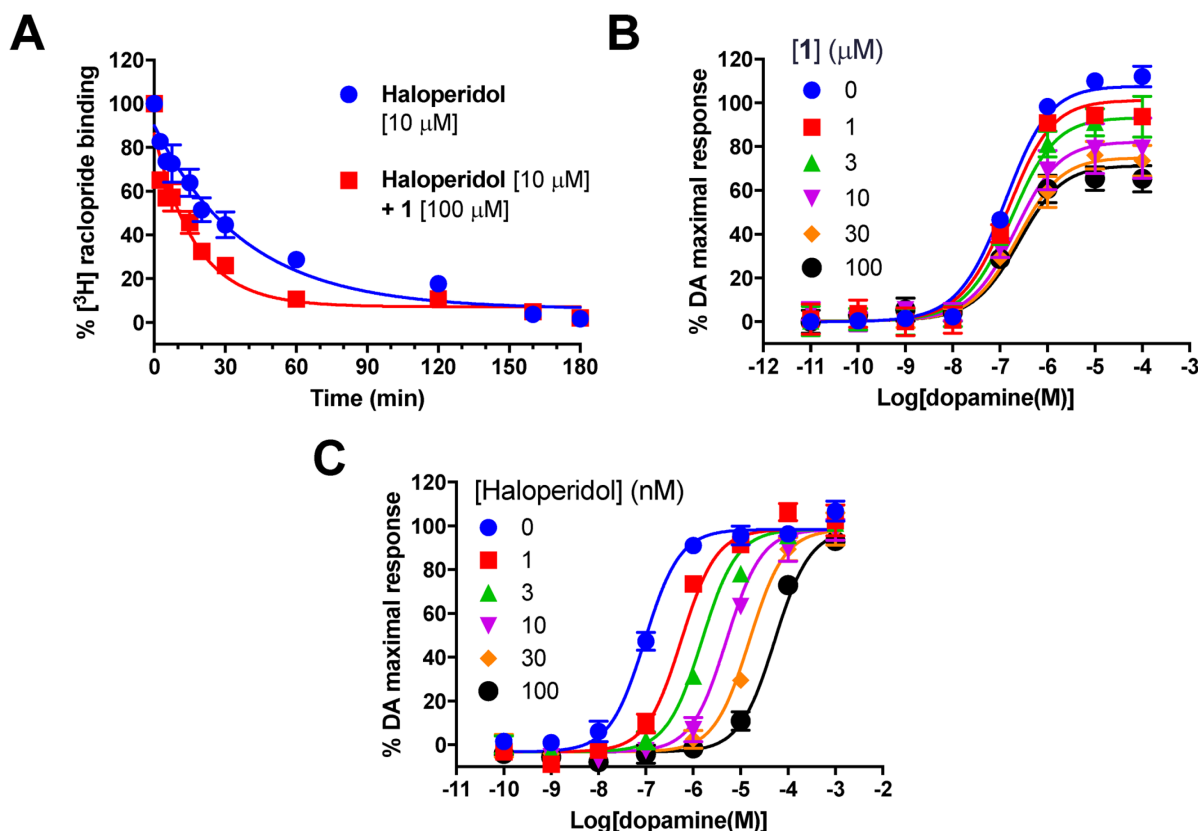


Figure 3. Compound **1** displays allosteric pharmacology at the D₂R. (A) **1** acts to increase the rate of dissociation of [³H]raclopride from the hD₂R expressed in FlpIN CHO membranes consistent with an allosteric mode of action (Table 2). (B) In an assay measuring inhibition of forskolin-stimulated cAMP production using a BRET biosensor, **1** acts to cause limited depression in the maximal response of dopamine with more modest effects upon dopamine potency (these data were fitted with an operational model of allostery to derive values of affinity and cooperativity, Table 4). In contrast increasing concentrations of haloperidol (C) causes a limitless dextral shift in dopamine potency with no effect on dopamine maximal response consistent with competitive antagonism and can be fit with a Gaddum–Schild model to derive a value of affinity pA₂ = 9.67 ± 0.10. Data are the mean ± SEM of three independent experiments performed in duplicate.

Table 2. Compounds 1 and 19 Act To Increase the Rate of [³H]Raclopride Dissociation from Membrane Homogenates of FlpIn CHO Cells Stably Expressing the D₂R^a

	<i>k</i> _{off} (min ⁻¹)		<i>t</i> _{1/2} (min)	
	haloperidol	haloperidol + modulator	haloperidol	haloperidol + modulator
1	0.020 ± 0.004	0.038 ± 0.005*	34.2	18.1
19	0.014 ± 0.001	0.038 ± 0.003*	49.2	18.2

^aValues represent the mean ± SEM from at least three independent experiments performed in quadruplicate. *Analysis with a Student's *t*-test revealed that [³H]raclopride displayed a significantly higher (*p* < 0.05) *k*_{off} in the presence of haloperidol plus modulator as compared to haloperidol alone.

one of either *m*-trifluoromethylaniline or *N,N*-diethylamine to reveal fragment-like low molecular weight analogues (**47a** and **47b**, respectively). While both maintained affinity at the D₂R, the latter compound was only able to partially displace [³H]raclopride and a value of $\alpha = 0.10$ could be determined reflecting moderate negative cooperativity. Excitingly, our finding that **47a** and **47b** are analogues both devoid of the fused system and morpholinomethyl moieties that maintain affinity indicates that the scaffold of **1** can be “pruned back” to reveal modulators of the D₂R with low molecular weights and high ligand efficiencies. A further two

compounds were synthesized that comprised the morpholinobutyl moiety but were devoid of the fused cyclohexane system and were substituted with either *m*-trifluoromethylaniline or *N,N*-diethylamine (**43a** and **43b**, respectively). Affinity was maintained for these analogues showing that the fused cyclohexane may be removed from the scaffold without detriment. It is interesting to note that **44** displayed 100-fold improved affinity ($K_B = 1 \mu\text{M}$) from its parent analogue **14j** ($K_B = 120 \mu\text{M}$), demonstrating the *N,N*-diethylamino substituent is favorable over the *m*-trifluoromethyl substituted aryl system. Similarly, upon introduction of this amine to **33a**, compound **33b** gained a 3-fold improvement in affinity ($K_B = 35 \mu\text{M}$) but acted to completely displace [³H]raclopride suggestive of higher negative cooperativity or a competitive mode of interaction. This is consistent with our observation that while **23a** partially displaced [³H]raclopride, compound **23b** was able to completely displace the radioligand. In summary, then, our exploration of the thienopyrimidine scaffold of **1** revealed that a vast array of modifications are tolerated in terms of affinity for the D₂R but that subtle modifications to the 4-position may modulate the degree of negative cooperativity between the allosteric ligand and orthosteric probe [³H]raclopride. As the degree of negative cooperativity on [³H]raclopride binding significantly changed upon *N,N*-diethylamino substitution (**19**), resulting in the incomplete displacement of the radioligand, we sought to obtain

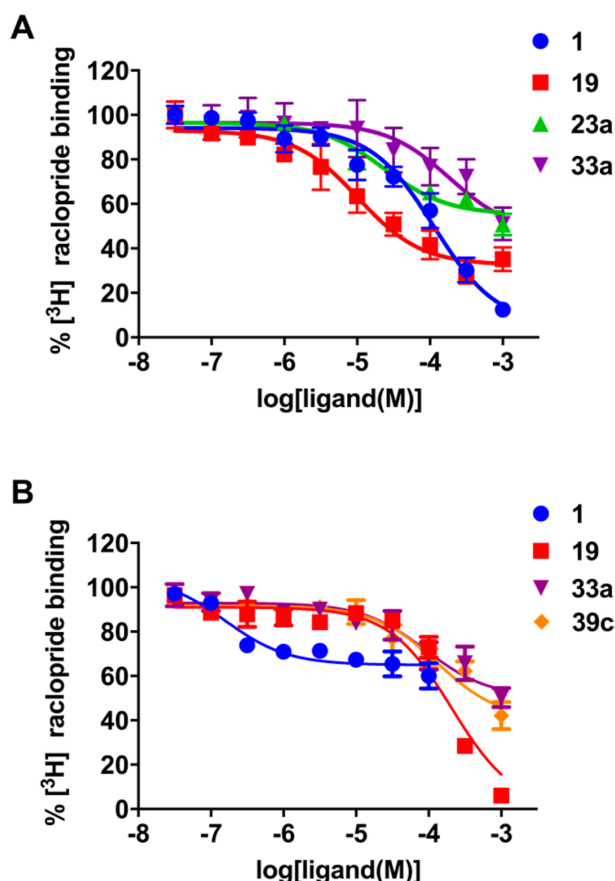


Figure 4. Analogues of **1** act to partially displace orthosteric radioligand binding at the D₂R and D₃R. (A) In equilibrium radioligand binding experiments, **1** acts to completely displace [³H]raclopride from the hD₂L₁R expressed in FlpIN CHO membranes, an effect consistent with a competitive mode of binding or an allosteric mode of binding that exerts high negative cooperativity with [³H]raclopride (Table 1). In contrast compounds **19**, **23a**, and **33a** act to only partially displace [³H]raclopride at the highest concentration consistent with an allosteric mode of action and moderate negative cooperativity (these data were fitted with an allosteric ternary complex model to derive estimates of affinity (K_B) and cooperativity with [³H]raclopride (α), Table 1). (B) **1** acts to partially displace [³H]raclopride from the hD₃R expressed in FlpIN CHO membranes at the highest concentration measured, whereas **19** completely displaces [³H]raclopride from the D₃R (Table 3). Data are the mean \pm SEM of three independent experiments performed in duplicate.

additional confirmation of an allosteric mode of interaction. The profile of **19** was further explored through radioligand binding dissociation kinetic experiments. In the presence of **19**, the dissociation rate of the [³H]raclopride from the D₂R again significantly increased (Table 2). This experiment provided further validation of the allosteric mode of action of **1** and its structural analogues.

Finally, we sought to assess receptor subtype selectivity at the D₃R versus the D₂R; accordingly, equilibrium radioligand binding experiments were conducted on **1** and a further seven structural analogues (**19**, **23a**, **33a**, **39c**, **40c**, **43b**, and **44**, Table 3). Molecules were selected based upon their profiles at the D₂R acquired from [³H]raclopride binding experiments at this receptor, where some showed increased binding affinities and divergent cooperativity profiles. Interestingly, two compounds displayed

selectivity for the D₂R over the D₃R **39c** (30-fold selectivity) and **44** (10-fold selectivity). In contrast, compounds **1**, **19**, and **23a** displayed selectivity toward the D₃R (57-fold, 23-fold, 140-fold, respectively). All other compounds displayed no significant subtype selectivity (**33a**, **40**, **43b**). It is interesting to note that many compounds assayed at the D₃R saw strikingly different levels of negative cooperativity with [³H]raclopride binding compared to that observed at the D₂R (Table 3, Figure 4B). For example, at the D₂R, **19** only partially displaces [³H]raclopride at the highest concentration measured; however, at the D₃R it completely displaces [³H]raclopride at the highest concentration despite having a lower functional binding affinity ($K_B = 89.7 \mu\text{M}$) (Table 3, Figure 4B). As **1** was identified via virtual ligand screening using a D₃R crystal structure, it is unsurprising that **1** displayed subtype selectivity for this receptor. However, our study has identified D₂R-selective compounds that may be used as a starting point for the future development of D₂R subtype-selective ligands.

Functional Analysis (cAMP) of Analogues of 1. We extended our characterization of these compounds to their effect upon dopamine action in the cAMP assay described above. Interestingly, all compounds above were shown to retain activity in our equilibrium radioligand binding experiments, yet many failed to have any effects upon dopamine binding and/or signaling efficacy within the same concentration range. This observation is likely an example of probe dependence whereby these ligands exert negative cooperativity on raclopride binding but display neutral cooperativity upon dopamine binding and efficacy. In agreement with this hypothesis, while our binding assay found that **1** displayed a robust effect upon [³H]raclopride binding, our functional data suggest that **1** acts to modulate dopamine efficacy but has little effect upon dopamine affinity.

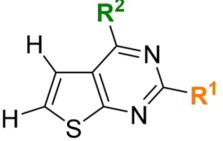
We first examined modifications to the 5,6-fused cyclohexane system of **1** (Table 4). We found that increasing the fused ring size to greater than six carbons renders these analogues inactive in this functional assay (**14b,c**), while the five-membered cyclopentane system (**14a**) maintained functional affinity ($K_B = 11.4 \mu\text{M}$) but changed the nature of the cooperativity whereby we observed a modulatory effect on dopamine affinity ($\alpha = 0.13$) rather than modulation of efficacy ($\beta = 1$). Both 6-phenyl substitution (**14d**) and modifications to the 5-position with phenyl (**14e**) or cyclohexyl (**14g**) substituents resulted in a loss of activity. Activity was maintained for the 6-cyclohexyl substituted analogue (**14i**, $K_B = 5.4 \mu\text{M}$, Figure 5A), but in contrast to the action of **1** that modulates dopamine efficacy, this ligand acted to modulate dopamine affinity only ($\alpha = 0.13$) (Table 4, Figure 5A). 5,6-Dimethyl substitution (**14h**), as well as removal of the fused functionality entirely (**14j**), rendered these analogues inactive in our functional assays, thus indicating a small window in which **1** can be modified surrounding the 5,6-positions and still maintain allosteric pharmacology with dopamine. Removal of the CF₃ substituent on the aryl ring of **1** (**16a**, Table 5) or replacement with 3-F (**16b**), 3-OMe (**16c**), or 3-OH (**17**) had no effect upon functional affinity. However, the addition of methoxy or hydroxy substituents resulted in additional modulatory effects upon dopamine affinity ($\alpha = 0.19$ and $\alpha = 0.06$, respectively).

We then focused on the importance of the aryl ring within **1** by replacing the phenyl ring with acyclic aliphatic amines (Table 6). These analogues still maintained a hydrogen-bond donor-acceptor but lacked the aromatic moiety in this region. The *N*-methylamino analogue (**18**) was inactive, whereas the *N,N*-diethylamino analogue (**19**) saw a 6-fold increase in functional affinity and a 4-fold increase in negative cooperativity with dopamine efficacy

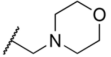
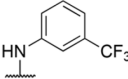
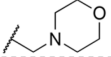
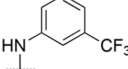
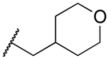
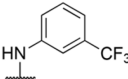
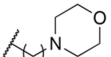
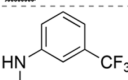
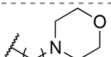
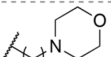
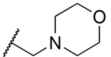
Table 3. Ability of **1** and Derivatives of **1** To Displace the Radiolabeled Antagonist [³H]Raclopride at the D₂R eExpressed in FlpIn CHO Cells



1, 19, 23a, 33a, 39c, 40c



43b, 44

	R ¹	R ²	^a pK _B (K _B , μM)	D ₂ /D ₃ selectivity	^b log α (α)
1			6.54 ± 0.27 (0.3)	57	-0.40 ± 0.04 (0.39)
19		N(CH ₂ CH ₃) ₂	3.85 ± 0.16 (140)	23	-
23a	H		6.65 ± 0.21 (0.2)	140	-0.39 ± 0.03 (0.06)
33a			4.28 ± 0.23 (52)	2	-0.44 ± 0.23 (0.37)
39c			3.97 ± 0.18 (106)	0.03	-0.69 ± 0.20 (0.20)
40		N(CH ₂ CH ₃) ₂	4.99 ± 0.05 (10)	1.6	-
43b		N(CH ₂ CH ₃) ₂	6.06 ± 0.03 (0.9)	3.5	-
44		N(CH ₂ CH ₃) ₂	4.95 ± 0.06 (11)	0.1	-

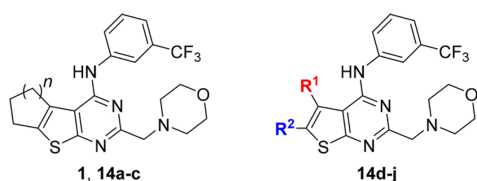
^aEstimate of the negative logarithm of the equilibrium dissociation constant ± SEM determined by radioligand binding. ^bEstimate of the logarithm of the net cooperativity factor between the modulator and [³H]raclopride. Values represent the mean ± SEM from at least three independent experiments performed in duplicate.

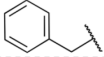
(K_B = 660 nM, β = 0.08, Figure 5B). To further probe the effects of this substituent, we tested an additional analogue of **19** in which the fused cyclohexane system was removed entirely while maintaining the *N,N*-diethyl functionality (**44**). While the analogue bearing no substitution at the 5- and 6-position (**14j**) displayed no activity in this functional assay, to our surprise compound **44** maintained affinity (K_B = 3 μM) as well as robust negative cooperativity with dopamine affinity and efficacy (α = 0.08, β = 0.24). Interestingly, due to the presence of the *N,N*-dimethylamino functionality, 6-benzyl substitution (**15**) no longer rendered the molecule inactive, as seen previously with **14f** (Table 4), but instead caused affinity and negative allosteric cooperativity to be maintained (Table 6). Together, these data demonstrate that the nature of the 4-substituent (aromatic or acyclic aliphatic amine) has significant effects upon negative cooperativity with dopamine. Isosteric replacement of the secondary amine with an ether (**20**, Table 6) did not affect affinity in our binding assay; moreover this compound showed no activity in the functional assay highlighting the importance of the secondary amine contained within **1** and the potential requirement of a hydrogen-bond donor-acceptor at the 4-position for cooperativity with dopamine.

Our binding experiments revealed that modifications at the 2-position of the thienopyrimidine can influence the degree of

negative cooperativity between the modulator and [³H]raclopride. Therefore, we examined the functional impact of removing the morpholinomethyl moiety with respect to varying substituents at the 4-position. Maintaining the *m*-(trifluoromethyl)anilino substituent (**23a**) did not affect functional affinity but resulted in a 3-fold increase in the modulatory effect upon dopamine efficacy (β = 0.10, Table 7). The *N,N*-diethylamino substituent (**23b**) not only maintained functional affinity (K_B = 1 μM) but gave rise to almost complete attenuation of dopamine signaling at a concentration of 10 μM indicative of a very high negative modulatory effect upon dopamine efficacy (Figure 5C, Table 7). Interestingly, the pyrimidinone analogue (**21**) was inactive and is in agreement with our finding that the secondary amine is a key structural determinant of cooperativity.

We next focused on the nonfunctionalized methylene spacer group within **1** and the importance of linker length (Table 7). Increasing linker length by one carbon atom had no effect on affinity; however the nature of allostery was altered as **39a** modulated dopamine affinity with little effect upon dopamine efficacy (α = 0.23). Further extension of linker length by one carbon **39b** engendered an additional modulatory effect upon dopamine efficacy (K_B = 1.39 μM, α = 0.21, β = 0.40). Moreover, further extension of the linker **39c** was observed to not only increase functional affinity (K_B = 611 nM) but also increase

Table 4. Functional Parameters for Analogues of **1** with Chemical Modifications to the 5,6-Fused System Derived from cAMP BRET Assay


	<i>n</i>	R ¹	R ²	^a p <i>K</i> _B (<i>K</i> _B , μM)	^b Log <i>a</i> (<i>a</i>)	^c Log β (<i>β</i>)
1	2	-	-	5.41 ± 0.22 (3.87)	= 0	-0.55 ± 0.08 (0.28)
14a	1	-	-	4.95 ± 0.40 (11.4)	-0.90 ± 0.32 (0.13)	= 0
14b	3	-	-		nd	
14c	4	-	-		nd	
14d	-	H			nd	
14e	-		H		nd	
14f	-	H			nd	
14g	-		H		nd	
14h	-	CH ₃	CH ₃		nd	
14i	-	H		5.27 ± 0.17 (5.37)	-0.90 ± 0.11 (0.13)	= 0
14j	-	H	H		nd	

^aEstimate of the negative logarithm of the equilibrium dissociation constant determined in a cAMP functional assay. ^bEstimate of the logarithm of the net cooperativity factor between the modulator and dopamine. ^cEstimate of the logarithm of the modulatory effect upon efficacy factor induced by the allosteric modulator. nd = inactive at concentrations up to 100 μM. Values represent the mean ± SEM from at least three independent experiments performed in duplicate.

negative cooperativity with dopamine efficacy ($\beta = 0.03$). The addition of the *N,N*-diethylamino substituent (**40**) resulted in a similar affinity as determined for **39c** but displayed pharmacology best fit with a competitive model (Table 7).

Interestingly, isosteric replacement of the morpholino nitrogen with a methine group (**33a**) caused a 10-fold increase in functional affinity ($K_B = 622$ nM), as well as enhancing the negative allosteric modulatory effect upon dopamine efficacy ($\beta = 0.13$). This finding suggests that the ionizable nitrogen within **1** is not a structural requirement to maintain modulatory activity at the D₂R. However, the *N,N*-diethylamino substitution (**33b**) was not tolerated in conjunction with the tetrahydropyran as the compound was inactive in this functional assay. Isosteric replacement of the morpholino oxygen for a methylene group via the incorporation of piperidine (**26**) maintained functional affinity ($K_B = 6.52$ μM) but saw a reduction in negative allosteric cooperativity ($\alpha = 0.49$, $\beta = 0.68$) compared to **33a**.

We also investigated the impact of bis-functionalization of **1** with respect to incorporating various amines at the 4-position of **1** in this functional assay (Table 8). Two analogues of **1** that incorporate the morpholinobutyl substituent, in conjunction with removal of the fused cyclohexane system, together with one of either *m*-CF₃-anilino (**43a**) or *N,N*-diethylamino substituents

(**43b**) maintained functional affinity ($K_B = 1.3$ μM and 1.4 μM, respectively) comparable to **1** but now displayed a higher level of negative cooperativity with both dopamine affinity and efficacy (Table 8). These data further indicate that linker length extension of the morpholine moiety acts to increase negative cooperativity with dopamine.

In agreement with our binding data, analogues of **1** devoid of both the morpholinomethyl and fused cyclohexane moieties but incorporating one of either *m*-(trifluoromethyl)aniline (**47a**) or *N,N*-diethylamine (**47b**, Figure 5D) maintained functional affinity and displayed robust negative cooperativity with dopamine efficacy and affinity despite the lack of a substituent at the 2-position or the presence of the fused cyclohexane system ($K_B = 1.3$ μM, $\alpha = 0.05$, $\beta = 0.15$ and $K_B = 1.4$ μM, $\alpha = 0.13$, $\beta = 0.06$, respectively, Table 8). These data demonstrate the utility of the thieno[2,3-*d*]pyrimidine scaffold as a NAM of the dopamine effect as “pruned back” analogues maintain negative allosteric cooperativity while preserving functional affinity relative to **1**. Through successive compound iterations, both the lipophilic ligand efficiency (LLE) and ligand efficiency (LE) of the scaffold have been enhanced significantly compared to that of **1**, with the most efficient compound being **47b** (Figure 6, LLE = 2.48, LE = 0.54). This reveals the versatility of the scaffold for further

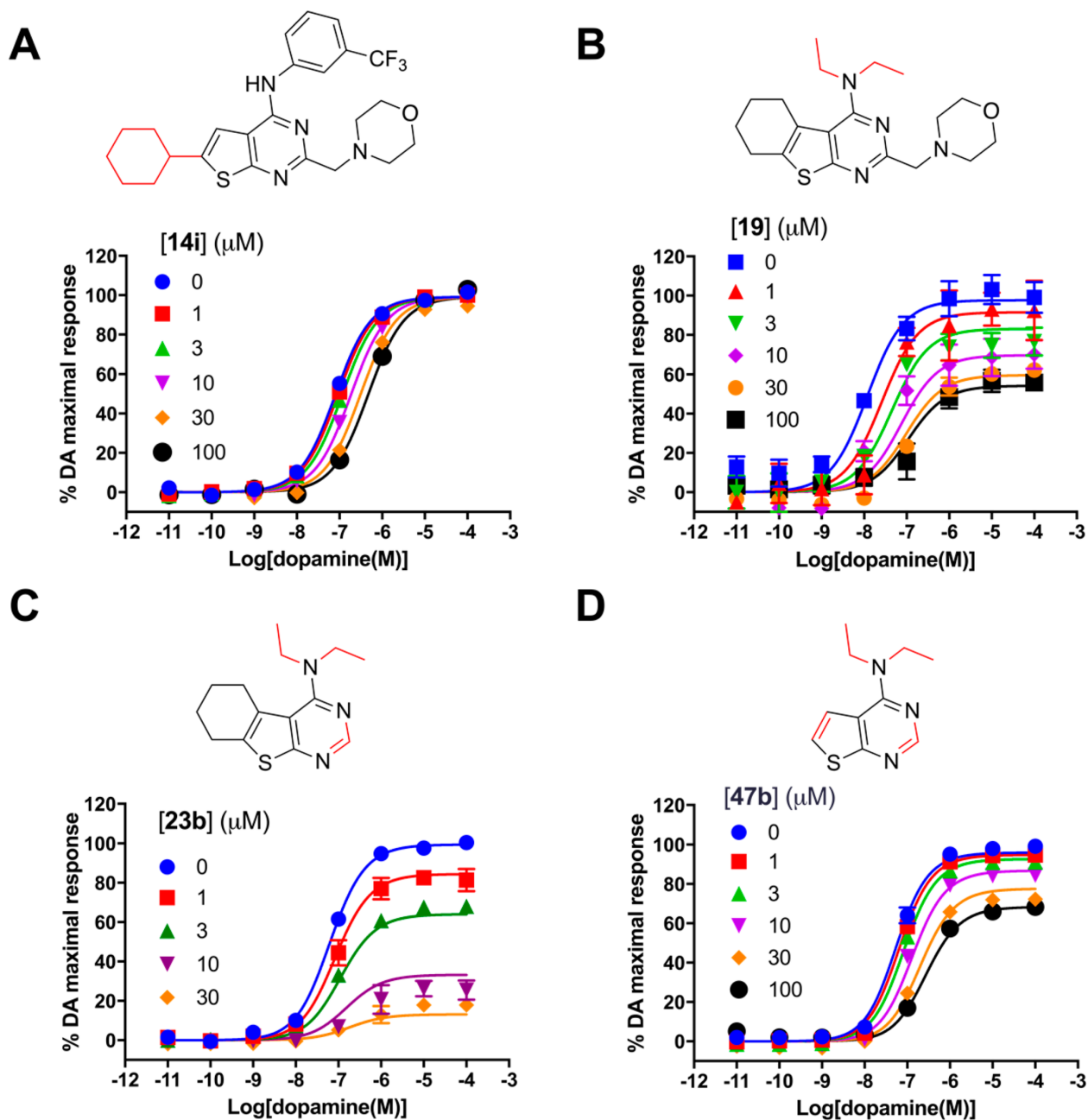
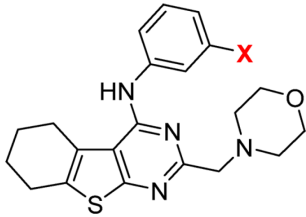


Figure 5. Exploration of the thieno[2,3-d]pyrimidine scaffold of **1** reveals small molecule modulators of the D₂L R with distinct functional effects. (A) Modification of the 5,6-fused system in the form of a 6-cyclohexane substitution (**14i**, Table 4) resulted in negative cooperativity upon dopamine affinity with no effect upon dopamine efficacy (B). Replacement of the phenyl ring of **1** with *N,N*-diethyl (**19**, Table 6) caused a 6-fold increase in affinity and 4-fold increase in negative cooperativity with dopamine. (C) Removal of the morpholinomethyl moiety along with incorporation of the *N,N*-diethylamino substitution (**23b**, Table 7) maintained affinity but resulted in a large increase in negative cooperativity with dopamine efficacy. (D) Remarkably, a fragment-like derivative devoid of both the morpholinomethyl and fused cyclohexane moieties but incorporating the *N,N*-diethylamino substitution (**47b**, Table 8) maintained functional affinity and displayed robust negative cooperativity with dopamine efficacy. All data are the mean \pm SEM of three independent experiments performed in duplicate. Data were fit using the operational model of allosterism to derive estimates of affinity and cooperativity with dopamine.

structural optimization and development of ligands that non-competitively modulate dopamine affinity and signaling efficacy at the D₂R. Collectively, these results demonstrate that analogues of **1** mediate their effects through an allosteric mode of action. While we were able to gain only relatively modest (10-fold) improvement in affinity, our SAR study revealed compounds with a range of modulatory effects upon dopamine efficacy and/or affinity.

Molecular Docking Studies. The recently solved structure of D₂R receptor (PDB code 6C38)³² provides an opportunity to accurately model the allosteric binding of compound **1** and a library of structurally diverse analogues. Specifically, we were interested in the interactions of these allosteric compounds with the orthosteric ligand, as reflected in the [³H]raclopride equilibrium binding assays (Table 1). While the D₂R structure

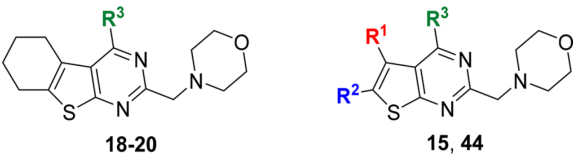
Table 5. Functional Parameters for Analogues of 1 with Modifications to Aryl Moiety

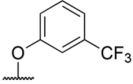


	X	pK _B (K _B , μM) ^a	log α (α) ^b	log β (β) ^c
1	CF ₃	5.41 ± 0.22 (3.87)	0	-0.55 ± 0.08 (0.28)
16a	H	5.13 ± 0.31 (7.46)	0	-0.95 ± 0.24 (0.11)
16b	F	5.08 ± 0.44 (8.39)	0	-0.40 ± 0.11 (0.40)
16c	OMe	5.10 ± 0.13 (8.02)	-0.73 ± 0.16 (0.19)	-0.53 ± 0.14 (0.29)
17	OH	5.55 ± 0.12 (2.81)	-1.22 ± 0.16 (0.06)	-3.0

^aEstimate of the negative logarithm of the equilibrium dissociation constant determined in a cAMP functional assay. ^bEstimate of the logarithm of the net cooperativity factor between the modulator and dopamine. ^cEstimate of the logarithm of the modulatory effect upon efficacy factor induced by the allosteric modulator. nd = inactive at concentrations up to 100 μM. Values represent the mean ± SEM from at least three independent experiments performed in duplicate.

Table 6. Functional Parameters for Analogues of 1 with Chemical Modifications to the 4-Position and 5,6-Fused System Derived from cAMP BRET Assay



	R ¹	R ²	R ³	^a pK _B (K _B , μM)	^b Log α (α)	^c Log β (β)
15	H		N(CH ₃) ₂	5.31 ± 0.15 (4.90)	-0.17 ± 0.14 (0.68)	-0.84 ± 0.10 (0.15)
18	-	-	NHCH ₃		nd	
19	-	-	N(CH ₂ CH ₃) ₂	6.18 ± 0.16 (0.662)	-0.17 ± 0.17 (0.68)	-1.10 ± 0.10 (0.08)
20	-	-			nd	
44	H	H	N(CH ₂ CH ₃) ₂	5.50 ± 0.10 (3.13)	-1.10 ± 0.16 (0.08)	-0.62 ± 0.15 (0.24)

^aEstimate of the negative logarithm of the equilibrium dissociation constant determined in a cAMP functional assay. ^bEstimate of the logarithm of the net cooperativity factor between the modulator and dopamine. ^cEstimate of the logarithm of the modulatory effect upon efficacy factor induced by the allosteric modulator. nd = inactive at concentrations up to 100 μM. Values represent the mean ± SEM from at least three independent experiments performed in duplicate.

was solved with the atypical antipsychotic drug risperidone, we first generated a conformational model of raclopride bound to the D₂R (D₂R^{Raclo}). Flexible docking of raclopride shows a pose similar to the pose of eticlopride found in the D₃R structure.⁹ Both raclopride and eticlopride are known to bind to the orthosteric pocket of the D₂R commonly occupied by dopamine; however, since it is bulkier than dopamine, the allosteric pocket in the D₂R^{Raclo} complex is shallower, as compared to the D₂R^{Dopa} complex.

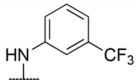
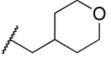
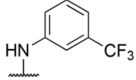
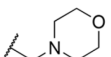
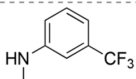
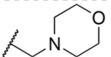
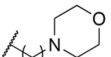
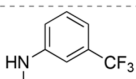
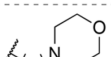
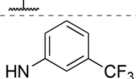
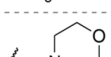
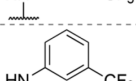
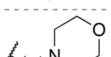
Docking of compound 1 in the D₂R^{Raclo} complex consistently yielded the best scoring pose shown in Figure 7. This pose is stabilized by a hydrogen bond between the ionized morpholine secondary amine and the oxygen atom of the side chain of S409^{7,36} (Ballesteros-Wenstein nomenclature³³), as well π-π stacking interactions of the thienopyrimidine moiety with Y408^{7,35} and

W100^{ECL1} side chains. In addition, the fused cyclohexane ring system is positioned in the hydrophobic subpocket located between helices V and VI formed by the residues I184ECL2, V190^{5,39}, H394^{6,55}, whereas the phenyl ring bearing the *m*-CF₃ substituent is placed between helices VI and VII, and ECL3 and is lined by the residues N396^{6,58}, N402^{ECL3}, P405^{7,32}, and Y408^{7,35} (Figure 7).

The key SAR data support the consistent binding pose of compound 1 and its analogues as illustrated in Figure 8 and Supporting Information Figure 2. First, we examined modifications to the fused cyclohexane system of 1 (14a-j). Most analogues bind in a similar mode, maintaining the key interactions of the scaffold (Supporting Information Figure 2A). At the same time, the docking illustrates a modest binding dependence on the size of this fused hydrophobic ring, as replacement of the

Table 7. Functional Parameters for Analogues of 1 with Chemical Modifications to the 2-Position Derived from cAMP BRET Assay



	R ¹	R ²	^a pK _B (K _B , μM)	^b Log α (α)	^c Log β (β)
21	H	OH		nd	
23a	H		4.60 ± 0.17 (25.4)	= 0	-1.02 ± 0.35 (0.10)
23b	H	N(CH ₂ CH ₃) ₂	5.72 ± 0.13 (1.92)	= 0	= -3.0
26			-5.16 ± 0.13 (6.98)	-0.46 ± 0.12 (0.34)	-0.22 ± 0.08 (0.60)
33a			6.22 ± 0.26 (0.622)	-0.89 ± 0.29 (0.13)	-0.63 ± 0.19 (0.23)
33b		N(CH ₂ CH ₃) ₂		nd	
39a			6.01 ± 0.17 (0.981)	-0.63 ± 0.05 (0.23)	= 0
39b			5.79 ± 0.11 (1.63)	-0.68 ± 0.12 (0.21)	-0.40 ± 0.08 (0.40)
39c			6.21 ± 0.11 (0.611)	-0.72 ± 0.18 (0.19)	-1.50 ± 0.15 (0.03)
40		N(CH ₂ CH ₃) ₂	5.80 ± 0.20 (1.77)	Schild Slope: 1.07 ± 0.11	

^aEstimate of the negative logarithm of the equilibrium dissociation constant ± SEM determined in an cAMP functional assay. ^bEstimate of the logarithm of the net cooperativity factor between the modulator and dopamine ± SEM determined in an cAMP functional assay. nd = inactive at concentrations up to 100 μM. Values represent the mean ± SEM from at least three independent experiments performed in duplicate.

cyclohexane with either cyclopentane (14a) or cycloheptane (14b) would make less favorable hydrophobic interactions, reducing allosteric binding affinity by approximately 2- to 4-fold (Figure 8A). Moreover, compounds that lack the fused ring system (14h,j) showed an even more pronounced decrease in binding, consistent with loss of interactions with this hydrophobic subpocket (Figure 8B).

Next, we examined compounds with variations to in the *m*-CF₃ substituent (16a–c, 17) positioned between helices VI and VII, and ECL3, but exposed to solvent. As the CF₃ substituent is favorable for solvent interactions, its removal in 16a explains the observed 6-fold decrease in binding for this compound. The reduction is much smaller for derivatives that have polar substituents in this position, 3-OH (17) and 3-OMe (16c) (Supporting Information Figure 2B).

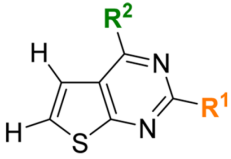
Next, we examined compounds with variations in *N*-(3-trifluoromethyl)phenylamino substituent (15, 18, 19). The docking poses place *N,N*-dimethylamino (15), *N*-methylamino (18), and *N,N*-diethylamino moieties (19) into the hydrophobic subpocket in the proximity of Y408^{7,35} and W100^{ECL1}, with 19 having the most extensive hydrophobic contacts. This is in agreement with an improved binding affinity for 19

(Supporting Information Figure 2C). The secondary amine of compound 1 is not engaged in any interactions, and its isosteric replacement to an ether (20) did not impact the predicted binding mode (Supporting Information Figure 2D) or its binding affinity (Table 1).

Interestingly, removal of the morpholinomethyl moiety (23a) maintained the π - π stacking interactions of the thienopyrimidine moiety with the Y408^{7,35} and W100^{ECL1}, though slightly shifting the scaffold, enabling an additional hydrogen bond interaction with T412^{7,39}. We hypothesize that though loss of the morpholine system abolished the interaction with the S409^{7,36} (Figure 8C), the new hydrogen bond at least partially compensated the loss, maintaining binding affinity of this analogue (Table 1). However, replacing morpholine with piperidine (26) leads to 2.5-fold decrease in affinity, reflecting replacement of a polar oxygen with a carbon in this solvent-exposed position (Supporting Information Figure 2E).

Moreover, removal of the tertiary amine in the morpholine ring abolishes the hydrogen bond interaction of 33a with S409^{7,36} (Figure 8D), with the importance of this hydrogen bond corroborated by a ~7-fold decrease in affinity for this compound (Table 1).

Table 8. Functional Parameters for Analogues of 1 with Bifunctionalization in Conjunction with Aromatic or Aliphatic 4-Substituted Amine



	R ¹	R ²	^a p <i>K</i> _B (<i>K</i> _B , μM)	^b Log α (α)	^c Log β (β)
43a			5.85 ± 0.10 (1.4)	-0.88 ± 0.16 (0.13)	-1.21 ± 0.16 (0.06)
43b		N(CH ₂ CH ₃) ₂	5.89 ± 0.09 (1.3)	-1.34 ± 0.21 (0.05)	-0.82 ± 0.18 (0.15)
47a	H		6.13 ± 0.21 (0.8)	-0.43 ± 0.06 (0.37)	= 0
47b	H	N(CH ₂ CH ₃) ₂	5.31 ± 0.07 (4.6)	= 0	-0.89 ± 0.04 (0.13)

^aEstimate of the negative logarithm of the equilibrium dissociation constant determined in a cAMP functional assay. ^bEstimate of the logarithm of the net cooperativity factor between the modulator and dopamine. ^cEstimate of the logarithm of the modulatory effect upon efficacy factor induced by the allosteric modulator. Values represent the mean ± SEM from at least three independent experiments performed in duplicate.

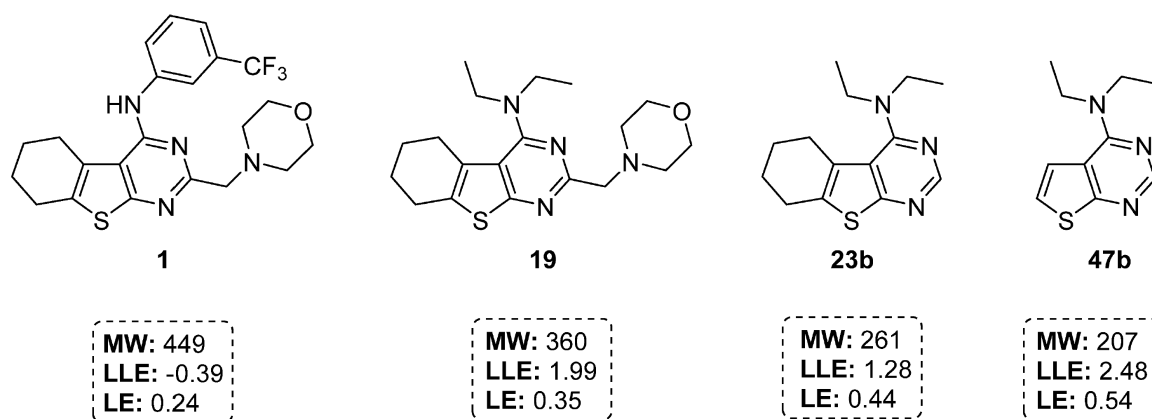


Figure 6. Lipophilic ligand efficiencies (LLE) and ligand efficiencies (LE) of 1, 19, 23b, and 47b calculated according to equilibrium dissociation constants derived from functional interaction experiments measuring cAMP accumulation. Multiple compound iterations have yielded improvements in the scaffold's efficiency through decreased molecular weight and functional binding affinity. This is particularly evident with compound 47b as it shows a marked improvement in both LLE and LE compared to that of 1, resulting in a promising fragment-like starting scaffold that can be elaborated through multiple vectors.

Furthermore, we evaluated the effect of elongating the methylene linker to the morpholine substituent (39a–c). In our model, increasing the linker length did not hinder the ability of the compounds to maintain crucial interactions, and even helped to improve complementarity of 39c with the binding pocket, in accordance with its improved affinity (Figure 8E).

Other docked analogues, characterized by morpholinomethyl deletion (23b), tetrahydropyranomethyl (33b), morpholinobutyl (40), and fused cyclohexane deletion (44), also maintained the crucial π – π stacking interactions with Y408^{ECL1} and W100^{ECL1} (Supporting Information Figure 2F). Similar poses were obtained for the two compounds 43a,b, comprising the morpholinobutyl moiety and four carbon linker but devoid of the fused cyclohexane system (Supporting Information Figure 2G).

Finally, we docked compounds devoid of the fused cyclohexane system and morpholinomethyl moieties but maintained

substitution with one of either *m*-trifluoromethylanilino or *N*,*N*-diethylamino (47a,b). This dramatically reduced the size of the scaffold but also maintained π – π stacking interactions with Y408^{ECL1} and W100^{ECL1} while shifting to gain a hydrogen bond interaction with T412^{ECL1} (Figure 8F), which is in agreement with only a minor loss of binding affinity (Table 1).

CONCLUSIONS

In this study, we report the pharmacological validation of a VLS hit, confirming it exerts its effect via an allosteric mode of action at the D₂R, as predicted by our initial modeling studies. We subsequently describe the design and characterization of a structurally novel series of dopamine D₂R NAMs based on this thieno[2,3-*d*]pyrimidine scaffold, demonstrating its scope for future development of D₂R NAMs. The impact of structural modification was assessed with respect to thienopyrimidine

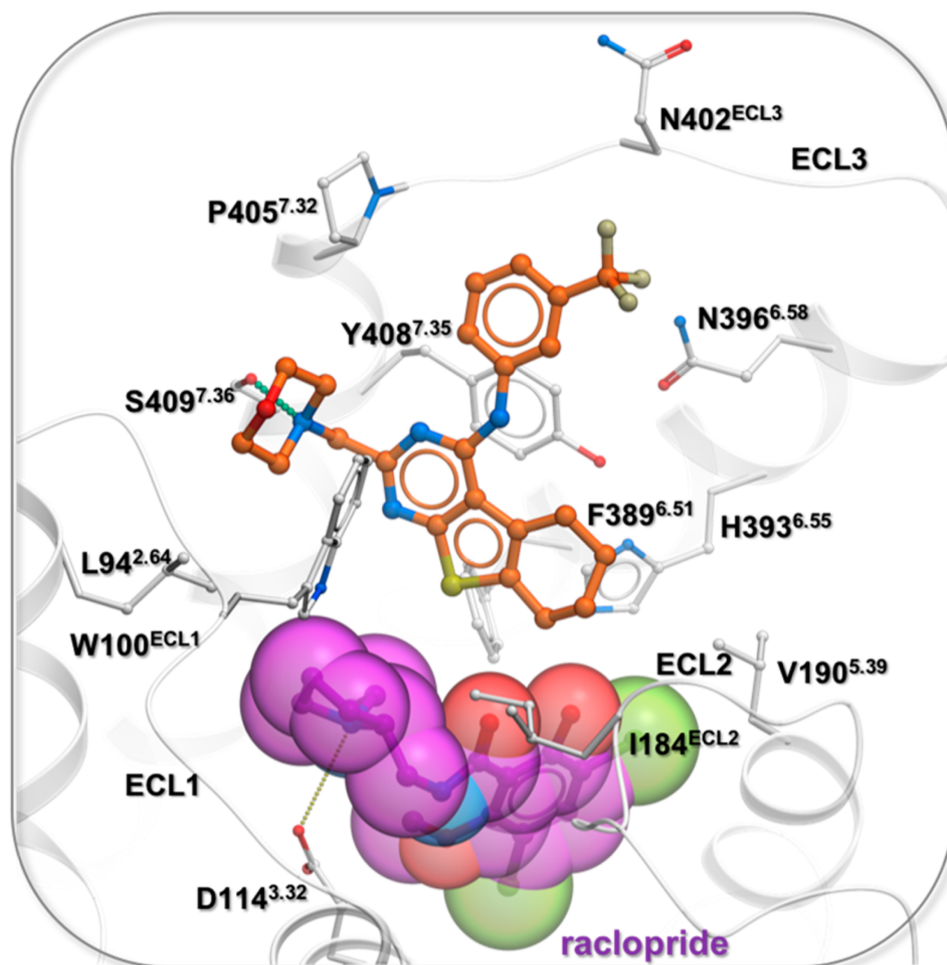


Figure 7. Compound **1** (orange carbon atoms) predicted binding mode in D₂R complex with raclopride. The D₂R^{Raclo} conformational model is based on raclopride (magenta carbon atoms) flexible docking into D₂R structure (PDB code 6C38) shown in light gray cartoon and stick presentation.

substituents (2-, 4-, 5-, and 6-positions), isosteric replacement of the aniline nitrogen with respect to hydrogen bonding, as well as the importance of bearing an ionizable nitrogen at differing linker lengths on the 2-substituent and its subsequent impact on the allosteric pharmacology of **1**. The majority of active compounds displayed comparable binding affinities to that of **1**. Rather, the structural modifications within this study had a profound effect upon the extent of modulation of dopamine binding and/or efficacy. Indeed, while **1** exerted its effect predominantly via negative modulation of dopamine efficacy, we identified analogues of **1** that displayed modulatory effects upon dopamine affinity (e.g., **14a**, **14i**, **39a**), and those that displayed modulatory effects upon both dopamine affinity and efficacy (e.g., **17**, **19**, **43a**). Maintaining a hydrogen-bond donor (secondary amine) at the 4-position was found to be a requirement for cooperativity with dopamine, as thienopyrimidinone analogues were inactive in our functional assay. Moreover, the ether analogue of **1** (**20**) was also inactive in our functional assay, suggesting this modification is not well tolerated. Most significantly, we show that this scaffold can be effectively “pruned back” of morpholinomethyl and fused cyclohexane moieties to reveal a low molecular weight fragment-like core with low μM functional affinity and very high lipophilic ligand efficiency (**47a,b**). Our molecular docking studies, using

the recently determined crystal structure as a template, provide some insight into the molecular determinants of this SAR. Thus, this minimal thieno[2,3-*d*]pyrimidine scaffold provides an attractive starting point for further structural interrogation and elaboration of the core scaffold to achieve high affinity, low molecular weight NAMs of the D₂R with varying effects upon dopamine binding and/or function.

■ EXPERIMENTAL SECTION

Chemistry: General Information and Synthetic Procedures.

Chemicals and solvents were purchased from standard suppliers and used without further purification. Davisil silica gel (40–63 μm) for flash column chromatography was supplied by Grace Davison Discovery Sciences (Victoria, Australia), and deuterated solvents were purchased from Cambridge Isotope Laboratories, Inc. (USA, distributed by Novachem PTY. Ltd., Victoria, Australia). Reactions were monitored by thin layer chromatography on commercially available precoated aluminum-backed plates (Merck Kieselgel 60 F₂₅₄). Visualization was by examination under UV light (254 and 366 nm). A solution of ninhydrin (in ethanol) was used to visualize primary and secondary amines. All organic extracts collected after aqueous workup procedures were dried over anhydrous MgSO₄ or Na₂SO₄ before gravity/vacuum filtering and evaporation to dryness. Organic solvents were evaporated in vacuo at ≤ 40 °C (water bath temperature). ¹H NMR and ¹³C NMR

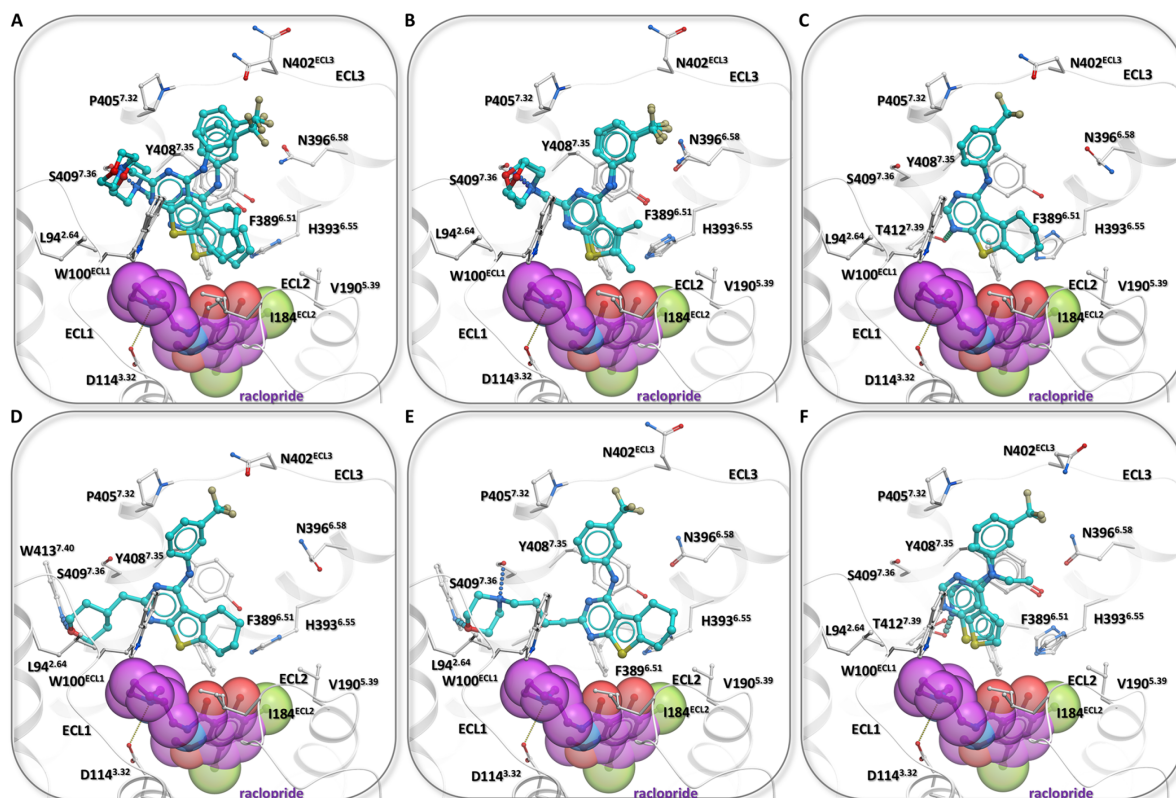


Figure 8. Compound 1 analogues (cyan carbon atoms) in complex with D₂R^{Raclo} (based on PDB code 6C38). Compounds with variation in the fused cyclohexane system: (A) compounds 14a,c. (B) Compounds 14h,j. (C) Compound devoid of morpholinomethyl moiety (23a). (D) Compound with tetrahydropyran moiety (33a). (E) Compounds with variations in alkyl linker length to the morpholine motif (39c). (F) Fragment-like compounds (47a,b).

spectra were recorded on a Bruker Avance Nanobay III 400 MHz Ultrashield Plus spectrometer at 400.13 and 100.62 MHz, respectively. Chemical shifts (δ) are recorded in parts per million (ppm) with reference to the chemical shift of the deuterated solvent. Coupling constants (J) are recorded in Hz, and the significant multiplicities are described by singlet (s), doublet (d), triplet (t), quadruplet (q), broad (br), multiplet (m), doublet of doublets (dd), and doublet of triplets (dt). Spectra were assigned using appropriate COSY, distortionless enhanced polarization transfer (DEPT), HSQC, and HMBSC sequences. LC-MS experiments were run to verify reaction outcome and purity using an Agilent 6120 series single quad coupled to an Agilent 1260 series HPLC. The following buffers were used: buffer A, 0.1% formic acid in buffer B, 0.1% formic acid in MeCN. The following gradient was used with a Poroshell 120 EC-C18 50 mm \times 3.0 mm, 2.7 μ m column and a flow rate of 0.5 mL/min and total run time of 5 min; 0–1 min 95% buffer A and 5% buffer B, from 1 to 2.5 min up to 0% buffer A and 100% buffer B, held at this composition until 3.8 min, 3.8–4 min 95% buffer A and 5% buffer B, held until 5 min at this composition. Mass spectra were acquired in positive and negative ion mode with a scan range of 100–1000 m/z . UV detection was carried out at 214 and 254 nm. All retention times (t_R) are quoted in minutes. All screening compounds were of >95% purity unless specified in the individual monologue. All NMR experiments were performed in CDCl₃ to permit comparison of the spectra of the various analogues. Experiments were performed in acetone-*d*₆, DMSO-*d*₆, or MeOH-*d*₄ if selected analogues lacked solubility in CDCl₃.

General Procedure A for the Gewald Synthesis of 2-Amino-3-carbomethoxythiophenes 5, 10a–c. To a stirred solution of ethyl cyanoacetate (1 equiv) in absolute ethanol was added sulfur powder (1 equiv), followed by the aldehyde or ketone (1 equiv) at rt under N₂ and the resulting mixture cooled to 0–5 °C. To this was added diethylamine (1 equiv) and the reaction mixture warmed to rt and subsequently

stirred at 50–55 °C for 5 h. The reaction was concentrated under reduced pressure and the residue was chromatographed on silica, eluting with petroleum ether/EtOAc (10:1) to give the desired compound as a solid or oil which can be recrystallized from an appropriate solvent as indicated.

General Procedure B for the Gewald Synthesis of 2-Amino-3-carbomethoxythiophenes 5, 10d–i. An equimolar mixture of powdered sulfur and morpholine was stirred until total dissolution of the sulfur. After, the ethyl cyanoacetate (1 equiv) and the aldehyde or ketone (1 equiv) were added to the reaction mixture, which was stirred at room temperature for ~18 h. After completion of the reaction, as monitored by TLC, the crude product was chromatographed on silica with an appropriate eluent as indicated to afford the desired compound which could be recrystallized from an appropriate solvent as indicated.

General Procedure C for the Preparation of 6, 11a–j, 31, 36a–c, 37b,c, 41. The required amino ethyl ester thiophene (1 equiv) and appropriate nitrile (1.2 equiv) were taken up in 1,4-dioxane, heated to 50 °C, and passed with dry HCl gas (Kipp's apparatus) until the starting material was absent in 3–24 h or a precipitate formed. The reaction mixture was filtered directly and the solid washed with *n*-hexane to obtain the desired compound. Depending on purity, the solid may be recrystallized from an appropriate solvent or reacted without further purification. Alternatively, the reaction mixture can be concentrated under reduced pressure and the residue chromatographed with an appropriate eluent as indicated.

General Procedure D for the Preparation of 7, 12a–j, 37a. The required 2-chlorothiopyrimidinone (1 equiv) was taken up in DMF. To this solution/suspension was added morpholine (2.5 equiv), and the resulting solution/suspension was stirred at 100 °C for 2–3 h. The reaction mixture was then cooled to room temperature or ~4 °C to induce crystallization of product. Any crystals were collected using vacuum filtration, washed with cold *i*-PrOH, and again recrystallized from

i-PrOH. In the case of present morpholinium hydrochloride, the solids were dissolved in CHCl₃, washed with 5% NaHCO₃ solution, water, brine and the organic extracts concentrated in vacuo. If no crystallization from reaction mixture was evident, the residue can be chromatographed on silica using 1% Et₃N/EtOAc unless otherwise indicated.

General Procedure E for the Preparation of Chloropyrimidines 8, 13a–j, 22, 25, 38a–c, 42, 46. The required thienopyrimidinone (1 equiv) was taken up in toluene. To this solution/suspension was added phosphorus oxychloride (4 equiv), *N,N*-dimethylformamide (cat.), and the solution/suspension was stirred at 100 °C. After TLC has indicated complete consumption of starting material, the reaction mixture was slowly introduced into a stirred suspension of ice–water and the pH adjusted to ~12 with 6 M NaOH. The aqueous phase was extracted with EtOAc, and the combined organic extracts were dried over anhydrous sodium sulfate and concentrated in vacuo. The resulting oil/solid, depending on purity, can be reacted without further purification or further purified using column chromatography (1:99 Et₃N/EtOAc) or recrystallized as indicated.

General Procedure F for the Synthesis of 1, 14a–j, 16a–c, 18–20, 23a,b, 33a,b, 39a–c, 40, 43a,b, 44, 47a,b. In a suitable microwave reaction vessel the required chloropyrimidine (1 equiv) was taken up in *i*-PrOH. To this was added the required amine (1.1 equiv) and the mixture irradiated under stirring at 120 °C for 1–2 h. Upon completion of the reaction, the mixture can be purified using silica gel chromatography to afford the compound. Similarly, any precipitate can be collected under vacuum and washed with cold *i*-PrOH to afford the desired compound.

2-(Morpholinomethyl)-*N*-(3-(trifluoromethyl)phenyl)-5,6,7,8-tetrahydrobenzo[4,5]thieno[2,3-*d*]pyrimidin-4-amine (1). General Procedure F. The residue was chromatographed on silica (1:99 MeOH/CHCl₃) which furnished the title compound as a white foam (160 mg, 70%). LCMS (*m/z*): 449.2 [M + H]⁺. HPLC: *t*_R 7.912 min. HRMS (*m/z*): C₂₃H₂₃F₃N₃OS requires 449.1671 [M + H]⁺; found 449.1661. ¹H NMR δ 8.17 (s, 1H), 7.93 (dd, *J* = 8.1, 1.6 Hz, 1H), 7.48 (t, *J* = 8.0 Hz, 1H), 7.34–7.31 (d, *J* = 7.7 Hz, 1H), 7.26 (s, 1H), 3.77 (s, 2H), 3.09 (t, *J* = 6.0 Hz, 2H), 2.87 (t, *J* = 6.0 Hz, 2H), 2.58 (s, 4H), 2.04–1.97 (m), 1.98–1.94 (m, 2H), 1.66 (dt, *J* = 11.2, 5.6 Hz, 4H). ¹³C NMR (CDCl₃) δ 167.5, 161.4, 154.2, 139.7, 135.0, 131.4 (q, *J* = 32.3 Hz), 129.5, 124.2, 124.1 (q, *J* = 272.4 Hz), 123.2, 119.7 (q, *J* = 3.8 Hz), 117.1 (q, *J* = 4.0 Hz), 115.1, 65.8, 54.8, 26.6, 26.0, 24.3, 22.7, 22.5.

2-Amino-4,5,6,7-tetrahydrobenzo[*b*]thiophene-3-carboxylate³³ (4). General Procedure A. The reaction mixture was kept for 30 min at 0 °C, and formed crystals were collected under vacuum filtration, washed with chilled ethanol (2 × 50 mL), and dried to give the title compound as bright yellow needles which were used as such for the next reaction without further purification (2.83 g, 80%). Mp: 110–114 °C. ¹H NMR (acetone-*d*₆) δ 6.88 (s, 2H), 4.21 (q, *J* = 7.1 Hz, 2H), 2.72–2.60 (m, 2H), 2.45 (m, 2H), 1.81–1.63 (m, 4H), 1.29 (t, *J* = 7.1 Hz, 3H). ¹³C NMR (acetone-*d*₆) δ 165.6, 162.9, 131.9, 116.2, 104.1, 58.7, 26.8, 24.1, 23.1, 22.7, 13.9. LCMS (*m/z*): 226.2 [M + H]⁺. HPLC: *t*_R 8.389 min. HRMS (*m/z*): C₁₁H₁₅NO₂S requires 225.0818 [M + H]⁺; found 225.0818.

2-(Chloromethyl)-5,6,7,8-tetrahydrobenzo[4,5]thieno[2,3-*d*]pyrimidin-4(3*H*)-one (6).¹⁶ General Procedure C. The reaction mixture was filtered directly and the solid washed with *n*-hexane to obtain the desired compound as a beige solid (4.21 g, 93%). LCMS (*m/z*): 255.1 [M + H]⁺. HPLC: *t*_R 6.858 min. HRMS (*m/z*): C₁₁H₁₁ClN₂OS requires 255.0354 [M + H]⁺; found 255.0353. ¹H NMR (DMSO-*d*₆) δ 12.72 (s, 1H), 4.56 (s, 2H), 2.85 (t, *J* = 5.8 Hz, 2H), 2.73 (t, *J* = 5.8 Hz, 2H), 1.76 (ddd, *J* = 7.5, 6.8, 4.4 Hz, 4H). ¹³C NMR (DMSO-*d*₆) δ 162.4, 158.6, 152.4, 133.7, 131.3, 122.1, 43.0, 25.6, 24.9, 22.8, 22.1.

2-(Morpholinomethyl)-5,6,7,8-tetrahydrobenzo[4,5]thieno[2,3-*d*]pyrimidin-4(3*H*)-one (7). General Procedure D. Reaction was cooled and crystals were collected under vacuum filtration to obtain the desired compound as a white crystalline solid (2.59 g, 70%). LCMS (*m/z*): 306.1 [M + H]⁺. HPLC: *t*_R 4.334 min. ¹H NMR (CDCl₃) δ 10.14 (s, 1H), 3.80–3.73 (m, 4H), 3.57 (s, 2H), 3.09–3.02 (m, 2H), 2.94 (t, *J* = 7.3 Hz, 2H), 2.63–2.57 (m, 4H), 2.51–2.40 (m, 2H). ¹³C NMR (CDCl₃) δ 168.6, 158.2, 152.2, 140.1, 138.7, 119.5, 66.7, 60.6, 53.6, 32.2, 29.5, 28.9, 27.

4-((4-Chloro-5,6,7,8-tetrahydrobenzo[4,5]thieno[2,3-*d*]pyrimidin-2-yl)methyl)morpholine (8). General Procedure E. The residue was chromatographed on silica (1:99 Et₃N/EtOAc) to afford the compound as a brown oil (270 mg, 67%). LCMS (*m/z*): 324.1 [M + H]⁺. HPLC: *t*_R 5.112 min. ¹H NMR (CDCl₃) δ 3.80 (s, 2H), 3.06 (t, *J* = 4.2 Hz, 2H), 2.84 (t, *J* = 4.2 Hz, 2H), 2.52–2.49 (m, 4H), 1.93–1.86 (m, 2H), 1.67–1.57 (m, 4H), 1.49–1.36 (m, 2H). ¹³C NMR (CDCl₃) δ 169.4, 161.4, 152.9, 138.9, 126.9, 126.9, 65.2, 54.7, 26.3, 26.0, 25.7, 24.1, 22.2.

Ethyl 2-Amino-5,6-dihydro-4*H*-cyclopenta[*b*]thiophene-3-carboxylate (10a).¹⁵ General Procedure A. The reaction was concentrated under reduced pressure and the residue eluted through a silica gel column (10:1 petroleum ether/EtOAc) to afford the compound as a yellow solid which later turned a dark brown (1.18 g, 37%).

General Procedure B. The reaction was concentrated under reduced pressure and the residue eluted through a silica gel column (10:1 petroleum ether/EtOAc) to afford the compound as a yellow solid which later turned brown (2.21 g, 44%). LCMS (*m/z*): 212.1 [M + H]⁺. HPLC: *t*_R 8.102 min. ¹H NMR (CDCl₃) δ 5.85 (s, 2H), 4.24 (q, *J* = 7.1 Hz, 2H), 2.82 (ddd, *J* = 7.9, 3.9, 1.9 Hz, 2H), 2.74–2.68 (m, 2H), 2.35–2.26 (m, 2H), 1.32 (t, *J* = 7.1 Hz, 1H). ¹³C NMR (CDCl₃) δ 166.4, 165.9, 142.8, 121.4, 103.0, 59.5, 30.9, 29.0, 27.4, 14.6.

Ethyl 2-Amino-5,6,7,8-tetrahydro-4*H*-cyclohepta[*b*]thiophene-3-carboxylate (10b). General Procedure A. The reaction was concentrated under reduced pressure and the residue chromatographed on silica (10:1 petroleum ether/EtOAc). The resulting residue was recrystallized from CHCl₃/petroleum ether to afford the desired compound as yellow crystals (1.55 g, 48%). LCMS (*m/z*): 240.2 [M + H]⁺. HPLC: *t*_R 8.791 min.

General Procedure B. The crude product was purified by silica gel column chromatography (10:1 petroleum ether/EtOAc) to afford the title compound as a yellow solid (3.87 g, 72%). ¹H NMR (CDCl₃) δ 5.76 (s, 2H), 4.28 (q, *J* = 7.1 Hz, 2H), 3.00–2.94 (m, 2H), 2.60–2.54 (m, 2H), 1.85–1.76 (m, 2H), 1.68–1.56 (m, 4H), 1.34 (t, *J* = 7.1 Hz, 3H). ¹³C NMR (CDCl₃) δ 166.1, 159.9, 138.0, 121.4, 107.6, 59.6, 32.2, 28.7, 28.7, 27.9, 27.0, 14.5.

Ethyl 2-Amino-4,5,6,7,8,9-hexahydrocycloocta[*b*]thiophene-3-carboxylate (10c). General Procedure A. The solvent was removed under reduced pressure and the residue eluted through a silica gel column (10:1 petroleum ether/EtOAc). The product was recrystallized from CHCl₃/petroleum ether to give the desired compound as yellow crystals (1.32 g, 37%). LCMS (*m/z*): 254.2 [M + H]⁺. HPLC: *t*_R 9.405 min.

General Procedure B. After completion of the reaction (24 h), as monitored by TLC, the mixture was concentrated under reduced pressure and the crude product was purified by silica gel column chromatography (10:1 petroleum ether/EtOAc) to afford the title compound as a yellow solid (2.63 g, 65%). ¹H NMR (CDCl₃) δ 5.94 (s, 1H), 4.27 (q, *J* = 7.1 Hz, 2H), 2.85–2.77 (m, 2H), 2.61–2.57 (m, 2H), 2.43–2.36 (m, 1H), 1.91–1.82 (m, 1H), 1.65–1.59 (m, 2H), 1.58–1.52 (m, 2H), 1.49–1.41 (m, 2H), 1.37–1.26 (m, 3H). ¹³C NMR (CDCl₃) δ 166.1, 161.5, 134.9, 120.2, 106.2, 59.5, 32.1, 29.9, 26.8, 26.6, 25.9, 25.7, 14.4.

Ethyl 2-Amino-5-phenylthiophene-3-carboxylate (10d). General Procedure B. After completion of the reaction, as monitored by TLC, the mixture was concentrated under reduced pressure and the crude product was purified by silica gel column chromatography (10:1 petroleum ether/EtOAc). This resulting brown solid was recrystallized from *i*-PrOH to afford the title compound as dark orange needles (6.30 g, 54%). LCMS (*m/z*): 248.1 [M + H]⁺. HPLC: *t*_R 7.946 min. ¹H NMR (CDCl₃) δ 7.47–7.42 (m, 2H), 7.36–7.30 (m, 2H), 7.25 (s, 1H), 7.23–7.18 (m, 1H), 6.02 (s, 2H), 4.31 (q, *J* = 7.1 Hz, 2H), 1.37 (t, *J* = 7.1 Hz, 3H). ¹³C NMR (CDCl₃) δ 165.5, 162.1, 134.1, 128.9, 126.7, 124.9, 124.8, 121.3, 108.1, 60.0, 14.6.

Ethyl 2-Amino-4-phenylthiophene-3-carboxylate (10e). General Procedure B. The reaction mixture was concentrated under reduced pressure, and the crude product was purified by silica gel column chromatography (10:1 petroleum ether/EtOAc). This resulting yellow solid was recrystallized from *i*-PrOH to afford the title compound as yellow crystals (4.88 g, 49%). LCMS (*m/z*): 248.1 [M + H]⁺. HPLC: *t*_R 7.379 min. ¹H NMR (CDCl₃) δ 7.33–7.28 (m, 5H), 6.10 (s, 2H), 6.07 (s, 2H), 4.04 (q, *J* = 7.1 Hz, 2H), 0.93 (t, *J* = 7.1 Hz, 3H). ¹³C NMR

(CDCl₃, δ 165.8, 163.9, 141.7, 138.6, 129.0, 127.3, 126.9, 105.6, 59.5, 13.7.

Ethyl 2-Amino-5-benzylthiophene-3-carboxylate (10f). General Procedure B. After completion of the reaction, as monitored by TLC, the mixture was concentrated under reduced pressure and the crude product chromatographed on silica (10:1 petroleum ether/EtOAc) to afford the title compound as a yellow oil (2.71 g, 35%). LCMS (*m/z*): 262.1 [M + H]⁺. HPLC: *t_R* 8.633 min. ¹H NMR (CDCl₃, δ 7.30–7.26 (m, 2H), 7.23–7.18 (m, 3H), 6.69 (t, *J* = 1.0 Hz, 1H), 5.83 (s, 2H), 4.22 (q, *J* = 7.1 Hz, 2H), 3.87 (s, 2H), 1.30 (t, *J* = 7.1 Hz, 1H). ¹³C NMR (CDCl₃, δ 165.4, 162.3, 139.9, 128.5, 128.49, 126.5, 125.1, 122.8, 106.1, 59.6, 36.0, 14.5.

Ethyl 2-Amino-4-cyclohexylthiophene-3-carboxylate (10g). General Procedure B. After completion of the reaction, as monitored by TLC, the reaction mixture was concentrated under reduced pressure and the crude product purified by silica gel column chromatography (10:1 petroleum ether/EtOAc). Collected fractions were concentrated under reduced pressure and placed in the freezer for 2 h. Formed solids were collected under vacuum and washed with petroleum ether to afford the compound as clear crystals (3.56 g, 38%). LCMS (*m/z*): 254.2 [M + H]⁺. HPLC: *t_R* 8.936 min. ¹H NMR (CDCl₃, δ 6.06 (s, 2H), 5.85 (s, 1H), 4.29 (q, *J* = 7.1 Hz, 2H), 3.03 (tt, *J* = 11.4, 2.5 Hz, 1H), 1.97 (d, *J* = 12.0 Hz, 2H), 1.80 (d, *J* = 12.6 Hz, 2H), 1.73 (d, *J* = 12.5 Hz, 1H), 1.37 (t, *J* = 7.2 Hz, 3H), 1.28–1.15 (m, 3H). ¹³C NMR (CDCl₃, δ 166.2, 164.5, 147.4, 100.6, 59.7, 39.4, 34.1, 27.1, 26.6, 14.1.

Ethyl 2-Amino-4,5-dimethylthiophene-3-carboxylate (10h). General Procedure B. After completion of the reaction, as monitored by TLC, the mixture was concentrated under reduced pressure and the crude product was purified by silica gel column chromatography (10:1 petroleum ether/EtOAc) to afford the title compound as a pale yellow solid which was recrystallized from *i*-PrOH (3.41 g, 38%). LCMS (*m/z*): 200.1 [M + H]⁺. HPLC: *t_R* 7.265 min. ¹H NMR (CDCl₃, δ 5.90 (s, 2H), 4.27 (q, *J* = 7.1 Hz, 2H), 2.16 (d, *J* = 0.7 Hz, 3H), 2.15 (d, *J* = 0.7 Hz, 2H), 1.34 (t, *J* = 7.1 Hz, 3H). ¹³C NMR (CDCl₃, δ 166.2, 161.0, 130.4, 113.9, 107.0, 59.7, 14.9, 14.5, 12.4.

Ethyl 2-Amino-5-cyclohexylthiophene-3-carboxylate (10i). General Procedure B. After completion of the reaction, as monitored by TLC, the mixture was concentrated under reduced pressure and the crude product was chromatographed on silica (10:1 petroleum ether/EtOAc) to afford the title compound as a gold oil (3.05 g, 73%). LCMS (*m/z*): 254.2 [M + H]⁺. HPLC: *t_R* 8.918 min. ¹H NMR (CDCl₃, δ 6.62 (d, *J* = 1.1 Hz, 1H), 5.79 (s, 2H), 4.25 (q, *J* = 7.1 Hz, 2H), 2.57–2.48 (m, 1H), 2.00–1.91 (m, 2H), 1.82–1.76 (m, 2H), 1.72–1.65 (m, 1H), 1.36–1.29 (m, 7H), 1.23–1.13 (m, 1H). ¹³C NMR (CDCl₃, δ 165.6, 160.9, 133.3, 119.1, 106.2, 59.6, 39.0, 34.9, 26.4, 26.0, 14.6.

Ethyl 2-Aminothiophene-3-carboxylate (10j).³⁴ Triethylamine (7.34 mL, 52.6 mmol) was added dropwise over 10 min to a mixture of 2,5-dihydroxy-1,4-dithiane (8.09 g, 52.6 mmol), ethyl cyanoacetate (11.2 mL, 105 mmol), and dimethylformamide (40 mL). The mixture was stirred at 45 °C for 30 min, diluted with 0.4 M acetic acid, and extracted with ether. The ethereal layer was dried over sodium sulfate. The residue was eluted through a silica gel column (10:1 petroleum ether/EtOAc) and the resulting fractions collected, concentrated under reduced pressure, and cooled at 4 °C to afford the compound as a light yellow crystalline solid (5.00 g, 55%). LCMS (*m/z*): 172.1 [M + H]⁺. HPLC: *t_R* 6.123 min. ¹H NMR (CDCl₃, δ 6.98 (d, *J* = 5.8 Hz, 1H), 6.18 (d, *J* = 5.8 Hz, 1H), 4.27 (q, *J* = 7.1 Hz, 2H), 1.34 (t, *J* = 7.1 Hz, 3H). ¹³C NMR (CDCl₃, δ 165.5, 162.7, 126.6, 107.2, 106.9, 59.8, 14.6.

2-(Chloromethyl)-3,5,6,7-tetrahydro-4H-cyclopenta[4,5]-thieno[2,3-*d*]pyrimidin-4-one (11a). General Procedure C. The precipitate was collected and washed with cold 1,4-dioxane to afford the compound as a beige solid (2.56 g, 70%). LCMS (*m/z*): 292.1 [M + H]⁺. HPLC: *t_R* 4.216 min. ¹H NMR (DMSO-*d*₆, δ 12.72 (s, 1H), 4.54 (s, 2H), 2.97–2.85 (m, 4H), 2.37 (p, *J* = 7.2 Hz, 2H). ¹³C NMR (DMSO-*d*₆, δ 167.2, 157.9, 151.7, 139.7, 138.7, 119.3, 42.7, 29.1, 28.6, 27.5.

2-(Chloromethyl)-3,5,6,7,8,9-hexahydro-4H-cyclohepta[4,5]-thieno[2,3-*d*]pyrimidin-4-one (11b). General Procedure C. The precipitate was collected and washed with cold 1,4-dioxane to afford the compound as a white powder (5.00 g, 86%). LCMS (*m/z*): 269.1

[M + H]⁺. HPLC: *t_R* 7.039 min. ¹H NMR (DMSO-*d*₆, δ 12.71 (s, 1H), 4.57 (s, 2H), 3.31–3.21 (m, 2H), 2.86–2.79 (m, 2H), 1.90–1.78 (m, 2H), 1.69–1.49 (m, 4H). ¹³C NMR (DMSO-*d*₆, δ 160.4, 158.7, 151.7, 137.6, 136.6, 122.2, 42.6, 32.0, 29.1, 27.3, 27.1, 26.9.

2-(Chloromethyl)-5,6,7,8,9,10-hexahydrocycloocta[4,5]-thieno[2,3-*d*]pyrimidin-4(3H)-one (11c). General Procedure C. The precipitate was collected and washed with cold 1,4-dioxane to afford the compound as a white powder (3.01 g, 78%). LCMS (*m/z*): 283.0 [M + H]⁺. HPLC: *t_R* 7.426 min. ¹H NMR (DMSO-*d*₆, δ 12.68 (s, 1H), 4.55 (s, 2H), 3.06–2.99 (m, 2H), 2.90–2.82 (m, 2H), 1.59 (s, 4H), 1.41–1.36 (m, 2H), 1.29–1.19 (m, 2H). ¹³C NMR (DMSO-*d*₆, δ 161.6, 158.2, 151.7, 136.1, 133.8, 121.6, 42.6, 31.5, 29.8, 26.1, 25.4, 25.2, 24.3.

2-(Chloromethyl)-5-phenylthieno[2,3-*d*]pyrimidin-4(3H)-one (11d). General Procedure C. The bright orange suspension was filtered and the resulting solids were washed with cold 1,4-dioxane which afforded the desired compound as a yellow solid (4.33 g, 82%). LCMS (*m/z*): 277.1 [M + H]⁺. HPLC: *t_R* 6.476 min. ¹H NMR (DMSO-*d*₆, δ 12.71 (s, 1H), 7.55 (s, 1H), 7.53 (dd, *J* = 7.9, 1.3 Hz, 2H), 7.41–7.37 (m, 2H), 7.35 (dd, *J* = 6.6, 2.7 Hz, 1H). ¹³C NMR (DMSO-*d*₆, δ 165.3, 157.8, 153.1, 138.5, 135.1, 129.4, 127.6, 127.5, 121.8, 119.9, 42.5.

2-(Chloromethyl)-6-phenylthieno[2,3-*d*]pyrimidin-4(3H)-one (11e). General Procedure C. The precipitate was collected from the crude reaction mixture and washed with hot *i*-PrOH to afford the compound as a white solid which was used without the need for further purification (4.57 g, 64%). LCMS (*m/z*): 277.1 [M + H]⁺. HPLC: *t_R* 6.752 min. ¹H NMR (DMSO-*d*₆, δ 12.72 (1H), 7.80 (s, 1H), 7.78–7.73 (m, 2H), 7.45 (dd, *J* = 8.1, 6.7 Hz, 2H), 7.38–7.34 (m, 1H), 4.62 (s, 2H). ¹³C NMR (DMSO-*d*₆, δ 162.9, 157.6, 153.2, 140.4, 132.6, 129.3, 128.8, 125.8, 125.1, 117.3, 42.6.

6-Benzyl-2-(chloromethyl)thieno[2,3-*d*]pyrimidin-4(3H)-one (11f). General Procedure C. The solvents were removed under reduced pressure and the residue was chromatographed on silica (40% petroleum ether in EtOAc). The collected fractions were concentrated under reduced pressure and the resulting solid was recrystallized from CHCl₃ affording the compound as white-yellow crystals (2.74 g, quantitative yield). LCMS (*m/z*): 291.1 [M + H]⁺. HPLC: *t_R* 6.680 min. ¹H NMR (DMSO-*d*₆, δ 7.62 (s, 1H), 7.35–7.28 (m, 4H), 7.25 (dd, *J* = 11.1, 4.3 Hz, 1H), 7.16 (s, 1H), 4.54 (s, 2H), 4.20 (s, 2H). ¹³C NMR (DMSO-*d*₆, δ 163.1, 157.6, 152.5, 142.9, 139.5, 128.7, 128.6, 123.7, 119.1, 42.7, 35.6.

2-(Chloromethyl)-5-cyclohexylthieno[2,3-*d*]pyrimidin-4(3H)-one (11g). General Procedure C. The precipitate was collected from the crude reaction mixture and washed with 1,4-dioxane. This afforded the desired compound as a yellow solid which was used without the need for further purification (2.75 g, 70%). LCMS (*m/z*): 283.1 [M + H]⁺. HPLC: *t_R* 7.595 min. ¹H NMR (DMSO-*d*₆, δ 12.73 (s, 1H), 7.21 (s, 1H), 4.57 (s, 2H), 3.26 (t, *J* = 9.6 Hz, 1H), 1.95 (d, *J* = 9.8 Hz, 2H), 1.77 (d, *J* = 11.6 Hz, 2H), 1.70 (d, *J* = 12.9 Hz, 1H), 1.41–1.28 (m, 4H), 1.22 (dt, *J* = 24.7, 9.6 Hz, 1H). ¹³C NMR (DMSO-*d*₆, δ 164.6, 158.3, 152.6, 144.8, 120.9, 116.6, 42.5, 37.9, 33.1, 26.3, 25.8.

2-(Chloromethyl)-5,6-dimethylthieno[2,3-*d*]pyrimidin-4(3H)-one (11h). General Procedure C. The precipitate was collected from the crude reaction mixture and washed with hot CHCl₃ to afford the compound as a yellow solid (3.38 g, 84%). LCMS (*m/z*): 229.0 [M + H]⁺. HPLC: *t_R* 5.717 min. ¹H NMR (DMSO-*d*₆, δ 12.69 (s, 1H), 4.55 (s, 2H), 2.36 (d, *J* = 0.8 Hz, 3H), 2.34 (d, *J* = 0.7 Hz, 1H). ¹³C NMR (DMSO-*d*₆, δ 161.2, 158.4, 151.9, 130.4, 128.8, 122.4, 42.6, 12.7, 12.7.

2-(Chloromethyl)-6-cyclohexylthieno[2,3-*d*]pyrimidin-4(3H)-one (11i). General Procedure C. The precipitate was collected from the crude reaction under vacuum filtration and washed with cold 1,4-dioxane. The remaining filtrate was concentrated, reduced under pressure and the resulting residue chromatographed on silica (40:60 EtOAc/petroleum ether) to afford the compound as a yellow solid (2.56 g, 64%). LCMS (*m/z*): 283.0 [M + H]⁺. HPLC: *t_R* 7.614 min. ¹H NMR (DMSO-*d*₆, δ 12.67 (s, 1H), 7.09 (d, *J* = 0.5 Hz, 1H), 4.57 (s, 2H), 2.89–2.78 (m, 1H), 1.97 (d, *J* = 8.5 Hz, 2H), 1.76 (d, *J* = 2.3 Hz, 2H), 1.65 (d, *J* = 12.5 Hz, 1H), 1.46–1.28 (m, 4H), 1.24–1.15 (m, 1H). ¹³C NMR (DMSO-*d*₆, δ 161.9, 157.7, 152.3, 149.8, 123.6, 116.1, 42.7, 38.9, 34.5, 25.7, 25.3.

2-(Chloromethyl)thieno[2,3-*d*]pyrimidin-4(3H)-one (11j). General Procedure C. The reaction mixture was concentrated under

reduced pressure and the residue chromatographed on silica (50:50 petroleum ether/EtOAc) which afforded the compound as a pale white solid (1.58 g, 21%). LCMS (m/z): 201.0 [M + H]⁺. HPLC: t_R 4.394 min. ¹H NMR (DMSO-*d*₆) δ 7.62 (d, J = 5.8 Hz, 1H), 7.40 (d, J = 5.8 Hz, 1H), 4.58 (s, 2H). ¹³C NMR (DMSO-*d*₆) δ 163.8, 157.9, 152.8, 124.8, 123.6, 121.6, 42.7.

2-(Morpholinomethyl)-3,5,6,7-tetrahydro-4H-cyclopenta[4,5]thieno[2,3-d]pyrimidin-4-one (12a). General Procedure D. The residue was chromatographed on silica (1:99 Et₃N/EtOAc) affording the compound as a beige solid (2.52 g, 86%). LCMS (m/z): 292.1 [M + H]⁺. HPLC: t_R 4.216 min. HRMS (m/z): C₁₄H₁₇N₃O₂S requires 292.112 [M + H]⁺; found 292.114. ¹H NMR (CDCl₃) δ 10.14 (s, 1H), 3.80–3.73 (m, 4H), 3.57 (s, 2H), 3.09–3.02 (m, 2H), 2.94 (t, J = 7.3 Hz, 2H), 2.63–2.57 (m, 4H), 2.51–2.40 (m, 2H). ¹³C NMR (CDCl₃) δ 168.6, 158.2, 152.2, 140.1, 138.7, 119.5, 66.7, 60.6, 53.6, 29.5, 28.9, 27.

2-(Morpholinomethyl)-3,5,6,7,8,9-hexahydro-4H-cyclohepta[4,5]thieno[2,3-d]pyrimidin-4-one (12b). General Procedure D. A precipitate was collected and recrystallized from CHCl₃/*i*-PrOH affording the compound as a white fluffy solid (3.29 g, 83%). LCMS (m/z): 320.1 [M + H]⁺. HPLC: t_R 5.186 min. HRMS (m/z): C₁₆H₂₁N₃O₂S requires 320.1433 [M + H]⁺; found 320.1427. ¹H NMR (CDCl₃) δ 10.09 (s, 1H), 3.83–3.70 (m, 4H), 3.55 (s, 2H), 3.37–3.25 (m, 2H), 2.88–2.78 (m, 2H), 2.60 (s, 4H'), 1.89 (ddd, J = 8.3, 7.5, 4.3 Hz, 2H), 1.74–1.63 (m, 4H). ¹³C NMR (CDCl₃) δ 161.8, 158.9, 137.8, 137.2, 130.1, 122.8, 66.8, 60.7, 53.6, 32.6, 30.1, 28.1, 27.8, 27.4.

2-(Morpholinomethyl)-5,6,7,8,9,10-hexahydrocycloocta[4,5]thieno[2,3-d]pyrimidin-4(3H)-one (12c). General Procedure D. A precipitate was collected and recrystallized from CHCl₃/*i*-PrOH to afford the compound as a white fluffy solid (1.75 g, 63%). LCMS (m/z): 334.1 [M + H]⁺. HPLC: t_R 5.489 min. HRMS (m/z): C₁₇H₂₃N₃O₂S requires 334.1592 [M + H]⁺; found 334.1584. ¹H NMR (CDCl₃) δ 10.17 (s, 1H), 3.81–3.71 (m, 4H), 3.54 (s, 2H), 3.13–3.05 (m, 2H), 2.90–2.81 (m, 2H), 2.67–2.51 (m, 4H), 1.78–1.61 (m, 4H), 1.45 (dd, J = 9.9, 4.7 Hz, 2H), 1.37–1.25 (m, 2H). ¹³C NMR (CDCl₃) δ 163.1, 158.6, 152.4, 136.3, 134.4, 122.2, 66.9, 60.8, 53.7, 31.9, 30.3, 27.1, 26.1, 25.8, 25.2.

2-(Morpholinomethyl)-6-phenylthieno[2,3-d]pyrimidin-4(3H)-one (12d). General Procedure D. Upon cooling of the reaction mixture, a precipitate formed which was collected under vacuum and washed with cold *i*-PrOH affording the compound as a white solid (2.71 g, 91%). LCMS (m/z): 328.1 [M + H]⁺. HPLC: t_R 5.092 min. HRMS (m/z): C₁₇H₁₇N₃O₂S requires 328.1118 [M + H]⁺; found 328.1114. ¹H NMR (DMSO-*d*₆) δ 10.85 (s, 1H), 7.78 (s, 1H), 7.78–7.73 (m, 2H), 7.46 (dd, J = 8.2, 6.8 Hz, 2H), 7.41–7.34 (m, 2H), 3.64–3.55 (m, 4H), 3.48 (s, 2H), 2.50 (dd, J = 6.1, 3.0 Hz, 4H). ¹³C NMR (DMSO-*d*₆) δ 163.3, 157.8, 155.1, 139.3, 132.8, 129.3, 128.6, 125.8, 124.7, 117.1, 66.1, 60.4, 53.0.

2-(Morpholinomethyl)-5-phenylthieno[2,3-d]pyrimidin-4(3H)-one (12e). General Procedure D. A precipitate was collected under vacuum and recrystallized from CHCl₃/*i*-PrOH to afford the desired compound as bright yellow crystals (2.67 g, 83%). LCMS (m/z): 328.1 [M + H]⁺. HPLC: t_R 4.853 min. HRMS (m/z): C₁₇H₁₇N₃O₂S requires 328.1123 [M + H]⁺; found 328.1114. ¹H NMR (CDCl₃) δ 10.61 (s, 1H), 7.58–7.54 (m, 2H), 7.44–7.35 (m, 3H), 7.10 (s, 1H), 3.71–3.66 (m, 4H), 3.53 (s, 2H), 2.56–2.50 (m, 4H). ¹³C NMR (CDCl₃) δ 166.7, 158.4, 154.2, 139.6, 135.4, 129.5, 127.9, 127.9, 120.3, 66.8, 60.7, 53.6.

6-Benzyl-2-(morpholinomethyl)thieno[2,3-d]pyrimidin-4(3H)-one (12f). General Procedure D. The residue was recrystallized from CHCl₃/*i*-PrOH to afford the compound as beige crystals (2.47 g, 78%). LCMS (m/z): 342.1 [M + H]⁺. HPLC: t_R 5.208 min. HRMS (m/z): C₁₈H₁₉N₃O₂S requires 342.1278 [M + H]⁺; found 342.1271. ¹H NMR (CDCl₃) δ 10.09 (s, 1H), 7.35–7.30 (m, 4H), 7.26 (dt, J = 5.0, 1.4 Hz, 3H), 7.13 (t, J = 1.1 Hz, 1H), 4.15 (s, 2H), 3.78–3.74 (m, 4H), 3.55 (s, 2H), 2.61–2.54 (m, 4H). ¹³C NMR (CDCl₃) δ 164.8, 157.8, 153.2, 142.4, 138.8, 128.9, 128.8, 127.1, 123.9, 119.2, 66.8, 60.7, 53.7, 36.9.

5-Cyclohexyl-2-(morpholinomethyl)thieno[2,3-d]pyrimidin-4(3H)-one (12g). General Procedure D. *i*-PrOH was introduced to a cooled reaction mixture and the resulting precipitate collected to afford

the compound as bright yellow crystals (1.56 g, 63% yield). LCMS (m/z): 334.1 [M + H]⁺. HPLC: t_R 5.715 min. HRMS (m/z): C₁₇H₂₃N₃O₂S requires 334.1587 [M + H]⁺; found 334.1584. ¹H NMR (CDCl₃) δ 10.15 (s, 1H), 6.82 (s, 1H), 3.79–3.72 (m, 4H), 3.56 (s, 2H), 3.35 (tt, J = 11.6, 2.8 Hz, 1H), 2.62–2.56 (m, 4H), 2.05 (d, J = 11.7 Hz, 2H), 1.86–1.71 (m, 3H), 1.54–1.41 (m, 2H), 1.33 (tt, J = 7.3, 3.5 Hz, 2H), 1.29–1.18 (m, 1H). ¹³C NMR (CDCl₃) δ 166.1, 158.5, 153.3, 146.0, 121.3, 115.2, 66.9, 60.6, 53.7, 38.7, 33.8, 26.8, 26.4.

5,6-Dimethyl-2-(morpholinomethyl)thieno[2,3-d]pyrimidin-4(3H)-one (12h). General Procedure D. Upon cooling of the reaction mixture, a formed precipitate was collected and washed with petroleum ether to afford the desired compound as a bright yellow solid (2.74 g, 88%). LCMS (m/z): 280.2 [M + H]⁺. HPLC: t_R 4.198 min. HRMS (m/z): C₁₃H₁₇N₃O₂S requires 280.1119 [M + H]⁺; found 280.1114. ¹H NMR (CDCl₃) δ 10.13 (s, 1H), 3.79–3.71 (m, 4H), 3.53 (s, 2H), 2.63–2.56 (m, 4H), 2.46 (d, J = 0.6 Hz, 3H), 2.37 (s, 3H). ¹³C NMR (CDCl₃) δ 162.7, 158.7, 152.6, 130.3, 129.5, 122.9, 66.9, 60.7, 53.7, 13.2, 13.1.

6-Cyclohexyl-2-(morpholinomethyl)thieno[2,3-d]pyrimidin-4(3H)-one (12i). General Procedure D. The solids were filtered from the cooled reaction mixture and recrystallized from *i*-PrOH to afford the compound as white fluffy crystals (2.57 g, 60%). LCMS (m/z): 334.2 [M + H]⁺. HPLC: t_R 5.603 min. HRMS (m/z): C₁₇H₂₃N₃O₂S requires 334.1593 [M + H]⁺; found 334.1584. ¹H NMR (CDCl₃) δ 10.17 (s, 1H), 7.13 (d, J = 1.0 Hz, 1H), 3.79–3.71 (m, 4H), 3.55 (s, 2H), 2.83–2.73 (m, 1H), 2.61–2.53 (m, 4H), 2.10–2.02 (m, 2H), 1.83 (dd, J = 9.9, 2.9 Hz, 2H), 1.73 (ddd, J = 9.6, 5.6, 1.5 Hz, 1H), 1.50–1.32 (m, 4H), 1.30–1.18 (m, 1H). ¹³C NMR (CDCl₃) δ 163.5, 158.0, 152.8, 150.2, 123.7, 115.8, 66.9, 60.8, 53.7, 39.9, 34.9, 26.3, 25.9.

2-(Morpholinomethyl)thieno[2,3-d]pyrimidin-4(3H)-one (12j). General Procedure D. The residue was chromatographed on silica (1:99 Et₃N/EtOAc) which afforded the compound as a gold solid (1.10 g, 58%). LCMS (m/z): 252.1 [M + H]⁺. HPLC: t_R 3.009 min. HRMS (m/z): C₁₁H₁₃N₃O₂S requires 252.0803 [M + H]⁺; found 252.0801. ¹H NMR (CDCl₃) δ 10.28 (s, 1H), 7.44 (d, J = 5.8 Hz, 1H), 7.21 (d, J = 5.8 Hz, 1H), 3.78–3.73 (m, 4H), 3.57 (s, 2H), 2.63–2.55 (m, 4H). ¹³C NMR (CDCl₃) δ 165.3, 158.2, 153.8, 123.7, 123.1, 121.9, 66.8, 60.7, 53.7.

4-((4-Chloro-6,7-dihydro-5H-cyclohepta[4,5]thieno[2,3-d]pyrimidin-2-yl)methyl)morpholine (13a). General Procedure E. The residue was chromatographed on silica (1:99 Et₃N/EtOAc) to afford the compound as a brown oil (270 mg, 67%). LCMS (m/z): 310.1 [M + H]⁺. HPLC: t_R 5.230 min. ¹H NMR (CDCl₃) δ 3.85 (s, 1H), 3.78–3.75 (m, 2H), 3.17–3.11 (m, 2H), 3.07–3.02 (m, 2H), 2.63–2.56 (m, 4H), 2.56–2.47 (m, 1H). ¹³C NMR (CDCl₃) δ 174.3, 160.5, 152.9, 144.6, 136.2, 124.6, 66.9, 64.9, 53.8, 30.3, 29.5, 27.5.

4-((4-Chloro-6,7,8,9-tetrahydro-5H-cyclohepta[4,5]thieno[2,3-d]pyrimidin-2-yl)methyl)morpholine (13b). General Procedure E. The residue was chromatographed on silica (1:99 Et₃N/EtOAc) to afford the compound as a gold oil (2.62 g, 70%). LCMS (m/z): 338.1 [M + H]⁺. HPLC: t_R 5.949 min. ¹H NMR (CDCl₃) δ 3.61 (s, 2H), 3.56–3.49 (m, 2H), 3.14–3.03 (m, 2H), 2.77–2.66 (m, 2H), 2.42–2.34 (m, 4H), 1.69 (dd, J = 11.3, 5.9 Hz, 2H), 1.51 (ddd, J = 10.7, 9.4, 5.4 Hz, 4H). ¹³C NMR (CDCl₃) δ 167.8, 159.4, 152.5, 143.1, 131.7, 126.7, 66.3, 64.1, 53.3, 31.4, 29.6, 27.6, 26.5, 26.0.

4-((4-Chloro-5,6,7,8,9,10-hexahydrocycloocta[4,5]thieno[2,3-d]pyrimidin-2-yl)methyl)morpholine (13c). General Procedure E. The residue was chromatographed on silica (1:99 Et₃N/EtOAc) to afford the compound as a gold oil (1.91 g, 67%). LCMS (m/z): 352.1 [M + H]⁺. HPLC: t_R 6.259 min. ¹H NMR (CDCl₃) δ 3.44 (s, 2H), 3.40–3.25 (m, 4H), 2.75–2.65 (m, 2H), 2.61–2.48 (m, 2H), 2.26–2.15 (m, 4H), 1.45–1.24 (m, 4H), 1.08 (dd, J = 9.5, 4.8 Hz, 2H), 0.91–0.84 (m, 2H). ¹³C NMR (CDCl₃) δ 168.2, 159.4, 152.0, 141.3, 128.4, 125.8, 65.9, 63.8, 53.0, 30.8, 29.4, 27.2, 25.5, 24.5, 24.1.

4-((4-Chloro-6-phenylthieno[2,3-d]pyrimidin-2-yl)methyl)morpholine (13d). General Procedure E. The residue was recrystallized from CHCl₃/petroleum ether to afford the compound as pale white crystals (2.45 g, 90%). LCMS (m/z): 346.1 [M + H]⁺. HPLC: t_R 6.418 min. ¹H NMR (DMSO-*d*₆) δ 8.08 (s, 1H), 7.96 (d, J = 6.9 Hz, 2H), 7.58–7.48 (m, 3H), 4.67 (s, 2H), 3.89 (s, 4H), 3.60–3.26 (m, 4H).

¹³C NMR (DMSO-*d*₆) δ 167.7, 153.5, 145.9, 131.7, 130.2, 130.1, 129.5, 126.8, 114.9, 63.4, 59.9, 51.8.

4-((4-Chloro-5-phenylthieno[2,3-*d*]pyrimidin-2-yl)methyl)morpholine (13e). General Procedure E. The residue was chromatographed on silica (1:99 Et₃N/EtOAc) which afforded the compound as a gold solid 1.02 g, 96%. LCMS (*m/z*): 346.1 [M + H]⁺. HPLC: *t*_R 5.595 min. ¹H NMR (DMSO-*d*₆) δ 7.95 (s, 1H), 7.68–7.29 (m, 5H), 3.80 (s, 2H), 3.63–3.53 (m, 4H), 2.55–2.51 (m, 4H). ¹³C NMR (DMSO-*d*₆) δ 169.72, 161.43, 153.8, 134.9, 134.7, 130.0, 128.2, 127.8, 127.5, 124.7, 66.2, 63.7, 53.1.

4-((6-Benzyl-4-chlorothieno[2,3-*d*]pyrimidin-2-yl)methyl)morpholine (13f). General Procedure E. The residue was recrystallized from CHCl₃/*i*-PrOH to afford the compound as pale yellow crystals (1.55 g, 70%). LCMS (*m/z*): 360.1 [M + H]⁺. HPLC: *t*_R 6.261 min. ¹H NMR (DMSO-*d*₆) δ 7.34 (d, *J* = 4.4 Hz, 1H), 4.35 (s, 2H), 3.76 (s, 2H), 3.60–3.50 (m, 4H), 2.56–2.44 (m, 4H). ¹³C NMR (DMSO-*d*₆) δ 168.5, 152.4, 148.2, 138.7, 128.8, 128.7, 127.9, 126.9, 116.8, 114.9, 67.1, 65.9, 52.9, 36.1.

4-((4-Chloro-5-cyclohexylthieno[2,3-*d*]pyrimidin-2-yl)methyl)morpholine (13g). General Procedure E. The residue was chromatographed on silica (1:99 Et₃N/EtOAc) which afforded the compound as a gold oil (1.14 g, 69%). LCMS (*m/z*): 352.1 [M + H]⁺. HPLC: *t*_R 6.418 min. ¹H NMR (CDCl₃) δ 7.21 (d, *J* = 0.7 Hz, 1H), 3.88 (s, 2H), 3.82–3.73 (m, 4H), 3.45–3.32 (m, 1H), 2.68–2.57 (m, 4H), 2.11 (d, *J* = 12.8 Hz, 2H), 1.87 (d, *J* = 12.9 Hz, 2H), 1.80 (d, *J* = 12.9 Hz, 1H), 1.53–1.35 (m, 4H), 1.33–1.19 (m, 1H). ¹³C NMR (CDCl₃) δ 171.4, 161.1, 154.5, 141.3, 125.7, 120.9, 66.9, 64.7, 53.9, 38.8, 34.4, 26.8, 26.2.

4-((4-Chloro-5,6-dimethylthieno[2,3-*d*]pyrimidin-2-yl)methyl)morpholine (13h). General Procedure E. The residue was recrystallized from CHCl₃/*i*-PrOH to afford the compound as pale white crystals (1.55 g, 70%). LCMS (*m/z*): 298.1 [M + H]⁺. HPLC: *t*_R 4.925 min. ¹H NMR (CDCl₃) δ 3.96 (s, 2H), 3.87–3.79 (m, 4H), 2.76 (s, 4H), 2.53 (d, *J* = 0.5 Hz, 3H), 2.50 (s, 3H). ¹³C NMR (CDCl₃) δ 168.9, 153.5, 136.4, 128.0, 125.1, 118.4, 66.3, 63.9, 53.4, 14.3, 14.2.

4-((4-Chloro-6-cyclohexylthieno[2,3-*d*]pyrimidin-2-yl)methyl)morpholine (13i). The residue was chromatographed on silica (1:99 Et₃N/EtOAc) affording the compound as a gold oil which later solidified under vacuum to produce a light yellow/white solid (1.64 g, 64%). LCMS (*m/z*): 352.1 [M + H]⁺. HPLC: *t*_R 6.663 min. ¹H NMR (CDCl₃) δ 7.05 (d, *J* = 1.1 Hz, 1H), 3.85 (s, 2H), 3.78–3.73 (m, 4H), 2.95–2.83 (m, 1H), 2.64–2.55 (m, 4H), 2.10 (dd, *J* = 13.4, 1.3 Hz, 2H), 1.91–1.83 (m, 2H), 1.80–1.71 (m, 1H), 1.57–1.35 (m, 4H), 1.32–1.21 (m, 1H). ¹³C NMR (CDCl₃) δ 168.6, 160.9, 155.3, 153.3, 128.7, 113.7, 66.9, 65.0, 53.8, 40.5, 34.8, 26.3, 25.8.

4-((4-Chlorothieno[2,3-*d*]pyrimidin-2-yl)methyl)morpholine (13j). General Procedure E. The residue was chromatographed on silica (1:99 Et₃N/EtOAc) which afforded the compound as a gold oil later solidifying under vacuum (1.12 g, 73%). LCMS (*m/z*): 270.0 [M + H]⁺. HPLC: *t*_R 1.169 min. ¹H NMR (CDCl₃) δ 7.58 (d, *J* = 6.0 Hz, 1H), 7.41 (d, *J* = 6.0 Hz, 1H), 3.91 (s, 2H), 3.81–3.74 (m, 4H), 2.70–2.60 (m, 4H). ¹³C NMR (CDCl₃) δ 169.5, 162.1, 155.1, 128.2, 127.9, 119.8, 66.9, 64.9, 53.9.

2-(Morpholinomethyl)-*N*-(3-(trifluoromethyl)phenyl)-6,7-dihydro-5*H*-cyclopenta[4,5]thieno[2,3-*d*]pyrimidin-4-amine (14a). General Procedure F. The residue was chromatographed on silica (1:99 Et₃N/EtOAc) and the resulting residue recrystallized from CHCl₃/petroleum ether to afford the title compound as a white powder (127 mg, 52%). LCMS (*m/z*): 435.1 [M + H]⁺. HPLC: *t*_R 6.750 min. HRMS (*m/z*): C₂₁H₂₁F₃N₄O requires 435.1467 [M + H]⁺; found 435.1464. ¹H NMR (acetone-*d*₆) δ 8.49 (s, 1H), 8.13 (d, *J* = 8.2 Hz, 1H), 7.86 (s, 1H), 7.58 (t, *J* = 8.0 Hz, 1H), 7.40 (d, *J* = 7.7 Hz, 1H), 3.68 (s, 2H), 3.66–3.59 (m, 4H), 3.31 (ddd, *J* = 5.7, 3.5, 1.7 Hz, 2H), 3.09–2.99 (m, 2H), 2.63–2.58 (m, 4H), 2.58–2.49 (m, 2H). ¹³C NMR (acetone-*d*₆) δ 173.4, 161.6, 154.7, 141.3, 137.8, 131.1 (q, *J* = 32.0 Hz), 130.2, 125.3 (q, *J* = 272.1 Hz), 125.1, 119.9 (d, *J* = 3.9 Hz), 118.2 (d, *J* = 4.1 Hz), 113.4, 67.5, 65.8, 54.5, 30.1, 29.6, 28.5.

2-(Morpholinomethyl)-*N*-(3-(trifluoromethyl)phenyl)-6,7,8,9-tetrahydro-5*H*-cyclohepta[4,5]thieno[2,3-*d*]pyrimidin-4-amine (14b). General Procedure F. The residue was chromatographed on silica (1:99 Et₃N/EtOAc) to afford the title compound as a gold oil

(90.3 mg, 12%). LCMS (*m/z*): 463.1 [M + H]⁺. HPLC: *t*_R 7.226 min. HRMS (*m/z*): C₂₁H₂₁F₃N₄O requires 463.1782 [M + H]⁺; found 463.1774. ¹H NMR (CDCl₃) δ 8.10 (s, 1H), 7.75 (dd, *J* = 8.1, 1.7 Hz, 1H), 7.45 (t, *J* = 7.9 Hz, 1H), 7.33 (d, *J* = 7.8 Hz, 1H), 7.22 (s, 1H), 3.76–3.73 (m, 4H), 3.74 (s, 2H), 3.16–3.08 (m, 2H), 2.93–2.89 (m, 2H), 2.67–2.59 (m, 4H), 1.98–1.78 (m, 4H), 1.88–1.79 (m, 2H). ¹³C NMR (CDCl₃) δ 166.4, 160.1, 154.1, 139.6, 138.9, 131.3 (q, *J* = 32.4 Hz), 129.4, 129.3, 124.1 (q, *J* = 272.5 Hz), 123.6, 119.9 (q, *J* = 3.8 Hz), 117.5 (q, *J* = 3.9 Hz), 116.4, 67.0, 65.1, 53.8, 30.4, 30.3, 29.1, 26.9, 26.4.

2-(Morpholinomethyl)-*N*-(3-(trifluoromethyl)phenyl)-5,6,7,8,9,10-hexahydrocycloocta[4,5]thieno[2,3-*d*]pyrimidin-4-amine (14c). General Procedure F. The residue was chromatographed on silica (1:99 Et₃N/EtOAc) to afford the compound as gold oil (60.2 mg, 11%). LCMS (*m/z*): 477.2 [M + H]⁺. HPLC: *t*_R 7.442 min. HRMS (*m/z*): C₂₄H₂₇F₃N₄O requires 477.194 [M + H]⁺; found 477.193. ¹H NMR (CDCl₃) δ 8.23 (s, 1H), 7.77 (dd, *J* = 8.1, 1.7 Hz, 1H), 7.46 (t, *J* = 7.9 Hz, 1H), 7.35 (s, 1H), 7.32 (d, *J* = 5.8 Hz, 1H), 3.77 (s, 2H), 3.78–3.74 (m, 4H), 3.07 (dd, *J* = 11.8, 5.5 Hz, 2H), 2.95–2.88 (m, 2H), 2.69–2.62 (m, 4H), 1.92–1.81 (m, 2H), 1.78–1.69 (m, 2H), 1.60–1.51 (m, 2H), 1.39 (dd, *J* = 10.5, 5.3 Hz, 2H). ¹³C NMR (CDCl₃) δ 167.0, 160.3, 153.9, 139.6, 138.3, 131.4 (q, *J* = 32.5 Hz), 129.4, 126.5, 124.1 (d, *J* = 272.5 Hz), 123.45, 119.9 (q, *J* = 3.8 Hz), 117.4 (q, *J* = 3.9 Hz), 115.2, 67.1, 65.3, 53.9, 31.7, 30.1, 28.0, 26.3, 26.2, 25.2.

2-(Morpholinomethyl)-6-phenyl-*N*-(3-(trifluoromethyl)phenyl)thieno[2,3-*d*]pyrimidin-4-amine (14d). General Procedure F. The residue was chromatographed on silica (1:99 Et₃N/EtOAc) to afford the title compound as a gold solid (244 mg, 51%). LCMS (*m/z*): 471.1 [M + H]⁺. HPLC: *t*_R 7.124 min. HRMS (*m/z*): C₂₄H₂₁F₃N₄O requires 471.1467 [M + H]⁺; found 471.1461. ¹H NMR (DMSO-*d*₆) δ 9.88 (s, 1H), 8.58 (s, 1H), 8.25 (s, 1H), 8.18 (d, *J* = 8.18 Hz, 1H), 7.73 (d, *J* = 7.5 Hz, 2H), 7.62 (t, *J* = 8.0 Hz, 1H), 7.53 (t, *J* = 7.6 Hz, 2H), 7.43 (t, *J* = 7.8 Hz, 2H), 3.66 (s, 2H), 3.62–3.57 (m, 4H), 2.58–2.52 (m, 4H). ¹³C NMR (DMSO-*d*₆) δ 166.6, 161.5, 153.8, 140.5, 139.2, 133.0, 129.7, 129.4, 129.4 (d, *J* = 31.4 Hz) 128.8, 125.8, 124.3 (q, *J* = 272.4 Hz), 123.7, 118.9 (d, *J* = 3.8 Hz), 116.8, 116.6 (d, *J* = 4.1 Hz), 114.9, 66.2, 64.8, 53.3.

2-(Morpholinomethyl)-5-phenyl-*N*-(3-(trifluoromethyl)phenyl)thieno[2,3-*d*]pyrimidin-4-amine (14e). General Procedure F. The residue was chromatographed on silica (1:29:70 Et₃N/petroleum ether/EtOAc) to afford the compound as a gold oil (307 mg, 75%). LCMS (*m/z*): 471.1 [M + H]⁺. HPLC: *t*_R 7.195 min. HRMS (*m/z*): C₂₄H₂₁F₃N₄O requires 471.1465 [M + H]⁺; found 471.1461. ¹H NMR (CDCl₃) δ 8.08 (s, 1H), 7.60 (dd, *J* = 6.4, 2.5 Hz, 3H), 7.55 (d, *J* = 2.2 Hz, 1H), 7.54 (d, *J* = 3.8 Hz, 1H), 7.34 (t, *J* = 7.9 Hz, 1H), 7.25 (dd, *J* = 13.4, 5.5 Hz, 2H), 7.21 (s, 1H), 7.01 (s, 1H), 3.85 (s, 2H), 3.82–3.77 (m, 4H), 2.76–2.66 (m, 4H). ¹³C NMR (CDCl₃) δ 168.5, 161.9, 154.6, 139.3, 135.9, 133.77, 131.33 (q, *J* = 32.2 Hz), 129.6, 129.4, 129.3 (d, *J* = 2.8 Hz), 123.3 (q, *J* = 272.2 Hz), 122.3, 121.5, 119.6 (q, *J* = 3.8 Hz), 116.5 (q, *J* = 4.0 Hz), 113.3, 67.0, 65.3, 53.8.

6-Benzyl-2-(morpholinomethyl)-*N*-(3-(trifluoromethyl)phenyl)thieno[2,3-*d*]pyrimidin-4-amine (14f). General Procedure F. The reaction precipitate was collected under vacuum and washed with cold *i*-PrOH to afford the compound as a white solid (37.5 mg, 55%). LCMS (*m/z*): 485.2 [M + H]⁺. HPLC: *t*_R 7.162 min. HRMS (*m/z*): C₂₅H₂₃F₃N₄O requires 485.1624 [M + H]⁺; found 485.1617. ¹H NMR (DMSO-*d*₆) δ 10.39 (s, 1H), 8.36 (d, *J* = 8.5 Hz, 1H), 8.19 (s, 1H), 7.92 (s, 1H), 7.61 (t, *J* = 8.0 Hz, 1H), 7.45 (d, *J* = 7.7 Hz, 1H), 7.39–7.33 (m, 4H), 7.30–7.25 (m, 1H), 4.52 (s, 2H), 4.30 (s, 2H), 3.89 (s, 4H), 3.40 (s, 4H). ¹³C NMR (DMSO-*d*₆) δ 166.2, 153.9, 142.6, 139.9, 139.2, 129.8, 129.4, 129.1, 128.7, 128.7, 126.8, 125.3, 124.2 (q, *J* = 272.3 Hz), 119.6, 117.6 (d, *J* = 3.9 Hz), 117.4, 116.8, 63.2, 59.8, 51.8, 36.2.

5-Cyclohexyl-2-(morpholinomethyl)-*N*-(3-(trifluoromethyl)phenyl)thieno[2,3-*d*]pyrimidin-4-amine (14g). General Procedure F. The residue was chromatographed on silica (1:29:70 Et₃N/petroleum ether/EtOAc) to afford the title compound as a yellow oil which later solidified under vacuum (260 mg, 66%). LCMS (*m/z*): 477.2 [M + H]⁺. HPLC: *t*_R 7.618 min. HRMS (*m/z*): C₂₄H₂₇F₃N₄O requires 477.1937 [M + H]⁺; found 477.193. ¹H NMR (CDCl₃) δ 8.33

(s, 1H), 7.75 (dd, *J* = 8.0, 0.9 Hz, 1H), 7.49 (t, *J* = 7.9 Hz, 1H), 7.37 (d, *J* = 6.6 Hz, 2H), 7.01 (s, 1H), 3.80 (s, 2H), 3.79–3.75 (m, 4H), 2.86 (t, *J* = 9.6 Hz, 1H), 2.74–2.62 (m, 4H), 2.23 (d, *J* = 10.4 Hz, 2H), 2.04–1.98 (m, 2H), 1.89 (d, *J* = 12.9 Hz, 1H), 1.64–1.47 (m, 4H), 1.45–1.31 (m, 1H). ¹³C NMR (CDCl₃) δ 169.7, 161.2, 154.7, 139.6, 138.8, 131.6 (q, *J* = 32.3 Hz), 129.6, 124.2 (q, *J* = 272.4 Hz), 123.2, 120.1 (q, *J* = 3.8 Hz), 117.3 (q, *J* = 4.0 Hz), 117.2, 114.1, 67.1, 65.2, 53.9, 41.3, 34.2, 26.9, 26.1.

5,6-Dimethyl-2-(morpholinomethyl)-*N*-(3-(trifluoromethyl)phenyl)thieno[2,3-*d*]pyrimidin-4-amine (14h). General Procedure F. The residue was chromatographed on silica (1:29:70 Et₃N/petroleum ether/EtOAc) to afford the title compound as a gold oil (214 mg, 40%). LCMS (*m/z*): 423.2 [M + H]⁺. HPLC: *t*_R 6.577 min. HRMS (*m/z*): C₂₀H₂₁F₃N₄O₂S requires 423.1464 [M + H]⁺; found 423.1461. ¹H NMR (CDCl₃) δ 8.20 (s, 1H), 7.81 (dd, *J* = 8.1, 1.2 Hz, 1H), 7.46 (t, *J* = 8.0 Hz, 1H), 7.38 (s, 1H), 7.34 (d, *J* = 7.8 Hz, 1H), 3.78–3.75 (m, 6H), 2.68–2.63 (m, 4H), 2.60 (s, 3H), 2.47 (s, 3H). ¹³C NMR (CDCl₃) δ 166.8, 160.5, 154.3, 139.5, 131.9, 131.4 (q, *J* = 32.3 Hz), 129.5, 123.8 (q, *J* = 272.2 Hz), 123.5 (d, *J* = 1.2 Hz), 120.0 (q, *J* = 3.8 Hz), 117.4 (q, *J* = 4.0 Hz), 116.1, 67.1, 65.3, 53.9, 14.6, 13.7.

6-Cyclohexyl-2-(morpholinomethyl)-*N*-(3-(trifluoromethyl)phenyl)thieno[2,3-*d*]pyrimidin-4-amine (14i). General Procedure F. The residue was chromatographed on silica (1:99 Et₃N/EtOAc) to afford the compound as a white solid (258 mg, 54%). LCMS (*m/z*): 477.2 [M + H]⁺. HPLC: *t*_R 7.666 min. HRMS (*m/z*): C₂₄H₂₇F₃N₄O₂S requires 477.1942 [M + H]⁺; found 477.193. ¹H NMR (400 MHz, DMSO-*d*₆) δ 9.72 (s, 1H), 8.57 (s, 1H), 8.17 (d, *J* = 8.3 Hz, 1H), 7.62 (d, *J* = 0.9 Hz, 1H), 7.59 (d, *J* = 8.1 Hz, 1H), 7.39 (d, *J* = 7.7 Hz, 1H), 3.64 (s, 2H), 3.61–3.56 (m, 4H), 2.90 (tt, *J* = 10.8, 5.5 Hz, 1H), 2.56–2.51 (m, 4H), 2.07 (d, *J* = 9.7 Hz, 2H), 1.81 (dd, *J* = 9.3, 3.0 Hz, 2H), 1.71 (d, *J* = 12.7 Hz, 1H), 1.51–1.35 (m, 4H), 1.26 (ddd, *J* = 17.7, 10.6, 6.0 Hz, 1H). ¹³C NMR (DMSO-*d*₆) δ 165.9, 160.5, 153.4, 148.5, 140.7, 129.7, 129.3 (d, *J* = 31.4 Hz), 124.3 (q, *J* = 272.1 Hz), 123.6, 118.7 (d, *J* = 3.8 Hz), 116.5 (d, *J* = 4.0 Hz), 115.6, 113.5, 66.2, 64.7, 53.2, 39.1, 34.4, 25.6, 25.4.

2-(Morpholinomethyl)-*N*-(3-(trifluoromethyl)phenyl)thieno[2,3-*d*]pyrimidin-4-amine (14j). General Procedure F. The precipitate was filtered and washed with cold *i*-PrOH affording the compound as a brown solid (199 mg, 45%). LCMS (*m/z*): 395.1 [M + H]⁺. HPLC: *t*_R 5.894 min. HRMS (*m/z*): C₁₈H₁₇F₃N₄O₂S requires 395.1106 [M + H]⁺; found 395.1148. ¹H NMR (DMSO-*d*₆) δ 10.68 (s, 1H), 8.43 (d, *J* = 8.5 Hz, 1H), 8.29 (d, *J* = 5.9 Hz, 2H), 7.82 (d, *J* = 6.0 Hz, 1H), 7.62 (t, *J* = 8.0 Hz, 1H), 7.46 (d, *J* = 7.7 Hz, 1H), 4.56 (s, 2H), 3.92 (s, 4H), 3.40 (s, 4H). ¹³C NMR (DMSO-*d*₆) δ 166.6, 154.7, 139.9, 129.7, 129.2 (d, *J* = 31.6 Hz), 128.8, 125.4, 124.7, 124.2 (q, *J* = 272.4 Hz), 120.3, 119.7 (d, *J* = 3.9 Hz), 117.7 (d, *J* = 3.9 Hz), 116.4, 63.3, 59.8, 51.9.

6-Benzyl-*N,N*-dimethyl-2-(morpholinomethyl)thieno[2,3-*d*]pyrimidin-4-amine (15). General Procedure F. The residue was chromatographed on silica (1:99 Et₃N/EtOAc) to afford the compound as a gold oil (91 mg, 33%). LCMS (*m/z*): 369.2 [M + H]⁺. HPLC: *t*_R 6.012 min, 93% purity (214 nm). HRMS (*m/z*): C₂₀H₂₄N₄O₂S requires 369.1747 [M + H]⁺; found 369.1744. ¹H NMR (CDCl₃) δ 7.30 (dd, *J* = 9.7, 4.8 Hz, 1H), 7.26–7.20 (m, 3H), 7.11 (s, 1H), 4.14 (s, 2H), 3.80–3.72 (m, 4H), 3.69 (s, 2H), 3.32 (s, 6H), 2.71–2.60 (m, 1H). ¹³C NMR (CDCl₃) δ 169.6, 160.7, 160.0, 157.6, 139.1, 138.2, 128.6, 128.5, 126.7, 118.7, 114.5, 66.8, 65.0, 53.6, 39.8, 36.9.

2-(Morpholinomethyl)-*N*-phenyl-5,6,7,8-tetrahydrobenzo[4,5]thieno[2,3-*d*]pyrimidin-4-amine (16a). General Procedure F. The residue was eluted through a silica gel column (99:1 EtOAc/Et₃N) and proceeded to afford the title compound as a light pink oil which later solidified at room temperature (48.8 mg, 20%). Mp: 129–135 °C. LCMS (*m/z*): 381.2 [M + H]⁺. HPLC: *t*_R 6.294 min. HRMS (*m/z*): C₂₁H₂₄N₄O₂S requires 381.1748 [M + H]⁺; found 381.1744. ¹H NMR (CDCl₃) δ 7.76–7.72 (m, 2H), 7.39–7.33 (m, 2H), 7.17 (s, 1H), 7.13–7.07 (m, 1H), 3.80–3.77 (m, 4H), 3.76 (s, 2H), 3.10–3.02 (m, *J* = 6.0 Hz, 2H), 2.88–2.78 (m, 2H), 2.69–2.62 (m, 4H), 2.02–1.96 (m, 2H), 1.96–1.89 (m, 2H). ¹³C NMR (CDCl₃) δ 167.0, 160.7, 154.7, 138.9, 134.4, 128.9, 124.4, 123.5, 120.5, 114.9, 67.0, 65.1, 53.9, 26.5, 25.5, 22.6, 22.5.

***N*-(3-Fluorophenyl)-2-(morpholinomethyl)-5,6,7,8-tetrahydrobenzo[4,5]thieno[2,3-*d*]pyrimidin-4-amine (16b).** General Procedure F. Chromatographed on silica (1:99 EtOAc/Et₃N) to give the final product as a yellow/orange solid (90.2 mg, 17%). Mp: 141–150 °C. LCMS (*m/z*): 399.2 [M + H]⁺. HPLC: *t*_R 6.569 min. HRMS (*m/z*): C₂₁H₂₃FN₄O₂S requires 399.1654 [M + H]⁺; found 399.1649. ¹H NMR (CDCl₃) δ 7.97 (dt, *J* = 11.5, 2.1 Hz, 1H), 7.32–7.26 (m, 1H), 7.24–7.19 (m, 2H), 6.80 (td, *J* = 8.2, 1.7 Hz, 1H), 3.83–3.80 (m, 4H), 3.80 (s, 2H), 3.06 (t, *J* = 5.7 Hz, 2H), 2.86 (t, *J* = 5.7 Hz, 2H), 2.72–2.65 (m, 4H), 2.02–1.97 (m, 2H), 1.97–1.91 (m, 2H). ¹³C NMR (CDCl₃) δ 165.8 (d, *J* = 247.2 Hz), 161.9, 160.7, 154.4, 140.7 (d, *J* = 11.2 Hz), 134.9, 129.9 (d, *J* = 9.7 Hz), 124.3, 115.2 (d, *J* = 2.7 Hz), 115.1, 109.9 (d, *J* = 21.6 Hz), 107.78 (d, *J* = 27.1 Hz), 67.1, 65.1, 53.9, 26.5, 25.6, 22.6, 22.5.

***N*-(3-Methoxyphenyl)-2-(morpholinomethyl)-5,6,7,8-tetrahydrobenzo[4,5]thieno[2,3-*d*]pyrimidin-4-amine (16c).** General Procedure F. This residue was purified using column chromatography (50:50 petroleum ether/EtOAc) to afford the final product as a yellow oil (60.5 mg, 18%). ¹H NMR (CDCl₃) δ 7.65 (s, 1H, H), 7.25 (t, *J* = 8.1 Hz, 1H), 7.18 (s, 1H), 7.12 (ddd, *J* = 8.2, 2.1, 0.8 Hz, 1H), 6.65 (ddd, *J* = 8.2, 2.5, 0.8 Hz, 1H), 3.86 (s, 3H), 3.81–3.76 (m, *J* = 8.3, 3.5 Hz, 6H), 3.06 (t, *J* = 5.9 Hz, 2H), 2.84 (t, *J* = 5.9 Hz, 2H), 2.67 (s, 4H), 2.03–1.96 (m, 2H), 1.96–1.89 (m, 2H). LCMS (*m/z*): 411.3 [M + H]⁺. HPLC: *t*_R 6.521 min. HRMS (*m/z*): C₂₂H₂₆N₄O₂S requires 411.1853 [M + H]⁺; found 411.1849. ¹³C NMR (CDCl₃) δ 167.0, 160.2, 154.6, 140.2, 134.6, 129.6, 124.4, 115.1, 112.5, 108.7, 106.6, 66.9, 65.2, 60.4, 55.3, 53.8, 26.4, 25.5, 22.6, 22.4.

3-((2-(Morpholinomethyl)-5,6,7,8-tetrahydrobenzo[4,5]thieno[2,3-*d*]pyrimidin-4-yl)amino)phenol (17). To a solution of *N*-(3-methoxyphenyl)-2-(morpholinomethyl)-5,6,7,8-tetrahydrobenzo[4,5]thieno[2,3-*d*]pyrimidin-4-amine (195 mg, 475 μmol) in DCM (4.00 mL) at 0 °C was added BBr₃ (1 M in DCM) (2.37 mL, 2.37 mmol). The mixture was stirred at rt under a N₂ environment overnight and then poured into ice–water. The solution was adjusted to pH 6 by addition of sat. NaHCO₃. The DCM was removed under reduced pressure and the aqueous residue extracted with EtOAc (3 × 20 mL). The combined organic extracts were washed with brine, dried (Na₂SO₄), filtered, and concentrated in vacuo. The resulting residue was eluted through a silica gel column (5:95 MeOH/DCM) to give the title compound as a white/gray solid (100 mg, 53%). Mp: 98–105 °C. LCMS (*m/z*): 397.2 [M + H]⁺. HPLC: *t*_R 5.850 min. HRMS (*m/z*): C₂₁H₂₄N₄O₂S requires 397.1699 [M + H]⁺; found 397.1693. ¹H NMR (CDCl₃) δ 8.37 (s, 1H), 7.73 (t, *J* = 2.0 Hz, 1H), 7.14 (s, 1H), 7.11 (t, *J* = 8.1 Hz, 1H), 6.87 (ddd, *J* = 8.0, 2.0, 0.7 Hz, 1H), 6.56 (ddd, *J* = 8.1, 2.3, 0.7 Hz, 1H), 3.79 (s, 2H), 3.78–3.73 (m, 4H), 2.98 (t, *J* = 5.4 Hz, 2H), 2.80–2.72 (m, 6H), 1.98–1.83 (m, 4H). ¹³C NMR (CDCl₃) δ 166.4, 160.3, 157.4, 154.5, 139.8, 134.4, 129.7, 124.6, 115.1, 111.5, 111.1, 108.3, 66.8, 64.0, 52.8, 26.4, 25.5, 22.5, 22.4.

***N*-Methyl-2-(morpholinomethyl)-5,6,7,8-tetrahydrobenzo[4,5]thieno[2,3-*d*]pyrimidin-4-amine (18).** General Procedure F. Upon completion of reaction the reaction vessel was stored at –4 °C overnight. Precipitates were collected and washed with cold *i*-PrOH to afford the compound as light brown crystals (300 mg, 76%). LCMS (*m/z*): 319.1 [M + H]⁺. HPLC: *t*_R 5.162 min. HRMS (*m/z*): C₁₆H₂₂N₄O₂S requires 319.1593 [M + H]⁺; found 319.1587. ¹H NMR (CDCl₃) δ 5.23 (dd, *J* = 9.4, 5.2 Hz, 1H), 3.82–3.74 (m, 4H), 3.71 (s, 2H), 3.10 (d, *J* = 4.8 Hz, 3H), 2.92–2.85 (m, 2H), 2.82–2.75 (m, 2H), 2.70–2.65 (m, 4H), 1.98–1.81 (m, 4H). ¹³C NMR (CDCl₃) δ 165.9, 161.0, 158.0, 132.8, 125.2, 114.6, 67.1, 65.4, 53.9, 28.1, 26.5, 25.5, 22.7.

***N,N*-Diethyl-2-(morpholinomethyl)-5,6,7,8-tetrahydrobenzo[4,5]thieno[2,3-*d*]pyrimidin-4-amine (19).** General Procedure F. The reaction mixture was concentrated under reduced pressure and the residue chromatographed on silica (5% MeOH–DCM) to afford the compound as a gold oil (299 mg, 90%). LCMS (*m/z*): 361.2 [M + H]⁺. HPLC: *t*_R 5.162 min. HRMS (*m/z*): C₁₉H₂₈N₄O₂S requires 361.2055 [M + H]⁺; found 361.2057. ¹H NMR (CDCl₃) δ 3.71 (t, *J* = 4.7 Hz, 6H), 3.41 (q, *J* = 7.0 Hz, 4H), 2.90–2.76 (m, 4H), 2.65–2.55 (m, 4H), 1.92–1.82 (m, 2H), 1.79–1.68 (m, 2H), 1.08 (t, *J* = 7.0 Hz, 6H). ¹³C NMR (CDCl₃) δ 168.9, 161.7, 159.1, 133.7, 127.4, 120.0, 66.9, 65.0, 53.6, 44.7, 26.6, 25.8, 23.1, 22.9, 12.5.

4-((4-(3-(Trifluoromethyl)phenoxy)-5,6,7,8-tetrahydrobenzo[4,5]thieno[2,3-d]pyrimidin-2-yl)methyl)morpholine **16** (20). A mixture of 4-((4-chloro-5,6,7,8-tetrahydrobenzo[4,5]thieno[2,3-d]pyrimidin-2-yl)methyl)morpholine (350 mg, 1.08 mmol), 3-(trifluoromethyl)phenol (135 μ L, 1.11 mmol), K₂CO₃ (299 mg, 2.16 mmol), and tris[2-(2-methoxyethoxy)ethylamine (TRIDENT) (34.0 μ L, 108 μ mol) was taken up in *i*-PrOH and irradiated at 40 W for 6 h in an 8 mL pressure tube. The reaction mixture was diluted with water and extracted with DCM. The combined organic extracts were dried and concentrated in vacuo. The residue was chromatographed on silica (1:99 Et₃N/EtOAc) to afford the title compound as pale yellow oil (351 mg, 72%). LCMS (*m/z*): 450.1 [M + H]⁺. HPLC: *t*_R 7.432 min. HRMS (*m/z*): C₂₂H₂₂F₃N₃O₂S requires 450.1468 [M + H]⁺; found 450.1458. ¹H NMR (CDCl₃) δ 7.56–7.48 (m, 3H), 7.41 (dt, *J* = 7.4, 1.7 Hz, 1H), 3.72–3.60 (m, 6H), 3.04 (t, *J* = 4.8 Hz, 2H), 2.85 (t, *J* = 4.8 Hz, 2H), 2.54–2.50 (m, 4H), 1.96–1.85 (m, 4H). ¹³C NMR (CDCl₃) δ 169.6, 162.2, 160.5, 152.7, 136.2, 131.9 (q, *J* = 32.9 Hz), 130.0, 126.8, 125.3 (d, *J* = 0.8 Hz), 123.7 (q, *J* = 272.4 Hz), 122.0 (q, *J* = 3.8 Hz), 119.1 (q, *J* = 3.9 Hz), 117.5, 66.8, 64.3, 53.6, 25.8, 25.6, 22.9, 22.4.

5,6,7,8-Tetrahydrobenzo[4,5]thieno[2,3-d]pyrimidin-4(3H)-one **21**. Ethyl-2-amino-4,5,6,7-tetrahydrobenzothioephene-3-carboxylate (4.05 g, 17.8 mmol) was taken up in formamide (20 mL) and heated to 170 °C under a nitrogen atmosphere. The heating was continued for 12 h and the progress of the reaction was monitored by TLC. The reaction mixture was allowed to cool to rt, and the precipitated solids were collected and washed with petroleum spirits to afford the compound as brown crystals (3.12 g, 85%). LCMS (*m/z*): 207.1 [M + H]⁺. HPLC: *t*_R 5.537 min. HRMS (*m/z*): C₁₀H₁₀N₂O₂S requires 207.0585 [M + H]⁺; found 207.0587. ¹H NMR (DMSO-*d*₆) δ 7.99 (s, 1H), 2.86 (t, *J* = 5.9 Hz, 2H), 2.73 (t, *J* = 5.8 Hz, 2H), 1.88–1.64 (m, 4H). ¹³C NMR (DMSO-*d*₆) δ 162.4, 157.6, 144.8, 132.1, 130.8, 122.6, 25.3, 24.4, 22.4, 21.7.

4-Chloro-5,6,7,8-tetrahydrobenzo[4,5]thieno[2,3-d]pyrimidine **22**. General Procedure E. The residue was chromatographed on silica (99:1 EtOAc/Et₃N) which afforded the compound as a gold solid (1.85 g, 68%). LCMS (*m/z*): 225.1 [M + H]⁺. HPLC: *t*_R 8.139 min. ¹H NMR (CDCl₃) δ 8.70 (s, 1H), 3.09 (t, *J* = 4.3 Hz, 2H), 2.88 (dd, *J* = 5.0, 3.5 Hz, 2H), 1.92 (dt, *J* = 6.1, 2.9 Hz, 4H). ¹³C NMR (CDCl₃) δ 169.02, 153.3, 151.7, 139.7, 128.9, 127.3, 26.4, 26.2, 22.5, 22.3.

N-(3-(Trifluoromethyl)phenyl)-5,6,7,8-tetrahydrobenzo[4,5]thieno[2,3-d]pyrimidin-4-amine **23a**. General Procedure F. The crude reaction was concentrated under reduced pressure and the residue chromatographed on silica eluting with (1:29:70 Et₃N/petroleum ether/EtOAc) to afford the compound as an oil which later solidified under vacuum to give a beige solid (265 mg, 68%). LCMS (*m/z*): 350.1 [M + H]⁺. HPLC: *t*_R 8.367 min. HRMS (*m/z*): C₁₇H₁₄F₃N₃S requires 350.0936 [M + H]⁺; found 350.0933. ¹H NMR (CDCl₃) δ 8.52 (s, 1H), 7.96 (s, 1H), 7.91 (d, *J* = 8.2 Hz, 1H), 7.48 (t, *J* = 8.0 Hz, 1H), 7.36 (d, *J* = 7.8 Hz, 1H), 7.22 (s, 1H), 3.08 (t, *J* = 6.0 Hz, 1H), 2.86 (t, *J* = 6.0 Hz, 1H), 2.05–1.91 (m, 4H). ¹³C NMR (CDCl₃) δ 166.7, 15.6, 152.4, 139.3, 135.5, 131.5 (d, *J* = 32.4 Hz), 129.64, 126.1 (d, *J* = 1.0 Hz), 124.1 (q, *J* = 272.5 Hz), 120.3 (q, *J* = 3.8 Hz), 117.5 (q, *J* = 3.9 Hz), 116.8, 26.6, 25.6, 22.6, 22.4.

N,N-Diethyl-5,6,7,8-tetrahydrobenzo[4,5]thieno[2,3-d]pyrimidin-4-amine **23b**. General Procedure F. The solution was concentrated in vacuo and the residue chromatographed on silica (4:1 EtOAc/petroleum ether) which afforded the desired compound as a light gold oil that solidified under high vacuum to give a pale yellow solid (233 mg, 80%). Mp: 60–62 °C. LCMS (*m/z*): 262.1 [M + H]⁺. HPLC: *t*_R 6.281 min. HRMS (*m/z*): C₁₄H₁₉N₃S requires 262.1376 [M + H]⁺; found 262.1372. ¹H NMR (CDCl₃) δ 8.50 (s, 1H), 3.46 (q, *J* = 7.1 Hz, 4H), 2.96–2.82 (m, 4H), 1.97–1.90 (m, 2H), 1.84–1.76 (m, 2H), 1.13 (t, *J* = 7.1 Hz, 6H). ¹³C NMR (CDCl₃) δ 168.3, 162.1, 151.3, 134.2, 127.7, 122.1, 44.9, 26.6, 25.8, 23.0, 22.9, 12.4.

2-(Piperidin-1-ylmethyl)-5,6,7,8-tetrahydrobenzo[4,5]thieno[2,3-d]pyrimidin-4(3H)-one **24**. General Procedure D. The reaction mixture was poured into water. The formed precipitates were collected under vacuum filtration and recrystallized from DMF.

The mother liquor was extracted with EtOAc, washed with water, brine, and the combined organic extracts were concentrated in vacuo. The residue was chromatographed on silica (1:99 MeOH/EtOAc) to afford the target compound as cream white solid (350 mg, 73%). Mp: 182–184 °C. LCMS (*m/z*): 304.2 [M + H]⁺. HPLC: *t*_R 5.228 min. HRMS (*m/z*): C₁₆H₂₁N₃O₂S requires 303.1356 [M + H]⁺; found 303.14. ¹H NMR δ 9.95 (s, 1H), 3.46 (s, 2H), 3.04–2.97 (m, 2H), 2.77–2.73 (m, 2H), 2.54–2.44 (m, 4H), 1.92–1.78 (m, 4H), 1.62 (m, 4H), 1.48 (d, *J* = 5.2 Hz, 2H). ¹³C NMR (CDCl₃) δ 163.7, 158.3, 153.8, 132.8, 131.5, 121.9, 60.8, 54.8, 25.9, 25.6, 25.1, 23.7, 23.0, 22.3.

4-Chloro-2-(piperidin-1-ylmethyl)-5,6,7,8-tetrahydrobenzo[4,5]thieno[2,3-d]pyrimidine **25**. General Procedure E. The residue was eluted through a silica gel column (99:1 EtOAc/Et₃N) which proceeded to give the compound as a golden oil (154 mg, 41%). LCMS (*m/z*): 324.1 [M + H]⁺. HPLC: *t*_R 6.231 min. HRMS (*m/z*): C₁₆H₂₀ClN₃S requires 322.114 [M + H]⁺; found 322.1139. ¹H NMR (CDCl₃) δ 3.80 (s, 2H), 3.06 (t, *J* = 4.2 Hz, 2H), 2.84 (t, *J* = 4.2 Hz, 2H), 2.52–2.49 (m, 4H), 1.93–1.86 (m, 4H), 1.67–1.57 (m, 4H), 1.49–1.36 (m, 2H). ¹³C NMR (CDCl₃) δ 169.4, 161.4, 152.9, 138.9, 126.9, 126.9, 65.2, 54.7, 26.3, 26.0, 25.7, 24.1, 22.5, 22.2.

2-(Piperidin-1-ylmethyl)-N-(3-(trifluoromethyl)phenyl)-5,6,7,8-tetrahydrobenzo[4,5]thieno[2,3-d]pyrimidin-4-amine **26**. General Procedure F. This residue was purified on silica gel (99:1 EtOAc/Et₃N) to give the final product as a yellow oil which later solidified at room temperature (100 mg, 24%). Mp: 121–126 °C. LCMS (*m/z*): 447.3 [M + H]⁺. HPLC: *t*_R 7.602 min. HRMS (*m/z*): C₂₃H₂₅F₃N₄S requires 447.1828 [M + H]⁺; found 447.1825. ¹H NMR δ 8.17 (s, 1H), 7.93 (dd, *J* = 8.1, 1.6 Hz, 1H), 7.48 (t, *J* = 8.0 Hz, 1H), 7.34–7.31 (d, *J* = 7.7 Hz, 1H), 7.26 (s, 1H), 3.77 (s, 2H), 3.09 (t, *J* = 6.0 Hz, 2H), 2.87 (t, *J* = 6.0 Hz, 2H), 2.58 (s, 4H), 2.04–1.97 (m), 1.98–1.94 (m, 2H), 1.66 (dt, *J* = 11.2, 5.6 Hz, 4H), 1.48–1.39 (m, 2H). ¹³C NMR (CDCl₃) δ 167.5, 161.4, 154.2, 139.7, 135.0, 131.4 (q, *J* = 32.3 Hz), 129.5, 124.2, 124.1 (q, *J* = 272.4 Hz), 123.2, 119.7 (q, *J* = 3.8 Hz), 117.1 (q, *J* = 4.0 Hz), 115.1, 65.8, 54.8, 26.6, 26.0, 25.7, 24.3, 22.7, 22.5.

2-(Tetrahydro-4H-pyran-4-ylidene)acetonitrile **29**. To a suspension of sodium hydride (60% mineral dispersion oil) (2.37 g, 59.3 mmol) in diethyl ether (150 mL) cooled to 0 °C was added diethyl cyanomethylphosphonate (9.55 mL, 59.3 mmol) dropwise followed by a solution of tetrahydro-4H-pyran-4-one (5.00 mL, 53.9 mmol) in diethyl ether (150 mL). After the addition was completed the reaction was warmed to room temperature and stirred overnight. H₂O and EtOAc were added, the organic layer was separated, washed with brine, dried over Na₂SO₄, filtered, and concentrated in vacuo to provide the compound as a brown oil. The crude oil was then subjected to vacuum distillation (20 mbar) to reveal the title compound as a transparent oil which crystallized upon standing. This distillate was dissolved in hot petroleum ether and left in the fridge overnight to recrystallize. The crystals were collected and dried to afford the desired compound as a white crystalline solid (2.56 g, 39%). LCMS (*m/z*): 124.2 [M + H]⁺. HPLC: *t*_R 3.390 min. ¹H NMR (CDCl₃) δ 5.19–5.16 (m, 1H), 3.81–3.71 (m, 4H), 2.67–2.60 (m, 2H), 2.43–2.37 (m, 2H). ¹³C NMR (CDCl₃) δ 162.7, 116.2, 93.6, 68.3, 68.1, 35.9, 33.7.

2-(Tetrahydro-2H-pyran-4-yl)acetonitrile **30**. To a solution of 2-(tetrahydro-4H-pyran-4-ylidene)acetonitrile (2.65 g, 20.8 mmol) in ethyl acetate (25 mL) and acetic acid (1 mL) stirred under N₂ was added 10% Pd/C (84.0 mg, 4.17 mmol). The reaction mixture was evacuated under reduced pressure, purged with hydrogen, and stirred for 5 h at rt under 1 atm of pressure. TLC showed consumption of the starting material after 5 h. The reaction was filtered (Celite) and the filtrate was concentrated in vacuo to provide the compound as pale yellow oil which was used for the next reaction without any further purification (2.61 g, quantitative yield). ¹H NMR (CDCl₃) δ 4.04–3.98 (m, 2H), 3.40 (td, *J* = 11.9, 2.1 Hz, 2H), 2.32 (d, *J* = 6.8 Hz, 2H), 1.93 (qdd, *J* = 10.8, 7.0, 3.9 Hz, 2H), 1.75 (ddd, *J* = 12.6, 3.5, 1.6 Hz, 2H), 1.51–1.38 (m, 2H). ¹³C NMR (CDCl₃) δ 118.1, 67.3, 32.3, 32.1, 24.4.

2-((Tetrahydro-2H-pyran-4-yl)methyl)-5,6,7,8-tetrahydrobenzo[4,5]thieno[2,3-d]pyrimidin-4(3H)-one **31**. General Procedure C. The reaction mixture was filtered directly and the solid washed with petroleum ether to obtain the desired compound as a beige solid

(4.23 g, 93%). Mp: 250–252 °C. LCMS (*m/z*): 255.1 [M + H]⁺. HPLC: *t_R* 6.858 min. HRMS (*m/z*): C₁₁H₁₁ClN₂O₂S requires 255.0354 [M + H]⁺; found 255.0353. ¹H NMR (DMSO-*d*₆) δ 7.44 (s, 1H), 4.56 (s, 2H), 2.85 (t, *J* = 5.8 Hz, 2H), 2.73 (t, *J* = 5.8 Hz, 2H), 1.76 (ddd, *J* = 7.5, 6.8, 4.4 Hz, 4H). ¹³C NMR (DMSO-*d*₆) δ 163.1, 158.5, 156.0, 131.0, 130.5, 120.4, 66.8, 40.8, 33.8, 32.2, 25.3, 24.4, 22.5, 21.8.

4-Chloro-2-((tetrahydro-2H-pyran-4-yl)methyl)-5,6,7,8-tetrahydrobenzo[4,5]thieno[2,3-*d*]pyrimidin-4(3H)-one (32). General Procedure E. The residue was chromatographed on silica (1:99 Et₃N/EtOAc) to afford the compound as a gold oil (350 mg, 24%). LCMS (*m/z*): 323.2 [M + H]⁺. HPLC: *t_R* 9.066 min, >95% purity (254 nm). ¹H NMR (CDCl₃) δ 3.93 (dd, *J* = 11.5, 2.4 Hz, 2H), 3.38 (td, *J* = 11.7, 2.3 Hz, 2H), 3.06 (d, *J* = 2.1 Hz, 2H), 2.91 (d, *J* = 7.2 Hz, 2H), 2.85 (d, *J* = 2.1 Hz, 2H), 2.28–2.17 (m, 1H), 1.90 (dt, *J* = 6.0, 2.9 Hz, 4H), 1.60–1.52 (m, 2H), 1.51–1.39 (m, 2H). ¹³C NMR (CDCl₃) δ 169.3, 163.4, 152.9, 138.2, 126.9, 126.3, 67.8, 45.7, 35.1, 32.8, 26.3, 25.9, 22.5, 22.3.

2-((Tetrahydro-2H-pyran-4-yl)methyl)-*N*-(3-(trifluoromethyl)phenyl)-5,6,7,8-tetrahydrobenzo[4,5]thieno[2,3-*d*]pyrimidin-4-amine (33a). General Procedure F. The crude reaction mixture was evaporated under reduced pressure and the residue chromatographed on silica (1% MeOH/CHCl₃) which furnished the title compound as a white foam (160 mg, 48%). LCMS (*m/z*): 448.2 [M + H]⁺. HPLC: *t_R* 7.945 min. HRMS (*m/z*): C₂₃H₂₄F₃N₃O₂S requires 448.1673 [M + H]⁺; found 448.1665. ¹H NMR (CDCl₃) δ 8.31 (s, 1H), 7.72 (dd, *J* = 8.1, 1.7 Hz, 1H), 7.47 (t, *J* = 7.9 Hz, 1H), 7.36–7.33 (m, 1H), 7.24 (s, 1H), 3.95 (dd, *J* = 11.5, 2.4 Hz, 2H), 3.41 (td, *J* = 11.8, 2.1 Hz, 2H), 3.07 (t, *J* = 6.0 Hz, 2H), 2.84 (dd, *J* = 13.1, 6.7 Hz, 4H), 2.26 (dq, *J* = 15.1, 7.5, 3.7 Hz, 1H), 2.03–1.90 (m, 4H), 1.63 (dd, *J* = 13.0, 1.9 Hz, 2H), 1.52–1.43 (m, 2H). ¹³C NMR (CDCl₃) δ 167.3, 163.4, 154.2, 139.5, 134.3, 131.3, (q, *J* = 32.2 Hz), 124.3, 124.1, (q, *J* = 272.5 Hz) 123.0, 119.7, (q, *J* = 3.8 Hz), 117.2, (q, *J* = 4.0 Hz), 114.5, 67.9, 46.2, 34.9, 32.9, 26.5, 25.5, 22.6, 22.5.

***N,N*-Diethyl-2-((tetrahydro-2H-pyran-4-yl)methyl)-5,6,7,8-tetrahydrobenzo[4,5]thieno[2,3-*d*]pyrimidin-4-amine (33b).** General Procedure F. Chromatographed on silica (50:50 petroleum ether/EtOAc) furnishing the target compound as a gold oil (150 mg, quantitative yield). LCMS (*m/z*): 360.2 [M + H]⁺. HPLC: *t_R* 6.664 min. HRMS (*m/z*): C₂₆H₂₉N₃O₂S requires 360.2107 [M + H]⁺; found 360.2104. ¹H NMR (CDCl₃) δ 3.94 (dd, *J* = 11.4, 2.4 Hz, 2H), 3.44 (dd, *J* = 14.1, 7.1 Hz, (m, 4H), 3.42–3.34 (m, 2H), 2.89 (t, *J* = 5.9 Hz, 2H), 2.84 (t, *J* = 6.3 Hz, 2H), 2.79 (d, *J* = 7.2 Hz, 2H), 2.27–2.15 (m, 1H), 1.96–1.88 (m, 2H), 1.81–1.74 (m, 2H), 1.59 (dd, *J* = 13.0, 1.7 Hz, 2H), 1.44 (ddd, *J* = 11.9, 10.3, 6.0 Hz, m, 2H), 1.12 (t, *J* = 7.0 Hz, 6H). ¹³C NMR (CDCl₃) δ 168.9, 162.0, 161.9, 132.9, 127.6, 119.6, 68.1, 45.9, 44.9, 34.9, 33.0, 26.7, 25.8, 23.1, 23.0, 12.5.

4-Morpholinobutanenitrile³⁶ (35b). Morpholine (3.66 mL, 42.3 mmol) and 4-chlorobutanenitrile (2.00 mL, 21.6 mmol) were taken up in toluene (30 mL) and stirred at reflux temperature for 7 h. The reaction mixture was filtered directly, and the solids were washed with CH₂Cl₂. The filtrate was acidified with 1 M KHSO₄ solution and extracted with further CH₂Cl₂, and the organic extracts were discarded. The aqueous phase was then adjusted to pH 12 with 1 M NaOH and extracted with CH₂Cl₂ (3 × 25 mL). The organic extracts were dried over anhydrous Na₂SO₄ and concentrated in vacuo to yield the compound as a transparent oil which was utilized without further purification (2.12 g, 65%). LCMS (*m/z*): 155.1 [M + H]⁺. ¹H NMR (CDCl₃) δ 3.77–3.66 (m, 4H), 2.53–2.37 (m, 8H), 1.83 (p, *J* = 6.9 Hz, 2H). ¹³C NMR (CDCl₃) δ 119.8, 66.9, 56.7, 53.5, 22.5, 14.9.

5-Morpholinopentanenitrile³⁶ (35c). Morpholine (6.93 mL, 80.4 mmol) and 5-chlorovaleronitrile (4.50 mL, 40.2 mmol) were taken up in toluene (50 mL) and stirred at reflux temperature for 8 h. The reaction mixture was filtered directly and the solids were washed with CH₂Cl₂. The filtrate was acidified with 1 M KHSO₄ solution and extracted with further CH₂Cl₂, and the organic extracts were discarded. The aqueous phase was then adjusted to pH 12 with 1 M NaOH and extracted with CH₂Cl₂ (3 × 30 mL). The organic extracts were dried over anhydrous Na₂SO₄ and concentrated in vacuo to yield the compound as a transparent oil which was utilized without further purification (2.93 g, 43%). LCMS (*m/z*): 169.2 [M + H]⁺. ¹H NMR

(CDCl₃) δ 3.77–3.61 (m, 4H), 2.52–2.29 (m, 8H), 1.80–1.57 (m, 4H). ¹³C NMR (CDCl₃) δ 119.7, 67.0, 57.8, 53.7, 25.4, 23.4, 17.1.

2-(2-Chloroethyl)-5,6,7,8-tetrahydrobenzo[4,5]thieno[2,3-*d*]pyrimidin-4(3H)-one (36a). General Procedure C. The reaction was allowed to cool and the precipitate was collected, washed with cold 1,4-dioxane, triturated with petroleum ether, filtered, and dried to afford the compound as a beige powder (4.95 g, 83%). LCMS (*m/z*): 269.1 [M + H]⁺. HPLC: *t_R* 6.677 min. ¹H NMR (DMSO-*d*₆) δ 12.38 (s, 1H), 3.98 (t, *J* = 6.6 Hz, 2H), 3.09 (t, *J* = 6.6 Hz, 2H), 2.84 (t, *J* = 5.8 Hz, 2H), 2.71 (t, *J* = 5.8 Hz, 2H), 1.83–1.67 (m, 4H). ¹³C NMR (DMSO-*d*₆) δ 162.6, 158.4, 154.2, 131.6, 130.7, 120.8, 41.5, 36.6, 25.3, 24.4, 22.5, 21.8.

2-(3-Chloropropyl)-5,6,7,8-tetrahydrobenzo[4,5]thieno[2,3-*d*]pyrimidin-4(3H)-one (36b). General Procedure C. The reaction mixture was allowed to cool and the formed precipitate was collected and washed with cold 1,4-dioxane to yield a light brown solid (3.16 g, 60%). LCMS (*m/z*): 283.1 [M + H]⁺. HPLC: *t_R* 7.018 min. ¹H NMR (DMSO-*d*₆) δ 12.29 (s, 1H), 3.70 (t, *J* = 6.5 Hz, 1H), 2.85 (t, *J* = 5.8 Hz, 2H), 2.78–2.73 (m, 2H), 2.73–2.68 (m, 2H), 2.15 (dq, *J* = 13.6, 6.6 Hz, 2H), 1.77 (ddt, *J* = 8.6, 5.2, 2.6 Hz, 4H). ¹³C NMR (DMSO-*d*₆) δ 162.6, 158.5, 156.4, 131.2, 130.6, 120.6, 44.6, 30.9, 29.3, 25.3, 24.4, 22.5, 21.8.

2-(4-Chlorobutyl)-5,6,7,8-tetrahydrobenzo[4,5]thieno[2,3-*d*]pyrimidin-4(3H)-one (36c). The reaction mixture was allowed to cool and water (150 mL) was added. The precipitate was collected, washed with MeOH, and recrystallized from DMF to afford the compound as light brown crystals (6.56 g, 83% yield). LCMS (*m/z*): 297.1 [M + H]⁺. HPLC: *t_R* 7.276 min. ¹H NMR (DMSO-*d*₆) δ 12.22 (s, 1H), 3.66 (t, *J* = 6.3 Hz, 2H), 2.85 (t, *J* = 6.0 Hz, 2H), 2.71 (t, *J* = 5.8 Hz, 2H), 2.61 (t, *J* = 7.2 Hz, 2H), 1.86–1.68 (m, 8H). ¹³C NMR (DMSO-*d*₆) δ 163.1, 158.5, 157.0, 131.2, 130.5, 120.4, 45.0, 32.9, 31.3, 25.2, 24.4, 24.1, 22.5, 21.8.

2-(2-Morpholinoethyl)-5,6,7,8-tetrahydrobenzo[4,5]thieno[2,3-*d*]pyrimidin-4(3H)-one (37a). General Procedure D. Residue chromatographed on silica (1:99 Et₃N/EtOAc) to yield the compound as a white solid (800 mg, 56%). LCMS (*m/z*): 320.1 [M + H]⁺. HPLC: *t_R* 4.909 min. HRMS (*m/z*): C₁₆H₂₃N₃O₂S requires 320.1433 [M + H]⁺; found 320.1427. ¹H NMR (CDCl₃) δ 12.51 (s, 1H), 3.82–3.71 (m, 4H), 2.96 (t, *J* = 5.9 Hz, 2H), 2.89–2.83 (m, 2H), 2.84–2.78 (m, 2H), 2.74 (t, *J* = 5.9 Hz, 2H), 2.62–2.56 (q, *J* = 3.8 Hz, 4H), 1.90–1.73 (m, 4H). ¹³C NMR (CDCl₃) δ 163.9, 159.7, 155.6, 132.6, 131.3, 121.4, 66.9, 55.7, 53.2, 30.1, 25.6, 25.2, 23.1, 22.4.

2-(3-Morpholinopropyl)-5,6,7,8-tetrahydrobenzo[4,5]thieno[2,3-*d*]pyrimidin-4(3H)-one³⁷ (37b). General Procedure C. The reaction mixture was filtered directly and the solids washed with petroleum ether to obtain the desired compound as a fluffy beige solid (3.51 g, 80%). LCMS (*m/z*): 334.1 [M + H]⁺. HPLC: *t_R* 4.925 min. HRMS (*m/z*): C₁₇H₂₃N₃O₂S requires 334.1586 [M + H]⁺; found 334.1584. ¹H NMR (DMSO-*d*₆) δ 11.54 (s, 1H), 3.99–3.81 (m, 4H), 3.42 (d, *J* = 12.3 Hz, 2H), 3.15–3.07 (m, 2H), 3.06–3.01 (m, 2H), 2.85 (t, *J* = 5.5 Hz, 2H), 2.70 (t, *J* = 7.2 Hz, 4H), 2.17 (dq, *J* = 15.4, 7.6 Hz, 2H), 1.86–1.69 (m, 4H). ¹³C NMR (DMSO-*d*₆) δ 162.9, 158.9, 156.5, 131.7, 131.0, 121.1, 63.5, 55.5, 51.3, 31.2, 25.7, 24.9, 22.9, 22.2, 20.8.

2-(4-Morpholinobutyl)-5,6,7,8-tetrahydrobenzo[4,5]thieno[2,3-*d*]pyrimidin-4(3H)-one (37c). General Procedure C. The reaction mixture was filtered directly and the solids collected and washed with hot *i*-PrOH to afford the desired compound as a white solid (2.34 g, 57%). LCMS (*m/z*): 348.2 [M + H]⁺. HPLC: *t_R* 5.034 min. HRMS (*m/z*): C₁₈H₂₅N₃O₂S requires 348.1749 [M + H]⁺; found 348.1740. ¹H NMR (DMSO-*d*₆) δ 11.36 (s, 1H), 3.99–3.77 (m, 4H), 3.36 (d, *J* = 12.2 Hz, 2H), 3.13–2.93 (m, 2H), 2.83 (t, *J* = 5.6 Hz, 2H), 2.70 (t, *J* = 5.5 Hz, 2H), 2.64 (t, *J* = 6.8 Hz, 2H), 1.86–1.63 (m, 8H). ¹³C NMR (DMSO-*d*₆) δ 162.6, 158.5, 157.1, 131.3, 130.7, 120.6, 63.2, 55.5, 50.9, 33.1, 25.4, 24.5, 24.0, 22.6, 22.1, 21.9.

4-(2-(4-Chloro-5,6,7,8-tetrahydrobenzo[4,5]thieno[2,3-*d*]pyrimidin-2-yl)ethyl)morpholine (38a). General Procedure E. The residue was chromatographed on silica (1:99 Et₃N/EtOAc) to afford the compound as a gold oil (270 mg, 78%). LCMS (*m/z*): 338.1 [M + H]⁺. HPLC: *t_R* 5.824 min. ¹H NMR (CDCl₃) δ 3.87–3.52 (m, 4H), 3.29–3.12 (m, 2H), 3.05 (s, 2H), 2.98–2.89 (m, 2H), 2.85 (s, 2H), 2.59–2.50

(m, 4H), 1.94–1.84 (m, 4H). ¹³C NMR (CDCl₃) δ 169.4, 163.3, 152.9, 138.1, 126.9, 126.4, 67.0, 57.2, 53.4, 35.9, 26.3, 25.9, 22.5, 22.3.

4-(3-(4-Chloro-5,6,7,8-tetrahydrobenzo[4,5]thieno[2,3-d]pyrimidin-2-yl)propyl)morpholine (38b). General Procedure E. The residue was chromatographed on silica (1:99 Et₃N/EtOAc) to afford the compound as a gold oil (1.06 g, 67%). LCMS (*m/z*): 352.1 [M + H]⁺. HPLC: *t_R* 5.938 min. ¹H NMR (CDCl₃) δ 3.66–3.61 (m, 4H), 3.08–2.95 (m, 4H), 2.88–2.78 (m, 2H), 2.47–2.37 (m, 4H), 2.11–2.00 (m, 2H), 1.91 (dt, *J* = 6.0, 2.9 Hz, 4H). ¹³C NMR (CDCl₃) δ 169.4, 164.8, 152.8, 137.9, 126.9, 126.2, 66.9, 58.4, 53.6, 26.3, 25.9, 25.4, 22.5, 22.2.

4-(4-(4-Chloro-5,6,7,8-tetrahydrobenzo[4,5]thieno[2,3-d]pyrimidin-2-yl)butyl)morpholine (38c). General Procedure E. The residue was chromatographed on silica (1:99 Et₃N/EtOAc) to afford the compound as a gold oil (1.42 g, 88%). LCMS (*m/z*): 366.1 [M + H]⁺. HPLC: *t_R* 6.255 min. ¹H NMR (CDCl₃) δ 3.75–3.63 (m, 4H), 3.07–3.02 (m, 2H), 3.02–2.97 (m, 2H), 2.87–2.82 (m, 2H), 2.44–2.34 (m, 6H), 1.98–1.79 (m, 6H), 1.62–1.53 (m, 2H). ¹³C NMR (CDCl₃) δ 169.4, 164.9, 152.9, 138.0, 126.9, 126.2, 66.9, 58.7, 53.7, 26.5, 26.2, 26.2, 25.9, 22.5, 22.2.

2-(2-Morpholinoethyl)-N-(3-(trifluoromethyl)phenyl)-5,6,7,8-tetrahydrobenzo[4,5]thieno[2,3-d]pyrimidin-4-amine (39a). General Procedure F. The crude reaction mixture was concentrated under reduced pressure and the residue chromatographed on silica (1:99 Et₃N/EtOAc). The product was isolated and found to have coeluted with a reaction byproduct (*m/z*: 347.2 [M + H]⁺), this mixture was concentrated under reduced pressure, and the resulting bright yellow solid was suspended in Et₂O. The solids were collected under vacuum filtration and washed with Et₂O to afford the desired compound as pale yellow crystalline solid (233 mg, 27%). LCMS (*m/z*): 463.2 [M + H]⁺. HPLC: *t_R* 7.025 min. HRMS (*m/z*): C₂₃H₂₅F₃N₄O requires 463.1783 [M + H]⁺; found 463.1774. ¹H NMR (CDCl₃) δ 8.28 (s, 1H), 7.71 (dd, *J* = 7.9, 1.5 Hz, 1H), 7.44 (t, *J* = 7.9 Hz, 1H), 7.35–7.31 (m, 1H), 7.23 (s, 1H), 3.87–3.60 (m, 2H), 3.12–3.04 (m, 4H), 2.97–2.91 (m, 2H), 2.84 (t, *J* = 6.0 Hz, 2H), 2.59–2.49 (m, 4H), 2.07–1.89 (m, 4H). ¹³C NMR (CDCl₃) δ 167.4, 163.3, 154.4, 139.6, 134.4, 131.4 (q, *J* = 32.3 Hz), 129.4, 124.4, 124.1 (q, *J* = 27.2 Hz), 123.2, 119.8 (q, *J* = 3.8 Hz), 117.4 (q, *J* = 4.0 Hz), 114.7, 67.2, 57.4, 53.6, 36.3, 26.6, 25.6, 22.6, 22.5.

2-(3-Morpholinopropyl)-N-(3-(trifluoromethyl)phenyl)-5,6,7,8-tetrahydrobenzo[4,5]thieno[2,3-d]pyrimidin-4-amine (39b). General Procedure F. The residue was chromatographed on silica (1:99 Et₃N/EtOAc) to afford the title compound as a light brown oil which later solidified under high vacuum to give a dark white solid (383 mg, 56%). LCMS (*m/z*): 477.2 [M + H]⁺. HPLC: *t_R* 6.671 min. HRMS (*m/z*): C₂₄H₂₇F₃N₄O requires 477.1937 [M + H]⁺; found 477.1930. ¹H NMR (CDCl₃) δ 8.24 (s, 1H), 7.78 (dd, *J* = 8.2, 1.8 Hz, 1H), 7.45 (t, *J* = 7.9 Hz, 1H), 7.36–7.31 (m, 1H), 7.22 (s, 1H), 3.70–3.66 (m, 4H), 3.07 (t, *J* = 6.0 Hz, 2H), 2.96–2.88 (m, 2H), 2.84 (t, *J* = 6.0 Hz, 2H), 2.44 (dd, *J* = 8.4, 6.6 Hz, 6H), 2.13–1.89 (m, 6H). ¹³C NMR (CDCl₃) δ 167.3, 164.7, 154.3, 139.5, 134.1, 131.3, (q, *J* = 32.1 Hz), 129.3, 124.3, 124.1, (q, *J* = 27.2 Hz), 123.1, 119.7, (q, *J* = 3.9 Hz), 117.2, (q, *J* = 4.0 Hz), 114.5, 67.1, 58.5, 53.6, 37.1, 26.5, 25.5, 25.2, 22.5, 22.4.

2-(4-Morpholinobutyl)-N-(3-(trifluoromethyl)phenyl)-5,6,7,8-tetrahydrobenzo[4,5]thieno[2,3-d]pyrimidin-4-amine (39c). General Procedure F. The residue was chromatographed on silica (1:99 Et₃N/EtOAc) to afford the title compound as a pale yellow crystalline solid (400 mg, 59%). LCMS (*m/z*): 491.2 [M + H]⁺. HPLC: *t_R* 6.671 min. HRMS (*m/z*): C₂₅H₂₉F₃N₄O requires 491.2102 [M + H]⁺; found 491.2087. ¹H NMR (CDCl₃) δ 8.30 (s, 1H), 7.74 (dd, *J* = 8.2, 1.8 Hz, 1H), 7.46 (t, *J* = 7.9 Hz, 1H), 7.35–7.31 (m, 1H), 7.22 (s, 1H), 3.76–3.62 (m, 4H), 3.06 (t, *J* = 6.0 Hz, 2H), 2.94–2.88 (m, 2H), 2.84 (t, *J* = 6.0 Hz, 2H), 2.47–2.33 (m, 6H), 1.97 (dddd, *J* = 23.5, 21.1, 13.6, 8.1 Hz, 6H), 1.59 (tt, *J* = 9.8, 6.6 Hz, 2H). ¹³C NMR (CDCl₃) δ 167.3, 164.8, 154.2, 139.5, 134.1, 131.26, (q, *J* = 32.2 Hz), 129.3, 124.07, (q, *J* = 27.2 Hz), 123.0, 119.6, (q, *J* = 3.8 Hz), 117.19, (q, *J* = 4.0 Hz), 114.4, 67.0, 58.9, 53.7, 38.9, 26.5, 26.2, 25.5, 22.5, 22.4.

N,N-Diethyl-2-(4-morpholinobutyl)-5,6,7,8-tetrahydrobenzo[4,5]thieno[2,3-d]pyrimidin-4-amine (40). General Procedure F. Pale yellow solid (145 mg, 94%). Mp: 60–62 °C. LCMS (*m/z*):

403.3 [M + H]⁺. HPLC: *t_R* 5.370 min. HRMS (*m/z*): C₂₂H₃₄N₄O requires 403.2532 [M + H]⁺; found 405.2326. ¹H NMR (CDCl₃) δ 3.76–3.65 (m, 4H), 3.44 (q, *J* = 7.0 Hz, 4H), 2.94–2.79 (m, 6H), 2.45 (d, *J* = 3.8 Hz, 4H), 2.39 (dd, *J* = 8.6, 7.0 Hz, 2H), 1.96–1.88 (m, 2H), 1.87–1.81 (m, 2H), 1.78 (dtd, *J* = 8.9, 5.9, 2.9 Hz, 2H), 1.63–1.52 (m, 2H), 1.12 (t, *J* = 7.0 Hz, 6H). ¹³C NMR (CDCl₃) δ 168.9, 163.5, 162.1, 132.8, 127.6, 119.6, 66.9, 58.9, 53.7, 44.8, 38.8, 26.8, 26.5, 26.1, 25.9, 23.2, 23.1, 12.6.

2-(4-Morpholinobutyl)thieno[2,3-d]pyrimidin-4(3H)-one (41). General Procedure C. The reaction vessel was decanted leaving a dark solid mass. The vessel was washed with 1,4-dioxane, and the solids were collected and stirred in hot 1,4-dioxane to wash away any 1,4-dioxane soluble impurities. The crude solid was chromatographed on silica (5% MeOH/DCM) affording the desired compound as a fluffy beige solid (1.22 g, 57%). LCMS (*m/z*): 294.2 [M + H]⁺. HPLC: *t_R* 3.664 min. HRMS (*m/z*): C₁₄H₁₉N₃O₂S requires 294.1277 [M + H]⁺; found 294.1271. ¹H NMR (CDCl₃) δ 7.44 (d, *J* = 5.8 Hz, 1H), 7.19 (d, *J* = 5.8 Hz, 1H), 3.78–3.73 (m, 4H), 2.87 (t, *J* = 7.5 Hz, 2H), 2.51–2.48 (m, 2H), 2.47–2.43 (m, 2H), 1.90 (dt, *J* = 15.1, 7.5 Hz, 2H), 1.70–1.61 (m, 2H). ¹³C NMR (CDCl₃) δ 166.0, 160.1, 157.8, 122.3, 122.2, 121.4, 66.4, 58.1, 53.4, 45.8, 34.4, 25.3, 25.2.

4-(4-Chlorothieno[2,3-d]pyrimidin-2-yl)butyl)morpholine (42). General Procedure D. The residue was chromatographed on silica (1:99 Et₃N-EtOAc) which afforded the desired compound as a golden oil (485 mg, 51%). LCMS (*m/z*): 312.2 [M + H]⁺. HPLC: *t_R* 4.734 min. ¹H NMR (CDCl₃) δ 7.52 (d, *J* = 6.0 Hz, 1H), 7.39 (d, *J* = 6.0 Hz, 1H), 3.73–3.69 (m, 4H), 3.10–3.02 (m, 2H), 2.46–2.42 (m, 4H), 2.42–2.37 (m, 2H), 1.92 (dt, *J* = 15.5, 7.7 Hz, 2H), 1.60 (ddd, *J* = 17.9, 8.6, 6.7 Hz, 2H). ¹³C NMR (CDCl₃) δ 169.6, 166.5, 154.9, 127.2, 127.1, 119.9, 67.1, 58.9, 53.9, 38.9, 26.7, 26.3.

2-(4-Morpholinobutyl)-N-(3-(trifluoromethyl)phenyl)thieno[2,3-d]pyrimidin-4-amine (43a). General Procedure F. The solvent was concentrated in vacuo and the brown residue was chromatographed on silica (98:1:1 EtOAc/MeOH/Et₃N) furnishing the target compound as a transparent oil, later turning into a white powder under high vacuum (201 mg, 80%). LCMS (*m/z*): 437.2 [M + H]⁺. HPLC: *t_R* 5.670 min. HRMS (*m/z*): C₂₁H₂₃F₃N₄O requires 437.1621 [M + H]⁺; found 437.1617. ¹H NMR (CDCl₃) δ 8.33 (t, *J* = 1.8 Hz, 1H), 7.80 (dd, *J* = 8.1, 0.8 Hz, 1H), 7.47 (t, *J* = 7.9 Hz, 1H), 7.40 (s, 1H), 7.36 (d, *J* = 7.8 Hz, 1H), 7.31 (d, *J* = 6.0 Hz, 1H), 7.25 (d, *J* = 6.0 Hz, 1H), 3.73–3.67 (m, 4H), 3.00–2.94 (m, 2H), 2.46–2.34 (m, *J* = 13.7, 6.1 Hz, 6H), 1.98–1.88 (m, 2H), 1.64–1.55 (m, 2H). ¹³C NMR (CDCl₃) δ 168.4, 166.2, 154.4, 139.5, 131.31 (q, *J* = 32.3 Hz), 129.4, 123.9 (q, *J* = 27.2 Hz), 123.4, 123.3, 120.0 (q, *J* = 3.7 Hz), 117.6 (q, *J* = 4.0 Hz), 116.6, 114.8, 67.0, 58.8, 53.7, 39.1, 26.2.

N,N-Diethyl-2-(4-morpholinobutyl)thieno[2,3-d]pyrimidin-4-amine (43b). General Procedure F. The solvents were evaporated under reduced pressure and the residue was chromatographed on silica (3:2 EtOAc/petroleum ether) furnishing the desired compound as a gold oil (178 mg, 89%). LCMS (*m/z*): 349.2 [M + H]⁺. HPLC: *t_R* 4.108 min. HRMS (*m/z*): C₁₈H₂₈N₄O requires 349.2063 [M + H]⁺; found 349.2057. ¹H NMR (CDCl₃) δ 7.26 (d, *J* = 6.2 Hz, 1H), 7.09 (d, *J* = 6.2 Hz, 1H), 3.74 (q, *J* = 7.1 Hz, 4H), 3.70 (dd, *J* = 7.8, 3.1 Hz, 4H), 2.81 (t, *J* = 7.5 Hz, 2H), 2.44–2.41 (m, 4H), 2.40–2.35 (m, 2H), 1.86 (dt, *J* = 15.3, 7.6 Hz, 2H), 1.58 (tt, *J* = 9.8, 6.6 Hz, 2H), 1.31 (t, *J* = 7.0 Hz, 6H). ¹³C NMR (CDCl₃) δ 169.9, 165.2, 156.9, 121.2, 119.3, 112.5, 67.1, 59.1, 53.8, 43.9, 38.9, 26.7, 26.3, 13.4.

N,N-Diethyl-2-(morpholinomethyl)thieno[2,3-d]pyrimidin-4-amine (44). General Procedure F. The solution was concentrated under reduced pressure and the residue chromatographed on silica (4:1 EtOAc/petroleum ether) affording the desired compound as a light brown oil (125 mg, 94%). Mp: 60–62 °C. LCMS (*m/z*): 262.1 [M + H]⁺. HPLC: *t_R* 6.281 min. HRMS (*m/z*): C₁₅H₂₂N₄O requires 307.1589 [M + H]⁺; found 307.1587. ¹H NMR (CDCl₃) δ 7.29 (d, *J* = 6.2 Hz, 1H), 7.15 (d, *J* = 6.2 Hz, 1H), 3.80–3.77 (m, 4H), 3.76 (dd, *J* = 12.4, 5.5 Hz, 4H), 3.71 (s, 2H), 2.75–2.59 (m, 4H), 1.31 (t, *J* = 7.0 Hz, 3H). ¹³C NMR (CDCl₃) δ 169.9, 160.9, 156.8, 121.1, 120.2, 113.1, 66.9, 65.2, 53.8, 44.0, 13.4.

Thieno[2,3-d]pyrimidin-4(3H)-one (45). Ethyl 2-aminothiophene-3-carboxylate (1.25 g, 7.30 mmol) was taken up in formamide

(15 mL) and heated to 170 °C under a N₂ atmosphere. The heating was continued for 5 h, in which the progress of the reaction was monitored by LC/MS. The crude reaction mixture was diluted with EtOAc and extracted with aqueous 1 M HCl solution (3 × 30 mL). The organic extracts were discarded, the aqueous phase adjusted to approximately pH 10 and further extracted with EtOAc (3 × 30 mL). The organic extracts were collected and dried over anhydrous sodium sulfate and the solvent was concentrated under reduced pressure affording the compound as a yellow solid (845 mg, 76%). LCMS (*m/z*): 153.1 [M + H]⁺. HPLC: *t_R* 3.424 min. ¹H NMR (DMSO-*d*₆) δ 12.50 (s, 1H), 8.14 (s, 1H), 7.59 (d, *J* = 5.8 Hz, 1H), 7.41 (d, *J* = 5.8 Hz, 1H). ¹³C NMR (DMSO-*d*₆) δ 164.6, 157.9, 146.1, 125.1, 124.3, 122.1.

4-Chlorothieno[2,3-d]pyrimidine (46). General Procedure E. The black crude residue was chromatographed on silica (60:40 EtOAc/petroleum ether) to afford the compound as a fluffy beige solid (695 mg, 77%). LCMS (*m/z*): 170.9 [M + H]⁺. HPLC: *t_R* 5.394 min. ¹H NMR (CDCl₃) δ 8.88 (s, 1H), 7.64 (d, *J* = 6.0 Hz, 1H), 7.46 (d, *J* = 6.0 Hz, 1H). ¹³C NMR (CDCl₃) δ 168.8, 155.0, 152.8, 129.6, 128.4, 119.2.

N-(3-(Trifluoromethyl)phenyl)thieno[2,3-d]pyrimidin-4-amine (47a). General Procedure F. The solvent was evaporated under reduced pressure and the residue was chromatographed on silica (70:29:1 petroleum ether/EtOAc/Et₃N). This afforded the target compound as a white/pale yellow solid (225 mg, 65%). Mp: 60–62 °C. LCMS (*m/z*): 296.0 [M + H]⁺. HPLC: *t_R* 6.842 min. HRMS (*m/z*): C₁₃H₈F₃N₃S requires 296.0466 [M + H]⁺; found 296.0464. ¹H NMR (400 MHz, DMSO-*d*₆) δ 9.92 (s, 1H), 8.60 (s, 1H), 8.33 (t, *J* = 2.0 Hz, 1H), 8.23 (dd, *J* = 8.1, 2.0 Hz, 1H), 7.93 (d, *J* = 6.0 Hz, 1H), 7.80 (d, *J* = 6.0 Hz, 1H), 7.63 (t, *J* = 8.0 Hz, 1H), 7.44 (ddt, *J* = 7.8, 1.7, 0.9 Hz, 1H). ¹³C NMR (DMSO-*d*₆) δ 166.8, 154.5, 152.9, 140.3, 129.7, 129.3 (d, *J* = 31.5 Hz), 124.5, 124.3 (q, *J* = 272.6 Hz), 119.4, 119.2 (q, *J* = 3.7 Hz), 117.2, 116.9 (q, *J* = 4.0 Hz).

N,N-Diethylthieno[2,3-d]pyrimidin-4-amine (47b). General Procedure F. The bright blue crude reaction was evaporated of any volatile solvents and the resulting residue chromatographed on silica (50:50 petroleum ether/EtOAc) affording the compound as a light green powder (223 mg, 91%). LCMS (*m/z*): 208.1 [M + H]⁺. HPLC: *t_R* 4.098 min. HRMS (*m/z*): C₁₀H₁₃N₃S requires 208.0984 [M + H]⁺; found 208.0903. ¹H NMR (CDCl₃) δ 8.43 (s, 1H), 7.32 (d, *J* = 6.2 Hz, 1H), 7.19 (d, *J* = 6.2 Hz, 1H), 3.76 (q, *J* = 7.1 Hz, 4H), 1.33 (t, *J* = 7.1 Hz, 6H). ¹³C NMR (CDCl₃) δ 169.1, 157.1, 153.1, 121.4, 120.5, 114.8, 44.1, 13.3.

Pharmacological Characterization. Materials. Dulbecco's modified Eagle's medium, Flp-In CHO cells, and hygromycin B were purchased from Invitrogen (Carlsbad, CA). Fetal bovine serum (FBS) was purchased from ThermoTrace (Melbourne, VIC, Australia). [³H]Raclopride, GF/C 96-well filter plates, and MicroScint-0 were from PerkinElmer (Boston, MA). All other reagents were purchased from Sigma-Aldrich (St. Louis, MO).

Cell Culture. FlpIn Chinese hamster ovary (CHO) cells (Invitrogen, Carlsbad, CA, USA) stably expressing the hD_{2L}R were grown and maintained in Dulbecco's modified Eagle's medium (DMEM) supplemented with 10% fetal bovine serum (FBS) and 200 μg/mL of hygromycin-B and maintained at 37 °C in a humidified incubator containing 5% CO₂.

[³H]Raclopride Binding Assay. The membranes of FlpIn CHO cells expressing the hD_{2L}R were prepared as previously described.³⁸ Radioligand inhibition assays were performed by co-incubating membrane homogenates (15 μg of protein) with varying concentrations of test compound in binding buffer (20 mM HEPES, 100 mM NaCl, 6 mM MgCl₂, 1 mM EGTA, 1 mM EDTA; pH 7.4) containing 0.5 nM of [³H]raclopride to a final volume of 300 μL in the absence or presence of the competing compounds, and incubated at 25 °C for 2–3 h. Each test compound was dissolved in dimethyl sulfoxide and diluted in the binding buffer into 10 half-log₁₀ serial dilutions: final test concentrations ranged from 10⁻³ M to 10⁻⁷ M. All compound concentrations were tested in duplicate. Nonspecific binding was determined using 10 μM haloperidol (Sigma-Aldrich, St. Louis, MO). In the kinetic binding assay, the dissociation of [³H]raclopride was started after being incubated for 60 min. Binding was terminated by fast flow filtration over GF/C

membrane unfilter plates (PerkinElmer) using a Uniplate 96-well harvester (PerkinElmer) followed by five washes with ice-cold 0.9% NaCl. MicroScint-0 (50 μL/well) was added, plates were sealed (TopSeal), and radioactivity was measured in a MicroBeta2 LumijET MicroBeta counter (PerkinElmer). The affinity (*K_d*) of [³H]raclopride at the D_{2L}R determined in saturation binding assays is 1.07 ± 0.12 nM, and the *B_{max}* value is 1.51 ± 0.26 pmol/mg protein.

Cell Culture and Transfection for cAMP Assay. FlpIn CHO cells stably expressing the human dopamine D_{2L} receptor were maintained in DMEM supplemented with 5% fetal calf serum (FBS) and 0.2 mg/mL hygromycin at 37 °C in a humidified incubator supplied with 5% CO₂. For transfection, the cells were grown in 10 cm culture dishes until subconfluent. A mixture of 4 μg of plasmid DNA containing BRET-based cAMP (CAMYEL) biosensor construct²⁹ and 25 μg of 20 kDa linear polyethylene imine (PEI) in 500 μL 150 mM NaCl was added into a dish of cells.

cAMP Measurement. The cellular cAMP levels were measured with the CAMYEL BRET-based biosensor for cAMP.²⁹ One day after transfection, cells were trypsinized and seeded in white 96-well microplates. The cells were then cultured for an additional day, rinsed twice with Hanks' balanced salt solution (HBSS) and were then incubated in fresh HBSS. The *Renilla* luciferase (*RLuc*) substrate coelenterazine-h was added to reach a final concentration of 5 μM. The cells were stimulated with dopamine in the presence of 10 μM forskolin (final concentration). For the antagonism assay, the antagonists were added 30 min prior to stimulation. The BRET signals were measured using a BMG Lumistar counter 30 min after stimulation. The BRET signal (BRET ratio) was determined by calculating the ratio of the light emitted at 535 ± 30 nm (YFP) to the light emitted at 475 ± 30 nm (RLuc).

Data Analysis. Computerized nonlinear regression, statistical analyses and simulations were performed using Prism 6.0 (GraphPad Prism 6.0b software, San Diego, CA).

Analysis of Radioligand Binding Experiments. Competition-binding curves between [³H]raclopride and **1** and analogues of **1** were fitted to the allosteric ternary complex model using the following equation.²⁷

$$Y = \frac{\frac{[A]}{K_A}}{\frac{[A]}{K_A} + \left(\frac{1 + \frac{[B]}{K_B}}{1 + \alpha \frac{[B]}{K_B}} \right)} \quad (1)$$

where *Y* is percentage (vehicle control) binding; [A] and [B] are the concentrations of [³H]raclopride and modulator, respectively; *K_A* and *K_B* are the equilibrium dissociation constants of [³H]raclopride and modulator, respectively; and *α* is the cooperativity between [³H]-raclopride and modulator. Values of *α* > 1 denote positive cooperativity, values of <1 (but >0) denote negative cooperativity, and values of 1 denote neutral cooperativity. For analogues of **1** that displayed incomplete displacement of [³H]raclopride, a value of *α* could be determined experimentally. However, for analogues that acted to completely displace the radioligand then we could not distinguish an allosteric mode of action (with high negative cooperativity) from a competitive mode of interaction. In these cases, we fit the above model fixing the value of *α* to assume high negative cooperativity (*α* = 0.0001). Values of *K_B* determined using this fit did not deviate significantly from values of affinity derived using a competitive model.

Radioligand binding dissociation kinetic data were analyzed and fit to an exponential decay equation using nonlinear regression to determine the rate constant.

$$\text{total binding} = \text{NS} + (\text{total} - \text{NS}) e^{-k_{\text{off}}t} \quad (2)$$

where NS is nonspecific binding and *t* is time expressed in minutes. The dissociation rate constant (*k_{off}*) is expressed in units of inverse, min⁻¹. The half-life for dissociation is also calculated as ln(2)/*k_{off}* or 0.6931/*k_{off}*.

Analysis of Functional Data. All concentration–response data were fitted to the following modified four-parameter Hill equation to derive potency estimates.³⁹

$$E = \text{basal} + \frac{(E_{\max} - \text{basal})[A]^{nH}}{[A]^{nH} + EC_{50}^{nH}} \quad (3)$$

where E is the effect of the system, nH is the Hill slope, and EC_{50} is the concentration of agonist $[A]$ that gives the midpoint response between basal and maximal effect of dopamine or other agonists (E_{\max}), which are the lower and upper asymptotes of the response, respectively.

To determine the mode of interaction of **1** and derivatives of **1** at the D₂R in relation to the agonist dopamine, data were fit to both a competitive and allosteric model and the best fit was compared statistically. A logistic equation of competitive agonist–antagonist interaction was globally fitted to data from functional experiments measuring the interaction between dopamine and all analogues of **1**:

$$\text{response} = \text{bottom} + \frac{(E_{\max} - \text{bottom})}{1 + \left(\frac{10^{-pEC_{50} \left[1 + \left(\frac{[B]/10^{-K_B} \right)^s \right]}}{[A]} \right)^{nH}} \quad (4)$$

where s represents the Schild slope for the antagonist and pA_2 represents the negative logarithm of the molar concentration of antagonist that makes it necessary to double the concentration of agonist needed to elicit the original submaximal response obtained in the absence of antagonist. The same data describing the interaction between all analogues of **1** and dopamine were also analyzed using a complete operational model of allosterism and agonism according to eq 5:²⁷

$$E = \frac{E_m(\tau_A[A](K_B + \alpha\beta[B]) + \tau_B[B]K_A)^{nH}}{([A]K_B + K_AK_B + K_A[B] + \alpha[A][B])^{nH} + (\tau_A[A](K_B + \alpha\beta[B]) + \tau_B[B]K_A)^{nH}} \quad (5)$$

where E_m is the maximum possible cellular response, $[A]$ and $[B]$ are the concentrations of orthosteric and allosteric ligands, respectively, K_A and K_B are the equilibrium dissociation constant of the orthosteric and allosteric ligands, respectively, τ_A and τ_B (constrained to -100) are operational measures of orthosteric and allosteric ligand efficacy (which incorporate both signal efficiency and receptor density), respectively, α is the binding cooperativity parameter between the orthosteric and allosteric ligand, and β denotes the magnitude of the allosteric effect of the modulator on the efficacy of the orthosteric agonist. K_A was constrained to 617 nM and represents a value of functional affinity determined by an operational model of agonism applied to dose–response data of dopamine in the presence of increasing concentrations of the alkylating agent phenoxybenzamine. For compounds that caused a limited rightward shift of the dopamine dose–response curve but no decrease in E_{\max} , data were fit using an operational model of allosterism where $\log \beta$ was constrained to 0 to represent neutral cooperativity with dopamine efficacy. For compounds that produced an unlimited decrease in the maximal response of dopamine $\log \beta$ was constrained to -3 .

For each of the compounds the two equations (models) were then compared for their fit using an extra-sum-of-squares F test. All of the data points and values shown in the figures and tables are the mean \pm SEM of at least three separate experiments performed in duplicate unless otherwise stated.

Molecular Docking Simulations. The D₂R crystal structure (PDB code 6C38)³² was prepared by the regularization algorithm implemented in ICM-Pro molecular modeling software.⁴⁰ Raclopride was docked into the orthosteric pocket of the D₂R using an energy-based docking protocol implemented in the ICM-Pro software.⁴⁰ The best energy binding pose predicted for raclopride in the D₂R was found to be similar to the binding pose of closely related eticlopride in the cocrystallized complex with the D₃R.⁹ The D₂R–raclopride complex was further optimized using biased probability Monte Carlo (BPMC) optimization of the surrounding residues in the proximity of 5 Å of ligand. In the final D₂R–raclopride complex, the rmsd between common atoms of raclopride and the crystallographic pose of eticlopride did not exceed 0.5 Å.

Compound **1** and its 33 analogues were docked into the D₃R–raclopride complex using an energy-based docking protocol implemented in the ICM-Pro software.^{40,41} Compounds were generated from

2D representations, and their 3D geometry was optimized using MMFF-94 force field. The docking was performed in the rectangular box that comprised the whole extracellular part of the receptor above raclopride, including the extracellular loops. Docking simulations used BPMC optimization of the compounds' internal coordinates in the pre-calculated grid energy potentials of the receptor. The exhaustive sampling of the compound conformational space was done with the thoroughness parameter set to 10 and at least three independent docking runs performed for each compound. The final docking poses were selected based on optimal ligand receptor interactions and ICM binding scores.

For D₃R docking, we used the previously published D₃R–eticlopride crystal structure (PDB code 3PBL),⁹ where raclopride was docked in place of eticlopride. Compound **1** and its eight analogues were then docked into D₃R–raclopride complex. Due to the hypothesized high flexibility of the E90^{2.65} residue side chain, it was set up as “explicitly flexible group” during the docking. Further docking method was used as above-mentioned.

■ ASSOCIATED CONTENT

5 Supporting Information

The Supporting Information is available free of charge on the ACS Publications website at DOI: 10.1021/acs.jmedchem.7b01565.

Figures showing multiple sequence alignment of dopamine receptors and molecular docking studies (PDF)
Molecular formula strings and some data (CSV)

■ AUTHOR INFORMATION

Corresponding Authors

*J.R.L.: phone, +61 3 9903 9095; e-mail, rob.lane@monash.edu.

*B.C.: phone, +61 9903 9556; e-mail, ben.capuano@monash.edu.

ORCID

Barrie Kellam: 0000-0003-0030-9908

Shailesh N. Mistry: 0000-0002-2252-1689

Vsevolod Katrich: 0000-0003-3883-4505

Peter J. Scammells: 0000-0003-2930-895X

Ben Capuano: 0000-0001-5434-0180

Notes

The authors declare no competing financial interest.

■ ACKNOWLEDGMENTS

This research was supported by a National Health and Medical Research Council (NHMRC) Project Grant APP1049564.

■ ABBREVIATIONS USED

cAMP, cyclic adenosine monophosphate; D₂R, dopamine D₂ receptor; D₃R, dopamine D₃ receptor; DA, dopamine; GPCR, G-protein-coupled receptor; FGA, first-generation antipsychotic; SGA, second-generation antipsychotic; EPS, extrapyramidal symptoms; NAM, negative allosteric modulator; VLS, virtual ligand screening; SAR, structure–activity relationship; CHO, Chinese hamster ovary; cAMP, cyclic adenosine monophosphate; BRET, bioluminescence resonance energy transfer; FBS, fetal bovine serum; HBSS, Hanks' balanced salt solution; SEM, standard error of mean; DMF, *N,N*-dimethylformamide; POCl₃, phosphorus oxychloride; *i*-PrOH, isopropyl alcohol; EtOAc, ethyl acetate; DCM, dichloromethane; MWI, microwave irradiation; TRIDENT, tris[2-(2-methoxyethoxy)ethyl]amine

■ REFERENCES

(1) Seeman, P. Targeting the dopamine D₂ receptor in schizophrenia. *Expert Opin. Ther. Targets* 2006, 10, 515–531.

- (2) Davis, K. L.; Kahn, R. S.; Ko, G.; Davidson, M. Dopamine in schizophrenia: a review and reconceptualization. *Am. J. Psychiatry* **1991**, *148*, 1474–1486.
- (3) Boyd, K. N.; Mailman, R. B. Dopamine receptor signaling and current and future antipsychotic drugs. *Handb. Exp. Pharmacol.* **2012**, *212*, 53–86.
- (4) Newcomer, J. W. Second-generation (atypical) antipsychotics and metabolic effects: a comprehensive literature review. *CNS Drugs* **2005**, *19*, 1–93.
- (5) Rossi, M.; Fasciani, I.; Marampon, F.; Maggio, R.; Scarselli, M. The first negative allosteric modulator for dopamine D2 and D3 Receptors, SB269652 may lead to a new generation of antipsychotic drugs. *Mol. Pharmacol.* **2017**, *91*, 586–594.
- (6) Kenakin, T.; Miller, L. J. Seven transmembrane receptors as shapeshifting proteins: the impact of allosteric modulation and functional selectivity on new drug discovery. *Pharmacol. Rev.* **2010**, *62*, 265–304.
- (7) May, L. T.; Christopoulos, A. Allosteric modulators of G-protein-coupled receptors. *Curr. Opin. Pharmacol.* **2003**, *3*, 551–556.
- (8) Lane, J. R.; Chubukov, P.; Liu, W.; Canals, M.; Cherezov, V.; Abagyan, R.; Stevens, R. C.; Katritch, V. Structure-based ligand discovery targeting orthosteric and allosteric pockets of dopamine receptors. *Mol. Pharmacol.* **2013**, *84*, 794–807.
- (9) Chien, E. Y.; Liu, W.; Zhao, Q.; Katritch, V.; Han, G. W.; Hanson, M. A.; Shi, L.; Newman, A. H.; Javitch, J. A.; Cherezov, V.; Stevens, R. C. Structure of the human dopamine D3 receptor in complex with a D2/D3 selective antagonist. *Science* **2010**, *330*, 1091–1095.
- (10) Silvano, E.; Millan, M. J.; Mannoury la Cour, C.; Han, Y.; Duan, L.; Griffin, S. A.; Luedtke, R. R.; Aloisi, G.; Rossi, M.; Zazzeroni, F.; Javitch, J. A.; Maggio, R. The tetrahydroisoquinoline derivative SB269,652 is an allosteric antagonist at dopamine D3 and D2 receptors. *Mol. Pharmacol.* **2010**, *78*, 925–934.
- (11) Wood, M.; Ates, A.; Andre, V. M.; Michel, A.; Barnaby, R.; Gillard, M. In vitro and in vivo identification of novel positive allosteric modulators of the human dopamine D2 and D3 receptor. *Mol. Pharmacol.* **2016**, *89*, 303–312.
- (12) Kumar, V.; Moritz, A. E.; Keck, T. M.; Bonifazi, A.; Ellenberger, M. P.; Sibley, C. D.; Free, R. B.; Shi, L.; Lane, J. R.; Sibley, D. R.; Newman, A. H. Synthesis and pharmacological characterization of novel trans-cyclopropylmethyl-linked bivalent ligands that exhibit selectivity and allosteric pharmacology at the dopamine D3 receptor (D3R). *J. Med. Chem.* **2017**, *60*, 1478–1494.
- (13) Manglik, A.; Lin, H.; Aryal, D. K.; McCorvy, J. D.; Dengler, D.; Corder, G.; Levit, A.; Kling, R. C.; Bernat, V.; Hubner, H.; Huang, X. P.; Sassano, M. F.; Giguere, P. M.; Lober, S.; Duan, D.; Scherrer, G.; Kobilka, B. K.; Gmeiner, P.; Roth, B. L.; Shoichet, B. K. Structure-based discovery of opioid analgesics with reduced side effects. *Nature* **2016**, *537*, 185–190.
- (14) Carlsson, J.; Coleman, R. G.; Setola, V.; Irwin, J. J.; Fan, H.; Schlessinger, A.; Salji, A.; Roth, B. L.; Shoichet, B. K. Ligand discovery from a dopamine D3 receptor homology model and crystal structure. *Nat. Chem. Biol.* **2011**, *7*, 769–778.
- (15) Sabnis, R. W.; Rangnekar, D. W.; Sonawane, N. D. 2-Aminothiophenes by the gewald reaction. *J. Heterocycl. Chem.* **1999**, *36*, 333–345.
- (16) Bogolubsky, A. V.; Ryabukhin, S. V.; Stetsenko, S. V.; Chupryna, A. A.; Volochnyuk, D. M.; Tolmachev, A. A. Synthesis of thieno[2,3-*d*]pyrimidin-2-ylmethanamine combinatorial library with four diversity points. *J. Comb. Chem.* **2007**, *9*, 661–667.
- (17) Bozorov, K.; Zhao, J. Y.; Elmuradov, B.; Pataer, A.; Aisa, H. A. Recent developments regarding the use of thieno[2,3-*d*]pyrimidin-4-one derivatives in medicinal chemistry, with a focus on their synthesis and anticancer properties. *Eur. J. Med. Chem.* **2015**, *102*, 552–573.
- (18) Wilding, B.; Faschauner, S.; Klempier, N. A practical synthesis of 5-functionalized thieno[2,3-*d*]pyrimidines. *Tetrahedron Lett.* **2015**, *56*, 4486–4489.
- (19) Wu, C.-H.; Coumar, M. S.; Chu, C.-Y.; Lin, W.-H.; Chen, Y.-R.; Chen, C.-T.; Shiao, H.-Y.; Rafi, S.; Wang, S.-Y.; Hsu, H.; Chen, C.-H.; Chang, C.-Y.; Chang, T.-Y.; Lien, T.-W.; Fang, M.-Y.; Yeh, K.-C.; Chen, C.-P.; Yeh, T.-K.; Hsieh, S.-H.; Hsu, J. T. A.; Liao, C.-C.; Chao, Y.-S.; Hsieh, H.-P. Design and synthesis of tetrahydropyridothieno[2,3-*d*]pyrimidine scaffold based epidermal growth factor receptor (EGFR) kinase inhibitors: the role of side chain chirality and michael acceptor group for maximal potency. *J. Med. Chem.* **2010**, *53*, 7316–7326.
- (20) Hesse, S.; Perspicace, E.; Kirsch, G. Microwave-assisted synthesis of 2-aminothiophene-3-carboxylic acid derivatives, 3H-thieno[2,3-*d*]pyrimidin-4-one and 4-chlorothieno[2,3-*d*]pyrimidine. *Tetrahedron Lett.* **2007**, *48*, 5261–5264.
- (21) Bugge, S.; Kaspersen, S. J.; Sundby, E.; Hoff, B. H. Route selection in the synthesis of C-4 and C-6 substituted thienopyrimidines. *Tetrahedron* **2012**, *68*, 9226–9233.
- (22) Jang, M.-Y.; Jonghe, S. D.; Belle, K. V.; Louat, T.; Waer, M.; Herdewijn, P. Synthesis, immunosuppressive activity and structure–activity relationship study of a new series of 4-*N*-piperazinyl-thieno[2,3-*d*]pyrimidine analogues. *Bioorg. Med. Chem. Lett.* **2010**, *20*, 844–847.
- (23) Forero, J. S. B.; de Carvalho, E. M.; Jones Junior, J.; da Silva, F. M. A new protocol for the synthesis of 2-aminothiophenes through the Gewald reaction in solvent-free conditions. *Heterocycl. Lett.* **2011**, *1*, 1–67.
- (24) Baricordi, N.; Benetti, S.; Bertolasi, V.; De Risi, C.; Pollini, G. P.; Zamberlan, F.; Zanirato, V. 1,4-Dithiane-2,5-diol as an efficient synthon for a straightforward synthesis of functionalized tetrahydrothiophenes via sulfa-Michael/aldol-type reactions with electrophilic alkenes. *Tetrahedron* **2012**, *68*, 208–213.
- (25) Lilienkamp, A.; Karkola, S.; Alho-Richmond, S.; Koskimies, P.; Johansson, N.; Huhtinen, K.; Vihko, K.; Wähälä, K. Synthesis and biological evaluation of 17 β -hydroxysteroid dehydrogenase type 1 (17 β -HSD1) inhibitors based on a thieno[2,3-*d*]pyrimidin-4(3H)-one core. *J. Med. Chem.* **2009**, *52*, 6660–6671.
- (26) Shonberg, J.; Draper-Joyce, C.; Mistry, S. N.; Christopoulos, A.; Scammells, P. J.; Lane, J. R.; Capuano, B. Structure-activity study of *N*-((trans)-4-(2-(7-cyano-3,4-dihydroisoquinolin-2(1H)-yl)ethyl)-cyclohexyl)-1H-indole-2-carboxamide (SB269652), a bitopic ligand that acts as a negative allosteric modulator of the dopamine D2 receptor. *J. Med. Chem.* **2015**, *58*, 5287–5307.
- (27) Christopoulos, A.; Kenakin, T. G protein-coupled receptor allostery and complexing. *Pharmacol. Rev.* **2002**, *54*, 323–374.
- (28) Christopoulos, A.; Changeux, J. P.; Catterall, W. A.; Fabbro, D.; Burris, T. P.; Cidlowski, J. A.; Olsen, R. W.; Peters, J. A.; Neubig, R. R.; Pin, J. P.; Sexton, P. M.; Kenakin, T. P.; Ehler, F. J.; Spedding, M.; Langmead, C. J. International Union of Basic and Clinical Pharmacology. XC. multisite pharmacology: recommendations for the nomenclature of receptor allostery and allosteric ligands. *Pharmacol. Rev.* **2014**, *66*, 918–947.
- (29) Jiang, L. I.; Collins, J.; Davis, R.; Lin, K. M.; DeCamp, D.; Roach, T.; Hsueh, R.; Rebres, R. A.; Ross, E. M.; Taussig, R.; Fraser, I.; Sternweis, P. C. Use of a cAMP BRET sensor to characterize a novel regulation of cAMP by the sphingosine 1-phosphate/G13 pathway. *J. Biol. Chem.* **2007**, *282*, 10576–10584.
- (30) Leach, K.; Sexton, P. M.; Christopoulos, A. Allosteric GPCR modulators: taking advantage of permissive receptor pharmacology. *Trends Pharmacol. Sci.* **2007**, *28*, 382–389.
- (31) Christopoulos, A. Assessing the distribution of parameters in models of ligand-receptor interaction: to log or not to log. *Trends Pharmacol. Sci.* **1998**, *19*, 351–357.
- (32) Wang, S.; Che, T.; Levit, A.; Shoichet, B. K.; Wacker, D.; Roth, B. L. Structure of the D2 dopamine receptor bound to the atypical antipsychotic drug risperidone. *Nature* **2018**, *555*, 269–273.
- (33) Nirogi, R. V. S.; Kambhampati, R. S.; Kothmirkar, P.; Arepalli, S.; Pamuleti, N. R. G.; Shinde, A. K.; Dubey, P. K. Convenient and efficient synthesis of some novel fused thieno pyrimidines using gewald's reaction. *Synth. Commun.* **2011**, *41*, 2835–2851.
- (34) Rashmi, P.; Nargund, L. V.; Hazra, K.; Chandra, J. N. Thienopyrimidines as novel inhibitors of Mycobacterium tuberculosis: synthesis and in-vitro studies. *Arch. Pharm.* **2011**, *344*, 459–465.
- (35) Brindani, N.; Rasso, G.; Dell'Amico, L.; Zambrano, V.; Pinna, L.; Curti, C.; Sartori, A.; Battistini, L.; Casiraghi, G.; Pelosi, G.; Greco, D.; Zanardi, F. Organocatalytic, asymmetric eliminative [4 + 2] cyclo-

addition of allylidene malononitriles with enals: rapid entry to cyclohexadiene-embedding linear and angular polycycles. *Angew. Chem., Int. Ed.* **2015**, *54*, 7386–7390.

(36) Frankel, M.; Mosher, H. S.; Whitmore, F. C. Addition reactions of 1-cyano-1,3-butadiene. *J. Am. Chem. Soc.* **1950**, *72*, 81–83.

(37) Shibinskaya, M. O.; Kutuzova, N. A.; Mazepa, A. V.; Lyakhov, S. A.; Andronati, S. A.; Zubritsky, M. J.; Galat, V. F.; Lipkowski, J.; Kravtsov, V. C. Synthesis of 6-aminopropyl-6*H*-indolo[2,3-*b*]quinoxaline Derivatives. *J. Heterocyclic Chem.* **2012**, *49*, 678–682.

(38) Klein Herenbrink, C.; Sykes, D. A.; Donthamsetti, P.; Canals, M.; Coudrat, T.; Shonberg, J.; Scammells, P. J.; Capuano, B.; Sexton, P. M.; Charlton, S. J.; Javitch, J. A.; Christopoulos, A.; Lane, J. R. The role of kinetic context in apparent biased agonism at GPCRs. *Nat. Commun.* **2016**, *7*, 10842.

(39) Motulsky, H. J. C. *Fitting Models to Biological Data Using Linear and Nonlinear Regression: A Practical Guide to Curve Fitting*; GraphPad Software, Inc.: San Diego CA, 2003.

(40) Neves, M. A. C.; Totrov, M.; Abagyan, R. Docking and scoring with ICM: the benchmarking results and strategies for improvement. *J. Comput.-Aided Mol. Des.* **2012**, *26*, 675–686.

(41) Abagyan, R.; Orry, A.; Rausch, E.; Totrov, M. *ICM-Pro User Guide*; MolSoft LLC: La Jolla, CA, 2017.

Supplementary Information

A Thieno[2,3-d]pyrimidine Scaffold is a Novel Negative Allosteric Modulator of the Dopamine D₂ Receptor

Tim J. Fyfe,^{†,§,||} Barbara Zarzycka,[‡] Herman D. Lim,[§] Barrie Kellam,^{||} Shailesh N. Mistry,^{||} Vsevolod Katrich,^{‡,≠} Peter J. Scammells,[†] J. Robert Lane,^{*,§} Ben Capuano^{*,†}

[†]Medicinal Chemistry, and [§]Drug Discovery Biology, Monash Institute of Pharmaceutical Sciences, Monash University, Parkville, Victoria 3052, Australia

^{||}School of Pharmacy, Centre for Biomolecular Sciences, University of Nottingham, Nottingham NG7 2RD, U.K

[‡]Department of Biological Sciences, Bridge Institute, University of Southern California, Los Angeles, CA 90089, United States.

[≠]Department of Chemistry, Bridge Institute, University of Southern California, Los Angeles, CA 90089, United States.

Table of Contents

Figure 1	Multiple sequence alignment of dopamine receptors.....	111-112
Figure 2	Molecular docking studies of analogues of compound 1 in complex with D ₂ R ^{Raclo}	114-115
Figure 3	Molecular docking studies and selectivity profiles of compound 1 and its analogues in complex with D ₃ R ^{Raclo}	117-118

The overall sequence identity of the full-length dopamine receptors constitutes only 12%, with sequence identity of the D₂R vs D₁R, D₃R, D₄R, and D₅R of 25.3%, 57.0%, 34.1%, and 26.6%, respectively (Figure 1a).

More importantly, the predicted allosteric pocket amongst the dopamine receptors is relatively low with the overall conservation of 17% (Figure 1c). Thus, low conservation of the predicted allosteric pocket amongst the dopamine receptors does suggest potential selectivity profile of D₂R optimized compounds. However, the D₂R and D₃R are the most closely related receptors, with the sequence identity of the predicted allosteric binding pocket of 88%. Thus, obtaining the high selectivity profile allosteric modulators for these receptors might be challenging.

Additionally, the D₄R shares only 44% sequence identity, while D₁R and D₅R are not closely related, exhibiting only 25% sequence identity (Figure 1c). Thus, it is expected that the selectivity profile amongst these dopamine receptors will be higher. The recently obtained crystal structure of the D₄R receptor showed significant differences of the predicted allosteric binding site, suggesting that our optimized compounds might have the higher selectivity profile over D₄R than over D₃R.

a



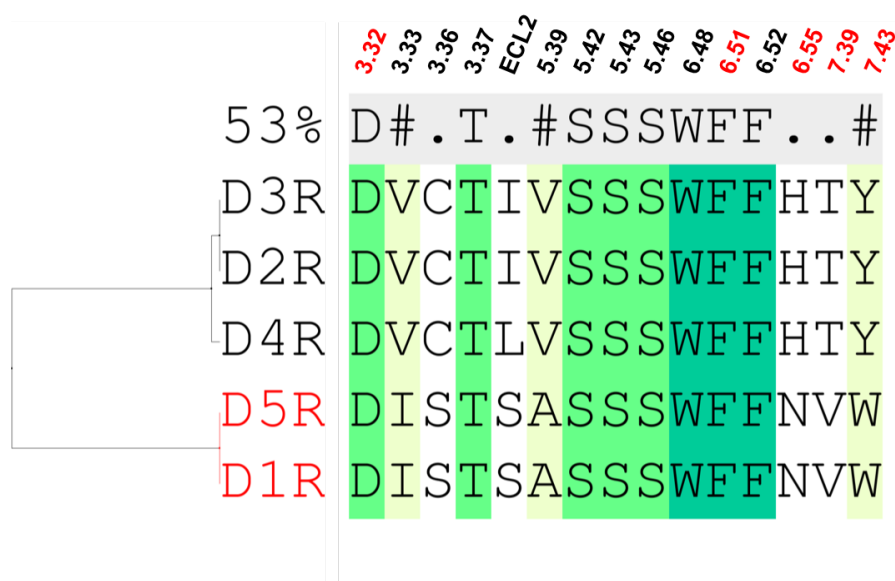
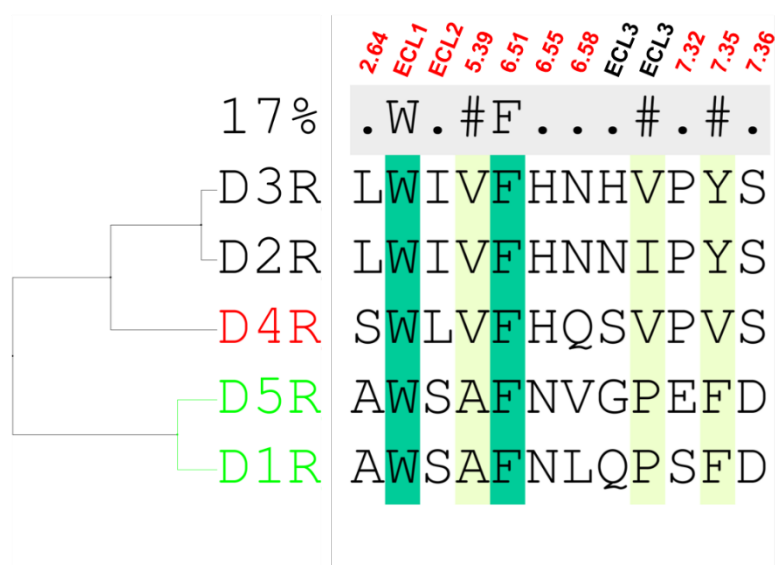
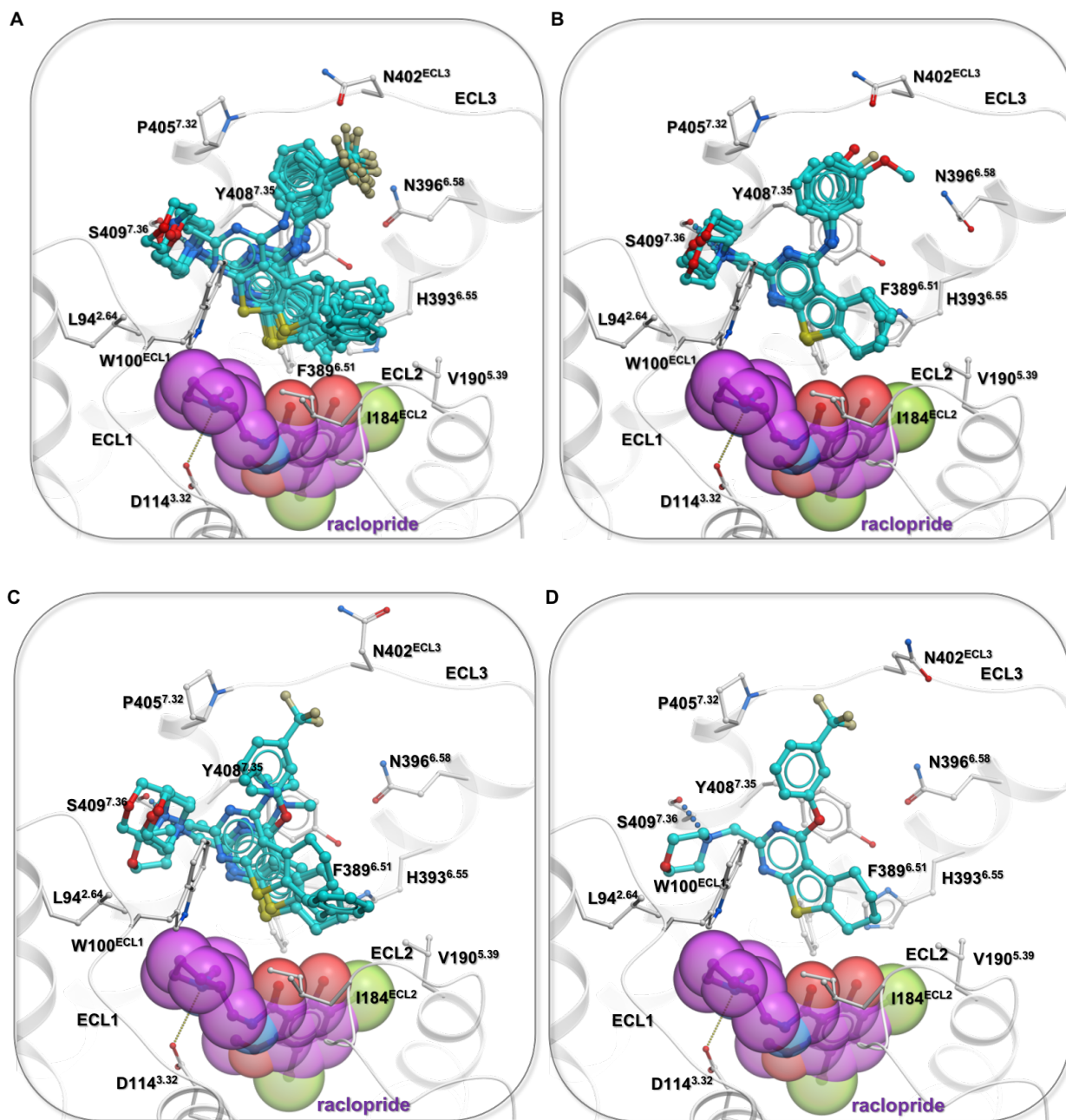
b**c**

Figure 1. Multiple sequence alignment of dopamine receptors. Alignments are coloured by the consensus strength, fully conserved residues (dark green), partially conserved residues (light green). **(a)** Full-length sequences. Overall sequence identity is 12%. Sequence identity of the D₂R vs D₁R, D₃R, D₄R, and D₅R are 25.3%, 57.0%, 34.1%, and 26.6%, respectively. **(b)** The orthosteric binding pockets. Overall sequence identity is 53.0%. Sequence identity of the D₂R vs D₁R, D₃R, D₄R, and D₅R are 53.0%, 100%, 100%, and 53.0%, respectively. **(c)** The predicted allosteric binding pockets. Overall sequence identity is 17%. Sequence identity of the D₂R vs D₁R, D₃R, D₄R, and D₅R are 25.0%, 88.0%, 44.0%, and 25.0%, respectively. Residues numbering is indicated above the alignment. The unique residues which create either orthosteric or allosteric pockets (black), residues that create both orthosteric and allosteric binding pockets (red).

Molecular docking studies.



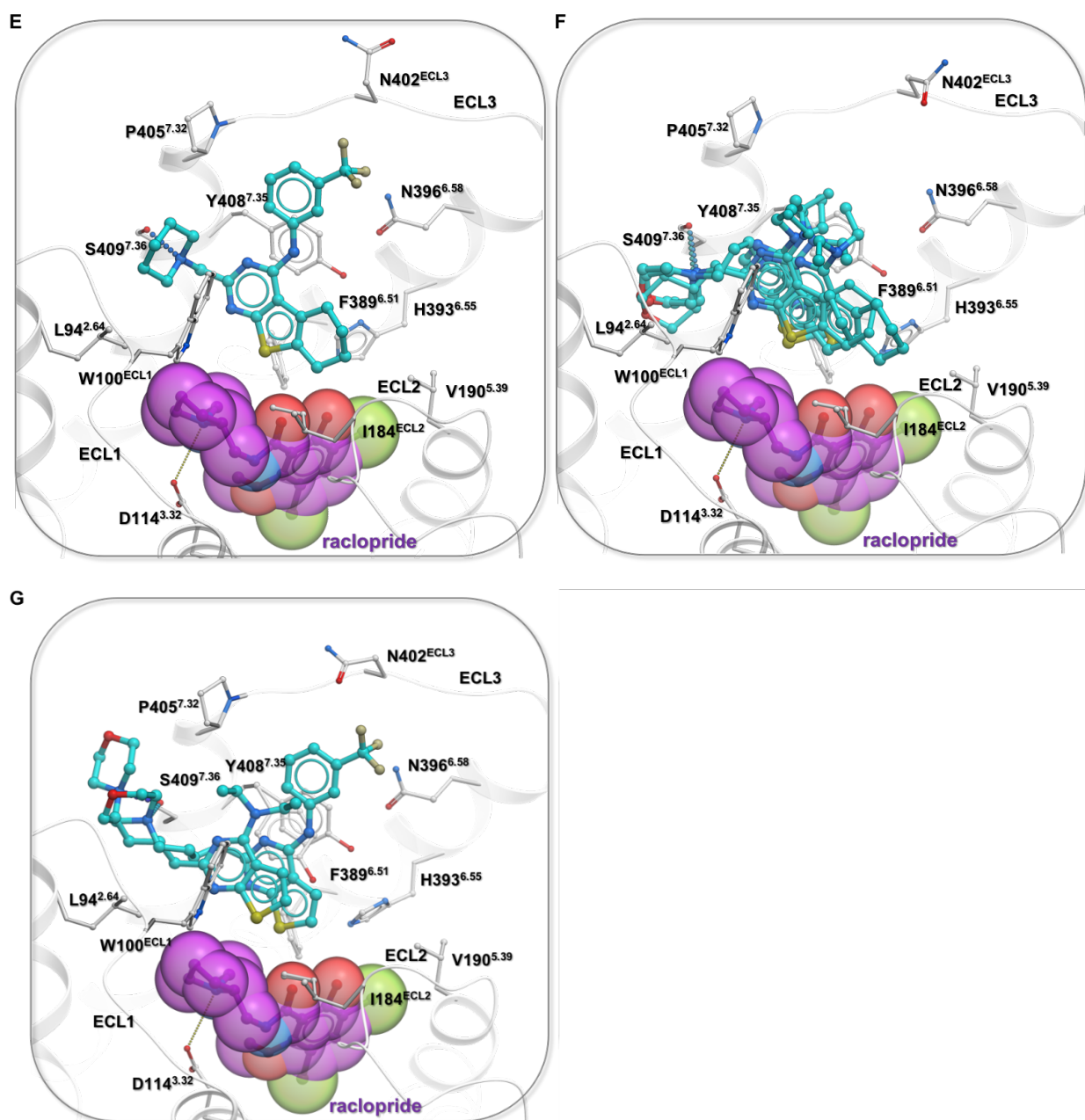


Figure 2. Compound 1 analogues in complex with D₂R^{Raclo}. Compounds with variation in the fused cyclohexane system. (A) Compounds **14a-j**. (B) Compounds with the variations in the *m*-CF₃ substituent (**16a-c**, **17**). (C) Compounds with the variations in the *N*-(3-trifluoromethyl)phenylamino system (**15**, **18**, **19**). (D) Compound with isosteric replacement to an ether linkage (**20**). (E) Piperidine analogue (**26**). (F) Compounds with morpholinomethyl, tetrahydropyranomethyl, morpholinobutyl, and fused cyclohexane deletion, respectively (**23b**, **33b**, **40**, **44**). (G) Compounds with morpholinobutyl moiety, but devoid of the fused cyclohexane system, and substituted with either *m*-trifluoromethylanilino or *N,N*-diethylamino (**43a-b**).

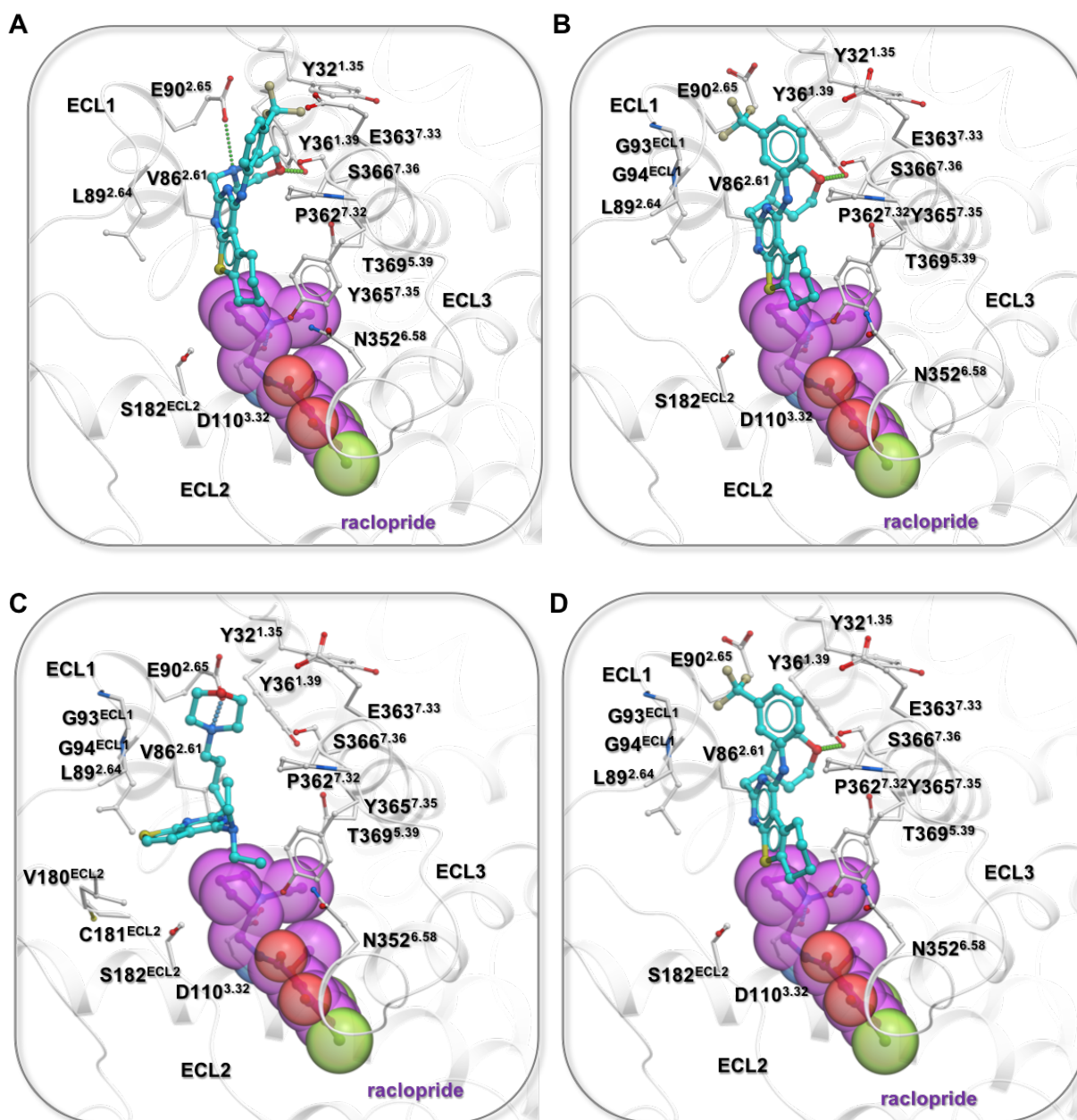
Selectivity

The predicted allosteric binding sites of the D₂R and D₃R show significant structural differences. Thus, predicted binding pose of compound **1** in complex with D₃R is stabilized by distinct interactions such as salt bridge between the ionized morpholine secondary amine and E90^{2.65} residue, and hydrogen bond between the oxygen atom of the morpholine ring and Y36^{1.39} residue. Additionally, the phenyl ring bearing the *m*-CF₃ substituent creates hydrophobic ring-ring interaction with Pro362^{7.32} residue. While the fused cyclohexane ring system is positioned in the hydrophobic sub-pocket located between helices VI, VII, and ECL2, creating pronounced hydrophobic ring-ring interaction with Y365^{7.35} residue (Figure 3a). This pose is characterized by the strong electrostatic interaction might explain the low micro molar binding affinity and ~57-fold higher selectivity for D₃R over D₂R (Table 3).

Interestingly, the abovementioned pose of compound **1** is supported by the SAR of its analogues (Table 3). Firstly, the compound with the tetrahydropyran moiety (**33a**), cannot create a salt bridge with E90^{2.65} residue, which is in agreement with the loss of affinity by ~170 fold (Figure 3b). Interestingly, this compound does not show selectivity, which can be explained by the model in which it loses the crucial interactions either with E90^{2.65} residue or S409^{7.36} residue for D₃R or D₂R, respectively, and none of the pose is significantly preferable.

Additionally, the pose of compound **1** in complex with D₃R can be supported by the SAR of analogues (**23a**) and (**43b**) which show low micro molar binding affinities (Table 3). Interestingly, the crucial interactions can be maintained when introducing the butylene linker, removing the fused cyclohexane system, and changing the *m*-CF₃-phenylamino substituent with *N,N*-diethylamino (**43b**) which is in accordance with low micro molar binding affinity (Figure 3c). However, since the crucial interactions of the compound (**43b**) can also be maintained in D₂R complex, (**43b**) does not show the selectivity profile (Table 3). Remarkably, upon removal of the morpholinomethyl moiety (**23a**), (Figure 3d), the salt bridge is missing, but the compound is slightly shifted thus creating a new hydrogen bond interaction with Y36^{1.39} residue and pi-pi stacking interactions with Y32^{1.35}, and additionally displays a perfect shape complementarity with the binding pocket, which might be reflected by ~140 fold selectivity for D₃R over D₂R (Table 3). Additionally, compound (**19**) with the variation in the *N*-(3-trifluoromethyl)phenylamino system can maintain the salt bridge interaction with E90^{2.65} residue, however, its morpholine ring is pointing outside the binding pocket and it loses the hydrophobic ring-ring interaction with Y365^{7.35}. This is reflected by the high binding affinity (140 μM) and therefore selectivity for D₂R over D₃R (by ~23 fold). Interestingly, compound (**39c**) with a variation in alkyl linker length to the morpholine motif and maintained fused system cannot create the salt bridge with E90^{2.65} residue and maintain the identified interactions characterized for compound (**1**) (Figure 3e). This observation is in accordance with its comparatively weak binding affinity (Table 3). However,

the same compound in complex with D₂R can perfectly maintain the crucial interactions in accordance with low μ M binding affinity (Table 1). Thus, compound (39c) shows ~30-fold selectivity for D₂R over D₃R.



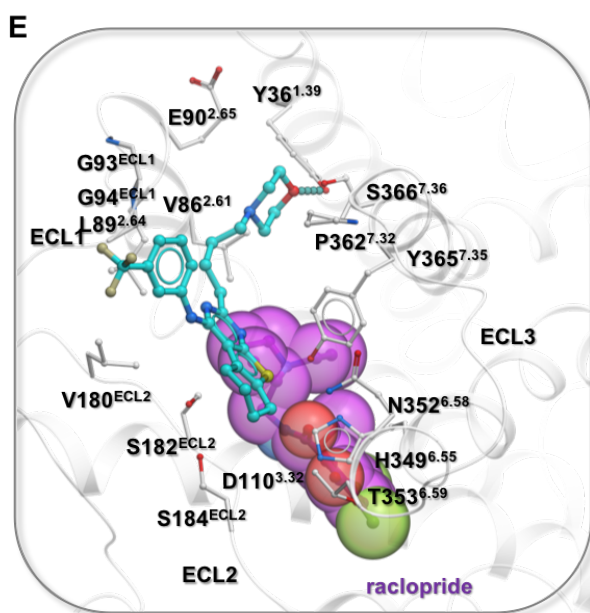
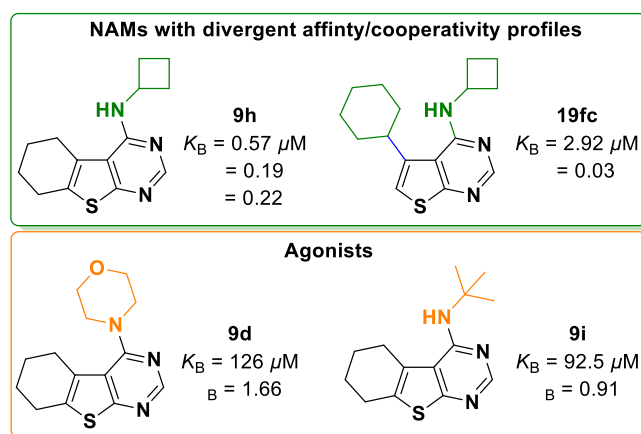
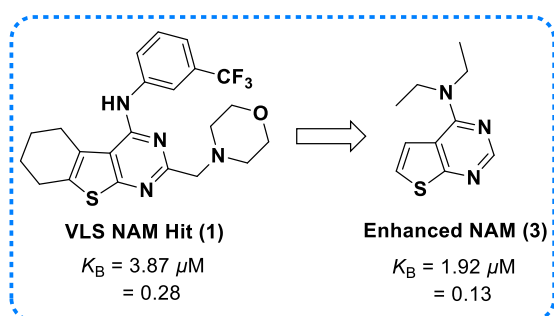


Figure 3. Compound 1 and its analogues in complex with D₃R^{Raclo}. (A) Compounds (1). (B) Compound with tetrahydropyran moiety (33a). (C) Compound with morpholinobutyl moiety, but devoid of the fused cyclohexane system, substituted with *N,N*-diethylamino, and four carbon linker (43b). (D) Compound devoid of morpholinomethyl moiety (23a) (E) Compounds with variations in alkyl linker length (butylene) to the morpholine motif (39c).

Chapter 3 – Subtle Modifications to a Thieno[2,3-*d*]pyrimidine Scaffold Yield Negative Allosteric Modulators and Agonists of the Dopamine D₂ Receptor

Graphical Abstract





Contents lists available at ScienceDirect

European Journal of Medicinal Chemistry

journal homepage: <http://www.elsevier.com/locate/ejmech>



Research paper

Subtle modifications to a thieno[2,3-d]pyrimidine scaffold yield negative allosteric modulators and agonists of the dopamine D₂ receptor

Tim J. Fyfe^{a, b, c}, Barrie Kellam^c, Shailesh N. Mistry^c, Peter J. Scammells^a, J. Robert Lane^{b, 1, **, *}, Ben Capuano^{a, *}

^a Medicinal Chemistry, Monash Institute of Pharmaceutical Sciences, Monash University, Parkville, Victoria, 3052, Australia

^b Drug Discovery Biology, Monash Institute of Pharmaceutical Sciences, Monash University, Parkville, Victoria, 3052, Australia

^c School of Pharmacy, Centre for Biomolecular Sciences, University of Nottingham, Nottingham, NG7 2RD, UK

ARTICLE INFO

Article history:

Received 25 November 2018

Received in revised form

24 January 2019

Accepted 24 January 2019

Available online 11 February 2019

Keywords:

Negative allosteric modulators

Dopamine D₂ receptor

Thieno[2,3-d]pyrimidines

NAMs

Agonists

ABSTRACT

We recently described a structurally novel series of negative allosteric modulators (NAMs) of the dopamine D₂ receptor (D₂R) based on thieno[2,3-d]pyrimidine **1**, showing it can be structurally simplified to reveal low molecular weight, fragment-like NAMs that retain robust negative cooperativity, such as **3**. Herein, we report the synthesis and functional profiling of analogues of **3**, placing specific emphasis on examining secondary and tertiary amino substituents at the 4-position, combined with a range of substituents at the 5/6-positions (e.g. aromatic/aliphatic carbocycles). We identify analogues with diverse pharmacology at the D₂R including NAMs with sub- μ M affinity (**9h**) and, surprisingly, low efficacy partial agonists (**9d** and **9i**).

Crown Copyright © 2019 Published by Elsevier Masson SAS. All rights reserved.

1. Introduction

The D₂R is a class A G protein-coupled receptor (GPCR) implicated in the pathophysiology and treatment of a number of central nervous system (CNS) disorders, including schizophrenia (SCZ). As

such, drugs targeting this receptor have traditionally targeted the orthosteric site - where the endogenous ligand DA binds. Clinically used antipsychotic drugs (APDs) targeting this site act as D₂R antagonists or low efficacy partial agonists, and are termed typical or atypical APDs based on their propensity to cause extrapyramidal side effects. Unfortunately, the efficacy of these drugs is largely limited to the positive symptoms of this disorder. Typical APDs are associated with extra-pyramidal motor symptoms (EPS) and hyperprolactinaemia, which are mediated by blockade of D₂R signalling in the nigrostriatal and tuberoinfundibular DA pathways, respectively [1–6]. Atypical APDs show a reduced incidence of EPS, but display other off-target side-effects mediated through the interaction with other aminergic receptors, including metabolic disorders and weight gain [7].

Alternative approaches to target the D₂R have emerged via the identification of homo- and heterodimeric complexes [8]. Such complexes in specific tissues may provide novel pharmacological targets for compounds with distinctive functional profiles and improved therapeutic windows [9–11]. Another proposition which entails targeting binding sites topographically distinct from the orthosteric site of GPCRs might also be advantageous. Negative

Abbreviations: cAMP, cyclic adenosine monophosphate; D₂R, dopamine D₂ receptor; D₃R, dopamine D₃ receptor; dopamine, DA; GPCR, G protein-coupled receptor; EPS, extrapyramidal symptoms; NAM, negative allosteric modulator; PAM, positive allosteric modulator; VLS, virtual ligand screening; SAR, structure-activity relationship; CHO, Chinese hamster ovary; BRET, bioluminescence resonance energy transfer; FBS, foetal bovine serum; HBSS, Hank's Balanced Salt Solution; SEM, standard error of mean; DMF, N,N-dimethylformamide; POCl₃, phosphorus oxychloride; i-PrOH, isopropyl alcohol; EtOAc, ethyl acetate; DCM, dichloromethane; MWI, microwave irradiation.

* Corresponding author.

** Corresponding author.

E-mail addresses: rob.lane@nottingham.ac.uk (J.R. Lane), ben.capuano@monash.edu (B. Capuano).

¹ Current addresses: Division of Pharmacology, Physiology and Neuroscience, School of Life Sciences, Queen's Medical Centre, University of Nottingham, Nottingham, NG7 2UH, UK and Centre of Membrane Protein and Receptors, Universities of Birmingham and Nottingham, UK.

<https://doi.org/10.1016/j.ejmech.2019.01.061>

0223-5234/Crown Copyright © 2019 Published by Elsevier Masson SAS. All rights reserved.

allosteric modulators (NAMs) of the D₂R may represent a safer therapeutic approach for the treatment of SCZ symptoms. A D₂R NAM with limited negative cooperativity with DA may display antipsychotic efficacy but avoid EPS through partial blockade of the D₂R akin to the action of atypical partial agonist APDs such as aripiprazole [12]. Furthermore, as a NAM will allow DA to bind, the spatiotemporal pattern of DA signalling is more likely to be maintained. Finally, NAMs may display greater selectivity for the D₂R over other targets via the targeting of less evolutionarily conserved sites and consequently reduced off target toxicities. Drug-like (NAMs) of DA receptors have recently been identified including the scaffold that is the focus of the present study [13–19].

Our previous study described the pharmacological validation of a virtual ligand screen hit (**1**, Fig. 1), confirming that it binds with low μM functional affinity and exerts its effect via negative allosteric cooperativity, primarily by modulation of dopamine signalling efficacy [18]. Based on the scaffold of **1**, we synthesised a small library of structural analogues to further understand key molecular features that were responsible for changes in affinity and negative allosteric cooperativity. Of several promising analogues identified, **2** (Fig. 1) maintained low μM affinity ($K_B = 1.92 \mu\text{M}$) and significantly attenuated DA signalling efficacy ($\beta = 0.001$). This compound was devoid of the morpholinomethyl moiety present on **1**, and also incorporated replacement of the ((3-trifluoromethyl)phenyl) amino-substituent with an *N,N*-diethylamino motif. In addition to this, our previous work focused on assessing various substituents at the 5/6-positions (e.g. phenyl, cyclohexyl) in place of the fused cyclohexane system. Moreover, we discovered that the scaffold could be structurally simplified, to reveal a low molecular weight fragment-like starting point that maintained μM affinity and negative cooperativity (MW = 207, $K_B = 4.56 \mu\text{M}$, $\beta = 0.13$) (**3**, Fig. 1). Thus, we identified an appropriate starting point for further structural interrogation and elaboration of the core scaffold using **2** and **3** as our lead compounds with the aim to identify higher affinity NAMs.

To this end, we sought to investigate the influence of varying the nature (both aliphatic and aromatic) of the 4-amino moiety of **2** (series 1, Fig. 2). In addition, a second series of compounds was designed to further explore the effect of 5/6-thiophene substitution with respect to altering functionality at the 4-position (series 2, Fig. 2). This would permit further refinement of the structural determinants of D₂R affinity and negative cooperativity. Through the parallel synthesis of an additional thirty-seven structural analogues of **2**, we have identified molecules that exert a range of modulatory behaviour including, surprisingly, derivatives that display agonism. To confirm a D₂R-mediated mechanism of action, all compounds with agonist profiles together with selected NAMs were assessed for their ability to modulate our functional readout in the absence

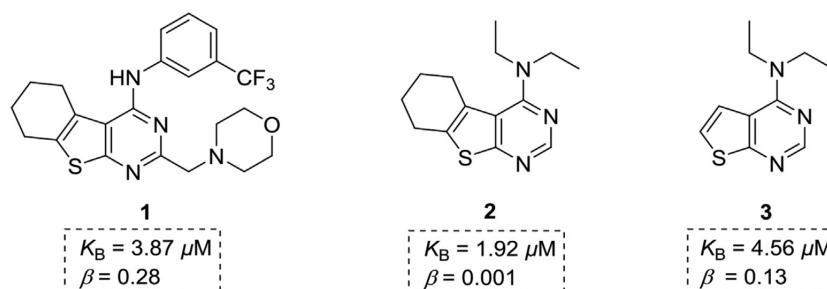


Fig. 1. Promising structural analogues of **1** arising from a preliminary structure-activity relationship (SAR) investigation. Compound **1** was identified from a virtual ligand screen and formed the basis of our previous SAR study [18]. Compound **2** significantly attenuates DA signalling efficacy at a concentration of $10 \mu\text{M}$ ($K_B = 1.92 \mu\text{M}$, $\beta = 0.001$). Compound **3** retains negative allosteric cooperativity despite being a structurally simplified fragment-like analogue (MW: 207, $K_B = 4.56 \mu\text{M}$, $\beta = 0.13$) of **1**.

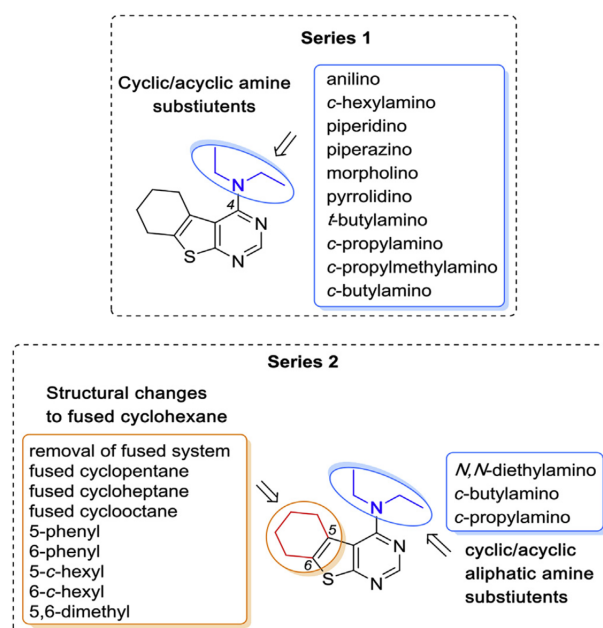


Fig. 2. Areas of structural modification conducted during SAR investigation of **2**.

of the D₂R.

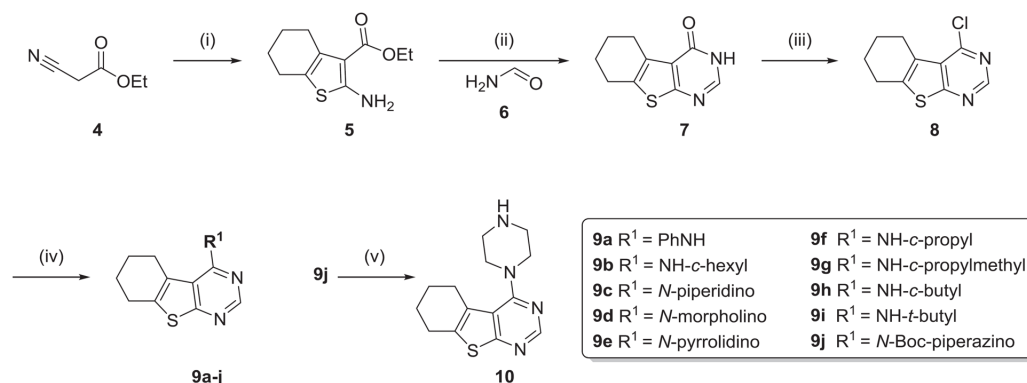
2. Chemistry

The synthesis of all compounds generally followed established methods for the synthesis of **1** and other related compounds previously reported by our research group [18]. Each compound detailed in this study was easily accessed in four-five steps (Schemes 1–3). Briefly, Scheme 1 depicts the synthesis of selected analogues (**9a–j**), beginning with Gewald [20] chemistry to facilitate the one-pot construction of the ethyl 2-amino-4,5,6,7-tetrahydrobenzo[*b*]thiophene-3-carboxylate (**5**) [18], followed by cyclisation with formamide (**6**) to afford the corresponding 5,6,7,8-tetrahydrobenzo[4,5]thieno[2,3-*d*]pyrimidinone (**7**) [18]. POCl₃ was employed to convert pyrimidinone **7** to the corresponding key intermediate chloropyrimidine **8** [18], followed by nucleophilic aromatic substitution (S_NAr) with the desired amine, in the presence of Hünig's base in propan-2-ol. This methodology afforded compounds **9a–j** in high purity after a simple work-up and/or chromatography.

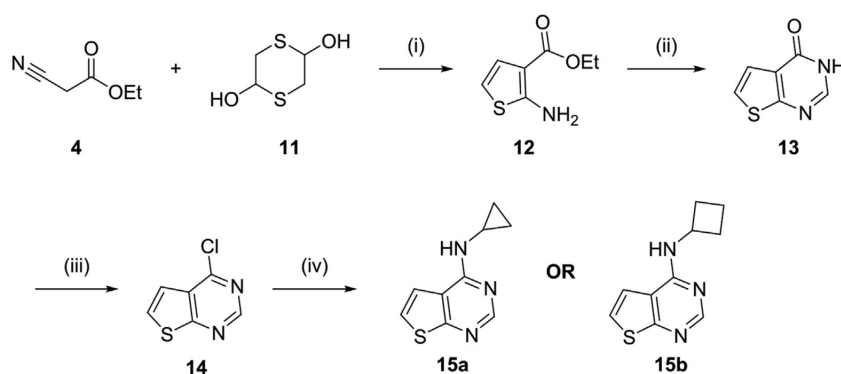
Chapter 3: Subtle Modifications to a Thieno[2,3-d]pyrimidine Scaffold Yield NAMs & Agonists of the D₂R

476

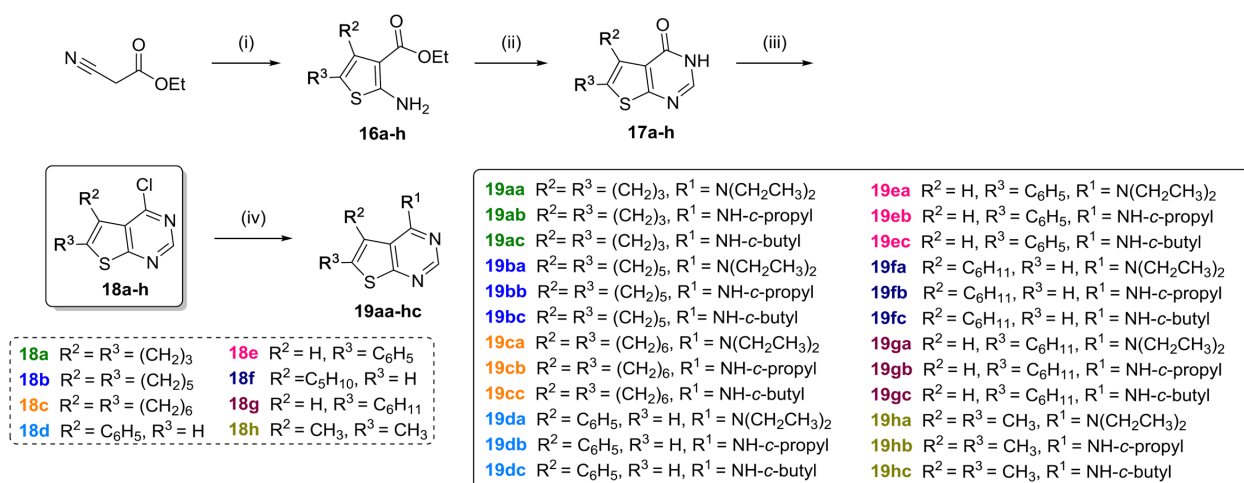
T.J. Fyfe et al. / European Journal of Medicinal Chemistry 168 (2019) 474–490



Scheme 1. Synthesis of Analogues of **2** Modified at the 4-Position^a. ^aReagents and conditions: (i) S₈, cyclohexanone, morpholine, rt, ~18 h, 81%; (ii) 170 °C, 12 h, 85%; (iii) POCl₃, DMF_(cat.), toluene, 4 h, 68%; (iv) amine, DIPEA, *i*-PrOH, reflux, 1–3 h, 68–88%; (v) TFA, DCM, rt, 4 h, 96%.



Scheme 2. Synthesis of Thieno[2,3-d]pyrimidine Analogues of **2**^a. ^aReagents and conditions: (i) Et₃N, DMF, 45 °C, 0.5 h, 55%; (ii) formamide (neat), 170 °C, 12 h, 76%; (iii) POCl₃, DMF_(cat.), toluene, 100 °C 4 h, 77%; (iv) amine, DIPEA, *i*-PrOH, 100 °C, 1–3 h, 76% (**15a**), 79% (**15b**).



Scheme 3. Synthesis of Functionalised Analogues of **2**^a. ^aReagents and conditions: (i) aldehyde or ketone, S₈, morpholine, rt 12–24 h, 38–84%, **16a–h**; (ii) formamide, 170 °C, 12 h, 75–85%, **17a–h**; (iii) POCl₃, DMF_(cat.), toluene, 100 °C, 3–5 h, 77–91%, **18a–h**; (iv) amine, DIPEA, *i*-PrOH, MWI, 1–3 h, 71–93%, **19aa–hc**.

2.1. Analogues of **2** varied at the 4-(*N,N*-diethylamino) substituent

Compound **2** was originally synthesised as an analogue of **1** to

observe the effect of simultaneously removing the morpholino-methyl moiety whilst incorporating a 4-(*N,N*-diethylamino) group in the context of retaining the tricyclic structure of the 5,6,7,8-

tetrahydrobenzo[4,5]thieno[2,3-*d*]pyrimidine. As this molecule was found to be a potent NAM of DA efficacy at the D₂R, an additional series of compounds was synthesised to investigate further changes to the 4-position of the pyrimidine ring (Scheme 1). Preliminary modifications included incorporating 6-membered secondary aromatic and aliphatic amino substituents (e.g. anilino (**9a**) and cyclohexylamino (**9b**)) together with 6-membered cyclic aliphatic tertiary amine moieties, including piperidino (**9c**), morpholino (**9d**) and piperazino (**10**), followed by the smaller pyrrolidino (**9e**) to assess the influence of a five-membered cyclic aliphatic system. The piperazino analogue **10** was obtained via the S_NAr reaction between commercially available *N*-Boc piperazine and **8** under microwave conditions as outlined previously (Scheme 1) to afford **9j** as a crystalline solid requiring no further purification. Standard trifluoroacetic acid-mediated *N*-Boc de-protection followed by an alkaline work-up furnished **10**. This molecule is unique relative to its counterparts in that it will impart a positive charge at physiological pH. Moreover, we investigated both monocyclic (cyclopropylamino (**9f**), cyclopropylmethylamino (**9g**), cyclobutylamino (**9h**)) and acyclic aliphatic secondary amine substituent (*tert*-butylamino (**9i**)). The *tert*-butylamino substituent was installed to assess the effect of an acyclic aliphatic secondary amine as a comparison to *N,N*-diethylamino. These syntheses were all achieved using chemistry as previously outlined (Scheme 1), and successfully afforded ten analogues (**9a-i**, and **10**) in yields varying from 68 to 88% following S_NAr of **8** with the appropriate amine.

2.2. Fragment analogues of **3**

We previously reported a low molecular weight fragment (*N,N*-diethylthieno[2,3-*d*]pyrimidin-4-amine, (**3**)) that retains low μM functional binding affinity and negative allosteric cooperativity at the D₂R ($K_B = 4.56 \mu\text{M}$, $\beta = 0.13$, Fig. 1) [18]. This molecule was originally synthesised using a deletion strategy to examine the effect of switching from a 5,6,7,8-tetrahydrobenzo[4,5]thieno[2,3-*d*]pyrimidine to the corresponding thieno[2,3-*d*]pyrimidine scaffold, in conjunction with incorporating a tertiary aliphatic amine at the 4-position. As such, we generated two additional analogues of **3** bearing 4-cyclopropylamino and 4-cyclobutylamino substituents. Their synthesis is depicted in Scheme 2 and begins with the construction of ethyl 2-aminothiophene-3-carboxylate (**12**) [18] using ethyl cyanoacetate (**4**) and 1,4-dithiane-2,5-diol (**11**) under modified Gewald conditions. Refluxing **12** in neat formamide afforded the corresponding pyrimidinone (**13**) [18] in good yield. Subsequent chemistry as outlined previously included deoxychlorination to give **14** [18], followed by S_NAr with cyclopropylamine or cyclobutylamine to afford the corresponding analogues **15a** and **15b**, respectively.

2.3. Single modifications to the 5,6,7,8-tetrahydrobenzo[4,5]thieno[2,3-*d*]pyrimidine moiety of **2** whilst varying the nature of the 4-substituent

Our previously reported SAR study of **1** focused on structural modifications to the fused cyclohexane system, including switching from a 5,6,7,8-tetrahydrobenzo[4,5]thieno[2,3-*d*]pyrimidine to the corresponding thieno[2,3-*d*]pyrimidine, 5- and 6-aryl substitution, 5- and 6-cyclohexyl substitution, 5,6-dimethyl substitution, as well as incorporation of fused cyclopentane, cycloheptane, and cyclo-octane systems [18]. These structural modifications were mostly employed in the presence of a 3-(trifluoromethyl)anilino substituent at the 4-position, and a 2-morpholinomethyl substituent. Only the fused cyclopentane and the 6-cyclohexyl modifications preserved the allosteric pharmacology seen with this scaffold, while the other structural modifications rendered the corresponding

molecule functionally inactive. This study, however, had demonstrated the encouraging effects of incorporating *N,N*-diethylamino, cyclopropylamino, or cyclobutylamino to the 4-position of the pyrimidine core, increasing functional affinity as well as maintaining the magnitude of negative allosteric cooperativity whilst bearing the fused cyclohexane system (Series 1, Fig. 2). To this end, we wanted to evaluate combining the structural modifications to the thiophene, whilst concurrently incorporating the aforementioned 4-amino substituents (Series 2, Fig. 2). These compounds would further refine the SAR and provide insight into the design of further high affinity NAMs. These modifications are depicted in Fig. 2 and their chemical synthesis is outlined in Scheme 3. All compounds were accessed using established chemistry as detailed in our previous work, beginning with construction of the appropriate thiophene via Gewald [20] chemistry (**16a-h**) [18], formation of the corresponding pyrimidinones (**17a-h**) [18] and chloropyrimidines (**18a-h**) [18], followed by S_NAr with the appropriate amine to furnish a further twenty-four analogues (**19aa-hc**).

3. Pharmacology

3.1. Functional and off-target analyses of analogues of **2** using a BRET biosensor for cAMP

To measure the effect of these compounds upon the functional response of the D₂R when stimulated by DA we made use of a BRET biosensor of cAMP. This assay measures inhibition of forskolin-stimulated cAMP accumulation through activation of the long isoform of the human D₂R (hD_{2L}R) stably expressed in FlpIn CHO cells and provides a robust measurement of D₂R Gα_{i/o} activation to allow estimates of functional binding affinities and quantify the magnitude of modulatory effects [18]. Application of an operational model of allosterism to the DA concentration–response data obtained in the presence and absence of increasing concentrations of our test compounds yielded an estimate of their affinity for the unoccupied receptor (K_B), cooperativity with DA affinity (α) and modulation of DA efficacy (β), plus the intrinsic efficacy of the allosteric ligand (τ_B) [21]. Values of α or $\beta < 1$ signify negative modulatory effects with DA, and values of α or $\beta > 1$ signify positive modulatory effects. Logarithms of affinity and cooperativity values are normally distributed, whereas the absolute values (antilogarithms) are not [22]. Thus, all interpretation of the SAR described below (Tables 1–3) refer to the logarithmic values. For ease of interpretation, however, the allosteric parameter antilogarithms are also highlighted in the main text for selected key analogues. As reported previously, the lead compound **2** acted as a NAM at the D₂R, with low μM functional affinity ($K_B = 1.92 \mu\text{M}$, Table 1) [18]. The depression in the DA dose–response curve caused by increasing concentrations of **2** is characteristic of the action of a NAM of agonist efficacy and β was fixed to 0.001 when fitting these data to signify high negative cooperativity (Fig. 3A, Table 1).

To our surprise, we identified molecules based on this NAM scaffold that now appear to display agonism. It was important, then, to confirm that these effects are D₂R mediated. Luciferase assays may identify false positive ‘hits’ through a variety of mechanisms, for example, by inhibition of the luciferase enzyme [23–25]. To allow us to discriminate between D₂R-mediated activities and any non-specific effects (Supplementary Fig. 1), all compounds observed to display D₂R agonism in our cAMP assay were selected for further analysis (**9c-d**, **9i**, **15a-b**, **19ac**, **19ca**, **19da**, **19db**, **19dc**, **19ec**, and **19ha**). In addition, a number of other compounds were selected, namely the parent NAMs **1** and **2**, together with NAMs **9h**, **19bb**, **19fb**, and **19fc**. We measured their ability to modulate the BRET signal in FlpIn CHO cells transfected with the CAMYEL biosensor [26], but not expressing the D₂R. All compounds were

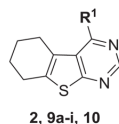
Chapter 3: Subtle Modifications to a Thieno[2,3-d]pyrimidine Scaffold Yield NAMs & Agonists of the D₂R

478

T.J. Fyfe et al. / European Journal of Medicinal Chemistry 168 (2019) 474–490

Table 1

Functional parameters derived from cAMP BRET assay for analogues of **1** modified with various amines at the 4-position.



#	R ¹	pK _B (K _B , μM) ^a	Logτ _B (τ _B) ^b	Log α (α) ^c	Log β (β) ^d
2		5.72 ± 0.13 (1.92)	= -3.0	=	= -3.0
9a		nd			
9b		nd			
9c		4.23 ± 0.13 (59.3)	NSE	= 0	= 0
9d		3.90 ± 0.27 (126)	-0.22 ± 0.15 (1.66)	= 0	= 0
9e		5.37 ± 0.13 (4.23)		= 0	-0.76 ± 0.06 (0.17)
9f		6.05 ± 0.09 (0.88)		= 0	-1.48 ± 0.08 (0.03)
9g		5.92 ± 0.19 (1.19)		-0.06 ± 0.14 (0.86)	-0.54 ± 0.08 (0.29)
9h		6.25 ± 0.12 (0.57)		-0.72 ± 0.12 (0.19)	-0.65 ± 0.07 (0.22)
9i		4.03 ± 0.31 (92.5)	-0.04 ± 0.15 (0.91)	= 0	= 0
10		4.70 ± 0.09 (20.0)		= -3.0	= 0

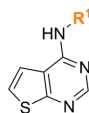
^a Estimate of the negative logarithm of the equilibrium dissociation constant as determined in a cAMP functional assay.

^b Estimate of the logarithm of the net cooperativity factor between the modulator and dopamine as determined in a cAMP functional assay.

^c Estimate of the intrinsic efficacy of the modulator. nd = inactive at concentrations up to 100 μM. NSE, non-specific effect, compound determined to inhibit forskolin-stimulated cAMP accumulation in the absence of the D₂R. Values represent the mean ± S.E.M. from at least three independent experiments performed in duplicate.

Table 2

Functional parameters derived from cAMP BRET assay for fragment analogues of **2** with modifications to the 4-position.



#	R ¹	pK _B (K _B , μM) ^a	Logτ _B (τ _B) ^b	Log α (α) ^c	Log β (β) ^d
3		5.31 ± 0.07 (4.6)		= 0	-0.89 ± 0.04 (0.13)
15a		4.67 ± 0.08 (21.4)	-0.65 ± 0.07 (0.22)	= -3.0	= 0
15b		5.13 ± 0.19 (7.38)	-0.32 ± 0.06 (0.48)	= 0	= 0

^a Estimate of the negative logarithm of the equilibrium dissociation constant determined in a cAMP functional assay.

^b Estimate of the logarithm of the net cooperativity factor between the modulator and dopamine determined in a cAMP functional assay.

^c Estimate of the intrinsic efficacy of the modulator. nd = inactive at concentrations up to 100 μM. Values represent the mean ± S.E.M. from at least three independent experiments performed in duplicate.

Chapter 3: Subtle Modifications to a Thieno[2,3-d]pyrimidine Scaffold Yield NAMs & Agonists of the D₂R

T.J. Fyfe et al. / European Journal of Medicinal Chemistry 168 (2019) 474–490

479

Table 3
Functional parameters derived from cAMP BRET assay for analogues of **2** with modifications to the 5/6-fused system and 4-position.

#	<i>n</i>	R ¹	R ²	R ³	pK _B (K _B , μM) ^a	Logτ _B (τ _B) ^b	Log α (α) ^c	Log β (β) ^d
2	2				5.72 ± 0.13 (1.92)	−3.0	0	−3.0
19aa	1				6.13 ± 0.14 (0.74)		0	−0.85 ± 0.07 (0.14)
19ab	1				5.22 ± 0.14 (6.01)		−0.13 ± 0.11 (0.75)	−0.55 ± 0.06 (0.28)
19ac	1				3.99 ± 0.50 (102)	−0.25 ± 0.29 (0.57)	0	0
19ba	3				nd			
19bb	3				5.53 ± 0.07 (2.96)		0	−1.30 ± 0.07 (0.05)
19bc	3				6.04 ± 0.13 (0.91)		0	−1.22 ± 0.09 (0.06)
19ca	4				4.84 ± 0.13 (14.5)	NSE	0	−3.0
19cb	4				6.27 ± 0.18 (0.53)		0	−1.00 ± 0.11 (0.10)
19cc	4				5.40 ± 0.26 (3.98)		0	−0.58 ± 0.09 (0.26)
19da	−			H	4.22 ± 0.33 (60.0)	−0.57 ± 0.14 (0.27)	−3.0	0
19db	−			H	5.72 ± 0.22 (1.93)	−0.47 ± 0.09 (0.32)	−3.0	0
19dc	−			H	3.89 ± 0.52 (137)	−0.41 ± 0.31 (0.39)	−3.0	0
19ea	−		H		6.04 ± 0.23 (0.90)		0	−3.0
19eb	−		H		5.92 ± 0.17 (6.35)		−0.22 ± 0.10 (0.60)	−0.37 ± 0.05 (0.43)
19ec	−		H		5.35 ± 0.24 (4.50)	0.55 ± 0.10 (0.28)	0	0
19fa	−			H	nd			
19fb	−			H	4.93 ± 0.16 (11.6)		0	−1.04 ± 0.19 (0.09)
19fc	−			H	5.53 ± 0.13 (2.92)		0	−1.55 ± 0.19 (0.03)
19ga	−		H		nd			
19gb	−		H		nd			
19gc	−		H		nd			
19ha	−		CH ₃	CH ₃	4.71 ± 0.30 (19.5)	−0.61 ± 0.11 (0.24)	0	0

(continued on next page)

Table 3 (continued)

#	n	R ¹	R ²	R ³	pK _B (K _B , μM) ^a	Logτ _B (τ _B) ^b	Log α (α) ^c	Log β (β) ^d
19hb	–		CH ₃	CH ₃	nd			
19hc	–		CH ₃	CH ₃	5.54 ± 0.16 (2.88)			–0.90 ± 0.08 (0.13)

^a Estimate of the negative logarithm of the equilibrium dissociation constant determined in a cAMP functional assay.

^b Estimate of the logarithm of the net cooperativity factor between the modulator and dopamine determined in a cAMP functional assay.

^c Estimate of the intrinsic efficacy of the modulator determined in a cAMP functional assay. nd = inactive at concentrations up to 100 μM. NSE – non-specific effect, compound determined to inhibit forskolin-stimulated cAMP accumulation in the absence of the D₂R. Values represent the mean ± S.E.M. from at least three independent experiments performed in duplicate.

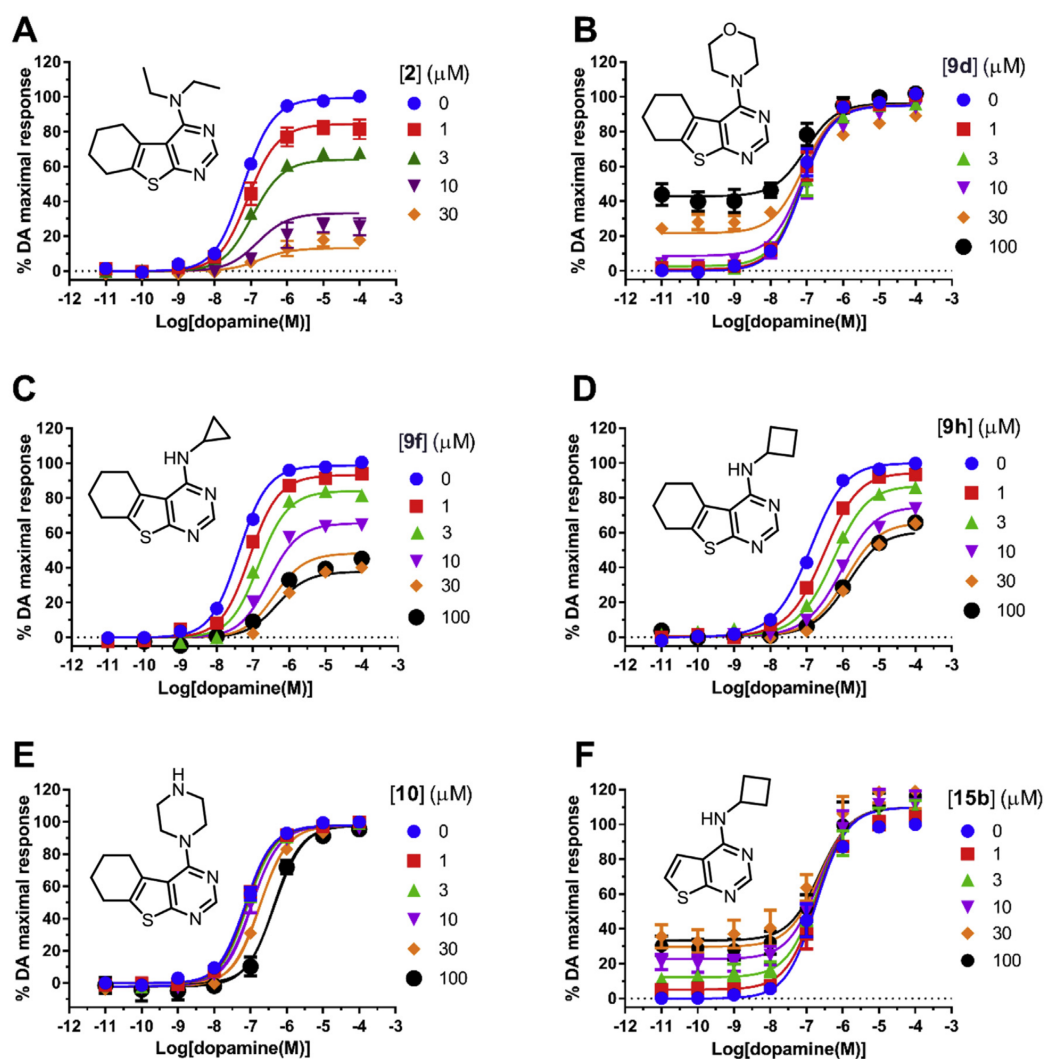


Fig. 3. Modification to the thieno[2,3-d]pyrimidine scaffold 4-substituent results in analogues with distinct functional effects at the hD₂R. (A) *N,N*-Diethylamino substitution confers negative allosteric cooperativity on DA signalling efficacy (**2**). (B) Introduction of the cyclic tertiary aliphatic morpholino moiety confers allosteric agonism (**9d**). (C, D) Introduction of cyclopropylamino or cyclobutylamino substituents to the 4-position in conjunction with the fused cyclohexane system results in analogues with sub-μM affinities that maintain negative allosteric cooperativity (**9f**, **9h**). (E) Introduction of the piperazino moiety (**10**) converts allosteric to competitive pharmacology. (F) Removal of the fused cyclohexane in conjunction with a cyclobutylamino substituent converts allosteric pharmacology to agonism (**15b**). All data used in these graphs are detailed in Tables 1 and 2 and are presented as mean ± SEM from three independent experiments performed in duplicate.

measured up to a concentration of 100 μM in both the presence and absence of forskolin (10 μM). DA (10 μM) was also used as a control. Two compounds (**9c**, **19ca**) were found to display effects independent of any action at the D₂R. Importantly, the original VLS hit (**1**), representative NAMs (**2**, **9h**, **19bb**, **19fb**, and **19fc**), as well as all other agonists exert an effect dependent on the presence of the D₂R.

4. Results and discussion

4.1. Functional analysis of 5,6,7,8-tetrahydrobenzo[4,5]thieno[2,3-*d*]pyrimidine analogues of **2**

We first examined the effect of introducing various monocyclic/acyclic aliphatic amines to the 4-position of the core scaffold whilst still bearing the fused cyclohexane system. This was based on our finding that **2**, bearing a 4-(*N,N*-diethylamino) substituent, displayed high negative cooperativity. As outlined in Table 1, anilino (**9a**) and cyclohexylamino (**9b**) substituents rendered the corresponding analogues functionally inactive. Substitution with the smaller cyclopropylamino substituent (**9f**) resulted in a modest increase in functional affinity ($K_B = 0.88 \mu\text{M}$) and maintenance of a negative modulatory effect on DA efficacy ($\beta = 0.03$, Fig. 3C). The cyclopropylmethylamino analogue (**9g**) maintained a functional affinity ($K_B = 1.19 \mu\text{M}$) similar to that of **2**, but more modest modulatory effects upon dopamine efficacy ($\beta = 0.29$). Introduction of a cyclobutylamino substituent (**9h**) not only maintained this negative modulatory action, but acted to increase affinity ($K_B = 0.57 \mu\text{M}$, $\alpha = 0.19$, $\beta = 0.22$, Fig. 3D). Conversely, the *tert*-butylamino analogue (**9i**) lost ~50-fold functional affinity relative to **2** ($K_B = 92.5 \mu\text{M}$), but now, surprisingly, exerted agonism ($\tau_B = 0.91$). It is interesting to note that introduction of the *tert*-butylamino moiety (**9i**) abolished negative cooperativity, whereas the *N,N*-diethylamino substituent (**2**) confers a high degree of negative allosteric modulatory effects upon dopamine efficacy. These data demonstrate that the ring size and nature of the substituent at the 4-position are crucial for both affinity and negative modulatory action. We found that larger 6-membered cyclic substituents bearing secondary amines, both of aromatic and aliphatic nature, are not tolerated, whereas three- and four-membered cyclic substituents (cyclopropylamino and cyclobutylamino, respectively) increase affinity and maintain modulatory properties in conjunction with the fused cyclohexane system. We next examined the effect of substituents bearing tertiary amines by incorporating various cyclic amines. The piperidino analogue (**9c**) decreased the functional affinity by 10-fold ($K_B = 59.3 \mu\text{M}$), and was devoid of any modulatory effect on DA but, surprisingly, appeared to exert an intrinsic response in its own right. However, our assay using FlpIn CHO cells that do not express the D₂R revealed that this is effect is most likely an off target effect (Supplementary Fig. 1). The morpholino analogue (**9d**) further decreased the functional affinity, some ~65-fold ($K_B = 126 \mu\text{M}$), but also displayed agonism ($\tau_B = 1.66$) with negligible modulatory action on DA an effect that required the expression of the D₂R (Fig. 3B). Interestingly, isosteric replacement of the morpholine O with NH to give the piperazino analogue (**10**), significantly changed the pharmacology as concentrations of **10** caused no decrease in DA maximal response, whilst acting to cause a limitless rightward shift in the DA dose-response curve. Such a pattern could be consistent with either very high negative cooperativity with DA affinity, or conversely, a competitive mode of action. Accordingly, these data could also be fit with a model of competitive antagonism ($pA_2 = 4.67 \pm 0.09$, Schild slope: 1.06 ± 0.12 , Fig. 3E). If this molecule is indeed competitive with DA we speculate that the presence of the piperazino ionisable nitrogen atom at physiological pH may potentially confer greater affinity for the orthosteric binding pocket, consequently converting the

pharmacology from allosteric to competitive. Decreasing the ring size by one carbon relative to **9c** to give pyrrolidine analogue (**9e**), maintained functional affinity ($K_B = 4.23 \mu\text{M}$), and displayed robust negative allosteric modulatory effects upon DA efficacy ($\beta = 0.17$).

4.2. Functional analysis of thieno[2,3-*d*]pyrimidine fragment analogues of **2**

We recently reported that incorporating an *N,N*-diethylamino substituent to the 4-position of the thieno[2,3-*d*]pyrimidine scaffold devoid of both the 2-morpholinomethyl moiety and fused cyclohexane systems (**3**), resulted in a low molecular weight fragment-like NAM of the D₂R (Fig. 1) [18]. As 4-cyclopropylamino and 4-cyclobutylamino substituents on the thieno[2,3-*d*]pyrimidine moiety conferred sub- μM analogues with robust negative cooperativity, we further examined the effect of introducing these substituents to the 4-position of **3** in place of the *N,N*-diethylamino functionality (Table 2). We found that introducing the cyclopropylamino substituent (**15a**) did not affect functional affinity, however caused a limitless rightward shift in the DA dose-response curve in addition to stimulating a modest agonist response in its own right. If cooperativity values of α and β were constrained to -3.0 and 0 , respectively, we could derive a value of affinity and efficacy ($K_B = 21.4 \mu\text{M}$, $\tau_B = 0.22$, Table 2). However, this pattern of ligand action is also consistent with that of a competitive low efficacy partial agonist. Furthermore, introduction of a cyclobutylamino substituent (**15b**) maintained affinity but abolished modulatory effects and engendered agonism ($K_B = 7.38 \mu\text{M}$, $\tau_B = 0.48$, Table 2, Fig. 3F). Thus, relatively subtle structural modifications significantly change pharmacology, from compounds which negatively modulate the behaviour of DA from a secondary binding site, to molecules that activate the receptor with no cooperativity. Of note, the D₂R orthosteric agonists pramipexole and sumanirole are both low molecular weight heterocyclic compounds bearing acyclic secondary amines.

4.3. Functional analysis (cAMP) of fused cyclohexane modified analogues of **2**

Our previous study revealed that incorporating various substituents (fused cyclopentane, cycloheptane, cyclooctane, 5- and 6-cyclohexyl, 5- and 6-phenyl, 5,6-dimethyl) to the 5-/6-positions of the thieno[2,3-*d*]pyrimidine generally rendered the corresponding analogues functionally inactive. However, these substituents were all previously examined on molecules also bearing 2-morpholinomethyl and 4-(3-(trifluoromethyl)anilino) substituents. As such, we further extended our study to monitor the effect of incorporating favourable amino substituents (*N,N*-diethylamino, cyclopropylamino, or cyclobutylamino) onto the 4-position of the thieno[2,3-*d*]pyrimidine whilst being devoid of the 2-morpholinomethyl moiety present in **1**, and bearing variation in the nature of substituents at the 5- and/or 6-positions (Table 3).

4.3.1. Fused cyclopentane analogues

Our previous work revealed converting the fused cyclohexane system of **1** to the homologous cyclopentane system had no adverse impact on functional affinity, nor the degree of negative cooperativity. Molecular docking studies conducted using the D₂R crystal structure as a template suggest that such fused hydrophobic rings interact with a hydrophobic subpocket located between helices V and VI formed by the residues I184^{ECL2}, V190^{5.39}, H394^{6.55} (where superscript numbers refer to Ballesteros-Weinstein numbering system [27]) [18,28]. However, these interactions were predicted for compounds bearing a fused hydrophobic ring in conjunction with additional substituents located at the 2-position

(morpholinomethyl) and 4-position (3-(trifluoromethyl)anilino). As these groups were now altered, we wanted to re-examine the importance of this ring system for such compounds. The *N,N*-diethylamino analogue (**19aa**) displayed an increase in functional affinity ($K_B = 0.74 \mu\text{M}$) relative to **1** and acted to negatively modulate DA signalling efficacy ($\beta = 0.14$, Fig. 4A). The cyclopropylamino analogue (**19ab**) maintained low μM affinity ($K_B = 6.01 \mu\text{M}$) and similarly acted as a NAM of DA efficacy ($\beta = 0.28$). Conversely, the cyclobutylamino analogue (**19ac**) displayed a >15-fold decrease in functional affinity ($K_B = 102 \mu\text{M}$) and acted as an agonist ($\tau_B = 0.57$). These data were surprising as **9h**, the corresponding fused cyclohexane variant of **19ac**, displayed sub- μM affinity at the D₂R and acted as a NAM of DA efficacy.

4.3.2. Larger homologous fused rings (cycloheptane and cyclooctane)

Increasing the hydrophobic ring size by one carbon relative to **1** was previously shown to abolish D₂R activity, potentially due to the hydrophobic allosteric pocket failing to accommodate such extended ring sizes [18]. Likewise, further expansion of the hydrophobic ring by one additional carbon in the presence of the 3-(trifluoromethyl)anilino substituent also previously rendered the corresponding analogue inactive [18]. In the presence of a fused cycloheptane system devoid of the 2-morpholinomethyl substituent, incorporation of the 4-(*N,N*-diethylamino) group (**19ba**) similarly abolished activity. However, the cyclopropylamino analogue **19bb** ($K_B = 2.96 \mu\text{M}$, $\beta = 0.05$, Fig. 4B) and cyclobutylamino

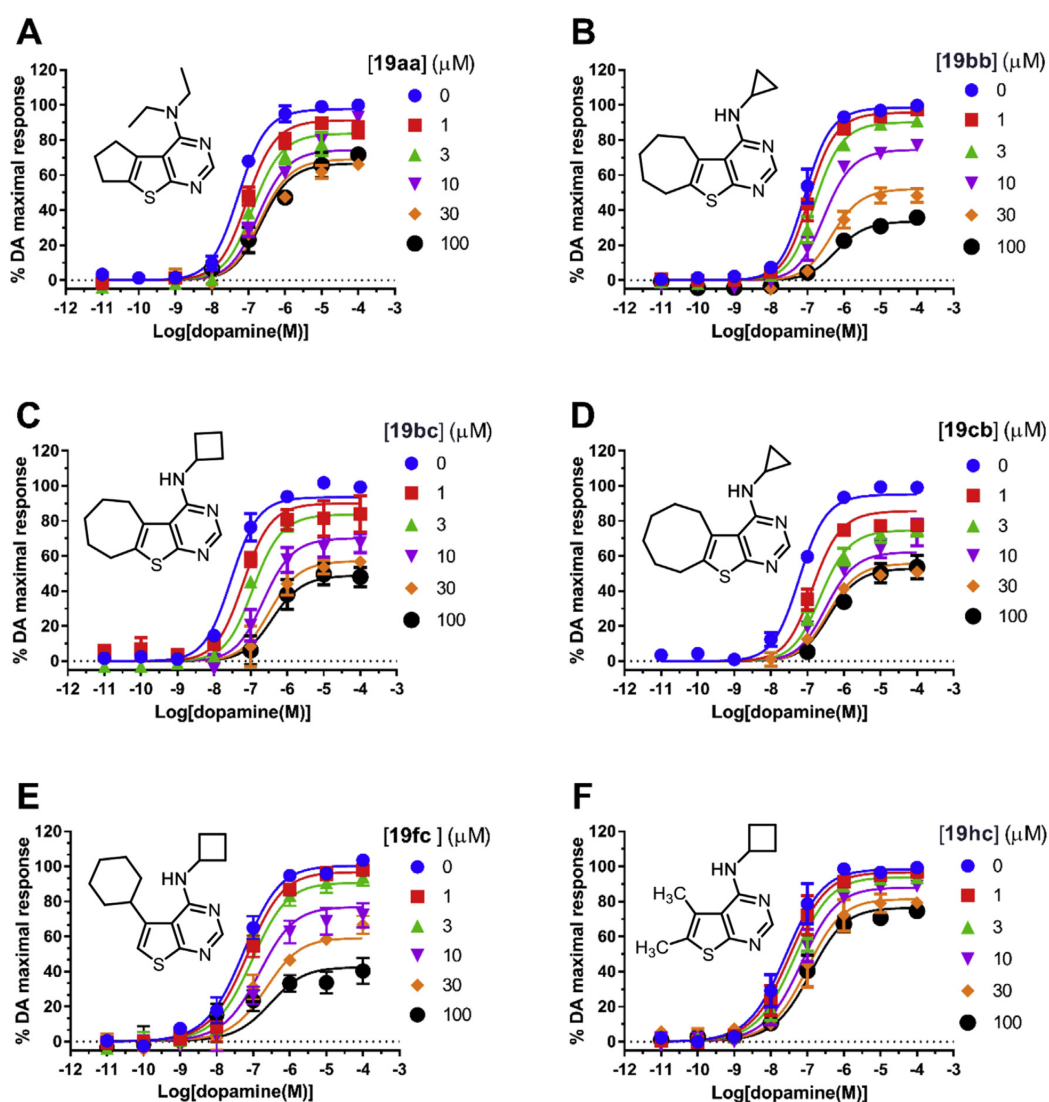


Fig. 4. Various aliphatic amino substituents at the 4-position can recover allosteric pharmacology. Most modifications to the 5- and 6-positions of the thienopyrimidine were previously found to be detrimental to the activity of the target compound. However, these activities can be recovered and even enhanced when using *N,N*-diethylamino, cyclopropylamino or cyclobutylamino substituents at the 4-position. (A) Fused cyclopentane with 4-(*N,N*-diethylamino) substituent (**19aa**, $K_B = 0.74 \mu\text{M}$, $\beta = 0.14$). (B) Fused cycloheptane with 4-(cyclopropylamino) substituent (**19bb**, $K_B = 2.96 \mu\text{M}$, $\beta = 0.05$). (C) Fused cycloheptane with 4-(cyclobutylamino) substituent (**19bc**, $K_B = 0.91 \mu\text{M}$, $\beta = 0.06$). (D) Fused cyclooctane with 4-(cyclobutylamino) substituent (**19cb**, $K_B = 0.53 \mu\text{M}$, $\beta = 0.10$). (E) 5-Cyclohexyl with 4-(cyclobutylamino) substituent (**19fc**, $K_B = 2.92 \mu\text{M}$, $\beta = 0.03$). (F) 5,6-Dimethyl with 4-(cyclobutylamino) substituent (**19hc**, $K_B = 2.88 \mu\text{M}$, $\beta = 0.13$). All data used in these graphs are detailed in Table 3 and are presented as mean \pm SEM from three independent experiments performed in duplicate.

analogue **19bc** ($K_B = 0.91 \mu\text{M}$, $\beta = 0.06$, Fig. 4C) remained NAMs of DA efficacy at the D₂R, with μM and sub- μM affinities, respectively. Interestingly, all cyclooctane analogues in this study maintained activity at the D₂R. The *N,N*-diethylamino analogue **19ca** maintained low μM affinity ($K_B = 14.5 \mu\text{M}$) and negatively modulated DA signalling efficacy whilst exerting a slight degree of agonism unlike the inactive structural analogue **19ba** bearing the fused cycloheptane system. However, this agonism proved to be a non-specific effect (Supplementary Fig. 1). To our surprise the cyclopropylamino analogue **19cb** displayed the highest improvement in affinity seen for any analogue of **1** to date, some 10-fold compared to **2**, coupled with robust negative modulation of DA signalling efficacy ($K_B = 0.53 \mu\text{M}$, $\beta = 0.10$, Fig. 4D). Introduction of a cyclobutylamino substituent (**19cc**) had no effects on affinity compared to **2** and this compound still acted as a NAM of DA efficacy ($K_B = 3.98 \mu\text{M}$, $\beta = 0.26$).

4.3.3. 5-Phenyl substituted analogues

Installing a phenyl substituent at the 5-position of **1** in the presence of the 4-(3-(trifluoromethyl)anilino) substituent had previously been shown to abolish activity [18]. Surprisingly, the *N,N*-diethylamino analogue (**19da**) not only lost >10-fold affinity, but caused a limitless rightward shift of the DA concentration response-curve, instead displaying weak agonism. From this limited set of data, however, its mode of action cannot be conclusively determined (i.e. allosteric agonist versus low efficacy competitive partial agonist). In order to derive a value of affinity and efficacy, cooperativity values of α and β were constrained to -3.0 and 0 , respectively ($K_B = 60.0 \mu\text{M}$, $\tau_B = 0.27$). Additionally, both the cyclopropylamino analogue (**19db**) ($K_B = 1.93 \mu\text{M}$, $\tau_B = 0.32$) and cyclobutylamino analogue (**19dc**) ($K_B = 137 \mu\text{M}$, $\tau_B = 0.39$) lost their modulatory effect upon DA and instead behaved as agonists.

4.3.4. 6-Phenyl substituted analogues

Converting the fused cyclohexane system of **1** to the corresponding 6-phenyl-substituted thiophene in the presence of 3-(trifluoromethyl)anilino was previously not tolerated [18]. However, in the presence of 4-(*N,N*-diethylamino), **19ea** showed improved functional affinity ($K_B = 0.90 \mu\text{M}$) relative to **1** and was a NAM of DA efficacy. The cyclopropylamino analogue **19eb** also maintained affinity and negative allosteric cooperativity ($K_B = 6.35 \mu\text{M}$, $\alpha = 0.60$, $\beta = 0.43$). Conversely, the cyclobutylamino analogue **19ec** no longer negatively modulated the action of DA but instead also acted as a weak agonist ($K_B = 4.50 \mu\text{M}$, $\tau_B = 0.28$). These data further demonstrate that the nature of the amine at the 4-position can dramatically affect the type of functional behaviour exerted by this scaffold at the D₂R.

4.3.5. 5-Cyclohexyl substituted analogues

Integration of a 5-cyclohexyl substituent into the scaffold of **1** was previously shown to abolish activity [18]. In line with these data, the *N,N*-diethylamino analogue (**19fa**) was also inactive. However, despite this, analogues **19fb** ($K_B = 11.6 \mu\text{M}$, $\beta = 0.09$) and **19fc** ($K_B = 2.92 \mu\text{M}$, $\beta = 0.03$, Fig. 4E) were both NAMs of DA efficacy at the D₂R. These data indicate that incorporation of a 5-cyclohexyl substituent may be favourable depending on the nature of substituents at the 2- and 4-positions.

4.3.6. 6-Cyclohexyl substituted analogues

Modifying the thiophene with a cyclohexyl substituent at the 6-position of **1** maintained low μM affinity and negative allosteric cooperativity [18]. This substituent changed observed pharmacology from negative modulation of DA efficacy (β) to negative modulation of DA affinity (α). However, we found that

incorporating the cyclohexyl substituent into analogues devoid of the 2-morpholinomethyl moiety (**19ga-c**) abolished activity regardless of the nature of the 4-substituent.

4.3.7. 5,6-Dimethyl substituted analogues

This structural modification in conjunction with the 4-(3-(trifluoromethyl)anilino) group was previously shown to abolish activity at the D₂R [18]. In the presence of an *N,N*-diethylamino in the 4-position, however, **19ha** maintained low μM affinity ($K_B = 19.5 \mu\text{M}$) but failed to have any effects on DA binding and function, instead displaying agonism ($\tau_B = 0.24$). Conversely, the cyclopropylamino analogue (**19hb**) was inactive in our functional assay, while the cyclobutylamino analogue (**19hc**) maintained low μM affinity and was a NAM of DA efficacy ($K_B = 2.88 \mu\text{M}$, $\beta = 0.13$, Fig. 4F).

Our data reveal that relatively subtle structural changes can cause a change in pharmacology from that of a NAM to that of a weak D₂R agonist. With two exceptions, the actions of the ligands described within this study are mediated through interaction with the D₂R. The phenomenon whereby subtle modifications to a small molecule allosteric scaffold act to modulate modes of pharmacology, presumably via a change in receptor conformation, have been coined as “molecular switches” [29]. This phenomenon has been documented for allosteric ligands targeting multiple GPCR and non-GPCR targets, including muscarinic acetylcholine receptors (mAChRs) [30–32], as well as kinase [33] and phospholipase [34,35] allosteric ligands. Molecular switches have been reported to encompass a number of subtle structural changes, for example, stereochemistry, ring size and simple aryl substitution (i.e. fluoro vs methyl) to afford compounds with diverse pharmacology (e.g. positive and negative allosteric modulators, partial antagonists, and agonists). Indeed it is not surprising that such changes to allosteric ligands can cause dramatic changes in pharmacology given that similarly subtle changes to orthosteric ligands can convert agonists to antagonists. However, for those compounds that displayed agonism rather than the NAM activity of **1**, the nature of this agonism i.e. whether it is non-competitive (allosteric) or competitive (orthosteric), cannot be conclusively confirmed due to their low D₂R affinity. Thus it is not clear whether such compounds bind to the same allosteric site as **1**, and are examples of molecular switching, or whether the relatively subtle structural changes investigated within this study confer the ability to engage the orthosteric site [18]. Indeed, our recent paper proposed that the allosteric binding site of **1** was in close proximity to the orthosteric site.

In summary, it is clear that the nature of substituents at the thieno[2,3-*d*]pyrimidine 4-, 5- and 6-positions play a crucial role in both binding affinity and functional activity (e.g. anilino (**9a**) and cyclohexylamino (**9b**) at the 4-position are not tolerated). However, other 6-membered substituents (morpholino (**9d**) and piperazino (**10**)) convert NAMs to agonists and competitive antagonists, respectively. Moreover, smaller acyclic and cyclic at the 4-position (*N,N*-diethylamino (**2**), cyclopropylamino (**9f**), cyclopropylmethylamino (**9g**) and cyclobutylamino (**9h**)) are tolerated, with all compounds retaining modulatory activity as well as **9h** showing a 10-fold increase in affinity. Decreasing the fused ring size whilst bearing the cyclobutylamino substituent (**19ac**) abolishes any negative modulatory effects, and instead confers agonism. However the *N,N*-diethylamino (**19aa**) and cyclopropylamino (**19ab**) counterparts retain negative modulatory action. Interestingly, increasing the ring size (cycloheptane (**19bc**), cyclooctane (**19cc**)) while bearing the cyclobutylamino substituent maintains negative modulatory action. However, introduction of the *N,N*-diethylamino substituent to the cycloheptane analogue (**19ba**) completely abolishes activity. Additionally, introduction of a phenyl

ring to the 5-position in the presence of any amine converts all analogues (**19da-c**) to agonists. In most cases, a cyclohexyl substituent at this position appears favourable (**19fb-c**) as these compounds retain affinity and cooperativity, whereas an *N,N*-diethylamino substituent (**19fa**) abolishes activity. A phenyl substituent at the 6-position, however, is tolerated in the presence of *N,N*-diethylamino (**19ea**) and cyclopropylamino (**19eb**), yet, with cyclobutylamino (**19ec**), this yields an agonist. Installing a cyclohexyl moiety at the 6-position abolishes activity for **19ga-c**, whereas the activity profile of analogues bearing a 5,6-dimethyl substituent are highly dependent on the amine present at the 4-position (*N,N*-diethylamino (**19ha**) = agonist, cyclopropylamino (**19hb**) = inactive, and cyclobutylamino (**19hc**) = NAM). All NAMs identified were modulators of agonist efficacy, whereby structural modifications did not confer modulation of agonist affinity.

5. Conclusions

In this study, we report the functional characterisation of a small library of structural analogues based on a thieno[2,3-*d*]pyrimidine scaffold that we have previously shown to act as D₂R NAMs. The impact of structural modification was initially assessed with respect to the type of amine substituent at the 4-position in the presence of the 5,6,7,8-tetrahydrobenzo[4,5]thieno[2,3-*d*]pyrimidine moiety (series 1). Having identified favourable amines from series 1, we further extended our study to the analysis of various substituents in place of the 5/6-fused cyclohexane system in conjunction with one of three selected amines (series 2) at the 4-position. While many of these derivatives maintained NAM activity, some, surprisingly acted as D₂R agonists. It is not clear from the present data if this change in activity relates to a switch from an allosteric to an orthosteric mode of engagement or whether these compounds bind to the same allosteric site yet display distinct pharmacological effects. Future studies are needed to address this but such efforts are complicated by the relatively low affinity of these ligands. In the presence of a fused cyclohexane system, small cyclic aliphatic amines (cyclopropylamino, cyclobutylamino) were found to be vital for negative modulatory action. Two of the highest affinity NAMs to arise from this scaffold were identified, **9h** ($K_B = 0.57 \mu\text{M}$, fused cyclohexane moiety) and **19cb** ($K_B = 0.53 \mu\text{M}$, fused cyclopentane moiety), that contain cyclobutylamino and cyclopropylamino substituents, respectively. Conversely, larger heterocyclic substituents (morpholino) and acyclic amines (*tert*-butylamino) conferred agonism and abolished modulatory activity (**9d** and **9i**, respectively). In combination with a range of different substituents at the 5/6-positions, however, small cyclic/acyclic aliphatic amines gave a range of analogues with differential functional pharmacology, ranging from NAMs of DA efficacy, to agonists and compounds with no apparent functional activity. Taken together, this study demonstrates that the pharmacology of analogues functionalised at the 4-, 5-, and 6-positions of the thieno[2,3-*d*]pyrimidine core is difficult to predict, resulting in shallow SAR. Such observations are consistent with SAR studies of allosteric modulators of other GPCR targets, highlighting the challenges associated with GPCR allosteric ligand design.

6. Experimental section

6.1. General methods for chemistry

Chemicals and solvents were purchased from standard suppliers and used without further purification. Davisil silica gel (40–63 μm) for flash column chromatography was supplied by Grace Davison Discovery Sciences (Victoria, Australia), and deuterated solvents were purchased from Cambridge Isotope Laboratories, Inc. (USA,

distributed by Novachem PTY. Ltd., Victoria, Australia). Reactions were monitored by thin layer chromatography on commercially available precoated aluminum-backed plates (Merck Kieselgel 60 F₂₅₄). Visualization was by examination under UV light (254 and 366 nm). A solution of ninhydrin (in ethanol) was used to visualize primary and secondary amines. All organic extracts collected after aqueous workup procedures were dried over anhydrous Na₂SO₄ before gravity/vacuum filtering and evaporation to dryness. Organic solvents were evaporated *in vacuo* at $\leq 40^\circ\text{C}$ (water bath temperature). ¹H NMR and ¹³C NMR spectra were recorded on a Bruker Avance Nanobay III 400 MHz Ultrashield Plus spectrometer at 400.13 and 100.62 MHz, respectively. Chemical shifts (δ) are recorded in parts per million (ppm) with reference to the chemical shift of the deuterated solvent. Coupling constants (*J*) are recorded in Hz, and the significant multiplicities described by singlet (s), doublet (d), triplet (t), quadruplet (q), broad (br), multiplet (m), doublet of doublets (dd), and doublet of triplets (dt). Spectra were assigned using appropriate COSY, distortionless enhanced polarization transfer (DEPT), HSQC, and HMBC sequences. All NMR experiments were performed in CDCl₃ to permit comparison of the spectra of the various analogues. Experiments were performed in acetone-*d*₆, DMSO-*d*₆, or MeOH-*d*₄ where selected analogues lacked solubility in CDCl₃. LCMS experiments were run using one of two systems to verify reaction outcome and purity. System A was the default unless otherwise stated. System A consisted of the following: an Agilent 6100 series single quad coupled to an Agilent 1200 series HPLC instrument using the following buffers: buffer A, 0.1% formic acid in H₂O; buffer B, 0.1% formic acid in MeCN. The following gradient was used with a Phenomenex Luna 3 μm C8(2) 15 mm \times 4.6 mm column and a flow rate of 0.5 mL/min and total run time of 12 min: 0–4 min 95% buffer A and 5% buffer B, 4–7 min 0% buffer A and 100% buffer B, 7–12 min 95% buffer A and 5% buffer B. Mass spectra were acquired in positive and negative ion modes with a scan range of 0–1000 *m/z* at 5 V. UV detection was carried out at 254 nm. System B consisted of the following: an Agilent 6120 series single quad coupled to an Agilent 1260 series HPLC instrument. The following buffers were used; buffer A, 0.1% formic acid in H₂O; buffer B, 0.1% formic acid in MeCN. The following gradient was used with a Poroshell 120 EC-C18 50 mm \times 3.0 mm, 2.7 μm column and a flow rate of 0.5 mL/min and total run time of 5 min: 0–1 min 95% buffer A and 5% buffer B, from 1 to 2.5 min up to 0% buffer A and 100% buffer B, held at this composition until 3.8 min, 3.8–4 min 95% buffer A and 5% buffer B, held until 5 min at this composition. Mass spectra were acquired in positive and negative ion modes with a scan range of 100–1000 *m/z*. UV detection was carried out at 214 and 254 nm. All retention times (*t_R*) are quoted in minutes. System C: Analytical reverse-phase HPLC was performed on a Waters HPLC system coupled directly to a photodiode array detector and fitted with a Phenomenex Luna C8 (2) 100 Å column (150 mm \times 4.6 mm, 5 μm) using a binary solvent system: solvent A, 0.1% TFA/H₂O; solvent B, 0.1% TFA/80% CH₃CN/H₂O. Gradient elution was achieved using 100% solvent A to 100% solvent B over 20 min at a flow rate of 1 mL/min. All compounds subjected to biological testing were found to be >95% pure by HPLC at two wavelengths (λ of 254 and 214 nm).

6.2. General synthetic procedures

6.2.1. General procedure A for the synthesis of **9a-j**, **15a-b**, **19aa-hc**

In a suitable microwave reaction vessel the required chloropyrimidine (1 equiv.) was taken up in *i*-PrOH. To this was added the required amine (1.1 equiv.) and the mixture irradiated under stirring at 120 °C for 1–2 h. Upon completion of the reaction, the mixture was directly purified using FCC to afford the compound. Similarly, any precipitate could be collected under vacuum and

washed several time with cold *i*-PrOH to afford the desired compound.

6.2.1.1. *N*-Phenyl-5,6,7,8-tetrahydrobenzo[4,5]thieno[2,3-d]pyrimidin-4-amine (9a). General procedure A. Purification by FCC (eluent, 1:1 EtOAc/PE) afforded 105 mg of a white amorphous solid (84%). LCMS (*m/z*): 281.9 [M+H]⁺. HPLC: *t*_R 6.244 min, >95% purity (214 & 254 nm). HRMS (*m/z*): C₁₆H₁₅N₃S requires 282.1071 [M+H]⁺; found 282.1059. ¹H NMR (CDCl₃) δ 8.48 (s, 1H), 7.64 (dt, *J* = 8.8, 1.7 Hz, 2H), 7.41–7.34 (m, 2H), 7.17–7.10 (m, 2H), 3.06 (dd, *J* = 8.1, 3.9 Hz, 2H), 2.85 (dd, *J* = 8.0, 3.9 Hz, 2H), 2.03–1.89 (m, 4H). ¹³C NMR (CDCl₃) δ 166.3, 155.0, 152.6, 138.5, 134.7, 129.1, 124.8, 124.0, 121.3, 116.6, 26.5, 25.5, 22.5, 22.4.

6.2.1.2. *N*-Cyclohexyl-5,6,7,8-tetrahydrobenzo[4,5]thieno[2,3-d]pyrimidin-4-amine (9b). General procedure A. Purification by FCC (eluent, 1:1 EtOAc/PE) afforded 115 mg of a beige amorphous solid (82%). LCMS (*m/z*): 288.2 [M+H]⁺. HPLC: *t*_R 6.383 min, >95% purity (214 & 254 nm). HRMS (*m/z*): C₁₆H₂₁N₃S requires 288.1533 [M+H]⁺; found 288.1529. ¹H NMR (CDCl₃) δ 8.35 (s, 1H), 4.23–4.12 (m, 1H), 2.91 (dd, *J* = 6.8, 5.1 Hz, 2H), 2.79 (dd, *J* = 8.1, 3.7 Hz, 2H), 2.12–2.03 (m, 2H), 1.96–1.85 (m, 4H), 1.75 (ddd, *J* = 13.3, 8.8, 5.0 Hz, 2H), 1.69–1.61 (m, 1H), 1.55–1.42 (m, 2H), 1.32–1.21 (m, 3H). ¹³C NMR (CDCl₃) δ 165.3, 156.9, 153.3, 132.9, 125.5, 116.0, 48.9, 33.3, 26.5, 25.8, 25.5, 24.8, 22.7, 22.6.

6.2.1.3. 4-(Piperidin-1-yl)-5,6,7,8-tetrahydrobenzo[4,5]thieno[2,3-d]pyrimidine (9c). General procedure A. Purification by FCC (eluent, 1:1 EtOAc/PE) afforded 95.2 mg of a white amorphous solid (68%). LCMS (*m/z*): 274.1 [M+H]⁺. HPLC: *t*_R 6.478 min, >95% purity (214 & 254 nm). HRMS (*m/z*): C₁₅H₁₉N₃S requires 274.1374 [M+H]⁺; found 274.1372. ¹H NMR (CDCl₃) δ 8.51 (s, 1H), 3.36–3.28 (m, 4H), 2.96–2.91 (m, 2H), 2.90–2.85 (m, *J* = 6.3, 1.6 Hz, 2H), 1.97–1.90 (m, 2H), 1.81 (ddd, *J* = 12.1, 5.9, 2.6 Hz, 2H), 1.77–1.71 (m, 4H), 1.69–1.62 (m, 2H). ¹³C NMR (CDCl₃) δ 168.1, 162.9, 151.6, 134.4, 127.7, 121.5, 51.8, 26.7, 25.8, 25.7, 24.4, 23.1, 22.9.

6.2.1.4. 4-(5,6,7,8-Tetrahydrobenzo[4,5]thieno[2,3-d]pyrimidin-4-yl)morpholine (9d). General procedure A. Purification by FCC (eluent, 1:1 EtOAc/PE) afforded 161 mg of a white amorphous solid (88%). LCMS (*m/z*): 275.9 [M+H]⁺. HPLC: *t*_R 5.179 min, >95% purity (214 & 254 nm). HRMS (*m/z*): C₁₄H₁₇N₃OS requires 275.1065 [M+H]⁺; found 275.1087. ¹H NMR (400 MHz, CDCl₃) δ 8.46 (s, 1H), 3.82–3.77 (m, 4H), 3.36–3.31 (m, 4H), 2.87–2.77 (m, 4H), 1.91–1.84 (m, 2H), 1.79–1.71 (m, 2H). ¹³C NMR (CDCl₃) δ 168.4, 162.1, 151.5, 135.5, 126.9, 121.4, 66.6, 51.1, 26.7, 25.8, 22.9, 22.8.

6.2.1.5. 4-(Pyrrolidin-1-yl)-5,6,7,8-tetrahydrobenzo[4,5]thieno[2,3-d]pyrimidine (9e). General procedure A. Purification by FCC (eluent, 1:1 EtOAc/PE) afforded 109 mg of a white amorphous solid (82%). LCMS (*m/z*): 260.0 [M+H]⁺. HPLC: *t*_R 5.270 min, >95% purity (214 & 254 nm). HRMS (*m/z*): C₁₄H₁₇N₃S requires 259.1112 [M+H]⁺; found 259.1138. ¹H NMR (CDCl₃) δ 8.33 (s, 1H), 3.72–3.65 (m, 4H), 2.90–2.81 (m, 4H), 1.95–1.86 (m, 6H), 1.78–1.71 (m, 2H). ¹³C NMR (CDCl₃) δ 167.7, 158.8, 150.9, 132.2, 127.5, 117.9, 50.9, 29.2, 25.8, 25.5, 23.3, 22.8.

6.2.1.6. *N*-Cyclopropyl-5,6,7,8-tetrahydrobenzo[4,5]thieno[2,3-d]pyrimidin-4-amine (9f). General procedure A. Purification by FCC (eluent, 1:1 EtOAc/PE) afforded 105 mg of a white amorphous solid (87%). LCMS (*m/z*): 246.0 [M+H]⁺. HPLC: *t*_R 4.864 min, >95% purity (214 & 254 nm). HRMS (*m/z*): C₁₃H₁₅N₃S requires 246.0954 [M+H]⁺; found 246.0981. ¹H NMR (CDCl₃) δ 8.47 (s, 1H), 5.51 (s, 1H), 2.96–2.89 (m, 1H), 2.83 (td, *J* = 5.9, 1.9 Hz, 2H), 2.78 (td, *J* = 6.0, 1.9 Hz, 2H), 1.95–1.83 (m, 4H), 0.95–0.90 (m, 2H), 0.61–0.57 (m,

2H). ¹³C NMR (CDCl₃) δ 165.2, 158.3, 153.1, 133.4, 125.3, 116.2, 26.4, 25.4, 23.9, 22.5, 22.4, 7.6.

6.2.1.7. *N*-(Cyclopropylmethyl)-5,6,7,8-tetrahydrobenzo[4,5]thieno[2,3-d]pyrimidin-4-amine (9g). General procedure A. Purification by FCC (eluent, 1:1 EtOAc/PE) afforded 88 mg of a light yellow amorphous solid (85%). LCMS (*m/z*): 260.0 [M+H]⁺. HPLC: *t*_R 5.519 min, >95% purity (214 & 254 nm). HRMS (*m/z*): C₁₄H₁₇N₃S requires 260.1215 [M+H]⁺; found 260.1216. ¹H NMR (CDCl₃) δ 8.36 (s, 1H), 5.40 (s, 1H), 2.97–2.91 (m, *J* = 8.0, 4.1, 1.7 Hz, 1H), 2.82–2.78 (m, 2H), 1.98–1.85 (m, 4H), 1.20–1.08 (m, 1H), 0.62–0.55 (m, 2H), 0.33–0.28 (m, 2H). ¹³C NMR (CDCl₃) δ 165.3, 157.4, 153.1, 133.1, 125.5, 116.1, 46.1, 26.4, 25.5, 22.7, 22.6, 10.8, 3.5.

6.2.1.8. *N*-Cyclobutyl-5,6,7,8-tetrahydrobenzo[4,5]thieno[2,3-d]pyrimidin-4-amine (9h). General procedure A. Purification by FCC (eluent, 1:1 EtOAc/PE) afforded 101 mg of a white amorphous solid (88%). LCMS (*m/z*): 260.0 [M+H]⁺. HPLC: *t*_R 5.612 min, >95% purity (214 & 254 nm). HRMS (*m/z*): C₁₄H₁₇N₃S requires 260.1213 [M+H]⁺; found 260.1213. ¹H NMR (CDCl₃) δ 8.37 (s, 1H), 5.41 (d, *J* = 6.2 Hz, 1H), 4.76–4.64 (m, 1H), 2.93 (td, *J* = 5.9, 1.6 Hz, 2H), 2.81 (dd, *J* = 9.8, 3.7 Hz, 2H), 2.50 (dddd, *J* = 13.6, 7.7, 3.7, 2.7 Hz, 2H), 1.99–1.85 (m, 6H), 1.85–1.76 (m, 2H). ¹³C NMR (CDCl₃) δ 165.5, 156.6, 153.2, 133.3, 125.4, 115.9, 46.2, 31.8, 26.5, 25.5, 22.7, 22.6, 15.4.

6.2.1.9. *N*-(*tert*-Butyl)-5,6,7,8-tetrahydrobenzo[4,5]thieno[2,3-d]pyrimidin-4-amine (9i). General procedure A. Purification by FCC (eluent, 1:1 EtOAc/PE) afforded 114 mg of a white amorphous solid (85%). LCMS (*m/z*): 262.0 [M+H]⁺. HPLC: *t*_R 4.623 min, >95% purity (214 & 254 nm). HRMS (*m/z*): C₁₄H₁₉N₃S requires 261.1312 [M+H]⁺; found 261.1294. ¹H NMR (CDCl₃) δ 8.34 (s, 1H), 5.28 (s, 1H), 2.88 (td, *J* = 5.9, 1.6 Hz, 2H), 2.78 (dd, *J* = 9.8, 3.7 Hz, 2H), 1.95–1.82 (m, 4H), 1.53 (s, 9H). ¹³C NMR (CDCl₃) δ 165.1, 157.3, 152.6, 132.7, 125.2, 116.4, 52.3, 29.2, 26.5, 25.5, 22.7, 22.5.

6.2.1.10. *tert*-Butyl-4-(5,6,7,8-tetrahydrobenzo[4,5]thieno[2,3-d]pyrimidin-4-yl)piperazine-1-carboxylate (9j). General procedure A. Purification by FCC (eluent, 1:1 EtOAc/PE) afforded 244 mg of a white amorphous solid (84%). LCMS (*m/z*): 375.2 [M+H]⁺. HPLC: *t*_R 7.500 min, >95% purity (214 & 254 nm). ¹H NMR (CDCl₃) δ 8.45 (s, 1H), 3.53 (dd, *J* = 6.1, 4.1 Hz, 4H), 3.30–3.25 (m, 4H), 2.82 (ddd, *J* = 9.2, 7.8, 3.7 Hz, 4H), 1.90–1.83 (m, 2H), 1.77–1.69 (m, 2H), 1.41 (s, 9H). ¹³C NMR (CDCl₃) δ 168.5, 162.3, 154.9, 151.6, 135.6, 127.0, 121.6, 80.1, 28.5, 26.7, 25.8, 23.1, 22.8.

6.2.1.11. 4-(Piperazin-1-yl)-5,6,7,8-tetrahydrobenzo[4,5]thieno[2,3-d]pyrimidine (10). *tert*-Butyl-4-(5,6,7,8-tetrahydrobenzo[4,5]thieno[2,3-d]pyrimidin-4-yl)piperazine-1-carboxylate (163 mg, 435 μmol) was dissolved in DCM. To this solution was added trifluoroacetic acid (5.00 mL, 65.3 mmol) and the reaction mixture was stirred at r.t. for 3 h. The solvents were evaporated and the residue the residue was taken up in H₂O (20 mL) and added to a separating funnel. The aqueous solution was washed with Et₂O (3 × 30 mL), and the aqueous phase made alkaline with the addition of 2 M NaOH solution. This phase was then extracted with DCM (3 × 30 mL) and the organic extracts collected and dried over anhydrous Na₂SO₄ to afford 115 mg of the corresponding amine free base as a white amorphous solid (96%). LCMS (*m/z*): 274.9 [M+H]⁺. HPLC: *t*_R 4.623 min, >95% purity (214 & 254 nm). HRMS (*m/z*): C₁₄H₁₈N₃S requires 275.1334 [M+H]⁺; found 275.1334. ¹H NMR (CDCl₃) δ 8.52 (s, 1H), 3.41–3.34 (m, 4H), 3.07–3.03 (m, 4H), 2.95–2.91 (m, 2H), 2.90–2.85 (m, 2H), 2.05 (s, 1H), 1.97–1.90 (m, 2H), 1.84–1.78 (m, 2H). ¹³C NMR (CDCl₃) δ 168.3, 162.5, 151.5, 135.0, 127.2, 121.4, 51.9, 45.7, 26.8, 25.8, 23.0, 22.8.

- 6.2.1.12. *N*-Cyclopropylthieno[2,3-d]pyrimidin-4-amine (**15a**). General procedure A. Purification by FCC (eluent, 1:1 EtOAc/PE) afforded 77.1 mg of a white amorphous solid (76%). LCMS (*m/z*): 191.9 [M+H]⁺. HPLC: *t_R* 3.290 min, >95% purity (214 & 254 nm). HRMS (*m/z*): C₉H₉N₃S requires 192.0587 [M+H]⁺; found 192.0590. ¹H NMR (CDCl₃) δ 8.55 (s, 1H), 7.35 (d, *J* = 5.2 Hz, 1H), 7.27 (d, *J* = 6.0 Hz, 1H), 5.92 (s, 1H), 3.03–2.97 (m, 1H), 0.99–0.93 (m, 2H), 0.74–0.68 (m, 2H). ¹³C NMR (CDCl₃) δ 167.3, 158.6, 153.9, 122.8, 118.4, 116.2, 24.6, 8.2.
- 6.2.1.13. *N*-Cyclobutylthieno[2,3-d]pyrimidin-4-amine (**15b**). General procedure A. Purification by FCC (eluent, 1:1 EtOAc/PE) afforded 85.1 mg of a white amorphous solid (79%). LCMS (*m/z*): 206.0 [M+H]⁺. HPLC: *t_R* 3.952 min, >95% purity (214 & 254 nm). HRMS (*m/z*): C₁₄H₁₇N₃S requires 206.0744 [M+H]⁺; found 206.0746. ¹H NMR (CDCl₃) δ 8.50 (s, 1H), 7.27 (d, *J* = 5.9 Hz, 1H), 7.17 (d, *J* = 6.0 Hz, 1H), 5.53 (d, *J* = 5.9 Hz, 1H), 4.81–4.71 (m, 1H), 2.57–2.46 (m, 2H), 2.07–1.92 (m, 2H), 1.85–1.75 (m, 2H). ¹³C NMR (CDCl₃) δ 166.7, 156.3, 154.2, 123.0, 117.2, 116.1, 46.4, 31.7, 15.3.
- 6.2.1.14. *N,N*-Diethyl-6,7-dihydro-5H-cyclopenta[4,5]thieno[2,3-d]pyrimidin-4-amine (**19aa**). General procedure A. Purification by FCC (eluent, 1:1 EtOAc/PE) afforded 115 mg of a white amorphous solid (78%). LCMS (*m/z*): 248.1 [M+H]⁺. HPLC: *t_R* 5.295 min, >95% purity (214 & 254 nm). HRMS (*m/z*): C₁₃H₁₇N₃S requires 248.1217 [M+H]⁺; found 248.1216. ¹H NMR (CDCl₃) δ 8.35 (s, 1H), 3.59 (q, *J* = 7.1 Hz, 4H), 3.06–2.99 (m, 2H), 2.94 (ddt, *J* = 8.2, 6.6, 1.8 Hz, 2H), 2.44–2.34 (m, 2H), 1.19 (t, *J* = 7.0 Hz, 6H). ¹³C NMR (CDCl₃) δ 173.3, 159.4, 151.3, 138.2, 136.0, 116.0, 43.7, 32.4, 29.8, 28.1, 13.1.
- 6.2.1.15. *N*-Cyclopropyl-6,7-dihydro-5H-cyclopenta[4,5]thieno[2,3-d]pyrimidin-4-amine (**19ab**). General procedure A. Purification by FCC (eluent, 1:1 EtOAc/PE) afforded 105 mg of a white amorphous solid (77%). LCMS (*m/z*): 232.1 [M+H]⁺. HPLC: *t_R* 4.629 min, >95% purity (214 & 254 nm). HRMS (*m/z*): C₁₂H₁₃N₃S requires 232.0903 [M+H]⁺; found 232.0903. ¹H NMR (CDCl₃) δ 8.49 (s, 1H), 5.28 (s, 1H), 2.98 (t, *J* = 7.2 Hz, 4H), 2.92 (td, *J* = 6.6, 3.7 Hz, 1H), 2.57–2.47 (m, 2H), 0.97–0.91 (m, 2H), 0.64–0.58 (m, 2H). ¹³C NMR (CDCl₃) δ 170.7, 157.7, 153.2, 138.9, 134.2, 133.1, 29.5, 29.2, 27.9, 23.8, 7.6.
- 6.2.1.16. *N*-Cyclobutyl-6,7-dihydro-5H-cyclopenta[4,5]thieno[2,3-d]pyrimidin-4-amine (**19ac**). General procedure A. Purification by FCC (eluent, 1:1 EtOAc/PE) afforded 90.1 mg of a white amorphous solid (83%). LCMS (*m/z*): 246.1 [M+H]⁺. HPLC: *t_R* 5.373 min, >95% purity (214 & 254 nm). HRMS (*m/z*): C₁₃H₁₅N₃S requires 246.0466 [M+H]⁺; found 246.0464. ¹H NMR (CDCl₃) δ 8.37 (s, 1H), 5.16 (d, *J* = 6.7 Hz, 1H), 4.77–4.65 (m, 1H), 3.06–2.96 (m, 4H), 2.60–2.45 (m, 4H), 1.99–1.86 (m, 2H), 1.84–1.75 (m, 2H). ¹³C NMR (CDCl₃) δ 155.8, 153.2, 138.6, 134.3, 113.1, 45.9, 31.8, 29.5, 29.2, 27.9, 15.2.
- 6.2.1.17. *N,N*-Diethyl-6,7,8,9-tetrahydro-5H-cyclohepta[4,5]thieno[2,3-d]pyrimidin-4-amine (**19ba**). General procedure A. Purification by FCC (eluent, 1:1 EtOAc/PE) afforded 99.4 mg of a white amorphous solid (86%). LCMS (*m/z*): 276.0 [M+H]⁺. HPLC: *t_R* 6.323 min, >95% purity (214 & 254 nm). HRMS (*m/z*): C₁₅H₂₁N₃S requires 276.1526 [M+H]⁺; found 276.1529. ¹H NMR (CDCl₃) δ 8.40 (s, 1H), 3.36 (q, *J* = 7.1 Hz, 4H), 2.98–2.93 (m, 2H), 2.82–2.78 (m, 2H), 1.87–1.80 (m, 2H), 1.68–1.62 (m, 2H), 1.56 (ddd, *J* = 11.4, 6.0, 2.8 Hz, 2H), 1.03 (t, *J* = 7.1 Hz, 7H). ¹³C NMR (CDCl₃) δ 166.3, 161.7, 150.9, 138.2, 132.6, 121.6, 44.5, 32.8, 30.4, 28.7, 27.6, 27.4, 12.3.
- 6.2.1.18. *N*-Cyclopropyl-6,7,8,9-tetrahydro-5H-cyclohepta[4,5]thieno[2,3-d]pyrimidin-4-amine (**19bb**). General procedure A. Purification by FCC (eluent, 1:1 EtOAc/PE) afforded 101 mg of a white amorphous solid (88%). LCMS (*m/z*): 274.2 [M+H]⁺. HPLC: *t_R* 5.709 min, >95% purity (214 & 254 nm). HRMS (*m/z*): C₁₅H₁₉N₃S requires 274.1374 [M+H]⁺; found 274.1372. ¹H NMR (CDCl₃) δ 8.48 (s, 1H), 5.53 (s, 1H), 2.97–2.90 (m, *J* = 5.7, 3.4 Hz, 4H), 2.90–2.84 (m, 4H), 1.93–1.86 (m, 2H), 1.82 (td, *J* = 11.7, 7.2 Hz, 2H), 0.97–0.89 (m, 2H), 0.64–0.57 (m, 2H). ¹³C NMR (CDCl₃) δ 164.2, 158.4, 152.8, 137.37, 130.2, 117.5, 30.48, 30.32, 29.0, 27.1, 26.4, 24.2, 7.7.
- 6.2.1.19. *N*-Cyclobutyl-6,7,8,9-tetrahydro-5H-cyclohepta[4,5]thieno[2,3-d]pyrimidin-4-amine (**19bc**). General procedure A. Purification by FCC (eluent, 1:1 EtOAc/PE) afforded 100 mg of a white amorphous solid (88%). LCMS (*m/z*): 274.0 [M+H]⁺. HPLC: *t_R* 5.908 min, >95% purity (214 & 254 nm). HRMS (*m/z*): C₁₅H₁₉N₃S requires 274.1371 [M+H]⁺; found 274.1372. ¹H NMR (CDCl₃) δ 8.35 (s, 1H), 5.40 (d, *J* = 6.3 Hz, 1H), 4.74–4.63 (m, 1H), 3.04–2.99 (m, 2H), 2.87 (dd, *J* = 6.7, 4.3 Hz, 2H), 2.55–2.45 (m, 2H), 2.03–1.69 (m, 10H). ¹³C NMR (CDCl₃) δ 164.4, 156.5, 152.8, 136.9, 130.2, 117.1, 46.4, 31.8, 30.4, 28.9, 27.2, 26.4, 22.5, 15.5.
- 6.2.1.20. *N,N*-Diethyl-5,6,7,8,9,10-hexahydrocycloocta[4,5]thieno[2,3-d]pyrimidin-4-amine (**19ca**). General procedure A. Purification by FCC (eluent, 1:1 EtOAc/PE) afforded 113 mg of a white amorphous solid (79%). LCMS (*m/z*): 290.2 [M+H]⁺. HPLC: *t_R* 7.076 min, >95% purity (214 & 254 nm). HRMS (*m/z*): C₁₆H₂₃N₃S requires 290.1689 [M+H]⁺; found 290.1685. ¹H NMR (CDCl₃) δ 8.57 (s, 1H), 3.43 (q, *J* = 7.1 Hz, 4H), 3.05–3.01 (m, 2H), 2.93–2.89 (m, 2H), 1.78–1.71 (m, 2H), 1.57 (tt, *J* = 8.4, 6.2 Hz, 2H), 1.49–1.42 (m, 2H), 1.16–1.11 (m, *J* = 8.3, 3.6 Hz, 2H), 1.09 (t, *J* = 7.1 Hz, 6H). ¹³C NMR (CDCl₃) δ 168.0, 162.4, 151.2, 138.5, 129.8, 121.6, 45.5, 31.8, 31.2, 27.9, 26.2, 25.4, 24.6, 12.3.
- 6.2.1.21. *N*-Cyclopropyl-5,6,7,8,9,10-hexahydrocycloocta[4,5]thieno[2,3-d]pyrimidin-4-amine (**19cb**). General procedure A. Purification by FCC (eluent, 1:1 EtOAc/PE) afforded 75.2 mg of a white amorphous solid (77%). LCMS (*m/z*): 274.2 [M+H]⁺. HPLC: *t_R* 5.709 min, >95% purity (214 & 254 nm). HRMS (*m/z*): C₁₅H₁₉N₃S requires 274.1374 [M+H]⁺; found 274.1372. ¹H NMR (CDCl₃) δ 8.52 (d, *J* = 3.2 Hz, 1H), 5.57 (s, 1H), 3.01–2.94 (m, 1H), 2.87 (dd, *J* = 12.3, 5.1 Hz, 4H), 1.75–1.66 (m, 4H), 1.57–1.48 (m, 2H), 1.38–1.27 (m, 2H), 0.99–0.92 (m, 2H), 0.62–0.57 (m, 2H). ¹³C NMR (CDCl₃) δ 164.9, 157.9, 152.9, 136.6, 127.5, 116.3, 31.6, 29.9, 27.8, 26.1, 25.2, 23.9, 7.7.
- 6.2.1.22. *N*-Cyclobutyl-5,6,7,8,9,10-hexahydrocycloocta[4,5]thieno[2,3-d]pyrimidin-4-amine (**19cc**). General procedure A. Purification by FCC (eluent, 1:1 EtOAc/PE) afforded 122 mg of a white amorphous solid (86%). LCMS (*m/z*): 288.2 [M+H]⁺. HPLC: *t_R* 6.266 min, >95% purity (214 & 254 nm). HRMS (*m/z*): C₁₆H₂₁N₃S requires 288.1531 [M+H]⁺; found 288.1531. ¹H NMR (CDCl₃) δ 8.39 (s, 1H), 5.48 (d, *J* = 6.6 Hz, 1H), 4.80–4.67 (m, 1H), 2.95–2.90 (m, 2H), 2.90–2.85 (m, 2H), 2.57–2.47 (m, 2H), 1.98–1.86 (m, 2H), 1.86–1.74 (m, 4H), 1.74–1.65 (m, 2H), 1.57–1.49 (m, 2H), 1.35 (dt, *J* = 10.7, 6.1 Hz, 2H). ¹³C NMR (CDCl₃) δ 165.1, 156.1, 152.8, 136.3, 127.5, 115.9, 46.1, 31.8, 31.6, 29.9, 27.8, 26.1, 25.2, 15.3.
- 6.2.1.23. *N,N*-Diethyl-5-phenylthieno[2,3-d]pyrimidin-4-amine (**19da**). General procedure A. Purification by FCC (eluent, 1:1 EtOAc/PE) afforded 94.1 mg of a white amorphous solid (86%). LCMS (*m/z*): 283.9 [M+H]⁺. HPLC: *t_R* 6.1389 min, >95% purity (214 & 254 nm). HRMS (*m/z*): C₁₆H₁₇N₃S requires 284.1213 [M+H]⁺; found 284.1216. ¹H NMR (CDCl₃) δ 8.55 (s, 1H), 7.44–7.38 (m, 4H), 7.37–7.32 (m, 1H), 7.18 (s, 1H), 3.16 (q, *J* = 7.1 Hz, 4H), 0.89 (t, *J* = 7.1 Hz, 6H). ¹³C NMR (CDCl₃) δ 170.1, 160.9, 152.11, 136.8, 136.4, 128.4, 128.1, 127.6, 120.5, 115.6, 43.7, 12.3.
- 6.2.1.24. *N*-Cyclopropyl-5-phenylthieno[2,3-d]pyrimidin-4-amine (**19db**). General procedure A. Purification by FCC (eluent, 1:1

EtOAc/PE) afforded 98.3 mg of a white amorphous solid (86%). LCMS (*m/z*): 267.9 [M+H]⁺. HPLC: *t_R* 5.308 min, >95% purity (214 & 254 nm). HRMS (*m/z*): C₁₅H₁₃N₃S requires 268.0830 [M+H]⁺; found 268.0903. ¹H NMR (CDCl₃) δ 8.60 (s, 1H), 7.51–7.47 (m, 3H), 7.43–7.38 (m, 2H), 7.07 (s, 1H), 5.11 (s, 1H), 2.87–2.80 (m, 1H), 0.80–0.74 (m, 2H), 0.29–0.24 (m, 2H). ¹³C NMR (CDCl₃) δ 166.9, 158.6, 154.4, 136.2, 134.7, 129.3, 129.1, 128.9, 120.5, 114.27, 23.7, 7.3.

6.2.1.25. *N*-Cyclobutyl-5-phenylthieno[2,3-d]pyrimidin-4-amine (**19dc**). General procedure A. Purification by FCC (eluent, 1:1 EtOAc/PE) afforded 85.1 mg of a white amorphous solid (75%). LCMS (*m/z*): 281.9 [M+H]⁺. HPLC: *t_R* 6.183 min, >95% purity (214 & 254 nm). HRMS (*m/z*): C₁₆H₁₅N₃S requires 282.1059 [M+H]⁺; found 282.1059. ¹H NMR (CDCl₃) δ 8.48 (s, 1H), 7.54–7.49 (m, 5H), 7.46 (dd, *J* = 6.7, 2.7 Hz, 2H), 7.07 (s, 1H), 5.10 (d, *J* = 5.5 Hz, 1H), 4.62–4.50 (m, 1H), 2.37–2.27 (m, 2H), 1.73–1.59 (m, 2H), 1.57–1.44 (m, 2H). ¹³C NMR (CDCl₃) δ 166.9, 156.4, 154.2, 136.2, 134.7, 129.4, 128.89, 128.7, 120.0, 113.9, 45.7, 31.2, 15.2.

6.2.1.26. *N,N*-Diethyl-6-phenylthieno[2,3-d]pyrimidin-4-amine (**19ea**). General procedure A. Purification by FCC (eluent, 1:1 EtOAc/PE) afforded 96.8 mg of a white amorphous solid (84%). LCMS (*m/z*): 284.0 [M+H]⁺. HPLC: *t_R* 6.080 min, >95% purity (214 & 254 nm). HRMS (*m/z*): C₁₆H₁₇N₃S requires 284.1213 [M+H]⁺; found 284.1216. ¹H NMR (CDCl₃) δ 8.41 (s, 1H), 7.65–7.61 (m, 2H), 7.48 (s, 1H), 7.45–7.40 (m, 2H), 7.37–7.32 (m, 1H), 3.79 (q, *J* = 7.1 Hz, 4H), 1.36 (t, *J* = 7.1 Hz, 6H). ¹³C NMR (CDCl₃) δ 168.9, 156.9, 153.2, 138.1, 134.1, 129.2, 128.4, 126.3, 116.8, 116.4, 44.2, 13.4.

6.2.1.27. *N*-Cyclopropyl-6-phenylthieno[2,3-d]pyrimidin-4-amine (**19eb**). General procedure A. Purification by FCC (eluent, 1:1 EtOAc/PE) afforded 99.1 mg of a white amorphous solid (90%). LCMS (*m/z*): 267.9 [M+H]⁺. HPLC: *t_R* 5.407 min, >95% purity (214 & 254 nm). HRMS (*m/z*): C₁₅H₁₃N₃S requires 268.0830 [M+H]⁺; found 268.0903. ¹H NMR (401 MHz, CDCl₃) δ 8.53 (s, 1H), 7.65–7.61 (m, 1H), 7.49 (s, 1H), 7.44–7.38 (m, 1H), 7.37–7.32 (m, 1H), 5.79 (s, 1H), 3.06–2.99 (m, 1H), 1.01–0.95 (m, 1H), 0.74–0.70 (m, 1H). ¹³C NMR (101 MHz, CDCl₃) δ 166.8, 158.2, 153.9, 140.7, 133.6, 129.2, 128.7, 126.4, 117.7, 113.3, 24.6, 8.2.

6.2.1.28. *N*-Cyclobutyl-6-phenylthieno[2,3-d]pyrimidin-4-amine (**19ec**). General procedure A. Purification by FCC (eluent, 1:1 EtOAc/PE) afforded 108 mg of a white amorphous solid (92%). LCMS (*m/z*): 281.9 [M+H]⁺. HPLC: *t_R* 5.940 min, >95% purity (214 & 254 nm). HRMS (*m/z*): C₁₆H₁₅N₃S requires 282.1058 [M+H]⁺; found 282.1059. ¹H NMR (CDCl₃) δ 8.48 (s, 1H), 7.65–7.62 (m, 2H), 7.45–7.39 (m, 2H), 7.37–7.31 (m, 2H), 5.47 (d, *J* = 7.2 Hz, 1H), 4.83–4.72 (m, 1H), 2.63–2.41 (m, 2H), 2.07–1.95 (m, 2H), 1.87–1.77 (m, 2H). ¹³C NMR (CDCl₃) δ 166.1, 155.9, 154.1, 140.9, 133.6, 129.2, 128.7, 126.3, 117.6, 112.5, 46.4, 31.7, 15.3.

6.2.1.29. 5-Cyclohexyl-*N,N*-diethylthieno[2,3-d]pyrimidin-4-amine (**19fa**). General procedure A. Purification by FCC (eluent, 1:1 EtOAc/PE) afforded 115 mg of a white amorphous solid (81%). LCMS (*m/z*): 290.2 [M+H]⁺. HPLC: *t_R* 7.189 min, >95% purity (214 & 254 nm). HRMS (*m/z*): C₁₆H₂₃N₃S requires 290.1689 [M+H]⁺; found 290.1685. ¹H NMR (CDCl₃) δ 8.58 (s, 1H), 7.02 (s, 1H), 3.47 (q, *J* = 7.1 Hz, 1H), 3.17–3.06 (m, *J* = 2.9 Hz, 1H), 1.98 (dd, *J* = 12.7, 1.3 Hz, 1H), 1.89–1.82 (m, 1H), 1.81–1.73 (m, 1H), 1.48–1.20 (m, 1H), 1.13 (t, *J* = 7.1 Hz, 1H). ¹³C NMR (CDCl₃) δ 169.8, 163.3, 151.6, 141.6, 119.9, 117.3, 45.0, 38.4, 34.8, 26.9, 26.2, 12.4.

6.2.1.30. 5-Cyclohexyl-*N*-cyclopropylthieno[2,3-d]pyrimidin-4-amine (**19fb**). General procedure A. Purification by FCC (eluent, 1:1 EtOAc/PE) afforded 87.8 mg of a white amorphous solid (88%). LCMS

(*m/z*): 274.2 [M+H]⁺. HPLC: *t_R* 6.073 min, >95% purity (214 & 254 nm). HRMS (*m/z*): C₁₆H₁₅N₃S requires 274.1375 [M+H]⁺; found 274.1372. ¹H NMR (CDCl₃) δ 8.55 (s, 1H), 6.87 (s, 1H), 5.57 (s, 1H), 3.07–2.99 (m, 1H), 2.59 (dd, *J* = 13.5, 5.5 Hz, 1H), 2.06 (t, *J* = 11.0 Hz, 2H), 1.95 (t, *J* = 10.5 Hz, 2H), 1.83 (d, *J* = 12.7 Hz, 1H), 1.50–1.38 (m, 4H), 1.30 (ddd, *J* = 13.7, 12.5, 4.9 Hz, 1H), 1.01–0.95 (m, 2H), 0.63–0.56 (m, 2H). ¹³C NMR (CDCl₃) δ 167.7, 158.6, 153.5, 139.7, 115.6, 115.3, 40.9, 33.9, 26.7, 25.9, 24.1, 7.7.

6.2.1.31. *N*-Cyclobutyl-5-cyclohexylthieno[2,3-d]pyrimidin-4-amine (**19fc**). General procedure A. Purification by FCC (eluent, 1:1 EtOAc/PE) afforded 115 mg of a white amorphous solid (81%). LCMS (*m/z*): 288.2 [M+H]⁺. HPLC: *t_R* 6.820 min, >95% purity (214 & 254 nm). HRMS (*m/z*): C₁₆H₂₁N₃S requires 288.1531 [M+H]⁺; found 288.1529. ¹H NMR (CDCl₃) δ 8.43 (s, 1H), 6.85 (s, 1H), 5.51 (d, *J* = 6.3 Hz, 1H), 4.79–4.69 (m, 1H), 2.74–2.66 (m, 1H), 2.60–2.50 (m, 2H), 2.15 (d, *J* = 8.2 Hz, 2H), 2.02–1.90 (m, 4H), 1.91–1.81 (m, 5H), 1.53–1.40 (m, 5H), 1.34 (ddd, *J* = 12.5, 8.2, 3.5 Hz, 1H). ¹³C NMR (CDCl₃) δ 167.8, 156.6, 153.5, 139.8, 115.2, 46.2, 41.0, 33.9, 31.7, 26.8, 26.0, 15.4.

6.2.1.32. 6-Cyclohexyl-*N,N*-diethylthieno[2,3-d]pyrimidin-4-amine (**19ga**). General procedure A. Purification by FCC (eluent, 1:1 EtOAc/PE) afforded 113 mg of a white amorphous solid (91%). LCMS (*m/z*): 290.0 [M+H]⁺. HPLC: *t_R* 6.559 min, >95% purity (214 & 254 nm). HRMS (*m/z*): C₁₆H₂₃N₃S requires 290.1683 [M+H]⁺; found 290.1685. ¹H NMR (CDCl₃) δ 8.37 (s, 1H), 6.96 (d, *J* = 1.0 Hz, 1H), 3.73 (q, *J* = 7.1 Hz, 4H), 2.83 (tt, *J* = 11.2, 3.5 Hz, 1H), 2.10–2.04 (m, 2H), 1.89–1.82 (m, 2H), 1.79–1.71 (m, 1H), 1.55–1.35 (m, 4H), 1.32 (t, *J* = 7.1 Hz, 6H), 1.30–1.19 (m, 1H). ¹³C NMR (CDCl₃) δ 167.9, 156.6, 152.5, 146.9, 115.4, 115.3, 44.07, 40.3, 35.1, 26.4, 25.9, 13.6.

6.2.1.33. 6-Cyclohexyl-*N*-cyclopropylthieno[2,3-d]pyrimidin-4-amine (**19gb**). General procedure A. Purification by FCC (eluent, 1:1 EtOAc/PE) afforded 84.8 mg of a white amorphous solid (87%). LCMS (*m/z*): 274.0 [M+H]⁺. HPLC: *t_R* 5.986 min, >95% purity (214 & 254 nm). HRMS (*m/z*): C₁₅H₁₉N₃S requires 274.1369 [M+H]⁺; found 274.1372. ¹H NMR (CDCl₃) δ 8.49 (s, 1H), 6.94 (s, 1H), 5.63 (s, 1H), 2.97 (qd, *J* = 6.7, 3.6 Hz, 1H), 2.81 (td, *J* = 10.9, 3.2 Hz, 1H), 2.06 (d, *J* = 10.6 Hz, 2H), 1.87–1.81 (m, 2H), 1.74 (d, *J* = 12.7 Hz, 1H), 1.52–1.33 (m, 4H), 1.31–1.20 (m, 1H), 0.97–0.91 (m, 2H), 0.70–0.64 (m, 2H). ¹³C NMR (CDCl₃) δ 157.7, 153.3, 149.7, 116.5, 111.8, 40.2, 35.01, 26.3, 25.9, 24.5, 8.15.

6.2.1.34. *N*-Cyclobutyl-6-cyclohexylthieno[2,3-d]pyrimidin-4-amine (**19gc**). General procedure A. Purification by FCC (eluent, 1:1 EtOAc/PE) afforded 101 mg of a white amorphous solid (88%). LCMS (*m/z*): 288.0 [M+H]⁺. HPLC: *t_R* 6.377 min, >95% purity (214 & 254 nm). HRMS (*m/z*): C₁₆H₂₁N₃S requires 288.1528 [M+H]⁺; found 288.1529. ¹H NMR (CDCl₃) δ 8.43 (s, 1H), 6.80 (d, *J* = 1.0 Hz, 1H), 5.31 (d, *J* = 7.2 Hz, 1H), 4.80–4.67 (m, 1H), 2.86–2.77 (m, 1H), 2.55–2.45 (m, 2H), 2.11–2.04 (m, 2H), 2.03–1.91 (m, 2H), 1.89–1.71 (m, 5H), 1.53–1.33 (m, 4H), 1.32–1.20 (m, 1H). ¹³C NMR (CDCl₃) δ 165.4, 155.5, 153.4, 149.9, 116.4, 111.1, 46.3, 40.2, 35.0, 31.8, 26.4, 25.9, 15.3.

6.2.1.35. *N,N*-Diethyl-5,6-dimethylthieno[2,3-d]pyrimidin-4-amine (**19ha**). General procedure A. Purification by FCC (eluent, 1:1 EtOAc/PE) afforded 82.3 mg of a white amorphous solid (71%). LCMS (*m/z*): 236.0 [M+H]⁺. HPLC: *t_R* 5.322 min, >95% purity (214 & 254 nm). HRMS (*m/z*): C₁₂H₁₇N₃S requires 236.1212 [M+H]⁺; found 236.1216. ¹H NMR (CDCl₃) δ 8.50 (s, 1H), 3.46 (q, *J* = 7.1 Hz, 4H), 2.43 (d, *J* = 0.8 Hz, 3H), 2.41 (d, *J* = 0.7 Hz, 3H), 1.12 (t, *J* = 7.1 Hz, 6H). ¹³C NMR (CDCl₃) δ 167.2, 162.0, 151.1, 131.3, 124.9, 122.3, 44.8, 13.9, 13.7, 12.3.

6.2.1.36. *N*-Cyclopropyl-5,6-dimethylthieno[2,3-d]pyrimidin-4-amine (**19hb**). General procedure A. Purification by FCC (eluent, 1:1 EtOAc/PE) afforded 101 mg of a white amorphous solid (93%). LCMS (*m/z*): 220.1 [M+H]⁺. HPLC: *t*_R 5.322 min, >95% purity (214 & 254 nm). HRMS (*m/z*): C₁₁H₁₃N₃S requires 220.0898 [M+H]⁺; found 220.0903. ¹H NMR (CDCl₃) δ 8.49 (s, 1H), 5.65 (s, 1H), 2.98–2.91 (m, 1H), 2.41 (s, 6H), 0.97–0.91 (m, 2H), 0.63–0.58 (m, 2H). ¹³C NMR (CDCl₃) δ 164.6, 158.4, 153.2, 130.2, 122.9, 117.2, 24.1, 14.5, 13.5, 7.7.

6.2.1.37. *N*-Cyclobutyl-5,6-dimethylthieno[2,3-d]pyrimidin-4-amine (**19hc**). General procedure A. Purification by FCC (eluent, 1:1 EtOAc/PE) afforded 85.5 mg of a white amorphous solid (73%). LCMS (*m/z*): 234.0 [M+H]⁺. HPLC: *t*_R 5.940 min, >95% purity (214 & 254 nm). HRMS (*m/z*): C₁₆H₁₅N₃S requires 234.1056 [M+H]⁺; found 234.1059. ¹H NMR (CDCl₃) δ 8.37 (s, 1H), 5.55 (d, *J* = 5.9 Hz, 1H), 4.81–4.59 (m, 1H), 2.54–2.48 (m, 2H), 2.46 (s, 3H), 2.41 (d, *J* = 0.6 Hz, 3H), 1.98–1.86 (m, 2H), 1.86–1.76 (m, 2H). ¹³C NMR (CDCl₃) δ 164.8, 156.5, 153.1, 129.8, 123.0, 116.8, 46.2, 31.8, 15.4, 14.5, 13.5.

6.3. Pharmacological characterisation

6.3.1. Materials

Dulbecco's modified Eagle's medium, Flp-In CHO cells, and hygromycin B were purchased from Invitrogen (Carlsbad, CA). Fetal bovine serum (FBS) was purchased from ThermoTrace (Melbourne, VIC, Australia). All other reagents were purchased from Sigma Aldrich (St. Louis, MO).

6.3.2. Cell culture and transfection for cAMP assay

FlpIn CHO cells stably expressing the human dopamine D_{2L} receptor (or WT FlpIn CHO cells for off-target screening assay) were maintained in DMEM supplemented with 5% foetal calf serum (FBS) and 0.2 mg/mL hygromycin at 37 °C in a humidified incubator supplied with 5% CO₂.

6.3.3. cAMP measurement (interaction & off-target assay)

The cellular cAMP levels were measured with the CAMYEL BRET-based biosensor for cAMP [26]. One day after transfection, cells were trypsinised and seeded in white 96-well microplates. The cells were then cultured for an additional day, rinsed twice with Hank's Balanced Salt Solution (HBSS) and were then incubated in fresh HBSS. The *Renilla* luciferase (*RLuc*) substrate coelenterazine-h was added to reach a final concentration of 5 μM.

Interaction assay: FlpIn CHO cells stably expressing the human

measured using a BMG Lumistar counter 30 min after stimulation. The BRET signal (BRET ratio) was determined by calculating the ratio of the light emitted at 535 ± 30 nm (YFP) to the light emitted at 475 ± 30 nm (RLuc).

6.3.4. Data analysis

Computerized nonlinear regression, statistical analyses and simulations were performed using Prism 6.0 (GraphPad Prism 6.0b Software, San Diego, CA).

6.3.5. Analysis of functional data

All concentration-response data were fitted to the following modified four-parameter Hill equation to derive potency estimates [36].

$$E = Basal + \frac{(E_{max} - Basal) \cdot [A]^{nH}}{[A]^{nH} + EC_{50}^{nH}} \quad (1)$$

where E is the effect of the system, nH is the Hill slope and EC₅₀ is the concentration of agonist [A] that gives the midpoint response between basal and maximal effect of dopamine or other agonists (E_{max}), which are the lower and upper asymptotes of the response, respectively.

To determine the mode of interaction of **1** and analogues of **1** at the D₂R in relation to the agonist dopamine, data were fit to both a competitive and allosteric model and the best fit compared statistically. A logistic equation of competitive agonist-antagonist interaction was globally fitted to data from functional experiments measuring the interaction between dopamine and all analogues of **1**:

$$Response = Bottom + \frac{(E_{max} - Bottom)}{1 + \left(\frac{10^{-pEC_{50}} \left[1 + \left(\frac{[B]}{10^{-pK_B}} \right)^s \right]^{nH}}{[A]} \right)^{nH}} \quad (2)$$

where *s* represents the Schild slope for the antagonist and pA₂ represents the negative logarithm of the molar concentration of antagonist that makes it necessary to double the concentration of agonist needed to elicit the original submaximal response obtained in the absence of antagonist. The same data describing the interaction between all analogues of **1** and dopamine were also analyzed using a complete operational model of allosterism and agonism according to equation (3) [37].

$$E = \frac{E_m(\tau_A[A](K_B + \alpha\beta[B]) + \tau_B[B]K_A)^{nH}}{([A]K_B + K_A K_B + K_A[B] + \alpha[A][B])^{nH} + (\tau_A[A](K_B + \alpha\beta[B]) + \tau_B[B]K_A)^{nH}} \quad (3)$$

dopamine D_{2L} receptor were stimulated with dopamine in the presence of 10 μM forskolin (final concentration). For the antagonism assay, the allosteric antagonists were added 30 min prior to stimulation. The BRET signals were measured using a BMG Lumistar counter 30 min after stimulation. The BRET signal (BRET ratio) was determined by calculating the ratio of the light emitted at 535 ± 30 nm (YFP) to the light emitted at 475 ± 30 nm (RLuc).

Off-target assay using non-hD_{2L}R-expressing Flp-In CHO cells: The allosteric antagonists (1–100 μM), and dopamine (10 μM) were added 30 min prior to stimulation in the presence or absence of 10 μM forskolin (final concentration). The BRET signals were

where E_m is the maximum possible cellular response, [A] and [B] are the concentrations of orthosteric and allosteric ligands, respectively, K_A and K_B are the equilibrium dissociation constant of the orthosteric and allosteric ligands, respectively, τ_A and τ_B (constrained to -100) are operational measures of orthosteric and allosteric ligand efficacy (which incorporate both signal efficiency and receptor density), respectively, α is the binding cooperativity parameter between the orthosteric and allosteric ligand, and β denotes the magnitude of the allosteric effect of the modulator on the efficacy of the orthosteric agonist. K_A was constrained to 617 nM, and represents a value of functional affinity determined by

an operational model of agonism applied to concentration-response data of dopamine in the presence of increasing concentrations of the alkylating agent phenoxybenzamine. For compounds that caused a limited rightward shift of the dopamine dose-response curve but no decrease in E_{max} , data were fit using an operational model of allostery where $\text{Log}\beta$ was constrained to 0 to represent neutral cooperativity with dopamine efficacy. For compounds that produced an unlimited decrease in the maximal response of dopamine $\text{Log}\beta$ was constrained to -3 .

For each of the compounds the two equations (models) were then compared for their fit using an extra-sum-of-squares F test. All of the data points and values shown in the figures and tables are the mean \pm S.E.M. of at least three separate experiments performed in duplicate unless otherwise stated.

Notes

The authors declare no competing financial interest.

Acknowledgments

This research was supported by a National Health and Medical Research Council Project Grant Number APP1049564.

Appendix A. Supplementary data

Supplementary data to this article can be found online at <https://doi.org/10.1016/j.ejmech.2019.01.061>.

References

- N. Ginovart, S. Kapur, Role of dopamine D(2) receptors for antipsychotic activity, *Handb. Exp. Pharmacol.* 212 (2012) 27–52.
- S. Miyamoto, N. Miyake, L.F. Jarskog, W.W. Fleischacker, J.A. Lieberman, Pharmacological treatment of schizophrenia: A critical review of the pharmacology and clinical effects of current and future therapeutic agents, *Mol. Psychiatr.* 17 (2012) 1206–1227.
- H.Y. Meltzer, Update on typical and atypical antipsychotic drugs, *Annu. Rev. Med.* 64 (2013) 393–406.
- S. Leucht, C. Corves, D. Arbt, R.R. Engel, C. Li, J.M. Davis, Second-generation versus first-generation antipsychotic drugs for schizophrenia: A meta-analysis, *Lancet* 373 (2009) 31–41.
- L. Farde, A.L. Nordstrom, F.A. Wiesel, S. Pauli, C. Halldin, G. Sedvall, Positron emission tomographic analysis of central D1 and D2 dopamine receptor occupancy in patients treated with classical neuroleptics and clozapine. Relation to extrapyramidal side effects, *Arch. Gen. Psychiatr.* 49 (1992) 538–544.
- M.G. Caron, M. Beaulieu, V. Raymond, B. Gagne, J. Drouin, R.J. Lefkowitz, F. Labrie, Dopaminergic receptors in the anterior pituitary gland. Correlation of [³H]dihydroergocryptine binding with the dopaminergic control of prolactin release, *J. Biol. Chem.* 253 (1978) 2244–2253.
- J.W. Newcomer, Second-generation (atypical) antipsychotics and metabolic effects: A comprehensive literature review, *CNS Drugs* 19 (2005) 1–93.
- R. Maggio, F. Novi, M. Scarselli, G.U. Corsini, The impact of G-protein-coupled receptor hetero-oligomerization on function and pharmacology, *FEBS J.* 272 (2005) 2939–2946.
- R. Maggio, M. Scarselli, M. Capannolo, M.J. Millan, Novel dimensions of D3 receptor function: Focus on heterodimerisation, transactivation and allosteric modulation, *Eur. Neuropsychopharmacol.* 25 (2015) 1470–1479.
- R. Maggio, M.J. Millan, Dopamine D2-D3 receptor heteromers: Pharmacological properties and therapeutic significance, *Curr. Opin. Pharmacol.* 10 (2010) 100–107.
- M. Carli, S. Kolachalam, S. Aringhieri, M. Rossi, L. Giovannini, R. Maggio, M. Scarselli, Dopamine D2 receptors dimers: How can we pharmacologically target them? *Curr. Neuropharmacol.* 16 (2018) 222–230.
- M. Rossi, I. Fasciani, F. Marampon, R. Maggio, M. Scarselli, The first negative allosteric modulator for dopamine D2 and D3 Receptors, SB269652 may lead to a new generation of antipsychotic drugs, *Mol. Pharmacol.* 91 (2017) 586–594.
- E. Silvano, M.J. Millan, C. Mannoury la Cour, Y. Han, L. Duan, S.A. Griffin, R.R. Luedtke, G. Aloisi, M. Rossi, F. Zazzeroni, J.A. Javitch, R. Maggio, The tetrahydroquinoline derivative SB269,652 is an allosteric antagonist at dopamine D3 and D2 receptors, *Mol. Pharmacol.* 78 (2010) 925–934.
- J. Shonberg, C. Draper-Joyce, S.N. Mistry, A. Christopoulos, P.J. Scammells, J.R. Lane, B. Capuano, Structure-activity study of *N*-((trans)-4-(2-(7-cyano-3,4-dihydroisoquinolin-2(1*H*)-yl)ethyl)cyclohexyl)-1*H*-indole-2-carboxamide (SB269652), a bitopic ligand that acts as a negative allosteric modulator of the dopamine D2 receptor, *J. Med. Chem.* 58 (2015) 5287–5307.
- J.R. Lane, P. Donthamsetti, J. Shonberg, C.J. Draper-Joyce, S. Dentry, M. Michino, L. Shi, L. Lopez, P.J. Scammells, B. Capuano, P.M. Sexton, J.A. Javitch, A. Christopoulos, A new mechanism of allostery in a G protein-coupled receptor dimer, *Nat. Chem. Biol.* 10 (2014) 745–752.
- V. Kumar, A.E. Moritz, T.M. Keck, A. Bonifazi, M.P. Ellenberger, C.D. Sibley, R.B. Free, L. Shi, J.R. Lane, D.R. Sibley, A.H. Newman, Synthesis and pharmacological characterization of novel trans-cyclopropylmethyl-linked bivalent ligands that exhibit selectivity and allosteric pharmacology at the dopamine D3 receptor (D3R), *J. Med. Chem.* 60 (2017) 1478–1494.
- J.R. Lane, P. Chubukov, W. Liu, M. Canals, V. Cherezov, R. Abagyan, R.C. Stevens, V. Katritch, Structure-based ligand discovery targeting orthosteric and allosteric pockets of dopamine receptors, *Mol. Pharmacol.* 84 (2013) 794–807.
- T.J. Fyfe, B. Zarzycka, H.D. Lim, B. Kellam, S.N. Mistry, V. Katritch, P.J. Scammells, J.R. Lane, B. Capuano, A thieno[2,3-d]pyrimidine scaffold is a novel negative allosteric modulator of the dopamine D2 receptor, *J. Med. Chem.* 62 (2018) 174–206.
- A. Kopinathan, C. Draper-Joyce, M. Szabo, A. Christopoulos, P.J. Scammells, J.R. Lane, B. Capuano, Subtle modifications to the indole-2-carboxamide motif of the negative allosteric modulator *N*-((trans)-4-(2-(7-cyano-3,4-dihydroisoquinolin-2(1*H*)-yl)ethyl)cyclohexyl)-1*H*-indole-2-carboxamide (SB269652) yield dramatic changes in pharmacological activity at the dopamine D2 receptor, *J. Med. Chem.* 62 (2018) 371–377.
- K. Gewald, E. Schinke, H. Böttcher, Heterocyclen aus CH-aciden nitrilen, VIII. 2-Amino-thiophene aus methylenaktiven nitrilen, carbonylverbindungen und schwefel, *Chem. Ber.* 99 (1966) 94–100.
- K. Leach, P.M. Sexton, A. Christopoulos, Allosteric GPCR modulators: Taking advantage of permissive receptor pharmacology, *Trends Pharmacol. Sci.* 28 (2007) 382–389.
- A. Christopoulos, Assessing the distribution of parameters in models of ligand-receptor interaction: To log or not to log, *Trends Pharmacol. Sci.* 19 (1998) 351–357.
- J. Inglese, R.L. Johnson, A. Simeonov, M. Xia, W. Zheng, C.P. Austin, D.S. Auld, High-throughput screening assays for the identification of chemical probes, *Nat. Chem. Biol.* 3 (2007) 466–479.
- D.S. Auld, N.T. Southall, A. Jadhav, R.L. Johnson, D.J. Diller, A. Simeonov, C.P. Austin, J. Inglese, Characterization of chemical libraries for luciferase inhibitory activity, *J. Med. Chem.* 51 (2008) 2372–2386.
- L.H. Heitman, J.P. van Veldhoven, A.M. Zweemer, K. Ye, J. Brussee, I.J. AP, False positives in a reporter gene assay: Identification and synthesis of substituted *N*-pyridin-2-ylbenzamides as competitive inhibitors of firefly luciferase, *J. Med. Chem.* 51 (2008) 4724–4729.
- L.L. Jiang, J. Collins, R. Davis, K.M. Lin, D. DeCamp, T. Roach, R. Hsueh, R.A. Rebres, E.M. Ross, R. Taussig, I. Fraser, P.C. Sternweis, Use of a cAMP BRET sensor to characterize a novel regulation of cAMP by the sphingosine 1-phosphate/G13 pathway, *J. Biol. Chem.* 282 (2007) 10576–10584.
- J.A. Ballesteros, H. Weinstein, Integrated methods for the construction of three-dimensional models and computational probing of structure-function relations in G protein-coupled receptors, in: S.C. Sealfon (Ed.), *Methods Neurosci.*, vol. 25, Academic Press, 1995, pp. 366–428.
- S. Wang, T. Che, A. Levit, B.K. Shoichet, D. Wacker, B.L. Roth, Structure of the D2 dopamine receptor bound to the atypical antipsychotic drug risperidone, *Nature* 555 (2018) 269–273.
- S. Sharma, A.L. Rodriguez, P.J. Conn, C.W. Lindsley, Synthesis and SAR of a mGluR5 allosteric partial antagonist lead: unexpected modulation of pharmacology with slight structural modifications to a 5-(phenylethynyl)pyrimidine scaffold, *Bioorg. Med. Chem. Lett.* 18 (2008) 4098–4101.
- P.J. Conn, C.K. Jones, C.W. Lindsley, Subtype-selective allosteric modulators of muscarinic receptors for the treatment of CNS disorders, *Trends Pharmacol. Sci.* 30 (2009) 148–155.
- T.M. Bridges, J.E. Marlo, C.M. Niswender, C.K. Jones, S.B. Jadhav, P.R. Gentry, H.C. Plumley, C.D. Weaver, P.J. Conn, C.W. Lindsley, Discovery of the first highly M5-preferring muscarinic acetylcholine receptor ligand, an M5 positive allosteric modulator derived from a series of 5-trifluoromethoxy *N*-benzyl isatins, *J. Med. Chem.* 52 (2009) 3445–3448.
- T.M. Bridges, J. Phillip Kennedy, M.J. Noetzel, M.L. Breining, P.R. Gentry, P.J. Conn, C.W. Lindsley, Chemical lead optimization of a pan Gq mAChR M1, M3, M5 positive allosteric modulator (PAM) lead. Part II: Development of a potent and highly selective M1, PAM, *Bioorg. Med. Chem. Lett.* 20 (2010) 1972–1975.
- C.W. Lindsley, Z. Zhao, W.H. Leister, R.G. Robinson, S.F. Barnett, D. Defeo-Jones, R.E. Jones, G.D. Hartman, J.R. Huff, H.E. Huber, M.E. Duggan, Allosteric Akt (PKB) inhibitors: Discovery and SAR of isozyme selective inhibitors, *Bioorg. Med. Chem. Lett.* 15 (2005) 761–764.
- S.A. Scott, P.E. Selvy, J.R. Buck, H.P. Cho, T.L. Criswell, A.L. Thomas, M.D. Armstrong, C.L. Arteaga, C.W. Lindsley, H.A. Brown, Design of isoform-selective phospholipase D inhibitors that modulate cancer cell invasiveness, *Nat. Chem. Biol.* 5 (2009) 108–117.
- R.R. Lavieri, S.A. Scott, P.E. Selvy, K. Kim, S. Jadhav, R.D. Morrison, J.S. Daniels, H.A. Brown, C.W. Lindsley, Design, synthesis, and biological evaluation of

Chapter 3: Subtle Modifications to a Thieno[2,3-d]pyrimidine Scaffold Yield NAMs & Agonists of the D₂R

490

T.J. Effe et al. / *European Journal of Medicinal Chemistry* 168 (2019) 474–490

- halogenated *N*-(2-(4-oxo-1-phenyl-1,3,8-triazaspiro[4.5]decan-8-yl)ethyl) benzamides: Discovery of an isoform-selective small molecule phospholipase D2 inhibitor, *J. Med. Chem.* 53 (2010) 6706–6719.
- [36] H.J.C. Motulsky, in: *Fitting Models to Biological Data Using Linear and Nonlinear Regression: a Practical Guide to Curve Fitting*, Graphpad Software Inc., San Diego CA, 2003.
- [37] A. Christopoulos, T. Kenakin, G protein-coupled receptor allostereism and complexing, *Pharmacol. Rev.* 54 (2002) 323–374.

Supplementary Information

Subtle Modifications to a Thieno[2,3-d]pyrimidine Scaffold Yield Negative Allosteric Modulators and Agonists of the Dopamine D₂ Receptor

Tim J. Fyfe,^{†,§,||} Barrie Kellam,^{||} Shailesh N. Mistry,^{||} Peter J. Scammells,[†] J. Robert Lane,^{*,‡} Ben Capuano^{*,†}

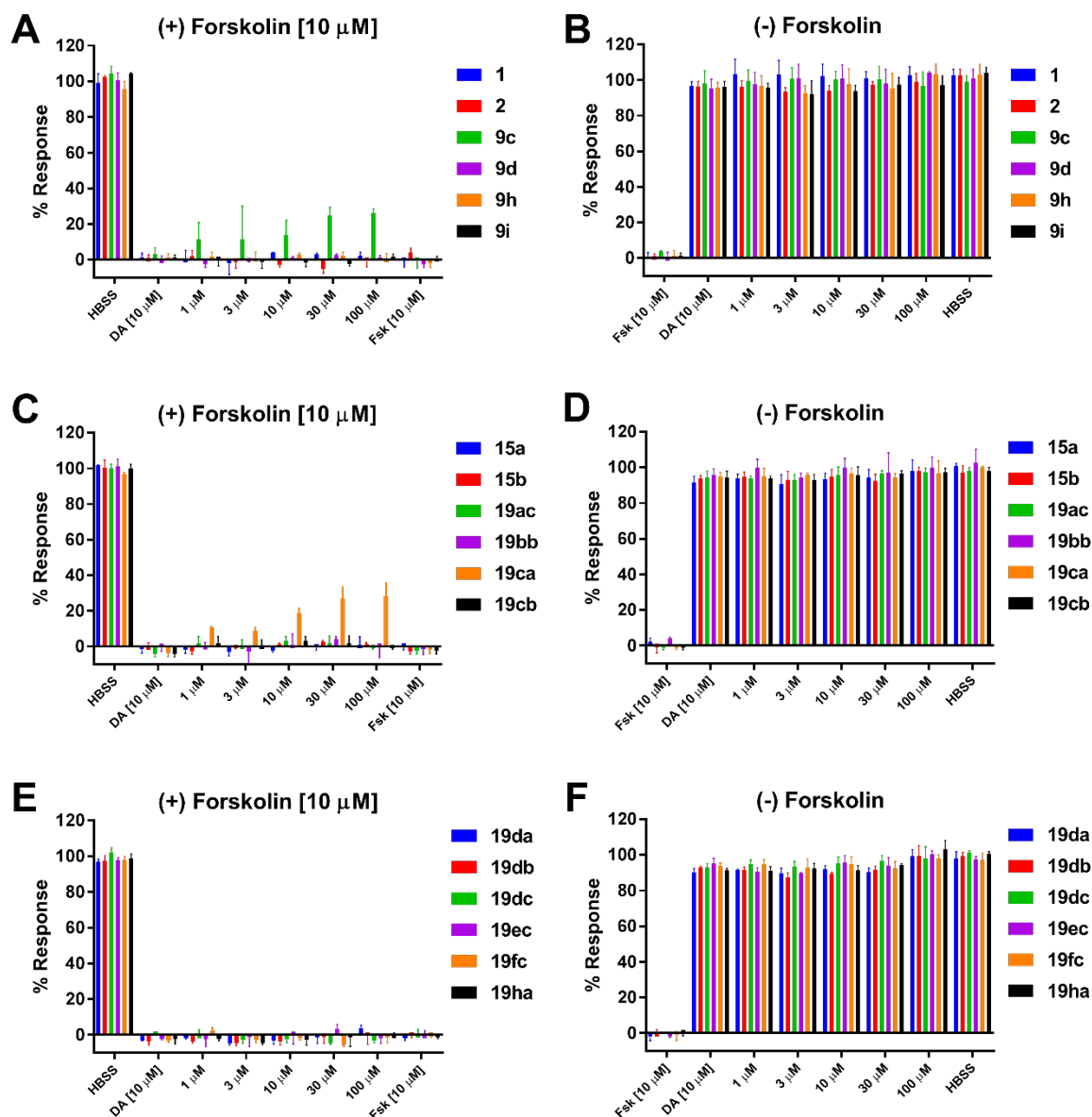
[†]Medicinal Chemistry, and [§]Drug Discovery Biology, Monash Institute of Pharmaceutical Sciences, Monash University, Parkville, Victoria 3052, Australia

^{||}School of Pharmacy, Centre for Biomolecular Sciences, University of Nottingham, Nottingham NG7 2RD, U.K.

[‡]School of Life Sciences, Queen's Medical Centre, University of Nottingham, Nottingham NG7 2UH, U.K.

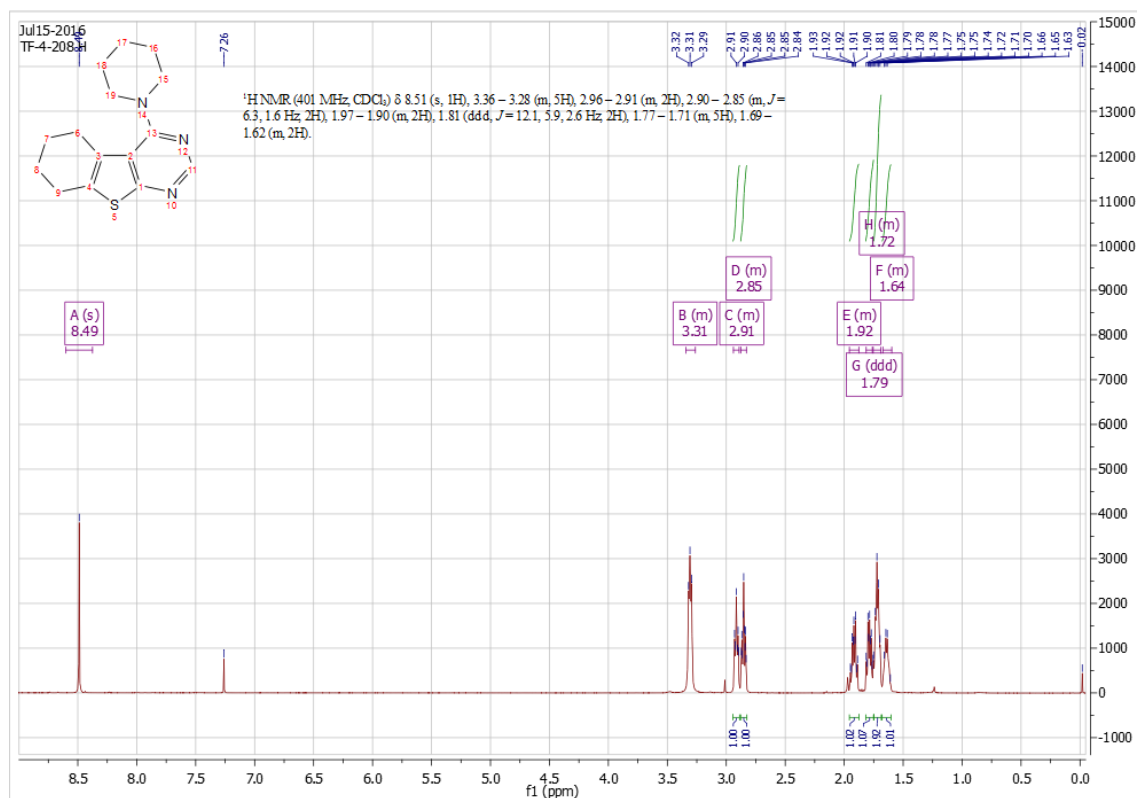
Table of Contents

Figure 1	Off-target screening graphs for compounds 1 , 2 , 9c-d , 9h-i , 15a-b , 19ac , 19bb , 19ca , 19da , 19db , 19dc , 19fb , 19fc , 19ec , and 9ha	139
Figure 2A-B	¹ H & ¹³ C NMR spectra for 9c	140
Figure 3A-D	¹ H & ¹³ C NMR, HRMS spectra & analytical HPLC trace for 9d	141-143
Figure 4A-D	¹ H & ¹³ C NMR, HRMS spectra & analytical HPLC trace for 9h	144-146
Figure 5A-D	¹ H & ¹³ C NMR, HRMS spectra & analytical HPLC trace for 9i	147-149
Figure 6-13A-B	¹ H & ¹³ C NMR spectra for 9f , 10 , 15b , 19aa , 19ab , 19bc , 19ca , 19cb	150-157
Figure 14A-D	¹ H & ¹³ C NMR, HRMS spectra & analytical HPLC trace for 19fc	158-160
Figure 15A-B	¹ H & ¹³ C NMR spectra for 19hc	161

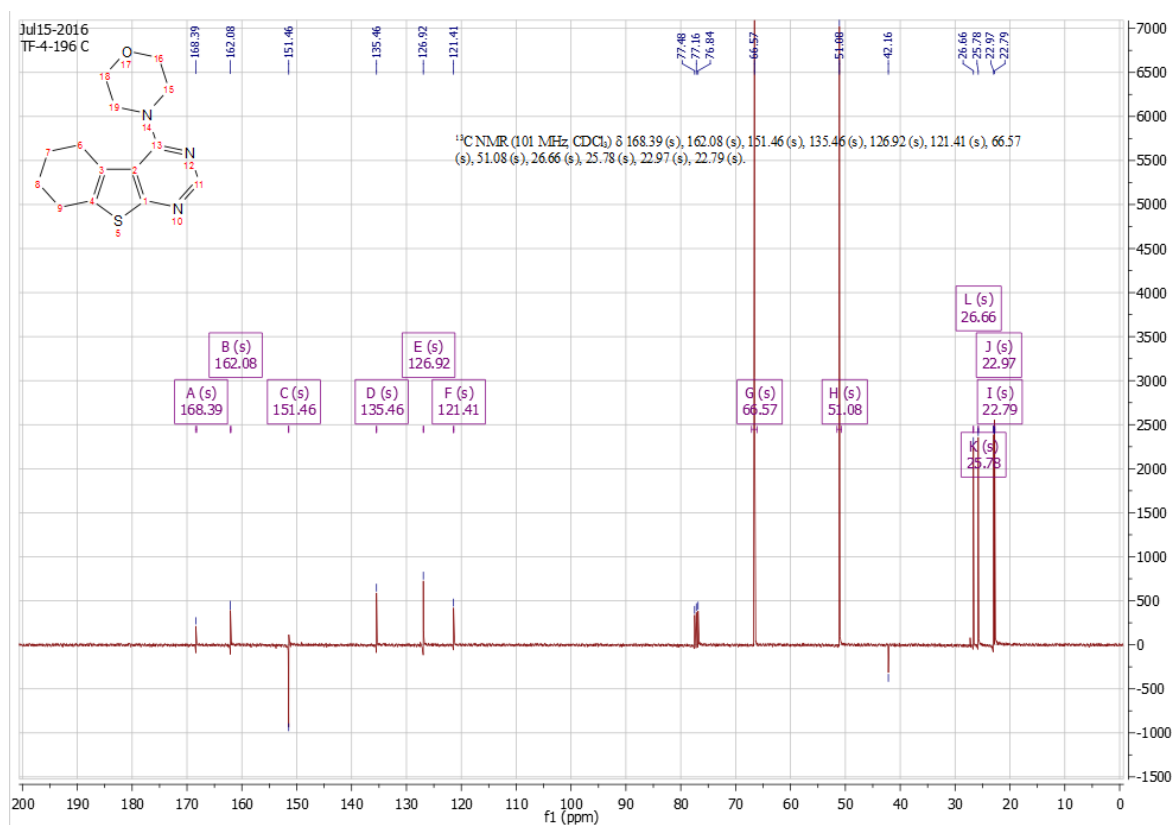


Supporting Figure 1. Measuring the Ability of thieno[2,3-*d*]pyrimidines to Modulate the BRET Signal in hD₂L_R Negative FlpIn CHO Cells Transfected with the CAMYEL Biosensor. All compounds observed to be agonists in our functional interaction assay, together with selected NAMs, were further assessed for their integrity. Compounds were measured both in the presence (panels **A**, **C**, **E**) and absence (panels **B**, **D**, **F**) of 10 μ M forskolin. The BRET signal obtained in the presence and absence of 10 μ M forskolin was normalised to 0 and 100%, respectively. (**A**) In the absence of the D₂R, compound **9c** was shown to cause a concentration-dependant change in the BRET signal, effecting a maximal 26% change at 100 μ M. (**C**) Compound **19ca** gave a similar response, effecting a maximal 28% change of the BRET signal at 100 μ M. All data used in these graphs are presented as mean \pm SEM from a minimum of three independent experiments performed in duplicate.

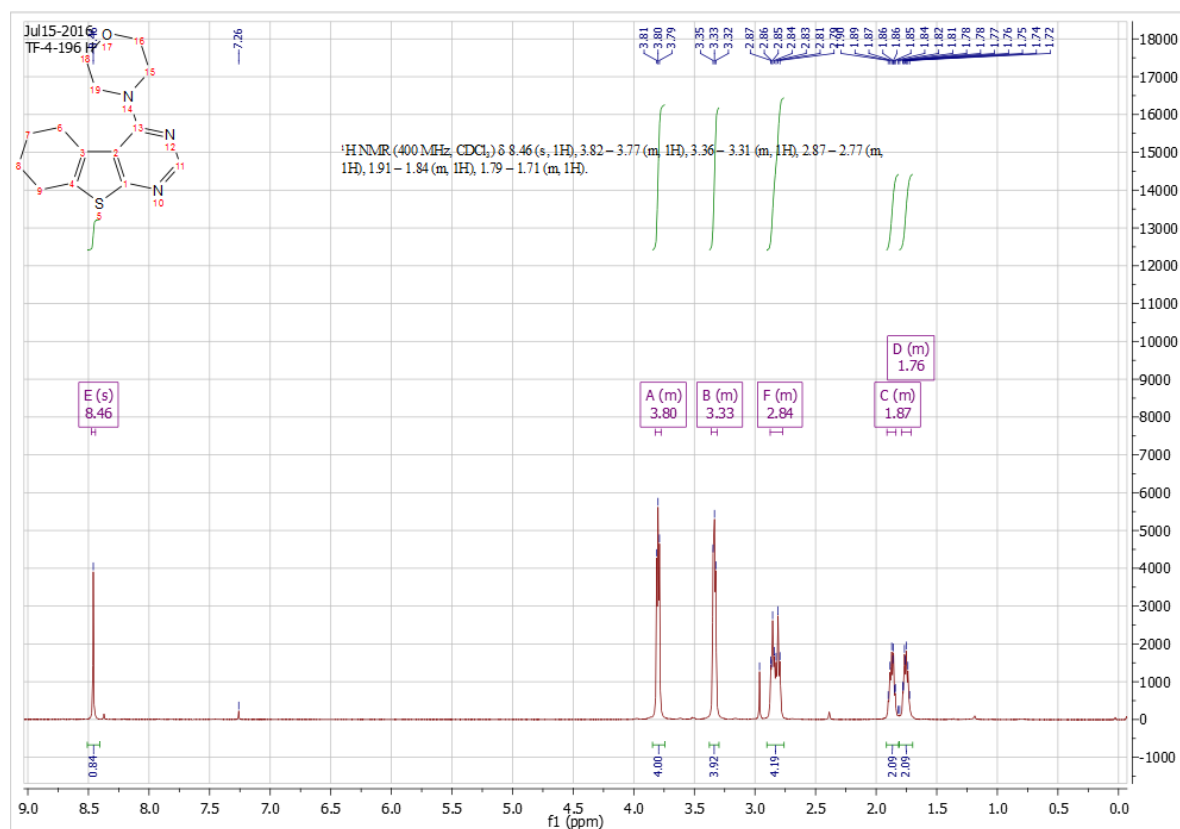
Supporting Figure 2A. ¹H NMR spectrum for compound 9c (non-specific inhibitor).



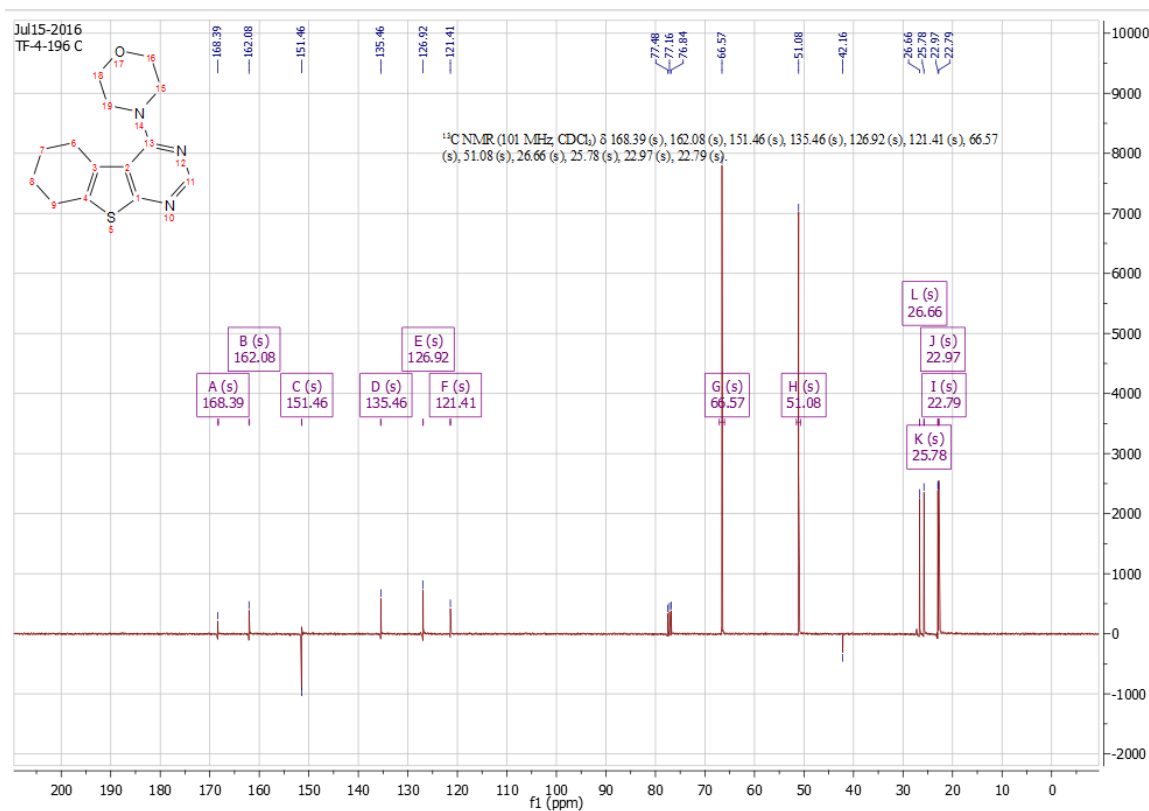
Supporting Figure 2B. ¹³C NMR spectrum for compound 9c (non-specific inhibitor).



Supporting Figure 3A. ¹H NMR spectrum for compound 9d.



Supporting Figure 3B. ¹³C NMR spectrum for compound 9d.



Supporting Figure 3C. HRMS spectrum (ESI) for compound 9d.

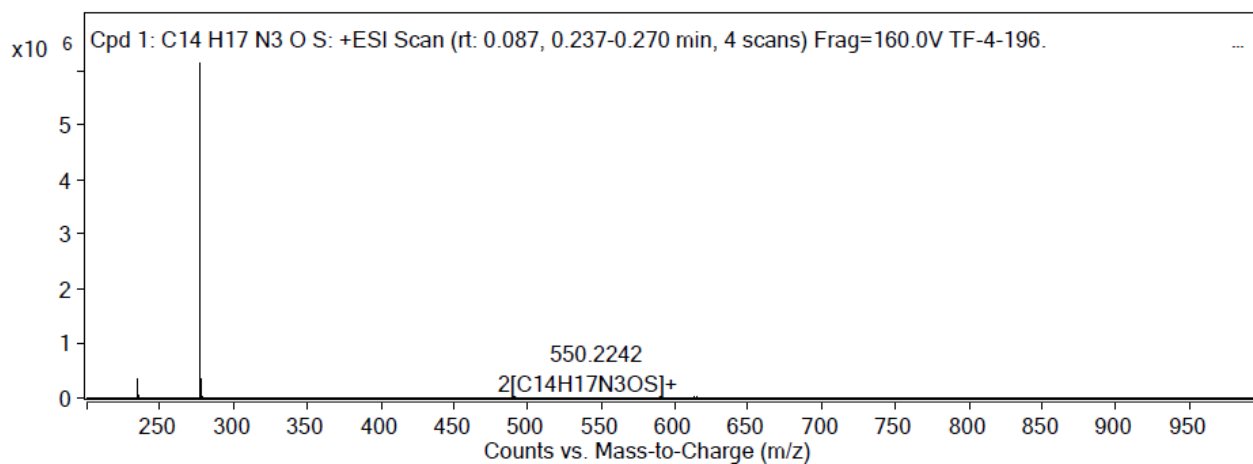
Qualitative Compound Report

Data File	TF-4-196.d	Sample Name	TF-4-196
Sample Type	Sample	Position	P2-D6
Instrument Name	Instrument 1	User Name	Dr Jason Dang
Acq Method	Monash_Direct.m	Acquired Time	27-Jul-16 1:07:38 PM
IRM Calibration Status	Success	DA Method	Monash_Accuracy.m
Comment			
Sample Group		Info.	
Formula	C14H17N3OS	Stream Name	LC 1
Acquisition SW Version	6200 series TOF/6500 series Q-TOF B.06.01 (B6172 SP1)		

Compound Table

Compound Label	RT	Mass	Abund	Formula	Tgt Mass	Diff (ppm)
Cpd 1: C14 H17 N3 O S	0.12	275.1097	6339693	C14 H17 N3 O S	275.1092	1.59

Compound Label	m/z	RT	Algorithm	Mass
Cpd 1: C14 H17 N3 O S	276.1168	0.12	Find By Formula	275.1097

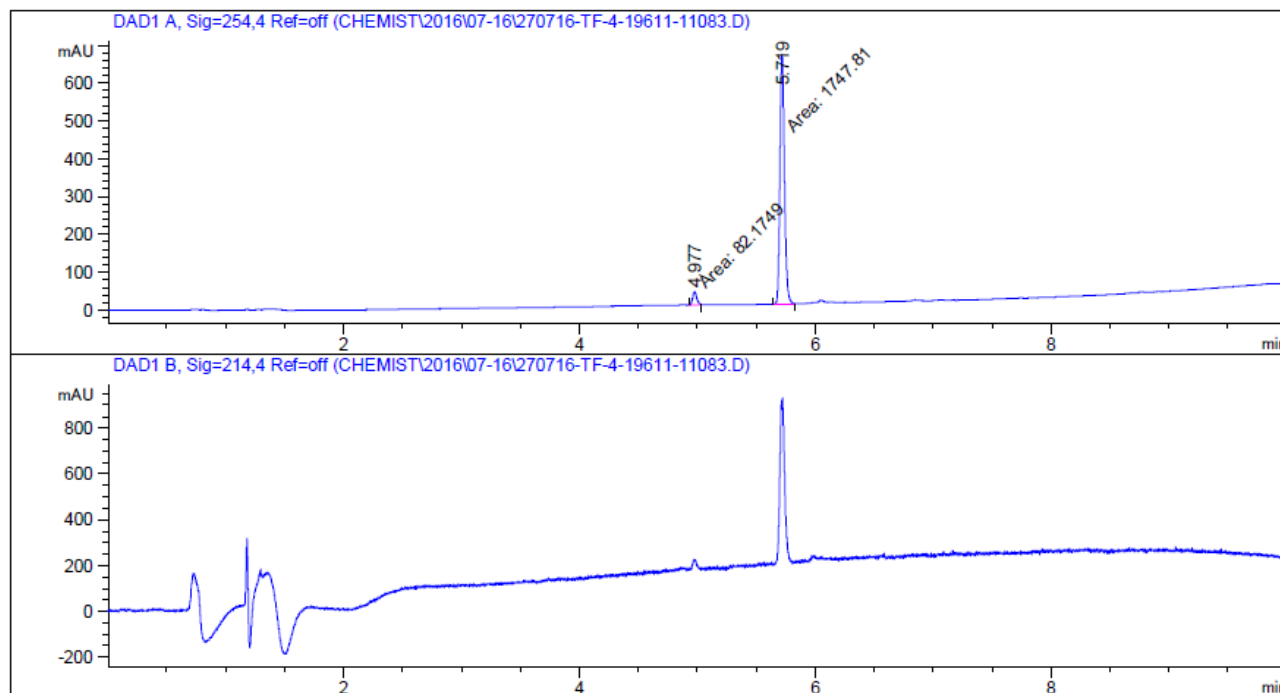


MS Spectrum Peak List

m/z	Calc m/z	Diff(ppm)	z	Abund	Formula	Ion
275.1065	275.1087	7.97	1	2193.46	C14H17N3OS	M+
276.1168	276.1165	-1.17	1	6339693.14	C14H17N3OS	(M+H)+
298.0975	298.0985	3.32	1	1438.13	C14H17N3OS	(M+Na)+

--- End Of Report ---

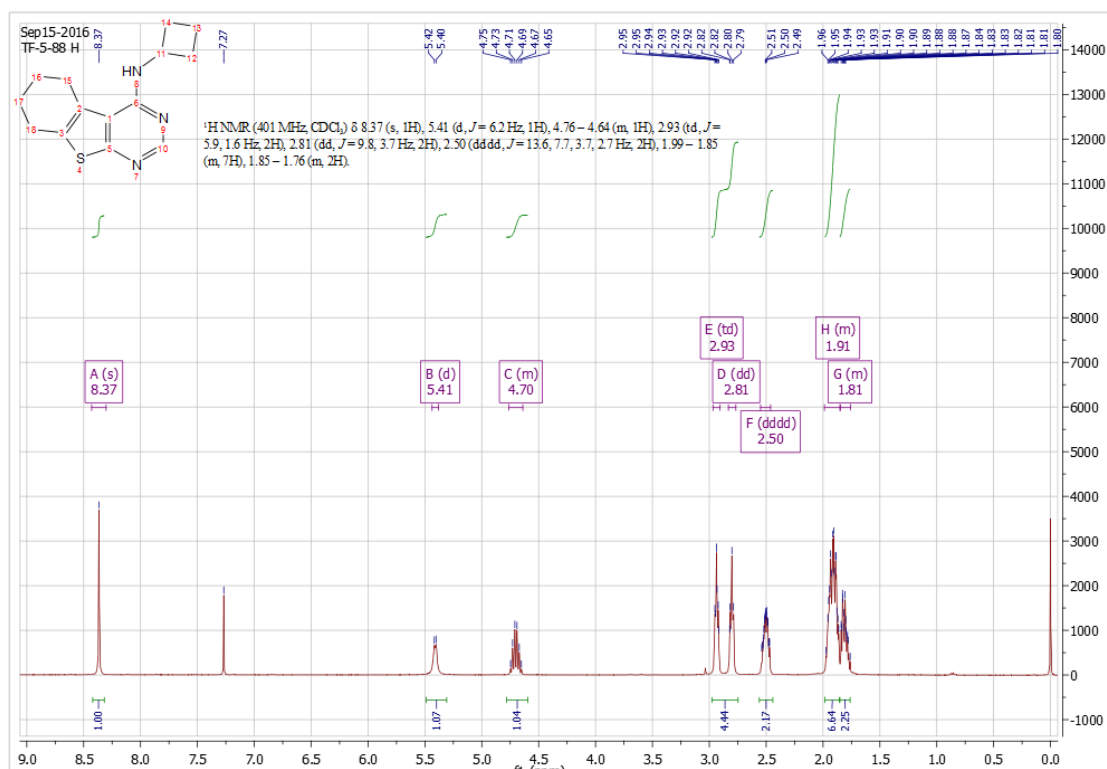
Supporting Figure 3D. Analytical HPLC trace for compound 9d.



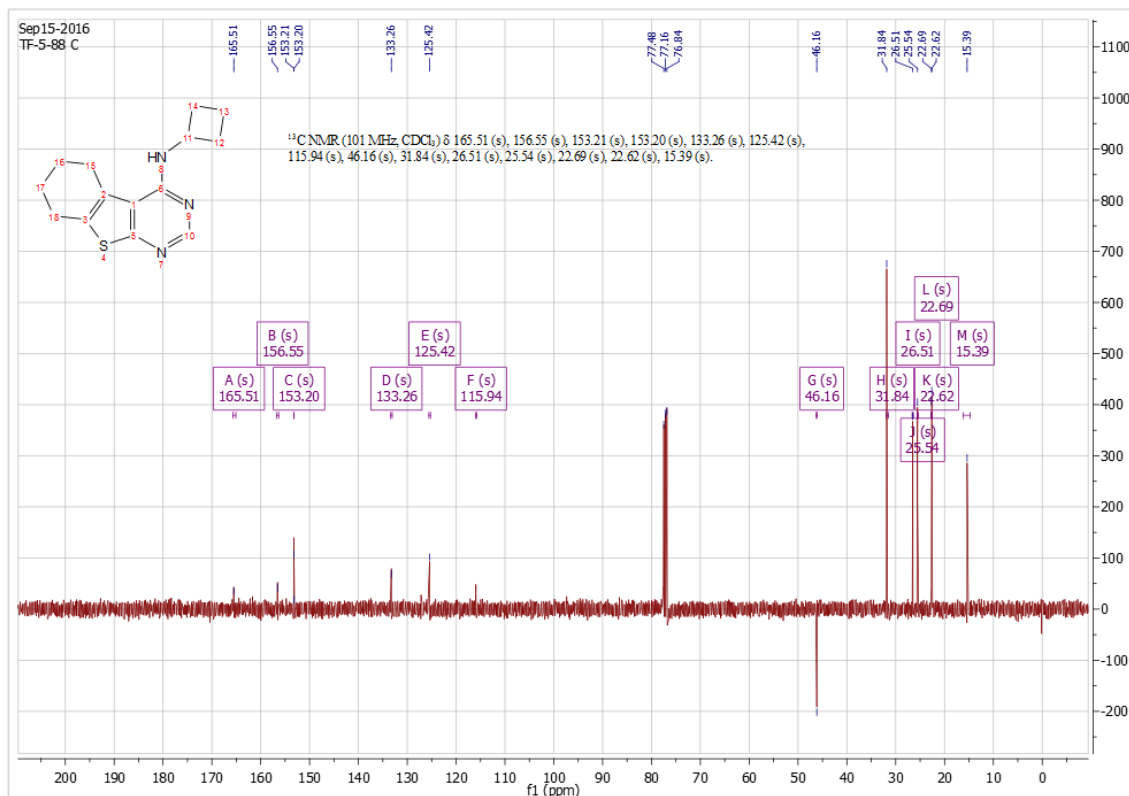
Signal 1: DAD1 A, Sig=254,4 Ref=off

Peak #	RetTime [min]	Type	Width [min]	Area [mAU*s]	Height [mAU]	Area %
1	4.977	MM	0.0399	82.17494	34.36274	4.4905
2	5.719	MM	0.0440	1747.80688	661.63831	95.5095

Supporting Figure 4A. ¹H NMR spectrum for compound 9h.



Supporting Figure 4B. ¹³C NMR spectrum for compound 9h.



Supporting Figure 4C. HRMS spectrum (ESI) for compound 9h

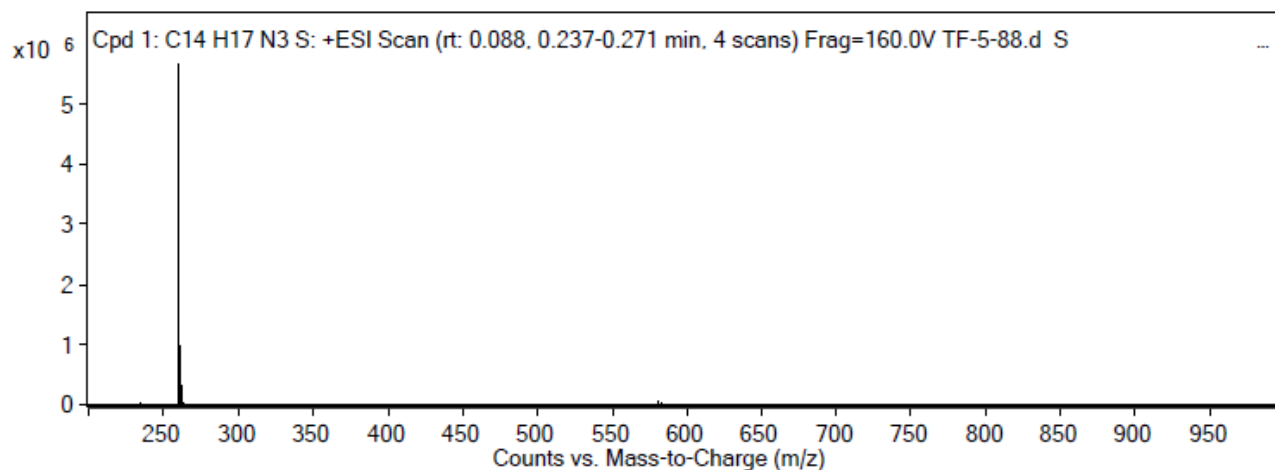
Qualitative Compound Report

Data File	TF-5-88.d	Sample Name	TF-5-88
Sample Type	Sample	Position	P1-B1
Instrument Name	Instrument 1	User Name	Dr Jason Dang
Acq Method	Monash_Direct.m	Acquired Time	23-Sep-16 2:58:45 PM
IRM Calibration Status	Success	DA Method	Monash_Accuracy.m
Comment		Info.	
Sample Group		Stream Name	LC 1
Formula	C ₁₄ H ₁₇ N ₃ S		
Acquisition SW Version	6200 series TOF/6500 series Q-TOF B.06.01 (B6172 SP1)		

Compound Table

Compound Label	RT	Mass	Abund	Formula	Tgt Mass	Diff (ppm)
Cpd 1: C ₁₄ H ₁₇ N ₃ S	0.121	259.1141	5689102	C ₁₄ H ₁₇ N ₃ S	259.1143	-0.67

Compound Label	m/z	RT	Algorithm	Mass
Cpd 1: C ₁₄ H ₁₇ N ₃ S	260.1213	0.121	Find By Formula	259.1141

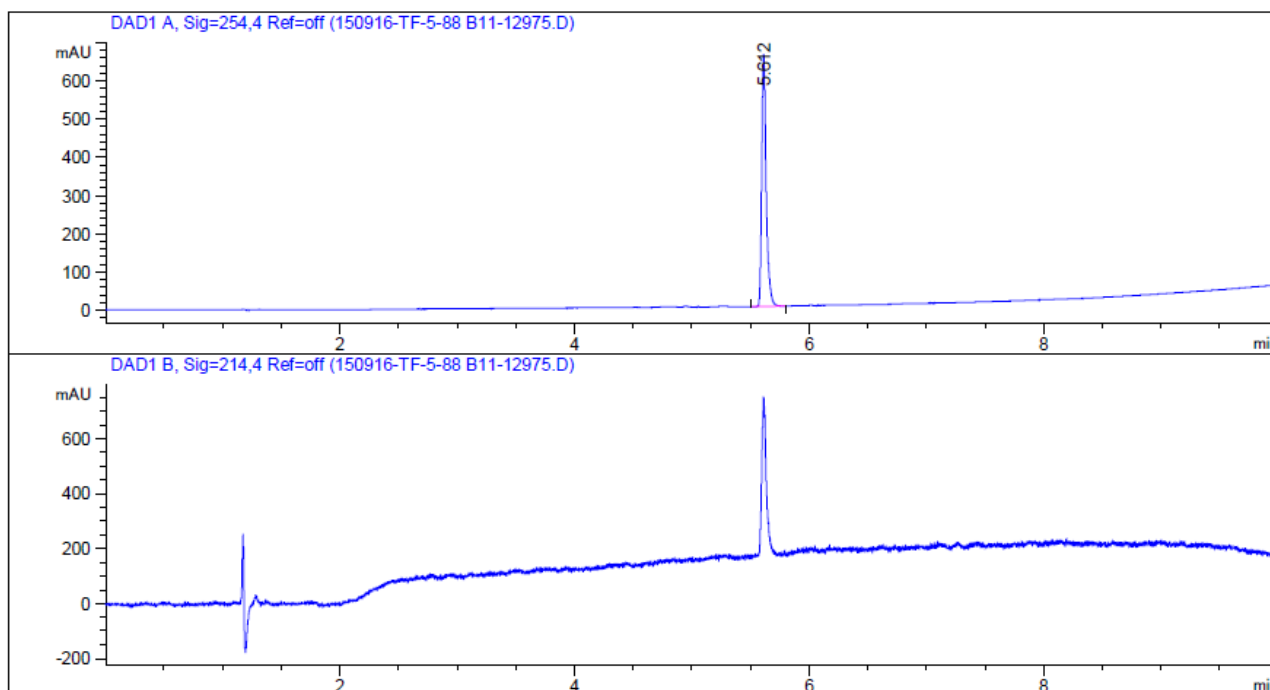


MS Spectrum Peak List

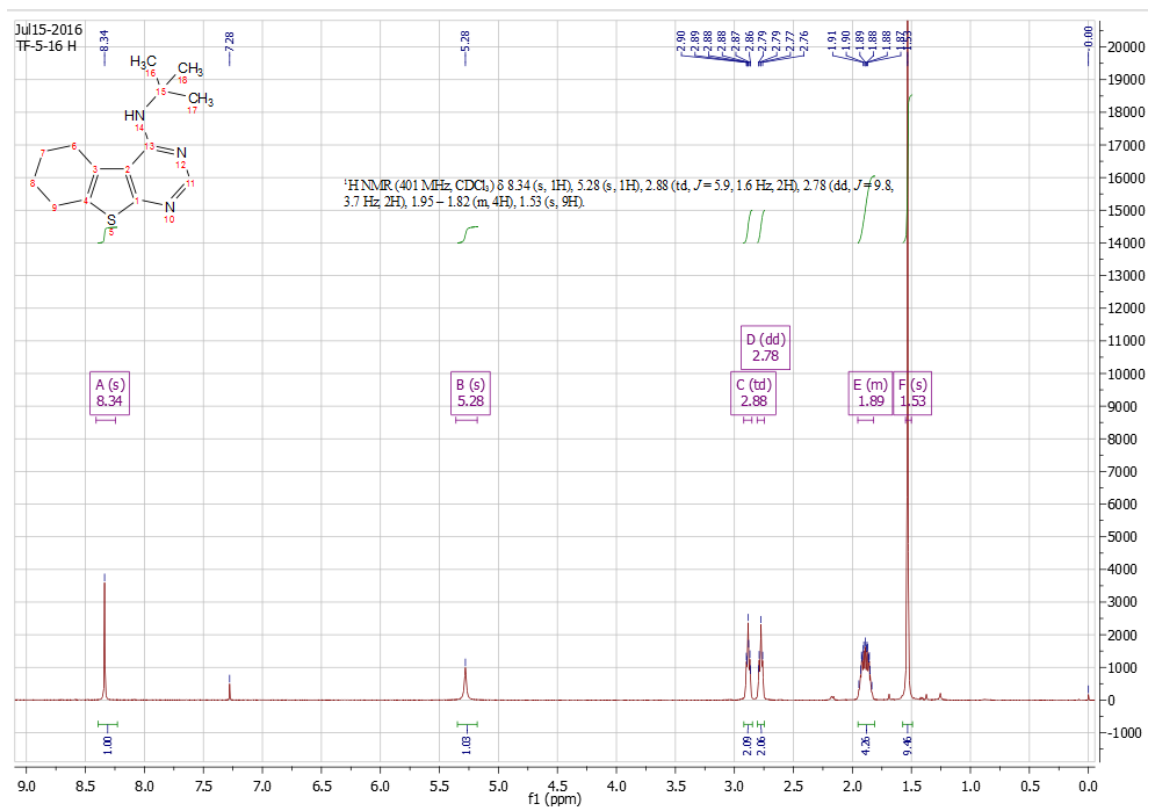
m/z	Calc m/z	Diff(ppm)	z	Abund	Formula	Ion
260.1213	260.1216	1.08	1	5689101.54	C ₁₄ H ₁₇ N ₃ S	(M+H) ⁺
261.1246	261.1244	-0.9	1	1006464.92	C ₁₄ H ₁₇ N ₃ S	(M+H) ⁺
282.103	282.1035	1.9	1	1321.78	C ₁₄ H ₁₇ N ₃ S	(M+Na) ⁺

--- End Of Report ---

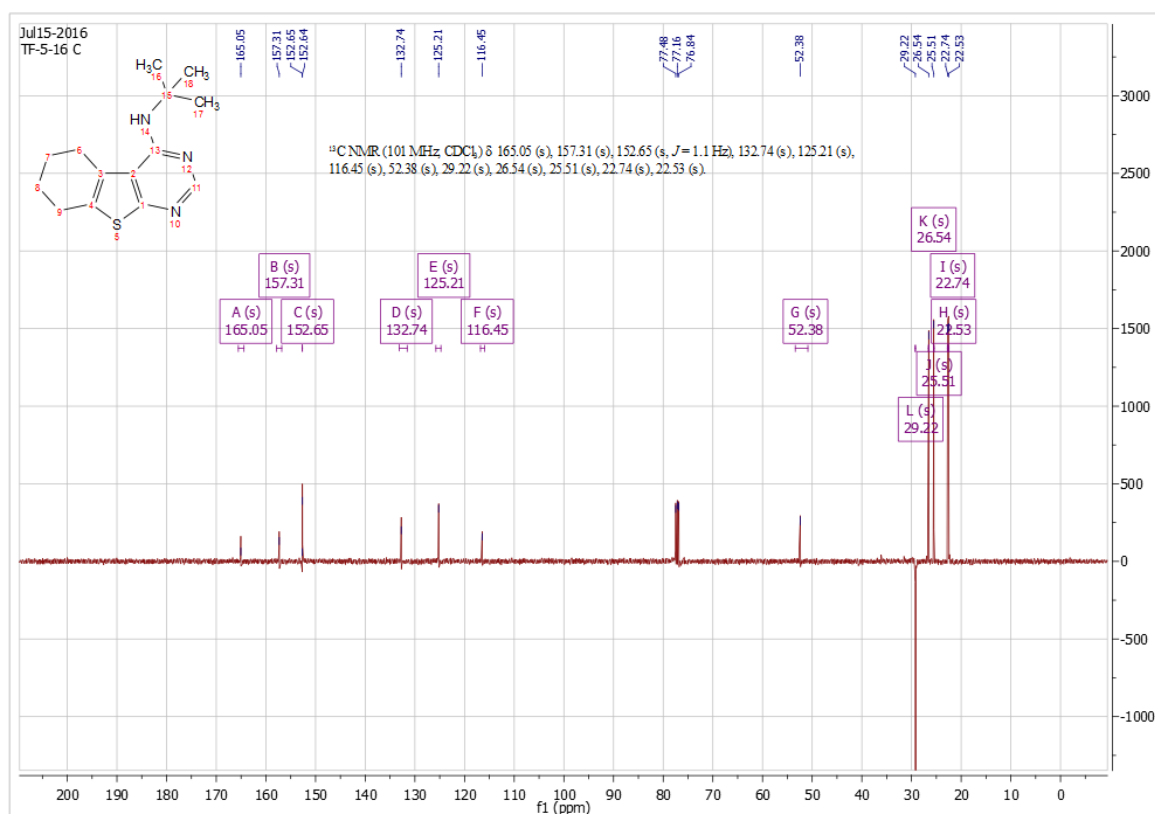
Supporting Figure 4D. Analytical HPLC trace for compound 9h.



Supporting Figure 5A. ¹H NMR spectrum for compound 9i.



Supporting Figure 5B. ¹³C NMR spectrum for compound 9i.



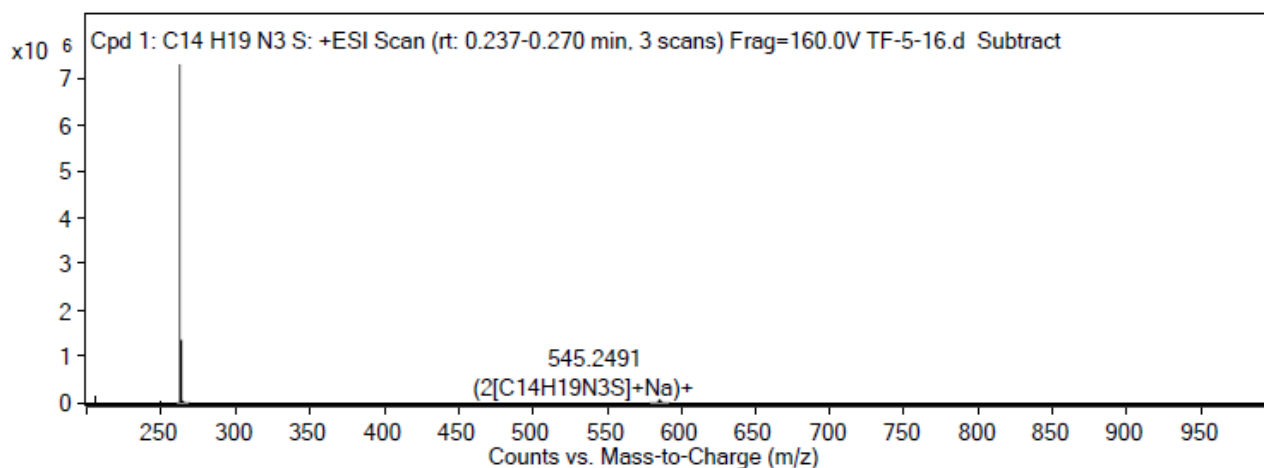
Supporting Figure 5C. HRMS spectrum (ESI) for compound 9i.

Qualitative Compound Report

Data File	TF-5-16.d	Sample Name	TF-5-16
Sample Type	Sample	Position	P2-C9
Instrument Name	Instrument 1	User Name	Dr Jason Dang
Acq Method	Monash_Direct.m	Acquired Time	27-Jul-16 12:47:53 PM
IRM Calibration Status	Success	DA Method	Monash_Accuracy.m
Comment			
Sample Group		Info.	
Formula	C ₁₄ H ₁₉ N ₃ S	Stream Name	LC 1
Acquisition SW Version	6200 series TOF/6500 series Q-TOF B.06.01 (B6172 SP1)		

Compound Table

Compound Label	RT	Mass	Abund	Formula	Tgt Mass	Diff (ppm)
Cpd 1: C ₁₄ H ₁₉ N ₃ S	0.12	261.131	7478110	C ₁₄ H ₁₉ N ₃ S	261.13	-4.14

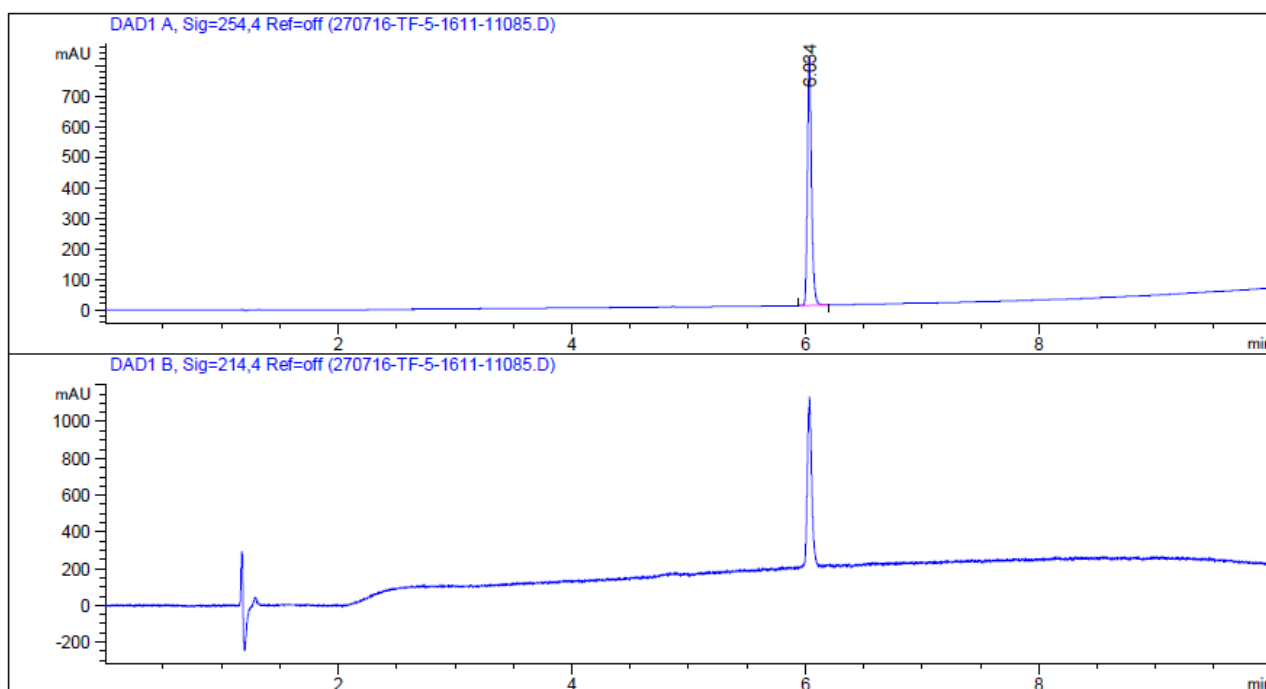


MS Spectrum Peak List

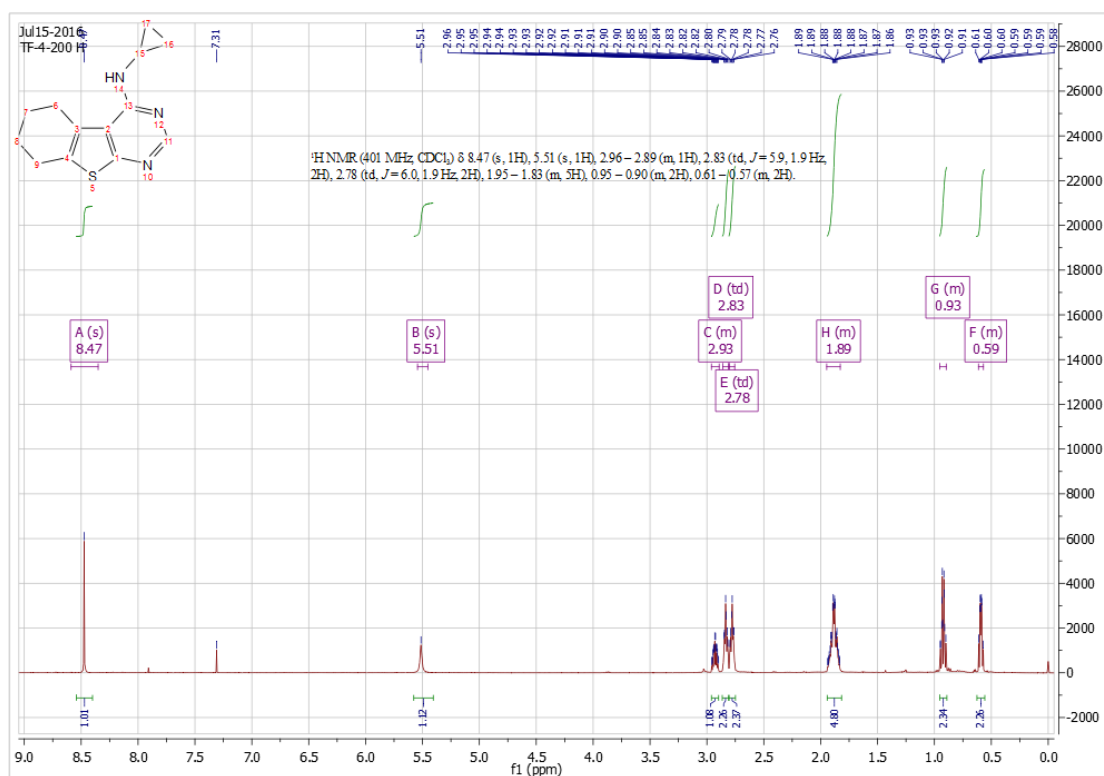
m/z	Calc m/z	Diff(ppm)	z	Abund	Formula	Ion
261.1312	261.1294	-6.83	1	1685.45	C ₁₄ H ₁₉ N ₃ S	M+
262.1382	262.1372	-3.79	1	7478110.4	C ₁₄ H ₁₉ N ₃ S	(M+H)+
284.1199	284.1192	-2.62	1	3529.13	C ₁₄ H ₁₉ N ₃ S	(M+Na)+

--- End Of Report ---

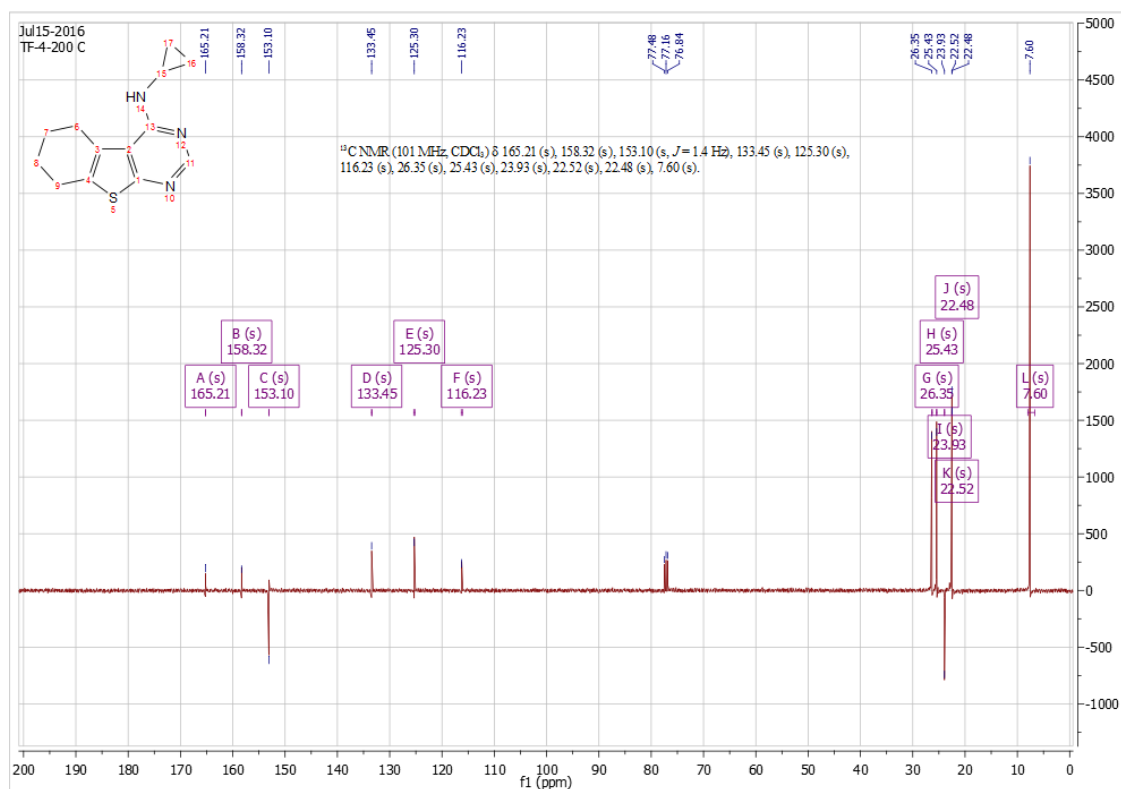
Supporting Figure 5D. Analytical HPLC trace for compound 9i.



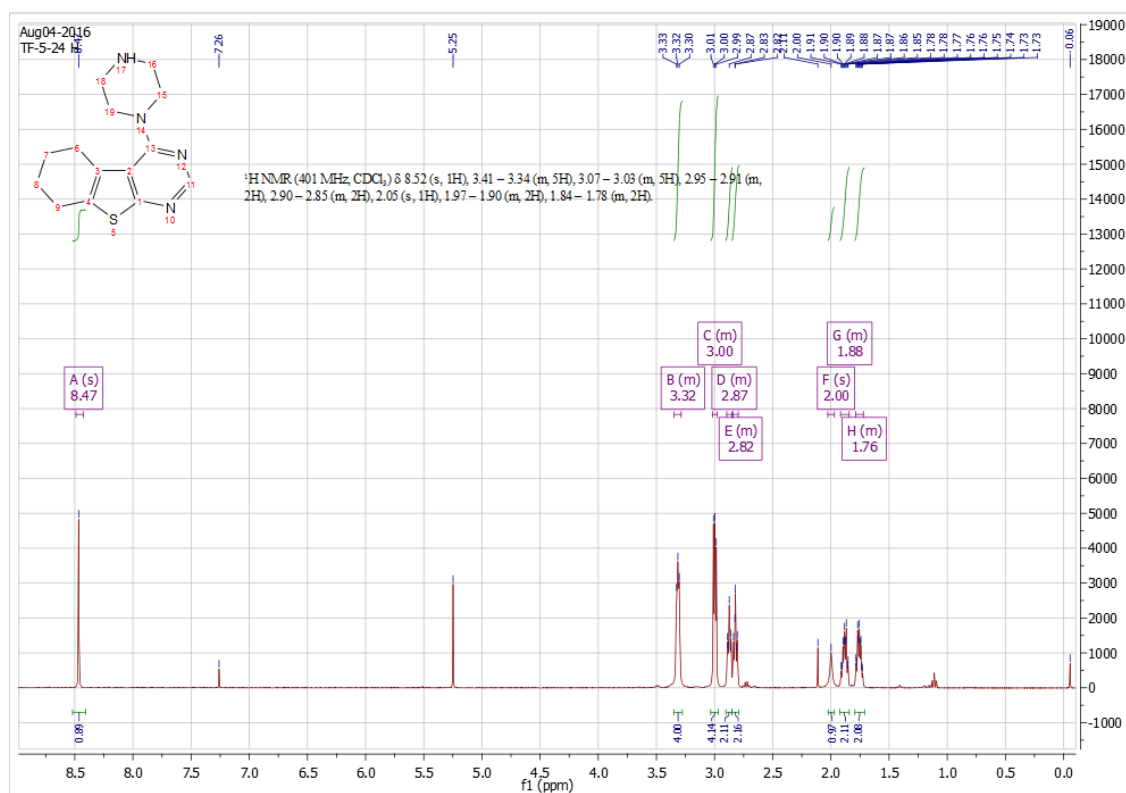
Supporting Figure 6A. ¹H NMR spectrum for compound 9f.



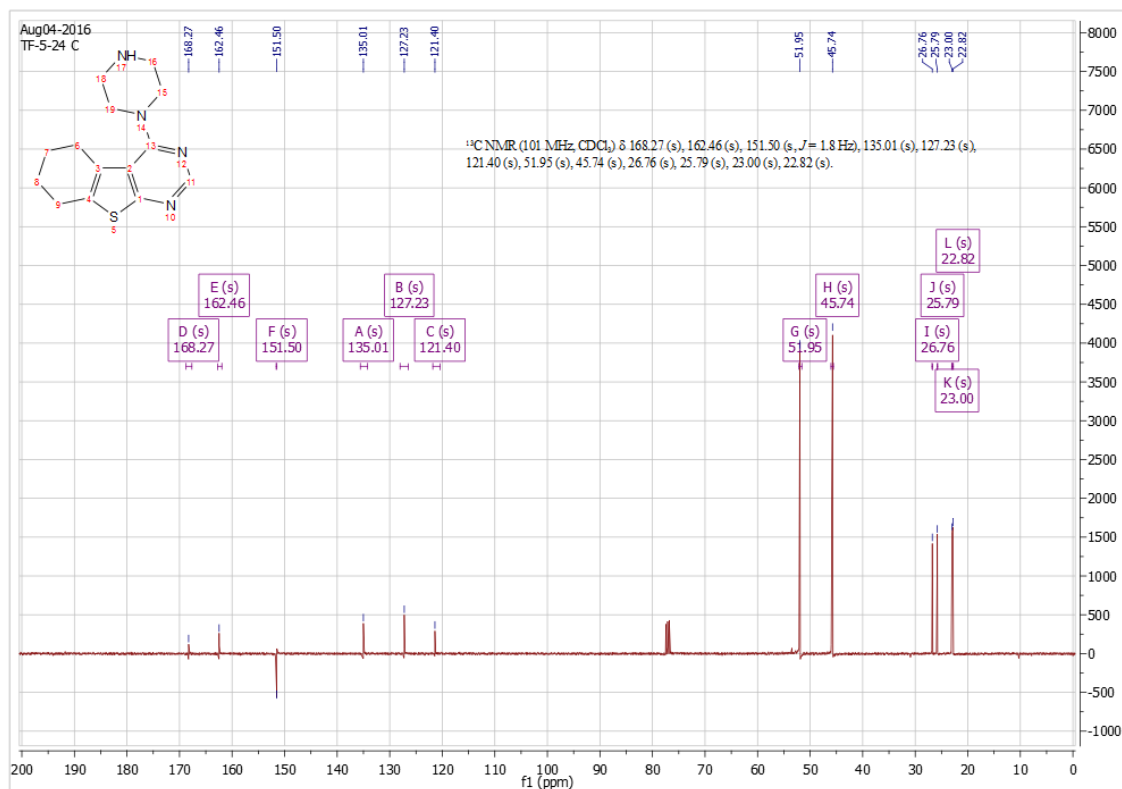
Supporting Figure 6B. ¹³C NMR spectrum for compound 9f.



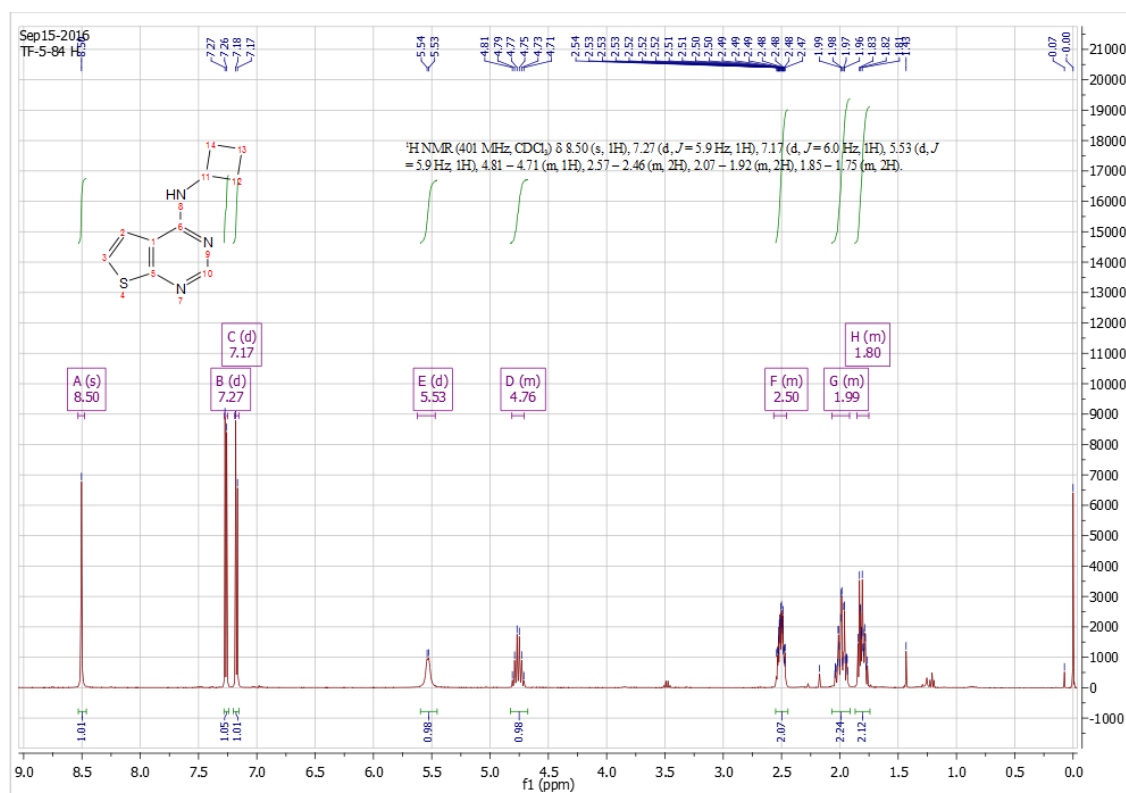
Supporting Figure 7A. ¹H NMR spectrum for compound 10.



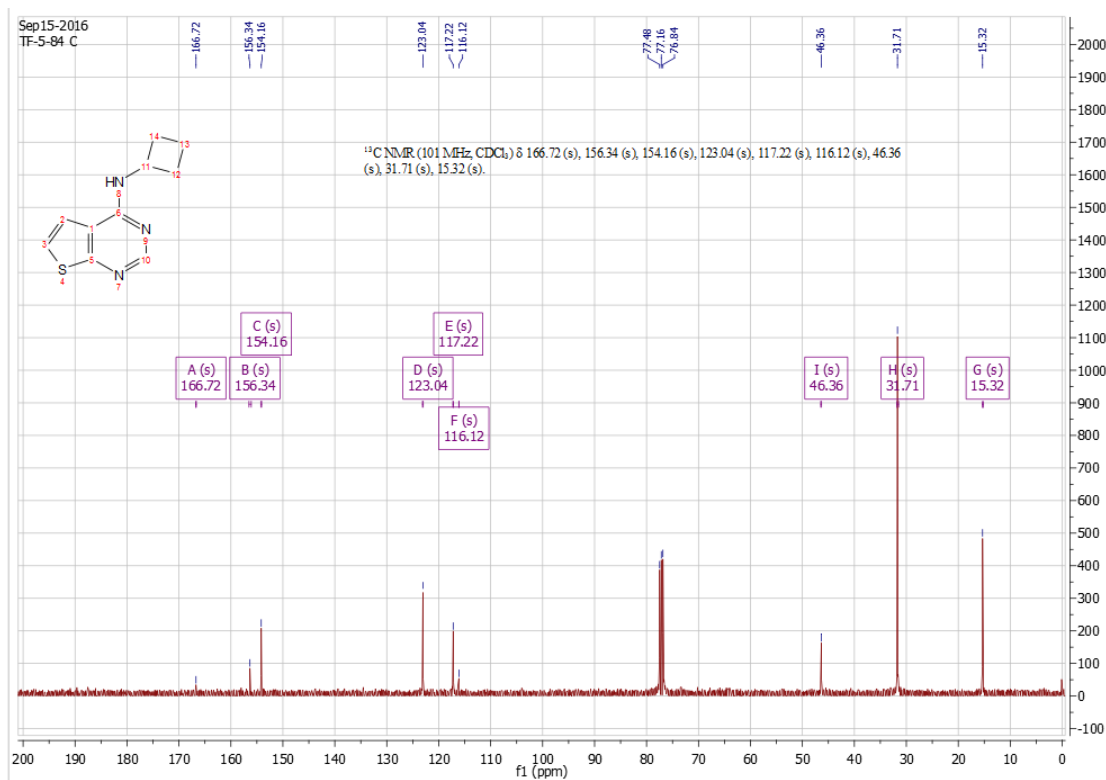
Supporting Figure 7B. ¹³C NMR spectrum for compound 10.



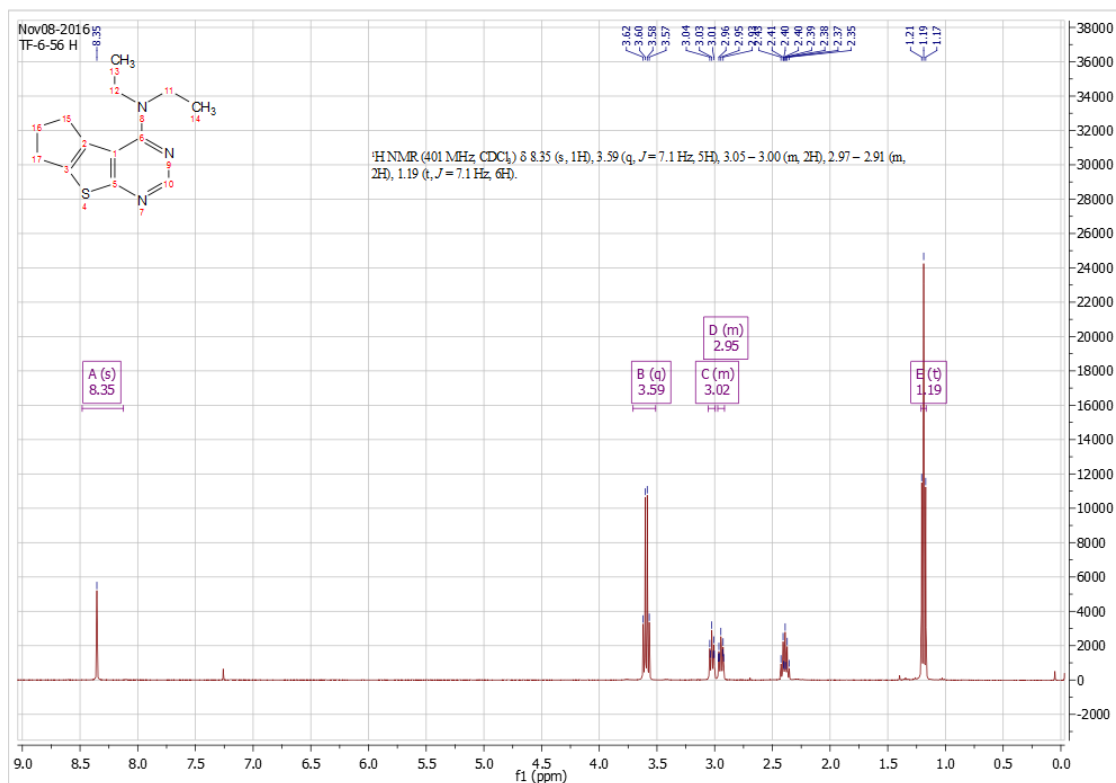
Supporting Figure 8A. ¹H NMR spectrum for compound 15b.



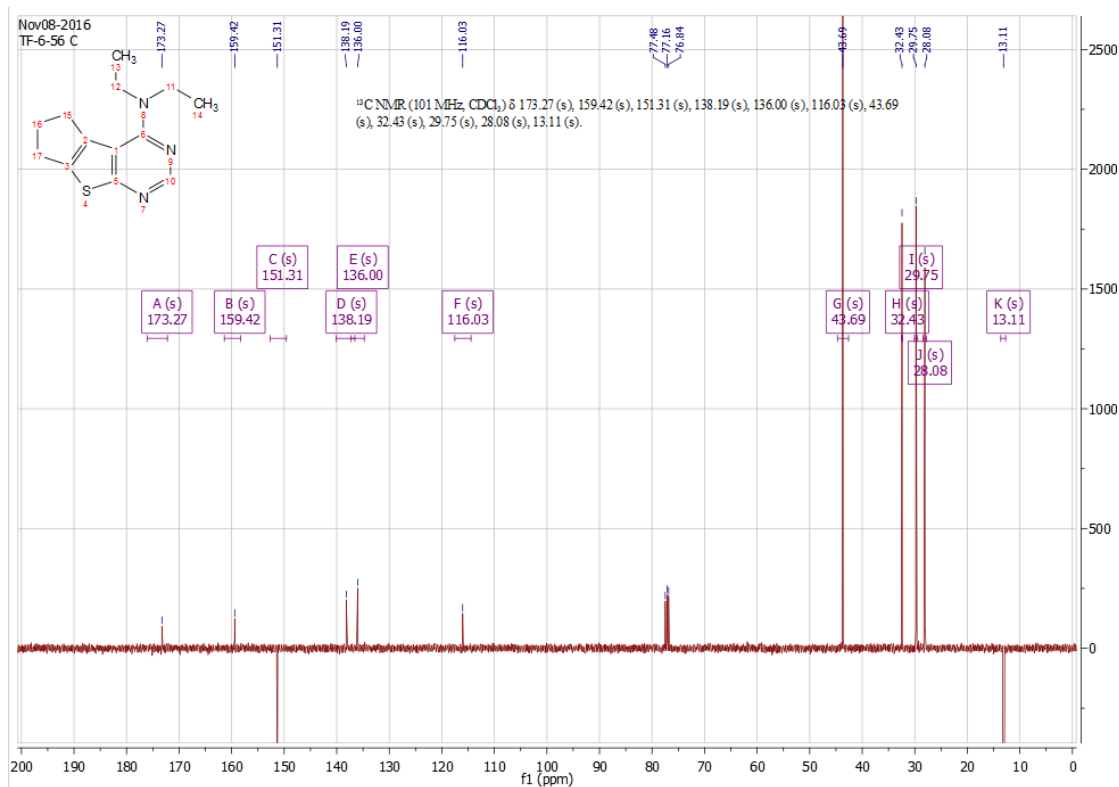
Supporting Figure 8B. ¹³C NMR spectrum for compound 15b.



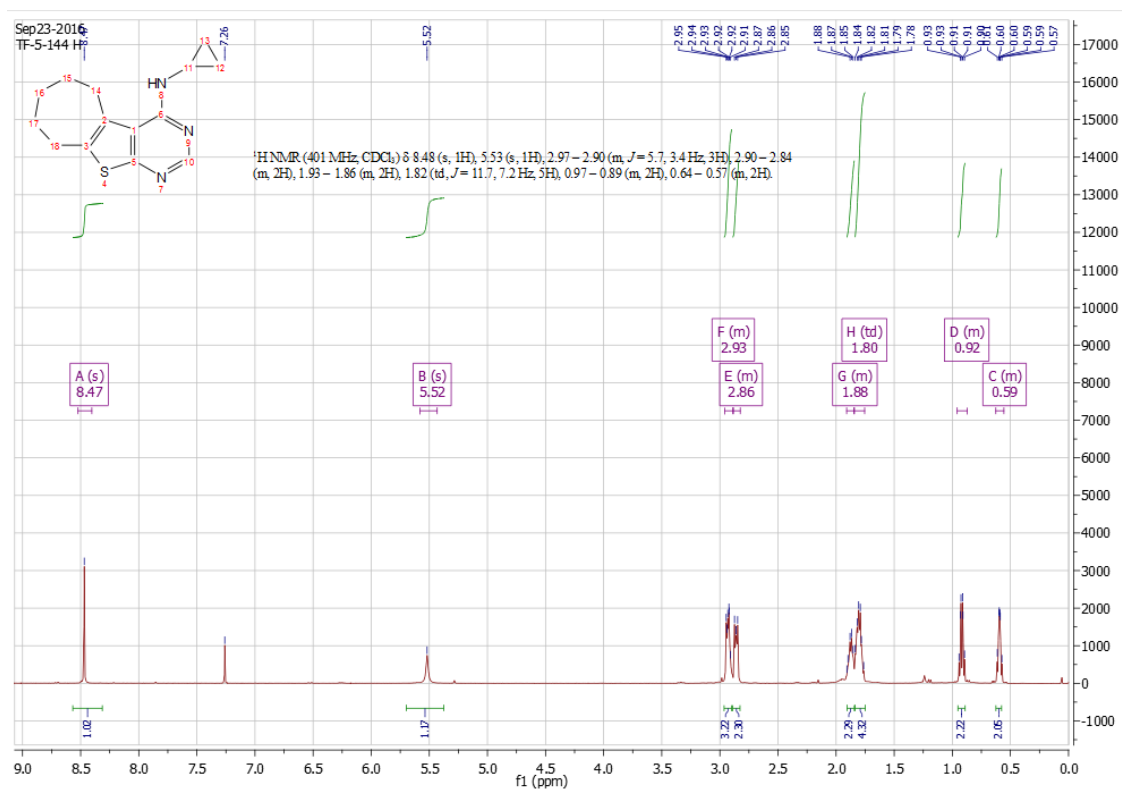
Supporting Figure 9A. ¹H NMR spectrum for compound 19aa.



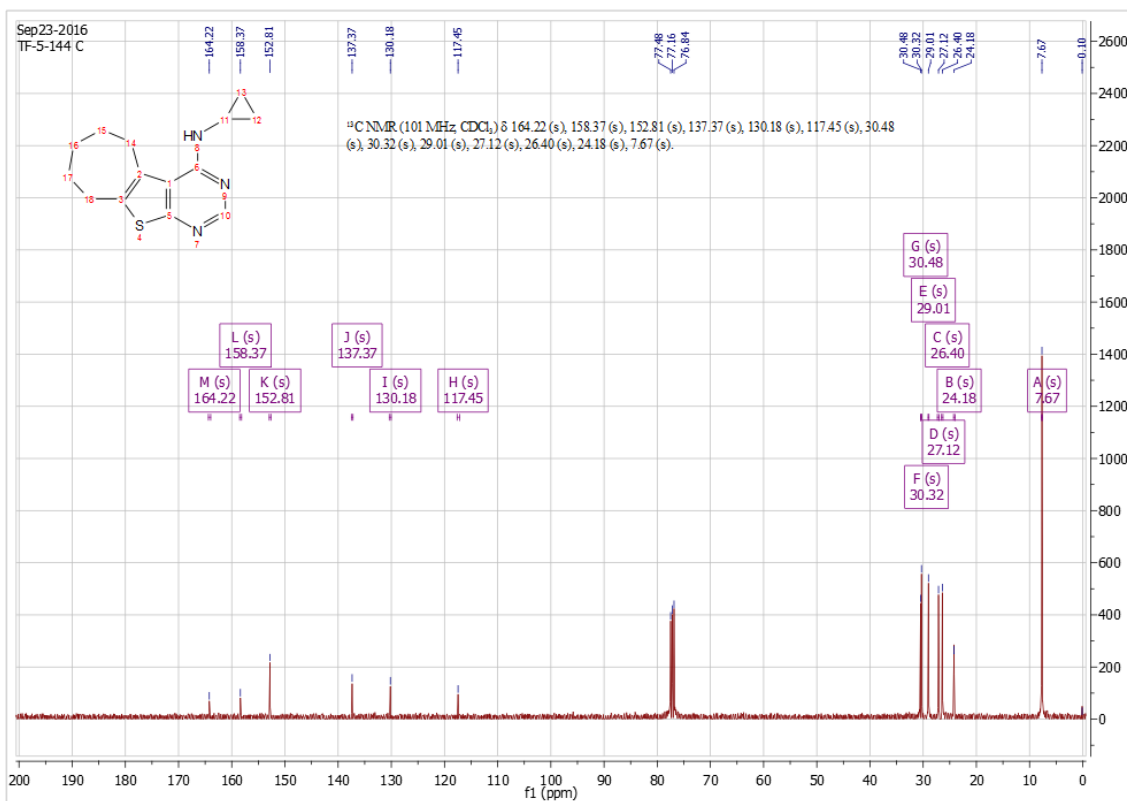
Supporting Figure 9B. ¹³C NMR spectrum for compound 19aa.



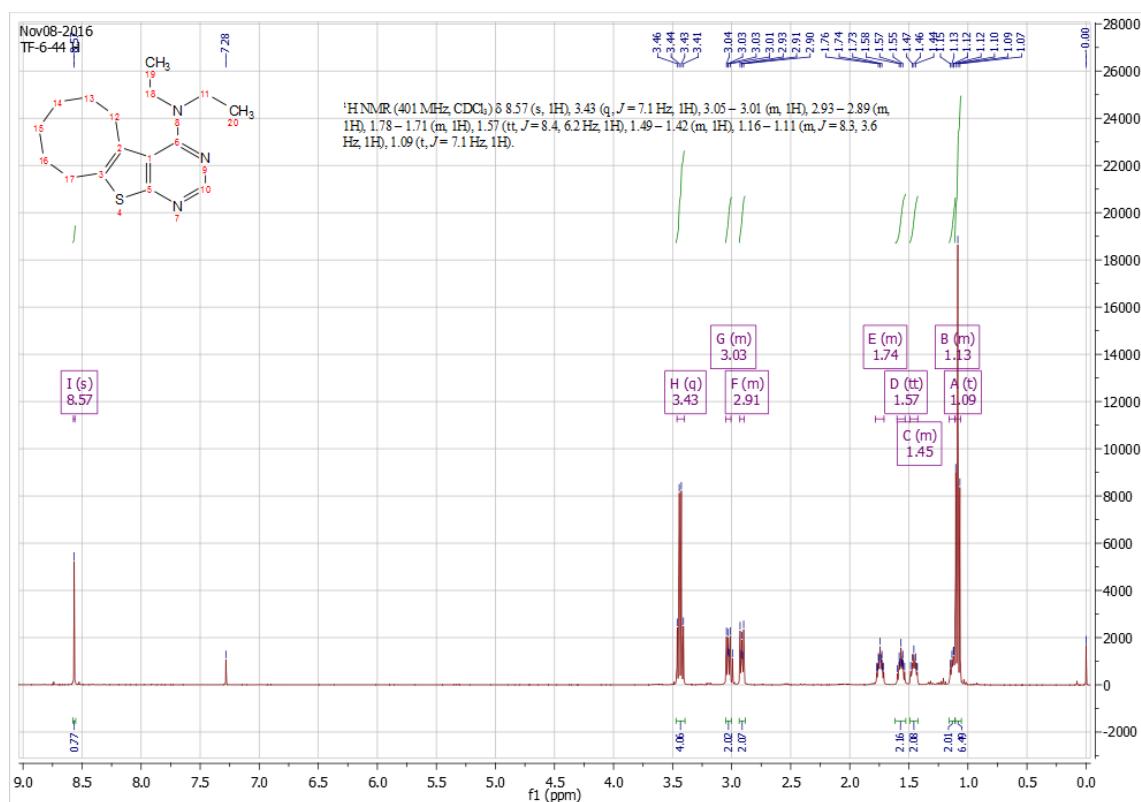
Supporting Figure 10A. ¹H NMR spectrum for compound 19bb.



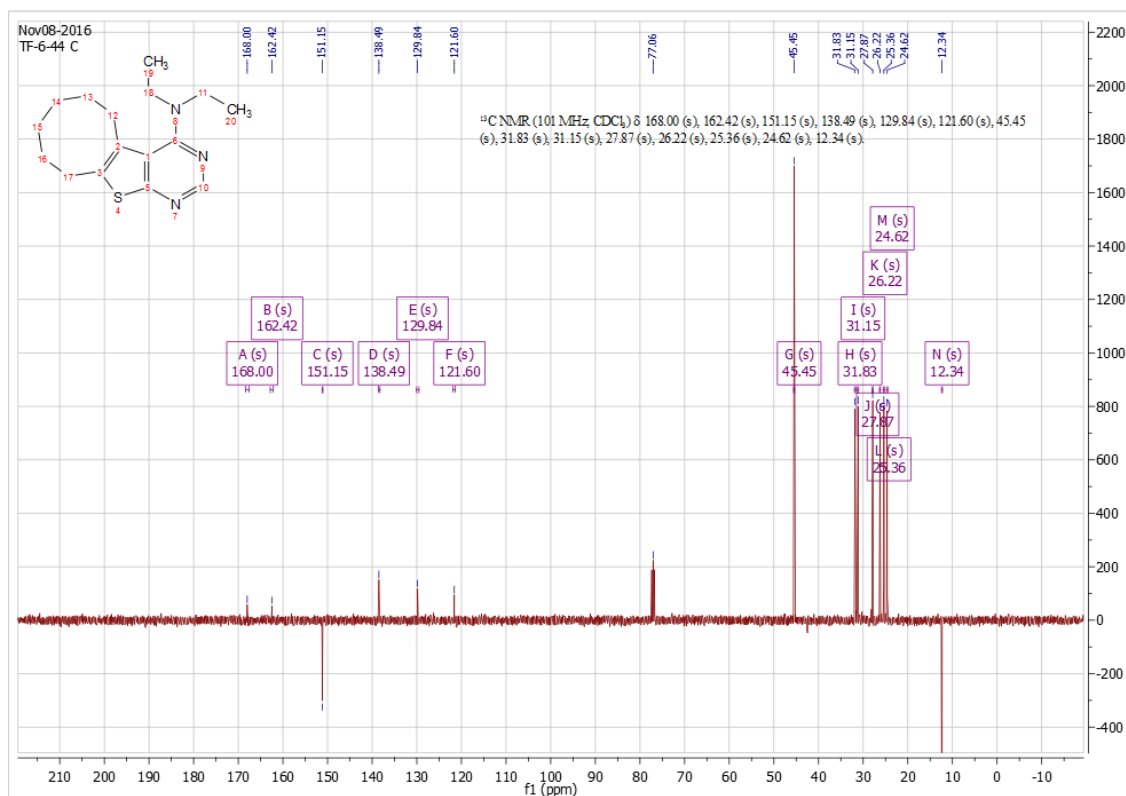
Supporting Figure 10B. ¹³C NMR spectrum for compound 19bb.



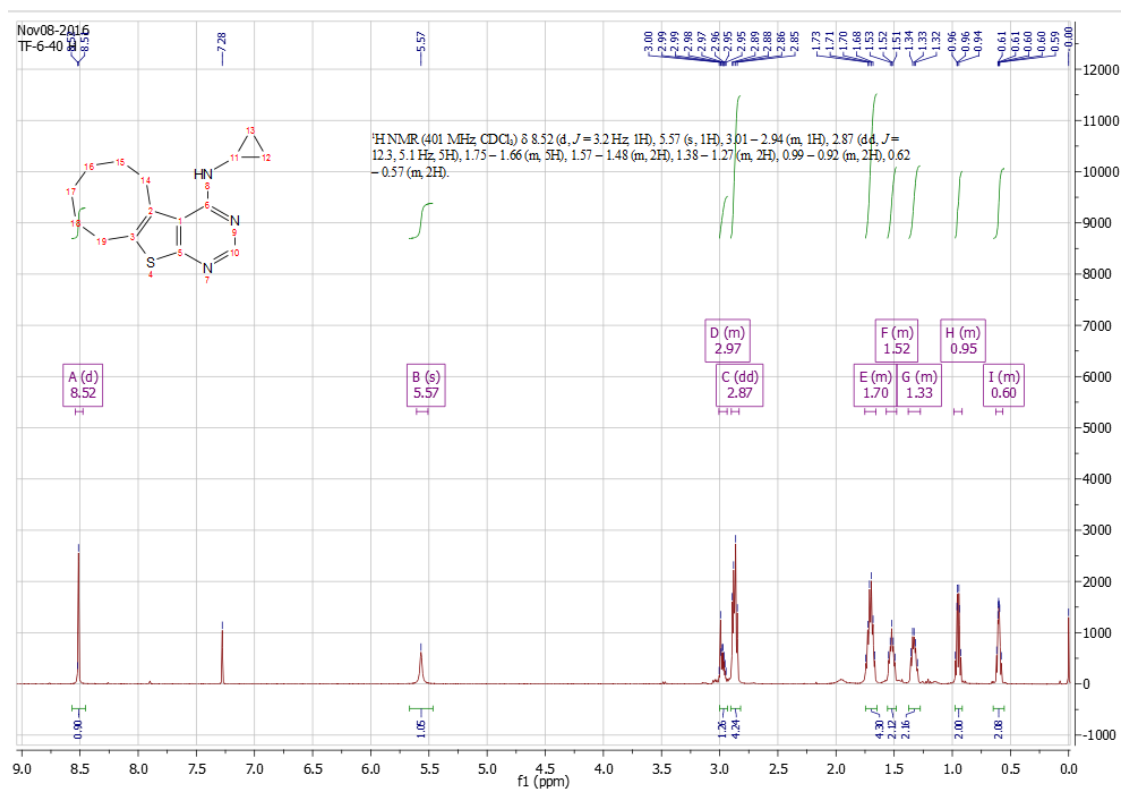
Supporting Figure 12A. ¹H NMR spectrum for compound 19ca (non-specific inhibitor).



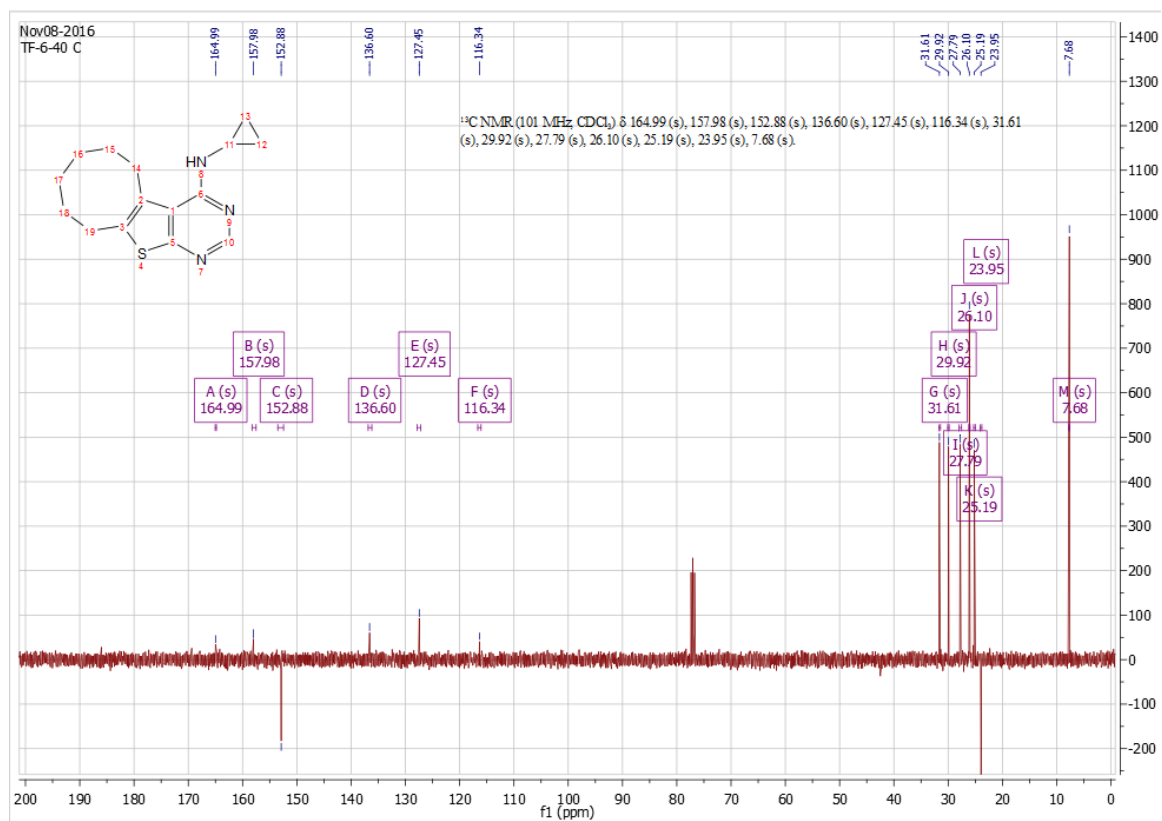
Supporting Figure 12B. ¹³C NMR spectrum for compound 19ca (non-specific inhibitor).



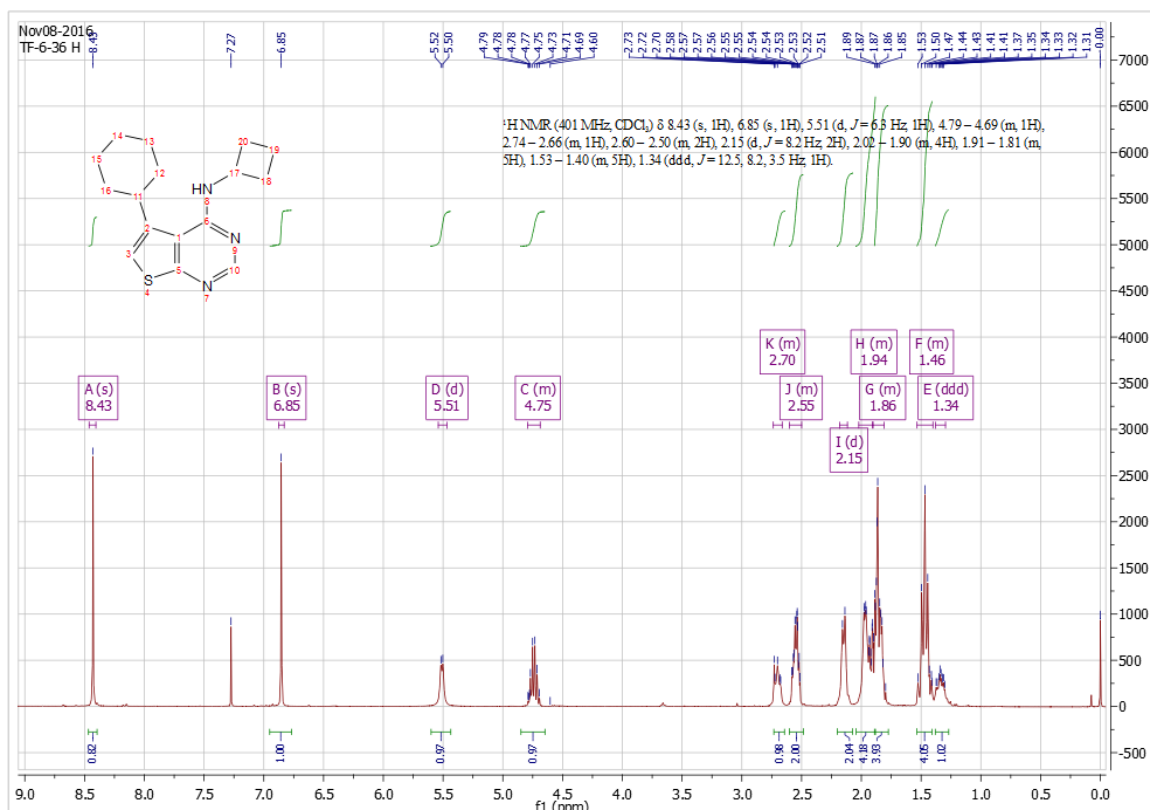
Supporting Figure 13A. ¹H NMR spectrum for compound 19cb.



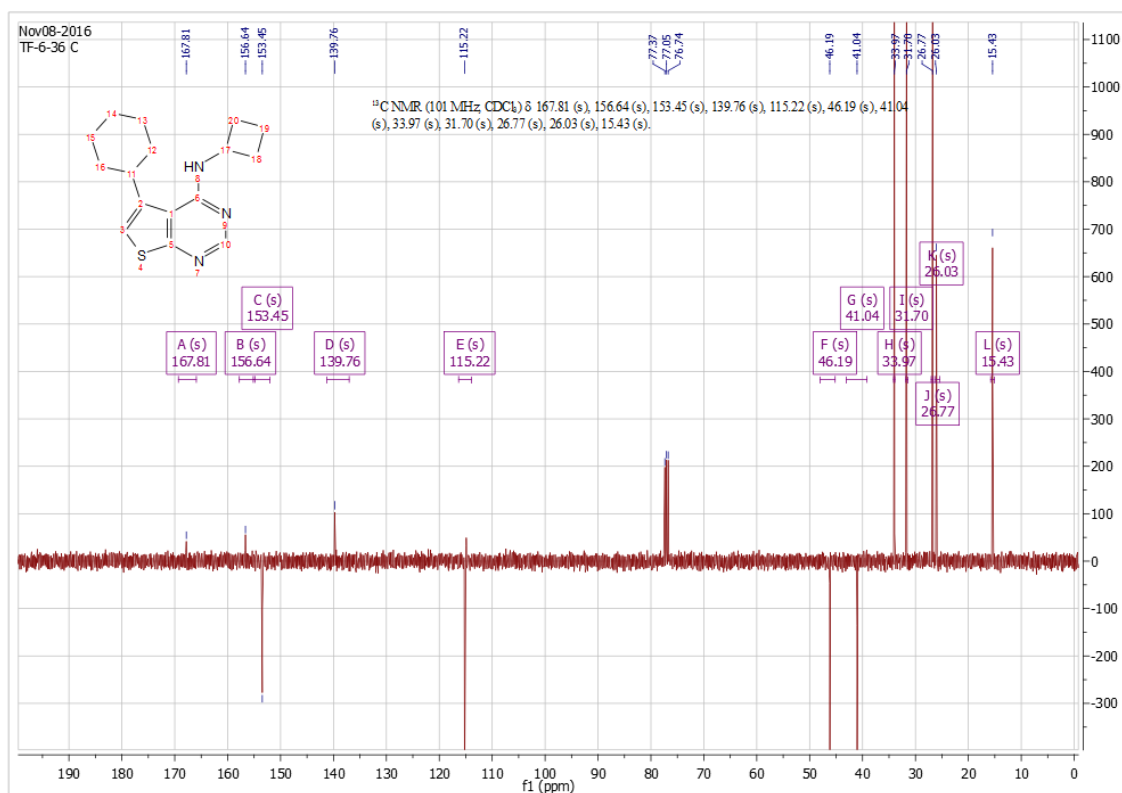
Supporting Figure 13B. ¹³C NMR spectrum for compound 19cb.



Supporting Figure 14A. ¹H NMR spectrum for compound 19fc.



Supporting Figure 14B. ¹³C NMR spectrum for compound 19fc.



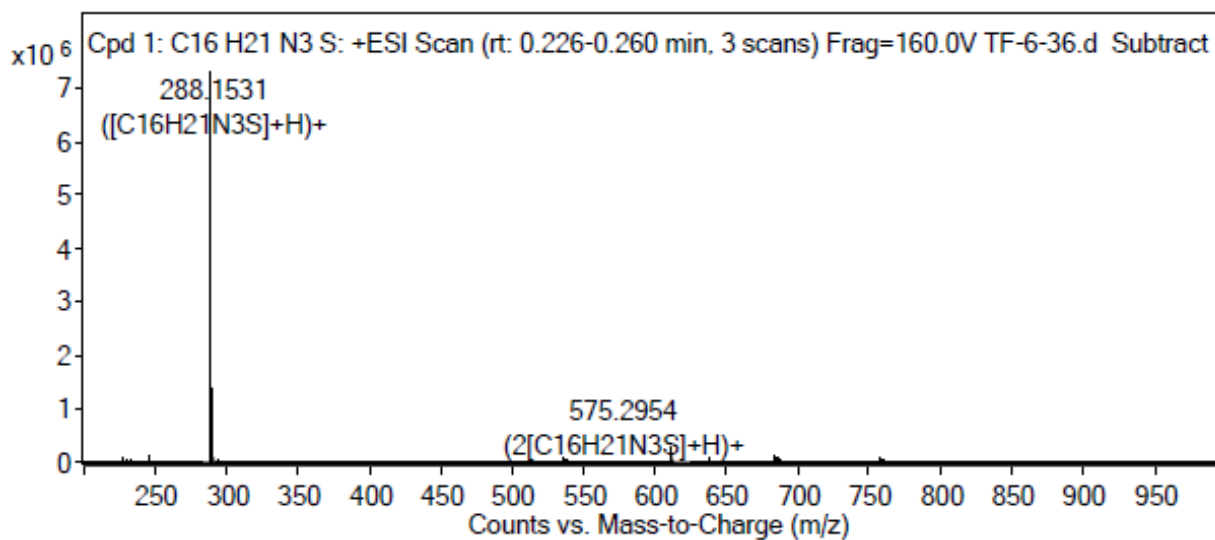
Supporting figure 14C. HRMS spectrum (ESI) for compound 19fc.

Qualitative Compound Report

Data File	TF-6-36.d	Sample Name	TF-6-36
Sample Type	Sample	Position	P1-C1
Instrument Name	Instrument 1	User Name	Dr Jason Dang
Acq Method	Monash_Direct.m	Acquired Time	10-Nov-16 12:54:56 PM
IRM Calibration Status	Success	DA Method	Monash_Accuracy.m
Comment		Info.	
Sample Group		Stream Name	LC 1
Formula	C ₁₆ H ₂₁ N ₃ S		
Acquisition SW Version	6200 series TOF/6500 series Q-TOF B.06.01 (B6172 SP1)		

Compound Table

Compound Label	RT	Mass	Abund	Formula	Tgt Mass	Diff (ppm)
Cpd 1: C ₁₆ H ₂₁ N ₃ S	0.11	287.146	7423478	C ₁₆ H ₂₁ N ₃ S	287.1456	1.18

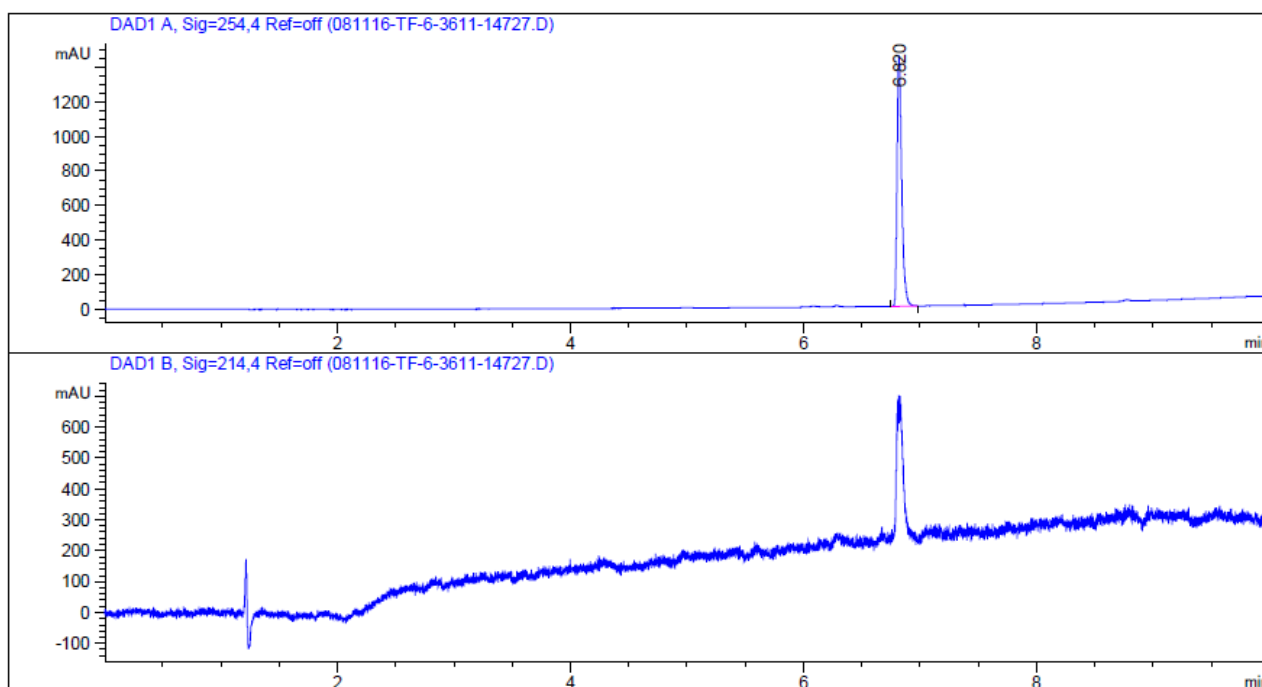


MS Spectrum Peak List

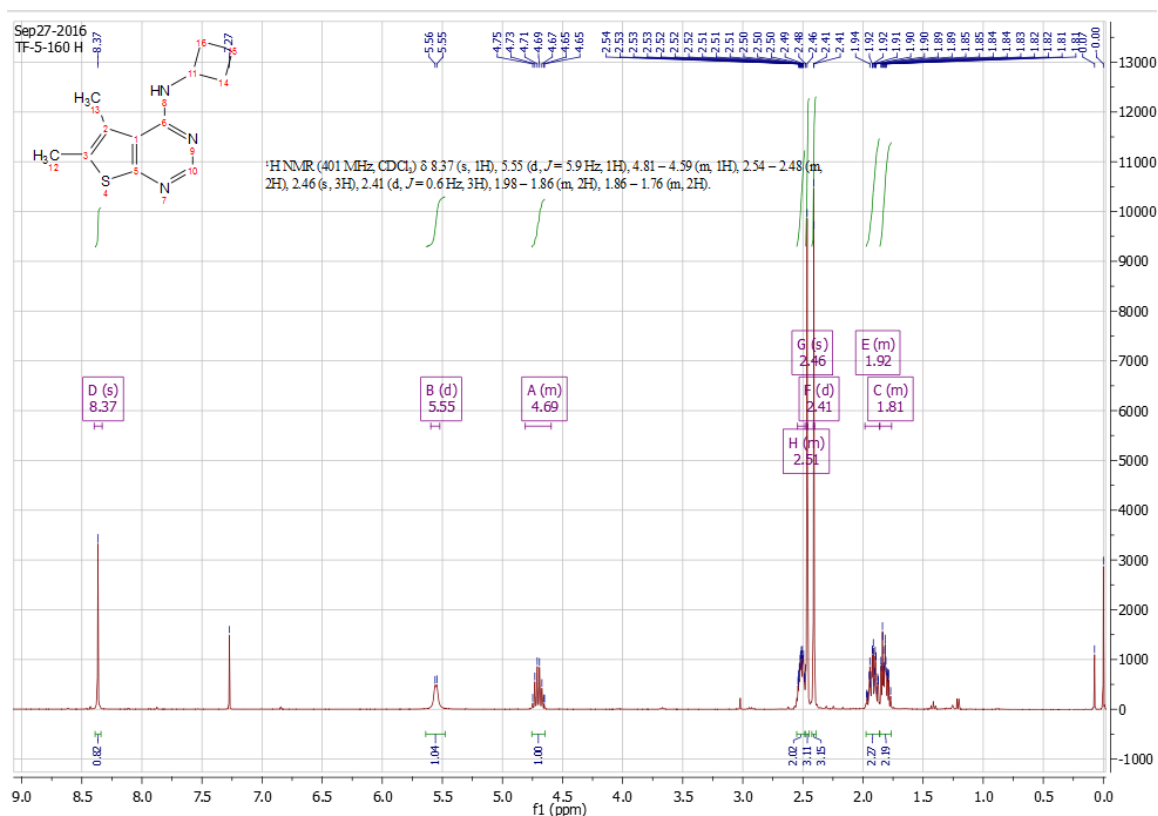
m/z	Calc m/z	Diff(ppm)	z	Abund	Formula	Ion
287.1456	287.1451	-1.85	1	2170.41	C ₁₆ H ₂₁ N ₃ S	M+
288.1531	288.1529	-0.82	1	7423477.68	C ₁₆ H ₂₁ N ₃ S	(M+H)+
310.1353	310.1348	-1.59	1	1924.29	C ₁₆ H ₂₁ N ₃ S	(M+Na)+

--- End Of Report ---

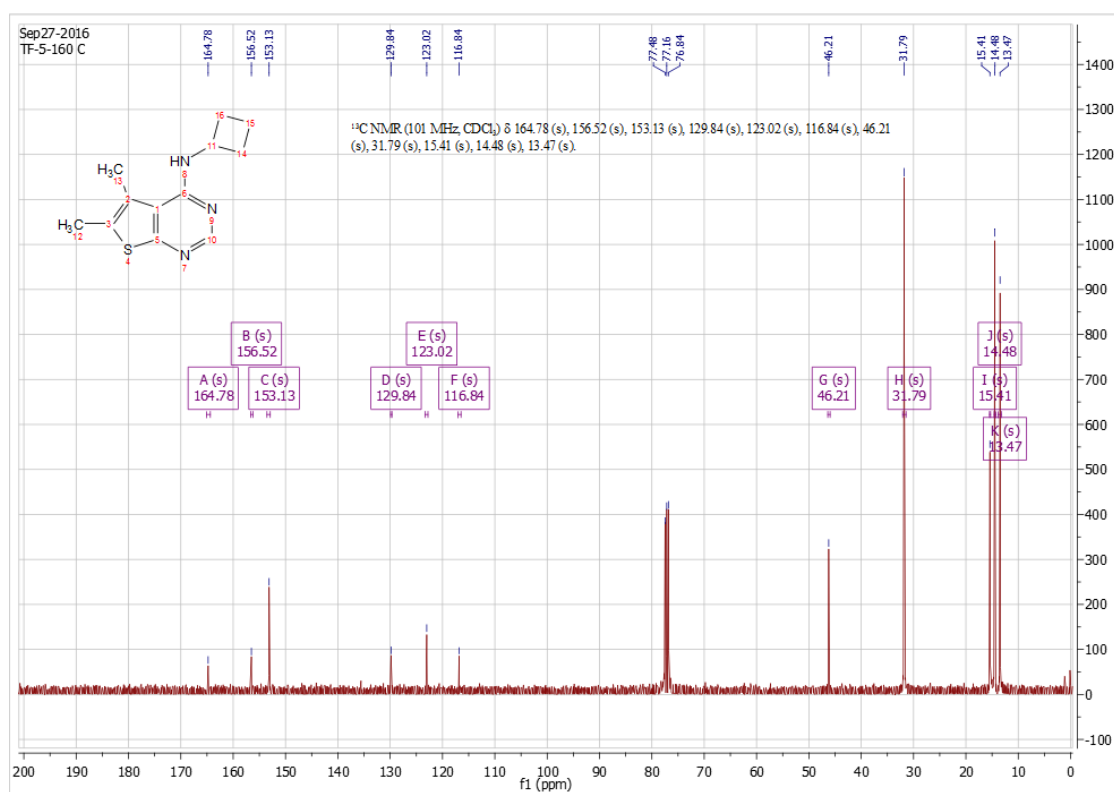
Supporting Figure 14D. Analytical HPLC trace for compound 19f.



Supporting Figure 15A. ¹H NMR spectrum for compound 19hc.



Supporting Figure 15B. ¹³C NMR spectrum for compound 19hc.

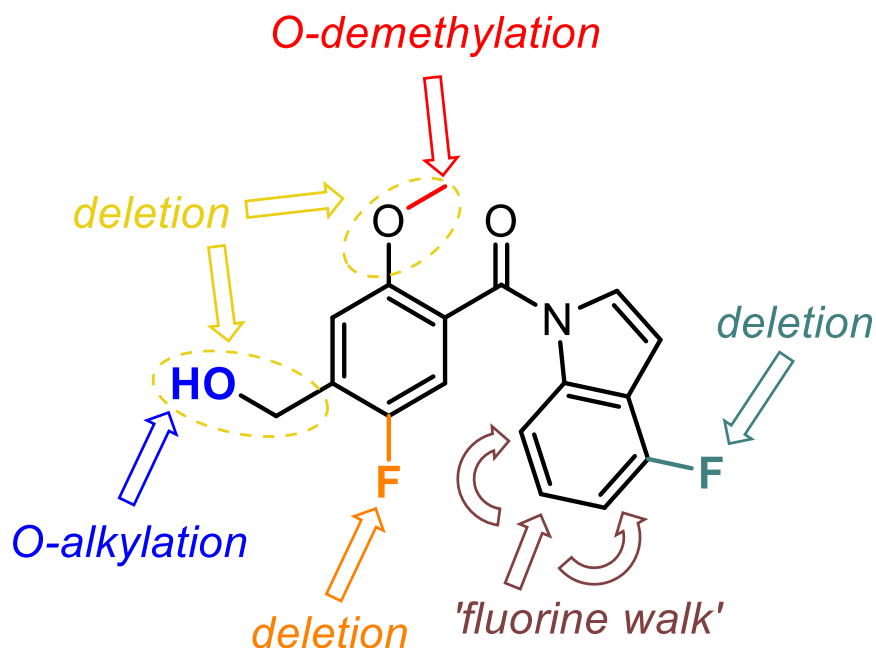


**Chapter 4 – Structure–Activity Relationship
Studies Toward the Synthesis of Irreversible
and Fluorescent Analogues of a Dopamine D₂
Receptor Positive Allosteric Modulator**

SAR Studies Toward the Synthesis of Irreversible and Fluorescent Analogues of a Dopamine D₂ Receptor Positive Allosteric Modulator

Tim J. Fyfe,^{†,‡} Peter J. Scammells,[†] J. Robert Lane,^{*,‡} Ben Capuano^{*,†}

[†]Medicinal Chemistry, and [‡]Drug Discovery Biology, Monash Institute of Pharmaceutical Sciences, Monash University, Parkville, Victoria 3052, Australia.



Abstract. Current therapeutic approaches for the treatment of the neurodegenerative disorder Parkinson's disease (PD) predominantly rely on the use of levodopa (LD) and agonists of the dopamine receptors (D₁₋₅Rs). Positive allosteric modulators (PAMs) of the D₂R may offer distinct advantages over these approaches including maintenance of endogenous temporal and spatial signalling, as well as enhanced receptor subtype selectivity. A D₂R PAM of agonist affinity (**2**) has recently been described. In order to understand its potentially novel binding mode to aid in the optimisation of D₂R PAMs, we examined the effect of subtle structural modification of **1** toward the design and synthesis of photoactivatable irreversible and fluorescent analogues. Herein, we describe a more efficient synthesis of **2** in fewer steps compared to literature, and describe initial structure-activity-relationships (SARs). Essentially all structural modifications to the core scaffold diminish PAM activity, highlighting the potential difficulty in developing dopaminergic allosteric modulators as small-molecule biochemical tools. Most notably, replacement of the methoxy substituent with hydrogen increases the degree of intrinsic efficacy 25-fold relative to **2**, and converts the corresponding compound into an allosteric agonist that maintains D₂R affinity, but shows decreased positive allosteric cooperativity.

Introduction. Due to the therapeutic potential of D₂R PAMs in pathologic conditions such as PD, understanding the mechanism of how such compounds modulate the binding and function of an orthosteric ligand is paramount in order to interpret these effects *in vivo*. For example, a PAM may potentiate orthosteric ligand affinity and/or efficacy, and it may be that one effect is desirable but the other is not. The limited amount of SAR information associated with the novel D₂R PAMs identified by Wood *et al.*, in particular compound **2** (Figure 1), provides much scope for further structural interrogation.¹ Accordingly, we aim to elucidate and understand the key structural features of **2** that underlie its distinct allosteric pharmacology. This will firstly be achieved via the generation of a series of analogues of **2** followed by their *in vitro* biochemical characterisation.

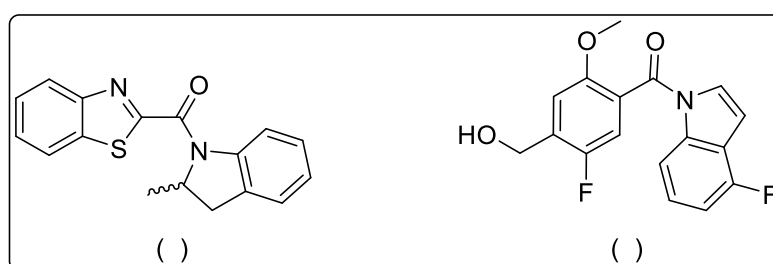


Figure 1. Novel D₂R PAM scaffolds reported from an HTS campaign by Wood *et al.*¹

Chemical Probes. In addition to understanding the effect of chemical structure and function for the purpose of identifying novel PAMs with various allosteric properties, elucidating the location where such compounds engage the D₂R is of great interest to permit future rational design. An ionisable nitrogen at physiological pH has been demonstrated to be a critical feature of all orthosteric monoaminergic receptor ligands as well as NAMs of the D₂R.^{2,3} In particular, the nitrogen of agonists, antagonists and NAMs, forms an ionic interaction with a highly conserved aspartate or glutamate residue in the DA receptors (D114^{3,32} and E95^{2,65}, respectively) (where the superscript refers to Ballesteros-Weinstein nomenclature)⁴, supported by numerous studies on allosteric compounds and recent crystals structures of the D₂-D₄R_s bound by orthosteric ligands.⁵⁻⁹ However, as **2** lacks an ionisable nitrogen, it is thought that this ligand may engage a distinct allosteric binding site compared to that of the traditional allosteric site on the D₂R. Accordingly, unmasking the ligand binding site of **2** would permit not only a better understanding of allosteric sites within this receptor, but may also permit structure-based allosteric drug design for the discovery of small molecule PAMs toward the symptomatic treatment of PD. Moreover, there is a need for selective pharmacological tools to probe poorly understood, existing, and novel receptor targets.¹⁰ This information may be obtained through the use of bifunctional molecular probes. Chemical probes are small molecules comprising a pharmacophore (e.g. PAM or NAM) that display affinity/selectivity for a given GPCR target, tethered to a functional group that exhibits specific properties (Figure 2). These properties may include

radiation or fluorescence,¹¹ as well as photo- and electrophilic-affinity labels that allow compounds to irreversibly bind to their targets via a reactive cross-linking moiety (also known as irreversible probes).¹² There are several resources that provide comprehensive overviews of irreversible probe chemical structures and their various applications in GPCR biology,¹³⁻¹⁷ as well as other protein and enzyme targets.¹⁸⁻²²

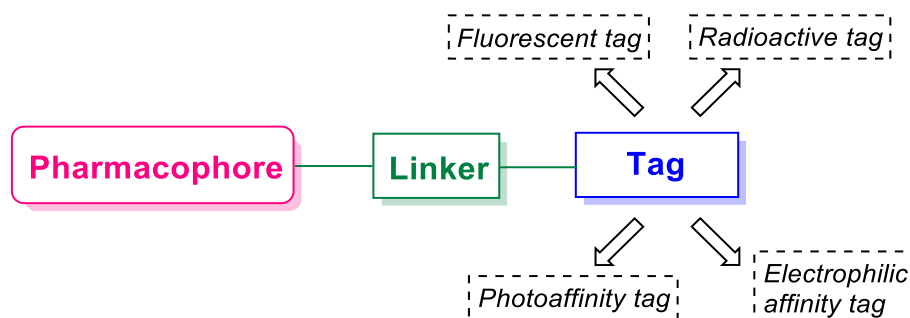


Figure 2. General design of bifunctional molecular probes. The active pharmacophore (orthosteric or allosteric) is either directly fused to a tag, or a connecting linker moiety may be employed.

Irreversible (also known as covalent or affinity) probes are categorised according to the type of pharmacophore and/or reactive group they contain. The pharmacophore drives receptor-target affinity and selectivity, whereas the reactive group is required to form a covalent bond with the receptor. Thus, defining the SAR of a chemical scaffold is beneficial for the accurate prediction of attachment locations that ensure parent pharmacological activity is retained. The inability of these ligands to dissociate from their targeted binding site allows them to be used as tools to provide insight into the structure and function of GPCRs using a variety of techniques.²³ This is particularly relevant from a drug discovery perspective, thus making the development of irreversible probes an attractive avenue to permit rational drug design. Furthermore, their ability to provide insight regarding key receptor-ligand interactions may have implications for understanding specific pharmacological functions such as those that govern functional selectivity. There are two common types of irreversible probes; chemoreactive or photoactivatable.

Chemoreactive Probes. Various electrophilic functional groups can be employed to generate chemoreactive tool compounds that are able to form a covalent bond with nucleophilic residues located in the binding pocket (Figure 3), and probes of this type may have both *in vitro* and *in vivo* applications. Electrophilic groups may be selected based on detailed knowledge of their reactivity and amino acid selectivity profiles, which may be determined through various computational approaches.²⁴⁻²⁶ Some common examples of these groups are detailed in Figure 4, including Michael acceptors,^{27,28} alkylating and sulfonylating agents,^{29,30} and isothiocyanates.³¹ Sulfonyl fluorides, for

example, have become important chemical biology and pharmacology tools, enabling the targeting of context-specific residues such as lysine and tyrosine to map enzyme binding sites and substrates.³² In order to incorporate these functionalities, synthetic strategies must be carefully devised in a manner such that they can be installed in the final stages of synthesis in order to avoid cross-reactivity. Chemoreactive probes, however, suffer from several shortcomings such as incomplete cross-linking³³ and reduced receptor activation when covalent binding leads to a loss of agonist efficacy.^{34,35} Moreover, such probes may be unpredictable and readily form irreversible covalent bonds in a non-selective manner.³⁶

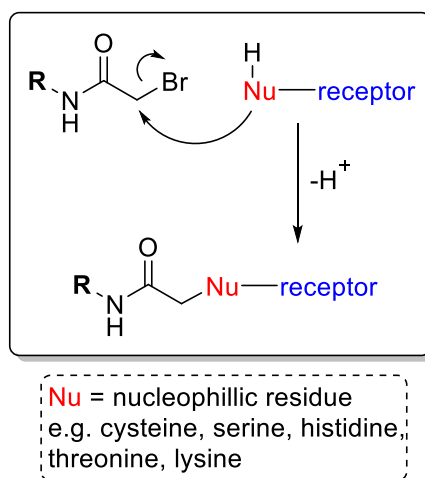


Figure 3. Mechanism of the covalent bond formation between the chemoreactive haloacetamide functional group and a nucleophilic residue located in the target binding pocket.

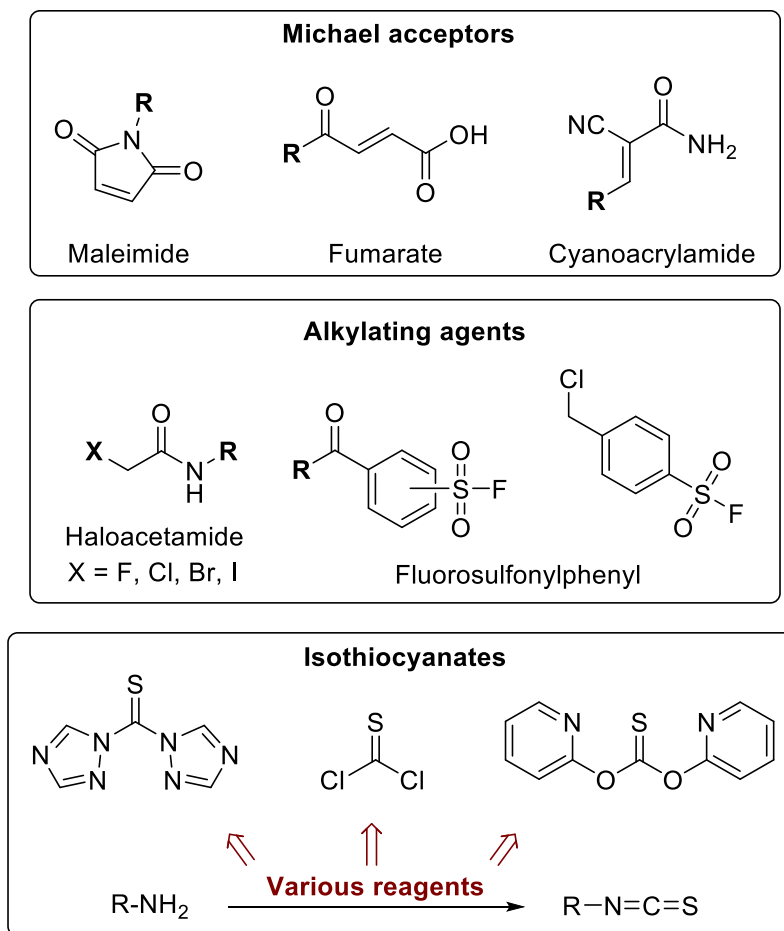


Figure 4. Select examples of chemoreactive functional groups and commercially available reagents used for synthesising chemoreactive probes containing isothiocyanate electrophilic affinity labels.

Despite this, chemoreactive probes have been utilised in structural and functional investigations of many GPCRs. Recently, chemoreactive probes containing a disulfide moiety were reported to have facilitated the crystallisation of the first agonist-bound GPCR crystal structure, in turn enabling the development of slow dissociating neurotransmitter analogues to be used as tools to facilitate crystallisation of other GPCRs.^{17,37} At the DA D₂R, the study of functional and behavioural effects of receptor blockade and calmodulin activity was enabled through the development of fluphenazine-*N*-mustard derivatives.^{38,39} In addition, phenoxybenzamine, *N*-ethoxycarbonyl-2-ethoxy-1,2-dihydroquinoline, and *N*-(*p*-isothiocyanatophenethyl)sipiperone have been used as chemoreactive probes to investigate D₂R function in both *in vivo* and *in vitro* settings.⁴⁰⁻⁴³

Photoreactive Probes. Conversely, photoreactive (or photoactivatable) functional groups must be chemically inert so that only upon UV photolysis a reactive species is produced (e.g. carbene, nitrene or diradical) that is then able to form a covalent bond with a neighbouring residue in close proximity

(Figure 5). This allows photoreactive probes to be employed in an *in vitro* receptor binding or functional assay at equilibrium, before being activated *in situ* resulting in target cross-linking.⁴⁴

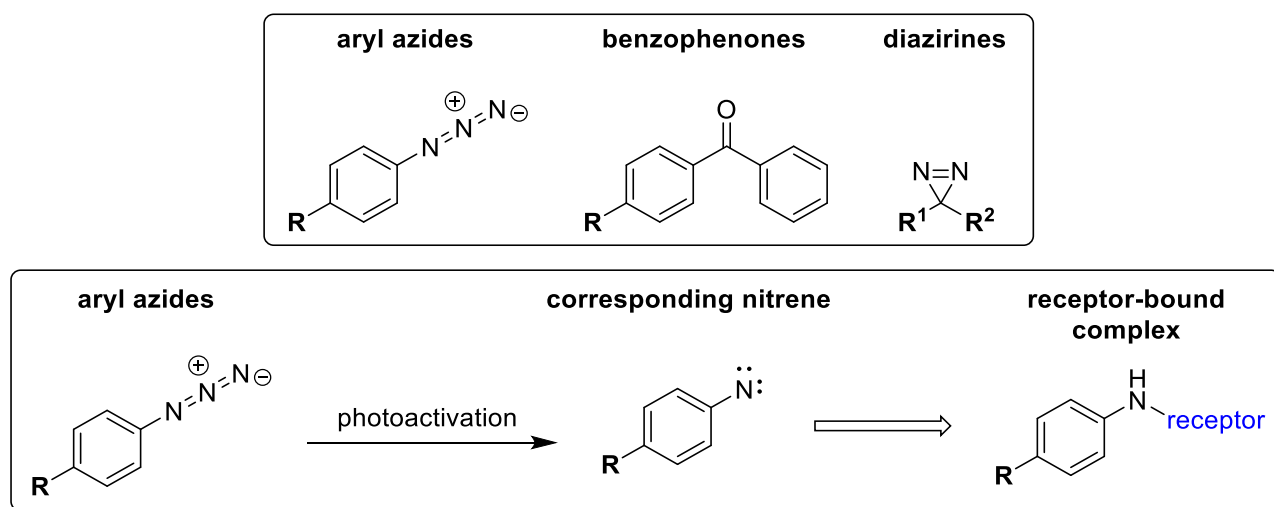


Figure 5. Common photoactivatable groups employed to synthesise photoreactive chemical probes followed by an example of the formed reactive species upon photoactivation of an aryl azide and its subsequent receptor-bound complex.

In contrast to their chemoreactive counterparts, photoreactive probes offer temporal control over reactivity which enhances the probability of capturing the receptor-ligand complex of interest. Furthermore, probes of this nature display greater synthetic tractability as their reactivity is dependent upon irradiation with ultra violet light. There is an extensive range of photoreactive groups that are at the disposal of the chemical biologist,⁴⁵ and some structural examples, namely aryl azides, benzophenones, and diazirines are detailed in Figure 5.^{46,47} Although benzophenones are chemically stable and display high cross-linking efficiency, their steric bulk may adversely affect their receptor-ligand interaction resulting in reduced accuracy. Alternatively, the smaller diazirines and aryl azides may be considered an attractive prospect due to their size. Unfortunately, the synthesis of diazirines can be difficult and time consuming therefore posing a major drawback for their use. In contrast, aryl azides are readily accessible targets which can be accessed from anilines via an intermediate diazonium salt upon treatment with sodium azide. Alternatively, aromatic azides may also be prepared from anilines upon treatment with commercially available *tertiary*-butyl nitrite and azidotrimethylsilane.⁴⁸ In addition, aryl azides may be prepared from the appropriate aryl halide upon treatment with sodium azide under copper iodide and diamine catalysis in the presence of a sodium ascorbate oxidant.⁴⁹ One limitation to their use, though, is their requirement for irradiation at wavelengths of 250-350 nm, which can potentially cause non-specific tissue damage to the biological

system being tested.⁵⁰ However, for the purpose of preliminary *in vitro* studies, aryl azides provide an ideal starting point for the development of photoactivatable irreversible ligands.

Photoactivatable probes have demonstrated utility in the identification and characterisation of GPCR-ligand binding sites,^{15,51} as well as providing preliminary evidence for receptor dimerization,⁵² and facilitation of receptor purification subsequently aiding GPCR crystallisation.⁵³ In addition, orthosterically-targeted photoactivatable probes containing an azide functionality are well documented and have extended our knowledge of the D₂R in a variety of tissues.⁵⁴⁻⁵⁸ Thus, developing biochemical tool variants of **2** with defined photoactivatable functional groups may not only facilitate the identification of novel drug targets and key molecular interactions involved in the binding of the **2** to the D₂R, but may also help to probe the structure and function of these allosteric sites. This information could also identify novel conformations of the receptor and guide the development of new and improved allosteric modulators

Fluorescent Probes. Fluorescent probes have seen widespread use in real-time monitoring of ligand-receptor interactions, as well as the visualisation and interrogation of drug-receptor targets.⁵⁹⁻⁶⁶ There are, however, multiple challenges when developing fluorescent probes. The attachment of a large molecular weight fluorophore to a ligand of interest may result in a loss of target affinity, but might also affect the pharmacological properties of the ligand such that it is no longer PAM or NAM. Accordingly, there are many structural aspects to consider when designing fluorescently labelled ligands. The length and composition of the linker/spacer used between the ligand and the fluorophore is a key consideration.⁶⁷ These subtleties can affect not only the ability of the probe to engage its target effectively, but may also affect its physical properties such as solubility. Various options are available to modify such properties, including incorporating linkers with greater rigidity to avoid conformational flexibility in the binding site, as well as increasing hydrophilicity through use of polyethylene glycol linkers, for example, to enhance aqueous solubility. Most importantly, a thorough understanding of an optimal attachment point for the linker and fluorophore must be obtained through SAR studies as functionalising the wrong position on the pharmacophore may cause losses in affinity and efficacy, or a complete abolishment of activity.

Fluorophores are organic dyes that usually consist of a conjugated system that results in them being able to emit light of a different wavelength relative to their excitation wavelength. Many fluorophores are now commercially available with key components optimised so that they may be useful over a variety of different wavelengths and brightness, and that they promote photostability with reduced self-quenching. Fluorophore optimisation has been achieved through increasing or decreasing the extent of conjugation of the molecules and also creating more rigid structures through incorporation

of extra rings, as well as introducing substituents with different electronic or electrostatic properties, such as fluorines or sulfonates, respectively.⁶⁸ As outlined in Figure 6, there are a number of traditional fluorophores based on the scaffold of fluorescein, rhodamine, cyanine, and BODIPY, from which further derivatives have been developed and optimised. Fluorophores based on the structural core of fluorescein are commonly used as they display high molar absorptivity, good aqueous solubility, and fluorescence quantum yield, making them suitable for confocal microscopy and flow cytometry.⁶⁹ However photobleaching, quenching, and pH sensitivity have limited their use.^{70,71} Rhodamine-based fluorophores display greater pH stability and reduced photodegradation despite their structural similarity to fluoresceins, and may display increased sensitivity.^{72,73} Cyanine fluorophores consist of two aromatic or heterocyclic rings connected through a conjugated carbon-carbon system.⁶⁹ In an effort to increase aqueous solubility and brightness, sulfonate derivatives of cyanine fluorophores have been especially advantageous.⁷⁴ Finally, the structure of BODIPY fluorophores are based upon a 4,4-difluoro-4-bora-3a,4a-diaza-s-indacene core which may be further functionalised. BODIPY fluorophores and derivatives thereof offer many beneficial properties as they are highly fluorescent and are insensitive to solvent polarity and pH, making them ideal for use in biological labelling studies.⁷⁵ Furthermore, their large absorption coefficient and high fluorescence quantum yields make them suitable for many different applications and particularly for imaging purposes.⁷⁶

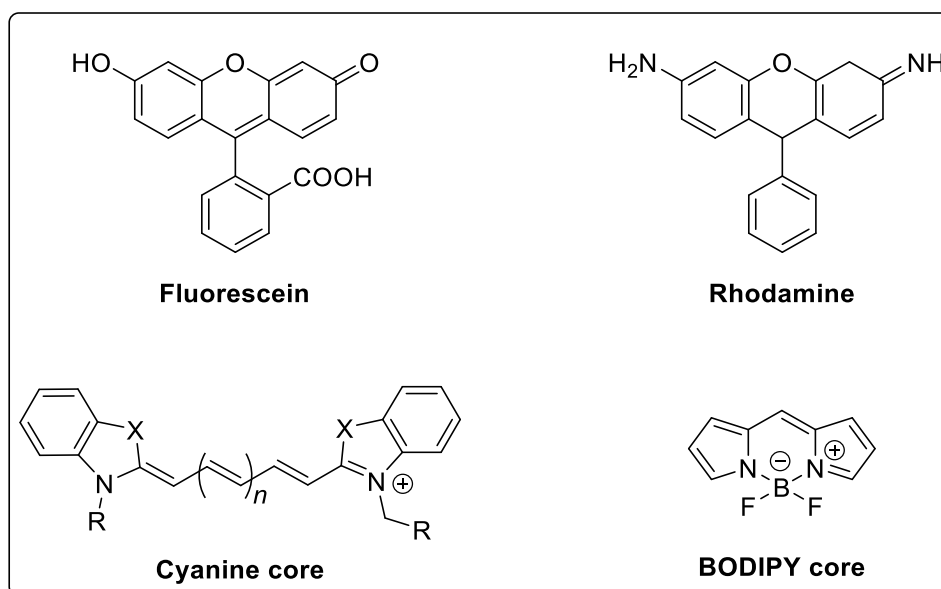


Figure 6. Scaffolds of xanthene-based fluorophores, fluorescein and rhodamine, the BODIPY (boron-dipyrromethene) core, and the representation of the general substitution pattern of cyanine-based fluorophores.

Many commercially available fluorophores contain specific functional groups such as *N*-hydroxysuccinimide active ester or imidoesters that permit their rapid incorporation into target molecules *via* nucleophilic substitution and subsequent amide bond formation. In order to modify **1** to give a potential fluorescent probe, an initial SAR evaluation of how the parent scaffold tolerates subtle structural changes will be used. At a cellular level, reversible fluorescent D₂R PAMs of this nature may have utility in the development of fluorescence-based ligand binding assays and receptor expression, localisation and trafficking studies. Selective fluorescent D₂R PAMs may also aid in the study of the D₂R in native cells and ultimately native tissue and whole animals, which is currently hindered by a lack of selective tools for detecting their expression. Moreover, fluorescent PAMs may serve as surrogate radioligands that can be used to determine fluorescent PAM affinity via saturation binding assays, and the affinity of non-fluorescent PAMs through competition binding assays. More recently, fluorescent histamine H₁-receptor antagonists have been developed for use in high-resolution confocal imaging, and to study ligand binding kinetics in living cells as well as membrane preparations, providing new opportunities for future drug discovery applications (Figure 7).⁷⁷

Considerable research efforts have been devoted to developing fluorescently labelled orthosteric probes that bind other class A GPCRs implicated in various CNS disorders, including adenosine,⁷⁸ muscarinic,⁷⁹ serotonin⁸⁰ and opioid^{81,82} receptors. Similar work conducted on DAR ligands is relatively limited in the literature. However, these studies have demonstrated both D₂R agonists⁸³ and antagonists^{84,85} to be amenable for fluorophore attachment, whereby these modifications retained the pharmacological profile of the parent ligands. Conversely, there is a current void in the literature surrounding the characterisation of fluorescently labelled allosteric ligands of the DARs.

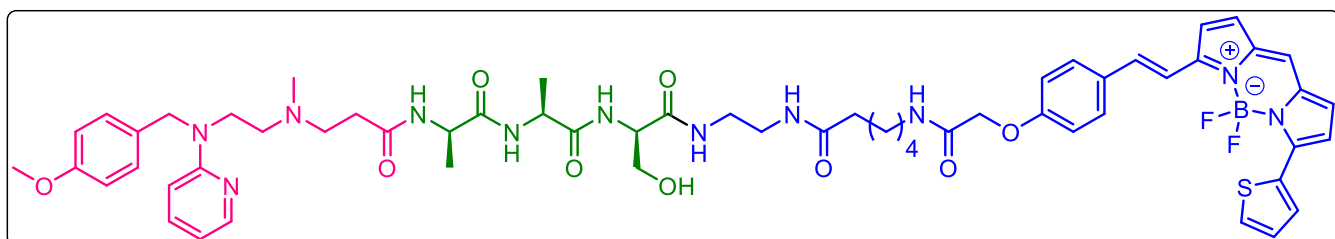


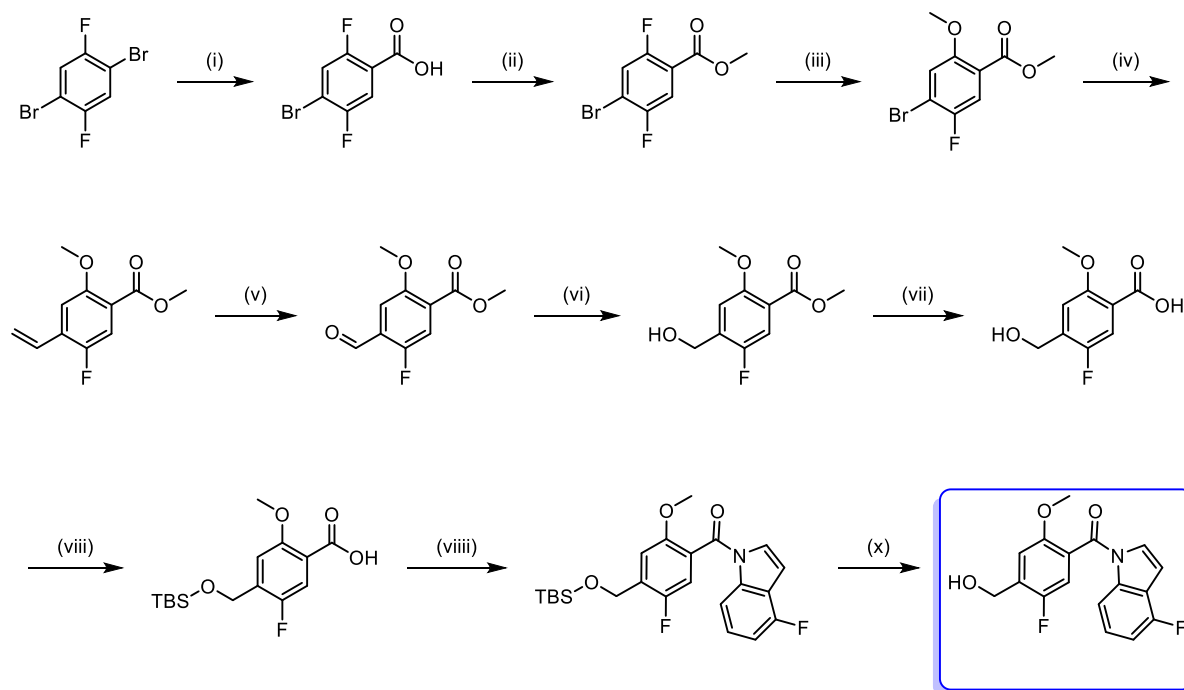
Figure 7. Chemical structure of representative broad-utility fluorescent probe of the histamine H₁ receptor based on the structure of the first-generation antihistamine, mepyramine, as reported by Stoddart *et al.*⁷⁷ The probe comprises three independent structural moieties, namely the parent mepyramine pharmacophore (red), a tripeptide linker (green) appended to a BODIPY derivative (BODIPY630/650-X) (blue).

In summary, the aims of this project were to gauge the amenability of the core scaffold to structural modification for the purpose of generating irreversible and fluorescent derivatives of **1**. If successful,

photoactivatable derivatives may help to facilitate studies toward the elucidation of their allosteric binding mode. Additionally, fluorescent derivatives may display potential for a variety of applications, including as fluorescent tracers to enable the characterisation of allosteric modulator binding kinetics. To be useful tools these derivatives must maintain both affinity for the receptor as well as PAM activity, and thus some preliminary structure-activity relationships would need to be established to permit the rational design of these biochemical tools.

Chemistry. In order to better understand potential linking points from which we could append a fluorophore or photoactivatable functional group whilst also gauging the importance of existing functionality, we designed and synthesised a focused library of derivatives of **2**. Initially, we re-synthesised **2** (Scheme 1) in order to further characterise its pharmacology, as well as make additional modifications to this molecule to understand the structural limitations of the scaffold. Following an adapted procedure from Wood *et al.*,¹ commercially available 1,4-dibromo-2,5-difluorobenzene **3** was treated with *n*-butyllithium at -78 °C, followed by treatment with solid CO₂ to afford the corresponding benzoic acid **4**. Fisher esterification via treatment of acid **4** with MeOH and thionyl chloride gave methyl ester **5**. Sodium methoxide was prepared from sodium metal and methanol and subsequently reacted with aryl fluoride **5** via nucleophilic aromatic substitution in DMF to install methyl ether **6**. Stille coupling conditions in the presence of Pd(PPh₃)₂Cl₂ were used to convert aryl bromide **6** to the corresponding terminal olefin **7**, followed by treatment with ozone in DCM *via* ozonolysis, affording the corresponding benzaldehyde **8** after reductive work-up with dimethyl sulfide. NaBH₄ was employed to effect reduction of the aldehyde **8** to the corresponding benzyl alcohol **9**. Next, ester saponification under alkaline conditions afforded carboxylic acid **10**. Treatment with *tert*-butyldimethylsilyl chloride (TBS-Cl) in the presence of imidazole, afforded the silyl-protected ether **11**. Next, the carboxylic acid **11** was treated with 4-fluoro-1*H*-indole in the presence of EDC and DMAP to afford the corresponding amide **12**. Finally, silyl ether de-protection proceeded smoothly in the presence of tetrabutylammonium fluoride (TBAF) and acetic acid and, after recrystallization from DCM/petroleum ether, afforded target compound **2**.

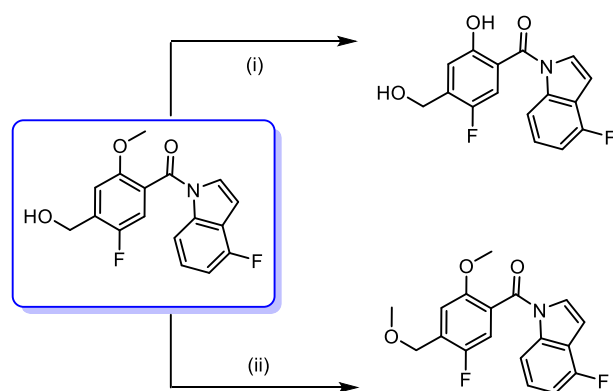
Scheme 1. Chemical Synthesis of **2** Using Literature Methodology^a



^aReagents and conditions: (i) *n*-BuLi, CO₂, Et₂O, -78 °C – rt, 75%; (ii) SOCl₂, MeOH, 0-60 °C, 3 h, 95%; (iii) NaOMe, dry DMF, rt, 18h, 75%; (iv) tributylvinylstannane, Pd(PPh₃)₂Cl₂, DMSO, 80 °C, 16 h, 70%; (v) O₃, dry DCM, dimethylsulfide, -78 °C, 6 h, 68%; (vi) NaBH₄, THF, rt, 3 h, 85%; (vii) LiOH, 55 °C, 4 h, 95%; (viii) TBS-Cl, imidazole, DMF, rt, 24 h, 75%; (viii) 4-fluoro-1*H*-indole, EDC, DMAP, dry 1,2-DCE, 0 °C – reflux, 65%; (x) TBAF, AcOH, THF, rt, 16 h, 75%.

Our SAR investigation into **2** placed specific emphasis on existing functionality present on the benzene ring at the 2-, 4-, and 5-positions (OMe, CH₂OH and F respectively). Initially we wanted to assess the effect of converting the OMe substituent to the corresponding phenol, as well as probe the importance of the primary alcohol through methylation. To achieve this, **2** was further functionalised to yield an additional two analogues (**13** and **14**, Scheme 2). To synthesise the phenol analogue, **2** was demethylated using borontribromide in DCM, providing the corresponding phenol **13** in moderate yield. In addition, **2** was alkylated with methyl iodide in the presence of silver(I) oxide to install the methoxymethyl moiety, which proceeded slowly under reflux conditions, eventually affording **14** in high yield.

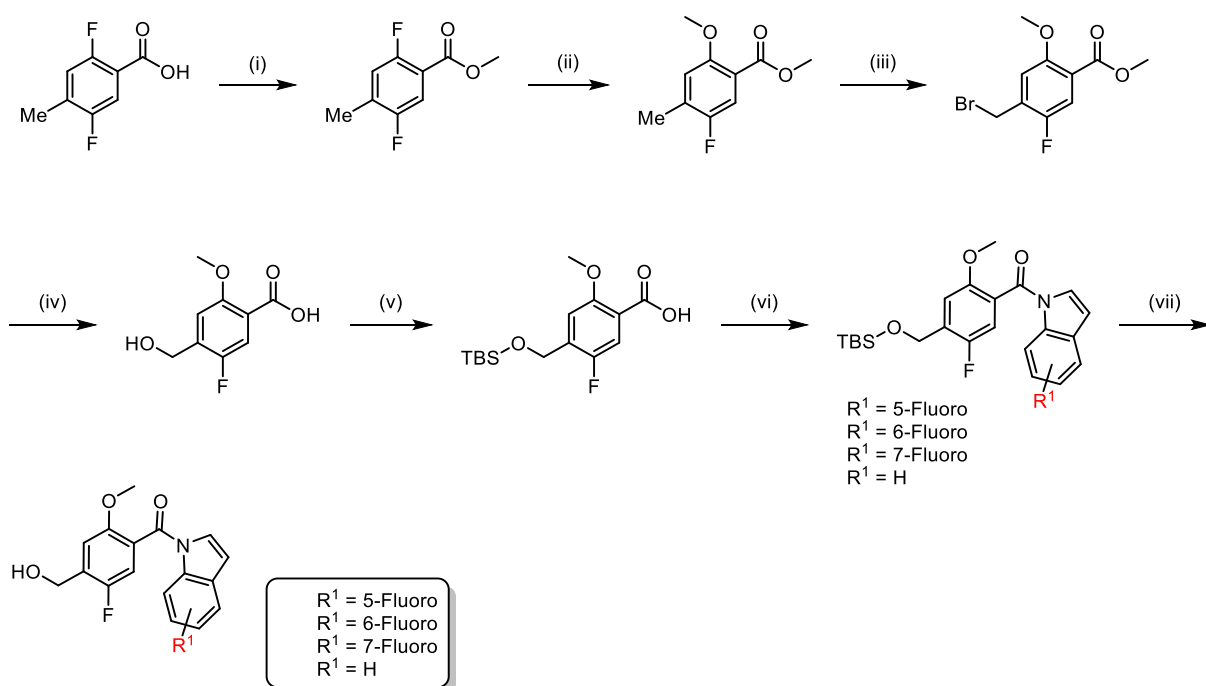
Scheme 2. Chemical Synthesis of Phenol and Methoxymethyl Ether Variants of 2^a



Reagents and conditions: (i) BBr₃, DCM, 0 °C, 3h, 71%; (ii) Ag₂O, MeI, reflux, 48 h, 94%.

In addition to these analogues, we wanted to assess the effect of alternate fluorine substitution on the indole, as well as a *des*-fluoro variant, by employing different indoles in the amide bond formation step. As the literature synthesis of **2** involves many synthetic steps including Stille coupling, ozonolysis and reduction, it was sought after to investigate a more appropriate synthesis, one in which contains fewer steps and is more conducive to the synthesis of structural analogues. Thus, an alternative 7-step synthetic pathway was established and is outlined in Scheme 3. The synthesis begins with the methyl esterification of commercially available 2,5-difluoro-4-methylbenzoic acid **15** using conditions outlined previously, to afford the corresponding ester **16**. Next, nucleophilic aromatic substitution was employed¹ to convert the aryl fluoride **16** to the corresponding methyl ether **17**. The tolyl substituent was then subjected to a 1,1'-azobis(cyclohexanecarbonitrile)-initiated radical bromination using *N*-bromosuccinimide in acetonitrile, affording the corresponding alkyl bromide **18**. Next, the one-pot hydrolysis of alkyl bromide **18** to the corresponding hydroxymethyl-substituted benzoic acid proceeded smoothly in the presence of sodium hydroxide at reflux to give **19**. TBS-protection of the alcohol was achieved using conditions as described earlier to give the corresponding silyl ether **20**, followed by EDC-mediated coupling with the appropriate indole in 1,2-dichloroethane to afford the corresponding amide products **21-24**. Finally, TBAF de-protection using conditions outlined previously were employed to afford the corresponding final analogues **21a-24a** in respectable yields.

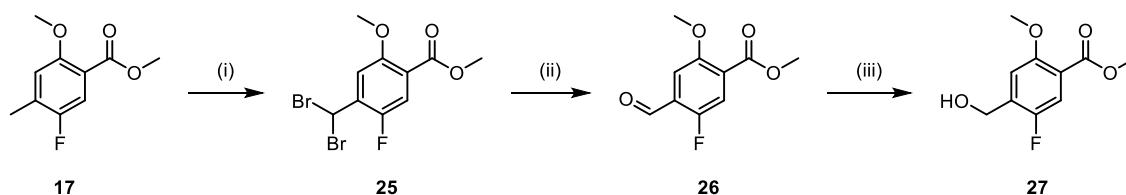
Scheme 3. Alternative Synthesis of **2** Using 2,5-Difluoro-4-Methylbenzoic Acid^a



^aReagents and conditions: (i) SOCl₂, MeOH, 0-60 °C, 3 h 95%; (ii) NaOMe, dry DMF, rt, 18h, 75%; (iii) NBS, azobisisobutyronitrile, MeCN, reflux, 3 h, 84%; (iv) NaOH, MeOH/H₂O, 100 °C, 4 h, 85% (v) TBS-Cl, imidazole, DMF, rt, 24 h, 75%; (vi) Indole, EDC, DMAP, dry 1,2-DCE, 0 °C – reflux, 45-80% (**21-24**); (vii) TBAF, AcOH, THF, rt, 16 h, 65-85% (**21a-24a**).

It is important to note that if careful stoichiometry is not adhered to with respect to the brominating agent, the aryl methyl will readily undergo dibromination. This results in the formation of a *gem*-dibromomethylarene intermediate **25**. However, this compound can be readily converted to the corresponding hydroxymethyl intermediate **27** in two steps as outlined in Scheme 4. Firstly, dibromomethyl compound (**25**) was stirred in neat DMSO at 120 °C, to effect transformation to the corresponding aldehyde **26** in excellent yield, followed by treatment with NaBH₄, to provide the corresponding alcohol, **27**.

Scheme 4. Synthesis of Key Intermediate 28 from Dibromo Side-Product^a



^aReagents and conditions: (i) NBS, azobisisobutyronitrile (cat.), MeCN, reflux, 3 h; (ii) DMSO, 120 °C, 24 h, 84%; (iii) NaBH₄, MeOH, rt, 3 h, 94%.

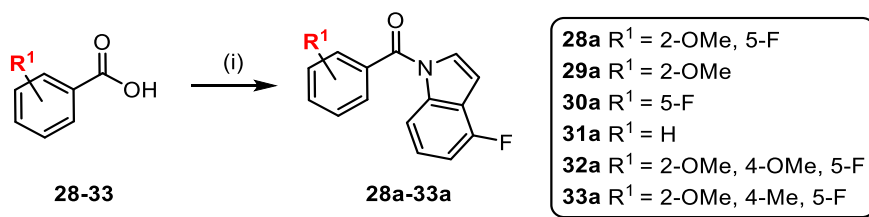
The next focus of the SAR study surrounding **2** was to examine the effects of removing substituents on the phenyl group (OMe, CH₂OH, F). All designed analogues devoid of the hydroxymethyl substituent could be easily accessed by reacting the appropriate commercially available benzoic acid with 4-fluoro-1*H*-indole (Scheme 5) using conditions outlined previously. Commercially available benzoic acids **28-33** used in the synthesis of corresponding analogues **28a-33a** are outlined in Table 1 and make specific reference to Scheme 5.

Table 1. Commercially Available Benzoic Acids Used for the Synthesis of Products 28a-33a.

CPD #	Benzoic acid	Product	CPD #	Benzoic acid	Product
28		28a	31		31a
29		29a	32		32a
30		30a	33		33a

All reactions proceeded smoothly to give the corresponding amide products **28a-33a** (Scheme 5).

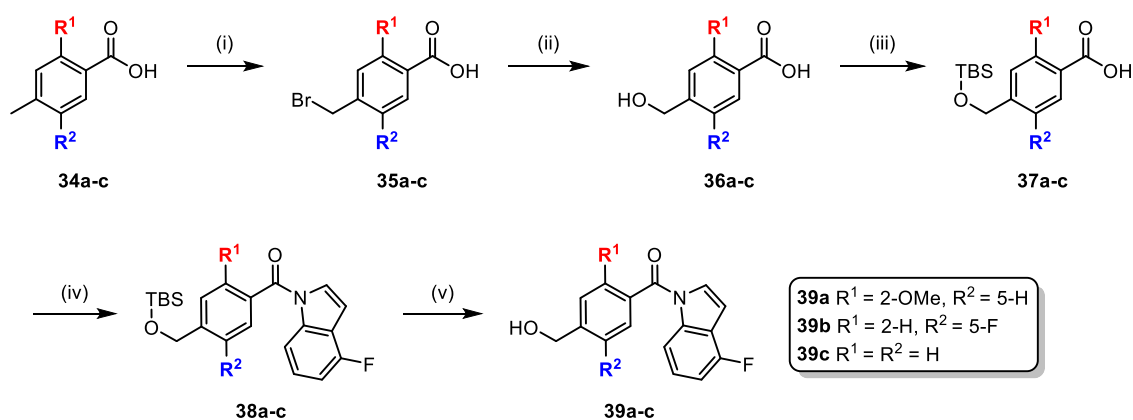
Scheme 5. Further Synthesis of Analogues of 2 Devoid of Hydroxymethyl Moiety^a



^aReagents and conditions: (i) 4-fluoro-1*H*-indole, EDC, DMAP, dry 1,2-DCE, 0 °C – reflux, 65-77% (**28a-33a**).

Further to these analogues, we wanted to assess the role of the hydroxymethyl functionality, both as a lone substituent, and in conjunction with the OMe and F substituents. To achieve this (Scheme 6), the appropriate commercially available toluic acid derivative (**34a-c**) was radically brominated using conditions outlined previously, to afford the corresponding alkyl halides **35a-c** in good yields. Nucleophilic displacement with sodium hydroxide proceeded smoothly to give compounds **36a-c** bearing the corresponding hydroxymethyl substituent at the 4-position. Alcohol protection was achieved with TBS-chloride using conditions described earlier to afford the corresponding silyl ethers **37a-c**, followed by EDC-mediated amide coupling with 4-fluoro-1*H*-indole again using conditions as outlined previously to afford amide products **38a-c** in respectable yields. Finally, TBAF de-protection in the presence of acetic acid in THF afforded the corresponding final products **39a-39c** in good yields.

Scheme 6. Further Synthesis of Analogues of 2 Containing Hydroxymethyl Functionality^a



^aReagents and conditions: (i) NBS, azobisisobutyronitrile, MeCN, reflux, 2-3.5 h, 65-80% (**35a-c**); (ii) NaOH, MeOH/H₂O, 100 °C, 4 h, 70-90% (**36a-c**); (iii) TBS-Cl, imidazole, DMF, rt, 24 h, 60-88% (**37a-c**); (iv) 4-fluoro-1*H*-indole, EDC, DMAP, dry 1,2-DCE, 0 °C – reflux, 65-77% (**38a-c**); (v) TBAF, AcOH, THF, rt, 16 h, 58-84% (**39a-c**).

Pharmacology. To validate and quantify the pharmacology of **2** in our laboratory, we utilised a BRET biosensor assay to measure inhibition of 10 μ M forskolin-stimulated cyclic adenosine monophosphate (cAMP) accumulation through G $\alpha_{i/o}$ G-protein activation by the hD_{2L}R stably expressed in FlpIn CHO cells. We initially conducted a series of cAMP inhibition assays in cells pre-treated with phenoxybenzamine (an alkylating agent used as an irreversible antagonist at the D₂R) (Figure 8A).⁸⁶ The concentration-response data for DA evaluated in cells treated or untreated with this alkylating agent were then fit to an operational model of receptor depletion in order to determine values of K_A and τ_A ($\log K_A = -6.21 \pm 0.13$, $\log \tau_A = 1.26 \pm 0.13$) for the agonist DA. These data were used to fit the data described below in which DA concentration-response curves in the absence or presence of increasing concentrations of **2** or derivatives were fit to an operational model of allostery.

In our functional assay the concentration-dependant response of DA was measured in the presence of increasing concentrations of **2**, where it was shown to act as a PAM at the hD_{2L}R. These data are reported in Table 2 and Figure 8B, and are presented as logarithms to base 10. For ease of interpretation, however, allosteric parameter antilogarithms are also highlighted in the main text for selected key derivatives. Application of an operational model of allostery to the concentration-response data yielded an estimate of affinity of **2** for the unoccupied receptor ($K_B = 4.68 \mu$ M), and its cooperativity with DA, where $\alpha\beta$ is the composite cooperativity parameter exerted upon DA binding and efficacy ($\alpha\beta = 54.2$). Values of $\alpha\beta > 1$ signify positive cooperativity with DA, and this equates to a maximal 54-fold increase upon the potency of DA in this assay. This model also permitted derivation of the molecules direct effect upon engaging with the receptor (termed allosteric agonism or intrinsic efficacy, denoted as τ_B) ($\tau_B = 0.53$). Thus, by using an assay measuring D₂R function, we have confirmed that **2** acts through a non-competitive mechanism to modulate the affinity of DA at the D₂R i.e. it is a PAM of agonist affinity whilst also displaying intrinsic efficacy in its own right.

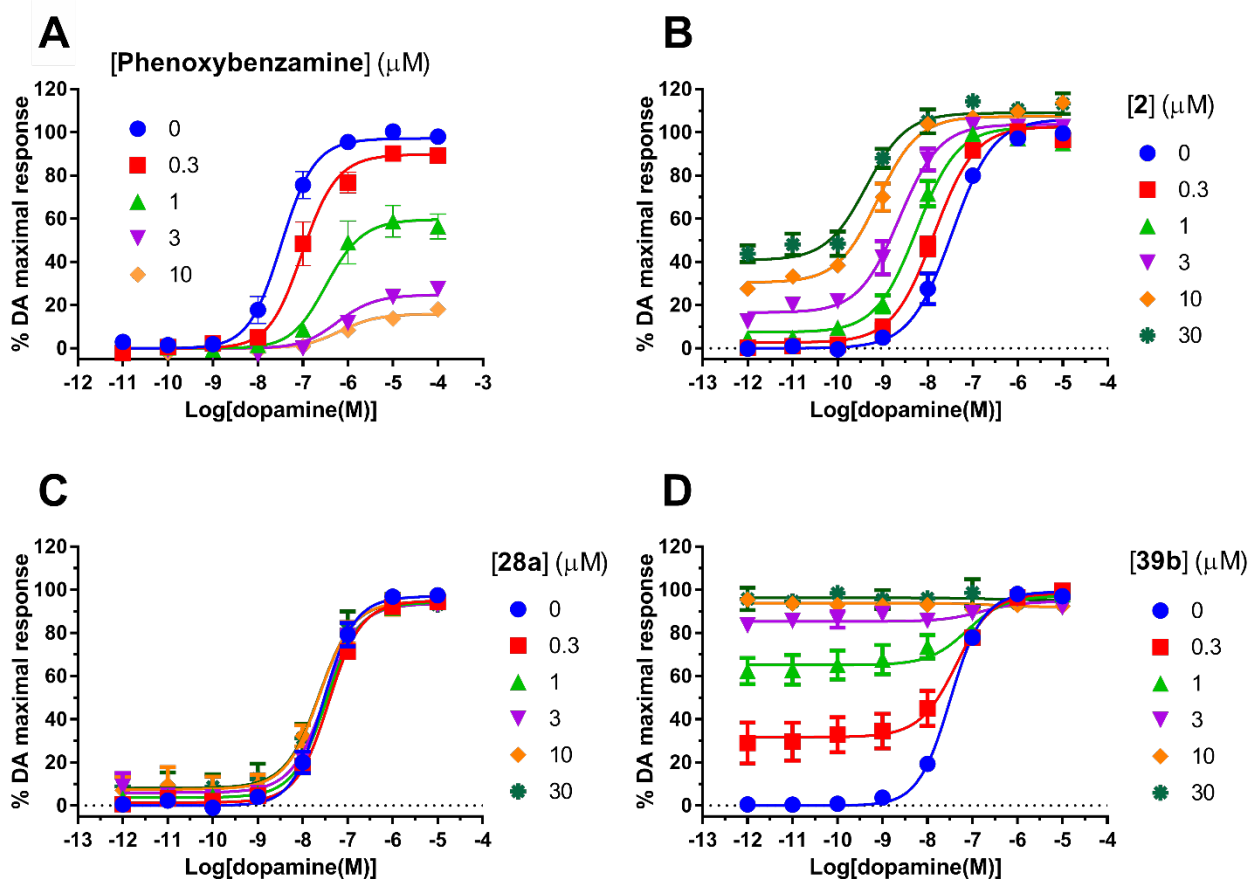
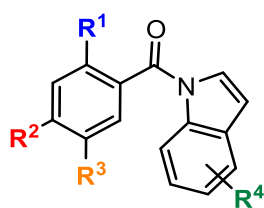


Figure 8. Derivation of Orthosteric Ligand Parameters. (A) The alkylating agent phenoxybenzamine displays a concentration-dependant inhibition of DA at the hD₂L_R (data fit to an operational model of receptor depletion in order to derive values of orthosteric ligand affinity (K_A) and intrinsic response (τ_A)). **Compound 2 and Structural Analogue 39b Display Distinct Allosteric Pharmacology at the hD₂L_R.** (B) In an assay measuring inhibition of forskolin-stimulated cAMP production using a BRET biosensor at the hD₂L_R, **2** acts to cause a limited potentiation of DA potency with no effect on the maximal response of DA consistent with positive allosteric modulation. (C) In contrast, **28a** (*des*-CH₂OH analogue) is now inactive at the hD₂L_R at a concentration of 30 μM. (D) Despite this, increasing concentrations of **39b** (*des*-OMe analogue) (up to 3 μM) effect a maximal response in their own right, with modest effects on DA potency and no effect on DA maximal response, consistent with allosteric agonism (data from panels B-C were fitted with an operational model of allostery to derive values of affinity, cooperativity and intrinsic efficacy, Table 2). Data is the mean ± SEM of three independent experiments performed in duplicate.

Functional Analysis (cAMP) of Analogues of 2. In order to explore the molecular features of **2** that are responsible for its allosteric activity, as well as gauge potential vectors for which we could append a fluorophore, we extended our functional characterisation to all additional analogues of **2** using the cAMP assay described above (Table 1). We first examined modifications to existing functionality on **2**. Converting the methyl ether to corresponding phenol (**13**) resulted in a slight decrease in functional affinity, whilst retaining a similar degree of allosteric agonism relative to **2** ($K_B = 31.0 \mu\text{M}$, $\tau_B = 0.58$). However, interestingly, this compound lost any modulatory effect on DA. Converting the hydroxymethyl to the corresponding methoxymethyl analogue (**14**), resulted in a 10-fold decrease in affinity and again abolished any modulatory effect, however resulted in a 3-fold increase in allosteric agonism ($K_B = 55.8 \mu\text{M}$, $\tau_B = 3.84$). We next examined the effect of modifications to the indole moiety of **2**. To allow us to derive a more accurate value of affinity and cooperativity for the 5-fluoro variant (**21a**), the value of intrinsic efficacy (τ_B) was constrained to 1. This modification caused a ~4-fold loss in affinity, coupled with a ~4-fold loss in allosteric cooperativity ($K_B = 19 \mu\text{M}$, $\alpha = 12$). On the other hand, the 6-fluoro variant (**22a**) lost ~10-fold affinity, together with a slight increase in the degree of allosteric agonism, however still retained positive modulatory effects on DA affinity, albeit >2-fold lower than **2** ($K_B = 41.7 \mu\text{M}$, $\tau_B = 0.76$, $\alpha = 21.0$). To enhance the accuracy of fit for data obtained for the 7-fluoro analogue (**23a**), the value of intrinsic efficacy (τ_B) was constrained to 1. This modification caused a ~37-fold loss in affinity relative to **2**, however modulatory effects were somewhat maintained ($K_B = 372 \mu\text{M}$, $\alpha = 45$). Interestingly, removal of the fluorine (**24a**) completely abolished activity. It is evident that both the presence and position of the fluoro substituent is absolutely critical to maintaining affinity and in particular, positive allosteric cooperativity. The effect of removing the hydroxymethyl substituent was the next area of focus, where it was also discovered to be integral to maintenance of affinity and positive modulatory effects. All combinations and permutations were explored, beginning with removal of the hydroxymethyl (**28a**) (Figure 8C), followed by removal of the hydroxymethyl and aryl fluoride (**29a**), removal of the hydroxymethyl and methyl ether (**30a**), as well as removal of all substituents on the phenyl ring (**31a**). These modifications rendered all of the corresponding analogues inactive. Substituting the hydroxymethyl moiety for a methyl ether (**32a**) or methyl (**33a**) also abolished functional activity. Notably, any modification to the primary alcohol has significant adverse effects on the activity and modulatory effect of the resulting compound. We next focused on maintaining the hydroxymethyl substituent whilst modifying the other substituents on the phenyl ring. Removal of the aryl fluoride (**39a**) resulted in a ~39-fold loss of functional affinity ($K_B = 182 \mu\text{M}$), however this modification acted to increase the degree of allosteric agonism and positive modulatory effects relative to **2** ($\tau_B = 10.0$, $\alpha = 354$). Removal of the methyl ether (**39b**) had dramatic effects on the allosteric pharmacology of **2**. The

effect on functional affinity was negligible ($K_B = 6.82 \mu\text{M}$), though this molecule now weakly potentiated DA affinity ($\alpha = 3.64$), however was now an efficacious allosteric agonist with a ~25-fold increase in intrinsic efficacy relative to **2** ($\tau_B = 12.5$), able to elicit an equivalent maximal response relative to that of DA at a concentration of $3 \mu\text{M}$ (Figure 8D). It is interesting to note that this compound is devoid of an ionisable nitrogen, yet is able to directly activate the receptor from a topographically distinct binding site. To our knowledge, this is one of the first reported compounds with this ability. Removing both the methyl ether and fluorine substituents simultaneously (**39c**) had slight effects on functional affinity ($K_B = 38.6 \mu\text{M}$) and allosteric agonism ($\tau_B = 0.58$), although diminishing any levels of positive allosteric cooperativity.

Table 2. Functional Parameters for 2 and Analogues of 2 Derived from Functional cAMP BRET Assay.



	R ¹	R ²	R ³	R ⁴	pK _B (K _B , μM) ^a	Logτ _B (τ _B) ^b	Log αβ (αβ) ^c
2	OMe	CH ₂ OH	F	4-F	5.33 ± 0.15 (4.68)	-0.28 ± 0.05 (0.53)	1.73 ± 0.19 (54.2)
13	OH	CH ₂ OH	F	4-F	4.51 ± 0.36 (31.0)	-0.24 ± 0.2 (0.58)	= 0
14	OMe	CH ₂ OMe	F	4-F	4.25 ± 0.37 (55.8)	0.18 ± 0.24 (1.51)	= 0
21a	OMe	CH ₂ OH	F	5-F	4.71 ± 0.09 (19)	= 0 (1)	1.08 ± 0.07 (12)
22a	OMe	CH ₂ OH	F	6-F	4.31 ± 0.34 (48.2)	-0.12 ± 0.21 (0.76)	1.32 ± 0.27 (21.0)
23a	OMe	CH ₂ OH	F	7-F	3.76 ± 0.19 (173)	= 0 (1)	1.66 ± 0.19 (45)
24a	OMe	CH ₂ OH	F	H		nd	
28a	OMe	H	F	4-F		nd	
29a	OMe	H	H	4-F		nd	

Chapter 4: SAR Studies Toward Irreversible & Fluorescent Analogues of a D₂R PAM

30a	H	H	F	4-F			nd
31a	H	H	H	4-F			nd
32a	OMe	OMe	F	4-F			nd
33a	OMe	CH ₃	F	4-F			nd
39a	OMe	CH ₂ OH	H	4-F	3.74 ± 0.71 (182)	0.99 ± 0.64 (10)	2.55 ± 0.71 (354)
39b	H	CH ₂ OH	F	4-F	5.17 ± 0.21 (6.82)	1.10 ± 0.20 (12.5)	0.56 ± 0.92 (3.64)
39c	H	CH ₂ OH	H	4-F	-4.41 ± 0.38 (38.6)	-0.23 ± 0.22 (0.58)	= 0

^aEstimate of the negative logarithm of the equilibrium dissociation constant determined in an cAMP functional assay.

^bEstimate of the intrinsic efficacy of the modulator. ^cEstimate of the logarithm of the net cooperativity factor between the modulator and dopamine. ^dEstimate of the logarithm of the modulatory effect upon efficacy factor induced by the allosteric modulator. nd = inactive at a concentration of 30 μM. Values represent mean ± S.E.M. from at least three independent experiments performed in duplicate.

Our data indicates that essentially any modification explored in this series of compounds has negative effects on not only the functional affinity of **2**, but also the degree of positive allosteric cooperativity upon DA affinity and the level of intrinsic agonism. This is currently not encouraging for the design of fluorescent derivatives of **2** bearing fluorophores linked through any of the currently substituted vectors of **2** (R¹ – R⁴). Work exploring the synthesis of irreversible azido derivatives of **2** and whether these analogues maintain allosteric pharmacology is currently underway in our laboratory.

Conclusions. In this study, we report the design, synthesis and characterisation of a series of compounds based on the scaffold of a novel D₂R PAM (**2**). This was achieved to further our understanding of the molecular features required for allostery at the D₂R, and to investigate an appropriate starting point toward the synthesis of irreversible and fluorescent analogues of **2** to aid in the elucidation of D₂R PAM allosteric binding modes. We have established a novel synthesis to access analogues of **2** in fewer synthetic steps compared to literature, and characterised all compounds in an assay measuring D₂R function. **2** was found to display low μM affinity for the D₂R and be a PAM of agonist affinity (54-fold potentiation of DA potency). We investigated the role of existing functionality on **2**, namely the A-ring substituents (OMe, CH₂OH, F) as well as the importance of the aryl fluoride and its position on the indole (B ring). A large proportion of analogues displayed an abolishment of activity (**24a**, **28a-33a**), and this was particularly evident when the hydroxymethyl

substituent of **2** was modified. An indolic fluoro substituent on the 4-position was determined to be optimal, while movement of this substituent to the 5-, 6-, and 7-positions reduced affinity and positive allosteric cooperativity (**21a-23a**). Removal of the aryl fluoride on the A-ring caused a ~39-fold loss in affinity, and increased the degree of allosteric agonism (**39a**). However, the most interesting compound to arise from this study was compound **39b**, as removal of the aryl methyl ether substituent caused a ~25-fold increase in allosteric agonism, whilst reducing the degree of positive modulatory effects and having no impact on the functional binding affinity. Unfortunately, the SAR obtained from this study demonstrates that the scaffold of **2** is not particularly amenable to structural modification. Thus, using **2** to develop fluorescent probe derivatives that retain their parent pharmacological profiles will likely fail. However, due to the relatively small size of the photoactivatable azide functionality, our data indicates some promise in regards to the successful development of such compounds. Accordingly, these data will be used to further guide the design and synthesis of irreversibly binding analogues of **2**.

Experimental section

Chemistry: General Information and Synthetic Procedures. Chemicals and solvents were purchased from standard suppliers and used without further purification. Davisil silica gel (40–63 μm) for flash column chromatography was supplied by Grace Davison Discovery Sciences (Victoria, Australia), and deuterated solvents were purchased from Cambridge Isotope Laboratories, Inc. (USA, distributed by Novachem PTY. Ltd., Victoria, Australia). Reactions were monitored by thin layer chromatography on commercially available precoated aluminum-backed plates (Merck Kieselgel 60 F₂₅₄). Visualization was by examination under UV light (254 and 366 nm). A solution of ninhydrin (in ethanol) was used to visualize primary and secondary amines. All organic extracts collected after aqueous workup procedures were dried over anhydrous MgSO₄ or Na₂SO₄ before gravity/vacuum filtering and evaporation to dryness. Organic solvents were evaporated *in vacuo* at ≤ 40 °C (water bath temperature). ¹H NMR and ¹³C NMR spectra were recorded on a Bruker Avance Nanobay III 400 MHz Ultrashield Plus spectrometer at 400.13 and 100.62 MHz, respectively. Chemical shifts (δ) are recorded in parts per million (ppm) with reference to the chemical shift of the deuterated solvent. Coupling constants (*J*) are recorded in Hz, and the significant multiplicities described by singlet (s), doublet (d), triplet (t), quadruplet (q), broad (br), multiplet (m), doublet of doublets (dd), and doublet of triplets (dt). Spectra were assigned using appropriate COSY, distortionless enhanced polarization transfer (DEPT), HSQC, and HMBC sequences. LC-MS were run to verify reaction outcome and purity using an Agilent 6120 series single quad coupled to an Agilent 1260 series HPLC. The following buffers were used: buffer A, 0.1% formic acid in; buffer B, 0.1% formic acid in MeCN.

The following gradient was used with a Poroshell 120 EC-C18 50 mm × 3.0 mm 2.7 μm column, and a flow rate of 0.5 mL/min and total run time of 5 min; 0–1 min 95% buffer A and 5% buffer B, from 1 to 2.5 min up to 0% buffer A and 100% buffer B, held at this composition until 3.8 min, 3.8–4 min 95% buffer A and 5% buffer B, held until 5 min at this composition. Mass spectra were acquired in positive and negative ion mode with a scan range of 100–1000 *m/z*. UV detection was carried out at 214 and 254 nm. All retention times (*t_R*) are quoted in minutes. All screening compounds were of >95% purity unless specified in the individual monologue. All NMR experiments were performed in CDCl₃ to permit comparison of the spectra of the various analogues. Experiments were performed in acetone-*d*₆, DMSO-*d*₆, or MeOH-*d*₄ if selected analogues lacked solubility in CDCl₃.

General Synthetic Procedures.

General Procedure A. TBS Protection of Primary Alcohols for the Synthesis of 11, 20, 37a-c.

TBSCl (2.0 eq.) was added to a stirred solution of primary alcohol (1.0 eq.), imidazole (3.0 eq.) and 4-dimethylaminopyridine (DMAP) (0.1 eq.) in *N,N*-dimethylformamide (DMF). The reaction mixture was stirred overnight at room temperature and then diluted with DCM, partitioned with saturated aqueous NH₄Cl, and extracted with DCM. The combined organic layers were dried (Na₂SO₄), filtered and concentrated *in vacuo*. The residue was purified by flash column chromatography (FCC) with an appropriate eluent as indicated.

General Procedure B. EDC-Mediated Coupling for the Synthesis of 12, 21-24, 28a-33a, 38a-c.

EDC (1.25 equiv.) was added to a solution carboxylic acid (1 eq.), appropriate indole (1 equiv.), and DMAP (1 eq.) in dry DCM. The reaction mixture was stirred for 16 h or until complete consumption of starting material was evident. The reaction was evaporated *in vacuo* and the residue purified by FCC using an appropriate eluent as indicated.

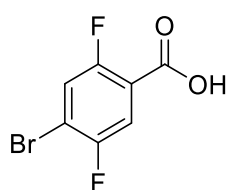
General Procedure C. TBAF Deprotection of Silyl Ethers for the Synthesis of 2, 21a-24a, 39a-c.

Tetra-*N*-butylammonium fluoride (1.2 eq.) was added dropwise to a stirred solution of silyl ether (1.0 eq.) and acetic acid (1.2 eq.) in tetrahydrofuran. The reaction mixture was stirred at room temperature overnight then diluted with dichloromethane, partitioned with ammonium chloride and extracted with dichloromethane. The combined organic layers were dried (Na₂SO₄), filtered and concentrated *in vacuo*. The residue was purified by FCC using an appropriate eluent as indicated.

General procedure D. Radical Bromination for the Synthesis of 18, 35a-c. To a solution of toluic acid derivative (1 eq.) in CCl₄ or MeCN (20 mL) were added *N*-bromosuccinimide (1.02 eq.) and (*E*)-1,1'-(diazene-1,2-diyl)bis(cyclohexane-1-carbonitrile) (0.15 eq.). After stirring at 90°C for 30 min

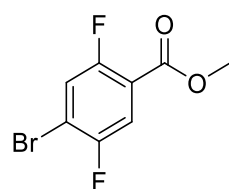
and at 100°C for 2.5 hr, the mixture was cooled to 0°C. The precipitate was collected by filtration and washed with *n*-hexanes and water to give a crude product. The crude product was dissolved in ethyl acetate (5 mL), and *n*-hexanes (10 mL) was added. The precipitated solid was collected by filtration, and dried under reduced pressure to give the desired alkyl halide. Similarly the reaction mixture could be directly concentrated *in vacuo* and purified by FCC with an appropriate eluent as indicated.

4-Bromo-2,5-difluorobenzoic acid (4).



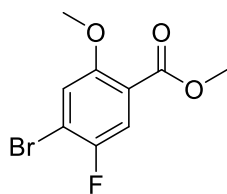
Under an nitrogen atmosphere, to a solution of 1,4-dibromo-2,5-difluorobenzene (7.00 g, 25.8 mmol) in dry Et₂O (120 mL) was added dropwise *n*-butyl lithium (2.5 M solution in *n*-hexanes) (10.8 mL, 27.0 mmol) at -78 °C, and the mixture was stirred at same temperature for 2 min. The mixture was added quickly to a stirred suspension of dry ice (~75 g) and Et₂O (80 mL), and the mixture was warmed up to room temperature. The precipitate was collected by filtration, and washed with Et₂O. The obtained solid was treated with water (50 mL) and 1 M HCl solution (70 mL), and extracted with Et₂O. The organic layer was washed with brine and dried. The desiccant was removed by filtration and the filtrate was evaporated *in vacuo*. The resulting residue was washed with *n*-hexanes, and dried *in vacuo* to obtain the desired compound as a pale yellow solid (4.35g, 72%). LCMS (*m/z*): 190.9 [M - H]⁺. HPLC: *t*_R 5.744 min, >95% purity (214 & 254 nm). ¹H NMR (*d*₆-DMSO) δ 7.88 (dd, *J* = 9.7, 5.6 Hz, 1H), 7.77 (dd, *J* = 8.7, 6.2 Hz, 1H). ¹³C NMR (*d*₆-DMSO) δ 163.4 (dd, *J* = 3.5, 1.8 Hz), 156.8 (dd, *J* = 257.1, 1.9 Hz), 154.5 (d, *J* = 239.7 Hz), 122.2 (d, *J* = 28.0 Hz), 120.2 (dd, *J* = 12.7, 6.4 Hz), 118.2 (d, *J* = 25.9 Hz), 113.6 (dd, *J* = 23.5, 10.4 Hz).

Methyl 4-bromo-2,5-difluorobenzoate (5).



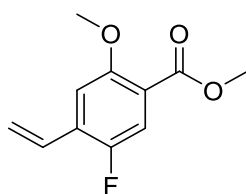
To a solution of 4-bromo-2,5-difluoro-benzoic acid (10.6 g, 44.7 mmol) in dry MeOH (140 mL) was added SOCl₂ (6.49 mL, 89.4 mmol) at 0 °C dropwise. After addition, the mixture was stirred at 70 °C for 3 h as indicated by TLC before the excess reagent was removed *in vacuo*. The residue was diluted with EtOAc and washed with saturated NaHCO₃ solution and brine. The organic phase was dried and concentrated *in vacuo* to give the desired compound as a yellow solid (10.4 g, 92%). HPLC: *t*_R 6.961 min, >95% purity (214 & 254 nm). ¹H NMR (CDCl₃) δ 7.70 (dd, *J* = 8.3, 6.0 Hz, 1H), 7.40 (dd, *J* = 9.3, 5.4 Hz, 1H), 3.94 (s, 3H). ¹³C NMR (CDCl₃) δ 163.2 (dd, *J* = 4.3, 1.8 Hz), 157.5 (dd, *J* = 230.2, 2.7 Hz), 155.1 (dd, *J* = 244.9, 2.8 Hz), 122.2 (d, *J* = 27.6 Hz), 119.1 – 118.2, 115.1 (d, *J* = 10.1 Hz), 114.8 (d, *J* = 9.8 Hz), 52.8.

Methyl 4-bromo-5-fluoro-2-methoxybenzoate (6).



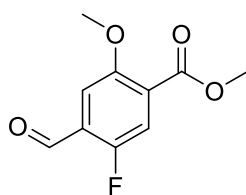
NaOMe (1.06 g, 19.6 mmol) (prepared from sodium metal (500 mg, 21.8 mmol) and MeOH (20 mL)) was introduced to a stirred solution of methyl 4-bromo-2,5-difluorobenzoate (4.09 g, 16.3 mmol) in anhydrous DMF (70 mL). The solution was stirred at rt for 16 h after which the reaction mixture was diluted with EtOAc (200 mL) and washed with H₂O (35 mL × 3). The organic layer was dried and concentrated *in vacuo* and the residue was purified by FCC (eluent, 1:10 EtOAc/PE) to afford the desired compound as a yellow crystalline solid (2.12 g, 52%). LCMS (*m/z*): 264.8 [M+H]⁺. HPLC: *t_R* 6.589 min, >95% purity (214 & 254 nm). ¹H NMR (CDCl₃) δ 7.58 (d, *J* = 8.6 Hz, 1H), 7.14 (d, *J* = 5.4 Hz, 1H), 3.88 (s, 3H), 3.88 (s, 3H). ¹³C NMR (CDCl₃) δ 164.3, 154.4, 154.2 (d, *J* = 243.8 Hz), 120.3 (d, *J* = 25.7 Hz), 118.4 (d, *J* = 6.0 Hz), 117.3, 116.05 (d, *J* = 23.1 Hz), 57.7.

Methyl 5-fluoro-2-methoxy-4-vinylbenzoate (7). A mixture of methyl 4-bromo-5-fluoro-2-



methoxybenzoate (1.14 g, 4.33 mmol), DMSO (15 mL), tributyl(vinyl)stannane (1.77 mL, 6.07 mmol) and trans-dichlorobis(triphenylphosphine) palladium(II) (456 mg, 650 μmol) was stirred under N₂ atmosphere at 80°C for 16 h and cooled. H₂O, EtOAc and PE (100, 140 and 70 mL, respectively) were added, the organic layer was separated and the aqueous phase extracted with a 2:1 mixture of EtOAc/PE. The organic layers were washed with H₂O, dried over anhydrous Na₂SO₄ and evaporated *in vacuo*. The resulting residue was purified by FCC (eluent, 1:5 EtOAc/PE). Fractions containing the target product were combined and evaporated *in vacuo* to give the title compound as a pale yellow oil (676 mg, 74%). LCMS (*m/z*): 211.1 [M+H]⁺. HRMS (*m/z*): C₁₁H₁₁FO₃: requires 211.0684. [M+H]⁺; found 211.0687. HPLC: *t_R* 6.636 min, >95% purity (214 & 254 nm). ¹H NMR (CDCl₃) δ 7.52 (d, *J* = 10.6 Hz, 1H), 7.02 (d, *J* = 5.9 Hz, 1H), 6.84 (dd, *J* = 17.7, 11.2 Hz, 1H), 5.91 (dd, *J* = 17.7, 0.7 Hz, 1H), 5.50 (dd, *J* = 11.2, 0.6 Hz, 1H), 3.91 (s, 3H), 3.88 (s, 3H). ¹³C NMR (101 MHz, CDCl₃) δ 165.2 (d, *J* = 2.2 Hz), 155.5 (s, *J* = 2.0 Hz), 153.7 (dd, *J* = 243.4, 1.5 Hz), 129.8 (d, *J* = 13.8 Hz), 128.9 (d, *J* = 3.0 Hz), 119.8 (d, *J* = 7.2 Hz), 118.9 (d, *J* = 5.0 Hz), 118.6, 110.3 (d, *J* = 3.5 Hz), 56.6, 52.1.

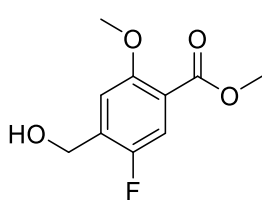
Methyl 5-fluoro-4-formyl-2-methoxybenzoate (8).



Methyl 5-fluoro-2-methoxy-4-vinylbenzoate (1.55 g, 7.37 mmol) was dissolved in DCM (25 mL) in a flask open to air. The reaction mixture was cooled to -78 °C and a stream of O₂(g) was passed through it for 5 min. At this time, O₃(g) was bubbled into the mixture until the color turned a dark brown/green and TLC indicated complete consumption of starting material. The resulting solution was then purged with O₂(g) for an additional 5 min before being treated with dimethylsulfide (1.64

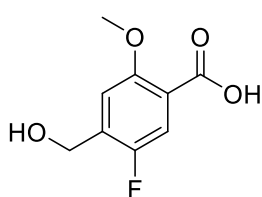
mL, 22.1 mmol) and allowed to warm to rt overnight. The mixture was concentrated *in vacuo* and purified using FCC (eluent, 3:1 DCM/PE) to afford the compound as a pale yellow solid (855 mg, 55 %). HRMS (*m/z*): C₁₅H₉F₂NO: requires 212.0481 [M+H]⁺; found 212.0479. HPLC: *t_R* 5.447 min, >95% purity (214 & 254 nm). ¹H NMR (CDCl₃) δ 10.37 (s, 1H), 7.58 (d, *J* = 10.0 Hz, 1H), 7.39 (d, *J* = 5.2 Hz, 1H), 3.93 (s, 3H), 3.93 (s, 3H). ¹³C NMR (CDCl₃) δ 186.5 (d, *J* = 6.1 Hz), 164.9 (d, *J* = 2.1 Hz), 158.3 (d, *J* = 252.3 Hz), 155.2 (d, *J* = 2.3 Hz), 127.2 (d, *J* = 7.5 Hz), 126.5 (d, *J* = 9.7 Hz), 119.6 (d, *J* = 24.4 Hz), 110.2 (d, *J* = 1.8 Hz), 56.8, 52.8.

Methyl 5-fluoro-4-(hydroxymethyl)-2-methoxybenzoate (9).



NaBH₄ (674 mg, 17.8 mmol) was added to a stirred solution of methyl 5-fluoro-4-formyl-2-methoxybenzoate (1.89 g, 8.91 mmol) in THF (70 mL). The reaction mixture was stirred for 2 h (TLC control). Sat. NaHCO₃ (50 mL) and EtOAc (100 mL) were added, the organic layer was separated and the aqueous phase extracted with EtOAc. The organic layer was dried over anhydrous Na₂SO₄ and evaporated *in vacuo*. The residue was purified by FCC (eluent, 1:1 EtOAc/PE). Fractions containing the target product were combined and evaporated *in vacuo* to afford the title compound as a translucent oil (1.75 g, 92%). LCMS (*m/z*): 214.9 [M+H]⁺. HPLC: *t_R* 4.787 min, >95% purity (214 & 254 nm). ¹H NMR (CDCl₃) δ 7.43 (d, *J* = 10.0 Hz, 1H), 7.06 (d, *J* = 5.7 Hz, 1H), 4.74 (s, 2H), 3.85 (s, 3H), 3.84 (s, 3H), 2.75 (s, 1H). ¹³C NMR (CDCl₃) δ 165.6, 155.8, 153.2 (d, *J* = 239.2 Hz), 133.9 (d, *J* = 16.3 Hz), 119.1 (d, *J* = 7.1 Hz), 117.9 (d, *J* = 24.8 Hz), 112.1 (d, *J* = 4.4 Hz), 58.7 (d, *J* = 3.9 Hz), 56.6, 52.3.

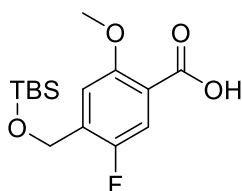
5-Fluoro-4-(hydroxymethyl)-2-methoxybenzoic acid (10).



A mixture of methyl 5-fluoro-4-(hydroxymethyl)-2-methoxybenzoate (2.00 g, 9.34 mmol), THF (40 mL), water (15 mL) and LiOH (483 mg, m 20.2 mmol) was stirred at rt for 3 h and then at 50°C for a further hour (TLC control). The organic solvent was evaporated under reduced pressure and the resulting aqueous solution acidified with concentrated HCl (~pH 1-2). The aqueous phase was then extracted with DCM (3 × 30 mL) and the organic extracts combined. Crystallisation of the product occurred upon standing at rt. The suspension was cooled to 0°C to induce further crystallisation of product. The crystals were collected under vacuum filtration and washed with ice cold DCM to afford a transparent crystalline solid. The aqueous phase was further extracted with EtOAc (2 × 25 mL), the organic extracts were dried over Na₂SO₄ and concentrated *in vacuo* to afford the corresponding free acid as a white solid (1.81 g, 97%). LCMS (*m/z*): 200.9 [M+H]⁺. HPLC: *t_R* 3.640 min, >95% purity (214 & 254 nm). ¹H NMR (MeOD) δ 7.48 (d, *J* = 10.1 Hz, 1H), 7.24 (d, *J* = 5.8 Hz, 1H), 4.70 (s, 2H),

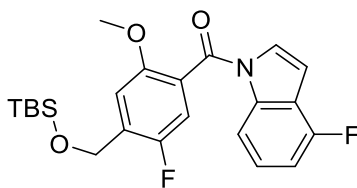
3.91 (s, 3H). ¹³C NMR (MeOD) δ 168.4 (d, *J* = 2.1 Hz), 156.9, 154.7 (d, *J* = 238.5 Hz), 135.8 (d, *J* = 16.6 Hz), 120.7 (d, *J* = 6.9 Hz), 118.6 (d, *J* = 24.9 Hz), 113.4 (d, *J* = 4.4 Hz), 58.6 (d, *J* = 4.0 Hz), 57.0.

4-(((*tert*-Butyldimethylsilyl)oxy)methyl)-5-fluoro-2-methoxybenzoic acid (11).



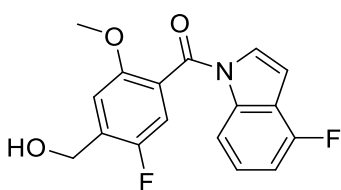
General procedure A using 5-fluoro-4-(hydroxymethyl)-2-methoxybenzoic acid. Purification by FCC (eluent, DCM/EtOAc, 70:30) gave 1.82 g of a white solid (69 %). (LCMS (*m/z*): 314.9 [M + H]⁺. HPLC: *t*_R 8.803 min, >95% purity (214 & 254 nm). ¹H NMR (CDCl₃) δ 7.64 (d, *J* = 10.0 Hz, 1H), 7.14 (d, *J* = 5.4 Hz, 1H), 4.69 (t, *J* = 1.0 Hz, 2H), 3.92 (s, 3H), 0.83 (s, 9H), -0.00 (s, 6H). ¹³C NMR (CDCl₃) δ 164.6, 154.5, 153.8 (d, *J* = 241.0 Hz), 136.7 (d, *J* = 16.7 Hz), 119.1 (d, *J* = 24.5 Hz), 116.9, 110.9 (d, *J* = 4.6 Hz), 58.8 (d, *J* = 4.2 Hz), 57.2, 25.9, -5.27.

(4-(((*tert*-Butyldimethylsilyl)oxy)methyl)-5-fluoro-2-methoxyphenyl)(4-fluoro-1*H*-indol-1-yl)methanone (12).



General procedure B using 4-(((*tert*-butyldimethylsilyl)oxy)methyl)-5-fluoro-2-methoxybenzoic. Purification with FCC (eluent, DCM/EtOAc, 3:1) gave a white solid (500 mg, 69%). LCMS (*m/z*): 432.3 [M + H]⁺. HPLC: *t*_R 9.373 min, >95% purity (214 & 254 nm). HRMS (*m/z*): C₂₃H₂₇F₂NO₃Si: requires 432.1813 [M+H]⁺; found 432.18.01. ¹H NMR (CDCl₃) δ 8.04 (d, *J* = 8.2 Hz, 1H), 7.13 (td, *J* = 8.2, 5.4 Hz, 1H), 7.06 (d, *J* = 5.5 Hz, 1H), 6.97 (d, *J* = 9.0 Hz, 1H), 6.87 (d, *J* = 3.8 Hz, 1H), 6.82 (ddd, *J* = 9.6, 8.1, 0.6 Hz, 1H), 6.49 (dd, *J* = 3.8, 0.5 Hz, 1H), 4.70 (s, 1H), 3.60 (s, 1H), 0.82 (s, *J* = 2.7 Hz, 4H), -0.00 (s, 2H). ¹³C NMR (CDCl₃) δ 166.0, 155.7 (d, *J* = 247.8 Hz), 153.3 (d, *J* = 239.3 Hz), 152.8, 137.7 (d, *J* = 9.2 Hz), 133.2 (d, *J* = 16.0 Hz), 127.4, 125.9 (d, *J* = 7.3 Hz), 123.2 (d, *J* = 6.9 Hz), 119.8 (d, *J* = 21.8 Hz), 115.7 (d, *J* = 24.8 Hz), 112.7 (d, *J* = 3.8 Hz), 110.9 (d, *J* = 4.7 Hz), 109.6 (d, *J* = 18.6 Hz), 104.5, 58.9 (d, *J* = 4.3 Hz), 56.3, 26.0, -5.2.

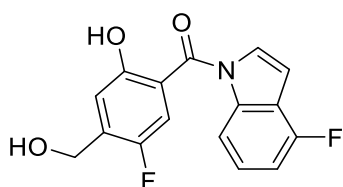
(4-Fluoro-1*H*-indol-1-yl)(5-fluoro-4-(hydroxymethyl)-2-methoxyphenyl)methanone (2).



General procedure C. Purification by FCC (eluent, DCM/EtOAc, 3:1) and recrystallization from DCM/PE gave a fluffy white solid (130 mg, 47%). LCMS (*m/z*): 318.1 [M + H]⁺. HPLC: *t*_R 7.093 min, >95% purity (214 & 254 nm). HRMS (*m/z*): C₁₇H₁₃F₂NO₃: requires 318.094 [M+H]⁺; found 318.0936. ¹H NMR (CDCl₃) δ 8.21 (d, *J* = 8.2 Hz, 1H), 7.31 (td, *J* = 8.2, 5.5 Hz, 1H), 7.16 (dd, *J* = 7.2, 4.3 Hz, 2H), 7.04 – 6.97 (m, 2H), 6.67 (dd, *J* = 3.8, 0.5 Hz, 1H), 4.85 (s, 2H), 3.78 (s, 3H), 2.18 (s, 1H). ¹³C NMR (CDCl₃) δ 165.9, 155.6 (d, *J* = 248.1 Hz), 153.8 (d, *J* = 241.3 Hz), 152.7 (d,

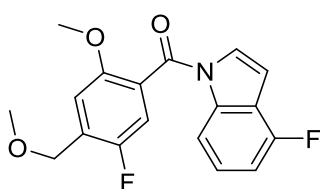
$J = 2.1$ Hz), 137.5 (d, $J = 9.2$ Hz), 132.2 (d, $J = 16.2$ Hz), 127.1, 125.9 (d, $J = 7.2$ Hz), 123.8 (d, $J = 6.9$ Hz), 119.7 (d, $J = 21.8$ Hz), 115.9 (d, $J = 25.1$ Hz), 112.6 (d, $J = 3.8$ Hz), 111.4 (d, $J = 4.5$ Hz), 109.6 (d, $J = 18.6$ Hz), 104.6, 58.8 (d, $J = 4.1$ Hz), 56.3.

(4-Fluoro-1*H*-indol-1-yl)(5-fluoro-2-hydroxy-4-(hydroxymethyl)phenyl)methanone (13).



To a solution of (4-fluoro-1*H*-indol-1-yl)(5-fluoro-4-(hydroxymethyl)-2-methoxyphenyl)methanone (75 mg, 236 μ mol) in DCM (10 mL) at 0 °C was added a solution of BBr₃ (1M in heptane) (1.18 mL, 1.18 mmol). The mixture was stirred at rt under a N₂ environment for three hours until TLC indicated complete consumption of the starting material. The reaction was poured into ice-water and the pH of the solution was adjusted to pH 6 by addition of saturated aqueous NaHCO₃. The DCM was removed under reduced pressure and the aqueous residue extracted with EtOAc (3 \times 20 mL). The combined organic extracts were washed with brine, dried (Na₂SO₄), filtered and concentrated *in vacuo*. The residue was purified by FCC (10:1 PE/EtOAc) to afford the title compound as a gold solid (51 mg, 71%). LCMS (m/z): 301.9 [M - H]⁺. HPLC: t_R 6.324 min, >95% purity (214 & 254 nm). HRMS (m/z): C₁₆H₁₁F₂NO₃: requires 302.0635 [M-H]⁻; found 302.0634. ¹H NMR (CDCl₃) δ 9.71 (s, 1H), 8.02 (d, $J = 8.3$ Hz, 1H), 7.42 (d, $J = 3.8$ Hz, 1H), 7.33 (td, $J = 8.2, 5.4$ Hz, 1H), 7.29 – 7.24 (m, $J = 9.0, 8.1$ Hz, 2H), 7.02 (ddd, $J = 9.5, 8.1, 0.6$ Hz, 1H), 6.82 (dd, $J = 3.8, 0.6$ Hz, 1H), 4.83 (d, $J = 2.8$ Hz, 2H), 1.95 (s, 1H). ¹³C NMR (101 MHz, CDCl₃) δ 169.6, 158.1, 155.9 (d, $J = 248.9$ Hz), 152.6 (d, $J = 240.1$ Hz), 138.1 (d, $J = 9.1$ Hz), 136.9 (d, $J = 16.6$ Hz), 127.3, 126.2 (d, $J = 7.4$ Hz), 119.7 (d, $J = 22.2$ Hz), 118.2 (d, $J = 4.2$ Hz), 116.3 (d, $J = 24.7$ Hz), 114.5 (d, $J = 6.9$ Hz), 112.3 (d, $J = 3.9$ Hz), 109.8 (d, $J = 18.6$ Hz), 105.2, 59.1 (d, $J = 3.9$ Hz).

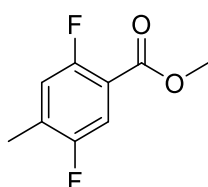
(4-Fluoro-1*H*-indol-1-yl)(5-fluoro-2-methoxy-4-(methoxymethyl)phenyl)methanone (14).



To a solution of (4-fluoro-1*H*-indol-1-yl)(5-fluoro-4-(hydroxymethyl)-2-methoxyphenyl)methanone (115 mg, 362 μ mol) in dry DCM (15 mL) was added Ag₂O (252 mg, 1.09 mmol) and MeI (135 μ L, 2.17 mmol). After stirring for 12 h at reflux temperature, additional MeI (1.35 μ L, 2.17 mmol) and Ag₂O (168 mg, 725 μ mol) was added. The reaction was stirred an additional 36 h at reflux and subsequently cooled. The mixture was filtered through Celite, evaporated under reduced pressure, and the residue purified by FCC (eluent, 1% MeOH/DCM) to afford the title compound as an opaque oil (113 mg, 94%). HRMS (m/z): C₁₈H₁₅F₂NO₃: requires 332.1098 [M+H]⁺; found 332.1093. LCMS (m/z): 331.9 [M+H]⁺. HPLC: t_R 7.842 min, >95% purity (214 & 254 nm). ¹H NMR (CDCl₃) δ 8.11 (d, $J = 8.2$ Hz, 1H), 7.19 (td, $J = 8.2, 5.4$ Hz, 1H), 7.07 (d, $J = 8.8$ Hz, 1H), 7.02 (d, $J = 5.4$ Hz, 1H), 6.92 (d, $J = 3.8$ Hz, 1H), 6.88 (ddd, $J = 9.6, 8.1, 0.6$ Hz, 1H), 6.55 (dd, $J = 3.8, 0.7$ Hz, 1H), 4.48 (dd,

$J = 1.2, 0.6$ Hz, 2H), 3.67 (s, 3H), 3.39 (s, 3H). ¹³C NMR (CDCl₃) δ 164.7, 154.5 (d, $J = 248.0$ Hz), 152.9 (d, $J = 241.7$ Hz), 151.6 (d, $J = 2.1$ Hz), 136.5 (d, $J = 9.3$ Hz), 128.7 (d, $J = 16.2$ Hz), 126.10, 124.8 (d, $J = 7.3$ Hz), 123.0 (d, $J = 7.0$ Hz), 118.6 (d, $J = 21.8$ Hz), 114.8 (d, $J = 25.4$ Hz), 111.5 (d, $J = 3.8$ Hz), 110.9 (d, $J = 4.3$ Hz), 108.4 (d, $J = 18.6$ Hz), 103.4, 66.6 (d, $J = 3.5$ Hz), 57.7, 55.3.

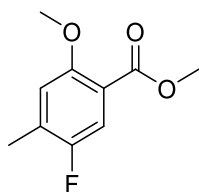
Methyl 2,5-difluoro-4-methylbenzoate (16).



To a solution of 4-bromo-2,5-difluoro-benzoic acid (15.0 g, 87.1 mmol) in dry MeOH (150 mL) was added SOCl₂ (12.6 mL, 174 mmol) at 0 °C dropwise. The mixture was stirred at 70 °C for 3 h and the excess reagent was removed *in vacuo*.

The residue was diluted with EtOAc and washed with saturated NaHCO₃ solution and brine. The organic phase was dried and concentrated to give 4-bromo-2,5-difluoro-benzoic acid methyl ester (14.5 g, 89%) as a darkened yellow oil that later solidified to give yellow crystals. LCMS (m/z): 186.9 [M+H]⁺. HPLC: t_R 6.579 min, >95% purity (214 & 254 nm). ¹H NMR (CDCl₃) δ 7.56 (dd, $J = 9.4, 5.9$ Hz, 1H), 6.97 (ddd, $J = 10.6, 6.0, 0.4$ Hz, 1H), 3.92 (s, 3H), 2.31 (d, $J = 1.7$ Hz, 3H). ¹³C NMR (CDCl₃) δ 164.0 (dd, $J = 4.2, 2.1$ Hz), 157.8 (dd, $J = 256.2, 2.4$ Hz), 156.7 (dd, $J = 242.1, 2.5$ Hz), 132.7 (dd, $J = 19.9, 8.9$ Hz), 119.5 (dd, $J = 24.9, 4.9$ Hz), 117.7 (dd, $J = 26.5, 1.8$ Hz), 116.9 (dd, $J = 12.1, 7.5$ Hz), 52.5, 15.0 (dd, $J = 3.0, 0.8$ Hz).

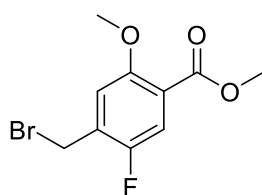
Methyl 4-bromo-5-fluoro-2-methoxybenzoate (17).



To a solution of methyl 4-bromo-2,5-difluorobenzoate (4.09 g, 16.3 mmol) in anhydrous DMF (70 mL) was added CH₃ONa (1.06 g, 19.6 mmol). The mixture solution was stirred at rt for 16 h. The reaction mixture was diluted with 200 mL EtOAc and washed with H₂O (35 mL \times 3). The organic layer was dried and

concentrated to be purified by FCC (eluent, 1:20 EtOAc/PE) to afford the title compound as a gold solid (14.2 g, 77%). LCMS (m/z): 199.0 [M+H]⁺. HPLC: t_R 6.324 min, >95% purity (214 & 254 nm). ¹H NMR (CDCl₃) δ 7.48 (d, $J = 9.7$ Hz, 1H), 6.77 (d, $J = 6.0$ Hz, 1H), 3.87 (s, 6H), 2.30 (d, $J = 1.8$ Hz, 3H). ¹³C NMR (CDCl₃) δ 165.6 (d, $J = 2.2$ Hz), 155.5 (d, $J = 2.0$ Hz), 154.8 (d, $J = 238.2$ Hz), 131.1, 130.9, 117.9 (d, $J = 25.6$ Hz), 115.2 (d, $J = 4.6$ Hz), 56.8, 52.2, 15.3 (d, $J = 3.0$ Hz).

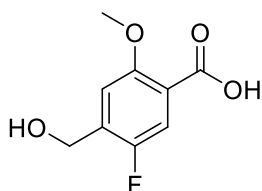
Methyl 4-(bromomethyl)-5-fluoro-2-methoxybenzoate (18).



General procedure D using methyl 4-bromo-5-fluoro-2-methoxybenzoate. The precipitated solid was collected by filtration, and dried under reduced pressure to give a white solid (2.45 g, 88%). LCMS (m/z): 277.0 [M+H]⁺. HPLC: t_R 6.486 min, >95% purity (214 & 254 nm). ¹H NMR (CDCl₃) δ 7.52 (d, $J = 9.7$ Hz, 1H), 6.97 (d, $J = 5.9$ Hz, 1H), 4.48 (d, $J = 1.0$ Hz, 2H), 3.90 (s, 3H), 3.89 (s, 3H). ¹³C NMR

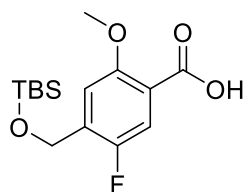
(CDCl₃) δ 165.2 (d, J = 2.1 Hz), 155.6 (d, J = 2.3 Hz), 153.9 (d, J = 243.6 Hz), 130.1 (d, J = 16.2 Hz), 121.3 (d, J = 7.0 Hz), 118.8 (d, J = 24.9 Hz), 114.6 (d, J = 2.8 Hz), 56.9, 52.5, 24.9 (d, J = 3.8 Hz).

5-Fluoro-4-(hydroxymethyl)-2-methoxybenzoic acid (19).



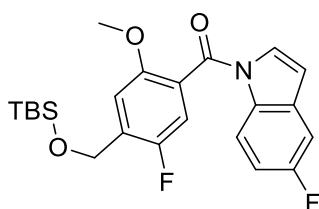
A mixture of methyl 4-(bromomethyl)-5-fluoro-2-methoxybenzoate (1.05 g, 3.79 mmol), THF (20 mL), H₂O (10 mL) and NaOH (758 mg, 19.0 mmol) was stirred at 60 °C for 8 h. The organic solvent was evaporated under reduced pressure and the resulting aqueous solution acidified with concentrated HCl (~pH 1-2). The aqueous phase was then extracted with DCM (3 x 30 mL) and the organic extracts combined and evaporated to dryness to afford the title compound as a white solid (685 mg, 90%). LCMS (m/z): 200.9 [M+H]⁺. HPLC: t_R 3.640 min, >95% purity (214 & 254 nm). ¹H NMR (MeOD) δ 7.48 (d, J = 10.1 Hz, 1H), 7.24 (d, J = 5.8 Hz, 1H), 4.70 (s, 2H), 3.91 (s, 3H). ¹³C NMR (MeOD) δ 168.4 (d, J = 2.1 Hz), 156.9, 154.7 (d, J = 238.5 Hz), 135.8 (d, J = 16.6 Hz), 120.7 (d, J = 6.9 Hz), 118.6 (d, J = 24.9 Hz), 113.4 (d, J = 4.4 Hz), 58.6 (d, J = 4.0 Hz), 57.0.

4-(((tert-Butyldimethylsilyl)oxy)methyl)-5-fluoro-2-methoxybenzoic acid (20).



General procedure A using 5-fluoro-4-(hydroxymethyl)-2-methoxybenzoic acid. Purification by FCC (eluent, DCM/EtOAc, 70:30) gave a white solid (1.66 g, 74 %). (LCMS (m/z): 314.9 [M+H]⁺. HPLC: t_R 8.803 min, >95% purity (214 & 254 nm). ¹H NMR (CDCl₃) δ 7.64 (d, J = 10.0 Hz, 1H), 7.14 (d, J = 5.4 Hz, 1H), 4.69 (t, J = 1.0 Hz, 2H), 3.92 (s, 3H), 0.83 (s, 9H), -0.00 (s, 6H). ¹³C NMR (CDCl₃) δ 164.6, 155.0, 154.6 (d, J = 1.9 Hz), 152.6, 136.7 (d, J = 16.7 Hz), 119.1 (d, J = 24.5 Hz), 116.9, 110.9 (d, J = 4.6 Hz), 58.8 (d, J = 4.2 Hz), 57.2, 25.9, -5.27.

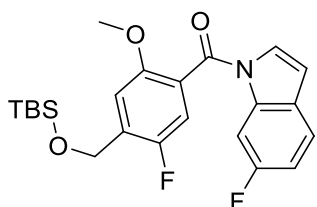
(4-(((tert-Butyldimethylsilyl)oxy)methyl)-5-fluoro-2-methoxyphenyl)(5-fluoro-1H-indol-1-yl)methanone (21).



General procedure B. Purification with FCC (eluent, DCM /EtOAc, 3:1) gave a white solid (101 mg, 72%). LCMS (m/z): 432.3 [M+H]⁺. HPLC: t_R 9.373 min, >95% purity (214 & 254 nm). ¹H NMR (CDCl₃) δ 8.43 (d, J = 8.2 Hz, 1H), 7.43 (td, J = 8.2, 5.4 Hz, 1H), 7.21 (d, J = 5.3 Hz, 1H), 7.01 (d, J = 9.0 Hz, 1H), 6.95 (d, J = 3.7 Hz, 1H), 6.88 (ddd, J = 10.1, 8.1, 0.8 Hz, 1H), 6.55 (dd, J = 3.9, 0.6 Hz, 1H), 4.72 (s, 1H), 3.70 (s, 1H), 0.88 (s, J = 2.9 Hz, 4H), -0.00 (s, 2H). ¹³C NMR (CDCl₃) δ 168.2, 156.4 (d, J = 247.6 Hz), 152.1 (d, J = 72.2 Hz), 138.2 (d, J = 9.2 Hz), 134.5 (d, J = 16.0 Hz), 128.1, 125.9 (d, J = 7.7 Hz), 123.9 (d, J = 6.9 Hz), 121.3 (d, J = 22.8 Hz),

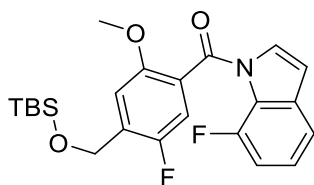
116.8 (d, $J = 24.9$ Hz), 111.7 (d, $J = 3.8$ Hz), 111.1 (d, $J = 4.9$ Hz), 109.2 (d, $J = 18.6$ Hz), 105.5, 59.2 (d, $J = 4.8$ Hz), 56.3, 28.0, -5.2.

(4-(((*tert*-Butyldimethylsilyl)oxy)methyl)-5-fluoro-2-methoxyphenyl)(6-fluoro-1*H*-indol-1-yl)methanone (22).



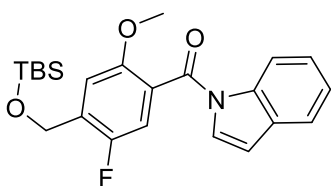
General procedure B. Purification with FCC (eluent, DCM /EtOAc, 3:1) gave a white solid (167 mg, 68%). LCMS (m/z): 432.3 $[M+H]^+$. HPLC: t_R 9.373 min, >95% purity (214 & 254 nm). ¹H NMR (CDCl₃) δ 8.21 (d, $J = 9.7$ Hz, 1H), 7.48 (dd, $J = 8.5, 5.3$ Hz, 1H), 7.23 (d, $J = 5.5$ Hz, 1H), 7.13 (d, $J = 9.0$ Hz, 1H), 7.05 (dd, $J = 10.9, 3.1$ Hz, 2H), 6.53 (d, $J = 3.5$ Hz, 2H), 4.97 – 4.72 (m, 2H), 3.78 (s, 3H), 1.00 (s, 9H), 0.17 (s, 6H). ¹³C NMR (CDCl₃) δ 167.5, 156.8, 155.2 (d, $J = 247.7$ Hz), 146.9, 137.8 (d, $J = 9.3$ Hz), 130.8, 127.7, 126.6 (d, $J = 7.3$ Hz), 122.7, 122.4, 121.8, 119.4, 114.3 (d, $J = 3.8$ Hz), 109.3 (d, $J = 18.5$ Hz), 109.1, 104.0, 64.6, 55.8, 26.1, -5.1.

(4-(((*tert*-Butyldimethylsilyl)oxy)methyl)-5-fluoro-2-methoxyphenyl)(7-fluoro-1*H*-indol-1-yl)methanone (23).



General procedure B. Purification with FCC (eluent, DCM /EtOAc, 3:1) gave a transparent oil (142 mg, 62%). LCMS (m/z): 432.3 $[M+H]^+$. HPLC: t_R 9.373 min, >95% purity (214 & 254 nm). ¹H NMR (CDCl₃) δ 8.04 (d, $J = 8.2$ Hz, 1H), 7.13 (td, $J = 8.2, 5.4$ Hz, 1H), 7.06 (d, $J = 5.5$ Hz, 1H), 6.97 (d, $J = 9.0$ Hz, 1H), 6.87 (d, $J = 3.8$ Hz, 1H), 6.82 (ddd, $J = 9.6, 8.1, 0.6$ Hz, 1H), 6.49 (dd, $J = 3.8, 0.5$ Hz, 1H), 4.70 (s, 1H), 3.60 (s, 1H), 0.82 (s, $J = 2.7$ Hz, 4H), -0.00 (s, 2H). ¹³C NMR (CDCl₃) δ 167.2, 157.4 (d, $J = 247.8$ Hz), 152.4 (d, $J = 72.2$ Hz), 137.7 (d, $J = 9.2$ Hz), 133.2 (d, $J = 16.0$ Hz), 127.4, 125.9 (d, $J = 7.3$ Hz), 123.2 (d, $J = 6.9$ Hz), 119.8 (d, $J = 21.8$ Hz), 115.7 (d, $J = 24.8$ Hz), 112.7 (d, $J = 3.8$ Hz), 110.9 (d, $J = 4.7$ Hz), 109.6 (d, $J = 18.6$ Hz), 104.5, 58.9 (d, $J = 4.3$ Hz), 56.3, 26.0, -5.2.

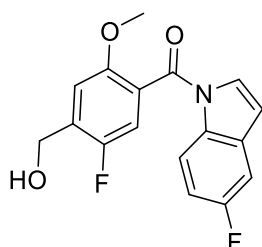
(4-(((*tert*-Butyldimethylsilyl)oxy)methyl)-5-fluoro-2-methoxyphenyl)(1*H*-indol-1-yl)methanone (24).



General procedure B. Purification with FCC (eluent, DCM /EtOAc, 3:1) gave 165 mg of a white solid (62%). LCMS (m/z): 414.2 $[M+H]^+$. HPLC: t_R 6.664 min, >95% purity (214 & 254 nm). ¹H NMR (CDCl₃) δ 8.27 (d, $J = 7.7$ Hz, 1H), 7.39 (d, $J = 7.5$ Hz, 1H), 7.23 – 7.17 (m, 1H), 7.13 (td, $J = 7.5, 1.0$ Hz, 1H), 7.06 (d, $J = 5.5$ Hz, 1H), 6.96 (d, $J = 9.1$ Hz, 1H), 6.89 (d, $J = 3.7$ Hz, 1H), 6.39 (d, $J = 3.8$ Hz, 1H), 4.70 (s, 2H), 3.60 (s, 3H), 0.82 (s, 9H), -0.00 (s, 6H). ¹³C NMR (CDCl₃) δ 165.9,

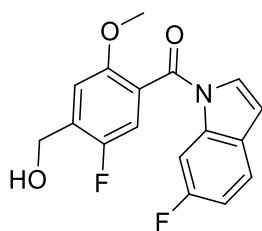
153.3 (d, $J = 240.4$ Hz), 152.8 (d, $J = 2.0$ Hz), 135.7, 132.8 (d, $J = 16.0$ Hz), 131.1, 127.4, 125.1, 124.2, 120.9, 116.6, 115.6 (d, $J = 24.8$ Hz), 110.9 (d, $J = 4.6$ Hz), 109.1, 58.9 (d, $J = 4.3$ Hz), 56.3, 26.0, 18.5, -5.2.

(5-Fluoro-1*H*-indol-1-yl)(5-fluoro-2-methoxy-4-(methoxymethyl)phenyl)methanone (21a).



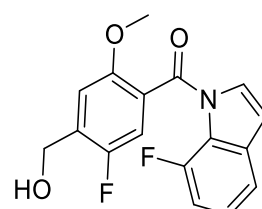
General procedure C. Purification by FCC (eluent, DCM/EtOAc, 3:1) and recrystallization from DCM/PE gave a white solid (62 mg, 85%). LCMS (m/z): 318.1 [M+H]⁺. HPLC: t_R 7.090 min, >95% purity (214 & 254 nm). HRMS (m/z): C₁₇H₁₃F₂NO₃: requires 318.094 [M+H]⁺; found 318.0934. ¹H NMR (CDCl₃) δ 8.42 (d, $J = 3.9$ Hz, 1H), 7.22 (dd, $J = 8.7, 2.5$ Hz, 1H), 7.18 – 7.14 (m, 2H), 7.13 – 7.05 (m, 2H), 6.52 (dd, $J = 3.8, 0.5$ Hz, 1H), 4.85 (d, $J = 5.6$ Hz, 2H), 3.79 (s, 3H), 2.01 (t, $J = 5.9$ Hz, 1H). ¹³C NMR (CDCl₃) δ 165.5, 160.1 (d, $J = 240.8$ Hz), 155.1, 152.8 (d, $J = 2.1$ Hz), 152.7, 132.2 (d, $J = 10.1$ Hz), 132.0 (d, $J = 2.7$ Hz), 131.9, 128.8, 117.7 (d, $J = 9.0$ Hz), 116.0 (d, $J = 25.1$ Hz), 112.8 (d, $J = 24.8$ Hz), 111.6 (d, $J = 4.5$ Hz), 108.9 (d, $J = 3.9$ Hz), 106.7 (d, $J = 24.0$ Hz), 59.1 (d, $J = 4.1$ Hz), 56.5.

(6-Fluoro-1*H*-indol-1-yl)(5-fluoro-2-methoxy-4-(methoxymethyl)phenyl)methanone (22a).



General procedure C. Purification by FCC (eluent, DCM/EtOAc, 3:1) and recrystallization from DCM/PE gave a white solid (45 mg, 51%). LCMS (m/z): 318.1 [M+H]⁺. HPLC: t_R 7.091 min, >95% purity (214 & 254 nm). HRMS (m/z): C₁₇H₁₃F₂NO₃: requires 318.094 [M+H]⁺; found 318.0932. ¹H NMR (MeOD) δ 7.38 (dd, $J = 7.8, 0.7$ Hz, 1H), 7.29 (d, $J = 2.8$ Hz, 1H), 7.27 (d, $J = 3.9$ Hz, 2H), 7.26 – 7.21 (m, 1H), 7.02 (ddd, $J = 12.2, 8.0, 0.6$ Hz, 1H), 6.67 (dd, $J = 3.7, 1.9$ Hz, 1H), 4.75 (s, 2H), 3.73 (s, 3H). ¹³C NMR (MeOD) δ 165.8, 155.1 (d, $J = 239.6$ Hz), 155.1, 151.7 (d, $J = 252.1$ Hz), 136.6 (d, $J = 4.1$ Hz), 135.3 (d, $J = 16.5$ Hz), 130.2, 125.8 (d, $J = 7.0$ Hz), 124.6 (d, $J = 3.3$ Hz), 124.5 (d, $J = 3.3$ Hz), 118.0 (d, $J = 3.7$ Hz), 117.6 (d, $J = 25.4$ Hz), 113.0 (d, $J = 4.5$ Hz), 112.5 (d, $J = 21.4$ Hz), 109.7 (d, $J = 1.7$ Hz), 58.6 (d, $J = 4.2$ Hz), 56.8.

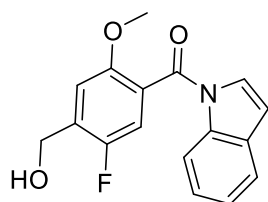
(7-Fluoro-1*H*-indol-1-yl)(5-fluoro-2-methoxy-4-(methoxymethyl)phenyl)methanone (23a).



General procedure C. Purification by FCC (eluent, DCM/EtOAc, 3:1) and recrystallization from DCM/PE gave 69 mg of a white solid (82%). LCMS (m/z): 318.1 [M+H]⁺. HPLC: t_R 7.088 min, >95% purity (214 & 254 nm). HRMS (m/z): C₁₇H₁₃F₂NO₃: requires 318.094 [M+H]⁺; found 318.0931. ¹H NMR (CDCl₃) δ 8.20 (d, $J = 9.7$ Hz, 1H), 7.48 (dd, $J = 8.6, 5.3$ Hz, 1H), 7.16 (d, $J = 3.5$ Hz, 1H), 7.14 (s, 1H), 7.07 (ddd, $J = 9.1, 8.6, 2.4$ Hz, 1H), 7.00 (d, $J = 3.8$ Hz, 1H), 6.53 (dd, $J = 3.8, 0.6$ Hz,

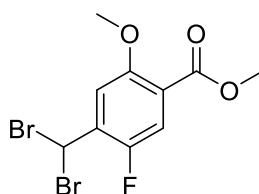
1H), 4.85 (s, 2H), 3.78 (s, 3H), 2.18 (s, 1H). ¹³C NMR (CDCl₃) δ 165.9 (d, *J* = 1.5 Hz), 161.4 (d, *J* = 241.1 Hz), 153.8 (d, *J* = 241.3 Hz), 152.7, 135.7 (d, *J* = 12.9 Hz), 132.1 (d, *J* = 16.2 Hz), 127.5 (d, *J* = 4.0 Hz), 123.9 (d, *J* = 6.9 Hz), 121.5 (d, *J* = 9.8 Hz), 115.9 (d, *J* = 25.1 Hz), 112.4 (d, *J* = 24.2 Hz), 111.5 (d, *J* = 4.5 Hz), 108.9, 104.2 (d, *J* = 28.7 Hz), 58.9 (d, *J* = 4.1 Hz), 56.4.

(5-Fluoro-4-(hydroxymethyl)-2-methoxyphenyl)(1*H*-indol-1-yl)methanone (24a).



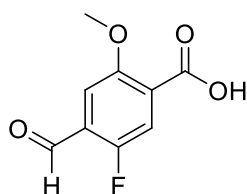
General procedure C. Purification by FCC (eluent, DCM/EtOAc, 3:1) and recrystallization from DCM/PE gave 42 mg of a white solid (74%). LCMS (*m/z*): 300.1 [M+H]⁺. HPLC: *t_R* 6.994 min, >95% purity (214 & 254 nm). HRMS (*m/z*): C₁₇H₁₃F₂NO₃: requires 300.0958 [M+H]⁺; found 300.0949. ¹H NMR (CDCl₃) δ 8.21 (d, *J* = 8.2 Hz, 1H), 7.31 (td, *J* = 8.2, 5.4 Hz, 1H), 7.16 (dd, *J* = 7.2, 4.6 Hz, 2H), 7.04 – 6.97 (m, 3H), 6.67 (dd, *J* = 3.8, 0.5 Hz, 1H), 4.85 (d, *J* = 3.0 Hz, 2H), 3.79 (s, *J* = 2.2 Hz, 3H), 2.08 (s, 1H). ¹³C NMR (CDCl₃) δ 165.9, 156.9, 154.8 (d, *J* = 239.2 Hz), 152.8 (d, *J* = 2.1 Hz), 152.7, 137.7 (d, *J* = 9.3 Hz), 132.2 (d, *J* = 16.2 Hz), 127.2, 126.1 (d, *J* = 7.3 Hz), 124.0 (d, *J* = 7.0 Hz), 119.8 (d, *J* = 21.8 Hz), 116.0 (d, *J* = 25.2 Hz), 112.7 (d, *J* = 3.9 Hz), 111.6 (d, *J* = 4.4 Hz), 109.7 (d, *J* = 18.6 Hz), 104.7, 59.1 (d, *J* = 4.1 Hz), 56.5.

Methyl 4-(dibromomethyl)-5-fluoro-2-methoxybenzoate (25). Product isolated from bromination



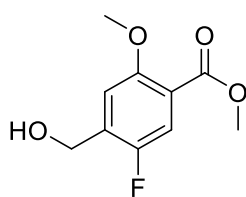
of methyl 5-fluoro-2-methoxy-4-methylbenzoate as a transparent oil (2.26 g, 25 %) (17). LCMS (*m/z*): 354.9 [M+H]⁺. HPLC: *t_R* 6.599 min, >95% purity (214 & 254 nm). ¹H NMR (CDCl₃) δ 7.46 (d, *J* = 10.0 Hz, 1H), 7.38 (d, *J* = 5.8 Hz, 1H), 6.89 (s, 1H), 3.97 (d, *J* = 6.3 Hz, 3H), 3.89 (s, 3H). ¹³C NMR (CDCl₃) δ 164.8, 155.8 (d, *J* = 2.2 Hz), 149.9 (d, *J* = 244.5 Hz), 133.3 (d, *J* = 13.7 Hz), 122.7 (d, *J* = 6.9 Hz), 118.7 (d, *J* = 25.0 Hz), 113.6, 56.9, 52.6, 34.0.

5-Fluoro-4-formyl-2-methoxybenzoic acid (26).



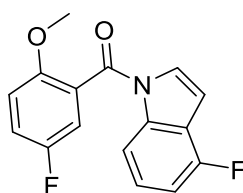
Methyl 4-(dibromomethyl)-5-fluoro-2-methoxybenzoate (2.25 g, 6.32 mmol) was taken up in DMSO (20 mL) and heated to 120 °C for 24 h. The reaction was diluted with EtOAc (50 mL) and washed with H₂O (4 × 35 mL), followed by brine (40 mL). The organic layer was dried (Na₂SO₄) and evaporated to dryness to give a brown residue which was purified by FCC (eluent, PE/EtOAc 10:1) to afford the title compound as a white solid (1.05 g, 84%). ¹H NMR (CDCl₃) δ 10.38 (s, 1H), 7.96 (d, *J* = 10.0 Hz, 1H), 7.50 (d, *J* = 5.0 Hz, 1H), 4.10 (s, 3H). ¹³C NMR (CDCl₃) δ 186.2 (d, *J* = 5.9 Hz), 164.2 (d, *J* = 1.7 Hz), 158.9 (d, *J* = 253.9 Hz), 154.5 (d, *J* = 2.4 Hz), 127.7 (d, *J* = 10.4 Hz), 124.6 (d, *J* = 7.6 Hz), 121.7 (d, *J* = 24.6 Hz), 110.6 (d, *J* = 1.8 Hz), 57.6.

5-Fluoro-4-(hydroxymethyl)-2-methoxybenzoic acid (27).



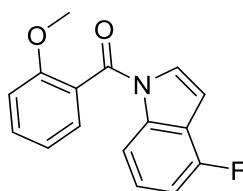
NaBH₄ (267 mg, 7.07 mmol) was added to a stirred solution of 5-fluoro-4-formyl-2-methoxybenzoic acid (1.00 g, 4.71 mmol) in MeOH (15 mL) at rt and the reaction was stirred for 3 h. The mixture was quenched with H₂O (5 mL) and evaporated to remove the MeOH. The residue was diluted with saturated aqueous NaHCO₃ solution and extracted with EtOAc (2 × 25 mL). The EtOAc extracts were washed with brine (30 mL), dried (Na₂SO₄) and evaporated to dryness to afford the compound as a white solid (949 mg, 94%). LCMS (*m/z*): 214.9 [M+H]⁺. HPLC: *t*_R 4.787 min, >95% purity (214 & 254 nm). ¹H NMR (CDCl₃) δ 7.43 (d, *J* = 10.0 Hz, 1H), 7.06 (d, *J* = 5.7 Hz, 1H), 4.74 (s, 2H), 3.85 (s, 3H), 3.84 (s, 3H), 2.75 (s, 1H). ¹³C NMR (CDCl₃) δ 165.6, 155.8, 153.2 (d, *J* = 239.2 Hz), 133.9 (d, *J* = 16.3 Hz), 119.1 (d, *J* = 7.1 Hz), 117.9 (d, *J* = 24.8 Hz), 112.1 (d, *J* = 4.4 Hz), 58.7 (d, *J* = 3.9 Hz), 56.6, 52.3.

(4-Fluoro-1*H*-indol-1-yl)(5-fluoro-2-methoxyphenyl)methanone (28a).



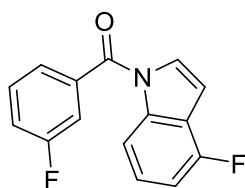
General procedure B. Purification with FCC (eluent, CHCl₃/PE, 3:1) gave 201 mg of a white solid (79%). LCMS (*m/z*): 287.9 [M+H]⁺. HPLC: *t*_R 7.796 min, >95% purity (214 & 254 nm). HRMS (*m/z*): C₁₆H₁₁F₂NO₂: requires 288.0835 [M+H]⁺; found 288.083. ¹H NMR (CDCl₃) δ 8.22 (d, *J* = 8.1 Hz, 1H), 7.31 (td, *J* = 8.2, 5.4 Hz, 1H), 7.26 – 7.21 (m, 1H), 7.19 (dd, *J* = 7.7, 2.9 Hz, 1H), 7.04 – 6.94 (m, 3H), 6.67 (dd, *J* = 3.8, 0.6 Hz, 1H), 3.76 (s, 3H). ¹³C NMR (CDCl₃) δ 165.9, 156.8 (d, *J* = 241.9 Hz), 155.7 (d, *J* = 248.1 Hz), 152.7, 137.7 (d, *J* = 9.2 Hz), 127.2, 126.1 (d, *J* = 7.3 Hz), 125.4 (d, *J* = 7.0 Hz), 118.8 (d, *J* = 22.9 Hz), 116.2 (d, *J* = 25.1 Hz), 112.9 (d, *J* = 7.8 Hz), 112.7 (d, *J* = 3.9 Hz), 109.7 (d, *J* = 18.6 Hz), 104.7, 56.5.

(4-Fluoro-1*H*-indol-1-yl)(2-methoxyphenyl)methanone (29a).



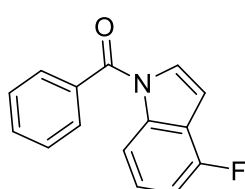
General procedure B. Purification with FCC (eluent, CHCl₃/PE, 3:1) gave a white solid (164 mg, 62%). LCMS (*m/z*): 269.9 [M+H]⁺. HPLC: *t*_R 7.726 min, >95% purity (214 & 254 nm). HRMS (*m/z*): C₁₆H₁₂FNO₂: requires 270.0929 [M+H]⁺; found 270.0925. ¹H NMR (CDCl₃) δ 8.22 (d, *J* = 7.9 Hz, 1H), 7.52 (t, *J* = 7.8 Hz, 1H), 7.45 (d, *J* = 6.6 Hz, 1H), 7.33 – 7.23 (m, 2H), 7.09 (t, *J* = 7.4 Hz, 1H), 7.05 – 6.95 (m, 3H), 6.7 (d, *J* = 3.5 Hz, 1H), 3.78 (s, 3H). ¹³C NMR (CDCl₃) δ 167.4, 156.5, 155.7 (d, *J* = 248.0 Hz), 132.6, 129.3, 127.54, 125.9 (d, *J* = 7.3 Hz), 124.6, 121.1, 119.8 (d, *J* = 21.8 Hz), 112.7, 111.7, 109.4 (d, *J* = 18.5 Hz), 104.2, 55.9.

(4-Fluoro-1*H*-indol-1-yl)(3-fluorophenyl)methanone (30a).



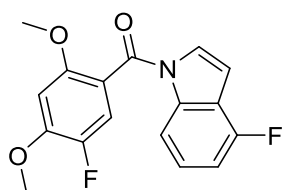
General procedure B. Purification with FCC (eluent, CHCl₃/PE, 3:1) gave 130 mg of a white solid (47%). General procedure B. LCMS (*m/z*): 257.9 [M+H]⁺. HPLC: *t_R* 7.898 min, >95% purity (214 & 254 nm). HRMS (*m/z*): C₁₅H₉F₂NO: requires 258.0729 [M+H]⁺; found 258.0725. ¹H NMR (CDCl₃) δ 8.17 (d, *J* = 8.3 Hz, 1H), 7.54 – 7.51 (m, 2H), 7.47 – 7.44 (m, 1H), 7.35 – 7.30 (m, 2H), 7.25 (d, *J* = 3.8 Hz, 1H), 7.01 (ddd, *J* = 9.6, 8.1, 0.6 Hz, 1H), 6.74 (dd, *J* = 3.8, 0.7 Hz, 1H). ¹³C NMR (CDCl₃) δ 167.3, 162.6 (d, *J* = 249.5 Hz), 155.8 (d, *J* = 248.4 Hz), 138.2 (d, *J* = 9.1 Hz), 136.3 (d, *J* = 7.1 Hz), 130.7 (d, *J* = 8.0 Hz), 127.3, 126.2 (d, *J* = 7.3 Hz), 125.1 (d, *J* = 3.2 Hz), 119.4 (d, *J* = 21.2 Hz), 116.5 (d, *J* = 23.4 Hz), 112.6 (d, *J* = 3.9 Hz), 109.7 (d, *J* = 18.5 Hz), 104.7.

(4-Fluoro-1*H*-indol-1-yl)(phenyl)methanone (31a).



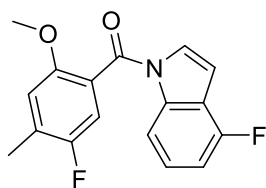
General procedure B. Purification with FCC (eluent, CHCl₃/PE, 3:1) gave a white solid (135 mg, 60%). LCMS (*m/z*): 239.9 [M+H]⁺. HPLC: *t_R* 7.841 min, >95% purity (214 & 254 nm). HRMS (*m/z*): C₁₅H₁₀FNO: requires 239.0759 [M+H]⁺; found 239.0741. ¹H NMR (CDCl₃) δ 8.18 (d, *J* = 8.3 Hz, 1H), 7.76 – 7.72 (m, 2H), 7.64 – 7.59 (m, 1H), 7.56 – 7.50 (m, 2H), 7.34 – 7.26 (m, 2H), 7.00 (ddd, *J* = 9.6, 8.1, 0.7 Hz, 1H), 6.72 (dd, *J* = 3.8, 0.7 Hz, 1H). ¹³C NMR (CDCl₃) δ 168.8 (C), 155.8 (d, *J* = 248.1 Hz), 138.3 (d, *J* = 9.2 Hz), 134.4, 132.3, 129.4, 128.8, 127.7, 125.9 (d, *J* = 7.3 Hz), 119.7 (d, *J* = 21.8 Hz), 112.6 (d, *J* = 3.9 Hz), 109.4 (d, *J* = 18.5 Hz), 104.2.

(4-Fluoro-1*H*-indol-1-yl)(5-fluoro-2,4-dimethoxyphenyl)methanone (32a).



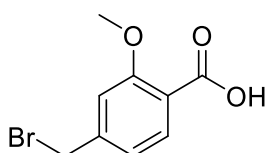
General procedure B. Purification with FCC (eluent, CHCl₃/PE, 3:1) gave a white solid (122 mg, 72%). LCMS (*m/z*): 318.1 [M+H]⁺. HPLC: *t_R* 7.761 min, >95% purity (214 & 254 nm). HRMS (*m/z*): C₁₇H₁₃F₂NO₃: requires 318.094 [M+H]⁺; 318.0936. ¹H NMR (CDCl₃) δ 8.17 (d, *J* = 8.3 Hz, 1H), 7.32 – 7.27 (m, 1H), 7.24 (d, *J* = 10.7 Hz, 1H), 7.08 (d, *J* = 3.8 Hz, 1H), 6.98 (ddd, *J* = 9.6, 8.1, 0.7 Hz, 1H), 6.66 (dd, *J* = 3.8, 0.5 Hz, 1H), 6.61 (d, *J* = 6.7 Hz, 1H), 3.99 (s, 1H), 3.77 (s, 1H). ¹³C NMR (CDCl₃) δ 165.9, 155.7 (d, *J* = 247.8 Hz), 153.8 (d, *J* = 2.0 Hz), 150.9 (d, *J* = 11.7 Hz), 146.7 (d, *J* = 241.4 Hz), 137.8 (d, *J* = 9.4 Hz), 127.5, 125.8 (d, *J* = 7.3 Hz), 119.8 (d, *J* = 21.9 Hz), 117.1 (d, *J* = 21.4 Hz), 115.7 (d, *J* = 5.4 Hz), 112.6 (d, *J* = 3.8 Hz), 109.4 (d, *J* = 18.6 Hz), 104.2, 98.3, 56.7, 56.6.

(4-Fluoro-1*H*-indol-1-yl)(5-fluoro-2-methoxy-4-methylphenyl)methanone (33a).



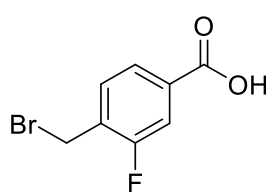
General procedure B. Purification with FCC (eluent, CHCl₃/PE, 3:1) gave a white solid (175 mg, 64%). LCMS (*m/z*): 301.9 [M+H]⁺. HPLC: *t_R* 7.827 min, >95% purity (214 & 254 nm). HRMS (*m/z*): C₁₇H₁₃F₂NO₂: requires 302.0993 [M+H]⁺; 302.0987. ¹H NMR (CDCl₃) δ 8.22 (d, *J* = 8.2 Hz, 1H), 7.30 (td, *J* = 8.2, 5.4 Hz, 1H), 7.14 (d, *J* = 8.7 Hz, 1H), 7.05 (d, *J* = 3.8 Hz, 1H), 6.99 (dd, *J* = 9.3, 8.4 Hz, 1H), 6.83 (d, *J* = 5.8 Hz, 1H), 6.66 (dd, *J* = 3.8, 0.6 Hz, 1H), 3.75 (s, 3H), 2.37 (d, *J* = 1.9 Hz, 3H). ¹³C NMR (CDCl₃) δ 166.1, 155.6 (d, *J* = 247.8 Hz), 155.3 (d, *J* = 240.1 Hz), 152.4 (d, *J* = 2.2 Hz), 137.7 (d, *J* = 9.4 Hz), 129.5 (d, *J* = 18.7 Hz), 127.4, 125.9 (d, *J* = 7.3 Hz), 122.6 (d, *J* = 6.8 Hz), 119.8 (d, *J* = 21.8 Hz), 115.9 (d, *J* = 26.1 Hz), 114.5 (d, *J* = 4.6 Hz), 112.7 (d, *J* = 3.9 Hz), 109.5 (d, *J* = 18.5 Hz), 104.4, 56.4, 15.4 (d, *J* = 3.2 Hz).

4-(Bromomethyl)-2-methoxybenzoic acid (35a).



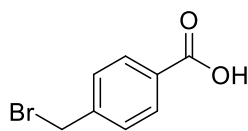
General procedure D. The precipitated solid was collected by filtration, and dried under reduced pressure to give 1.10 g of a white solid (74%). LCMS (*m/z*): 244.8 [M+H]⁺. HPLC: *t_R* 5.309 min, >95% purity (214 & 254 nm). ¹H NMR (CDCl₃) δ 8.13 (d, *J* = 8.0 Hz, 1H), 7.14 (dd, *J* = 8.0, 1.5 Hz, 1H), 7.09 (d, *J* = 1.3 Hz, 1H), 4.48 (s, 2H), 4.10 (s, 3H). ¹³C NMR (CDCl₃) δ 165.0, 158.3, 145.2, 134.5, 122.7, 117.7, 112.4, 56.9, 31.9.

4-(Bromomethyl)-3-fluorobenzoic acid (35b).



General procedure D. The precipitated solid was collected by filtration, and dried under reduced pressure to give 1.33 g of a white solid (70%). LCMS (*m/z*): 232.9 [M-H]⁻. HPLC: *t_R* 5.796 min, >95% purity (214 & 254 nm). ¹H NMR (CDCl₃) δ 7.89 (dd, *J* = 8.0, 1.5 Hz, 1H), 7.80 (dd, *J* = 10.0, 1.5 Hz, 1H), 7.52 (t, *J* = 7.6 Hz, 1H), 4.53 (s, 2H). ¹³C NMR (CDCl₃) δ 178.3, 160.4 (d, *J* = 251.3 Hz), 131.8 (d, *J* = 7.8 Hz), 131.5 (d, *J* = 3.1 Hz), 131.1 (d, *J* = 14.7 Hz), 126.3 (d, *J* = 3.7 Hz), 117.6 (d, *J* = 23.3 Hz), 29.7.

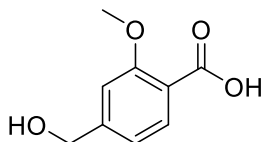
4-(Bromomethyl)benzoic acid (35c).



General procedure D. The precipitated solid was collected by filtration, and dried under reduced pressure to give a pale yellow solid (1.35 g, 86%). LCMS (*m/z*): 214.9 [M-H]⁻. HPLC: *t_R* 5.541 min, >95% purity (214 & 254 nm). ¹H

NMR (*d*₆-DMSO) δ 7.93 (d, *J* = 8.3 Hz, 2H), 7.57 (d, *J* = 8.4 Hz, 1H), 4.76 (s, 2H). ¹³C NMR (*d*₆-DMSO) δ 166.9, 142.8, 130.5, 129.7, 129.4, 29.5.

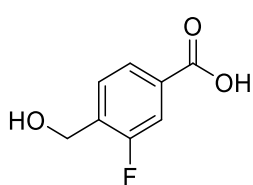
4-(Hydroxymethyl)-2-methoxybenzoic acid (36a).



4-(Bromomethyl)-2-methoxybenzoic acid (726 mg, 2.96 mmol) was taken up in an aqueous solution of K₂CO₃ (10%, 20 mL) and stirred at 70 °C for 30 min.

The reaction mixture was cooled and acidified with concentrated HCl. The resulting precipitate was filtered off, washed with H₂O and dried to afford 530 mg of a white solid (98%). LCMS (*m/z*): 181.8 [M-H]⁻. HPLC: *t*_R 3.306 min, >95% purity (214 & 254 nm). ¹H NMR (*d*₆-DMSO) δ 7.63 (d, *J* = 7.8 Hz, 1H), 7.08 – 7.07 (m, 1H), 6.94 (ddt, *J* = 7.9, 1.4, 0.7 Hz, 1H), 4.54 (s, 2H), 3.81 (s, 3H). ¹³C NMR (*d*₆-DMSO) δ 167.1, 158.4, 148.5, 130.9, 119.1, 117.6, 109.9, 62.5, 55.6.

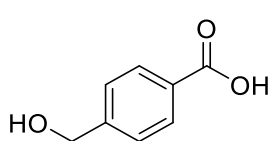
3-Fluoro-4-(hydroxymethyl)benzoic acid (36b).



4-(Bromomethyl)-3-fluorobenzoic acid (1.01 g, 4.33 mmol) was taken up in an aqueous solution of K₂CO₃ (10%, 25 mL) and stirred at 70 °C for 1.5 h. The reaction mixture was cooled and acidified with concentrated HCl. The resulting precipitate was filtered off, washed with H₂O and dried to afford a white solid

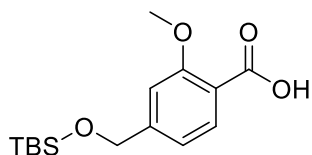
(684 mg, 93%). LCMS (*m/z*): 169.0 [M-H]⁻. HPLC: *t*_R 3.575 min, >95% purity (214 & 254 nm). ¹H NMR (*d*₆-DMSO) δ 7.79 (dd, *J* = 7.9, 1.4 Hz, 1H), 7.65 – 7.59 (m, 2H), 4.62 (s, 2H). ¹³C NMR (*d*₆-DMSO) δ 166.3 (d, *J* = 2.6 Hz), 159.1 (d, *J* = 244.9 Hz), 134.4 (d, *J* = 15.0 Hz), 131.4 (d, *J* = 7.3 Hz), 128.9 (d, *J* = 5.0 Hz), 125.3 (d, *J* = 3.1 Hz), 115.3 (d, *J* = 22.7 Hz), 56.6 (d, *J* = 4.2 Hz).

4-(Hydroxymethyl)benzoic acid (36c).



4-(Bromomethyl)benzoic acid (1.25 g, 5.81 mmol) was taken up in an aqueous solution of K₂CO₃ (10%, 25 mL) and stirred at 70 °C for 1.5 hr. The reaction mixture was cooled and acidified with concentrated HCl. The resulting precipitate was filtered off, washed with H₂O and dried to afford a white solid (687 mg, 78%). LCMS (*m/z*): 151.0 [M-H]⁻. HPLC: *t*_R 3.375 min, >95% purity (214 & 254 nm). ¹H NMR (*d*₆-DMSO) δ 7.91 (d, *J* = 8.1 Hz, 2H), 7.44 (d, *J* = 8.0 Hz, 2H), 4.58 (s, 2H). ¹³C NMR (*d*₆-DMSO) δ 167.8, 148.2, 129.7, 129.5, 126.7, 62.9.

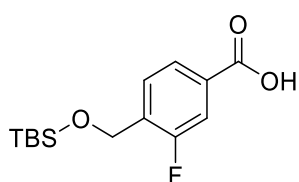
4-(((*tert*-Butyldimethylsilyl)oxy)methyl)-2-methoxybenzoic acid (37a).



General procedure A. Purification with FCC (eluent, 2:3 EtOAc/PE) gave a transparent oil (1.45 g, 77%). LCMS (*m/z*): 297.0 [M+H]⁺. HPLC: *t*_R 6.732 min, >95% purity (214 & 254 nm). ¹H NMR (CDCl₃) δ 7.98 (d, *J* =

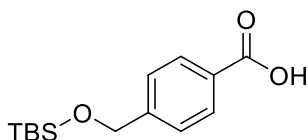
8.0 Hz, 1H), 7.00 (d, $J = 0.5$ Hz, 1H), 6.89 (ddt, $J = 8.0, 1.5, 0.8$ Hz, 1H), 4.67 (s, 2H), 3.94 (s, 3H), 0.84 (s, 9H), -0.00 (s, 6H). ¹³C NMR (CDCl₃) δ 165.8, 158.5, 149.8, 133.7, 119.1, 116.5, 108.9, 64.3, 56.6, 25.9, -5.19.

4-(((*tert*-Butyldimethylsilyl)oxy)methyl)-3-fluorobenzoic acid (37b).



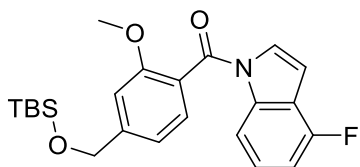
General procedure A. Purification with FCC (eluent, 2:3 EtOAc/PE) gave a white solid (687 mg, 68%). LCMS (m/z): 232.9 [M-H]⁻. HPLC: t_R 8.255 min, >95% purity (214 & 254 nm). ¹H NMR (CDCl₃) δ 7.79 (dd, $J = 8.0, 1.5$ Hz, 1H), 7.59 (dd, $J = 10.4, 1.5$ Hz, 1H), 7.50 (t, $J = 7.6$ Hz, 1H), 4.73 (s, 2H), 0.83 (s, 9H), -0.00 (s, 6H). ¹³C NMR (CDCl₃) δ 171.1, 159.3 (d, $J = 246.5$ Hz), 135.3 (d, $J = 14.4$ Hz), 129.7 (d, $J = 7.7$ Hz), 128.2 (d, $J = 4.7$ Hz), 126.2 (d, $J = 3.2$ Hz), 116.5 (d, $J = 23.0$ Hz), 59.0 (d, $J = 4.9$ Hz), 26.0, -5.25.

4-(((*tert*-Butyldimethylsilyl)oxy)methyl)benzoic acid (37c).



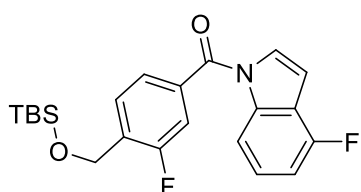
General procedure A. Purification with FCC (eluent, 2:3 EtOAc/PE) gave a white solid (375 mg, 80%). LCMS (m/z): 282.9 [M-H]⁻. HPLC: t_R 8.510 min, >95% purity (214 & 254 nm). ¹H NMR (CDCl₃) δ 7.97 (d, $J = 8.3$ Hz, 2H), 7.31 (d, $J = 8.4$ Hz, 2H), 4.70 (s, 2H), 0.84 (s, 9H), -0.00 (s, 6H). ¹³C NMR (CDCl₃) δ 172.3, 147.9, 130.4, 128.1, 125.9, 64.7, 26.1, -5.15.

(4-(((*tert*-Butyldimethylsilyl)oxy)methyl)phenyl)(4-fluoro-1*H*-indol-1-yl)methanone (38a).



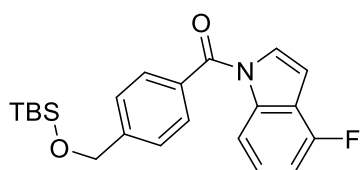
General procedure B. Purification with FCC (eluent, PE/EtOAc, 10:1) gave a white solid (375 mg, 43%). HRMS (m/z): C₂₃H₂₈FNO₃Si requires 414.1903 [M+H]⁺; found 414.1895. HPLC: t_R 6.732 min, >95% purity (214 & 254 nm). ¹H NMR (CDCl₃) δ 8.22 (d, $J = 8.3$ Hz, 1H), 7.41 (d, $J = 7.7$ Hz, 1H), 7.29 (td, $J = 8.3, 5.6$ Hz, 1H), 7.09 – 7.06 (m, 2H), 7.02 – 6.96 (m, 2H), 6.64 (dd, $J = 3.8, 0.7$ Hz, 1H), 4.82 (s, 2H), 3.79 (s, 3H), 0.98 (s, 9H), 0.15 (s, 6H). ¹³C NMR (CDCl₃) δ 167.5, 156.8, 155.7 (d, $J = 247.7$ Hz), 146.9, 137.8 (d, $J = 9.3$ Hz), 129.3, 127.7, 125.8 (d, $J = 7.3$ Hz), 122.9, 119.9, 119.7, 118.1, 112.7 (d, $J = 3.8$ Hz), 109.31 (d, $J = 18.5$ Hz), 109.0, 104.1, 64.6, 55.8, 26.1, -5.1.

(4-(((*tert*-Butyldimethylsilyl)oxy)methyl)-3-fluorophenyl)(4-fluoro-1*H*-indol-1-yl)methanone (38b).



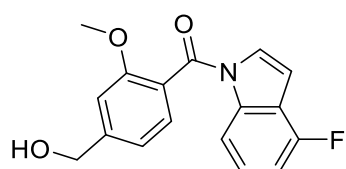
General procedure B. Purification with FCC (eluent, PE/EtOAc, 10:0.5) gave a white solid (184 mg, 3%). LCMS (m/z): 402.1 [M+H]⁺. HPLC: t_R 7.726 min, >95% purity (214 & 254 nm). ¹H NMR (CDCl₃) δ 8.01 (d, J = 8.3 Hz, 1H), 7.54 (t, J = 7.5 Hz, 1H), 7.38 (dd, J = 7.9, 1.6 Hz, 1H), 7.26 (dd, J = 10.0, 1.6 Hz, 1H), 7.2 (td, J = 8.2, 5.4 Hz, 1H), 7.12 (d, J = 3.8 Hz, 1H), 6.85 (ddd, J = 9.6, 8.1, 0.6 Hz, 1H), 6.58 (dd, J = 3.8, 0.7 Hz, 1H), 4.73 (s, 2H), 0.82 (s, 9H), 0.00 (s, 6H). ¹³C NMR (CDCl₃) δ 159.3 (d, J = 248.4 Hz), 155.8 (d, J = 248.2 Hz), 138.2 (d, J = 9.1 Hz), 134.4 (d, J = 7.1 Hz), 133.7, 133.5, 128.5 (d, J = 5.0 Hz), 127.4, 126.1 (d, J = 7.3 Hz), 125.2, 125.2, 119.8, 119.6, 115.9 (d, J = 23.3 Hz), 112.6 (d, J = 3.9 Hz), 109.6 (d, J = 18.5 Hz), 104.5, 58.8, 26.0, -5.2.

(4-(((*tert*-Butyldimethylsilyl)oxy)methyl)phenyl)(4-fluoro-1*H*-indol-1-yl)methanone (38c).



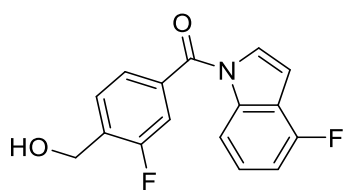
General procedure B. Purification with FCC (eluent, PE/EtOAc, 10:0.5) gave a white solid (210 mg, 58%). LCMS (m/z): 402.1 [M+H]⁺. HPLC: t_R 7.735 min, >95% purity (214 & 254 nm). ¹H NMR (CDCl₃) δ 8.02 (d, J = 8.3 Hz, 1H), 7.61 – 7.55 (m, 2H), 7.35 (d, J = 8.4 Hz, 2H), 7.19 – 7.13 (m, 2H), 6.85 (ddd, J = 9.6, 8.1, 0.6 Hz, 1H), 6.57 (dd, J = 3.8, 0.6 Hz, 1H), 4.70 (s, 2H), 0.83 (s, 9H), -0.00 (s, 6H). ¹³C NMR (CDCl₃) δ 168.8, 155.8 (d, J = 248.0 Hz), 146.4, 138.3 (d, J = 9.3 Hz), 132.8, 129.5, 127.8, 126.1, 125.8 (d, J = 7.3 Hz), 119.7 (d, J = 21.9 Hz), 112.6 (d, J = 3.9 Hz), 109.3 (d, J = 18.5 Hz), 103.9, 64.6, 26.1, -5.14.

(4-Fluoro-1*H*-indol-1-yl)(4-(hydroxymethyl)-2-methoxyphenyl)methanone (39a).



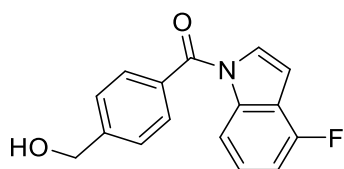
General procedure C. Purification with FCC (eluent, DCM/EtOAc, 3:1) gave the title compound as a white solid (270 mg, 93%). LCMS (m/z): 299.9 [M+H]⁺. HPLC: t_R 6.741 min, >95% purity (214 & 254 nm). HRMS (m/z): C₁₇H₁₄FNO₃: requires 300.1038 [M+H]⁺; found 300.103. HPLC: t_R 6.732 min, >95% purity (214 & 254 nm). ¹H NMR (CDCl₃) δ 8.21 (d, J = 8.3 Hz, 1H), 7.42 (d, J = 7.7 Hz, 1H), 7.29 (td, J = 8.2, 5.4 Hz, 1H), 7.08 (s, 1H), 7.06 – 7.03 (m, 2H), 6.99 (ddd, J = 9.6, 8.1, 0.6 Hz, 1H), 6.64 (dd, J = 3.8, 0.7 Hz, 1H), 4.79 (s, 2H), 3.79 (s, 3H), 2.05 (s, 1H). ¹³C NMR (CDCl₃) δ 167.4, 156.9, 155.7 (d, J = 244.3 Hz), 146.1, 137.7 (d, J = 9.3 Hz), 129.5, 127.5, 125.9 (d, J = 7.3 Hz), 123.6, 119.8 (d, J = 21.8 Hz), 118.9, 112.7 (d, J = 3.8 Hz), 109.7, 109.4 (d, J = 18.5 Hz), 104.2, 64.9, 55.9.

(4-Fluoro-1*H*-indol-1-yl)(3-fluoro-4-(hydroxymethyl)phenyl)methanone (39b).



General procedure C. Purification with FCC (eluent, DCM/EtOAc, 3:1) gave 88 mg of the title compound as a white solid (90%). LCMS (m/z): 288.0 [M+H]⁺. HPLC: t_R 6.913 min, >95% purity (214 & 254 nm). HRMS (m/z): C₁₆H₁₁F₂NO₂: requires 288.0758 [M+H]⁺; found 288.0753. ¹H NMR (CDCl₃) δ 8.16 (d, J = 8.3 Hz, 1H), 7.66 (t, J = 7.4 Hz, 1H), 7.54 (dd, J = 7.8, 1.3 Hz, 1H), 7.45 (dd, J = 9.9, 1.3 Hz, 1H), 7.33 (td, J = 8.2, 5.5 Hz, 1H), 7.26 (d, J = 2.6 Hz, 1H), 7.04 – 6.99 (m, 1H), 6.75 (d, J = 3.7 Hz, 1H), 4.89 (s, 2H), 2.03 (s, 1H). ¹³C NMR (CDCl₃) δ 161.3, 158.8, 155.8 (d, J = 248.5 Hz), 138.2 (d, J = 9.3 Hz), 135.2 (d, J = 7.2 Hz), 132.6 (d, J = 14.8 Hz), 129.3 (d, J = 4.9 Hz), 127.3, 126.2 (d, J = 7.3 Hz), 125.3 (d, J = 3.6 Hz), 119.7 (d, J = 21.9 Hz), 116.4 (d, J = 23.5 Hz), 112.6 (d, J = 3.9 Hz), 109.7 (d, J = 18.5 Hz), 104.7, 58.9 (d, J = 4.4 Hz).

(4-Fluoro-1*H*-indol-1-yl)(4-(hydroxymethyl)phenyl)methanone (39c).



General procedure C. Purification with FCC (eluent, DCM/EtOAc, 3:1) gave the title compound as a white solid (99 mg, 94%). LCMS (m/z): 270.0 [M+H]⁺. HPLC: t_R 6.678 min, >95% purity (214 & 254 nm). HRMS (m/z): C₁₆H₁₂FNO₂: requires 270.0852 [M+H]⁺; found 270.0842. ¹H NMR (CDCl₃) δ 8.16 (d, J = 8.3 Hz, 1H), 7.73 (d, J = 8.2 Hz, 2H), 7.53 (d, J = 8.3 Hz, 2H), 7.30 (ddd, J = 15.4, 8.8, 5.4 Hz, 2H), 7.00 (dd, J = 9.3, 8.5 Hz, 1H), 6.75 – 6.69 (m, 1H), 4.82 (s, 2H), 2.05 (s, 1H). ¹³C NMR (CDCl₃) δ 168.7, 155.8 (d, J = 248.2 Hz), 145.5, 138.2 (d, J = 9.2 Hz), 133.4, 129.7, 127.6, 126.9, 125.9 (d, J = 7.3 Hz), 119.7 (d, J = 21.9 Hz), 112.5 (d, J = 3.9 Hz), 109.4 (d, J = 18.5 Hz), 104.2, 64.7.

Pharmacological Characterisation. *Materials.* Dulbecco's modified Eagle's medium, Flp-In CHO cells, and hygromycin B were purchased from Invitrogen (Carlsbad, CA). Fetal bovine serum (FBS) was purchased from ThermoTrace (Melbourne, VIC, Australia). All other reagents were purchased from Sigma Aldrich (St. Louis, MO).

Cell culture. FlpIn Chinese Hamster Ovary (CHO) cells (Invitrogen, Carlsbad, CA, USA) stably expressing the hD_{2L}R were grown and maintained in Dulbecco's modified Eagle's medium (DMEM) supplemented with 10% fetal bovine serum (FBS), and 200 μ g/mL of Hygromycin-B, and maintained at 37 °C in a humidified incubator containing 5% CO₂.

Cell culture and transfection for cAMP assay: FlpIn CHO cells stably expressing the human dopamine D_{2L} receptor were maintained in DMEM supplemented with 5% foetal calf serum (FBS) and 0.2 mg/mL hygromycin at 37 °C in a humidified incubator supplied with 5% CO₂. For transfection, the cells were grown in 10 cm culture dishes until sub-confluent. A mixture of 4 µg plasmid DNA containing BRET-based cAMP (CAMYEL) biosensor construct⁸⁷ and 25 µg 20 kDa linear polyethylene imine (PEI) in 500 µL 150 mM NaCl was added into a dish of cells.

cAMP measurement: The cellular cAMP levels were measured with the CAMYEL BRET-based biosensor for cAMP.⁸⁷ One day after transfection, cells were trypsinized and seeded in white 96-well microplates. The cells were then cultured for an additional day, rinsed twice with Hank's Balanced Salt Solution (HBSS) and were then incubated in fresh HBSS. The *Renilla* luciferase (*RLuc*) substrate coelenterazine-h was added to reach a final concentration of 5 µM. The cells were stimulated with dopamine in the presence of 10 µM forskolin (final concentration). For the antagonism assay, the antagonists were added 30 min prior to stimulation. The BRET signals were measured using a BMG Lumistar counter 30 min after stimulation. The BRET signal (BRET ratio) was determined by calculating the ratio of the light emitted at 535 ± 30 nm (YFP) to the light emitted at 475 ± 30 nm (RLuc).

Data analysis. Computerized nonlinear regression, statistical analyses and simulations were performed using Prism 6.0 (GraphPad Prism 6.0b Software, San Diego, CA).

Analysis of functional data. All concentration-response data were globally fitted to the following operational model of allosterism and agonism (eq 1):⁸⁸

$$E = \frac{(E_m(\tau_A[A](K_B + \alpha\beta[B]) + \tau_B[B]K_A)^n)}{([A]K_B + K_AK_B + [B]K_A + \alpha[A][B])^n + (\tau_A[A](K_B + \alpha\beta[B]) + \tau_B[B]K_A)^n}$$

where E_m is the maximum possible cellular response, [A] and [B] are the concentrations of orthosteric and allosteric ligands, respectively, K_A and K_B are the equilibrium dissociation constant of the orthosteric and allosteric ligands, respectively, τ_A and τ_B are operational measures of orthosteric and allosteric ligand efficacy, respectively, α is the binding cooperativity parameter between the orthosteric and allosteric ligand, β denotes the magnitude of the allosteric effect of the modulator on

the efficacy of the orthosteric agonist, and n denotes the transducer slope that describes the underlying stimulus–response coupling of the ligand-occupied receptor to the signal pathway. The K_A for dopamine was determined through receptor depletion by phenoxybenzamine alkylation as follows; given the proportional relationship of R_T to measured τ , K_A is invariant with receptor depletion. Thus, unique estimates of K_A could be obtained by direct operational model fitting of the family of concentration-response curve for dopamine.^{89,90}

References

1. Wood, M.; Ates, A.; Andre, V. M.; Michel, A.; Barnaby, R.; Gillard, M. In vitro and in vivo identification of novel positive allosteric modulators of the human dopamine D2 and D3 receptor. *Mol. Pharmacol.* **2016**, *89*, 303-312.
2. Michino, M.; Beuming, T.; Donthamsetti, P.; Newman, A. H.; Javitch, J. A.; Shi, L. What can crystal structures of aminergic receptors tell us about designing subtype-selective ligands? *Pharmacol. Rev.* **2015**, *67*, 198-213.
3. Vaidehi, N.; Bhattacharya, S.; Larsen, A. B. Structure and dynamics of G-protein coupled receptors. *Adv. Exp. Med. Biol.* **2014**, *796*, 37-54.
4. Ballesteros, J. A.; Weinstein, H. Integrated methods for the construction of three-dimensional models and computational probing of structure-function relations in G protein-coupled receptors. In *Methods Neurosci.*, Sealfon, S. C., Ed. Academic Press: 1995; Vol. 25, pp 366-428.
5. Chien, E. Y.; Liu, W.; Zhao, Q.; Katritch, V.; Han, G. W.; Hanson, M. A.; Shi, L.; Newman, A. H.; Javitch, J. A.; Cherezov, V.; Stevens, R. C. Structure of the human dopamine D3 receptor in complex with a D2/D3 selective antagonist. *Science* **2010**, *330*, 1091-1095.
6. Wang, S.; Wacker, D.; Levit, A.; Che, T.; Betz, R. M.; McCorvy, J. D.; Venkatakrisnan, A. J.; Huang, X. P.; Dror, R. O.; Shoichet, B. K.; Roth, B. L. D4 dopamine receptor high-resolution structures enable the discovery of selective agonists. *Science* **2017**, *358*, 381-386.
7. Wang, S.; Che, T.; Levit, A.; Shoichet, B. K.; Wacker, D.; Roth, B. L. Structure of the D2 dopamine receptor bound to the atypical antipsychotic drug risperidone. *Nature* **2018**, *555*, 269-273.
8. Fyfe, T. J.; Zarzycka, B.; Lim, H. D.; Kellam, B.; Mistry, S. N.; Katritch, V.; Scammells, P. J.; Lane, J. R.; Capuano, B. A thieno[2,3-*d*]pyrimidine scaffold is a novel negative allosteric modulator of the dopamine D2 receptor. *J. Med. Chem.* **2018**, *62*, 174-206.
9. Draper-Joyce, C. J.; Michino, M.; Verma, R. K.; Klein Herenbrink, C.; Shonberg, J.; Kopinathan, A.; Scammells, P. J.; Capuano, B.; Thal, D. M.; Javitch, J. A.; Christopoulos, A.; Shi, L.; Lane, J. R. The structural determinants of the bitopic binding mode of a negative allosteric modulator of the dopamine D2 receptor. *Biochem. Pharmacol.* **2018**, *148*, 315-328.
10. Jorg, M.; May, L. T.; Mak, F. S.; Lee, K. C.; Miller, N. D.; Scammells, P. J.; Capuano, B. Synthesis and pharmacological evaluation of dual acting ligands targeting the adenosine A2A and dopamine D2 receptors for the potential treatment of Parkinson's disease. *J. Med. Chem.* **2015**, *58*, 718-738.
11. Ciruela, F.; Jacobson, K. A.; Fernández-Dueñas, V. Portraying G protein-coupled receptors with fluorescent ligands. *ACS Chem. Bio.* **2014**, *9*, 1918-1928.
12. Manuela, J.; J., S. P. Guidelines for the synthesis of small-molecule irreversible probes targeting G protein-coupled receptors. *ChemMedChem* **2016**, *11*, 1488-1498.
13. Baker, S. P.; Deyrup, M. D. Development of novel irreversible ligands. *Neuroprotocols* **1994**, *4*, 66-75.
14. Newman, A. H. Chapter 29. Irreversible ligands for drug receptor characterization. In *Annu. Rep. Med. Chem.*, Bristol, J. A., Ed. Academic Press: 1990; Vol. 25, pp 271-280.

15. Grunbeck, A.; Sakmar, T. P. Probing G protein-coupled receptor—ligand interactions with targeted photoactivatable cross-linkers. *Biochemistry* **2013**, *52*, 8625-8632.
16. Kotzyba-Hibert, F.; Kapfer, I.; Goeldner, M. Recent trends in photoaffinity labeling. *Angew. Chem. Int. Ed.* **1995**, *34*, 1296-1312.
17. Weichert, D.; Gmeiner, P. Covalent molecular probes for class A G protein-coupled receptors: Advances and applications. *ACS Chem. Bio.* **2015**, *10*, 1376-1386.
18. Das, J. Aliphatic diazirines as photoaffinity probes for proteins: Recent developments. *Chem. Rev.* **2011**, *111*, 4405-4417.
19. Noe, M. C.; Gilbert, A. M. Chapter twenty-seven - Targeted covalent enzyme inhibitors. In *Annu. Rep. Med. Chem.*, Desai, M. C., Ed. Academic Press: 2012; Vol. 47, pp 413-439.
20. Evans, M. J.; Cravatt, B. F. Mechanism-based profiling of enzyme families. *Chem. Rev.* **2006**, *106*, 3279-3301.
21. De Cesco, S.; Kurian, J.; Dufresne, C.; Mittermaier, A. K.; Moitessier, N. Covalent inhibitors design and discovery. *Eur. J. Med. Chem.* **2017**, *138*, 96-114.
22. Johnson, D. S.; Weerapana, E.; Cravatt, B. F. Strategies for discovering and derisking covalent, irreversible enzyme inhibitors. *Future Med. Chem.* **2010**, *2*, 949-964.
23. Doornbos, M. L. J.; Wang, X.; Vermond, S. C.; Peeters, L.; Pérez-Benito, L.; Trabanco, A. A.; Lavreysen, H.; Cid, J. M.; Heitman, L. H.; Tresadern, G.; Ijzerman, A. P. Covalent allosteric probe for the metabotropic glutamate receptor 2: design, synthesis, and pharmacological characterization. *J. Med. Chem.* **2019**, *62*, 223-233.
24. Flanagan, M. E.; Abramite, J. A.; Anderson, D. P.; Aulabaugh, A.; Dahal, U. P.; Gilbert, A. M.; Li, C.; Montgomery, J.; Oppenheimer, S. R.; Ryder, T.; Schuff, B. P.; Uccello, D. P.; Walker, G. S.; Wu, Y.; Brown, M. F.; Chen, J. M.; Hayward, M. M.; Noe, M. C.; Obach, R. S.; Philippe, L.; Shanmugasundaram, V.; Shapiro, M. J.; Starr, J.; Stroh, J.; Che, Y. Chemical and computational methods for the characterization of covalent reactive groups for the prospective design of irreversible inhibitors. *J. Med. Chem.* **2014**, *57*, 10072-10079.
25. Schmidt, T. C.; Welker, A.; Rieger, M.; Sahu, P. K.; Sotriffer, C. A.; Schirmeister, T.; Engels, B. Protocol for rational design of covalently interacting inhibitors. *Chemphyschem* **2014**, *15*, 3226-3235.
26. Shannon, D. A.; Weerapana, E. Covalent protein modification: the current landscape of residue-specific electrophiles. *Curr. Opin. Chem. Biol.* **2015**, *24*, 18-26.
27. Nijmeijer, S.; Engelhardt, H.; Schultes, S.; van de Stolpe, A. C.; Lusink, V.; de Graaf, C.; Wijnmans, M.; Haaksma, E. E.; de Esch, I. J.; Stachurski, K.; Vischer, H. F.; Leurs, R. Design and pharmacological characterization of VUF14480, a covalent partial agonist that interacts with cysteine 98(3.36) of the human histamine H₄ receptor. *Br. J. Pharmacol.* **2013**, *170*, 89-100.
28. Krishnan, S.; Miller, R. M.; Tian, B.; Mullins, R. D.; Jacobson, M. P.; Taunton, J. Design of reversible, cysteine-targeted michael acceptors guided by kinetic and computational analysis. *J. Am. Chem. Soc.* **2014**, *136*, 12624-12630.
29. Pitha, J.; Buchowiecki, W.; Milecki, J.; Kusiak, J. W. Affinity labels for beta-adrenoceptors: preparation and properties of alkylating beta-blockers derived from indole. *J. Med. Chem.* **1987**, *30*, 612-615.
30. Baraldi, P. G.; Cacciari, B.; Moro, S.; Romagnoli, R.; Ji, X.-d.; Jacobson, K. A.; Gessi, S.; Borea, P. A.; Spalluto, G. Fluorosulfonyl- and bis-(β -chloroethyl)amino-phenylamino functionalized pyrazolo[4,3-*e*]1,2,4-triazolo[1,5-*c*]pyrimidine derivatives: irreversible antagonists at the human A₃ adenosine receptor and molecular modeling studies. *J. Med. Chem.* **2001**, *44*, 2735-2742.
31. Davie, B. J.; Valant, C.; White, J. M.; Sexton, P. M.; Capuano, B.; Christopoulos, A.; Scammells, P. J. Synthesis and pharmacological evaluation of analogues of benzyl quinolone carboxylic acid (BQCA) designed to bind irreversibly to an allosteric site of the M₁ muscarinic acetylcholine receptor. *J. Med. Chem.* **2014**, *57*, 5405-5418.
32. Narayanan, A.; Jones, L. H. Sulfonyl fluorides as privileged warheads in chemical biology. *Chem. Sci.* **2015**, *6*, 2650-2659.

33. Kung, M. P.; Mu, M.; Zhuang, Z. P.; Kung, H. F. NCS-MPP (4-(2'-methoxy-phenyl)-1-[2'-(N-2"-pyridyl)-p-isothiocyanobenz amido]-ethyl-piperazine): a high affinity and irreversible 5-HT_{1A} receptor ligand. *Life Sci.* **1996**, *58*, 177-186.
34. Tsotinis, A.; Afroudakis, P. A.; Davidson, K.; Prashar, A.; Sugden, D. Design, synthesis, and melatonergic activity of new azido- and isothiocyanato-substituted indoles. *J. Med. Chem.* **2007**, *50*, 6436-6440.
35. Baker, S. P.; Liptak, A.; Pitha, J. Irreversible inactivation of the beta-adrenoreceptor by a partial agonist. Evidence for selective loss of the agonist high affinity binding sites. *J. Biol. Chem.* **1985**, *260*, 15820-15828.
36. Chandrasekaran, A.; Shen, L.; Lockhead, S.; Oganessian, A.; Wang, J.; Scatina, J. Reversible covalent binding of neratinib to human serum albumin in vitro. *Drug Metab. Lett.* **2010**, *4*, 220-227.
37. Weichert, D.; Kruse, A. C.; Manglik, A.; Hiller, C.; Zhang, C.; Hübner, H.; Kobilka, B. K.; Gmeiner, P. Covalent agonists for studying G protein-coupled receptor activation. *PNAS* **2014**, *111*, 10744.
38. Winkler, J. D.; Thermos, K.; Weiss, B. Differential effects of fluphenazine-*N*-mustard, on calmodulin activity and on D₁ and D₂ dopaminergic responses. *Psychopharmacology* **1987**, *92*, 285-291.
39. Chen, J. F.; Aloyo, V. J.; Qin, Z. H.; Weiss, B. Irreversible blockade of D₂ dopamine receptors by fluphenazine-*N*-mustard increases D₂ dopamine receptor mRNA and proenkephalin mRNA and decreases D₁ dopamine receptor mRNA and mu and delta opioid receptors in rat striatum. *Neurochem. Int.* **1994**, *25*, 355-366.
40. Xu, S. X.; Hatada, Y.; Black, L. E.; Creese, I.; Sibley, D. R. *N*-(*p*-isothiocyanatophenethyl)siperone, a selective and irreversible antagonist of D₂ dopamine receptors in brain. *J. Pharmacol. Exp. Ther.* **1991**, *257*, 608-615.
41. Thompson, T. L.; Bridges, S. R.; Weirs, W. J. Alteration of dopamine transport in the striatum and nucleus accumbens of ovariectomized and estrogen-primed rats following *N*-(*p*-isothiocyanatophenethyl) siperone (NIPS) treatment. *Brain Res. Bull.* **2001**, *54*, 631-638.
42. McDougall, S. A.; Rudberg, K. N.; Veliz, A.; Dhargalkar, J. M.; Garcia, A. S.; Romero, L. C.; Gonzalez, A. E.; Mohd-Yusof, A.; Crawford, C. A. Importance of D₁ and D₂ receptor stimulation for the induction and expression of cocaine-induced behavioral sensitization in preweanling rats. *Behav. Brain Res.* **2017**, *326*, 226-236.
43. Nilsson, C. L.; Ekman, A.; Hellstrand, M.; Eriksson, E. Inverse agonism at dopamine D₂ receptors. Haloperidol-induced prolactin release from GH4C1 cells transfected with the human D₂ receptor is antagonized by R(-)-*n*-propylnorapomorphine, raclopride, and phenoxybenzamine. *Neuropsychopharmacology* **1996**, *15*, 53-61.
44. Davie, B. J.; Sexton, P. M.; Capuano, B.; Christopoulos, A.; Scammells, P. J. Development of a photoactivatable allosteric ligand for the m₁ muscarinic acetylcholine receptor. *ACS Chem. Neurosci.* **2014**, *5*, 902-907.
45. Fleming, S. Chemical reagents in photoaffinity labeling. *Tetrahedron* **1995**, *51*, 12479-12520.
46. Wu, L.; Xu, B. Analysis of protein ligand-receptor binding by photoaffinity cross-linking. *Curr. Protoc. Protein Sci.* **2015**, *79*, 1-14.
47. Lapinsky, D. J. Tandem photoaffinity labeling–bioorthogonal conjugation in medicinal chemistry. *Bioorg. Med. Chem.* **2012**, *20*, 6237-6247.
48. Barral, K.; Moorhouse, A. D.; Moses, J. E. Efficient conversion of aromatic amines into azides: A one-pot synthesis of triazole linkages. *Org. Lett.* **2007**, *9*, 1809-1811.
49. Andersen, J.; Madsen, U.; Björkling, F.; Liang, X. Rapid synthesis of aryl azides from aryl halides under mild conditions. *Synlett* **2005**, *2005*, 2209-2213.
50. Smith, E.; Collins, I. Photoaffinity labeling in target- and binding-site identification. *Future Med. Chem.* **2015**, *7*, 159-183.
51. Brune, S.; Priel, S.; Wunsch, B. Structure of the sigma₁ receptor and its ligand binding site. *J. Med. Chem.* **2013**, *56*, 9809-9819.

52. Gomes, I.; Jordan, B. A.; Gupta, A.; Rios, C.; Trapaidze, N.; Devi, L. A. G protein coupled receptor dimerization: implications in modulating receptor function. *J. Mol. Med.* **2001**, *79*, 226-242.
53. Benovic, J. L. G-protein-coupled receptors signal victory. *Cell* **2012**, *151*, 1148-1150.
54. Niznik, H. B.; Guan, J. H.; Neumeyer, J. L.; Seeman, P. A photoaffinity ligand for dopamine D₂ receptors: azidocleobopride. *Mol. Pharmacol.* **1985**, *27*, 193-199.
55. Amlaiky, N.; Caron, M. G. Photoaffinity labeling of the D₂-dopamine receptor using a novel high affinity radioiodinated probe. *J. Biol. Chem.* **1985**, *260*, 1983-1986.
56. Kanety, H.; Fuchs, S. Immuno-photoaffinity labeling of the D₂-dopamine receptor. *Biochem. Biophys. Res. Commun.* **1988**, *155*, 930-936.
57. Niznik, H. B.; Dumbrille-Ross, A.; Guan, J. H.; Neumeyer, J. L.; Seeman, P. Dopamine D₂ receptors photolabeled by iodo-azido-cleobopride. *Neurosci. Lett.* **1985**, *55*, 267-272.
58. Wouters, W.; Van Dun, J.; Laduron, P. M. Photoaffinity labeling of human brain dopamine receptors. *Biochem. Pharmacol.* **1984**, *33*, 3517-3520.
59. Vernall, A. J.; Stoddart, L. A.; Briddon, S. J.; Hill, S. J.; Kellam, B. Highly potent and selective fluorescent antagonists of the human adenosine A₃ receptor based on the 1,2,4-triazolo[4,3-a]quinoxalin-1-one scaffold. *J. Med. Chem.* **2012**, *55*, 1771-1782.
60. Daly, C. J.; McGrath, J. C. Fluorescent ligands, antibodies, and proteins for the study of receptors. *Pharmacol. Ther.* **2003**, *100*, 101-118.
61. Briddon, S. J.; Kellam, B.; Hill, S. J. Design and use of fluorescent ligands to study ligand-receptor interactions in single living cells. *Methods Mol. Biol.* **2011**, *746*, 211-236.
62. Cottet, M.; Faklaris, O.; Falco, A.; Trinquet, E.; Pin, J.-P.; Mouillac, B.; Durroux, T. Fluorescent ligands to investigate GPCR binding properties and oligomerization. *Biochem. Soc. Trans.* **2013**, *41*, 148-153.
63. Stoddart, L. A.; Kilpatrick, L. E.; Briddon, S. J.; Hill, S. J. Probing the pharmacology of G protein-coupled receptors with fluorescent ligands. *Neuropharmacology* **2015**, *98*, 48-57.
64. Mitronova, G. Y.; Lukinavičius, G.; Butkevich, A. N.; Kohl, T.; Belov, V. N.; Lehnart, S. E.; Hell, S. W. High-affinity functional fluorescent ligands for human β -adrenoceptors. *Sci. Rep.* **2017**, *7*, 12319.
65. McGrath, J. C.; Arribas, S.; Daly, C. J. Fluorescent ligands for the study of receptors. *Trends. Pharm. Sci.* **1996**, *17*, 393-399.
66. Iliopoulos-Tsoutsouvas, C.; Kulkarni, R. N.; Makriyannis, A.; Nikas, S. P. Fluorescent probes for G-protein-coupled receptor drug discovery. *Expert Opin. Drug. Discov.* **2018**, *13*, 933-947.
67. Baker, J. G.; Middleton, R.; Adams, L.; May, L. T.; Briddon, S. J.; Kellam, B.; Hill, S. J. Influence of fluorophore and linker composition on the pharmacology of fluorescent adenosine A₁ receptor ligands. *Br. J. Pharmacol.* **2010**, *159*, 772-786.
68. Giepmans, B. N.; Adams, S. R.; Ellisman, M. H.; Tsien, R. Y. The fluorescent toolbox for assessing protein location and function. *Science* **2006**, *312*, 217-224.
69. Gonçalves, M. S. T. Fluorescent labeling of biomolecules with organic probes. *Chem. Rev.* **2009**, *109*, 190-212.
70. Song, L.; Varma, C. A.; Verhoeven, J. W.; Tanke, H. J. Influence of the triplet excited state on the photobleaching kinetics of fluorescein in microscopy. *Biophys. J.* **1996**, *70*, 2959-2968.
71. Martin, M. M.; Lindqvist, L. The pH dependence of fluorescein fluorescence. *J. Lumin.* **1975**, *10*, 381-390.
72. Brandtzaeg, P. Rhodamine conjugates: specific and nonspecific binding properties in immunohistochemistry. *Ann. N. Y. Acad. Sci.* **1975**, *254*, 35-54.
73. McKay, I. C.; Forman, D.; White, R. G. A comparison of fluorescein isothiocyanate and lissamine rhodamine (RB 200) as labels for antibody in the fluorescent antibody technique. *Immunology* **1981**, *43*, 591-602.
74. Wessendorf, M. W.; Brelje, T. C. Which fluorophore is brightest? A comparison of the staining obtained using fluorescein, tetramethylrhodamine, lissamine rhodamine, Texas red, and cyanine 3.18. *Histochemistry* **1992**, *98*, 81-85.

75. Karolin, J.; Johansson, L. B. A.; Strandberg, L.; Ny, T. Fluorescence and absorption spectroscopic properties of dipyrrometheneboron difluoride (BODIPY) derivatives in liquids, lipid membranes, and proteins. *JACS* **1994**, *116*, 7801-7806.
76. Ulrich, G.; Ziesse, R.; Harriman, A. The chemistry of fluorescent bodipy dyes: versatility unsurpassed. *Angew Chem. Int. Ed. Engl.* **2008**, *47*, 1184-1201.
77. Stoddart, L. A.; Vernall, A. J.; Bouzo-Lorenzo, M.; Bosma, R.; Kooistra, A. J.; de Graaf, C.; Vischer, H. F.; Leurs, R.; Briddon, S. J.; Kellam, B.; Hill, S. J. Development of novel fluorescent histamine H₁-receptor antagonists to study ligand-binding kinetics in living cells. *Sci. Rep.* **2018**, *8*, 1572.
78. Middleton, R. J.; Briddon, S. J.; Cordeaux, Y.; Yates, A. S.; Dale, C. L.; George, M. W.; Baker, J. G.; Hill, S. J.; Kellam, B. New fluorescent adenosine A₁-receptor agonists that allow quantification of ligand-receptor interactions in microdomains of single living cells. *J. Med. Chem.* **2007**, *50*, 782-793.
79. Daval, S. B.; Valant, C.; Bonnet, D.; Kellenberger, E.; Hibert, M.; Galzi, J.-L.; Ilien, B. Fluorescent derivatives of AC-42 to probe bitopic orthosteric/allosteric binding mechanisms on muscarinic M₁ receptors. *J. Med. Chem.* **2012**, *55*, 2125-2143.
80. Alonso, D.; Vázquez-Villa, H.; Gamo, A. M.; Martínez-Espesón, M. F.; Tortosa, M.; Viso, A.; Fernández de la Pradilla, R.; Junquera, E.; Aicart, E.; Martín-Fontecha, M.; Benhamú, B.; López-Rodríguez, M. L.; Ortega-Gutiérrez, S. Development of fluorescent ligands for the human 5-HT_{1A} receptor. *ACS Med. Chem. Lett.* **2010**, *1*, 249-253.
81. Schembri, L. S.; Stoddart, L. A.; Briddon, S. J.; Kellam, B.; Canals, M.; Graham, B.; Scammells, P. J. Synthesis, biological evaluation, and utility of fluorescent ligands targeting the μ -opioid receptor. *J. Med. Chem.* **2015**, *58*, 9754-9767.
82. Lam, R.; Gondin, A. B.; Canals, M.; Kellam, B.; Briddon, S. J.; Graham, B.; Scammells, P. J. Fluorescently labeled morphine derivatives for bioimaging studies. *J. Med. Chem.* **2018**, *61*, 1316-1329.
83. Barton, A. C.; Kang, H. C.; Rinaudo, M. S.; Monsma, F. J., Jr.; Stewart-Fram, R. M.; Macinko, J. A., Jr.; Haugland, R. P.; Ariano, M. A.; Sibley, D. R. Multiple fluorescent ligands for dopamine receptors. I. Pharmacological characterization and receptor selectivity. *Brain. Res.* **1991**, *547*, 199-207.
84. Madras, B. K.; Canfield, D. R.; Pfaelzer, C.; Vittimberga, F. J., Jr.; Difiglia, M.; Aronin, N.; Bakthavachalam, V.; Baidur, N.; Neumeyer, J. L. Fluorescent and biotin probes for dopamine receptors: D₁ and D₂ receptor affinity and selectivity. *Mol. Pharmacol.* **1990**, *37*, 833-839.
85. Bakthavachalam, V.; Baidur, N.; Madras, B. K.; Neumeyer, J. L. Fluorescent probes for dopamine receptors: synthesis and characterization of fluorescein and 7-nitrobenz-2-oxa-1,3-diazol-4-yl conjugates of D-1 and D-2 receptor ligands. *J. Med. Chem.* **1991**, *34*, 3235-3241.
86. Sibley, D. R.; Creese, I. Regulation of ligand binding to pituitary D-2 dopaminergic receptors. Effects of divalent cations and functional group modification. *J. Biol. Chem.* **1983**, *258*, 4957-4965.
87. Jiang, L. I.; Collins, J.; Davis, R.; Lin, K. M.; DeCamp, D.; Roach, T.; Hsueh, R.; Rebres, R. A.; Ross, E. M.; Taussig, R.; Fraser, I.; Sternweis, P. C. Use of a cAMP BRET sensor to characterize a novel regulation of cAMP by the sphingosine 1-phosphate/G13 pathway. *J. Biol. Chem.* **2007**, *282*, 10576-10584.
88. Leach, K.; Sexton, P. M.; Christopoulos, A. Allosteric GPCR modulators: taking advantage of permissive receptor pharmacology. *Trends Pharmacol. Sci.* **2007**, *28*, 382-389.
89. Keov, P.; López, L.; Devine, S. M.; Valant, C.; Lane, J. R.; Scammells, P. J.; Sexton, P. M.; Christopoulos, A. Molecular mechanisms of bitopic ligand engagement with the M(1) muscarinic acetylcholine receptor. *J. Biol. Chem.* **2014**, *289*, 23817-23837.
90. Black, J. W.; Leff, P.; Shankley, N. P.; Wood, J. An operational model of pharmacological agonism: the effect of E/[A] curve shape on agonist dissociation constant estimation. *Br. J. Pharmacol.* **1985**, *84*, 561-571.

Chapter 5 – Structure-Kinetic Profiling of Haloperidol Analogues at the Dopamine D₂ Receptor

Declaration for Thesis Chapter 5

The data presented in Chapter 5 contains research which is in manuscript format for submission to the *Journal of Medicinal Chemistry*

Declaration by candidate

In the case of Chapter 5, the nature and extent of my contribution to the work was the following:

Nature of Contribution	Contribution (%)
Design, synthesis, purification, characterisation and pharmacological testing of all analogues.	85
Main author of manuscript.	

The following co-authors contributed to the work. Co-authors who are students at Monash University must also indicate the extent of their contribution in percentage terms:

Name	Nature of Contribution	Contribution (%)*
David Sykes	Co-author of manuscript	
Steven J. Charlton	Co-author of manuscript	
Barrie Kellam	Co-author of manuscript	
Shailesh N. Mistry	Co-author of manuscript	
Peter J. Scammells	Co-author of manuscript	
J. Robert Lane	Co-author of manuscript	
Ben Capuano	Co-author of manuscript	

*Percentage contribution only shown for co-authors who were students at Monash University at the time of their contribution to this work

Candidates Signature:

Tim J. Fyfe

Date: 20/02/2019

Declaration by co-authors

The undersigned hereby certify that:

1. The above declaration correctly reflects the nature and extent of the candidate's contribution to this work, and the nature of the contribution of each of the co-authors.
2. They meet the criteria for authorship in that they have participated in the conception, execution, or interpretation, of at least that part of the publication in their field of expertise;
3. They take public responsibility for their part of the publication, except for the responsible author who accepts overall responsibility for the publication;
4. There are no other authors of the publication according to these criteria;
5. Potential conflicts of interest have been disclosed to (a) granting bodies. (b) the editor or publisher of journals or other publications, and (c) the head of the responsible academic unit; and
6. The original data are stored at the following locations(s) and will be held for at least five years from the date indicated below:

Department of Medicinal Chemistry, Monash Institute of Pharmaceutical Sciences, 381 Royal Parade, Parkville, Victoria, 3052, Australia.

Co-author signatures:

David Sykes:	Date: 20/02/2019
Steven J. Charlton:	Date: 20/02/2019
Barrie Kellam:	Date: 20/02/2019
Shailesh N. Mistry:	Date: 20/02/2019
Peter J. Scammells:	Date: 20/02/2019
J. Robert Lane:	Date: 20/02/2019
Ben Capuano:	Date: 20/02/2019

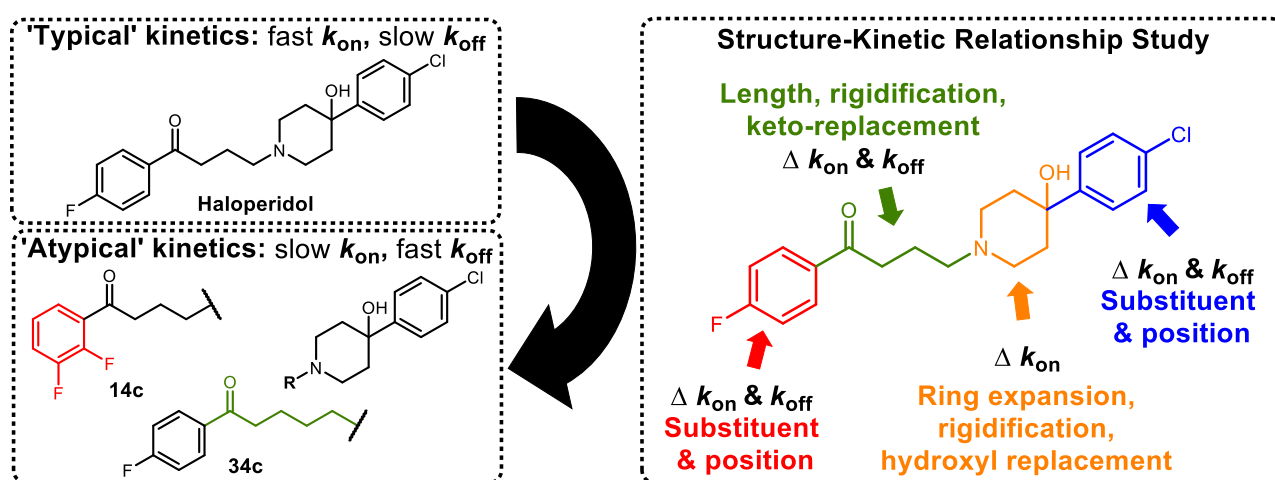
Structure-Kinetic Profiling of Haloperidol Analogues at the Dopamine D₂ Receptor

Tim J. Fyfe,^{†,‡,§} J. Robert Lane,[‡] Barrie Kellam,[‡] David Sykes,[‡] Ben Capuano,[†] Peter J. Scammells,[†] Steven J. Charlton,^{‡,*} and Shailesh N. Mistry^{‡,*}

[†]Medicinal Chemistry, and [§]Drug Discovery Biology, Monash Institute of Pharmaceutical Sciences, Monash University, Parkville, Victoria 3052, Australia.

[‡]School of Pharmacy, Centre for Biomolecular Sciences, University of Nottingham, Nottingham NG7 2RD, U.K.

^{*}School of Life Sciences, Queen's Medical Centre, University of Nottingham, Nottingham NG7 2UH, U.K.



Abstract. Haloperidol (**1**) is a “typical” butyrophenone antipsychotic drug (APD) with high propensity to cause on-target extrapyramidal side effects (EPS) and hyperprolactinemia relative to atypical APDs such as clozapine (**2**). Both drugs are antagonists at the dopamine D₂ receptor (D₂R), with contrasting kinetic profiles. Whilst **1** displays relatively fast association and slow dissociation at the D₂R, **2** exhibits relatively slow association and fast dissociation. Although **2** has a lower propensity for D₂R-mediated side effects, it is associated with severe off-target side effects. Both drugs have diverse polypharmacology, and a number of mechanisms have been proposed to explain the typical/atypical profile of APDs. We recently provided evidence that a slow dissociation rate from the D₂R predicts hyperprolactinemia, likely through insurmountable antagonism, whereas EPS were predicted by a fast association rate at the D₂R, resulting in a higher receptor rebinding potential. We suggested there may be an optimal kinetic profile where rebinding is sufficient for efficacy but insufficient to cause EPS. To further explore this hypothesis, we have conducted a detailed structure-kinetic study *via* kinetic binding parameter measurements of 50 structural analogues of **1** using a time-resolved Förster resonance energy transfer (TR-FRET) assay. Our study demonstrates that even subtle modifications to the core scaffold dramatically influences binding kinetic rate constants,

on the DA-serotonin antagonism theory. It suggests a role for the 5-HT_{2A} receptor in efficacy as well as decreased risk of EPS development.¹⁹ The relatively fast rate at which **2** dissociates from the D₂R has also been hypothesised to be the basis for its atypical profile and other related APDs. The rapid dissociation hypothesis postulates that the fast rate of APD dissociation from the D₂R contributes to the reduced side-effect profile of atypical APDs,²⁰ and was in part based on the consensus that APDs exhibit similar association rates (k_{on}) for the D₂R meaning that affinity is largely mediated by differences in dissociation rate (k_{off}).²¹

The incorporation of drug-receptor kinetic binding parameters into drug discovery programs is seen as increasingly important for the development of next generation therapeutics.²²⁻²⁹ Pharmacological experiments to derive estimates of APD kinetic rate constants have traditionally been carried out using mostly radiometric detection methods with limited assay throughput.^{21,30,31} However, we have recently developed a competition association assay using TR-FRET to determine ligand kinetic parameters of unlabelled D₂R agonists,^{32,33} and profiled an extensive series of clinical APDs under physiological temperature and sodium ion concentration in order to explore the kinetic basis for on-target side effects.³⁴ We found that association rates, but not dissociation rates, correlate with EPS, challenging the fast dissociation hypothesis.^{20,34} We proposed that rapid association rate leads to drug rebinding at the D₂R, maintaining a higher concentration of APD in the striatum and thus resulting in a more profound blockade of dopamine signalling.³⁴ In contrast, hyperprolactinaemia, which is related to the rate of reversal of APD-receptor occupancy (occurring via the phenomenon of insurmountable antagonism), was directly correlated with APD dissociation rate. In this study, **1** was shown to have fast k_{on} , slow k_{off} kinetics, whereas **2** was characterised by slow k_{on} , fast k_{off} kinetics. It is thought that the differences in kinetic rate constants may be a distinguishing factor in the corresponding clinical profile of these drugs.³⁴ This has led to an expanded kinetic hypothesis for APD side effects by considering both dissociation and association rates of drugs.³⁴ Optimising D₂R binding kinetics may permit the design of novel tools to rigorously test the kinetic hypothesis, as well as facilitate the potential generation of new APDs with an improved therapeutic profile.

Haloperidol (**1**), a typical APD, displays a lower affinity for the 5-HT_{2A} receptor and has fewer off-target side effects as compared to **2**, however it displays a kinetic profile at D₂Rs (fast k_{on} , slow k_{off}) that our recent study suggests may underlie its on-target side effect profile (i.e. a prevalence for EPS and hyperprolactinemia). In contrast, the atypical APD clozapine (**2**), displays a broad non-selective profile with affinity for many aminergic GPCRs, contributing to its off-target side effects such as weight gain. However, the latter's D₂R kinetic profile (slow k_{on} , fast k_{off}) is thought to contribute to the absence of debilitating "on-target" side effects; resulting in a lower incidence of EPS and reduced hyperprolactinemia.³⁴ We have therefore selected **1** as our model compound to interrogate and potentially optimise its kinetic profile towards that of **2**. We hypothesise that modification to the

scaffold of **1** will facilitate further understanding of the influence of molecular structure on the kinetic rate constants of D₂R ligands, toward the kinetic optimisation of novel APDs.

To this end, we herein describe the design and synthesis of 50 analogues of **1**, focusing on structural modification of four key moieties (figure 2) and use competition association kinetic binding methodology to determine their association and dissociation rates, and equilibrium affinities at the D₂R. We detail an extensive kinetic evaluation of **1**, showing that both the association and dissociation kinetics of this scaffold can vary considerably with subtle structural modification. Interestingly, we have identified previous analogues of **1**, among others, that may have been overlooked on the basis of affinity-driven scaffold optimisation, that possess favourable kinetic profiles. These data will help us interrogate the structure-kinetic relationships (SKR) of **1**, as well as expand our understanding of the kinetic hypothesis and the relationship between APD kinetic binding parameters and on-target side-effect profiles. Although the structure-activity relationships (SAR) surrounding the butyrophenone scaffold of APDs have been extensively studied in previous years,³⁵⁻⁴⁰ to our knowledge, these data represent the first reported SKR relating to analogues of **1**.

Chemistry. To begin our structure-kinetic study, we focused on modifying four distinct regions of **1**, namely the *para*-fluorophenyl (red box), ketone and alkyl linker (green box), piperidinol (orange box), and *para*-chlorophenyl (blue box) moieties, as depicted in **figure 2**. For completeness, we included both established and novel analogues of **1** in our approach, covering 50 compounds in totality.

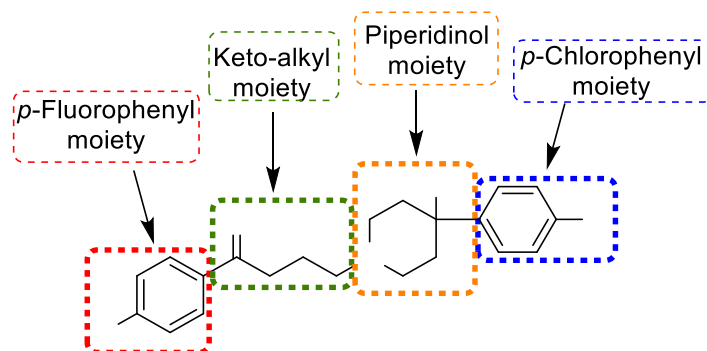
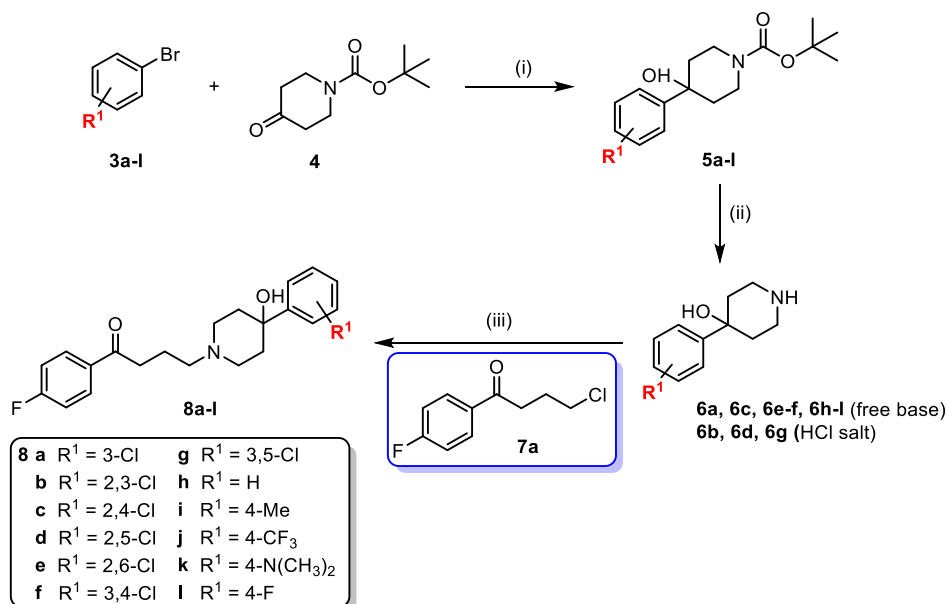


Figure 2. Structural regions of haloperidol (1) investigated as part of the SKR study.

Variation of para-chlorophenyl moiety of 1. In evaluating the positional effects of halogen substitution on the *p*-chlorophenyl moiety, we initially synthesised analogues bearing the chloro-substituent in the *ortho* (**8n**) and *meta* (**8a**) positions, as well as incorporation of all possible dichloro substitution patterns (2,3-diCl (**8b**); 2,4-diCl (**8c**); 2,5-diCl (**8d**); 2,6-diCl (**8e**); 3,4-diCl (**8f**); and 3,5-diCl (**8g**)). In addition, we wanted to assess the effects of halogen removal through the proteo analogue (**8h**), as well as alternative *para*-substituents, including methyl (**8i**), trifluoromethyl (**8j**),

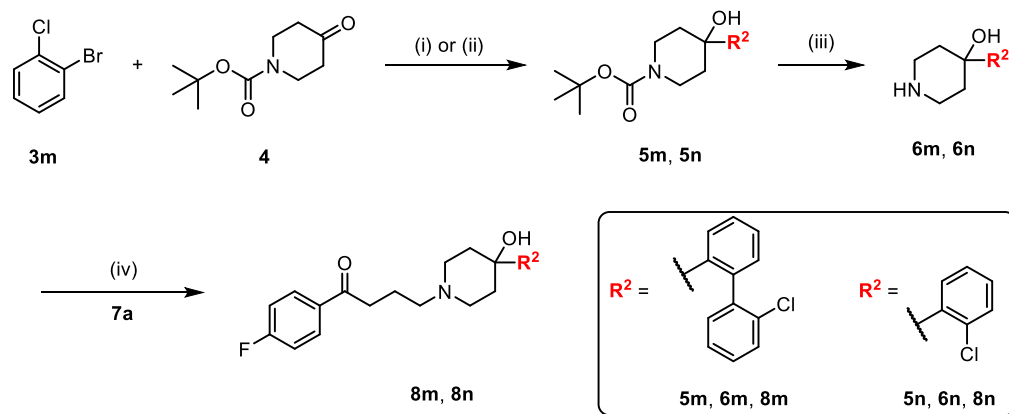
N,N-dimethylamino (**8k**) and fluoro (**8l**). The synthesis of these compounds is summarised in **scheme 1**. Firstly, the appropriately substituted bromobenzene (**3a-l**) underwent lithiation using *n*-BuLi, followed by treatment with commercially available *tert*-butyl 4-oxopiperidine-1-carboxylate (**4**) to afford the corresponding *N*-Boc-protected phenylpiperidinols (**5a-l**). HCl-mediated *N*-Boc-deprotection afforded the corresponding hydrochloride salts or free amines following basic work-up (**6a-l**). Finally, nucleophilic displacement of key intermediate 4-chloro-1-(4-fluorophenyl)butan-1-one (**7a**) with the appropriate substituted phenylpiperidinol (**6a-l**) was achieved by refluxing in toluene in the presence of KI and NaHCO₃, to afford the desired final analogues (**8a-l**).

Scheme 1. Synthesis of haloperidol (1) analogues with modification to *para*-chlorophenyl moiety^a



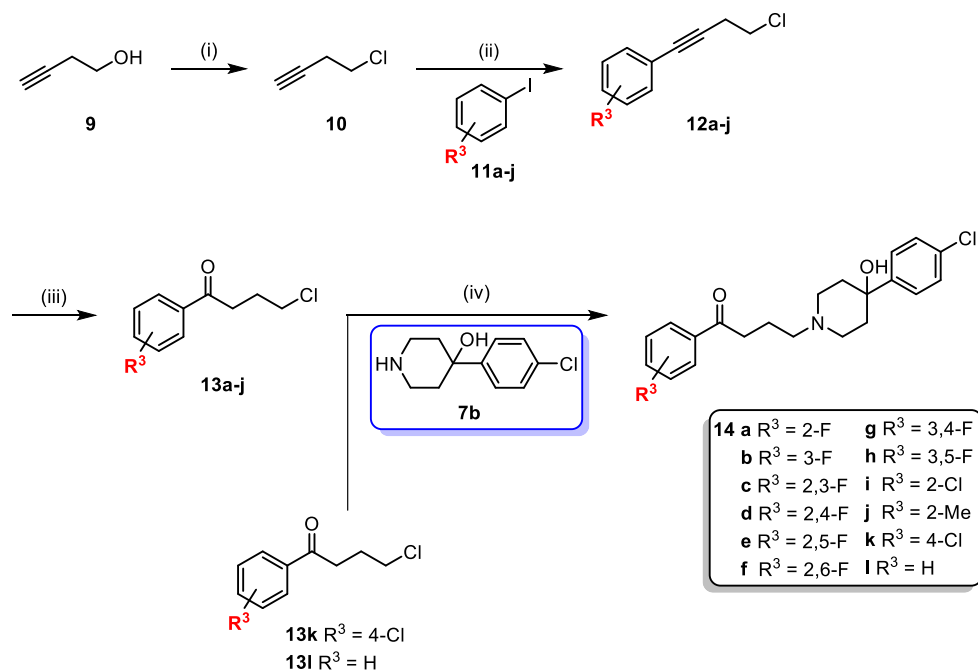
^aReagents and conditions: (i) *n*-BuLi, THF, -78 °C, 3-8 h, 50-88% (**5a-l**); (ii) HCl (4 M), 1,4-dioxane, 1-3 h, 75-98% (**6a**, **6c**, **6e-f**, **6h-l** (free base) **6b**, **6d**, **6g** (HCl salt)); (iii) NaHCO₃, KI, toluene, reflux, 24 h, 45-70% (**8a-l**).

Though established, the employed lithiation chemistry proved to be problematic towards the synthesis of the *o*-chloro analogue (**8n**, **scheme 2**). Standard conditions failed to deliver the desired *N*-Boc-protected piperidinol intermediate from **3m**, instead producing the biphenyl piperidinol (**5m**). Whilst unintended, this molecule would still provide additional information to our study and was *N*-Boc deprotected to give **6m**, followed by *N*-alkylation with **7a** using conditions outlined previously, to furnish biphenyl analogue (**8m**). In contrast, the desired *o*-chloro analogue was accessed in three steps using an alternative approach (**scheme 2**). Grignard addition of **3m** to **4** yielded *o*-chlorophenyl piperidinol intermediate **5n**, which underwent *N*-Boc deprotection to give **6n**. Final *N*-alkylation with **7a**, furnished **8n**.

Scheme 2. Synthesis of biphenyl side-product and *ortho*-Cl analogues of **1**^a

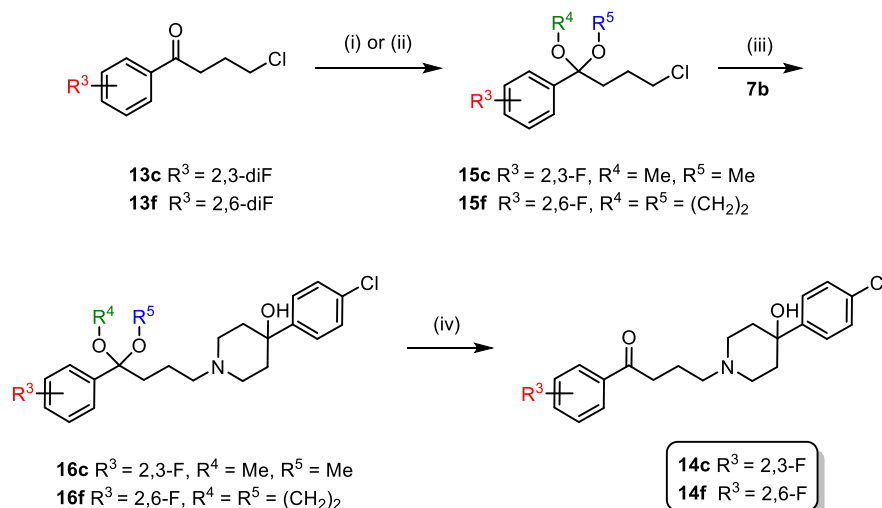
^aReagents and conditions: (i) *n*-BuLi, THF, -78 °C, 6 h, 55% (**5m**); (ii) Mg, I₂(cat.), Et₂O, 0 °C – reflux, 3 h, 54% (**5n**); (iii) HCl, 1,4-dioxane, rt, 2 h, 72-96% (**6m**, **6n**); (iii) NaHCO₃, KI, toluene, reflux, 24 h, 62-76% (**8m**, **8n**).

Variation of the p-fluorophenyl moiety of 1. To investigate positional effects of fluorine substitution in the butyrophenone phenyl ring on the kinetics of **1**, we generated analogues with all possible mono and di-fluoro substituents (2-F (**14a**); 3-F (**14b**); 2,3-diF (**14c**); 2,4-diF (**14d**); 2,5-diF (**14e**); 2,6-diF (**14f**); 3,4-diF (**14g**); 3,5-diF (**14h**), as well as two *ortho*-substituted analogues (2-Cl (**14i**) and 2-Me (**14j**)), a *para*-substituted analogue (4-Cl (**16k**)) and a *des*-fluoro variant (**14l**). As detailed in **scheme 3**, commercially available 3-butynol (**9**) was treated with SOCl₂ and catalytic pyridine at reflux temperature, followed by distillation to afford 4-chlorobut-1-yne (**10**). The appropriate iodobenzene (**11a-j**) was then employed in a Pd-catalysed Sonogashira cross-coupling reaction⁴¹ with **10**, affording the corresponding internal aryl alkynes (**12a-j**). Next, we utilised a TfOH-catalysed metal-free regioselective Markovnikov-type hydration protocol⁴² with 2,2,2-trifluoroethanol as solvent in the presence of H₂O, furnishing the corresponding aryl ketones (**13a-j**). Finally, *N*-alkylation of commercially available key intermediate **7b** with each synthesised alkyl chloride (**13a-b**, **13d-e**, **13g-j**) furnished final analogues **14a-b**, **14d-e**, and **14g-j**. Alternatively, 4-chloro-1-(4-chlorophenyl)butan-1-one (**13l**) was accessed via Friedel-Crafts acylation, followed by *N*-alkylation of **7b** to afford **14k**. Finally, commercially available 4-chloro-1-phenylbutan-1-one (**13l**) was aminated with **7b** to afford the *des*-fluoro analogue **14l**.

Scheme 3. Synthesis of analogues of 1 with modification to *p*-fluorophenyl moiety^a

^aReagents and conditions: (i) SOCl₂, pyridine, 0 °C – reflux, 30 min, 82%; (ii) PdCl₂(PPh₃)₂, CuI, Et₃N, 1,4-dioxane, 50 °C, 1-3 h, 45-85% (**12a-j**); (iii) TfOH, H₂O, CF₃CH₂OH, 60 °C, 3-8 h, 50-90% (**13a-j**); (iv) NaHCO₃, KI, toluene, reflux, 24 h, 50-82% (**14a-b, d-e, g-l**); **14c** and **14f** were detected but unable to be isolated in appreciable yield.

The synthesis of analogues containing 2,3-difluorophenyl (**14c**) and 2,6-difluorophenyl (**14f**) substituents were problematic. When attempting to *N*-alkylate key intermediate **7b** with the corresponding alkyl halides (**13c**, **13f**) major side-products due to a competing S_NAr reaction were observed, making purification of the target compounds by FCC and preparative HPLC extremely challenging. These side-products are believed to arise due to activation of the position *ortho* to the ketone moiety, when a fluoro-substituent is present. To circumvent the S_NAr reaction, syntheses of the affected analogues were modified to incorporate ketal protection/deprotection of the ketone, permitting nucleophilic displacement of the alkyl halide only (**scheme 4**). Beginning with ketal protection of **13c**, we employed a *p*TsOH-catalysed reaction with trimethyl orthoformate in MeOH at room temperature, to afford the corresponding dimethyl ketal (**15c**). Alternatively, **13f** was reacted with 1,2-ethanediol in the presence of catalytic *p*TsOH in toluene under Dean-Stark conditions, to afford the corresponding 1,3-dioxolane (**15f**). These compounds were then subjected to nucleophilic displacement using **7b** to furnish **16c** and **16f**, followed by acid-catalysed hydrolysis in acetone at reflux, affording final compounds **14c** and **14f**.

Scheme 4. Synthesis of 2,3- and 2,6-difluoro analogues of **1** using various protection strategies^a

^aReagents and conditions: (i) trimethylorthoformate, *p*-TsOH.H₂O, MeOH, rt, 12 h, 77% (**15c**); (ii) ethylene glycol, *p*-TsOH.H₂O, toluene, reflux (Dean-Stark), 16 h, 83% (**15f**); (iii) NaHCO₃, KI, toluene, reflux, 24 h, 71-77% (**16c**, **16f**); (iv) *p*-TsOH.H₂O, 15:1 acetone/H₂O, reflux, 48 h, 76-82% (**14c**, **14f**).

Variation of ketone and linker moiety of 1. We focused on replacement of the ketone group of **1** with a range of moieties, including ether, thioether and the corresponding carbinol (racemic). The ether- and thioether-variants of **1** were accessed using a literature procedure in three steps⁴³ (**17a-b**, Figure 3, Supplementary Scheme 1), whilst the corresponding secondary alcohol was afforded in two-steps also through literature procedure (**18**, Figure 3)⁴⁴ (Supplementary Scheme 2).

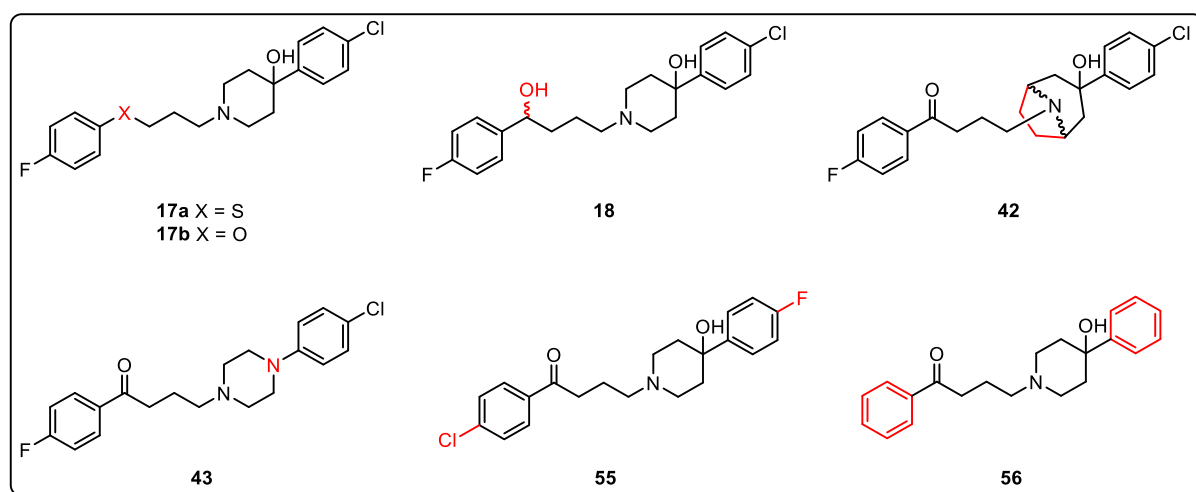
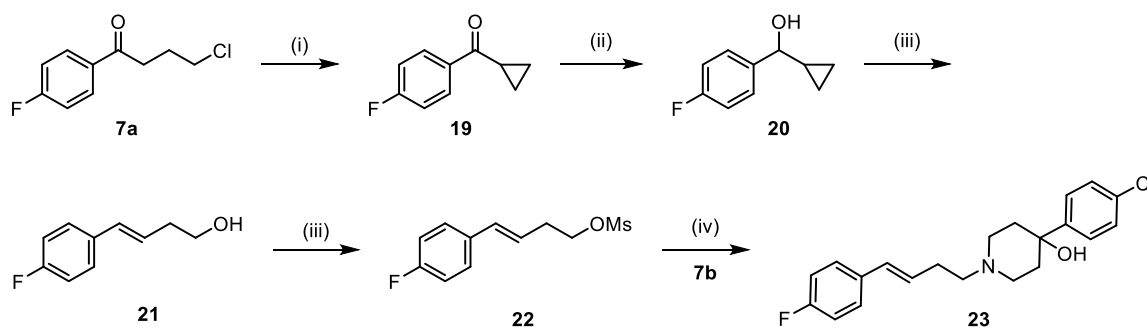


Figure 3. Literature analogues of 1 synthesised using various methodologies. (A) Ether- and thioether-analogues⁴³ (**17a-b**, respectively). (B) Racemic alcohol analogue⁴⁴ (**18**). (C) Tropanyl analogue³⁵ (**42**). (D) Piperazinyl analogue³⁵ (**43**). (E) Reverse substitution analogue⁴⁵ (**55**). (F) *des*-Halo analogue⁴⁶ (**56**).

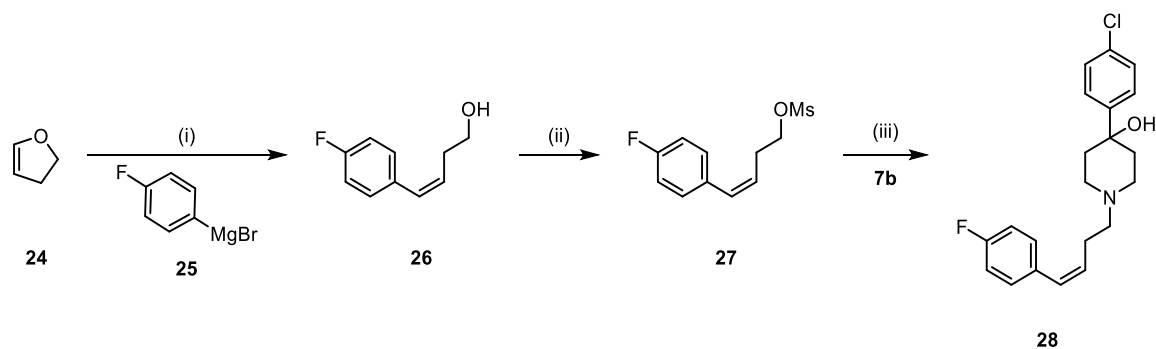
Our subsequent focus was to further understand the effect and importance of geometry on the kinetics of conformationally restricted analogues of **1**, via synthesis of both olefin geometric isomers. The *trans*-olefin **23** was accessed through a five step chemical synthesis as outlined in **scheme 5**, beginning with a one-pot base-mediated intramolecular enolate alkylation of key intermediate **7a**, to furnish cyclopropyl(4-fluorophenyl)methanone (**19**) in quantitative yield. Subsequent reduction with NaBH₄ afforded secondary alcohol **20**, followed by a vanadyl acetylacetonate-catalysed stereoselective isomerisation in chlorobenzene to yield (*E*)-4-(4-fluorophenyl)but-3-en-1-ol (**21**) as the exclusive geometric isomer. Compound **21** was subsequently activated with methanesulfonyl chloride to give mesylate **22**. This was followed by *N*-alkylation of **7b** using standard conditions, affording final olefin analogue **23**.

Scheme 5. Synthesis of *trans*-olefin analogue of **1**^a

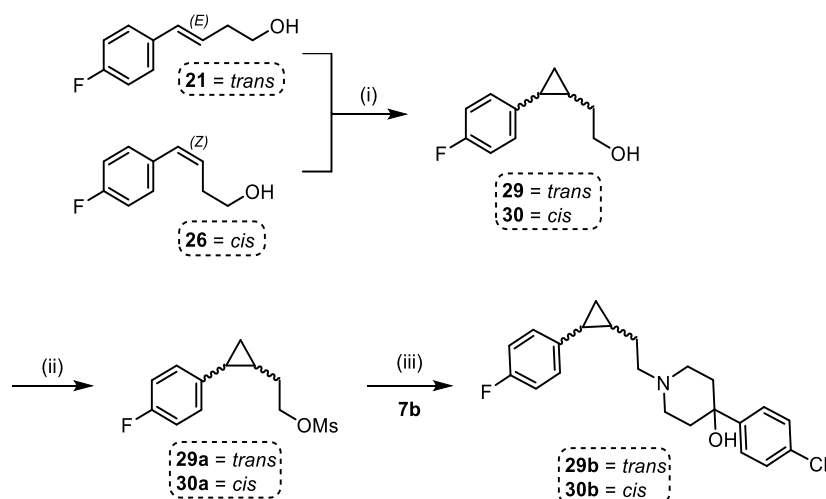


^aReagents and conditions: (i) NaOH, MeOH, 60 °C, 5 h, quantitative; (ii) NaBH₄, MeOH, 0 °C – rt, 3 h, 99%; (iii) VO(acac)₂, BHT, PhCl, 80 °C, 48 h, 35%; (iv) MsCl, DCM, Et₃N, rt, 3h, 88%; (v) NaHCO₃, KI, toluene, reflux, 24 h, 82%.

The *cis*-isomer **28**, was accessed through a three-step synthesis as outlined in **scheme 6**. Initially, Ni-catalysed stereoselective arylation of 2,3-dihydrofuran **24** with (4-fluorophenyl)magnesium bromide (**25**) at -30 °C, successfully afforded the *cis*-olefin **26** as the exclusive isomer. This compound was then mesylated using standard conditions to afford **27**, followed by *N*-alkylation of **7b** using conditions outlined previously, furnishing **28**. As outlined in **scheme 7**, both *trans* and *cis*-isomers (**21** and **26**, respectively) were treated with diethylzinc and diiodomethane using Simmons-Smith⁴⁷ conditions to access the corresponding racemic *trans*- and *cis*-cyclopropanes (**29** and **30**, respectively). This was followed by mesylation to give **29a** and **30a**, and subsequent *N*-alkylation of **7b** to afford racemic **29b** and **30b**.

Scheme 6. Synthesis of *cis*-olefin analogue of 1^a

^aReagents and conditions: (i) Ni[COD]₂, 1,3-bis-(2,6-diisopropylphenyl)imidazolium chloride, LiCl, THF, -30 °C, 8 h, 31%; (ii) MsCl, Et₃N, DCM, rt, 24 h, 90%; (iii) NaHCO₃, KI, toluene, reflux, 24 h, 75%.

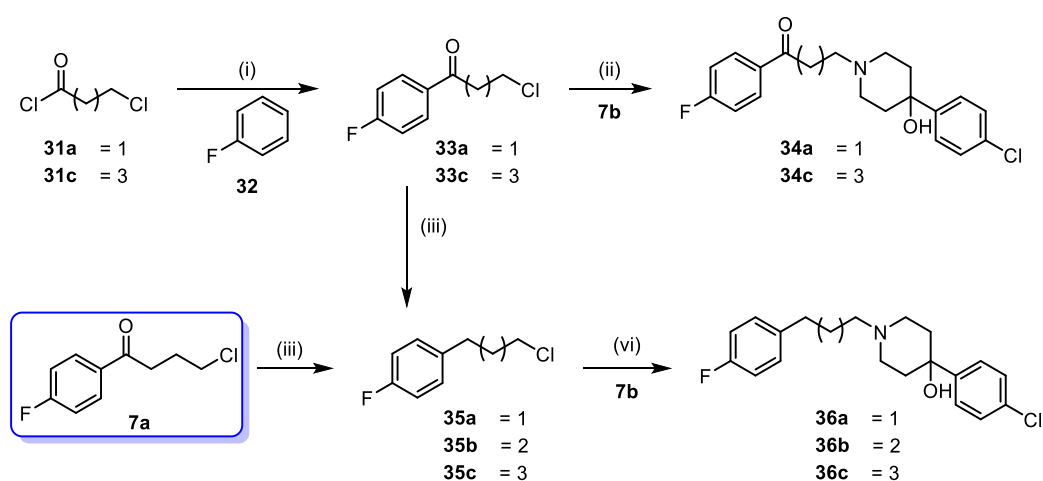
Scheme 7. Synthesis of both *trans*- and *cis*-cyclopropane enantiomers of 1^a

^aReagents and conditions: (i) Et₂Zn, CH₂I₂, DCM, 0 °C – rt, 24 h, 95-98% (**29**, **30**); (ii) MsCl, Et₃N, DCM, rt, 90-95% (**29a**, **30a**); (iii) NaHCO₃, KI, toluene, reflux, 24 h, 67-70% (**29b**, **30b**).

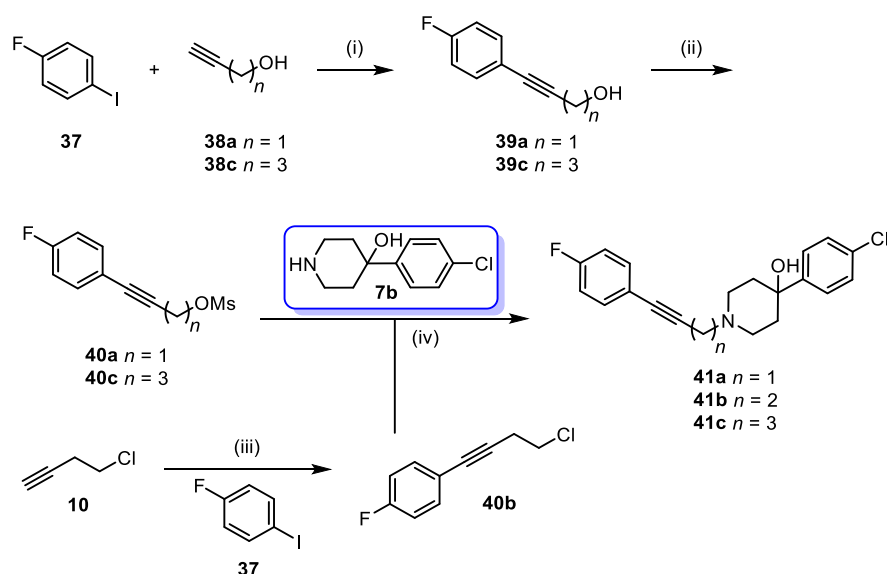
Next, we focused on the synthesis of both propiophenone and valerophenone analogues of **1** that maintained the ketone functionality (**scheme 8**). Beginning with Friedel-Crafts acylation chemistry, the appropriate commercially available acyl chloride (**31a**, **31c**) was reacted with fluorobenzene **32** in the presence of stoichiometric AlCl₃ to afford the corresponding phenones (**33a**, **33c**). This was followed by *N*-alkylation of **7b** to afford final analogues (**34a**, **34c**). In addition, we wanted to access the 1,3-propylene, 1,4-butylene and 1,5-pentylene analogues of **1** (**scheme 8**). To achieve this, phenones **33a**, **7a**, and **33c** were treated with triethylsilane in TFA, followed by evaporation and direct chromatographic purification to furnish the corresponding reduced intermediates **35a-c**. Lastly, *N*-alkylation of key intermediate **7b** furnished alkane analogues **36a-c**.

To assess analogues of **1** incorporating internal aromatic alkynes (**scheme 9**), 1-fluoro-4-iodobenzene (**37**) was initially subjected to modified Sonagashira conditions⁴⁸ using commercially available alcohols (**38a**, **38c**), affording aryl alkynes (**39a**, **39c**). Next, the alcohols were converted to their corresponding mesylates (**40a**, **40c**), followed by *N*-alkylation of **7b** with the appropriate mesylate to afford the corresponding final propynyl and pentynyl analogues (**41a** and **41c**, respectively). The butynyl analogue **41b** was accessed via the cross-coupling reaction between key intermediate **10** and 1-fluoro-4-iodobenzene (**37**), providing aryl alkyne intermediate **40b**, which underwent amination with **7b**.

Scheme 8. Synthesis of ketone and alkane analogues of **1**^a



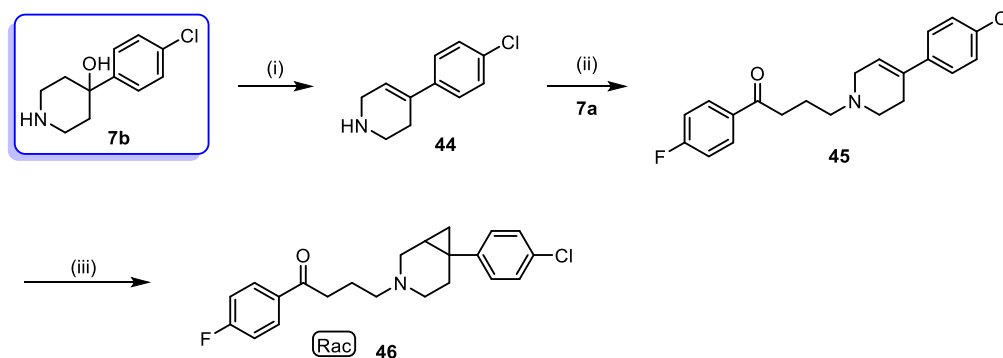
^aReagents and conditions: (i) AlCl₃, DCM, 0 °C – rt, 6 h, 85% (**33a**, **33c**); (ii) NaHCO₃, KI, toluene, reflux, 24 h, 75-90% (**34a**, **34c**); (iii) triethylsilane, trifluoroacetic acid, 0 °C, 2-3 h, 75-85% (**35a-c**); (iv) NaHCO₃, KI, toluene, reflux, 24 h, 72-91% (**36a-c**).

Scheme 9. Synthesis of internal alkyne analogues of **1**^a

^aReagents and conditions: (i) Pd(PPh₃)₂Cl₂, CuI, Et₃N, MeCN, rt, 5 h, 94% (**39a**, **39c**); (ii) methanesulfonyl chloride, Et₃N, DCM, 24 h, 93% (**40a**, **40c**); (iii) PdCl₂(PPh₃)₂, Et₃N, 1,4-dioxane, 50 °C, 3 h, 75% (**40b**); (iii) NaHCO₃, KI, toluene, reflux, 24 h, 68-74% (**41a-c**).

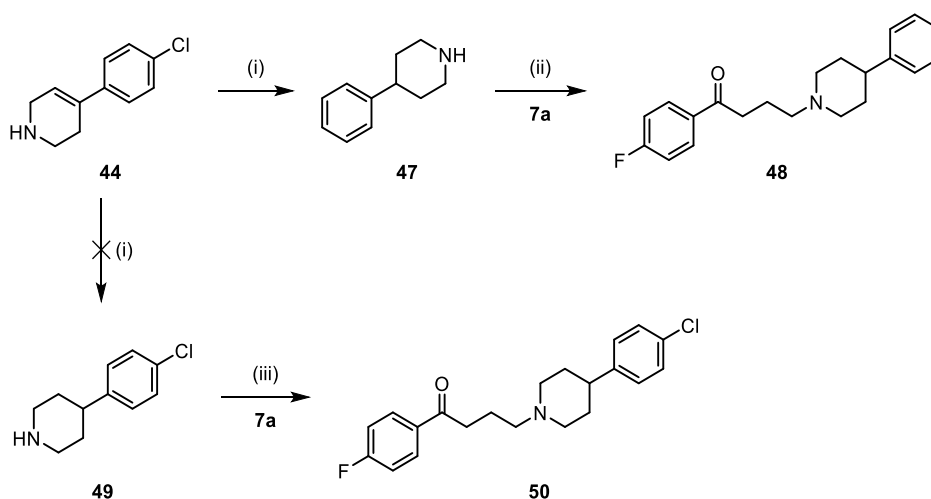
Variation of the piperidinol moiety of 1. Modification to the piperidinol moiety of **1** was another key interest in our SKR investigation. To observe the kinetic effect of introducing an ethylene bridge on the piperidinol, we synthesised tropanyl analogue **42** according to a literature procedure³⁷ (Figure 3, Supplementary Scheme 3), utilising *n*-BuLi in place of Grignard chemistry. We then sought to modify the tertiary alcohol group, beginning with synthesis of piperazinyl analogue **43** (Figure 3). This compound was accessed in two steps *via* the construction of the piperazine ring and subsequent *N*-alkylation with **7a**³⁵ (Supplementary Scheme 4).

Removing the tertiary alcohol within **1** to generate the corresponding 3,6-dihydropyridine (**45**) was our next focus, as well as further elaboration of the olefin to yield the corresponding cycloalkane derivative (**46**) (scheme 10). Key piperidinol intermediate **7b** was firstly dehydrated using neat concentrated HCl followed by an alkaline work-up to afford the 1,2,3,6-tetrahydropyridine (**44**). Displacement of **7a** with **44** furnished olefin **45**. This molecule was subsequently treated using Simmons-Smith⁴⁷ conditions, as outlined previously, to afford the corresponding cyclopropane analogue **46**.

Scheme 10. Synthesis of dihydropyridyl and fused cyclopropane analogues of 1^a

Reagents and conditions: (i) HCl (conc.), reflux, 5 h, quantitative; (ii) NaHCO₃, KI, toluene, reflux, 24 h, 65%; (iii) Et₂Zn, CH₂I₂, DCM, 0 °C – rt, 24 h, 75% (**46b**).

In addition, we synthesised two piperidine analogues of **1** (**scheme 11**). 1,2,3,6-Tetrahydropyridine intermediate **44** was subjected to a 10% Pd/C-catalysed hydrogenation using standard conditions, however resulted in dehalogenation of the aryl chloride to produce the corresponding unsubstituted phenylpiperidine **47**. Displacement of **7a** with **47** furnished the *des*-chlorophenyl piperidine analogue **48**. To circumvent dehalogenation, use of Adam's catalyst was explored but still resulted in dehalogenation. To this end, we sourced commercially available 4-(4-chlorophenyl)piperidine **49** and, following *N*-alkylation with **7a**, afforded the corresponding 4-chlorophenyl piperidine analogue **50**.

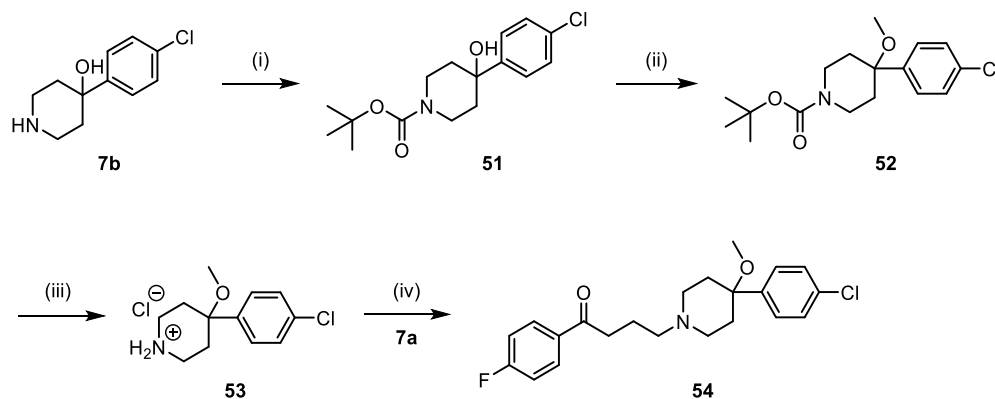
Scheme 11. Synthesis of phenyl piperidinyl analogues of 1^a

^aReagents and conditions: (i) 10% Pd/C, H_{2(g)}, MeOH, rt, 4 h, 95%; (ii) NaHCO₃, KI, toluene, reflux, 24 h, 68%; (iii) NaHCO₃, KI, toluene, reflux, 24 h, 70%.

Further emphasis was placed on the tertiary alcohol contained within **1**, where we sought to assess the impact of *O*-methylation (**scheme 12**). *N*-Boc-protection of key intermediate **7b** gave **51**, followed

by *O*-alkylation with methyl iodide to afford the corresponding methyl ether **52**. This was followed by *N*-Boc-deprotection to give secondary amine **53** as the hydrochloride salt. Final *N*-alkylation with key intermediate **7a** afforded compound **54**.

Scheme 12. Synthesis of methyl ether analogue of 1^a



^aReagents and conditions: (i) Boc₂O, Et₃N, DCM, rt, 4 h, 85%; (ii) NaH, MeI, DMF, rt, 24 h, 80%; (iii) HCl, 1,4-dioxane, rt, 2 h, 95%; (iv) NaHCO₃, KI, toluene, reflux, 24 h, 70%.

Dual modification to halo-aryl moieties of 1. Recent molecular dynamics (MD) simulations by Thomas *et al.*⁴⁹ were used to understand the ligand binding pathways of **1** and **2** at the D₂R/D₃R. The final stable pose of **1** was shown to occupy the same space as predicted in a number of molecular docking studies;⁵⁰⁻⁵² however, the molecular orientation was contradictory to these data by 180°, with the butyrophenone moiety buried most deeply in the receptor. Therefore, and due to confounding studies regarding the orientation of **1** at the D₂R, it was of interest to investigate the kinetic effects of modifying both phenyl moieties of **1** simultaneously. Accordingly, we synthesised a further two structural analogues of **1** (Figure 3, Supplementary Scheme 4). These modifications included swapping both aromatic termini (**55**), as well as removal of these aromatic substituents (**56**). **55** was synthesised according to a literature procedure following Friedel-Crafts acylation and *N*-alkylation.⁵³ Compound **56** was similarly accessed through literature methods (Figure 3, Supplementary Scheme 4).⁴⁶

Pharmacology. *Characterisation of PPHT-red binding.* Specific equilibrium binding of the agonist PPHT-red (Cisbio Bioassays) to human D_{2L} receptor (hD_{2L}R) was saturable and best described by the interaction of PPHT-red with a single population of binding sites (Supplementary Figure 1A). From these studies, the equilibrium dissociation constant (K_d) of the fluorescent ligand was determined to be 43.2 ± 0.37 nM. The binding kinetics of PPHT-red were characterised by monitoring the observed association rates at six different ligand concentrations (Supplementary Figure 1B). The observed rate of association was related to PPHT-red concentration in a linear fashion (Supplementary Figure 1C). Kinetic rate parameters for PPHT-red were calculated by globally fitting the association time courses, resulting in a k_{on} of $9.21 \pm 0.24 \times 10^6$ M⁻¹ min⁻¹ and k_{off} of 0.35 ± 0.01 min⁻¹. The resulting K_d (k_{off}/k_{on}) of 46.3 ± 0.15 nM was comparable to that obtained from equilibrium studies.

Characterisation of kinetic binding parameters of unlabelled analogues of 1 at the D₂R. The competition association binding method allows the characterisation of the kinetic rate parameters of unlabelled compounds (k_{on} , k_{off}) and the subsequent calculation of a kinetically-derived (k_{on}/k_{off}) equilibrium dissociation constant (K_d). The binding affinity of the various ligands for the hD_{2L}R were measured at equilibrium at 37 °C in a buffer containing 5'-guanylyl imidodiphosphate (GppNHp) (0.1 mM) to ensure that antagonist and tracer binding only occurred to the G protein-uncoupled form of the receptor. K_i values for compound **1**, **2**, and the 50 structural analogues studied are summarised in Tables 1-5, and representative competition curves are presented in Figure 4A. In these tables we have separated the analogues into five groups, those that have been modified at the *para*-chlorophenyl, *para*-fluorophenyl, piperidinol, ketone/alkyl linker, and concurrent phenyl ring moiety modification, as indicated in Figure 2. Representative kinetic competition curves for selected analogues are in Figures 4B-D. Association curves for PPHT-red alone and in the presence of competitor were globally fitted to Eq. 3 enabling the calculation of both k_{on} (k_3) and k_{off} (k_4) for each of the ligands, as reported in Tables 1-5. To validate the rate constants, we compared the kinetically derived dissociation constant (K_d) values (k_{on}/k_{off}) with the dissociation constant (K_i) obtained from equilibrium competition binding experiments (Figure 5). There was a good correlation between these two values for all compounds tested (two-tailed Pearson's correlation $r^2 = 0.99$, $p < 0.0001$), indicating that the parameters determined in the kinetic assay were in agreement with those determined at equilibrium.

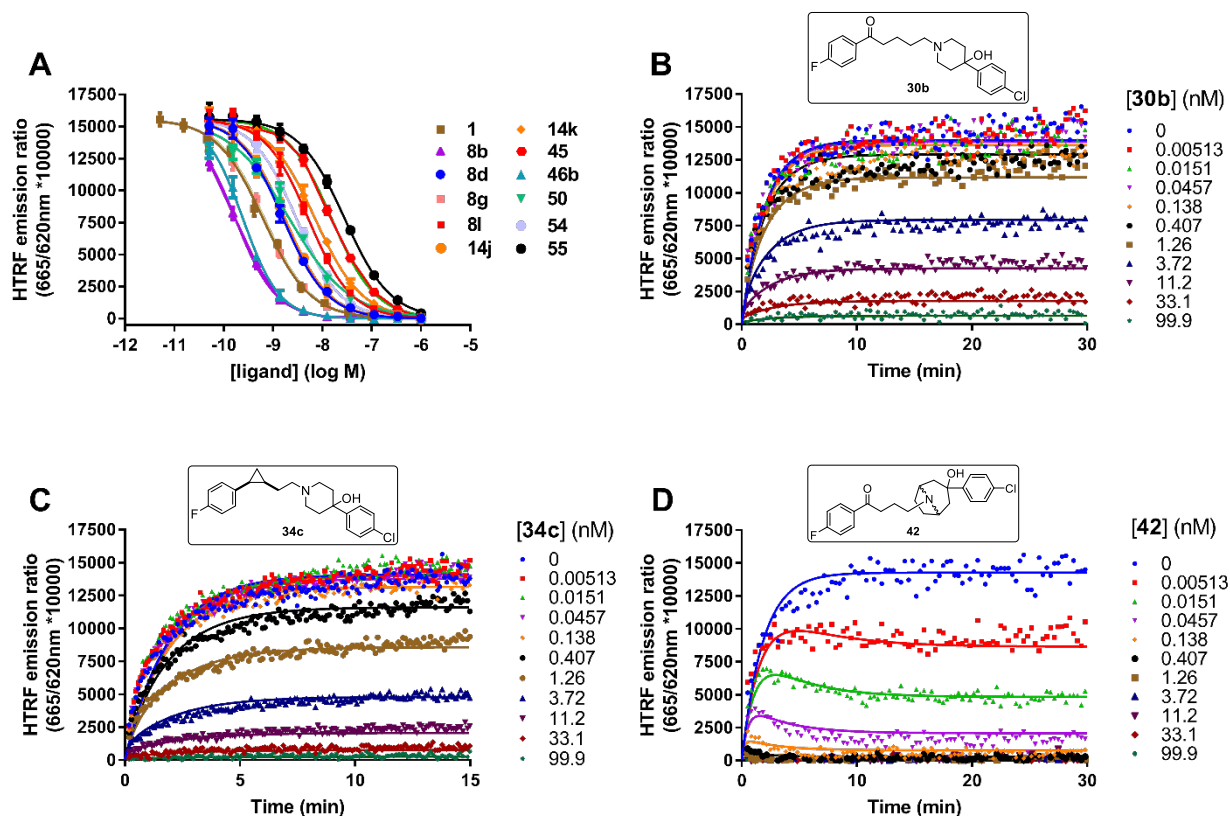


Figure 4. Equilibrium and competition association binding. (A) Competition between PPHT-red (12.5 nM) and increasing concentrations of **1** and representative analogues (**8b**, **8d**, **8g**, **8l**, **14j**, **14k**, **45**, **46**, **50**, **55**) at the hD₂L R. PPHT-red competition association curves in the presence of (B) **30b**; (C) **34c**; (D) **42**. All binding reactions were performed at 37 °C in the presence of GppNHp (100 μM) with non-specific binding levels determined by inclusion of haloperidol (10 μM). Kinetic and equilibrium data were fitted to the equations described in “Methods” section to calculate K_i , K_d , and k_{on} and k_{off} values for the unlabelled ligands: these are summarised in tables 1-5. Data are presented as singlet values from a representative of four.

Characterisation of the kinetic profile of 1 at the hD₂L R. The equilibrium affinities and kinetic rate constants of **1** and **2** have recently been determined using the aforementioned TR-FRET assay.³⁴ Prior to initiating an investigation into **1**, we also assessed its parameters and determined similar estimates in agreement with literature³⁴ ($k_{off} = 0.61 \pm 0.04 \text{ min}^{-1}$, $k_{on} = 1.29 \pm 0.21 \times 10^9 \text{ M}^{-1} \text{ min}^{-1}$, $pK_d = 9.31 \pm 0.05$, Table 1), validating our experimental conditions and further demonstrating that **1** is indeed a high affinity, fast k_{on} /slow k_{off} compound at the hD₂L R. Previous characterisation of **2** using the same experiment under identical test conditions showed it to have relatively slow k_{on} , fast k_{off} kinetic properties ($k_{on} = 8.23 \pm 1.42 \times 10^7 \text{ M}^{-1} \text{ min}^{-1}$, $k_{off} = 1.67 \pm 0.25 \text{ min}^{-1}$), and moderate affinity ($pK_d = 7.69 \pm 0.02$) consistent with literature estimates.^{34,54} These values are outlined in Tables 1-5 and all experimental structure-kinetic data will make specific reference to these data as a comparison.

Furthermore, compounds with fast k_{off} values approaching $>1.0 \text{ min}^{-1}$ were reassessed using a modified “online” injection protocol, whereby the hD₂L_R membrane homogenates were introduced using an online injector whilst simultaneously measuring TR-FRET binding. This is to avoid any delay between membrane addition and initial TR-FRET measurement, improving the quality of the non-linear fit for compounds with rapid equilibration kinetics and thus increasing our confidence in the rate parameter estimate. Characterisation of **1** using this methodology returned comparable estimates to the offline injection protocol. Additional data acquired for selected compounds using this methodology are located in Tables 2 and 3.

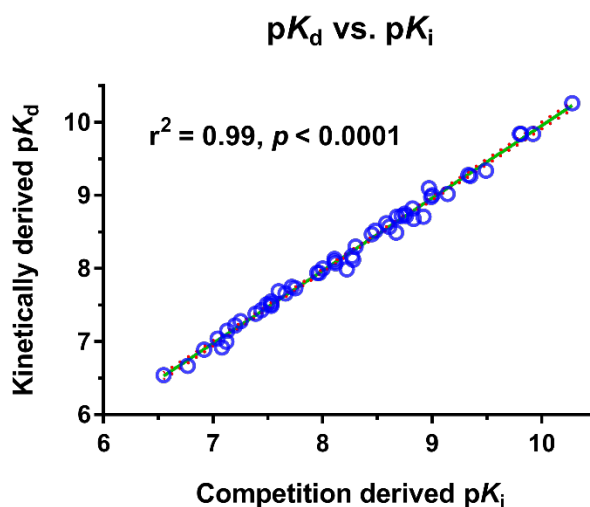


Figure 5. Correlating equilibrium and kinetically derived parameters for haloperidol (1**) and **51** structural analogues at the dopamine D₂ receptor.** Correlation between pK_i and kinetically derived pK_d for the 51 test ligands including haloperidol. pK_i values were taken from PPHT-red competition binding experiments at equilibrium as exemplified in Figure 4A. The values composing the kinetically derived pK_d ($k_{\text{off}}/k_{\text{on}}$) were taken from competition kinetic association experiments as exemplified in Figures 4B-D. All data used in these plots are detailed in Tables 1-5. Data are presented as mean \pm S.E.M. from four separate experiments.

Kinetic effects of variation of the para-chlorophenyl moiety of 1. Initially focusing on modification of the *para*-chlorophenyl moiety of **1**, we sought to assess the kinetic effect of all possible mono (**8a**, **8n**) and di-chlorophenyl substituents (**8b-g**), as well as variation of the *para*- substituent (**8h-m**) through the synthesis of 14 structural analogues (Table 1). These compounds exhibited a 17-fold variation in affinity, which was driven by interesting changes in kinetic parameters, spanning a >10 -fold variation in association rate ($k_{\text{on}} = 1.22 \pm 0.20 \times 10^8 \text{ M}^{-1} \text{ min}^{-1}$ to $2.95 \pm 0.30 \times 10^9 \text{ M}^{-1} \text{ min}^{-1}$), and a ~ 4 -fold variation in dissociation rate ($k_{\text{off}} = 0.30 \pm 0.01 \text{ min}^{-1}$ to $k_{\text{off}} = 1.25 \pm 0.09 \text{ min}^{-1}$).

The data show that analogues lacking an electron withdrawing group (EWG) (chloro) substituent at the *meta*- and *para*-positions have reduced binding affinity, and this loss is mirrored by a decrease in k_{on} and an increase in k_{off} relative to **1**. For example, the *ortho*-Cl analogue (**8n**) displayed an ~8-fold reduction in affinity resulting from a decreased k_{on} and increased k_{off} ($k_{\text{on}} = 3.54 \pm 0.16 \times 10^8 \text{ M}^{-1} \text{ min}^{-1}$, $k_{\text{off}} = 1.16 \pm 0.11 \text{ min}^{-1}$). This was also evident for the 2,6-diCl analogue (**8e**) losing ~6-fold affinity, also mediated by a slowed association and increased dissociation rate ($k_{\text{on}} = 5.07 \pm 0.47 \times 10^8 \text{ M}^{-1} \text{ min}^{-1}$, $k_{\text{off}} = 1.05 \pm 0.05 \text{ min}^{-1}$). This trend continued with the *des*-Cl analogue **8h**, as it also revealed a similar change in rate constants ($k_{\text{on}} = 1.22 \pm 0.20 \times 10^8 \text{ M}^{-1} \text{ min}^{-1}$, $k_{\text{off}} = 1.02 \pm 0.10 \text{ min}^{-1}$).

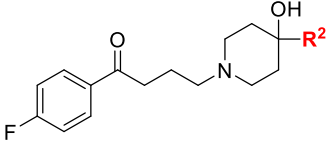
Addition of a strong electron donating group (EDG) (*N,N*-dimethylamino, **8k**) results in a >10-fold decrease in affinity ($\text{p}K_{\text{d}} = 8.12 \pm 0.04$) and again appears to be driven by a decrease in k_{on} and an increase in k_{off} ($k_{\text{on}} = 1.64 \pm 0.12 \times 10^8 \text{ M}^{-1} \text{ min}^{-1}$, $k_{\text{off}} = 1.25 \pm 0.09 \text{ min}^{-1}$), with this compound displaying a kinetic profile similar to that of **2**. Furthermore, other analogues bearing weakly electron donating substituents (e.g. *para*-tolyl analogue **8i**) saw a smaller decrease in affinity (~3-fold), similarly mediated by a change in both rate constants towards the profile of **2** ($k_{\text{on}} = 1.00 \pm 0.06 \times 10^9 \text{ M}^{-1} \text{ min}^{-1}$, $k_{\text{off}} = 0.98 \pm 0.02 \text{ min}^{-1}$).

Conversely, insertion of a *meta*-Cl substituent (exemplified by **8a**), despite decreasing affinity ~8-fold, acts only to decrease the k_{on} whilst having no effect on k_{off} ($k_{\text{on}} = 3.62 \pm 0.94 \times 10^8 \text{ M}^{-1} \text{ min}^{-1}$, $k_{\text{off}} = 0.64 \pm 0.10 \text{ min}^{-1}$), and this similarly applies to *para*-Cl substituents. The trend continued with 2,4-dichloro (**8c**) and 2,5-dichloro (**8d**) analogues, losing ~7-fold and 3-fold affinity, respectively. Again, this loss was largely mediated by a decreased association rate (**8c**: $k_{\text{on}} = 2.87 \pm 0.56 \times 10^8 \text{ M}^{-1} \text{ min}^{-1}$, $k_{\text{off}} = 0.70 \pm 0.16 \text{ min}^{-1}$; **8d**: $k_{\text{on}} = 5.29 \pm 0.36 \times 10^8 \text{ M}^{-1} \text{ min}^{-1}$, $k_{\text{off}} = 0.56 \pm 0.06 \text{ min}^{-1}$), relative to **1**. Interestingly, when the *ortho*- and *meta*-chloro substituents are combined (2,3-diCl analogue (**8b**)), affinity increases ~5-fold, and this is now predominantly mediated by both a ~2-fold increase in association rate and ~2-fold decrease in dissociation rate ($\text{p}K_{\text{d}} = 9.84 \pm 0.08$, $k_{\text{on}} = 2.20 \pm 0.30 \times 10^9 \text{ M}^{-1} \text{ min}^{-1}$, $k_{\text{off}} = 0.30 \pm 0.01 \text{ min}^{-1}$). Substitution with a strongly electron withdrawing *para*-CF₃ substituent (**8j**) maintained affinity, with no effect on the kinetic profile of the analogue relative to **1** ($k_{\text{on}} = 1.36 \pm 0.07 \times 10^9 \text{ M}^{-1} \text{ min}^{-1}$, $k_{\text{off}} = 0.62 \pm 0.02 \text{ min}^{-1}$). Furthermore, replacing the *para*-chloro substituent for a *para*-fluoro (**8l**) predominantly decreased k_{on} .

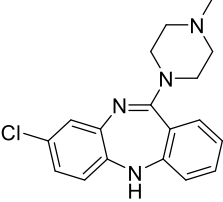
All compounds bearing an *ortho*-substituent (**8n**, **8c**, **8d**, **8e**, **8m**), with the exception of **8b**, displayed a reduced on-rate, indicating potential sensitivity to steric bulk at this position through resulting rotation of the phenyl group relative to the piperidinol. Interestingly, the 2,3-diCl analogue (**8b**), contains the privileged 2,3-dichlorophenylpiperidine pharmacophore known to confer high affinity in other molecules at both the D₂-like and 5HT receptors. This particular substitution pattern may therefore support a different binding mode. Both increased lipophilicity and steric bulk are preferred

at the *meta*- and *para*-positions of the ring, with the 4-position being optimal, which is supported by **8h** (4-fluoro) and **8l** (4-H) being less favoured. For the off-rate, the substituent effect is reversed in terms of increasing k_{off} ($o > m > p$). This parameter appears to be less impacted by steric factors, and instead the electronics may play a greater role (**8k**, **8i**, **8h**). In summary, these initial data provide insight into how structural modifications of haloperidol (**1**) impact upon individual kinetic parameters, demonstrating the potential for differential modification of rate constants towards the profile of clozapine (**2**) depending on the position and nature of the aryl substituents of the 4-phenylpiperidin-4-ol moiety.

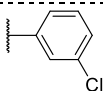
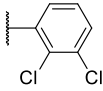
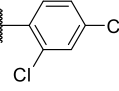
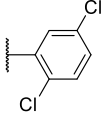
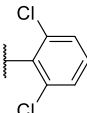
Table 1. Kinetic binding parameters for haloperidol (**1**), clozapine (**2**), and unlabelled analogues of **1** for human D_{2L} receptors estimated using TR-FRET assay.

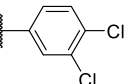
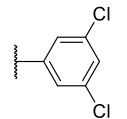
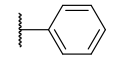
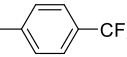
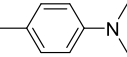
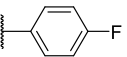
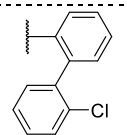


Haloperidol (**1**), **8a-8n**



Clozapine (**2**)

#	R ²	k_{on} (M ⁻¹ min ⁻¹) ^a	k_{off} (min ⁻¹) ^a	$t_{1/2}$ (min) ^a	pK _d ^a	pK _i ^b
1		1.29±0.21 × 10 ⁹	0.61±0.04	1.15±0.08	9.31±0.05	9.33±0.09
2 ³²	-	8.23±1.42 × 10 ⁷	1.67±0.25	0.41	7.69±0.02	7.60±0.02
8a		6.32±0.94 × 10 ⁸	0.64±0.10	1.19±0.22	9.00±0.05	9.00±0.03
8n		3.54±0.16 × 10 ⁸	1.16±0.11	0.61±0.05	8.49±0.03	8.67±0.09
8b		2.20±0.30 × 10 ⁹	0.30±0.01	2.28±0.04	9.84±0.08	9.92±0.03
8c		2.87±0.56 × 10 ⁸	0.70±0.16	1.15±0.24	8.62±0.02	8.58±0.01
8d		5.29±0.36 × 10 ⁸	0.56±0.06	1.27±0.11	8.98±0.02	8.99±0.01
8e		5.07±0.47 × 10 ⁸	1.05±0.05	0.67±0.05	8.68±0.04	8.83±0.08

8f		$2.95 \pm 0.30 \times 10^9$	0.42 ± 0.02	1.67 ± 0.11	9.84 ± 0.03	9.81 ± 0.04
8g		$6.58 \pm 0.67 \times 10^8$	0.43 ± 0.02	1.94 ± 0.30	9.27 ± 0.06	9.35 ± 0.04
8h		$1.22 \pm 0.20 \times 10^8$	1.02 ± 0.10	0.71 ± 0.08	8.07 ± 0.04	8.12 ± 0.02
8i		$1.00 \pm 0.06 \times 10^9$	0.98 ± 0.11	0.73 ± 0.07	9.02 ± 0.03	9.14 ± 0.08
8j		$1.36 \pm 0.07 \times 10^9$	0.62 ± 0.02	1.12 ± 0.04	9.34 ± 0.04	9.49 ± 0.10
8k		$1.64 \pm 0.12 \times 10^8$	1.25 ± 0.09	0.56 ± 0.03	8.12 ± 0.04	8.28 ± 0.09
8l		$2.61 \pm 0.24 \times 10^8$	0.78 ± 0.08	0.92 ± 0.11	8.52 ± 0.02	8.48 ± 0.01
8m		$3.25 \pm 0.77 \times 10^8$	0.82 ± 0.11	0.89 ± 0.12	8.57 ± 0.05	8.61 ± 0.03

^aThe rate constants k_{off} , k_{on} , the half-life ($t_{1/2}$), and the kinetically derived $\text{p}K_{\text{d}}$ were obtained from competition kinetic association experiments using PPHT-red. ^b $\text{p}K_{\text{i}}$ values were taken from PPHT-red competition binding experiments at equilibrium. Data are presented as mean \pm S.E.M. from four experiments performed in singlet.

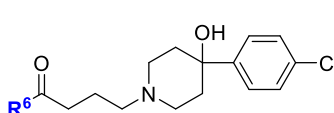
*Completed using online injection protocol.

Kinetic effects of variation of the para-fluorophenyl moiety of 1. We examined the effect of fluoro substituents at both *ortho*-(**14a**) and *meta*-(**14b**) positions of the phenone moiety, as well as all possible di-fluorophenyl substituents (**14c-h**), together with three additional *ortho*-analogues (*o*-Cl (**14i**), *o*-CH₃ (**14j**), *o*-Cl (**14k**)), and an unsubstituted analogue (**14l**). Modification to this moiety caused large decreases in affinity relative to **1**, spanning over 100-fold from $\text{p}K_{\text{d}} = 6.67 \pm 0.01$ (**14h**) to $\text{p}K_{\text{d}} = 8.75 \pm 0.02$ (**14l**), and is associated with a wide range of association and dissociation rate constants. These losses in affinity are mediated through concurrent changes in both k_{on} and k_{off} . This applies to all but the *para*-Cl analogue (**14k**), as it lost affinity 10-fold relative to **1**, but was largely mediated by a decreased rate of association ($k_{\text{on}} = 1.38 \pm 0.05 \times 10^8$, $k_{\text{off}} = 0.70 \pm 0.03 \text{ min}^{-1}$). The *des*-fluoro analogue (**14l**) maintained the highest affinity, and similar to the previous series, this was facilitated by a shift in both rate constants ($\text{p}K_{\text{d}} = 8.75 \pm 0.02$, $k_{\text{on}} = 6.33 \pm 1.06 \times 10^8 \text{ M}^{-1} \text{ min}^{-1}$, $k_{\text{off}} = 1.12 \pm 0.18 \text{ min}^{-1}$). Of the three *ortho*-substituted analogues (**14a** (*m*-F), **14i** (*m*-Cl)), **14j** (*m*-CH₃)), the fluoro substituent was the least favourable in terms of affinity, decreasing ~ 13 -fold relative to **1**, whereas the *ortho*-tolyl substituent only reduces affinity by 6-fold. However, these changes are likewise mediated by a decreased association rate and increased rate of dissociation. Notably, the *m*-Cl (**14i**) and *m*-CH₃ (**14j**) substituents have similar Van der Waals radii, but very different electronic

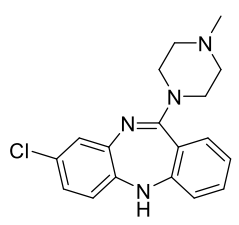
effects, thus highlighting a steric factor as being important. The *meta*-fluoro substituted analogue (**14b**) also dramatically reduced the affinity and was similarly driven by a decreased k_{on} and increased k_{off} ($k_{\text{on}} = 2.55 \pm 0.27 \times 10^7 \text{ M}^{-1} \text{ min}^{-1}$, $k_{\text{off}} = 1.08 \pm 0.21 \text{ min}^{-1}$).

Difluoro substitution of the phenyl group revealed no clear SKR and commonly caused substantial losses in binding affinity. However, unlike the previous chloro series, greater increases in the rate of dissociation were observed. Interestingly, using our online injection protocol, we identified compounds with even slower k_{on} values relative to **2**, coupled with equal to or faster k_{off} values, despite their affinities being lower than **2**. For example, the 2,3-(**14c**), 2,4-(**14d**) and 2,5-difluoro (**14e**) analogues of **1** ($\text{p}K_{\text{d}} = 7.28 \pm 0.04$, 6.92 ± 0.05 and 6.85 ± 0.04 , respectively) showed dissociation rates faster than any compound identified in the previous series ($k_{\text{off}} = 1.70 \pm 0.09 \text{ min}^{-1}$, $k_{\text{off}} = 1.36 \pm 0.21 \text{ min}^{-1}$ and $k_{\text{off}} = 1.49 \pm 0.36 \text{ min}^{-1}$, respectively). In conclusion, these preliminary data suggest that different fluorine substitution patterns dramatically reduce binding affinities, mediated through changes in both kinetic parameters. However, the relationship between the nature of substituents, the substitution pattern and the corresponding kinetic profile is unclear.

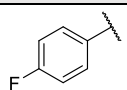
Table 2. Kinetic binding parameters of unlabelled analogues of 1 with modification to the *para*-fluorophenyl moiety for human D_{2L} receptors estimated using TR-FRET assay.

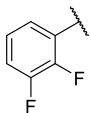
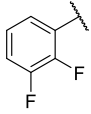
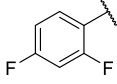
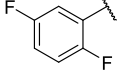
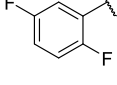
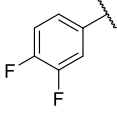
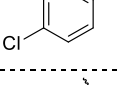


Haloperidol (**1**), **14a-l**



Clozapine (**2**)

#	R ⁶	$k_{\text{on}} (\text{M}^{-1} \text{ min}^{-1})$	$k_{\text{off}} (\text{min}^{-1})$	$t_{1/2} (\text{min})$	$\text{p}K_{\text{d}}$	$\text{p}K_{\text{i}}$
1		$1.29 \pm 0.21 \times 10^9$	0.61 ± 0.04	1.15 ± 0.08	9.31 ± 0.05	9.33 ± 0.09
2 ³²	-	$8.23 \pm 1.42 \times 10^7$	1.67 ± 0.25	0.41	7.69 ± 0.02	7.60 ± 0.02
14a		$9.93 \pm 1.44 \times 10^7$	1.04 ± 0.11	0.69 ± 0.02	7.99 ± 0.05	8.10 ± 0.15
14b		$2.55 \pm 0.27 \times 10^7$	0.96 ± 0.13	0.76 ± 0.09	7.43 ± 0.03	7.44 ± 0.03
14b*		$2.64 \pm 0.49 \times 10^7$	1.08 ± 0.21	0.70 ± 0.12	7.39 ± 0.01	7.42 ± 0.02

14c		$3.01 \pm 0.47 \times 10^7$	1.29 ± 0.26	0.60 ± 0.10	7.38 ± 0.02	7.39 ± 0.04
14c*		$3.24 \pm 0.34 \times 10^7$	1.70 ± 0.09	0.41 ± 0.10	7.28 ± 0.04	7.33 ± 0.04
14d		$1.07 \pm 0.02 \times 10^7$	1.36 ± 0.21	0.51 ± 0.07	6.92 ± 0.05	7.08 ± 0.10
14e		$1.15 \pm 0.20 \times 10^7$	1.14 ± 0.15	0.63 ± 0.08	7.00 ± 0.04	7.12 ± 0.12
14e*		$1.13 \pm 0.38 \times 10^7$	1.49 ± 0.36	0.58 ± 0.16	6.85 ± 0.04	6.95 ± 0.12
14f		$1.84 \pm 0.26 \times 10^7$	1.09 ± 0.12	0.66 ± 0.09	7.22 ± 0.05	7.20 ± 0.04
14g		$1.36 \pm 0.21 \times 10^8$	1.03 ± 0.20	0.75 ± 0.14	8.13 ± 0.03	8.11 ± 0.03
14h		$4.25 \pm 0.52 \times 10^6$	0.92 ± 0.13	0.79 ± 0.09	6.67 ± 0.01	6.77 ± 0.08
14i		$3.16 \pm 0.54 \times 10^8$	1.11 ± 0.25	0.76 ± 0.22	8.47 ± 0.03	8.45 ± 0.01
14j		$3.66 \pm 0.91 \times 10^8$	0.83 ± 0.21	1.01 ± 0.25	8.71 ± 0.25	8.82 ± 0.02
14k		$1.38 \pm 0.05 \times 10^8$	0.70 ± 0.03	1.00 ± 0.04	8.30 ± 0.02	8.30 ± 0.02
14l		$6.33 \pm 1.06 \times 10^8$	1.12 ± 0.18	0.67 ± 0.11	8.75 ± 0.02	8.75 ± 0.05

^aThe rate constants k_{off} , k_{on} , the half-life ($t_{1/2}$), and the kinetically derived pK_d were obtained from competition kinetic association experiments using PPHT-red. ^b pK_i values were taken from PPHT-red competition binding experiments at equilibrium. Data are presented as mean \pm S.E.M. from four experiments performed in singlet. *Completed using online injection protocol.

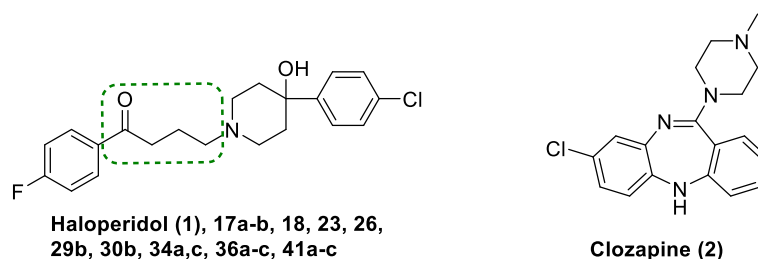
Kinetic effects of variation of ketone and linker moieties of 1. We next examined the effect of modification to the linker and ketone moieties of **1** through synthesis of a further 15 analogues. Specific linker-modified compounds included propiophenone (**34a**) and valerophenone (**34c**) analogues of **1**, alongside 3-5 carbon alkane (**36a-c**) and alkyne analogues (**41a-c**). In addition, a thorough analysis of modification to the ketone moiety was undertaken *via* synthesis of geometric

olefin isomers (**23**, **26**) and their corresponding cyclopropane derivatives (**29b**, **30b**), through to isosteric replacement with sulfur (**17a**) or oxygen (**17b**), as well as conversion of the ketone to the corresponding secondary alcohol (**18**).

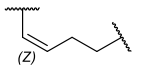
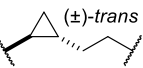
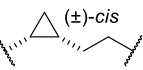
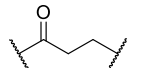
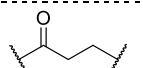
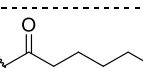
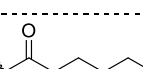
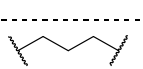
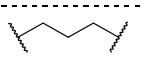
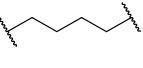
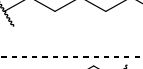
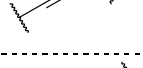
All compounds in this series lost binding affinity relative to **1** and, for the most part, this was mediated through a decrease in k_{on} and an increase in k_{off} . Converting the ketone to its corresponding secondary alcohol (**18**) (racemic), however, whilst engendering a 13-fold reduction in affinity compared to **1**, was exclusively caused by a slowed k_{on} ($\text{p}K_{\text{d}} = 7.04 \pm 0.01$, $k_{\text{on}} = 6.19 \pm 0.41 \times 10^6 \text{ M}^{-1} \text{ min}^{-1}$). Replacement of the carbonyl moiety with sulfur (**17a**) or oxygen (**17b**) modulated both kinetic binding parameters, though their respective association rates varied ~6-fold ($k_{\text{on}} = 4.99 \pm 0.59 \times 10^8 \text{ M}^{-1} \text{ min}^{-1}$ and $k_{\text{on}} = 1.22 \pm 0.35 \times 10^9 \text{ M}^{-1} \text{ min}^{-1}$, respectively). This difference may be due to the size of the S atom vs the O atom, whereby sulfur lone pairs are less efficient at donating into the aromatic ring compared to those on oxygen, which in turn may affect the rotation of the ring relative to the side chain. The *trans* alkene (**23**) lost ~10-fold affinity relative to **1**, and this was again predominantly due to a decreased k_{on} ($k_{\text{on}} = 6.39 \pm 0.88 \times 10^7 \text{ M}^{-1} \text{ min}^{-1}$). Interestingly, the *cis*- isomer (**26**) saw a further 5-fold reduction in affinity ($\text{p}K_{\text{d}} = 7.49 \pm 0.12$), however, this was predominantly due to a change in association rate, displaying a k_{on} almost 20-fold slower and a k_{off} 2-fold faster than **1** ($k_{\text{on}} = 3.35 \pm 0.72 \times 10^7 \text{ M}^{-1} \text{ min}^{-1}$, $k_{\text{off}} = 1.25 \pm 0.16 \text{ min}^{-1}$). This compound possesses a “slower on, faster off” profile resembling that of **2**. Further analysis of the racemic cycloalkane diastereomers was also interesting. Introduction of the *trans*-cyclopropane (**29b**) resulted in a ~10-fold increase in affinity relative to the parent *trans*-olefin **23**, which was predominantly due to a further ~10-fold increase in association rate ($k_{\text{on}} = 6.07 \pm 0.87 \times 10^8 \text{ M}^{-1} \text{ min}^{-1}$). Conversely, introduction of the *cis*-cyclopropane (**30b**) had no effects on affinity relative to the parent *cis*-olefin **28**; however, this substituent marginally decreased k_{on} whilst increasing the k_{off} and thus shifting the kinetic profile further towards that of **2** ($k_{\text{on}} = 4.47 \pm 0.47 \times 10^7 \text{ M}^{-1} \text{ min}^{-1}$, $k_{\text{off}} = 1.37 \pm 0.09 \text{ min}^{-1}$). These data indicate that *cis*-geometry is preferred as opposed to *trans*- with respect to this sub-set of compounds in reference to tuning the kinetic profile towards “slow on, fast off” characteristics, and demonstrates the importance of geometry in the corresponding pharmacological profile of APDs. Analysis of the propiophenone and valerophenone analogues of **1** returned further intriguing results. Decreasing the linker length by just one carbon (**34a**) relative to **1** resulted in dramatic changes in both association and dissociation rate constants ($k_{\text{on}} = 1.33 \pm 0.17 \times 10^7 \text{ M}^{-1} \text{ min}^{-1}$, $k_{\text{off}} = 1.95 \pm 0.32 \text{ min}^{-1}$). However, this compound lost affinity at the D₂R by >20-fold ($\text{p}K_{\text{d}} = 6.84 \pm 0.05$). Interestingly, the binding of **1** at the D₂R has been proposed to arise via a “handover” mechanism, whereby an initial key π -stacking interaction with Tyr^{7.35} (Ballesteros-Weinstein numbering scheme)⁵⁵ allows this residue to act as a pivot point from which the ligand can explore the extracellular vestibule, followed by formation of a salt-bridge with Asp^{3.32}.⁴⁹ This mechanism appears to be reliant upon an optimal (7.89 Å) intramolecular distance

between the *p*-fluorophenyl moiety of **1** and the protonated amine, thus changes in this distance through linker extension might be expected to influence orthosteric binding and the corresponding kinetic profile of the ligand. Perhaps the most exciting compound to arise from our study was the valerophenone analogue (**34c**). Despite losing affinity by >10-fold relative to **1**, this compound displayed a ~10-fold slower k_{on} and a >3.5-fold faster k_{off} than **1**. Furthermore, it retained greater D₂R affinity compared to **2**, with only a marginally faster k_{on} , and displayed a k_{off} that is ~1.4-fold faster ($pK_d = 7.89 \pm 0.01$, $k_{\text{on}} = 1.80 \pm 0.15 \times 10^8 \text{ M}^{-1} \text{ min}^{-1}$, $k_{\text{off}} = 2.35 \pm 0.19 \text{ min}^{-1}$). The alkane analogues of **1** (**36a-c**) exhibited a 10-fold variation in affinity with respect to one another, with the butylene analogue (**36b**) found to be optimal in terms of affinity conservation relative to **1** ($pK_d = 8.17 \pm 0.03$), despite all having >10-fold losses in affinity relative to **1**. Interestingly, although being of lower affinity than **2**, the propylene analogue (**36a**) was found to have a “slow on, fast off” kinetic profile ($pK_d = 7.18 \pm 0.06$, $k_{\text{on}} = 2.29 \pm 0.15 \times 10^7 \text{ M}^{-1} \text{ min}^{-1}$, $k_{\text{off}} = 1.54 \pm 0.07 \text{ min}^{-1}$). Finally, analysis of the 3-5-carbon alkyne analogues (**41a-c**) saw a 10-fold variation in affinity, with the pentyne analogue (**41c**) being optimal ($pK_d = 7.75 \pm 0.03$), as well as displaying the largest change in both rate constants towards that of **2** ($k_{\text{on}} = 6.41 \pm 0.80 \times 10^7$, $k_{\text{off}} = 1.15 \pm 0.15 \text{ min}^{-1}$).

Table 3. Kinetic binding parameters of unlabelled analogues of 1 with modifications to the ketone and linker moieties for human D_{2L} receptors estimated using TR-FRET assay.



#	Structure	k_{on} ($\text{M}^{-1} \text{ min}^{-1}$)	k_{off} (min^{-1})	$t_{1/2}$ (min)	pK_d	pK_i
1		$1.29 \pm 0.21 \times 10^9$	0.61 ± 0.04	1.15 ± 0.08	9.31 ± 0.05	9.33 ± 0.09
2 ³²	-	$8.23 \pm 1.42 \times 10^7$	1.67 ± 0.25	0.41	7.69 ± 0.02	7.60 ± 0.02
17a		$4.99 \pm 0.59 \times 10^8$	0.99 ± 0.15	0.74 ± 0.10	8.71 ± 0.04	8.68 ± 0.04
17b		$1.22 \pm 0.35 \times 10^9$	0.91 ± 0.12	0.81 ± 0.11	9.10 ± 0.08	8.97 ± 0.04
18		$6.19 \pm 0.41 \times 10^6$	0.57 ± 0.05	1.25 ± 0.13	7.04 ± 0.01	7.04 ± 0.02
23		$6.39 \pm 0.88 \times 10^7$	0.76 ± 0.13	0.74 ± 0.10	7.94 ± 0.03	7.95 ± 0.03

26		$3.35 \pm 0.72 \times 10^7$	1.25 ± 0.16	0.58 ± 0.09	7.49 ± 0.12	7.53 ± 0.06
29b		$6.07 \pm 0.87 \times 10^8$	0.92 ± 0.14	0.82 ± 0.14	8.82 ± 0.04	8.82 ± 0.04
30b		$4.47 \pm 0.47 \times 10^7$	1.37 ± 0.09	0.51 ± 0.03	7.51 ± 0.03	7.53 ± 0.03
34a		$1.03 \pm 0.18 \times 10^7$	1.27 ± 0.15	0.57 ± 0.07	6.89 ± 0.05	6.92 ± 0.02
34a*		$1.33 \pm 0.17 \times 10^7$	1.95 ± 0.32	0.43 ± 0.04	6.84 ± 0.05	6.88 ± 0.02
34c		$1.42 \pm 0.24 \times 10^8$	1.65 ± 0.30	0.48 ± 0.10	7.94 ± 0.04	7.97 ± 0.02
34c*		$1.80 \pm 0.15 \times 10^8$	2.35 ± 0.19	0.30 ± 0.03	7.89 ± 0.01	7.92 ± 0.02
36a		$2.45 \pm 0.26 \times 10^7$	1.33 ± 0.22	0.57 ± 0.10	7.28 ± 0.06	7.25 ± 0.03
36a*		$2.29 \pm 0.15 \times 10^7$	1.54 ± 0.07	0.46 ± 0.10	7.18 ± 0.06	7.21 ± 0.03
36b		$1.57 \pm 0.13 \times 10^8$	1.11 ± 0.05	0.63 ± 0.02	8.17 ± 0.03	8.27 ± 0.09
36c		$5.51 \pm 0.69 \times 10^7$	1.22 ± 0.15	0.60 ± 0.08	7.66 ± 0.03	7.66 ± 0.02
41a		$3.37 \pm 0.62 \times 10^6$	0.96 ± 0.14	0.77 ± 0.11	6.54 ± 0.01	6.55 ± 0.01
41b		$1.61 \pm 0.24 \times 10^7$	1.10 ± 0.21	0.69 ± 0.11	7.15 ± 0.05	7.13 ± 0.06
41c		$6.41 \pm 0.80 \times 10^7$	1.15 ± 0.15	0.65 ± 0.11	7.75 ± 0.03	7.72 ± 0.04

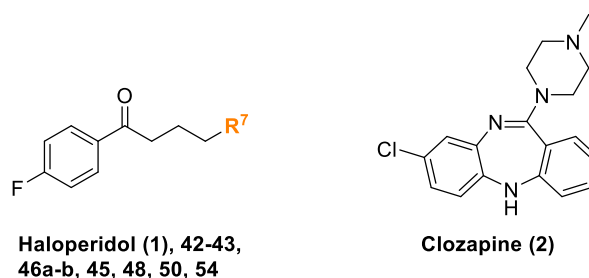
^aThe rate constants k_{off} , k_{on} , the half-life ($t_{1/2}$), and the kinetically derived $\text{p}K_{\text{d}}$ were obtained from competition kinetic association experiments using PPHT-red. ^b $\text{p}K_{\text{i}}$ values were taken from PPHT-red competition binding experiments at equilibrium. Data are presented as mean \pm S.E.M. from four experiments performed in singlet.

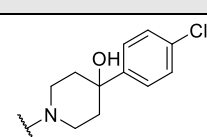
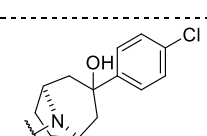
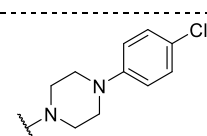
*Completed using online injection protocol.

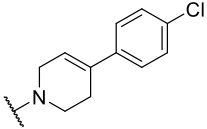
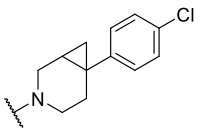
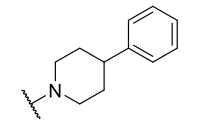
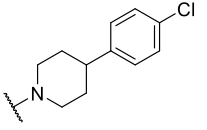
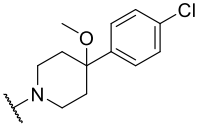
Kinetic effects of variation of the piperidinol moiety of 1. The kinetic effect of structural modifications to the 4-phenylpiperidin-4-ol moiety of **1** was explored through the synthesis of eight additional analogues. We observed the effects of introducing an ethylene bridge (**42**), as well as modification primarily to the tertiary alcohol through methyl ether formation (**54**) and its subsequent removal, generating a variety of compounds containing piperidinyl (**48**, **50**), piperazinyl (**43**), dihydropyridinyl (**45**), and cyclopropyl (**46**) functionalities. We observed a wide range of affinities that spanned a ~30-fold difference, and unlike the previous chemical series, modification to the piperidinol moiety for the most part had relatively negligible effects on the k_{off} , with the majority maintaining similar values

to that of **1** (Table 3). Instead, a decrease in affinity relative to **1** was largely facilitated by a decreased k_{on} . Notably, of the two analogues with higher affinities relative to **1**, these were instead largely mediated by an increase in k_{on} and decrease in k_{off} . For example, introducing the tropanyl moiety (**42**) conferred a ~10-fold increase in affinity which was equally driven by an increase in k_{on} and decrease in k_{off} ($\text{p}K_{\text{d}} = 10.26 \pm 0.06$, $k_{\text{on}} = 3.68 \pm 0.64 \times 10^9 \text{ M}^{-1} \text{ min}^{-1}$, $k_{\text{off}} = 0.19 \pm 0.02 \text{ min}^{-1}$). The cyclopropane variants (**46**) 5-fold improved affinity relative to **1** was also mediated by an increased k_{on} and decreased k_{off} ($\text{p}K_{\text{d}} = 9.84 \pm 0.02$, $k_{\text{on}} = 2.03 \pm 0.09 \times 10^9 \text{ M}^{-1} \text{ min}^{-1}$, $k_{\text{off}} = 0.30 \pm 0.01 \text{ min}^{-1}$). The improved affinities and decreased dissociation rates of **42** and **46** (tropanyl and cyclopropane analogues, respectively) can perhaps be rationalised through a major conformational difference induced by these substituents, resulting in a more entropically favourable binding event. From these preliminary data, it appears that modification to the piperidinol moiety is not particularly amenable to significant increases in the corresponding compounds rate of dissociation.

Table 4. Kinetic binding parameters of unlabelled analogues of **1 with modifications to the piperidinol moiety for human D_{2L} receptors estimated using TR-FRET assay.**

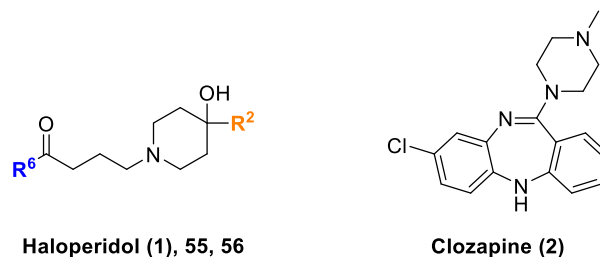


#	R ⁷	$k_{\text{on}} (\text{M}^{-1} \text{ min}^{-1})$	$k_{\text{off}} (\text{min}^{-1})$	$t_{1/2} (\text{min})$	$\text{p}K_{\text{d}}$	$\text{p}K_{\text{i}}$
1		$1.29 \pm 0.21 \times 10^9$	0.61 ± 0.04	1.15 ± 0.08	9.31 ± 0.05	9.33 ± 0.09
2 ³²	-	$8.23 \pm 1.42 \times 10^7$	1.67 ± 0.25	0.41	7.69 ± 0.02	7.60 ± 0.02
42		$3.68 \pm 0.64 \times 10^9$	0.19 ± 0.02	3.59 ± 0.39	10.26 ± 0.06	10.28 ± 0.08
43		$2.86 \pm 0.33 \times 10^7$	0.80 ± 0.07	0.89 ± 0.09	7.55 ± 0.04	7.53 ± 0.04

45		$6.52 \pm 0.46 \times 10^7$	0.65 ± 0.05	1.09 ± 0.09	8.00 ± 0.02	8.00 ± 0.02
46		$2.03 \pm 0.09 \times 10^9$	0.30 ± 0.01	2.35 ± 0.10	9.84 ± 0.02	9.80 ± 0.02
48		$8.99 \pm 0.37 \times 10^7$	0.71 ± 0.05	0.99 ± 0.07	8.10 ± 0.02	8.11 ± 0.03
50		$4.31 \pm 0.37 \times 10^8$	0.84 ± 0.09	0.86 ± 0.09	8.72 ± 0.03	8.76 ± 0.06
54		$3.60 \pm 0.22 \times 10^8$	0.68 ± 0.03	1.03 ± 0.05	8.72 ± 0.01	8.72 ± 0.01

^aThe rate constants k_{off} , k_{on} , the half-life ($t_{1/2}$), and the kinetically derived $\text{p}K_{\text{d}}$ were obtained from competition kinetic association experiments using PPHT-red. ^b $\text{p}K_{\text{i}}$ values were taken from PPHT-red competition binding experiments at equilibrium. Data are presented as mean \pm S.E.M. from four experiments performed in singlet.

Dual modifications to both phenyl moieties of 1. Finally, we assessed the effect of swapping the halogen substituents on each end of haloperidol (**1**) through compound (**55a**), as well as their simultaneous removal as exemplified by the *des*-halo analogue **56** (Table 5). These structural changes all decreased affinity, which was reflected by decreases in the corresponding k_{on} , with only minor effects on k_{off} relative to **1**. Swapping the halogen atoms on each ring (**55a**) caused a 16-fold loss in affinity ($\text{p}K_{\text{d}} = 7.73 \pm 0.02$), which was predominantly driven by a 16-fold decrease in k_{on} ($k_{\text{on}} = 4.17 \pm 0.28 \times 10^7 \text{ M}^{-1} \text{ min}^{-1}$). Finally, removal of both halogen atoms (**56**) simultaneously caused a ~18-fold loss in affinity ($\text{p}K_{\text{d}} = 7.51 \pm 0.01$), driven by a sole ~18-fold decrease in k_{on} relative to **1** ($k_{\text{on}} = 2.28 \pm 0.13 \times 10^7 \text{ M}^{-1} \text{ min}^{-1}$). This effect is unlike that of previous analogues bearing a *para*-halo substituent on only one of the two phenyl rings (**8h** and **14l**), whereby both k_{on} and k_{off} are altered (tables 1 and 2, respectively).

Table 5. Kinetic binding parameters of unlabelled bi-functionalised analogues of 1 for human D_{2L} receptors estimated using TR-FRET assay.

#	R ⁶	R ²	k_{on} (M ⁻¹ min ⁻¹)	k_{off} (min ⁻¹)	$t_{1/2}$ (min)	pK_d	pK_i
1			$1.29 \pm 0.21 \times 10^9$	0.61 ± 0.04	1.15 ± 0.08	9.31 ± 0.05	9.33 ± 0.09
2³²	-	-	$8.23 \pm 1.42 \times 10^7$	1.67 ± 0.25	0.41	7.69 ± 0.02	7.60 ± 0.02
55			$4.17 \pm 0.28 \times 10^7$	0.77 ± 0.05	0.91 ± 0.06	7.73 ± 0.02	7.75 ± 0.01
56			$2.28 \pm 0.13 \times 10^7$	0.71 ± 0.05	0.98 ± 0.07	7.51 ± 0.01	7.49 ± 0.01

^aThe rate constants k_{off} , k_{on} , the half-life ($t_{1/2}$), and the kinetically derived pK_d were obtained from competition kinetic association experiments using PPHT-red. ^b pK_i values were taken from PPHT-red competition binding experiments at equilibrium. Data are presented as mean \pm S.E.M. from four experiments performed in singlet. *Completed using online injection protocol.

Our studies show that modifying the scaffold of **1** produces compounds with a wide range of both association rates (spanning ~30-fold, from $k_{\text{on}} = 3.37 \pm 0.62 \times 10^6 \text{ M}^{-1} \text{ min}^{-1}$ to $3.68 \pm 0.64 \times 10^9 \text{ M}^{-1} \text{ min}^{-1}$) and dissociation rates (spanning >10-fold, from $k_{\text{off}} = 0.19 \pm 0.02 \text{ min}^{-1}$ to $2.35 \pm 0.19 \text{ min}^{-1}$), which constituted large variations in hD_{2L}R affinities (spanning over three orders of magnitude from $K_d = 288 \text{ nM}$ to 0.0549 nM). To further understand the relationship between kinetic rate constants and the affinity of D₂R ligands, we have correlated the kinetic binding data of these 50 compounds (k_{on} , k_{off}) with the derived equilibrium affinity estimates (pK_d) (Figure 6A). Our data confirms that pK_d is robustly correlated with association rate (see Figure 6A, Spearman's $r^2 = 0.96$, $p > 0.0001$), whereas pK_d is, to a much lesser extent, correlated with dissociation rate (Figure 6B). These data are in contrast to previous studies claiming the differences in APD affinities are determined entirely by how fast they dissociate from the D₂R.²¹ This is due to the fact that association rates have widely been assumed to be diffusion limited. Indeed, studies conducted at other systems, namely the M₃ muscarinic acetylcholine and A_{2A} adenosine receptors, have found correlations between k_{off} values and affinity.⁵⁶⁻⁵⁸ However, the association rate constants of a series of metabotropic glutamate

receptor 2 positive allosteric modulators were found to be strongly correlated to affinity, whereas dissociation rate constants were not.²⁴ This correlation has also been observed at the orexin OX₂ receptor and β_2 -adrenoreceptors for ligands with distinct chemotypes.^{59,60}

It is evident that modification to the scaffold of **1** and the corresponding changes in affinity are principally mediated by a change in the rate of association (Figure 6A). Though, our study highlights that particular structural moieties of **1** are more appropriate for the modification of both kinetic parameters towards a “slow on, fast off” profile. For example, when modification to the piperidinol moiety caused a loss in binding affinity relative to **1**, this was predominantly k_{on} mediated, whilst having negligible effects on k_{off} . However, modification of the *p*-fluorophenyl or linker moieties and subsequent losses in affinity saw greater changes in both kinetic rate constants, highlighting these areas as a focal point for future SKR investigations. In addition, we were able to derive preliminary SKR for the *p*-chlorophenyl moiety of **1**. From our kinetic data obtained from a limited amount of compound structural/chemical diversity, we determined that both the electronic nature and position of substituents on the aromatic ring dictate the corresponding kinetic profile. We found that *meta*- and *para*-EWG groups (depending on compound affinity), can either slow the k_{on} whilst having no effect on k_{off} (**8a**, **8c**, **8d**), or equally, slow the k_{on} whilst increasing k_{off} (**8b**, **8f**, **8g**). Conversely, compounds bearing *ortho*-Cl substituents and that are not *meta*- or *para*-substituted, act to slow the k_{on} but increase the k_{off} (**8e**, **8n**). This is also true for *para*-EDG substituents at these positions (**8h**, **8i**, **8k**). It may be possible to use such molecules as templates in an attempt to further increase affinity *via* decoration of the aromatic termini, whilst maintaining the attractive kinetic profile of **2**.

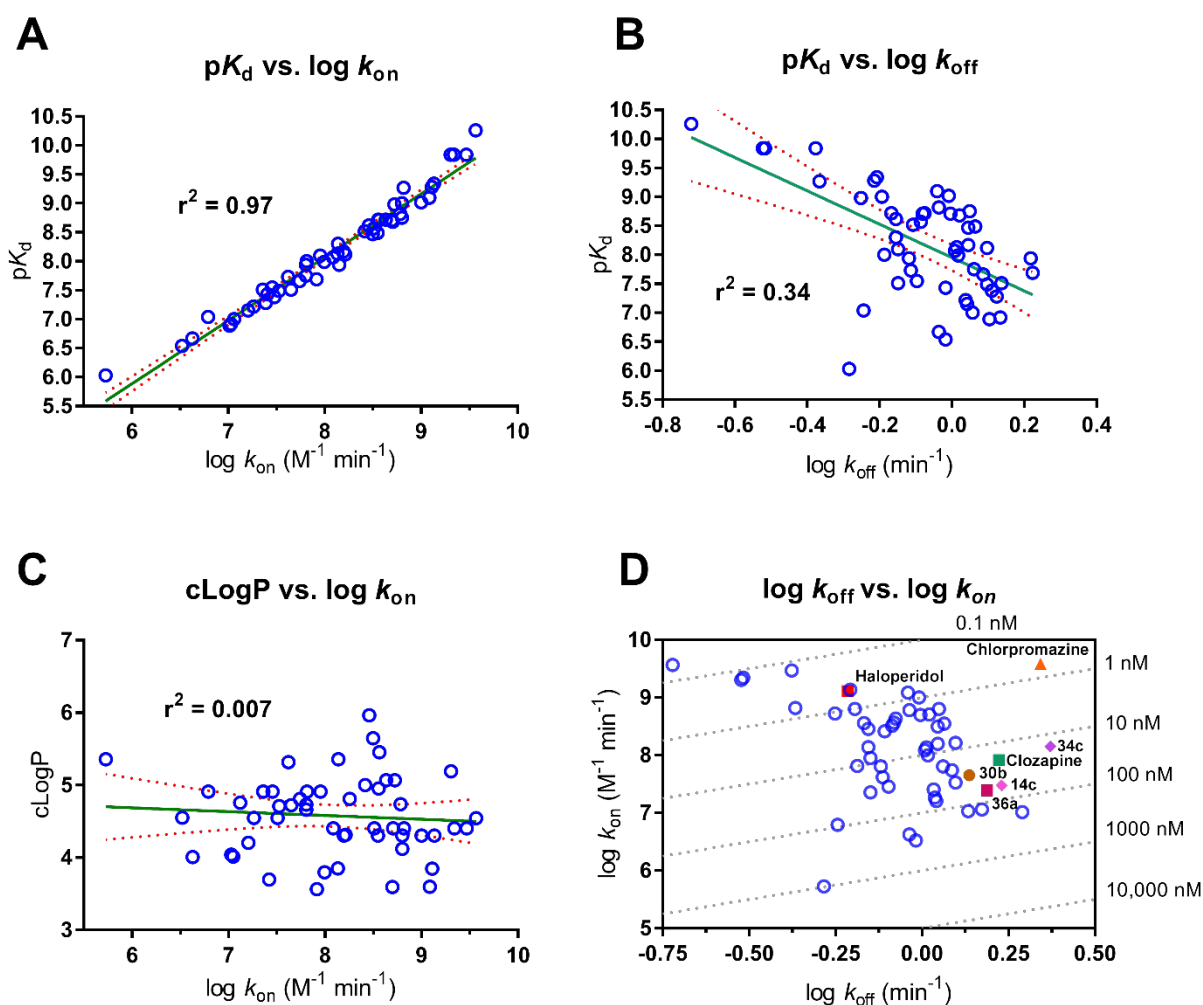


Figure 6. Correlating kinetically derived equilibrium dissociation constants vs. kinetic rate constants of haloperidol (1) and 51 structural analogues at the dopamine D₂ receptor. (A) A plot of $\log k_{on}$ vs. pK_d demonstrates a statistically significant correlation (two-tailed Pearson's correlation $r^2 = 0.96$, $p = < 0.0001$) between these two variables. (B) Conversely, a plot of pK_d vs. $\log k_{off}$ demonstrates a much poorer correlation (two-tailed Pearson's correlation $r^2 = 0.34$, $p = < 0.0001$) despite the traditional scientific consensus that APD affinity is solely driven by changes in k_{off} . (C) The observed association rate ($\log k_{on}$) and calculated partition coefficient ($cLogP$) show no correlation (two-tailed Pearson's correlation $r^2 = 0.007$, $p = 0.562$). The central line corresponds to the linear regression of the data, the dotted lines represent the 95% confidence intervals for the regression. (D) Representing the diversity in affinity and corresponding kinetic profiles for analogues of **1**. A plot of $\log k_{off}$ vs. $\log k_{on}$ represents a spectrum of compounds with various kinetic profiles (~ 10 -fold difference in k_{off} , ~ 30 -fold difference in k_{on}) identified from this study. Clozapine³⁴ (**2**) and typical APD chlorpromazine³⁴ are also included as reference points. These data identify several compounds with interesting 'slow on, fast off' kinetic profiles similar to **2** (**14c**, **30b**, **34c**, **36a**). Combinations of k_{on} and k_{off} that result in identical affinity (K_d) values are represented by *diagonal*

dotted lines. All data used in these plots apart from chlorpromazine are detailed in Tables 1-5. Data are presented as mean from at least four separate experiments.

The derived association rate of all compounds was further assessed for any potential correlation with physicochemical parameters such as clogP (Figure 6C) and topological polar surface area (tPSA) (Supplementary Figure 2), to which there was found to be no relationship. This is unsurprising as this study places particular emphasis on the kinetics of not only positional isomers between subsets of compounds, but close structural analogues which display very similar properties of size, lipophilicity and polarity. This further provides evidence that the observed changes to affinity and kinetic profile are not simply due to modification of physicochemical properties. These data are in contrast to previous observations at the D₂R reporting that compounds with fast dissociation rates are less lipophilic and have lower molecular weights.⁶¹ This is notable as additional micro-pharmacokinetic/pharmacodynamic mechanisms, such as ligand binding to the cell membrane, are known to play a role in target binding kinetics.⁶² Although it is widely accepted that increasing lipophilicity results in increased affinity, this study shows that for this subset of compounds this is not the case, highlighting that careful analysis of kinetic parameters is essential and also likely to be context/target dependent.

Our recent proposal to expand the kinetic hypothesis for APD side effects considers not only the dissociation rate (and therefore the propensity to display insurmountable antagonism), but the association rate and subsequent potential for receptor rebinding.³⁴ Based on this hypothesis, we proposed three broad classes of APDs in an attempt to explain how different kinetic characteristics have the potential to influence on-target side effects. *Class 1*: fast on/slow off compounds exemplified by haloperidol (**1**), *Class 2*: fast on/fast off compounds, namely chlorpromazine, an early typical APD and *Class 3*: slow on/fast off compounds exemplified by clozapine (**2**). A fast association rate will result in a higher receptor rebinding potential in the striatum and consequently high EPS potential. In contrast, slow dissociation at the level of the pituitary results in insurmountable antagonism leading to increased prolactin release (e.g. **1**). These data suggest that the profile of **1**, i.e. slow k_{on} /fast k_{off} kinetics as exhibited by **2**, is optimal for APDs targeting D₂Rs. Using the scaffold of **1**, we have shown that single structural modifications to one of four moieties produces structurally similar molecules with a spectrum of association and dissociation kinetic rate constants (Figure 6D), and several molecules have been identified (**14c**, **30b**, **34c**, **36a**) that display interesting profiles resembling that of **2**. Of the known literature compounds we tested (**14k-l**, **17a-b**, **18**, **42**, **43**, **55**, **56**), information regarding their EPS and hyperprolactinemia liabilities is absent. Our data highlights the importance of employing kinetic analyses in conjunction with other parameters toward the optimisation of APD drug leads.

The identification of substituents and structural drivers that modulate kinetic profiles for the butyrophenone scaffold through a concurrent increase in k_{on} and decrease in k_{off} , such as EDGs on the *p*-chlorophenyl moiety, difluoro-substituents on the *p*-fluorophenyl moiety, replacing the ketone for a *cis*-cyclopropane, or the simple alteration of the alkyl linker length, may be used to ‘fine tune’ the design of novel compounds structurally similar to **1** with enhanced kinetic parameters similar to that of atypical APD **2**. Collectively, these data represent the first reported kinetic characterisation of analogues of **1** and clearly demonstrate that incorporation of kinetic binding parameter analyses into APD discovery programs may facilitate the identification of D₂R antagonist APDs with an improved therapeutic window.

▪ CONCLUSIONS

In this study, we report the chemical synthesis and extensive kinetic profiling of 50 analogues of haloperidol (**1**) at the hD₂L_R, using a TR-FRET competition association kinetic binding assay, permitting the derivation of multiple equilibrium and kinetic parameters (pK_i , pK_d , k_{on} and k_{off}). The kinetic profile was assessed with respect to predominantly single modification of one of four structural moieties of **1**, namely the *p*-fluorophenyl, ketone and alkyl linker, piperidinol, and *p*-chlorophenyl moieties. Specifically, we observed the effect of both mono and di-halogen substituents on individual phenyl rings, as well as ketone and linker modified variants, incorporating *cis*- and *trans*-olefins and their corresponding cyclopropanes, together with numerous alkanes and alkynes. In addition, we investigated the effect of modification to the tertiary alcohol, as well as incorporation of piperazinyl, tetrahydropyridinyl and other piperidinyl moieties. Importantly, we show that there is no correlation between k_{on} and the physicochemical parameters clogP and TPSA, meaning that differences in kinetic profiles and corresponding compound affinities are not simply due to non-specific effects such as cell membrane binding. Moreover, we reveal that k_{on} is significantly correlated with pK_d , and is contrary to previous reports at the D₂R. Thus, we found that a loss in binding affinity is generally associated with a decrease in k_{on} . However, preliminary SKR derived for the *p*-chlorophenyl moiety of **1**, demonstrates that particular substitution patterns and the nature of aromatic substituents are more likely to concurrently decrease k_{on} whilst increasing k_{off} . For example, chloro substituents at the *ortho*-position modulate the kinetic parameters toward a slow k_{on} /fast k_{off} profile, whereas *meta* and/or *para*-chloro substituents can either decrease the k_{on} , whilst having no effect on k_{off} , or, equally, they may also simultaneously decrease $k_{\text{on}}/k_{\text{off}}$. The *p*-fluorophenyl and ketone/alkyl linker structural moieties of **1** were found to be important for mediating changes in both kinetic rate parameters, particularly the k_{off} , whilst the piperidinol moiety was more linked to changes in k_{on} only. For example, converting the aryl ketone to a *cis*-cyclopropane group or increasing/decreasing the linker length, significantly modulates both rate constants, whereas most modifications to the

piperidinol ring simply modulate the k_{on} . We show that with minimal variation this scaffold can effectively be converted to resemble the kinetic profile of **2**, a prototypical atypical APD, and we have identified a number of molecules (**14c**, **30b**, **34c**, **36a**) that display these improved profiles. These compounds may be used as tools to further explore the influence of kinetic rate parameters and their role in the corresponding clinical profile of APDs toward the development of novel efficacious treatments devoid of EPS and hyperprolactinemia propensities.

Chemistry: Materials and Methods. Chemicals and solvents of analytical and HPLC grade were purchased from commercial suppliers and used without further purification. Reactions were monitored by thin-layer chromatography on commercially available silica pre-coated aluminium-backed plates (Merck Kieselgel 60 F254). Visualisation was under UV light (254 nm and 366 nm), followed by staining with ninhydrin or KMnO₄ dips. Flash column chromatography was performed using silica gel 60, 230-400 mesh particle size (Sigma Aldrich). NMR spectra were recorded on a Bruker-AV 400. ¹H spectra were recorded at 400.13 Hz and ¹³C NMR spectra at 101.62 Hz. All ¹³C NMR are ¹H broadband decoupled. Solvents used for NMR analysis (reference peaks listed) were CDCl₃ supplied by Cambridge Isotope Laboratories Inc., ($\delta_H = 7.26$ ppm, $\delta_C = 77.16$) and CD₃OD supplied by VWR ($\delta_H = 3.31$ ppm and $\delta_C = 49.00$). Chemical shifts (δ) are recorded in parts per million (ppm) and coupling constants are recorded in Hz. The following abbreviations are used to describe signal shapes and multiplicities; singlet (s), doublet (d), triplet (t), quadruplet (q), broad (br), dd (doublet of doublets), ddd (double doublet of doublets), dtd (double triplet of doublets) and multiplet (m). Spectra were assigned using appropriate COSY and HSQC experiments. Processing of the NMR data was carried out using the NMR software Topspin 3.0. RP-HPLC-MS spectra were recorded on a Shimadzu UFLCXR system coupled to an Applied Biosystems API2000 and visualised at 254 nm (channel 1) and 220 nm (channel 2). RP-HPLC-MS was carried out using a Phenomenex Gemini® NX-C18 110 Å, column (50 mm × 2 mm × 3 μm) at a flow rate 0.5 mL/min over a 5-min period (Method A). Final products were one single peak and >95% pure. The retention time of the final product is reported using a gradient method of 5-95% solvent B in solvent A over 12 minutes. (Solvent A = 0.01% trifluoroacetic acid in H₂O, solvent B = 0.01% trifluoroacetic acid in CH₃CN (Method B). All high-resolution mass spectra (HRMS) were recorded on a Bruker microTOF mass spectrometer using MS electrospray ionization operating in positive ion mode. Preparative RP-HPLC was performed on a Waters 515 LC system and monitored using a Waters 996 photodiode array detector at wavelengths between 190 and 800 nm. Spectra were analysed using Millenium 32 software. Preparative RP-HPLC was performed using a Gemini® NX-C18 110 Å column (250 mm × 21.2 mm × 5 μm) at a flow rate of 20.0 mL/min using a gradient method of 5-95% B over 15 minutes (Solvent A = 0.01% trifluoroacetic acid in H₂O, solvent B = 0.01% trifluoroacetic in CH₃CN

(Method C)). Predicted partition coefficient (cLogP) values were calculated using Data Warrior 4.7.2, Actelion Pharmaceutical Ltd.

General Procedure A. *n*-Butyllithium mediated addition of aryllithiums to ketones for the preparation of 5a-m. To a stirred solution of substituted bromobenzene (**3a-l**) (1.35 equiv.) in THF at -78 °C was added *n*-butyllithium (1.30 equiv.) and the reaction maintained at -78 °C for 30 min. After this, a solution of ketone (1 equiv.) in THF was slowly introduced into the reaction and stirred at -78 °C for 2 h. The reaction was quenched with the addition of a saturated solution of NH₄Cl and transferred to a separating funnel and extracted with DCM (3 × 40 mL). The organic extracts were dried (anhydrous Na₂SO₄) and the residue purified by column chromatography using PE/EtOAc in a ratio as indicated to afford the desired compound.

General procedure B. *N*-Boc deprotection for the preparation of 6a-n. The *N*-Boc protected amine was taken up in 4 M HCl in 1,4-dioxane (20 mL) and stirred at r.t. for 2 h. The solvents were evaporated *in vacuo* to afford the corresponding amine hydrochloride. Alternatively, the residue could be taken up in H₂O (20 mL) and added to a separating funnel. The aqueous solution was washed with Et₂O (3 × 30 mL), and the aqueous phase made alkaline with the addition of 2 M NaOH solution. This phase was then extracted with DCM (3 × 30 mL) and the organic extracts collected, dried over anhydrous Na₂SO₄ and evaporated *in vacuo* to afford the corresponding amine free base.

General Procedure C. *N*-Alkylation for the preparation of 8a-n, 14a-l, 17a-b, 18, 23, 26, 29b, 30b, 34a, 34c, 36a-c, 41a-c, 42-43, 46a-b, 48, 50, 54, 55, 56. To a round-bottom flask or sealed microwave vessel was added the amine (1.1 equiv.), alkyl halide or mesylate (1 equiv.), KI (0.1 equiv.) and NaHCO₃ (2 equiv.) followed by toluene. This suspension was then heated at reflux temperature for 24 h. The reaction was filtered and evaporated to dryness followed by direct chromatographic purification using an appropriate eluent as indicated.

General Procedure D. Sonogashira cross-coupling of aryl iodides for the preparation of 12a-j, 40b. PdCl₂(PPh₃)₂ (1 mol %) and copper(I) iodide (2 mol %) were placed in a 50 mL round-bottomed flask equipped with a magnetic bar and then non-dried 1,4-dioxane (10 mL), the corresponding iodide (1.0 equiv.), 4-chloro-1-butyne (1.2 equiv.), and triethylamine (5.0 equiv.) were added. The flask was capped with a rubber septum, and the resulting mixture was magnetically stirred at 50 °C for 2-6 h. The reaction was diluted with Et₂O (100 mL) after cooling, removing the solids by filtration. The resulting solution was purified by column chromatography (petroleum ether) to yield the corresponding alkyne product.

General Procedure E. Sonogashira cross-coupling of aryl iodides for the preparation of 39a, 39c. To a N₂-degassed solution of CH₃CN and triethylamine (2.0 equiv.) were added alkyne (1.1 equiv.), the appropriate iodobenzene (1.0 equiv.), Pd(PPh₃)₂Cl₂ (2% mol) and CuI (2% mol), and the mixture was stirred at room temperature for 5 hr. The reaction was diluted with Et₂O, filtered, concentrated, and purified on silica gel (*n*-hexanes).

General Procedure F. Triflic acid-catalysed Markovnikov-type hydration of internal alkynes for the preparation of 13a-j. The purified alkyne was treated with triflic acid (0.5 equiv.) and H₂O (2 equiv) in 2,2,2-trifluoroethanol in a sealed vial equipped with a magnetic stirring bar, and stirred at 60 °C for 6 h. The reaction mixture was concentrated under reduced pressure and the corresponding ketone directly purified by FCC with an appropriate eluent as indicated.

General procedure G. Alcohol mesylation for the preparation of 22, 27, 29a, 30a, 40a, 40c. To a solution of alcohol (1 equiv.), Et₃N (2.5 equiv.), in DCM was added at room temperature MsCl (1.3 equiv.). The mixture was stirred at room temperature for 1.5-24 h until complete consumption of starting material was evident. The mixture was diluted with EtOAc, washed with H₂O, brine, and the organic fraction dried (Na₂SO₄). The solvents were removed *in vacuo* and the residue chromatographed on silica eluting with the appropriate solvent as indicated. Similarly, and in many cases, the residue could be used for the next reaction without the need for purification.

***tert*-Butyl 4-(4-chlorophenyl)-4-hydroxypiperidine-1-carboxylate (5a).** General procedure A. Purification by FCC (eluent: EtOAc/hexane 0-40%) gave 7.64 g of a white foam (74%). LCMS (*m/z*): 312.1 [M+H]⁺, *t*_R 2.95 min. ¹H NMR (CDCl₃) δ 7.43 – 7.38 (m, 2H), 7.34 – 7.30 (m, 2H), 4.08 – 3.91 (m, 2H), 3.21 (td, *J* = 13.0, 2.7 Hz, 2H), 1.94 (td, *J* = 13.3, 4.9 Hz, 2H), 1.75 (s, 1H), 1.69 (dq, *J* = 14.2, 2.8 Hz, 2H), 1.47 (s, 9H). ¹³C NMR (CDCl₃) δ 154.9, 146.7, 133.2, 128.7, 126.2, 79.8, 71.5, 39.9, 38.2, 28.6.

***tert*-Butyl 4-(3-chlorophenyl)-4-hydroxypiperidine-1-carboxylate (5b).** General procedure A. Purification by FCC (eluent: EtOAc/hexane 0-40%) gave 1.25 g of a white solid (69.1%). LCMS (*m/z*): 312.1 [M+H]⁺, *t*_R 2.95 min. ¹H NMR (CDCl₃) δ 7.51 (t, *J* = 1.8 Hz, 1H), 7.35 (dt, *J* = 7.6, 1.6 Hz, 1H), 7.30 (t, *J* = 7.6 Hz, 1H), 7.25 (dt, *J* = 7.7, 1.7 Hz, 1H), 4.03 (ddt, *J* = 13.4, 4.2, 1.7 Hz, 2H), 3.23 (td, *J* = 13.0, 2.7 Hz, 2H), 2.03 (s, 1H), 1.96 (td, *J* = 13.3, 4.9 Hz, 2H), 1.77 – 1.66 (m, 2H), 1.49 (s, 9H). ¹³C NMR (CDCl₃) δ 154.9, 150.4, 134.5, 129.8, 127.4, 125.2, 122.9, 79.8, 71.5, 39.9, 38.1, 28.6.

***tert*-Butyl 4-(2,3-dichlorophenyl)-4-hydroxypiperidine-1-carboxylate (5c).** General procedure A. Purification by FCC (eluent: EtOAc/hexane 0-40%) gave 1.87 g of a white solid (65.9%). LCMS (*m/z*): 346.1 [M+H]⁺, *t*_R 3.05 min. ¹H NMR (CDCl₃) δ 7.55 (dd, *J* = 8.0, 1.6 Hz, 1H), 7.49 (dd, *J* =

8.0, 1.6 Hz, 1H), 7.35 – 7.26 (m, 1H), 4.15 – 4.05 (m, 2H), 3.33 (td, $J = 13.0, 2.7$ Hz, 2H), 2.38 – 2.27 (m, 2H), 2.07 – 1.98 (m, 2H), 1.54 (s, 9H), 1.51 (s, 1H). ¹³C NMR (CDCl₃) δ 155.0, 145.7, 135.2, 130.2, 129.9, 127.7, 125.4, 79.7, 72.9, 39.9, 35.3, 28.6.

***tert*-Butyl 4-(2,4-dichlorophenyl)-4-hydroxypiperidine-1-carboxylate (5d).** General procedure A. Purification by FCC (eluent: EtOAc/hexane 0-40%) gave 1.30 g of a transparent oil (71%). LCMS (m/z): 346.1 [M+H]⁺, t_R 3.02 min. ¹H NMR (CDCl₃) δ 7.27 (d, $J = 8.0$ Hz, 2H), 7.03 (t, $J = 8.0$ Hz, 1H), 4.01 (s, 2H), 3.42 (s, 1H), 3.23 (s, 2H), 2.76 (td, $J = 13.2, 5.0$ Hz, 2H), 1.90 (d, $J = 12.9$ Hz, 2H), 1.44 (s, 9H). ¹³C NMR (CDCl₃) δ 155.0, 145.2, 133.4, 133.0, 129.9, 128.7, 127.7, 79.8, 72.4, 35.0, 28.6.

***tert*-Butyl 4-(2,5-dichlorophenyl)-4-hydroxypiperidine-1-carboxylate (5e).** General procedure A. Purification by FCC (eluent: EtOAc/hexane 0-40%) gave 1.48 g of a white solid (68%). LCMS (m/z): 346.3 [M+H]⁺, t_R 3.02 min. ¹H NMR (CDCl₃) δ 7.59 (d, $J = 2.5$ Hz, 1H), 7.29 (d, $J = 8.5$ Hz, 1H), 7.18 (dd, $J = 8.4, 2.5$ Hz, 1H), 4.09 – 4.00 (m, 2H), 3.28 – 3.21 (m, 2H), 2.83 (d, $J = 1.0$ Hz, 1H), 2.32 (td, $J = 13.3, 4.9$ Hz, 2H), 1.84 (d, $J = 13.4$ Hz, 2H), 1.47 (s, 9H). ¹³C NMR (CDCl₃) δ 155.0, 145.2, 133.4, 133.0, 129.9, 128.7, 127.7, 79.8, 72.4, 35.0, 28.6.

***tert*-Butyl 4-(2,6-dichlorophenyl)-4-hydroxypiperidine-1-carboxylate (5f).** General procedure A. Purification by FCC (eluent: EtOAc/hexane 0-40%) gave 1.72 g of a transparent oil (76%). LCMS (m/z): 346.1 [M+H]⁺, t_R 3.03 min. ¹H NMR (CDCl₃) δ 7.32 (d, $J = 8.0$ Hz, 2H), 7.12 – 7.03 (m, 1H), 4.02 (dd, $J = 13.2, 4.8$ Hz, 2H), 3.26 (td, $J = 12.9, 2.8$ Hz, 2H), 2.81 (td, $J = 13.2, 5.0$ Hz, 2H), 2.01 – 1.89 (m, 2H), 1.48 (s, 9H). ¹³C NMR (CDCl₃) δ 155.1, 140.1, 133.8, 132.1, 128.4, 79.6, 76.1, 39.9, 35.7, 28.6.

***tert*-Butyl 4-(3,4-dichlorophenyl)-4-hydroxypiperidine-1-carboxylate (5g).** General procedure A. Purification by FCC (eluent: EtOAc/hexane 0-40%) gave 1.25 g of a white foam (73.4%). LCMS (m/z): 346.2 [M+H]⁺, t_R 3.06 min. ¹H NMR (CDCl₃) δ 7.59 (d, $J = 2.2$ Hz, 1H), 7.38 (d, $J = 8.4$ Hz, 1H), 7.26 (dd, $J = 8.4, 2.2$ Hz, 1H), 3.97 (dt, $J = 12.9, 3.3$ Hz, 2H), 3.19 (t, $J = 12.9$ Hz, 2H), 1.86 (td, $J = 13.2, 4.8$ Hz, 2H), 1.71 – 1.65 (m, 2H), 1.46 (s, 1H), 1.44 (s, 9H). ¹³C NMR (CDCl₃) δ 154.9, 148.9, 132.4, 130.9, 130.3, 127.2, 124.3, 79.8, 70.9, 42.9, 36.6, 28.5.

***tert*-Butyl 4-(3,5-dichlorophenyl)-4-hydroxypiperidine-1-carboxylate (5h).** General procedure A. Purification by FCC (eluent: EtOAc/hexane 0-40%) gave 2.22 g of a white solid (78.2%). LCMS (m/z): 345.9 [M+H]⁺, t_R 3.09 min. ¹H NMR (CDCl₃) δ 7.35 (d, $J = 1.9$ Hz, 2H), 7.24 (t, $J = 1.9$ Hz, 1H), 4.01 (ddt, $J = 13.5, 4.7, 1.8$ Hz, 2H), 3.18 (td, $J = 13.1, 2.7$ Hz, 2H), 2.22 (s, 1H), 1.90 (td, $J = 13.3, 4.9$ Hz, 2H), 1.71 – 1.62 (m, 2H), 1.45 (s, 9H). ¹³C NMR (CDCl₃) δ 154.9, 151.9, 135.2, 127.3, 123.7, 79.9, 71.5, 39.8, 38.1, 28.6.

tert-Butyl 4-hydroxy-4-phenylpiperidine-1-carboxylate (5i). General procedure A. Purification by FCC (eluent: EtOAc/hexane 0-40%) gave 1.49 g of a white foam (76%). LCMS (*m/z*): 278.1 [M+H]⁺, *t_R* 2.83 min. ¹H NMR (CDCl₃) δ 7.53 – 7.45 (m, 2H), 7.43 – 7.33 (m, 2H), 7.34 – 7.24 (m, 1H), 4.03 (ddt, *J* = 13.3, 4.4, 1.8 Hz, 2H), 3.26 (td, *J* = 13.1, 2.7 Hz, 2H), 2.01 (td, *J* = 13.4, 4.9 Hz, 2H), 1.84 (s, 1H), 1.50 (s, 9H). ¹³C NMR (CDCl₃) δ 154.9, 148.1, 128.5, 127.2, 124.5, 79.5, 71.5, 39.9, 38.1, 28.5.

tert-Butyl 4-hydroxy-4-(*p*-tolyl)piperidine-1-carboxylate (5j). General procedure A. Purification by FCC (eluent: EtOAc/hexane 0-40%) gave 1.29 g of white foam (68%). LCMS (*m/z*): 292.2 [M+H]⁺, *t_R* 2.93 min. ¹H NMR (CDCl₃) δ 7.37 – 7.33 (m, 2H), 7.17 (dt, *J* = 7.9, 0.7 Hz, 2H), 3.99 (dt, *J* = 13.1, 2.6 Hz, 2H), 3.23 (td, *J* = 13.1, 2.7 Hz, 2H), 2.34 (s, 3H), 1.96 (td, *J* = 13.4, 4.9 Hz, 2H), 1.84 – 1.78 (m, 1H), 1.76 – 1.66 (m, 2H), 1.47 (s, 9H). ¹³C NMR (CDCl₃) δ 155.0, 145.3, 136.9, 129.2, 124.5, 79.6, 71.4, 40.0, 38.3, 28.6, 21.1.

tert-Butyl 4-hydroxy-4-(4-(trifluoromethyl)phenyl)piperidine-1-carboxylate (5k). General procedure A. Purification by FCC (eluent: EtOAc/hexane 0-40%) gave 1.43 g of a white foam (84%). LCMS (*m/z*): 346.2 [M+H]⁺, *t_R* 3.00 min. ¹H NMR (CDCl₃) δ 7.60 (m, 4H), 4.04 (ddt, *J* = 13.7, 4.6, 1.8 Hz, 2H), 3.22 (td, *J* = 13.0, 2.6 Hz, 2H), 1.98 (td, *J* = 13.3, 4.9 Hz, 2H), 1.75 – 1.66 (m, 2H), 1.47 (s, 9H), 1.35 – 1.27 (m, 1H). ¹³C NMR (CDCl₃) δ 154.9, 152.2 (d, *J* = 1.5 Hz), 129.6 (q, *J* = 32.5 Hz), 125.5 (q, *J* = 3.8 Hz), 125.1, 124.2 (q, *J* = 272.1 Hz), 79.9, 71.7, 39.8, 38.1, 28.6.

tert-Butyl 4-(4-(dimethylamino)phenyl)-4-hydroxypiperidine-1-carboxylate (5l). General procedure A. Purification by FCC (eluent: EtOAc/hexane 0-40%) gave 1.22 g of white solid (69%). LCMS (*m/z*): 321.0 [M+H]⁺, *t_R* 2.51 min. ¹H NMR (CDCl₃) δ 7.34 (d, *J* = 8.9 Hz, 2H), 6.73 (d, *J* = 8.5 Hz, 2H), 3.96 (s, 2H), 3.25 (t, *J* = 11.6 Hz, 2H), 2.94 (s, 6H), 2.03 – 1.88 (m, 2H), 1.79 – 1.71 (m, 2H), 1.47 (s, 9H). ¹³C NMR (CDCl₃) δ 155.1, 129.2, 128.3, 125.7, 112.6, 79.5, 71.1, 40.8, 28.6, 28.6.

tert-Butyl 4-(4-fluorophenyl)-4-hydroxypiperidine-1-carboxylate (5m). General procedure A. Purification by FCC (eluent: EtOAc/hexane 0-40%) gave 1.24 g of transparent oil (71%). ¹H NMR (CDCl₃) δ 7.42 – 7.35 (m, 2H), 6.94 (t, *J* = 8.7 Hz, 2H), 3.88 (dd, *J* = 12.8, 4.4 Hz, 2H), 3.22 – 3.09 (m, 2H), 3.07 (s, 1H), 1.83 (td, *J* = 13.2, 4.7 Hz, 2H), 1.64 (dd, *J* = 14.1, 2.5 Hz, 2H), 1.39 (s, 9H). ¹³C NMR (CDCl₃) δ 161.8 (d, *J* = 245.3 Hz), 154.9, 144.3 (d, *J* = 3.1 Hz), 126.4 (d, *J* = 7.9 Hz), 114.9 (d, *J* = 21.2 Hz), 79.6, 70.9, 38.1, 28.4.

tert-Butyl 4-(2'-chloro-[1,1'-biphenyl]-2-yl)-4-hydroxypiperidine-1-carboxylate (5n). General procedure A. Purification by FCC (eluent: EtOAc/hexane 0-40%) gave 700 mg of a white solid (55%). Reaction by-product from the attempted synthesis of TF-01-62. LCMS (*m/z*): 388.1 [M+H]⁺, *t_R* 3.12 min. ¹H NMR (CDCl₃) δ 7.51 (dd, *J* = 8.0, 1.3 Hz, 1H), 7.49 – 7.41 (m, 1H), 7.40 (td, *J* = 7.7,

1.6 Hz, 1H), 7.29 (dtd, $J = 10.5, 6.2, 5.6, 2.9$ Hz, 4H), 7.01 (dd, $J = 7.5, 1.5$ Hz, 1H), 3.89 (dddd, $J = 15.5, 13.2, 5.0, 2.6$ Hz, 2H), 3.06 (qd, $J = 12.4, 2.7$ Hz, 2H), 2.09 – 1.98 (m, 1H), 1.96 – 1.85 (m, 1H), 1.74 (ddd, $J = 13.8, 11.4, 2.7$ Hz, 2H), 1.44 (s, 9H). ¹³C NMR (CDCl₃) δ 154.9, 145.0, 142.9, 137.3, 133.5, 132.3, 131.0, 129.5, 128.8, 128.2, 126.9, 126.4, 126.3, 79.5, 73.6, 38.6, 38.2, 28.6.

tert-Butyl 4-(2-chlorophenyl)-4-hydroxypiperidine-1-carboxylate (5n). To a stirred solution of 1-bromo-2-chloro-benzene (609 μ L, 5.22 mmol) in Et₂O was added magnesium turnings (150 mg, 6.17 mmol), followed by catalytic iodide and the reaction stirred at room temperature for 2 h. This mixture was then cooled to 0°C, and treated with 4-oxopiperidine-1-carboxylic acid tert-butyl ester (946 mg, 4.75 mmol) dissolved in Et₂O (10 mL) and added to the reaction mixture slowly. The reaction was heated at reflux temperature for 3 h. The reaction was quenched with a saturated solution NH₄Cl and the aqueous phase extracted with EtOAc. The organic extracts were combined and dried over MgSO₄, filtered and evaporated *in vacuo*. The residue was purified by FCC (eluent: EtOAc/*n*-hexanes 0-40%) and gave 800 mg of a white foam (54%). LCMS (m/z): 312.2 [M+H]⁺, t_R 2.97 min. ¹H NMR (CDCl₃) δ 7.56 (dd, $J = 7.9, 1.8$ Hz, 1H), 7.30 (dd, $J = 7.8, 1.5$ Hz, 1H), 7.21 (td, $J = 7.6, 1.5$ Hz, 1H), 7.15 (td, $J = 7.5, 1.7$ Hz, 1H), 3.96 (dd, $J = 13.4, 4.8$ Hz, 2H), 3.22 (t, $J = 12.9$ Hz, 2H), 3.05 (s, 1H), 2.29 (td, $J = 13.2, 4.9$ Hz, 2H), 1.87 – 1.78 (m, 2H), 1.43 (s, 9H). ¹³C NMR (CDCl₃) δ 154.9, 143.5, 131.7, 131.5, 128.6, 127.2, 127.1, 79.5, 72.2, 39.8, 34.9, 28.5.

4-(3-Chlorophenyl)piperidin-4-ol (6a). General procedure B. Alkaline work-up afforded 660 mg of a white solid (97%). LCMS (m/z): 212.0 [M+H]⁺, t_R 0.74 min. ¹H NMR (CDCl₃) δ 7.52 (t, $J = 1.9$ Hz, 1H), 7.37 (dt, $J = 7.7, 1.5$ Hz, 1H), 7.29 (t, $J = 7.8$ Hz, 1H), 7.24 (dt, $J = 7.9, 1.7$ Hz, 1H), 3.10 (td, $J = 12.3, 2.6$ Hz, 2H), 2.99 – 2.90 (m, 2H), 2.42 (d, $J = 9.1$ Hz, 2H), 1.97 (td, $J = 13.2, 4.6$ Hz, 2H), 1.70 (dd, $J = 14.1, 2.5$ Hz, 2H). ¹³C NMR (CDCl₃) δ 151.2, 134.4, 129.8, 127.1, 125.2, 122.9, 71.4, 42.2, 39.1.

4-(2,3-Dichlorophenyl)-4-hydroxypiperidin-1-ium chloride (6b). General procedure B. Concentration *in vacuo* gave 685 mg of a beige solid (94%). LCMS (m/z): 246.0 [M+H]⁺, t_R 2.53 min. ¹H NMR (DMSO-*d*₆) δ 9.19 (d, $J = 55.0$ Hz, 2H), 7.75 (dd, $J = 8.1, 1.7$ Hz, 1H), 7.60 (dd, $J = 8.0, 1.6$ Hz, 1H), 7.40 (t, $J = 8.0$ Hz, 1H), 5.88 (s, 1H), 3.20 (s, 4H), 2.74 (dt, $J = 14.1, 8.9$ Hz, 2H), 1.80 (dd, $J = 14.3, 2.4$ Hz, 2H). ¹³C NMR (DMSO-*d*₆) δ 146.4, 133.4, 129.7, 128.8, 128.0, 126.8, 69.8, 30.5.

4-(2,4-Dichlorophenyl)piperidin-4-ol (6c). General procedure B. Alkaline work-up afforded 325 mg of a white solid (65 %). LCMS (m/z): 246.0 [M+H]⁺, t_R 2.65 min. ¹H NMR (CDCl₃) δ 7.27 (dd, $J = 8.0, 1.9$ Hz, 2H), 7.01 (td, $J = 8.0, 2.1$ Hz, 1H), 3.20 – 3.09 (m, 2H), 2.96 – 2.84 (m, 2H), 2.80 – 2.66 (m, 3H), 1.91 (dt, $J = 14.0, 2.4$ Hz, 2H). ¹³C NMR (CDCl₃) δ 140.9, 133.9, 131.9, 131.9, 127.9, 76.0, 42.1, 36.6.

4-(2,5-Dichlorophenyl)-4-hydroxypiperidin-1-ium chloride (6d). General procedure B. Concentration in vacuo gave 180 mg of a white solid (98%). LCMS (*m/z*): 246.2 [M+H]⁺, *t_R* 1.34 min. ¹H NMR (DMSO-*d*₆) δ 9.42 – 8.91 (m, 2H), 7.79 (d, *J* = 2.6 Hz, 1H), 7.45 (d, *J* = 8.4 Hz, 1H), 7.39 (dd, *J* = 8.5, 2.6 Hz, 1H), 5.98 (s, 1H), 3.23 – 3.11 (m, 4H), 2.77 (dt, *J* = 14.1, 9.0 Hz, 2H), 1.70 (d, *J* = 13.9 Hz, 2H). ¹³C NMR (DMSO-*d*₆) δ 146.1, 133.2, 132.1, 129.1, 128.8, 128.0, 69.4, 39.2, 30.3.

4-(2,6-Dichlorophenyl)piperidin-4-ol (6e). General procedure B. Alkaline work-up afforded 682 mg of a white solid (96%). LCMS (*m/z*): 246.0 [M+H]⁺, *t_R* 0.88 min. ¹H NMR (DMSO-*d*₆) δ 8.93 (d, *J* = 60.3 Hz, 2H), 7.45 (d, *J* = 7.9 Hz, 2H), 7.28 (dd, *J* = 8.4, 7.5 Hz, 1H), 5.67 (s, 1H), 3.21 (s, 4H), 2.90 – 2.76 (m, 2H), 2.16 (d, *J* = 13.7 Hz, 2H). ¹³C NMR (DMSO-*d*₆) δ 139.9, 133.6, 132.0, 129.2, 72.0, 32.1.

4-(3,4-Dichlorophenyl)piperidin-4-ol (6f). General procedure B. Alkaline work-up afforded 702 mg of a white solid (98%). LCMS (*m/z*): 246.0 [M+H]⁺, *t_R* 1.86 min. ¹H NMR (CDCl₃) δ 7.61 (d, *J* = 2.2 Hz, 1H), 7.40 (d, *J* = 8.4 Hz, 1H), 7.30 (dd, *J* = 8.4, 2.2 Hz, 1H), 3.07 (td, *J* = 12.3, 2.7 Hz, 2H), 2.97 – 2.90 (m, 2H), 2.21 (s, 2H), 1.94 (ddd, *J* = 13.6, 12.2, 4.8 Hz, 2H), 1.70 – 1.63 (m, 2H). ¹³C NMR (CDCl₃) δ 149.3, 132.4, 130.8, 127.1, 124.2, 71.2, 42.1, 38.9.

4-(3,5-Dichlorophenyl)-4-hydroxypiperidin-1-ium chloride (6g). General procedure B. Concentration in vacuo gave 755 mg of a white solid (93%). LCMS (*m/z*): 246.0 [M+H]⁺, *t_R* 2.62 min. ¹H NMR (DMSO-*d*₆) δ 9.03 (s, 2H), 7.52 (t, *J* = 1.9 Hz, 1H), 7.45 (d, *J* = 1.9 Hz, 2H), 5.79 (s, 1H), 3.17 (dtd, *J* = 22.5, 12.8, 11.9, 7.0 Hz, 4H), 2.26 (td, *J* = 13.5, 5.0 Hz, 2H), 1.74 (dd, *J* = 13.9, 2.3 Hz, 2H). ¹³C NMR (DMSO-*d*₆) δ 152.7, 134.0, 126.5, 123.7, 68.5, 33.9.

4-Phenylpiperidin-4-ol (6h). General procedure B. Alkaline work-up afforded 622 mg of a white solid (97%). LCMS (*m/z*): 178.2 [M+H]⁺, *t_R* 0.42 min. ¹H NMR (CDCl₃) δ 7.55 – 7.48 (m, 2H), 7.41 – 7.32 (m, 2H), 7.31 – 7.22 (m, 1H), 3.10 (dd, *J* = 12.2, 2.6 Hz, 2H), 2.98 – 2.89 (m, 2H), 2.22 (s, 2H), 2.00 (ddd, *J* = 13.5, 12.2, 4.6 Hz, 2H), 1.75 – 1.69 (m, 2H). ¹³C NMR (CDCl₃) δ 149.1, 128.4, 126.9, 124.6, 71.5, 42.4, 39.3.

4-(*p*-Tolyl)piperidin-4-ol (6i). General procedure B. Alkaline work-up afforded 621 mg of a white solid (95%). LCMS (*m/z*): 192.1 [M+H]⁺, *t_R* 0.62 min. ¹H NMR (CDCl₃) δ 7.37 (d, *J* = 8.3 Hz, 2H), 7.15 (d, *J* = 8.0 Hz, 2H), 3.07 (dd, *J* = 12.2, 2.7 Hz, 2H), 2.92 – 2.86 (m, 2H), 2.42 – 2.26 (m, 5H), 1.96 (td, *J* = 13.0, 4.6 Hz, 2H), 1.69 (dd, *J* = 14.1, 2.6 Hz, 2H). ¹³C NMR (CDCl₃) δ 146.2, 136.5, 129.1, 124.6, 71.2, 42.4, 39.3, 21.0.

4-(4-(Trifluoromethyl)phenyl)piperidin-4-ol (6j). General procedure B. Alkaline work-up afforded 702 mg of a light yellow solid (92%). LCMS (*m/z*): 246.1 [M+H]⁺, *t_R* 1.41-1.82 min. ¹H NMR

(CDCl₃) δ 7.66 – 7.56 (m, 4H), 3.11 (td, *J* = 12.3, 2.6 Hz, 2H), 3.01 – 2.92 (m, 2H), 2.20 – 2.07 (m, 2H), 2.01 (ddd, *J* = 13.5, 12.3, 4.8 Hz, 2H), 1.74 – 1.65 (m, 2H). ¹³C NMR (CDCl₃) δ 152.9, 129.3 (q, *J* = 32.4 Hz), 125.4 (q, *J* = 3.7 Hz), 125.1, 71.7, 42.3, 39.2.

4-(4-(Dimethylamino)phenyl)piperidin-4-ol (6k). General procedure B. Alkaline work-up afforded 675 mg of a light orange solid (98%). LCMS (*m/z*): 221.2 [M+H]⁺, *t_R* 0.31 min. ¹H NMR (CDCl₃) δ 7.40 – 7.31 (m, 2H), 6.76 – 6.68 (m, 2H), 3.09 (td, *J* = 12.1, 2.7 Hz, 2H), 2.93 (s, 6H), 2.90 (dt, *J* = 11.9, 3.5 Hz, 2H), 2.07 (s, 2H), 1.96 (ddd, *J* = 13.3, 11.9, 4.5 Hz, 2H), 1.77 – 1.68 (m, 2H). ¹³C NMR (CDCl₃) δ 149.6, 136.9, 125.4, 112.4, 70.9, 42.5, 40.7, 39.3.

4-(4-Fluorophenyl)piperidin-4-ol (6l). General procedure B. Alkaline work-up afforded 600 mg of a light yellow solid (92%). LCMS (*m/z*): 196.2 [M+H]⁺, *t_R* 0.42 min. ¹H NMR (CDCl₃) δ 7.47 – 7.42 (m, 2H), 7.01 (t, *J* = 8.7 Hz, 2H), 3.07 (td, *J* = 12.2, 2.6 Hz, 2H), 2.91 (ddd, *J* = 12.6, 4.2, 2.1 Hz, 2H), 1.95 (td, *J* = 13.0, 4.7 Hz, 2H), 1.69 (dd, *J* = 14.1, 2.6 Hz, 2H). ¹³C NMR (CDCl₃) δ 161.9 (d, *J* = 245.2 Hz), 144.9 (d, *J* = 3.0 Hz), 126.4 (d, *J* = 8.0 Hz), 115.1 (d, *J* = 21.1 Hz), 71.4, 42.5, 39.5.

4-(2'-Chloro-[1,1'-biphenyl]-2-yl)piperidin-4-ol (6m). General procedure B. Alkaline work-up afforded 200 mg of a white solid (95%). LCMS (*m/z*): 288.0 [M+H]⁺, *t_R* 2.06 min. ¹H NMR (CDCl₃) δ 7.61 (dd, *J* = 8.1, 1.3 Hz, 1H), 7.49 – 7.41 (m, 1H), 7.44 – 7.37 (m, 1H), 7.35 – 7.25 (m, 4H), 7.02 (dd, *J* = 7.6, 1.5 Hz, 1H), 3.05 – 2.95 (m, 2H), 2.90 – 2.81 (m, 2H), 2.37 (s, 2H), 2.09 (ddd, *J* = 13.9, 12.2, 4.6 Hz, 1H), 1.98 (ddd, *J* = 13.7, 12.2, 4.7 Hz, 1H), 1.78 (ddt, *J* = 13.5, 10.5, 2.7 Hz, 2H). ¹³C NMR (CDCl₃) δ 145.6, 143.1, 137.2, 133.4, 132.2, 131.1, 129.4, 128.6, 128.2, 126.7, 126.5, 126.2, 73.5, 39.2, 38.8.

4-(2-Chlorophenyl)piperidin-4-ol (6n). General procedure B. Alkaline work-up afforded 285 mg of a white solid (72 %). LCMS (*m/z*): 2121 [M+H]⁺, *t_R* 0.48 min. ¹H NMR (CDCl₃) δ 7.57 (dd, *J* = 7.9, 1.8 Hz, 1H), 7.34 (dd, *J* = 7.8, 1.5 Hz, 1H), 7.25 (td, *J* = 7.6, 1.5 Hz, 1H), 7.18 (td, *J* = 7.6, 1.8 Hz, 1H), 3.15 (td, *J* = 12.4, 2.7 Hz, 2H), 2.99 – 2.89 (m, 2H), 2.63 (s, 1H), 2.29 (ddd, *J* = 13.4, 12.3, 4.7 Hz, 2H), 1.96 – 1.86 (m, 2H). ¹³C NMR (CDCl₃) δ 144.2, 131.9, 131.8, 128.5, 127.3, 127.2, 72.4, 42.2, 36.3.

4-(4-Chlorophenyl)piperidin-4-ol (7b). General procedure B. Alkaline work-up afforded 1.62 g of a beige solid (96%). LCMS (*m/z*): 311.1 [M+H]⁺, *t_R* 0.76 min. ¹H NMR (CDCl₃) δ 7.43 – 7.38 (m, 2H), 7.32 – 7.27 (m, 2H), 3.05 (td, *J* = 12.3, 2.7 Hz, 2H), 2.91 – 2.84 (m, 2H), 2.18 (s, 2H, broad), 1.91 (ddd, *J* = 13.4, 12.2, 4.7 Hz, 2H), 1.71 – 1.60 (m, 2H). ¹³C NMR (CDCl₃) δ 147.7, 132.7, 128.5, 126.2, 71.3, 42.3, 39.3.

4-(4-(3-Chlorophenyl)-4-hydroxypiperidin-1-yl)-1-(4-fluorophenyl)butan-1-one (8a). General procedure C. Purification by FCC (eluent 20:0.5:0.1, EtOAc/MeOH/NH₄OH) gave 91 mg of the title

compound as a white solid (68%). LCMS (*m/z*): 376.2 [M+H]⁺, *t_R* 3.37 min. HRMS (*m/z*): C₂₁H₂₃ClFNO₂: requires 376.1505 [M+H]⁺; found 376.1546. ¹H NMR (CDCl₃) δ 8.02 (t, *J* = 6.7 Hz, 2H), 7.44 (s, 1H), 7.35 – 7.18 (m, 3H), 7.14 (t, *J* = 8.4 Hz, 2H), 2.98 (t, *J* = 7.0 Hz, 2H), 2.78 (d, *J* = 11.4 Hz, 2H), 2.55 – 2.35 (m, 4H), 2.06 – 1.90 (m, 5H), 1.67 (d, *J* = 13.6 Hz, 2H). ¹³C NMR (CDCl₃) δ 198.5, 165.7 (d, *J* = 254.5 Hz), 150.7, 134.4, 133.8 (d, *J* = 3.1 Hz), 130.8 (d, *J* = 9.2 Hz), 129.7, 127.2, 125.2, 122.9, 115.8 (d, *J* = 21.7 Hz), 71.3, 57.9, 49.4, 38.5, 36.4, 22.1.

4-(4-(2,3-Dichlorophenyl)-4-hydroxypiperidin-1-yl)-1-(4-fluorophenyl)butan-1-one (8b).

General procedure C. Purification by FCC (eluent 20:0.5:0.1, EtOAc/MeOH/NH₄OH) gave 82 mg of the title compound as a white solid (68%). LCMS (*m/z*): 410.3 [M+H]⁺, *t_R* 3.58 min. HRMS (*m/z*): C₂₁H₂₂Cl₂FNO₂: requires 410.1118 [M+H]⁺; found 410.1151. ¹H NMR (CDCl₃) δ 7.99 (dd, *J* = 8.6, 5.6 Hz, 2H), 7.41 (ddd, *J* = 16.5, 8.0, 1.5 Hz, 2H), 7.18 (t, *J* = 8.0 Hz, 1H), 7.11 (t, *J* = 8.6 Hz, 2H), 2.98 (t, *J* = 7.1 Hz, 3H), 2.94 (s, 1H), 2.81 (dt, *J* = 11.9, 3.2 Hz, 2H), 2.58 – 2.45 (m, 4H), 2.26 (td, *J* = 13.0, 4.4 Hz, 2H), 2.04 – 1.93 (m, 4H). ¹³C NMR (CDCl₃) δ 198.5, 165.7 (d, *J* = 254.4 Hz), 145.9, 134.9, 133.7 (d, *J* = 3.0 Hz), 130.8 (d, *J* = 9.2 Hz), 129.7, 127.5, 125.5, 115.7 (d, *J* = 21.8 Hz), 72.4, 57.7, 49.1, 36.3, 35.4, 21.8.

4-(2,4-Dichlorophenyl)-1-(4-(4-fluorophenyl)-4-oxobutyl)-4-hydroxypiperidin-1-ium 2,2,2-trifluoroacetate (8c).

General procedure C. Purification by preparative HPLC (Method C) afforded the title compound as a white solid (44 mg, 60%). LCMS (*m/z*): 410.3 [M+H]⁺, *t_R* 3.47 min. HRMS (*m/z*): C₂₁H₂₂Cl₂FNO₂: requires 410.1012 [M+H]⁺; found 410.1094. ¹H NMR (CDCl₃) δ 12.05 (s, 1H), 8.00 – 7.92 (m, 2H), 7.33 (d, *J* = 8.0 Hz, 2H), 7.12 (td, *J* = 8.2, 4.1 Hz, 2H), 5.59 (s, 1H), 3.58 (d, *J* = 11.3 Hz, 2H), 3.36 (q, *J* = 11.2 Hz, 2H), 3.28 – 3.10 (m, 6H), 2.35 (d, *J* = 14.1 Hz, 2H), 2.22 (p, *J* = 6.8 Hz, 2H). ¹³C NMR (CDCl₃) δ 196.78, 166.1 (d, *J* = 255.6 Hz), 137.8, 133.8, 132.7 (d, *J* = 3.1 Hz), 132.2, 130.8 (d, *J* = 9.5 Hz), 129.2, 116.0 (d, *J* = 21.9 Hz), 73.3, 56.7, 48.5, 35.1, 33.7, 18.2.

4-(4-(2,5-Dichlorophenyl)-4-hydroxypiperidin-1-yl)-1-(4-fluorophenyl)butan-1-one (8d).

General procedure C. Purification by FCC (eluent 20:0.5:0.1, EtOAc/MeOH/NH₄OH) gave 91 mg of the title compound as a white solid (70%). LCMS (*m/z*): 410.3 [M+H]⁺, *t_R* 3.65 min. HRMS (*m/z*): C₂₁H₂₂Cl₂FNO₂: requires 410.1012 [M+H]⁺; found 410.1093. ¹H NMR (CDCl₃) δ 8.04 – 7.94 (m, 2H), 7.53 (d, *J* = 2.5 Hz, 1H), 7.25 (d, *J* = 8.5 Hz, 1H), 7.17 – 7.07 (m, 3H), 2.97 (t, *J* = 7.0 Hz, 2H), 2.77 (dt, *J* = 10.8, 2.8 Hz, 3H), 2.51 – 2.42 (m, 4H), 2.28 (td, *J* = 13.0, 4.4 Hz, 2H), 1.96 (p, *J* = 7.1 Hz, 2H), 1.86 (dd, *J* = 13.7, 2.6 Hz, 2H). ¹³C NMR (CDCl₃) δ 198.7, 165.7 (d, *J* = 254.4 Hz), 145.6, 133.8 (d, *J* = 3.1 Hz), 133.2, 132.8, 130.8 (d, *J* = 9.1 Hz), 130.1, 128.4, 127.7, 115.7 (d, *J* = 21.8 Hz), 72.0, 57.7, 49.1, 36.3, 35.2, 21.9.

4-(4-(2,6-Dichlorophenyl)-4-hydroxypiperidin-1-yl)-1-(4-fluorophenyl)butan-1-one (8e).

General procedure C. Purification by FCC (eluent 20:0.5:0.1, EtOAc/MeOH/NH₄OH) gave 69 mg of

the title compound as a white solid (73%). LCMS (m/z): 410.72 [M+H]⁺, t_R 3.50 min. HRMS (m/z): C₂₁H₂₂Cl₂FNO₂: requires 410.1111 [M+H]⁺; found 410.1066. ¹H NMR (CDCl₃) δ 8.01 (dd, J = 8.7, 5.6 Hz, 2H), 7.29 (d, J = 7.9 Hz, 2H), 7.12 (t, J = 8.6 Hz, 2H), 7.04 (t, J = 8.0 Hz, 1H), 3.24 (s, 1H), 2.98 (t, J = 7.1 Hz, 2H), 2.81 – 2.69 (m, 4H), 2.54 – 2.48 (m, 2H), 2.45 (t, J = 7.1 Hz, 2H), 2.06 (d, J = 13.6 Hz, 2H), 1.97 (p, J = 7.1 Hz, 2H). ¹³C NMR (CDCl₃) δ 198.8, 165.7 (d, J = 254.1 Hz), 140.7, 134.0, 133.8 (d, J = 3.0 Hz), 132.0, 130.8 (d, J = 9.2 Hz), 128.2, 115.7 (d, J = 21.7 Hz), 75.8, 57.8, 49.2, 36.4, 36.2, 22.1.

4-(4-(3,4-Dichlorophenyl)-4-hydroxypiperidin-1-yl)-1-(4-fluorophenyl)butan-1-one (8f).

General procedure C. Purification by FCC (eluent 20:0.5:0.1, EtOAc/MeOH/NH₄OH) gave 84 mg of the title compound as a white solid (70%). LCMS (m/z): 410.2 [M+H]⁺, t_R 3.69 min. HRMS (m/z): C₂₁H₂₂Cl₂FNO₂: requires 410.1111 [M+H]⁺; found 410.1066. ¹H NMR (CDCl₃) δ 8.03 (dd, J = 8.7, 5.5 Hz, 2H), 7.55 (d, J = 2.1 Hz, 1H), 7.40 (d, J = 8.5 Hz, 1H), 7.31 – 7.23 (m, 1H), 7.16 (t, J = 8.6 Hz, 2H), 2.99 (t, J = 7.0 Hz, 2H), 2.80 (dt, J = 11.4, 2.9 Hz, 2H), 2.54 – 2.37 (m, 4H), 2.08 – 1.91 (m, 4H), 1.66 (dd, J = 14.1, 2.6 Hz, 2H). ¹³C NMR (CDCl₃) δ 198.4, 167.0, 164.5, 148.9, 133.8, 133.8, 132.5, 130.9, 130.8, 130.7, 130.3, 127.2, 124.3, 115.9, 115.7, 77.5, 77.2, 76.8, 71.1, 57.9, 49.3, 38.4, 36.3, 22.0.

4-(4-(3,5-Dichlorophenyl)-4-hydroxypiperidin-1-yl)-1-(4-fluorophenyl)butan-1-one (8g).

General procedure C. Purification by FCC (eluent 20:0.5:0.1, EtOAc/MeOH/NH₄OH) gave 92 mg of the title compound as a white solid (62%). LCMS (m/z): 410.7 [M+H]⁺, t_R 3.59 min. HRMS (m/z): C₂₁H₂₂Cl₂FNO₂: requires 410.1084 [M+H]⁺; found 410.1097. ¹H NMR (DMSO-*d*₆) δ 8.08 (dd, J = 8.5, 5.6 Hz, 2H), 7.41 (t, J = 1.9 Hz, 1H), 7.35 (t, J = 8.7 Hz, 2H), 7.28 (d, J = 1.9 Hz, 2H), 5.04 (s, 1H), 2.95 (t, J = 6.6 Hz, 2H), 2.57 (d, J = 10.9 Hz, 2H), 2.35 (t, J = 6.8 Hz, 2H), 2.29 (t, J = 11.4 Hz, 2H), 1.85 (t, J = 6.7 Hz, 2H), 1.58 (dt, J = 12.9, 6.4 Hz, 2H), 1.42 (d, J = 12.9 Hz, 2H). ¹³C NMR (DMSO-*d*₆) δ 198.2, 164.7 (d, J = 251.1 Hz), 154.7, 134.1 (d, J = 2.9 Hz), 133.7, 130.8 (d, J = 9.4 Hz), 125.8, 123.8, 115.6 (d, J = 21.7 Hz), 69.9, 57.2, 48.7, 37.5, 35.6, 22.2.

1-(4-Fluorophenyl)-4-(4-hydroxy-4-phenylpiperidin-1-yl)butan-1-one (8h).

General procedure C. Purification by FCC (eluent 20:0.5:0.1, EtOAc/MeOH/NH₄OH) gave 101 mg of the title compound as a white solid (88%). LCMS (m/z): 342.3 [M+H]⁺, t_R 2.92 min. HRMS (m/z): C₂₁H₂₄FNO₂: requires 342.1864 [M+H]⁺; found 342.1873. ¹H NMR (CDCl₃) δ 8.08 – 7.99 (m, 2H), 7.48 (dd, J = 7.6, 1.7 Hz, 2H), 7.36 (t, J = 7.7 Hz, 2H), 7.31 – 7.22 (m, 1H), 7.15 (t, J = 8.6 Hz, 2H), 3.00 (t, J = 7.1 Hz, 2H), 2.81 (dt, J = 11.7, 3.1 Hz, 2H), 2.56 – 2.42 (m, 4H), 2.05 (ddd, J = 28.3, 13.9, 5.8 Hz, 4H), 1.89 (s, 1H), 1.73 (dd, J = 14.2, 2.6 Hz, 2H). ¹³C NMR (CDCl₃) δ 198.5, 165.7 (d, J = 254.3 Hz), 148.5, 133.8 (d, J = 3.0 Hz), 130.8 (d, J = 9.3 Hz), 128.4, 127.1, 124.6, 115.7 (d, J = 21.7 Hz), 71.4, 57.9, 49.5, 38.5, 36.4, 22.0.

1-(4-Fluorophenyl)-4-(4-hydroxy-4-(*p*-tolyl)piperidin-1-yl)butan-1-one (8i). General procedure C. Purification by FCC (eluent 20:0.5:0.1, EtOAc/MeOH/NH₄OH) gave 84 mg of the title compound as a white solid (80%). LCMS (*m/z*): 356.2 [M+H]⁺, *t_R* 3.22 min. HRMS (*m/z*): C₂₂H₂₆FNO₂: requires 356.2067 [M+H]⁺; found 356.2068. ¹H NMR (CDCl₃) δ 8.01 (dd, *J* = 8.7, 5.6 Hz, 2H), 7.34 (d, *J* = 8.0 Hz, 2H), 7.18 – 7.08 (m, 4H), 2.98 (t, *J* = 7.1 Hz, 2H), 2.78 (dt, *J* = 12.1, 3.3 Hz, 2H), 2.52 – 2.40 (m, 4H), 2.33 (s, 3H), 2.09 – 1.94 (m, 5H), 1.70 (dd, *J* = 14.2, 2.6 Hz, 2H). ¹³C NMR (CDCl₃) δ 198.5, 165.7 (d, *J* = 254.3 Hz), 145.6, 136.7, 133.8 (d, *J* = 3.1 Hz), 130.8 (d, *J* = 9.3 Hz), 129.1, 124.6, 115.7 (d, *J* = 21.8 Hz), 71.1, 57.9, 49.6, 38.5, 36.4, 21.9, 21.1.

1-(4-Fluorophenyl)-4-(4-hydroxy-4-(4-(trifluoromethyl)phenyl)piperidin-1-yl)butan-1-one (8j). General procedure C. Purification by FCC (eluent 20:0.5:0.1, EtOAc/MeOH/NH₄OH) gave 65 mg of the title compound as a white solid (69%). LCMS (*m/z*): 410.2 [M+H]⁺, *t_R* 3.59 min. HRMS (*m/z*): C₂₂H₂₃F₄NO₂: requires 410.1756 [M+H]⁺; found 410.1778. ¹H NMR (CDCl₃) δ 8.00 (dd, *J* = 8.6, 5.5 Hz, 2H), 7.57 (s, 4H), 7.13 (t, *J* = 8.6 Hz, 2H), 2.99 (t, *J* = 7.0 Hz, 2H), 2.85 (d, *J* = 11.2 Hz, 2H), 2.57 – 2.45 (m, 4H), 2.17 – 1.90 (m, 5H), 1.79 – 1.63 (m, 2H). ¹³C NMR (CDCl₃) δ 198.4, 165.8 (d, *J* = 254.7 Hz), 152.3, 133.7 (d, *J* = 3.1 Hz), 129.4 (d, *J* = 32.4 Hz), 125.4 (q, *J* = 3.7 Hz), 125.2, 124.3 (q, *J* = 272.9 Hz), 115.8 (d, *J* = 21.9 Hz), 71.3, 57.9, 49.3, 38.2, 36.3, 21.7.

4-(4-(4-(Dimethylamino)phenyl)-4-hydroxypiperidin-1-yl)-1-(4-fluorophenyl)butan-1-one (8k). General procedure C. Purification by FCC (eluent 20:0.5:0.1, EtOAc/MeOH/NH₄OH) gave 60 mg of the title compound as a light orange solid (62%). LCMS (*m/z*): 385.4 [M+H]⁺, *t_R* 1.41 min. HRMS (*m/z*): C₂₃H₂₉FN₂O₂: requires 385.2310 [M+H]⁺; found 385.2274. ¹H NMR (CDCl₃) δ 7.99 (dd, *J* = 8.7, 5.6 Hz, 2H), 7.32 (d, *J* = 8.8 Hz, 2H), 7.12 (t, *J* = 8.6 Hz, 2H), 6.70 (d, *J* = 8.9 Hz, 2H), 3.01 (t, *J* = 7.0 Hz, 2H), 2.92 (s, 6H), 2.93 – 2.86 (m, 2H), 2.60 (dt, *J* = 14.8, 8.4 Hz, 4H), 2.14 (td, *J* = 13.3, 4.3 Hz, 2H), 2.02 (p, *J* = 7.3 Hz, 2H), 1.94 (s, 1H), 1.77 (dd, *J* = 14.3, 2.7 Hz, 2H). ¹³C NMR (CDCl₃) δ 198.2, 165.8 (d, *J* = 254.4 Hz), 149.8, 135.8, 133. (d, *J* = 3.0 Hz), 130.8 (d, *J* = 9.2 Hz), 125.5, 115.7 (d, *J* = 21.8 Hz), 112.5, 70.4, 57.5, 49.4, 40.7, 37.7, 36.3, 21.2.

1-(4-Fluorophenyl)-4-(4-(4-fluorophenyl)-4-hydroxypiperidin-1-yl)butan-1-one (8l). General procedure C. Purification by FCC (eluent 20:0.5:0.1, EtOAc/MeOH/NH₄OH) gave 80 mg of the title compound as a white solid (74%). LCMS (*m/z*): 360.3 [M+H]⁺, *t_R* 3.09 min. HRMS (*m/z*): C₂₁H₂₃F₂NO₂: requires 360.1697 [M+H]⁺; found 360.1777. ¹H NMR (CDCl₃) δ 8.12 – 7.96 (m, 2H), 7.44 – 7.36 (m, 2H), 7.13 (t, *J* = 8.6 Hz, 2H), 7.00 (t, *J* = 8.7 Hz, 2H), 2.98 (t, *J* = 7.0 Hz, 2H), 2.80 (dt, *J* = 11.7, 3.0 Hz, 2H), 2.55 – 2.41 (m, 4H), 2.02 (dt, *J* = 14.3, 10.2 Hz, 5H), 1.70 (dd, *J* = 14.2, 2.6 Hz, 2H). ¹³C NMR (CDCl₃) δ 198.5, 165.8 (d, *J* = 254.4 Hz), 161.9 (d, *J* = 245.3 Hz), 144.2 (d, *J* = 2.6 Hz), 133.8 (d, *J* = 3.3 Hz), 130.8 (d, *J* = 9.2 Hz), 126.4 (d, *J* = 8.0 Hz), 115.7 (d, *J* = 21.8 Hz), 115.1 (d, *J* = 21.1 Hz), 71.1, 57.9, 49.5, 38.5, 36.4, 21.9.

4-(2'-Chloro-[1,1'-biphenyl]-2-yl)-1-(4-(4-fluorophenyl)-4-oxobutyl)-4-hydroxypiperidin-1-ium 2,2,2-trifluoroacetate (8m). General procedure C. Purification by preparative HPLC (Method C) afforded 95 mg of the title compound as a transparent oil (76%). LCMS (m/z): 452.2 [M+H]⁺, t_R 4.00 min. HRMS (m/z): C₂₇H₂₇ClFNO₂: requires 452.1787 [M+H]⁺; found 452.1811. ¹H NMR (CDCl₃) δ 12.19 (s, 1H), 7.94 (dd, J = 8.6, 5.3 Hz, 2H), 7.53 (d, J = 8.0 Hz, 1H), 7.49 – 7.38 (m, 2H), 7.33 (ddd, J = 7.5, 5.1, 2.7 Hz, 2H), 7.25 (d, J = 7.6 Hz, 2H), 7.12 (t, J = 8.5 Hz, 2H), 7.02 (d, J = 7.5 Hz, 1H), 3.44 (dd, J = 26.7, 11.6 Hz, 2H), 3.22 – 2.99 (m, 6H), 2.71 – 2.58 (m, 1H), 2.46 (td, J = 14.0, 4.1 Hz, 1H), 2.35 (s, 1H), 2.15 (t, J = 7.2 Hz, 2H), 2.01 (dd, J = 30.5, 14.6 Hz, 2H). ¹³C NMR (CDCl₃) δ 196.7, 166.1 (d, J = 255.6 Hz), 142.3, 142.1, 137.1, 133.4, 132.8 (d, J = 3.0 Hz), 132.4, 130.9, 130.8 (d, J = 9.5 Hz), 129.6, 129.2, 128.8, 127.8, 126.7, 126.4, 116.0 (d, J = 21.9 Hz), 71.4, 56.6, 48.6, 35.9, 35.6, 35.1, 18.2.

4-(2-Chlorophenyl)-1-(4-(4-fluorophenyl)-4-oxobutyl)-4-hydroxypiperidin-1-ium 2,2,2-trifluoroacetate (8n). General procedure C. Purification by preparative HPLC (Method C) afforded 88 mg of the title compound as a white solid (62%). LCMS (m/z): 376.2 [M+H]⁺, t_R 3.37 min. HRMS (m/z): C₂₁H₂₃ClFNO: requires 376.1474 [M+H]⁺; found 376.1479. ¹H NMR (CDCl₃) δ 12.14 (s, 1H), 8.01 – 7.92 (m, 2H), 7.46 (dd, J = 7.7, 1.9 Hz, 1H), 7.37 (dd, J = 7.5, 1.8 Hz, 1H), 7.32 – 7.19 (m, 2H), 7.13 (t, J = 8.5 Hz, 2H), 4.05 (s, 1H), 3.58 (d, J = 11.5 Hz, 2H), 3.36 (q, J = 11.2 Hz, 2H), 3.15 (q, J = 6.5, 5.2 Hz, 4H), 2.67 (td, J = 13.9, 4.1 Hz, 2H), 2.31 (d, J = 14.1 Hz, 2H), 2.22 (p, J = 6.6 Hz, 2H). ¹³C NMR (CDCl₃) δ 196.6, 166.0 (d, J = 255.5 Hz), 140.6, 132.6 (d, J = 3.0 Hz), 131.9, 131.5, 130.7 (d, J = 9.4 Hz), 129.5, 127.7, 127.1, 115.9 (d, J = 22.0 Hz), 69.8, 56.6, 48.4, 35.0, 32.9, 18.1.

4-Chlorobut-1-yne (9). 3-Butynol (25.0 mL, 330 mmol) and pyridine (2.66 mL, 33 mmol) were placed in a 100 mL roundbottomed flask, and the mixture was cooled in an ice bath. Then, thionyl chloride (24.4 mL, 334 mmol) was added dropwise for 10 min. The flask was shaken occasionally during the addition, and after the thionyl chloride was added, the mixture was heated under reflux for 30 min. Fractional distillation of the products gave 4-chloro-1-butyne as a light-yellow liquid (24 mL, 82%). ¹H NMR (CDCl₃) δ 3.58 (t, J = 7.1 Hz, 2H), 2.63 (td, J = 7.1, 2.6 Hz, 2H), 2.07 (t, J = 2.7 Hz, 1H). ¹³C NMR (CDCl₃) δ 80.2, 70.5, 41.9, 22.8.

1-(4-Chlorobut-1-yn-1-yl)-2-fluorobenzene (12a). General procedure D. Purification by FCC (*n*-hexanes) gave 1.24 g of a yellow oil (72%). LCMS (m/z): 183.1 [M+H]⁺, t_R 3.05 min. ¹H NMR (CDCl₃) δ 7.47 – 7.40 (m, 1H), 7.34 – 7.26 (m, 1H), 7.15 – 7.03 (m, 2H), 3.73 (t, J = 7.2 Hz, 2H), 2.95 (t, J = 7.2 Hz, 2H). ¹³C NMR (CDCl₃) δ 162.9 (d, J = 251.0 Hz), 133.8 (d, J = 1.5 Hz), 129.9 (d, J = 7.9 Hz), 124.0 (d, J = 3.8 Hz), 115.6 (d, J = 21.0 Hz), 111.7 (d, J = 15.7 Hz), 91.2 (d, J = 3.3 Hz), 75.9 (d, J = 1.1 Hz), 42.1, 24.1.

1-(4-Chlorobut-1-yn-1-yl)-3-fluorobenzene (12b). General procedure D. Purification by FCC (*n*-hexanes) gave 1.55 g of a yellow oil (90%). LCMS (*m/z*): 183.0 [M+H]⁺, *t*_R 3.02 min. ¹H NMR (CDCl₃) δ 7.32 – 7.25 (m, 1H), 7.22 (dt, *J* = 7.7, 1.3 Hz, 1H), 7.14 (ddd, *J* = 9.5, 2.6, 1.4 Hz, 1H), 7.03 (tdd, *J* = 8.4, 2.7, 1.2 Hz, 1H), 3.71 (t, *J* = 7.2 Hz, 2H), 2.91 (t, *J* = 7.2 Hz, 2H). ¹³C NMR (CDCl₃) δ 162.6 (d, *J* = 246.3 Hz), 129.9 (d, *J* = 8.5 Hz), 127.7 (d, *J* = 3.1 Hz), 125.1 (d, *J* = 9.5 Hz), 118.6 (d, *J* = 22.7 Hz), 115.6 (d, *J* = 21.2 Hz), 86.9, 81.5 (d, *J* = 3.4 Hz), 42.1, 23.9.

1-(4-Chlorobut-1-yn-1-yl)-2,3-difluorobenzene (12c). General procedure D. Purification by FCC (*n*-hexanes) gave 1.65 g of a yellow oil (87%). LCMS (*m/z*): 201.1 [M+H]⁺, *t*_R 3.02 min. ¹H NMR (CDCl₃) δ 7.20 – 7.11 (m, 1H), 7.15 – 7.05 (m, 1H), 7.00 (dddd, *J* = 8.3, 7.8, 4.9, 1.6 Hz, 1H), 3.70 (t, *J* = 7.2 Hz, 2H), 2.93 (td, *J* = 7.2, 0.7 Hz, 2H). ¹³C NMR (CDCl₃) δ 151.3 (dd, *J* = 252.7, 13.4 Hz), 150.7 (dd, *J* = 248.3, 12.2 Hz), 128.5 (d, *J* = 3.4 Hz), 123.9 (dd, *J* = 7.3, 4.9 Hz), 117.4 (d, *J* = 17.5 Hz), 113.9 (dd, *J* = 12.3, 1.8 Hz), 92.6 (d, *J* = 3.8 Hz), 74.9 (dd, *J* = 4.6, 1.3 Hz), 41.9, 24.1.

1-(4-Chlorobut-1-yn-1-yl)-2,4-difluorobenzene (12d). General procedure D. Purification by FCC (*n*-hexanes) gave 1.72 g of a yellow oil (82.3%). LCMS (*m/z*): 201.1 [M+H]⁺, *t*_R 2.99 min. ¹H NMR (CDCl₃) δ 7.42 – 7.35 (m, 1H), 6.86 – 6.78 (m, 2H), 3.69 (t, *J* = 7.2 Hz, 2H), 2.91 (t, *J* = 7.2 Hz, 2H). ¹³C NMR (CDCl₃) δ 163.3 (dd, *J* = 253.7, 12.2 Hz), 162.6 (dd, *J* = 251.7, 11.3 Hz), 134.6 (dd, *J* = 9.7, 2.8 Hz), 111.6 (dd, *J* = 21.9, 3.8 Hz), 108.1 (dd, *J* = 16.0, 4.1 Hz), 104.3 (dd, *J* = 24.9, 0.2 Hz), 90.9 (dd, *J* = 3.4, 1.8 Hz), 75.0 (d, *J* = 1.4 Hz), 42.04, 24.1.

2-(4-Chlorobut-1-yn-1-yl)-1,4-difluorobenzene (12e). General procedure D. Purification by FCC (*n*-hexanes) gave 1.45 g of a yellow oil (70%). LCMS (*m/z*): 201.1 [M+H]⁺, *t*_R 3.00 min. ¹H NMR (CDCl₃) δ 7.10 (ddd, *J* = 8.5, 5.4, 2.9 Hz, 1H), 7.04 – 6.93 (m, 2H), 3.69 (t, *J* = 7.2 Hz, 2H), 2.92 (t, *J* = 7.2 Hz, 2H). ¹³C NMR (CDCl₃) δ 159.3 (d, *J* = 249.6 Hz), 158.2 (d, *J* = 242.8 Hz), 128.8 (d, *J* = 81.5 Hz), 119.8 (dd, *J* = 25.2, 1.9 Hz), 116.7 (dd, *J* = 10.6, 8.6 Hz), 116.5 (dd, *J* = 10.5, 8.5 Hz), 92.3 (d, *J* = 3.4 Hz), 75.1 (d, *J* = 2.6 Hz), 41.9, 24.1.

2-(4-Chlorobut-1-yn-1-yl)-1,3-difluorobenzene (12f). General procedure D. Purification by FCC (*n*-hexanes) gave 992 mg of a pink oil (53%). LCMS (*m/z*): 200.9 [M+H]⁺, *t*_R 2.97 min. ¹H NMR (CDCl₃) δ 7.32 – 7.20 (m, 1H), 6.96 – 6.86 (m, 2H), 3.74 (t, *J* = 7.3 Hz, 2H), 2.99 (t, *J* = 7.3 Hz, 2H). ¹³C NMR (CDCl₃) δ 163.5 (d, *J* = 253.2 Hz), 163.4 (d, *J* = 253.3 Hz), 129.6 (t, *J* = 10.0 Hz), 111.4 (dd, *J* = 4.5, 0.3 Hz), 111.2 (dd, *J* = 4.5, 1.2 Hz), 102.2 (t, *J* = 19.8 Hz), 96.2 (t, *J* = 3.1 Hz), 69.6 (t, *J* = 1.4 Hz), 41.8, 24.3.

4-(4-Chlorobut-1-yn-1-yl)-1,2-difluorobenzene (12g). General procedure D. Purification by FCC (*n*-hexanes) gave 1.53g of a yellow oil (81%). LCMS (*m/z*): 200.9 [M+H]⁺, *t*_R 3.03 min. ¹H NMR (CDCl₃) δ 7.21 (ddd, *J* = 10.9, 7.5, 2.0 Hz, 1H), 7.13 (dd, *J* = 4.6, 1.6 Hz, 1H), 7.08 (dt, *J* = 10.2, 8.2

Hz, 1H), 3.67 (t, $J = 7.1$ Hz, 2H), 2.86 (t, $J = 7.1$ Hz, 2H). ¹³C NMR (CDCl₃) δ 150.6 (dd, $J = 250.9$, 12.5 Hz), 150.0 (dd, $J = 248.7$, 13.0 Hz), 128.4 (dd, $J = 6.4$, 3.6 Hz), 120.8 (d, $J = 18.3$ Hz), 117.5 (d, $J = 17.8$ Hz), 86.5 (d, $J = 1.9$ Hz), 80.6 (t, $J = 2.3$ Hz), 42.1, 23.8.

1-(4-Chlorobut-1-yn-1-yl)-3,5-difluorobenzene (12h). General procedure D. Purification by FCC (*n*-hexanes) gave 1.61 g of a yellow oil (85%). LCMS (m/z): 200.9 [M+H]⁺, t_R 3.03 min. ¹H NMR (CDCl₃) δ 6.98 – 6.91 (m, 2H), 6.79 (tt, $J = 9.0$, 2.4 Hz, 1H), 3.70 (t, $J = 7.1$ Hz, 2H), 2.90 (t, $J = 7.1$ Hz, 2H). ¹³C NMR (CDCl₃) δ 162.8 (d, $J = 248.5$ Hz), 162.7 (d, $J = 248.6$ Hz), 125.9 (t, $J = 11.8$ Hz), 114.9 (d, $J = 7.4$ Hz), 114.7 (d, $J = 7.4$ Hz), 104.5 (t, $J = 25.4$ Hz), 88.2, 80.6 (t, $J = 3.9$ Hz), 41.94, 23.8.

1-Chloro-2-(4-chlorobut-1-yn-1-yl)benzene (12i). General procedure E. Purification by FCC (*n*-hexanes) gave 1.12 g of a light-yellow liquid (88%). LCMS (m/z): 200.4 [M+H]⁺, t_R 3.02 min. ¹H NMR (CDCl₃) δ 7.45 (dd, $J = 7.5$, 1.9 Hz, 1H), 7.38 (dd, $J = 7.9$, 1.5 Hz, 1H), 7.21 (dtd, $J = 16.1$, 7.4, 1.6 Hz, 2H), 3.72 (t, $J = 7.3$ Hz, 2H), 2.95 (t, $J = 7.3$ Hz, 2H). ¹³C NMR (CDCl₃) δ 136.0, 133.5, 129.3, 129.2, 126.5, 123.1, 91.3, 79.5, 42.1, 24.1.

1-(4-Chlorobut-1-yn-1-yl)-2-methylbenzene (12j). General procedure E. Purification by FCC (*n*-hexanes) gave 1.32 g of a transparent liquid (92%). LCMS (m/z): 179.1 [M+H]⁺, t_R 3.03 min. ¹H NMR (CDCl₃) δ 7.39 (dd, $J = 7.4$, 1.3 Hz, 1H), 7.23 – 7.17 (m, 2H), 7.17 – 7.07 (m, 1H), 3.71 (t, $J = 7.2$ Hz, 2H), 2.93 (t, $J = 7.2$ Hz, 2H), 2.44 (s, 3H). ¹³C NMR (CDCl₃) δ 140.4, 132.0, 129.5, 128.2, 125.6, 123.0, 89.7, 81.5, 42.5, 24.1, 20.8.

4-Chloro-1-(2-fluorophenyl)butan-1-one (13a). General procedure F. Purification by FCC (*n*-hexanes/EtOAc 10:0.1) gave 1.12 g of a yellow oil (82%). LCMS: t_R 2.91 min. ¹H NMR (CDCl₃) δ 7.87 (td, $J = 7.6$, 1.9 Hz, 1H), 7.52 (dddd, $J = 8.3$, 7.1, 5.0, 1.9 Hz, 1H), 7.23 (ddd, $J = 7.8$, 7.3, 1.1 Hz, 1H), 7.14 (ddd, $J = 11.3$, 8.3, 1.1 Hz, 1H), 3.66 (t, $J = 6.4$ Hz, 2H), 3.18 (td, $J = 6.9$, 3.1 Hz, 2H), 2.27 – 2.17 (m, 2H). ¹³C NMR (CDCl₃) δ 197.4 (d, $J = 4.0$ Hz), 162.2 (d, $J = 254.6$ Hz), 134.8 (d, $J = 9.1$ Hz), 130.7 (d, $J = 2.7$ Hz), 125.6 (d, $J = 13.0$ Hz), 124.6 (d, $J = 3.4$ Hz), 116.9 (d, $J = 24.0$ Hz), 44.6, 40.5 (d, $J = 7.8$ Hz), 26.8 (d, $J = 2.1$ Hz).

4-Chloro-1-(3-fluorophenyl)butan-1-one (13b). General procedure F. Purification by FCC (*n*-hexanes/EtOAc 10:0.1) gave 449 mg of a dark red oil (41%). LCMS (m/z): 201.1 [M+H]⁺, t_R 2.91 min. ¹H NMR (CDCl₃) δ 7.77 (ddd, $J = 7.8$, 1.6, 1.0 Hz, 1H), 7.66 (ddd, $J = 9.5$, 2.6, 1.5 Hz, 1H), 7.46 (td, $J = 8.0$, 5.5 Hz, 1H), 7.28 (tdd, $J = 8.3$, 2.7, 1.0 Hz, 1H), 3.69 (t, $J = 6.2$ Hz, 2H), 3.17 (t, $J = 6.9$ Hz, 2H), 2.27 – 2.20 (m, 2H). ¹³C NMR (CDCl₃) δ 197.7 (d, $J = 2.0$ Hz), 162.9 (d, $J = 248.0$ Hz), 138.9 (d, $J = 6.0$ Hz), 130.4 (d, $J = 7.6$ Hz), 123.9 (d, $J = 3.0$ Hz), 120.3 (d, $J = 21.4$ Hz), 114.8 (d, $J = 22.3$ Hz), 44.6, 35.5, 26.7.

4-Chloro-1-(2,3-difluorophenyl)butan-1-one (13c). General procedure F. Purification by FCC (*n*-hexanes/EtOAc 10:0.1) gave 745 mg of a yellow oil (81%). LCMS: *t*_R 2.94 min. ¹H NMR (CDCl₃) δ 7.61 (ddt, *J* = 7.8, 6.0, 1.7 Hz, 1H), 7.36 (dddd, *J* = 9.8, 8.2, 7.4, 1.8 Hz, 1H), 7.17 (tdd, *J* = 8.1, 4.6, 1.5 Hz, 1H), 3.66 (t, *J* = 6.3 Hz, 2H), 3.18 (td, *J* = 6.9, 3.1 Hz, 2H), 2.22 (dddd, *J* = 13.3, 6.9, 6.2, 0.8 Hz, 32H). ¹³C NMR (CDCl₃) δ 196.2 (dd, *J* = 3.8, 2.6 Hz), 151.1 (dd, *J* = 250.1, 14.0 Hz), 150.5 (dd, *J* = 256.7, 13.7 Hz), 127.5 (d, *J* = 9.9 Hz), 125.1 (dd, *J* = 3.6, 1.6 Hz), 124.5 (dd, *J* = 6.6, 4.5 Hz), 121.6 (dd, *J* = 17.5, 1.4 Hz), 44.4, 40.5 (d, *J* = 7.0 Hz), 26.6 (d, *J* = 2.0 Hz).

4-Chloro-1-(2,4-difluorophenyl)butan-1-one (13d). General procedure F. Purification by FCC (*n*-hexanes/EtOAc 10:0.1) gave 294 mg of a yellow oil (58%). LCMS: *t*_R 2.91 min. ¹H NMR (CDCl₃) δ 7.94 (td, *J* = 8.6, 6.6 Hz, 1H), 7.01 – 6.91 (m, 1H), 6.87 (ddd, *J* = 11.1, 8.6, 2.4 Hz, 1H), 3.65 (t, *J* = 6.3 Hz, 2H), 3.14 (td, *J* = 6.9, 3.3 Hz, 2H), 2.20 (dddd, *J* = 13.3, 6.9, 6.2, 0.8 Hz, 2H). ¹³C NMR (101 MHz, CDCl₃) δ 195.7 (d, *J* = 4.8 Hz), 165.9 (dd, *J* = 257.2, 12.4 Hz), 162.9 (dd, *J* = 257.5, 12.6 Hz), 132.7 (dd, *J* = 10.5, 4.3 Hz), 122.0 (dd, *J* = 13.2, 3.6 Hz), 112.4 (dd, *J* = 21.4, 3.4 Hz), 104.9 (dd, *J* = 27.9, 25.4 Hz), 44.5 (s), 40.3 (d, *J* = 7.8 Hz), 26.7 (d, *J* = 2.2 Hz).

4-Chloro-1-(2,5-difluorophenyl)butan-1-one (13e). General procedure F. Purification by FCC (*n*-hexanes/EtOAc 10:0.1) gave 384 mg of a clear oil (82%). LCMS: *t*_R 2.90 min. ¹H NMR (CDCl₃) δ 7.50 (ddd, *J* = 8.7, 5.5, 3.3 Hz, 1H), 7.18 (ddt, *J* = 9.0, 7.0, 3.6 Hz, 1H), 7.10 (ddd, *J* = 10.1, 9.0, 4.2 Hz, 1H), 3.62 (t, *J* = 6.3 Hz, 2H), 3.13 (td, *J* = 6.9, 3.2 Hz, 2H), 2.17 (pd, *J* = 6.6, 0.8 Hz, 2H). ¹³C NMR (CDCl₃) δ 195.8 (dd, *J* = 4.8, 1.3 Hz), 158.7 (dd, *J* = 244.6, 2.2 Hz), 158.1 (dd, *J* = 250.8, 2.4 Hz), 126.4 (dd, *J* = 15.8, 6.2 Hz), 121.4 (dd, *J* = 24.6, 9.4 Hz), 118.3 (dd, *J* = 27.4, 7.9 Hz), 116.4 (dd, *J* = 25.0, 3.3 Hz), 44.4, 40.3 (d, *J* = 8.2 Hz), 26.6 (d, *J* = 2.3 Hz).

4-Chloro-1-(2,6-difluorophenyl)butan-1-one (13f). General procedure F. Purification by FCC (*n*-hexanes/EtOAc 10:0.1) gave 408 mg of a clear oil (79%). LCMS (*m/z*): 219.1 [M+H]⁺, *t*_R 2.90 min. ¹H NMR (CDCl₃) δ 7.39 (tt, *J* = 8.4, 6.3 Hz, 1H), 6.94 (t, *J* = 8.2 Hz, 2H), 3.63 (t, *J* = 6.3 Hz, 2H), 3.06 (t, *J* = 7.0 Hz, 2H), 2.20 (p, *J* = 6.7 Hz, 2H). ¹³C NMR (CDCl₃) δ 196.6, 159.9 (d, *J* = 253.5 Hz), 159.9 (d, *J* = 253.7 Hz), 132.6 (t, *J* = 10.5 Hz), 112.4 – 112.3 (m), 112.21 – 112.06 (m), 44.2, 41.9 (t, *J* = 2.3 Hz), 26.5.

4-Chloro-1-(3,4-difluorophenyl)butan-1-one (13g). General procedure F. Purification by FCC (*n*-hexanes/EtOAc 10:0.1) gave 1.27 g of a yellow oil (78%). LCMS (*m/z*): 219.5 [M+H]⁺, *t*_R 2.94 min. ¹H NMR (CDCl₃) δ 7.87 – 7.78 (m, 1H), 7.78 (dtd, *J* = 6.5, 2.1, 1.0 Hz, 1H), 7.34 – 7.22 (m, 1H), 3.71 – 3.67 (m, 2H), 3.16 (t, *J* = 6.9 Hz, 2H), 2.30 – 2.20 (m, 2H). ¹³C NMR (CDCl₃) δ 196.5, 153.8 (dd, *J* = 257.1, 13.0 Hz), 150.6 (dd, *J* = 251.0, 13.0 Hz), 133.9 (t, *J* = 3.8 Hz), 125.1 (dd, *J* = 7.5, 3.6 Hz), 117.7 (d, *J* = 17.8 Hz), 117.4 (dd, *J* = 17.9, 1.9 Hz), 44.6, 35.3, 26.7.

4-Chloro-1-(3,5-difluorophenyl)butan-1-one (13h). General procedure F. Purification by FCC (*n*-hexanes/EtOAc 10:0.1) gave 309 mg of a red oil (72%). LCMS: *t*_R 2.96 min. ¹H NMR (CDCl₃) δ 7.53 – 7.42 (m, 2H), 7.02 (tt, *J* = 8.4, 2.4 Hz, 1H), 3.67 (t, *J* = 6.2 Hz, 2H), 3.13 (t, *J* = 6.9 Hz, 2H), 2.22 (tt, *J* = 6.8, 6.0 Hz, 2H). ¹³C NMR (CDCl₃) δ 196.47 (t, *J* = 2.4 Hz), 163.20 (dd, *J* = 251.1, 11.7 Hz), 139.71 (t, *J* = 7.4 Hz), 111.07 (dd, *J* = 18.9, 7.3 Hz), 108.63 (t, *J* = 25.4 Hz), 44.46, 35.61, 26.57.

4-Chloro-1-(2-chlorophenyl)butan-1-one (13i). General procedure F. Purification by FCC (*n*-hexanes/EtOAc 10:0.1) gave 1.12 g of a yellow oil (80%). LCMS (*m/z*): 217.1 [M+H]⁺, *t*_R 2.90 min. ¹H NMR (CDCl₃) δ 7.48 (dd, *J* = 7.5, 1.7 Hz, 1H), 7.44 – 7.36 (m, 2H), 7.32 (td, *J* = 7.2, 1.8 Hz, 1H), 3.65 (t, *J* = 6.3 Hz, 2H), 3.14 (t, *J* = 7.0 Hz, 2H), 2.21 (p, *J* = 6.7 Hz, 2H). ¹³C NMR (CDCl₃) δ 202.2, 139.3, 131.9, 130.9, 130.7, 128.9, 127.1, 44.4, 39.9, 26.9.

4-Chloro-1-(*o*-tolyl)butan-1-one (13j). General procedure F. Purification by FCC (*n*-hexanes/EtOAc 10:0.1) gave 900 mg of a yellow oil (74%). LCMS (*m/z*): 197.3 [M+H]⁺, *t*_R 2.90 min. ¹H NMR (CDCl₃) δ 7.68 (dd, *J* = 7.8, 1.4 Hz, 1H), 7.38 (td, *J* = 7.5, 1.4 Hz, 1H), 7.30 – 7.23 (m, 2H), 3.67 (t, *J* = 6.3 Hz, 2H), 3.10 (t, *J* = 6.9 Hz, 2H), 2.50 (s, 3H), 2.20 (p, *J* = 6.6 Hz, 2H). ¹³C NMR (CDCl₃) δ 203.1, 138.2, 137.8, 132.1, 131.5, 128.6, 125.9, 44.7, 38.3, 27.0, 21.5.

4-(4-Chlorophenyl)-1-(4-(2-fluorophenyl)-4-oxobutyl)-1,2,3,6-tetrahydropyridin-1-ium 2,2,2-trifluoroacetateone (14a). General procedure C. Purification by preparative HPLC (Method C) afforded 49 mg of white solid (45%). LCMS (*m/z*): 376.3 [M+H]⁺, *t*_R 3.34 min. HRMS (*m/z*): C₂₁H₂₃ClFNO₂: requires 376.1401 [M+H]⁺; found 376.1483. ¹H NMR (CDCl₃) δ 11.71 (s, 1H), 7.87 (td, *J* = 7.6, 1.8 Hz, 1H), 7.57 (tdd, *J* = 7.3, 5.0, 1.8 Hz, 1H), 7.41 (d, *J* = 8.5 Hz, 2H), 7.33 (d, *J* = 8.4 Hz, 2H), 7.29 – 7.22 (m, 1H), 7.17 (dd, *J* = 11.4, 8.3 Hz, 1H), 3.88 (s, 1H), 3.55 (d, *J* = 11.6 Hz, 2H), 3.34 (q, *J* = 11.2 Hz, 2H), 3.14 (tt, *J* = 6.6, 3.3 Hz, 4H), 2.53 (td, *J* = 14.1, 4.1 Hz, 2H), 2.26 – 2.14 (m, 2H), 1.94 (d, *J* = 14.4 Hz, 2H).

4-(4-(4-Chlorophenyl)-4-hydroxypiperidin-1-yl)-1-(3-fluorophenyl)butan-1-one (14b). General procedure C. Purification by FCC (eluent 20:0.5:0.1, EtOAc/MeOH/NH₄OH) gave 55 mg of a white solid (39%). LCMS (*m/z*): 376.1 [M+H]⁺, *t*_R 3.21 min. HRMS (*m/z*): C₂₁H₂₃ClFNO₂: requires 376.1474 [M+H]⁺; found 376.1480. ¹H NMR (Methanol-*d*₄) δ 7.89 (dt, *J* = 7.8, 1.2 Hz, 1H), 7.75 (ddd, *J* = 9.7, 2.7, 1.6 Hz, 1H), 7.63 – 7.51 (m, 3H), 7.45 – 7.35 (m, 3H), 3.61 (d, *J* = 11.9 Hz, 2H), 3.49 (td, *J* = 12.7, 2.8 Hz, 2H), 3.34 – 3.24 (m, 4H), 2.43 (td, *J* = 14.5, 4.4 Hz, 2H), 2.31 – 2.18 (m, 2H), 2.01 (dq, *J* = 15.3, 2.9 Hz, 2H). ¹³C NMR (Methanol-*d*₄) δ 198.9 (d, *J* = 2.3 Hz), 164.3 (d, *J* = 246.3 Hz), 147.0, 140.1 (d, *J* = 6.2 Hz), 134.23, 131.8 (d, *J* = 7.7 Hz), 129.5, 127.5, 125.2 (d, *J* = 3.0 Hz), 121.3 (d, *J* = 21.7 Hz), 115.5 (d, *J* = 22.8 Hz), 69.3, 50.3, 49.6, 36.4, 36.3, 19.6.

4-(4-(4-Chlorophenyl)-4-hydroxypiperidin-1-yl)-1-(2,3-difluorophenyl)butan-1-one (14c). A solution of 4-(4-chlorophenyl)-1-(4-(2,3-difluorophenyl)-4,4-dimethoxybutyl)piperidin-4-ol (110 mg, 250 μ mol) in 15 mL of 15:1 acetone:H₂O was treated with pTsOH (61.8 mg, 326 μ mol), and the mixture was heated at reflux for 48 h. The mixture was concentrated under reduced pressure. The residue was dissolved in EtOAc (20 mL) and poured into saturated NaHCO₃ (20 mL). The aqueous phase was extracted with EtOAc (2 \times 20 mL) and the combined extracts were dried (Na₂SO₄), and concentrated under reduced pressure. The residue was purified by FCC (SiO₂, 98:1 EtOAc:MeOH), affording the title compound as a beige solid (75 mg, 76%). LCMS (*m/z*): 394.2 [M+H]⁺, *t*_R 3.37 min. HRMS (*m/z*): C₂₁H₂₂ClF₂NO₂: requires 394.1380 [M+H]⁺; found 394.1390. ¹H NMR (CDCl₃) δ 7.62 (ddt, *J* = 7.9, 6.1, 1.8 Hz, 1H), 7.38 – 7.32 (m, 3H), 7.32 – 7.25 (m, 2H), 7.16 (tdd, *J* = 8.1, 4.5, 1.5 Hz, 1H), 3.01 (td, *J* = 7.0, 2.8 Hz, 2H), 2.82 – 2.76 (m, 2H), 2.51 – 2.38 (m, 4H), 2.05 – 1.79 (m, 5H), 1.66 (dd, *J* = 14.0, 2.7 Hz, 2H). ¹³C NMR (CDCl₃) δ 197.0 (dd, *J* = 6.3, 2.6 Hz), 151.1 (dd, *J* = 250.4, 14.8 Hz), 150.4 (dd, *J* = 256.2, 13.6 Hz), 147.0, 132.8, 128.5, 128.1 (d, *J* = 9.9 Hz), 126.2, 125.2 (dd, *J* = 3.5, 1.3 Hz), 124.3 (dd, *J* = 6.6, 4.5 Hz), 121.2 (d, *J* = 17.4 Hz), 71.2, 57.8, 49.4, 41.4 (d, *J* = 6.8 Hz), 38.5, 21.9.

4-(4-Chlorophenyl)-1-(4-(2,4-difluorophenyl)-4-oxobutyl)-4-hydroxypiperidin-1-ium 2,2,2-trifluoroacetate (14d). General procedure C. Purification by preparative HPLC (Method C) afforded 68 mg of a white solid (66%). LCMS (*m/z*): 394.3 [M+H]⁺, *t*_R 3.35 min. HRMS (*m/z*): C₂₁H₂₂ClF₂NO₂: requires 394.1380 [M+H]⁺; found 394.1387. ¹H NMR (CDCl₃) δ 11.54 (s, 1H), 7.53 (ddd, *J* = 8.6, 5.4, 3.3 Hz, 1H), 7.39 (d, *J* = 8.4 Hz, 2H), 7.31 – 7.20 (m, 3H), 7.15 (td, *J* = 9.5, 4.1 Hz, 1H), 4.83 (s, 1H), 3.47 (d, *J* = 10.2 Hz, 2H), 3.33 (q, *J* = 11.3 Hz, 2H), 3.11 (td, *J* = 6.4, 3.2 Hz, 4H), 2.45 (td, *J* = 14.0, 4.2 Hz, 2H), 2.18 (dq, *J* = 13.7, 6.7 Hz, 2H), 1.93 (d, *J* = 14.4 Hz, 2H). ¹³C NMR (CDCl₃) δ 195.1, 158.7 (dd, *J* = 245.1, 1.9 Hz), 158.3 (dd, *J* = 251.3, 2.2 Hz), 144.8, 133.6, 128.8, 126.1, 125.6 (dd, *J* = 15.4, 6.4 Hz), 122.1 (dd, *J* = 24.5, 9.6 Hz), 118.6 (dd, *J* = 27.2, 7.8 Hz), 116.4 (d, *J* = 27.9 Hz), 68.8, 56.5, 48.9, 39.9 (d, *J* = 9.0 Hz), 35.4, 18.1.

4-(4-Chlorophenyl)-1-(4-(2,5-difluorophenyl)-4-oxobutyl)-4-hydroxypiperidin-1-ium 2,2,2-trifluoroacetate (14e). General procedure C. Purification by preparative HPLC (Method C) afforded 60 mg of a white solid (66%). LCMS (*m/z*): 394.3 [M+H]⁺, *t*_R 3.35 min. HRMS (*m/z*): C₂₁H₂₂ClF₂NO₂: requires 394.1380 [M+H]⁺; found 394.1385. ¹H NMR (CDCl₃) δ 11.15 (s, 1H), 7.53 (ddd, *J* = 8.7, 5.4, 3.3 Hz, 1H), 7.38 (d, *J* = 8.3 Hz, 2H), 7.31 (d, *J* = 8.4 Hz, 2H), 7.23 (dq, *J* = 6.9, 3.1 Hz, 1H), 7.14 (td, *J* = 9.6, 4.1 Hz, 1H), 3.55 (d, *J* = 11.4 Hz, 2H), 3.33 (q, *J* = 11.3 Hz, 2H), 3.21 – 3.05 (m, 4H), 2.53 – 2.42 (m, 2H), 2.19 (t, *J* = 7.9 Hz, 2H), 1.9 (d, *J* = 14.5 Hz, 2H). ¹³C NMR (CDCl₃) δ 195.1, 158.6 (dd, *J* = 245.1, 1.9 Hz), 158.2 (dd, *J* = 251.0, 2.3 Hz), 144.2, 133.8, 128.9,

125.8, 122.0 (dd, $J = 24.5, 9.8$ Hz), 118.5 (dd, $J = 27.5, 8.0$ Hz), 116.4 (d, $J = 3.1$ Hz), 116.2 (d, $J = 2.8$ Hz), 69.0, 56.5, 48.9, 39.8 (d, $J = 8.9$ Hz), 35.3, 18.1.

4-(4-(4-Chlorophenyl)-4-hydroxypiperidin-1-yl)-1-(2,6-difluorophenyl)butan-1-one (14f). A solution of 4-(4-chlorophenyl)-1-(3-(2-(2,6-difluorophenyl)-1,3-dioxolan-2-yl)propyl)piperidin-4-ol (150 mg, 342 μ mol) in 15 mL of 15:1 acetone:H₂O was treated with pTsOH (84.7 mg, 445 μ mol), and the mixture was heated at reflux for 48 h. The mixture was concentrated under reduced pressure. The residue was dissolved in EtOAc (20 mL) and poured into saturated NaHCO₃ (20 mL). The aqueous phase was extracted with EtOAc (2 \times 20 mL) and the combined extracts were dried (Na₂SO₄), and concentrated under reduced pressure. The residue was purified by FCC (eluent, 98:1 EtOAc/MeOH), affording the title compound as a beige solid (110 mg, 82%). LCMS (m/z): 394.2 [M+H]⁺, t_R 3.27 min. HRMS (m/z): C₂₁H₂₂ClF₂NO₂: requires 394.1418 [M+H]⁺; found 394.1465. ¹H NMR (CDCl₃) δ 7.45 – 7.37 (m, 2H), 7.36 (td, $J = 8.4, 7.3, 5.3$ Hz, 1H), 7.32 – 7.25 (m, 2H), 6.94 (t, $J = 8.1$ Hz, 2H), 2.92 (t, $J = 7.1$ Hz, 2H), 2.79 (dt, $J = 11.7, 3.1$ Hz, 2H), 2.50 – 2.37 (m, 4H), 2.07 (td, $J = 13.2, 4.5$ Hz, 2H), 1.94 (p, $J = 7.2$ Hz, 3H), 1.69 (dd, $J = 14.0, 2.7$ Hz, 2H). ¹³C NMR (CDCl₃) δ 197.6, 159.9 (dd, $J = 253.1, 7.5$ Hz), 147.1, 132.8, 132.3 (t, $J = 10.4$ Hz), 128.5, 126.2, 118.5 (t, $J = 19.6$ Hz), 112.4 – 112.2 (m), 112.2 – 111.9 (m), 71.12, 57.6, 49.4, 42.9, 38.5, 21.3.

4-(4-(4-Chlorophenyl)-4-hydroxypiperidin-1-yl)-1-(3,4-difluorophenyl)butan-1-one (14g). General procedure C. Purification by FCC (eluent 20:0.5:0.1, EtOAc/MeOH/NH₄OH) gave 48 mg of a white solid (74%). LCMS (m/z): 364.2 [M+H]⁺, t_R 3.51 min. HRMS (m/z): C₂₁H₂₂ClF₂NO₂: requires 394.1380 [M+H]⁺; found 394.1388. ¹H NMR (CDCl₃) δ 7.82 (ddd, $J = 10.5, 7.7, 2.1$ Hz, 1H), 7.76 (ddd, $J = 8.8, 4.1, 1.8$ Hz, 1H), 7.37 (d, $J = 8.4$ Hz, 2H), 7.28 (d, $J = 8.7$ Hz, 2H), 7.28 – 7.18 (m, 1H), 2.95 (t, $J = 7.0$ Hz, 2H), 2.76 (d, $J = 12.2$ Hz, 2H), 2.49 – 2.34 (m, 4H), 2.03 – 1.90 (m, 4H), 1.80 (s, 1H), 1.66 (dd, $J = 14.2, 2.6$ Hz, 2H). ¹³C NMR (CDCl₃) δ 197.5, 153.6 (dd, $J = 256.7, 13.0$ Hz), 150.5 (dd, $J = 250.7, 12.9$ Hz), 147.0, 134.5 (t, $J = 3.8$ Hz), 132.9, 128.5, 126.2, 125.1 (dd, $J = 7.3, 3.6$ Hz), 117.7 – 117.6 (m), 117.5 – 117.4 (m), 71.1, 57.8, 49.4, 38.4, 36.3, 21.9.

4-(4-Chlorophenyl)-1-(4-(3,5-difluorophenyl)-4-oxobutyl)-4-hydroxypiperidin-1-ium 2,2,2-trifluoroacetate (14h). General procedure C. Purification by FCC (eluent 20:0.5:0.1, EtOAc/MeOH/NH₄OH) gave 42 mg of a white solid (44%). LCMS (m/z): 394.3 [M+H]⁺, t_R 3.44 min. HRMS (m/z): C₂₁H₂₂ClF₂NO₂: requires 394.1307 [M+H]⁺; found 394.1371. ¹H NMR (Methanol-*d*₄) δ 7.64 – 7.53 (m, 2H), 7.49 (d, $J = 8.4$ Hz, 2H), 7.36 (d, $J = 8.4$ Hz, 2H), 7.28 – 7.17 (m, 1H), 3.71 – 3.54 (m, 2H), 3.44 (td, $J = 12.8, 2.8$ Hz, 2H), 2.34 (td, $J = 14.1, 4.3$ Hz, 2H), 2.27 – 2.15 (m, 2H), 2.04 – 1.94 (m, 2H). ¹³C NMR (Methanol-*d*₄) δ 197.6, 164.6 (d, $J = 249.3$ Hz), 164.5 (d, $J = 249.3$ Hz), 147.0, 141.1 (t, $J = 7.5$ Hz), 134.2, 129.5, 127.4, 112.1 (d, $J = 7.2$ Hz), 111.9 (d, $J = 7.4$ Hz), 109.3 (t, $J = 26.0$ Hz), 69.2, 57.5, 36.6, 36.3, 19.4.

1-(2-Chlorophenyl)-4-(4-(4-chlorophenyl)-4-hydroxypiperidin-1-yl)butan-1-one (14i). General procedure C. Purification by FCC (eluent 20:0.5:0.1, EtOAc/MeOH/NH₄OH) gave 89 mg of a white solid (70%). LCMS (*m/z*): 392.2 [M+H]⁺, *t_R* 3.40 min. HRMS (*m/z*): C₂₁H₂₃Cl₂NO₂: requires 392.1106 [M+H]⁺; found 392.1184. ¹H NMR (CDCl₃) δ 7.47 (dd, *J* = 7.5, 1.7 Hz, 1H), 7.42 – 7.34 (m, 4H), 7.33 – 7.25 (m, 3H), 2.97 (t, *J* = 7.1 Hz, 2H), 2.77 (dt, *J* = 11.9, 3.0 Hz, 2H), 2.47 – 2.36 (m, 4H), 2.10 – 1.98 (m, 3H), 1.93 (p, *J* = 7.2 Hz, 2H), 1.68 (dd, *J* = 14.2, 2.6 Hz, 2H). ¹³C NMR (CDCl₃) δ 203.4, 147.1, 139.7, 132.8, 131.7, 130.9, 130.6, 128.9, 128.4, 126.9, 126.2, 71.1, 57.7, 49.4, 40.9, 38.5, 21.7.

4-(4-(4-Chlorophenyl)-4-hydroxypiperidin-1-yl)-1-(*o*-tolyl)butan-1-one (14j). General procedure C. Purification by FCC (eluent 20:0.5:0.1, EtOAc/MeOH/NH₄OH) gave 90 mg as a white solid (70%). LCMS (*m/z*): 372.3 [M+H]⁺, *t_R* 3.47 min. HRMS (*m/z*): C₂₂H₂₆ClNO₂: requires 372.1652 [M+H]⁺; found 372.1626. ¹H NMR (CDCl₃) δ 7.66 (d, *J* = 7.6 Hz, 1H), 7.39 (d, *J* = 8.5 Hz, 2H), 7.35 (d, *J* = 8.0 Hz, 1H), 7.28 (d, *J* = 8.6 Hz, 2H), 7.24 (d, *J* = 7.5 Hz, 2H), 2.92 (t, *J* = 7.1 Hz, 2H), 2.78 (dt, *J* = 12.0, 3.1 Hz, 2H), 2.49 (s, 3H), 2.50 – 2.36 (m, 4H), 2.04 (td, *J* = 13.3, 4.5 Hz, 2H), 1.93 (p, *J* = 7.2 Hz, 3H), 1.68 (dd, *J* = 14.1, 2.6 Hz, 2H). ¹³C NMR (CDCl₃) δ 204.4, 147.1, 138.3, 138.0, 132.8, 132.0, 131.2, 128.6, 128.4, 126.2, 125.7, 71.2, 57.9, 49.5, 39.5, 38.6, 21.9, 21.4.

4-(4-(4-Chlorophenyl)-4-hydroxypiperidin-1-yl)-1-phenylbutan-1-one (14k). General procedure C. Purification by FCC (eluent 20:0.5:0.1, EtOAc/MeOH/NH₄OH) gave 75mg of a white solid (75 mg, 79%). LCMS (*m/z*): 358.1 [M+H]⁺, *t_R* 3.21 min. HRMS (*m/z*): C₂₁H₂₄ClNO₂: requires 358.1558 [M+H]⁺; found 358.1579. ¹H NMR (CDCl₃) δ 7.98 (d, *J* = 8.3 Hz, 2H), 7.60 – 7.51 (m, 1H), 7.51 – 7.42 (m, 2H), 7.36 (d, *J* = 8.4 Hz, 2H), 7.32 – 7.22 (m, 2H), 3.00 (t, *J* = 7.0 Hz, 2H), 2.79 (dt, *J* = 12.0, 3.0 Hz, 2H), 2.51 – 2.37 (m, 4H), 2.07 – 1.92 (m, 5H), 1.65 (dd, *J* = 14.1, 2.6 Hz, 2H). ¹³C NMR (CDCl₃) δ 200.1, 147.1, 137.4, 132.9, 132.8, 128.7, 128.5, 128.2, 126.2, 71.2, 58.0, 49.4, 38.5, 36.4, 22.1.

1-(4-Chlorophenyl)-4-(4-(4-chlorophenyl)-4-hydroxypiperidin-1-yl)butan-1-one (14l). General procedure C. Purification by FCC (eluent 20:0.5:0.1, EtOAc/MeOH/NH₄OH) gave 68 mg of the title compound as a yellow solid (80%). LCMS (*m/z*): 392.4 [M+H]⁺, *t_R* 3.68 min. HRMS (*m/z*): C₂₁H₂₃Cl₂NO₂: requires 392.1106 [M+H]⁺; found 392.1174. ¹H NMR (CDCl₃) δ 7.92 (d, *J* = 8.6 Hz, 2H), 7.43 (d, *J* = 8.6 Hz, 2H), 7.35 (d, *J* = 8.7 Hz, 2H), 7.28 (d, *J* = 8.7 Hz, 2H), 2.96 (t, *J* = 7.0 Hz, 2H), 2.75 (dt, *J* = 12.2, 3.2 Hz, 2H), 2.50 – 2.35 (m, 4H), 2.06 – 1.90 (m, 4H), 1.73 (s, 1H), 1.65 (dd, *J* = 14.1, 2.6 Hz, 2H). ¹³C NMR (CDCl₃) δ 198.8, 147.1, 139.4, 135.7, 132.8, 129.7, 128.9, 128.5, 126.2, 71.2, 57.9, 49.4, 38.5, 36.4, 22.1.

1-(4-Chloro-1,1-dimethoxybutyl)-2,3-difluorobenzene (15c). 4-Chloro-1-(2,3-difluorophenyl)butan-1-one (450 mg, 2.06 mmol), was taken up in MeOH (15 mL) and treated with trimethyl orthoformate (450 mL, 4.12 mmol), *p*-toluenesulphonic acid monohydrate (7.83 mg, 41.2 mmol) and stirred for 3 hr at r.t. This was diluted with sat. aq. NaHCO₃ (20 mL), H₂O (20 mL) and extracted with EtOAc (3 x 15 mL). The organic extracts were combined, washed with brine (20 mL), dried over MgSO₄, filtered and concentrated in vacuo to afford 425 mg of the title compound as a light green oil (77%). LCMS (*m/z*): 265.8 [M+H]⁺, *t_R* 3.08 min. ¹H NMR (CDCl₃) δ 7.35 (ddt, *J* = 8.1, 6.4, 1.7 Hz, 1H), 7.14 (dddd, *J* = 9.9, 8.7, 7.1, 1.8 Hz, 1H), 7.06 (tdd, *J* = 8.1, 5.0, 1.6 Hz, 1H), 3.42 (t, *J* = 6.6 Hz, 2H), 3.19 (s, 6H), 2.22 – 2.13 (m, 2H), 1.54 – 1.42 (m, 2H). ¹³C NMR (CDCl₃) δ 151.1 (dd, *J* = 247.4, 13.6 Hz), 147.9 (dd, *J* = 253.0, 13.5 Hz), 129.8 (d, *J* = 7.3 Hz), 125.1 (dd, *J* = 3.7, 2.2 Hz), 123.5 (dd, *J* = 6.8, 4.8 Hz), 117.3 (d, *J* = 17.2 Hz), 101.8 (d, *J* = 3.2 Hz), 48.8, 44.8, 32.4 (d, *J* = 3.1 Hz), 27.3.

2-(3-Chloropropyl)-2-(2,6-difluorophenyl)-1,3-dioxolane (15f). A solution of 4-chloro-1-(2,6-difluorophenyl)butan-1-one (250 mg, 1.14 mmol), ethylene glycol (320 μL, 5.72 mmol), and *p*-TsOH.H₂O (10.9 mg, 57.2 μmol) in toluene (15 mL) was heated at reflux temperature with use of a Dean-Stark water trap for 16 h. The cooled reaction mixture was washed with NaOH (3 × 20 mL), followed by H₂O (2 × 20 mL) and dried (Na₂SO₄). The organic layer was removed *in vacuo* and the residue purified by FCC (5:95 EtOAc/PE) to afford 249 mg of a clear oil (83%). LCMS (*m/z*): 263.3 [M+H]⁺, *t_R* 2.91 min. ¹H NMR (CDCl₃) δ 7.23 (tt, *J* = 8.2, 5.3 Hz, 1H), 6.85 (t, *J* = 8.7 Hz, 2H), 4.12 – 4.03 (m, 2H), 3.93 – 3.84 (m, 2H), 3.56 (t, *J* = 6.8 Hz, 2H), 2.25 – 2.19 (m, 2H), 1.93 (dt, *J* = 14.1, 6.9 Hz, 2H). ¹³C NMR (CDCl₃) δ 160.6 (dd, *J* = 252.0, 7.6 Hz), 129.9 (t, *J* = 11.1 Hz), 117.7 (t, *J* = 14.7 Hz), 112.7 – 112.6 (m), 112.5 – 112.4 (m), 109.1 (t, *J* = 3.5 Hz), 64.9, 45.1, 36.5 (t, *J* = 1.8 Hz), 26.8.

4-(4-Chlorophenyl)-1-(4-(2,3-difluorophenyl)-4,4-dimethoxybutyl)piperidin-4-ol (16c). General procedure C. Purification by FCC (eluent 20:0.5:0.1, EtOAc/MeOH/NH₄OH) gave 130 mg as a transparent oil (71%). LCMS (*m/z*): 440.1 [M+H]⁺, *t_R* 2.39 min. ¹H NMR (CDCl₃) δ 7.40 (d, *J* = 8.7 Hz, 2H), 7.38 – 7.33 (m, 1H), 7.29 (d, *J* = 8.6 Hz, 2H), 7.12 (dtd, *J* = 9.6, 7.9, 1.8 Hz, 1H), 7.04 (tdd, *J* = 8.1, 5.0, 1.4 Hz, 1H), 3.18 (s, 6H), 2.66 (d, *J* = 11.4 Hz, 2H), 2.38 – 2.19 (m, 4H), 2.11 – 1.97 (m, 4H), 1.76 (s, 1H), 1.65 (dd, *J* = 14.1, 2.6 Hz, 2H), 1.29 – 1.16 (m, 2H). ¹³C NMR (CDCl₃) δ 151.1 (dd, *J* = 246.8, 13.8 Hz), 147.9 (dd, *J* = 252.8, 13.3 Hz), 146.9, 132.9, 130.1 (d, *J* = 7.1 Hz), 128.5, 126.2, 125.2 (t, *J* = 4.9, 2.3 Hz), 123.4 (dd, *J* = 12.0, 5.1 Hz), 117.1 (d, *J* = 17.2 Hz), 102.2 (t, *J* = 3.1 Hz), 71.1, 58.2, 49.4, 48.8, 38.4, 32.7 (d, *J* = 2.9 Hz), 21.4.

4-(4-Chlorophenyl)-1-(3-(2-(2,6-difluorophenyl)-1,3-dioxolan-2-yl)propyl)piperidin-4-ol (16f). General procedure C. Purification by FCC (eluent 20:0.5:0.1, EtOAc/MeOH/NH₄OH) gave 325 mg

as a transparent oil (77%). LCMS (*m/z*): 438.1 [M+H]⁺, *t_R* 2.39 min. ¹H NMR (CDCl₃) δ 7.42 (d, *J* = 8.6 Hz, 2H), 7.29 (d, *J* = 8.6 Hz, 2H), 7.25 – 7.17 (m, 1H), 6.89 – 6.79 (m, 2H), 4.12 – 4.02 (m, 2H), 3.93 – 3.86 (m, 2H), 2.78 (d, *J* = 11.3 Hz, 2H), 2.44 – 2.34 (m, 4H), 2.15 – 2.01 (m, 4H), 1.85 (s, 1H), 1.68 (d, *J* = 11.5 Hz, 4H). ¹³C NMR (CDCl₃) δ 160.7 (d, *J* = 251.7 Hz), 160.7 (d, *J* = 251.9 Hz), 147.1, 132.8, 129.7 (t, *J* = 11.0 Hz), 128.5, 126.2, 117.9 (t, *J* = 14.8 Hz), 112.6 (d, *J* = 7.2 Hz), 112.4 (d, *J* = 7.2 Hz), 109.5 (t, *J* = 3.5 Hz), 71.2, 64.9, 58.5, 49.4, 38.5, 37.2, 20.9.

4-(4-Chlorophenyl)-1-(3-((4-fluorophenyl)thio)propyl)piperidin-4-ol (17a). General procedure C. Purification by FCC (eluent 20:0.5:0.1, EtOAc/MeOH/NH₄OH) gave 67 mg of a white solid (77%). LCMS (*m/z*): 380.1 [M+H]⁺, *t_R* 3.73 min. HRMS (*m/z*): C₂₀H₂₃ClFNOS: requires 380.1276 [M+H]⁺; found 380.1308. ¹H NMR (CDCl₃) δ 7.43 (d, *J* = 8.6 Hz, 2H), 7.39 – 7.31 (m, 2H), 7.34 – 7.24 (m, 2H), 6.99 (t, *J* = 8.6 Hz, 2H), 2.92 (t, *J* = 7.3 Hz, 2H), 2.75 (dt, *J* = 11.8, 3.0 Hz, 2H), 2.50 (t, *J* = 7.3 Hz, 2H), 2.40 (td, *J* = 12.0, 2.4 Hz, 2H), 2.08 (td, *J* = 13.2, 4.5 Hz, 2H), 1.82 (p, *J* = 7.3 Hz, 2H), 1.70 (dd, *J* = 14.2, 2.6 Hz, 3H). ¹³C NMR (CDCl₃) δ 161.8 (d, *J* = 246.1 Hz), 146.9, 132.9, 132.3 (d, *J* = 8.0 Hz), 131.5 (d, *J* = 3.4 Hz), 128.5, 126.2, 116.1 (d, *J* = 21.8 Hz), 71.2, 57.4, 49.6, 38.6, 33.2, 26.8.

4-(4-Chlorophenyl)-1-(3-(4-fluorophenoxy)propyl)piperidin-4-ol (17b). General procedure C. Purification by FCC (eluent 20:0.5:0.1, EtOAc/MeOH/NH₄OH) gave 77 mg of a white solid (80%). LCMS (*m/z*): 364.2 [M+H]⁺, *t_R* 3.51 min. HRMS (*m/z*): C₂₀H₂₃ClFNO₂: requires 380.1474 [M+H]⁺; found 364.1492. ¹H NMR (CDCl₃) δ 7.44 (d, *J* = 8.7 Hz, 2H), 7.31 (d, *J* = 8.6 Hz, 2H), 6.96 (dd, *J* = 9.6, 7.7 Hz, 2H), 6.84 (dd, *J* = 9.1, 4.3 Hz, 2H), 3.98 (t, *J* = 6.3 Hz, 2H), 2.88 – 2.76 (m, 2H), 2.58 (t, *J* = 7.5 Hz, 2H), 2.51 – 2.39 (m, 2H), 2.11 (td, *J* = 13.2, 4.5 Hz, 2H), 2.03 – 1.93 (m, 2H), 1.73 (dd, *J* = 14.2, 2.7 Hz, 3H). ¹³C NMR (CDCl₃) δ 157.3 (d, *J* = 238.0 Hz), 155.2 (d, *J* = 2.1 Hz), 147.0, 132.9, 128.5, 126.3, 115.9 (d, *J* = 23.0 Hz), 115.6 (d, *J* = 7.8 Hz), 71.2, 67.1, 55.4, 49.6, 38.6, 27.1.

4-(4-Chlorophenyl)-1-(4-(4-fluorophenyl)-4-hydroxybutyl)piperidin-4-ol (18). General procedure C. Purification by FCC (20:1:0.1, EtOAc/MeOH/NH₄OH) gave 60 mg of the title compound as a white solid (67%). LCMS (*m/z*): 378.3 [M+H]⁺, *t_R* 3.05 min. HRMS (*m/z*): C₂₁H₂₅ClFNO₂: requires 378.1558 [M+H]⁺; found 378.1643. ¹H NMR (CDCl₃) δ 7.48 – 7.38 (m, 2H), 7.36 – 7.23 (m, 4H), 6.99 (t, *J* = 8.7 Hz, 2H), 4.67 – 4.61 (m, 1H), 3.07 – 2.99 (m, 1H), 2.89 – 2.79 (m, 1H), 2.64 (td, *J* = 12.1, 2.7 Hz, 1H), 2.58 – 2.47 (m, 3H), 2.22 (ddt, *J* = 18.7, 12.9, 4.7 Hz, 2H), 2.00 – 1.88 (m, 1H), 1.81 – 1.65 (m, 6H), 1.25 (s, 1H). ¹³C NMR (CDCl₃) δ 161.9 (d, *J* = 244.1 Hz), 146.4, 141.6 (d, *J* = 3.1 Hz), 133.2, 128.6, 127.4 (d, *J* = 8.0 Hz), 126.3, 115.1 (d, *J* = 21.2 Hz), 73.3, 70.9, 58.9, 50.2, 48.6, 40.2, 37.9, 37.7, 24.1.

Cyclopropyl(4-fluorophenyl)methanone (19). To a stirred solution of NaOH (1.82 g, 45.6 mmol) in H₂O (30 mL) at room temperature was added a solution of 4-chloro-1-(4-fluorophenyl)butan-1-

one (5.00 mL, 30.4 mmol) in THF (10 mL). After addition, the reaction temperature was increased to 60 °C and stirred for a further 5 hours. EtOAc and H₂O were added and the organic phase was washed with additional H₂O, brine, and dried (Na₂SO₄) followed by concentration *in vacuo* to yield the product as a light-yellow oil (5.00 g, quantitative). LCMS: *t*_R 2.73 min. ¹H NMR (CDCl₃) δ 8.08 – 7.99 (m, 2H), 7.19 – 7.09 (m, 2H), 2.62 (tt, *J* = 7.8, 4.6 Hz, 1H), 1.23 (ddt, *J* = 6.8, 4.6, 2.2 Hz, 2H), 1.04 (dq, *J* = 7.3, 3.6 Hz, 2H). ¹³C NMR (CDCl₃) δ 199.1, 165.7 (d, *J* = 254.0 Hz), 134.5 (d, *J* = 3.0 Hz), 130.7 (d, *J* = 9.2 Hz), 115.7 (d, *J* = 21.8 Hz), 17.2, 11.8.

Cyclopropyl(4-fluorophenyl)methanol (20). To a stirred solution of cyclopropyl(4-fluorophenyl)methanone (5.00 g, 30.5 mmol) in MeOH (40 mL) at 0° C was added NaBH₄ (1.50 g, 39.6 mmol) portion-wise. The reaction mixture was allowed to come to room temperature and stirred for a further 4 hours. To the reaction mixture was added to sat. aqueous NH₄Cl solution and EtOAc, the phases were separated, the aqueous phase was extracted twice with EtOAc, the combined organic phases were dried (Na₂SO₄), filtered, and concentrated *in vacuo* to afford 5.01 g of a gold oil (99%). LCMS (*m/z*): *t*_R 2.73 min. ¹H NMR (CDCl₃) δ 8.08 – 7.99 (m, 1H), 7.19 – 7.09 (m, 1H), 2.62 (tt, *J* = 7.8, 4.6 Hz, 1H), 1.23 (ddt, *J* = 6.8, 4.6, 2.2 Hz, 2H), 1.04 (dq, *J* = 7.3, 3.6 Hz, 2H). ¹³C NMR (CDCl₃) δ 199.1, 165.7 (d, *J* = 254.0 Hz), 134.5 (d, *J* = 3.0 Hz), 130.7 (d, *J* = 9.2 Hz), 115.7 (d, *J* = 21.8 Hz), 17.2, 11.8.

(E)-4-(4-Fluorophenyl)but-3-en-1-ol (21). To a mixture of vanadyl acetylacetonate (639 mg, 2.41 mmol), 2,6-di-*tert*-butyl-*p*-cresol (265 mg, 1.20 mmol), and chlorobenzene (40 mL) in a round-bottom flask was added solution of cyclopropyl(4-fluorophenyl)methanol (4.00 g, 24.1 mmol) in chlorobenzene (5.00 mL) and the resulting mixture was stirred at 80 °C. After 48 h, the reaction mixture was cooled to r.t. and filtered through a pad of Florisil. The solvent was evaporated and the residue was purified by FCC (eluent, 4:1 *n*-hexanes/EtOAc) to yield 1.41 g of a transparent oil (35%). LCMS: *t*_R 2.73 min. ¹H NMR (CDCl₃) δ 7.35 – 7.26 (m, 2H), 6.98 (t, *J* = 8.7 Hz, 2H), 6.45 (d, *J* = 15.9 Hz, 1H), 6.11 (dt, *J* = 15.8, 7.1 Hz, 1H), 3.74 (t, *J* = 6.3 Hz, 2H), 2.46 (qd, *J* = 6.4, 1.4 Hz, 2H), 2.04 (s, 1H). ¹³C NMR (CDCl₃) δ 162.2 (d, *J* = 246.2 Hz), 133.5 (d, *J* = 3.2 Hz), 131.6, 127.6 (d, *J* = 8.0 Hz), 126.3 (d, *J* = 2.3 Hz), 115.5 (d, *J* = 21.5 Hz), 62.1, 36.4.

(E)-4-(4-Fluorophenyl)but-3-en-1-yl methanesulfonate (22). General procedure G. Purification by FCC (eluent 4:1, PE/EtOAc) gave 152 mg of a transparent oil (83%). LCMS (*m/z*): *t*_R 2.79 min. ¹H NMR (CDCl₃) δ 7.35 – 7.28 (m, 2H), 6.99 (t, *J* = 8.7 Hz, 2H), 6.48 (dt, *J* = 15.8, 1.5 Hz, 1H), 6.07 (dt, *J* = 15.8, 7.0 Hz, 1H), 4.33 (t, *J* = 6.6 Hz, 2H), 3.01 (s, 3H), 2.65 (qd, *J* = 6.7, 1.4 Hz, 2H). ¹³C NMR (CDCl₃) δ 162.4 (d, *J* = 246.7 Hz), 133.1 (d, *J* = 3.2 Hz), 132.5, 127.8 (d, *J* = 7.9 Hz), 123.7 (d, *J* = 2.3 Hz), 115.6 (d, *J* = 21.6 Hz), 69.1, 37.7, 32.9.

(E)-4-(4-Chlorophenyl)-1-(4-(4-fluorophenyl)but-3-en-1-yl)piperidin-4-ol (23). General procedure C. Purification by FCC (20:1:0.1, EtOAc/MeOH/NH₄OH) gave 80 mg of a white solid (82%). LCMS (*m/z*): 360.3 [M+H]⁺, *t_R* 3.62 min. HRMS (*m/z*): C₂₁H₂₃ClFNO: requires 360.1452 [M+H]⁺; found 360.1541. ¹H NMR (CDCl₃) δ 7.48 – 7.40 (m, 2H), 7.35 – 7.26 (m, 4H), 6.98 (t, *J* = 8.7 Hz, 2H), 6.40 (d, *J* = 15.8 Hz, 1H), 6.12 (dt, *J* = 15.7, 6.9 Hz, 1H), 2.85 (dt, *J* = 11.9, 3.0 Hz, 2H), 2.59 – 2.51 (m, 2H), 2.49 – 2.39 (m, 4H), 2.13 (td, *J* = 13.2, 4.5 Hz, 2H), 1.91 (s, 1H), 1.73 (dd, *J* = 14.2, 2.6 Hz, 2H). ¹³C NMR (CDCl₃) δ 162.1 (d, *J* = 245.8 Hz), 147.1, 133.9 (d, *J* = 3.2 Hz), 132.9, 129.9, 128.5, 128.2 (d, *J* = 2.3 Hz), 127.5 (d, *J* = 7.8 Hz), 126.2, 115.5 (d, *J* = 21.5 Hz), 71.1, 58.5, 49.5, 38.6, 30.9.

(Z)-4-(4-Fluorophenyl)but-3-en-1-ol (26). An oven-dried round-bottom flask containing a stirring bar was charged with Ni(COD)₂ (319 mg, 10 mol%), 1,3-bis(2,6-diisopropylphenyl)imidazolium chloride (492 mg, 10 mol%) and LiCl (491 mg, 11.6 mmol). The flask was fitted with a rubber septum, evacuated and back-filled with argon (this sequence was repeated an additional two times). 2,3-Dihydrofuran (875 μL, 11.6 mmol) was added to the flask along with THF (15 mL). The reaction mixture was then cooled to -30 °C and stirred for 2 minutes. Then, (4-fluorophenyl)magnesium bromide (0.8 M solution in THF; 28.9 mL, 23.1 mmol) was added via syringe. The mixture was stirred at this temperature for 6 hours and then diluted with EtOAc (30 mL) and a solution of aqueous sat. NH₄Cl (20 mL). The separated organic layer was dried over anhydrous Na₂SO₄, filtered and concentrated *in vacuo*. The crude material was purified by FCC (eluent 4:1 *n*-hexanes/EtOAc) to afford 600 mg of a transparent oil (31%). LCMS: *t_R* 2.73 min. ¹H NMR (CDCl₃) δ 7.35 – 7.26 (m, 2H), 6.98 (t, *J* = 8.7 Hz, 2H), 6.45 (d, *J* = 15.9 Hz, 1H), 6.11 (dt, *J* = 15.8, 7.1 Hz, 1H), 3.74 (t, *J* = 6.3 Hz, 2H), 2.46 (qd, *J* = 6.4, 1.4 Hz, 2H). ¹³C NMR (CDCl₃) δ 161.8 (d, *J* = 246.1 Hz), 133.3 (d, *J* = 3.4 Hz), 130.6, 130.4 (d, *J* = 7.8 Hz), 128.3 (d, *J* = 1.5 Hz), 115.2 (d, *J* = 21.1 Hz), 62.5, 31.9.

(Z)-4-(4-Fluorophenyl)but-3-en-1-yl methanesulfonate (27). General procedure G. Compound degraded after attempted FCC purification (eluent 4:1 EtOAc/PE). Therefore, the compound was used for the next reaction without purification.

(Z)-4-(4-Chlorophenyl)-1-(4-(4-fluorophenyl)but-3-en-1-yl)-4-hydroxypiperidin-1-ium 2,2,2-trifluoroacetate (28). General procedure C. Purification by preparative HPLC (Method C) gave 65 mg of a white solid (75%). LCMS (*m/z*): 360.3 [M+H]⁺, *t_R* 3.65 min. HRMS (*m/z*): C₂₁H₂₃ClFNO: requires 360.1452 [M+H]⁺; found 360.1533. ¹H NMR (CDCl₃) δ 11.28 (s, 1H), 7.36 (d, *J* = 8.5 Hz, 2H), 7.29 (d, *J* = 8.5 Hz, 2H), 7.20 (dd, *J* = 8.5, 5.4 Hz, 2H), 7.05 (t, *J* = 8.6 Hz, 2H), 6.59 (d, *J* = 11.5 Hz, 1H), 5.89 (s, 1H), 5.50 (dt, *J* = 11.5, 7.1 Hz, 1H), 3.37 (d, *J* = 11.4 Hz, 2H), 3.23 (q, *J* = 11.2 Hz, 2H), 3.05 (dq, *J* = 9.2, 4.4 Hz, 2H), 2.75 (q, *J* = 7.7 Hz, 2H), 2.41 (td, *J* = 14.0, 4.2 Hz, 2H), 1.87

(d, $J = 14.4$ Hz, 2H). ¹³C NMR (CDCl₃) δ 161.9 (d, $J = 247.4$ Hz), 144.4, 133.6, 132.2, 132.1 (d, $J = 3.6$ Hz), 130.2 (d, $J = 8.0$ Hz), 128.8, 125.9, 124.4, 115.5 (d, $J = 21.5$ Hz), 68.7, 56.5, 48.9, 35.2, 23.1.

***trans*-2-(2-(4-Fluorophenyl)cyclopropyl)ethan-1-ol (29)**. A solution of (*E*)-4-(4-fluorophenyl)but-3-en-1-ol (250 mg, 1.50 mmol) in DCM (30 mL), was treated with Et₂Zn (0.9 M in hexanes; 8.36 mL, 7.52 mmol). After 10 minutes, the reaction mixture was cooled to 0 °C, and treated with a solution of CH₂I₂ (607 μ L, 7.52 mmol) in DCM (10 mL) drop-wise over 10 minutes and allowed to warm to ambient temperature. After 24 h, the reaction mixture was quenched slowly with sat. aqueous NH₄Cl and stirred for 10 minutes. The reaction mixture was extracted with DCM (3 x 20 mL), and the combined organic phases were washed with sat. aqueous NaHCO₃, dried (Na₂SO₄), filtered, and concentrated *in vacuo* to yield the desired cyclopropane as a transparent oil (265 mg, 98%). LCMS: t_R 2.67 min. ¹H NMR (CDCl₃) δ 7.00 (dd, $J = 8.6, 5.5$ Hz, 2H), 6.93 (dd, $J = 9.8, 7.6$ Hz, 2H), 3.76 (t, $J = 6.5$ Hz, 2H), 1.72 – 1.57 (m, 4H), 1.09 – 1.00 (m, 1H), 0.87 (dt, $J = 8.5, 5.0$ Hz, 1H), 0.80 (dt, $J = 8.7, 5.2$ Hz, 1H). ¹³C NMR (CDCl₃) δ 161.1 (d, $J = 243.0$ Hz), 139.0 (d, $J = 3.0$ Hz), 127.2 (d, $J = 7.9$ Hz), 115.1 (d, $J = 21.3$ Hz), 62.9, 37.3, 22.2, 20.1, 15.5.

***cis*-2-(2-(4-Fluorophenyl)cyclopropyl)ethan-1-ol (30)**. A solution of (*Z*)-4-(4-fluorophenyl)but-3-en-1-ol (250 mg, 1.50 mmol) in DCM (30 mL), was treated with Et₂Zn (0.9 M in hexanes; 8.36 mL, 7.52 mmol). After 10 minutes, the reaction mixture was cooled to 0 °C, and treated with a solution of CH₂I₂ (607 μ L, 7.52 mmol) in DCM (10 mL) drop-wise over 10 minutes and allowed to warm to ambient temperature. After 24 h, the reaction mixture was quenched slowly with sat. aqueous NH₄Cl and stirred for 10 minutes. The reaction mixture was extracted with DCM (3 x 20 mL), and the combined organic phases were washed with sat. aqueous NaHCO₃, dried (Na₂SO₄), and concentrated *in vacuo* to yield the desired cyclopropane as a yellow oil (271 mg, quantitative). LCMS (m/z): 181.3 [M+H]⁺, t_R 2.65 min. ¹H NMR (CDCl₃) δ 7.16 – 7.11 (m, 2H), 6.95 (t, $J = 8.7$ Hz, 2H), 3.56 (td, $J = 6.3, 2.5$ Hz, 2H), 2.11 (td, $J = 8.3, 5.8$ Hz, 1H), 1.58 (s, 1H), 1.43 – 1.31 (m, 1H), 1.19 – 1.05 (m, 2H), 1.01 (td, $J = 8.2, 4.9$ Hz, 1H), 0.65 (q, $J = 5.3$ Hz, 1H). ¹³C NMR (CDCl₃) δ 161.4 (d, $J = 243.7$ Hz), 134.8 (d, $J = 3.2$ Hz), 130.5 (d, $J = 7.8$ Hz), 114.8 (d, $J = 21.1$ Hz), 62.8, 31.9, 19.8, 15.4, 9.6.

***trans*-2-(2-(4-Fluorophenyl)cyclopropyl)ethyl methanesulfonate (29a)**. General procedure G. No purification required post work-up, giving 366 mg of a transparent oil (95%). LCMS (m/z): 259.4 [M+H]⁺, t_R 2.83 min. ¹H NMR (CDCl₃) δ 7.04 – 6.98 (m, 2H), 6.93 (dd, $J = 9.9, 7.6$ Hz, 2H), 4.32 (td, $J = 6.5, 1.5$ Hz, 2H), 2.96 (s, 3H), 1.83 (qd, $J = 6.7, 3.3$ Hz, 2H), 1.71 (dt, $J = 9.2, 4.9$ Hz, 1H), 1.10 – 1.00 (m, 1H), 0.92 (dt, $J = 8.5, 5.1$ Hz, 1H), 0.83 (dt, $J = 8.7, 5.3$ Hz, 1H). ¹³C NMR (CDCl₃) δ 161.2 (d, $J = 243.4$ Hz), 138.3 (d, $J = 3.1$ Hz), 127.3 (d, $J = 7.7$ Hz), 115.2 (d, $J = 21.3$ Hz), 69.8, 37.4, 33.8, 22.3, 19.4, 15.2.

cis-2-(2-(4-Fluorophenyl)cyclopropyl)ethyl methanesulfonate (30a). General procedure G. Purification by FCC (eluent 4:1, PE/EtOAc) gave 274 mg of a transparent oil (83%). LCMS: t_R 2.83 min. ¹H NMR (CDCl₃) δ 7.19 – 7.10 (m, 2H), 6.96 (t, J = 8.7 Hz, 2H), 4.20 – 4.04 (m, 2H), 2.92 (s, 3H), 2.18 (td, J = 8.6, 6.0 Hz, 1H), 1.56 (dq, J = 13.2, 6.6 Hz, 1H), 1.31 (dt, J = 14.4, 7.2 Hz, 1H), 1.22 – 1.15 (m, 1H), 1.05 (td, J = 8.4, 5.3 Hz, 1H), 0.69 (q, J = 5.6 Hz, 1H). ¹³C NMR (CDCl₃) δ 161.5 (d, J = 244.2 Hz), 134.1 (d, J = 3.1 Hz), 130.5 (d, J = 7.9 Hz), 115.1 (d, J = 21.2 Hz), 69.8, 37.3, 28.6, 19.9, 14.7, 9.5.

trans-4-(4-Chlorophenyl)-1-(2-(2-(4-fluorophenyl)cyclopropyl)ethyl)piperidin-4-ol (29b). General procedure C. Purification by FCC (20:1:0.1, EtOAc/MeOH/NH₄OH) gave 72 mg of a white solid (80%). LCMS (m/z): 374.3 [M+H]⁺, t_R 3.73 min. HRMS (m/z): C₂₂H₂₅ClFNO: requires 374.1609 [M+H]⁺; found 374.1690. ¹H NMR (CDCl₃) δ 7.46 – 7.39 (m, 2H), 7.33 – 7.26 (m, 2H), 7.00 (dd, J = 8.6, 5.5 Hz, 2H), 6.97 – 6.88 (m, 2H), 2.81 (dt, J = 11.5, 3.3 Hz, 2H), 2.54 (dd, J = 8.9, 6.9 Hz, 2H), 2.43 (ddd, J = 11.8, 9.7, 2.0 Hz, 2H), 2.10 (td, J = 13.3, 4.4 Hz, 3H), 1.71 (dd, J = 14.2, 2.7 Hz, 2H), 1.66 – 1.55 (m, 3H), 1.01 – 0.91 (m, 1H), 0.85 (dt, J = 8.4, 5.0 Hz, 1H), 0.77 (dt, J = 8.6, 5.2 Hz, 1H). ¹³C NMR (CDCl₃) δ 161.1 (d, J = 243.0 Hz), 147.1, 139.2 (d, J = 3.1 Hz), 132.8, 128.5, 127.2 (d, J = 7.7 Hz), 126.2, 115.1 (d, J = 21.3 Hz), 71.1, 58.5, 49.7, 49.6, 38.5 (d, J = 1.5 Hz), 32.1, 22.6, 21.6, 15.8.

cis-4-(4-Chlorophenyl)-1-(2-(2-(4-fluorophenyl)cyclopropyl)ethyl)piperidin-4-ol (30b). General procedure C. Purification by FCC (20:1:0.1, EtOAc/MeOH/NH₄OH) gave 49 mg of a white solid (66%). LCMS (m/z): 374.3 [M+H]⁺, t_R 3.73 min. HRMS (m/z): C₂₂H₂₅ClFNO: requires 374.1609 [M+H]⁺; found 374.1687. ¹H NMR (CDCl₃) δ 7.44 – 7.37 (m, 2H), 7.33 – 7.26 (m, 2H), 7.21 – 7.12 (m, 2H), 6.97 (t, J = 8.7 Hz, 2H), 2.70 – 2.59 (m, 2H), 2.51 – 2.40 (m, 1H), 2.42 – 2.29 (m, 2H), 2.25 (td, J = 13.3, 11.7, 3.8 Hz, 1H), 2.16 – 1.98 (m, 3H), 1.86 (s, 1H), 1.65 (dq, J = 14.2, 2.8 Hz, 2H), 1.34 (td, J = 11.9, 11.2, 5.4 Hz, 1H), 1.20 – 0.97 (m, 3H), 0.64 (q, J = 5.3 Hz, 1H). ¹³C NMR (CDCl₃) δ 161.2 (d, J = 243.5 Hz), 146.9, 134.8 (d, J = 3.0 Hz), 132.7, 130.4 (d, J = 7.7 Hz), 128.4, 126.1, 114.7 (d, J = 21.2 Hz), 70.9, 58.3, 49.6, 48.9, 38.2, 26.0, 20.1, 16.9, 9.7.

3-Chloro-1-(4-fluorophenyl)propan-1-one (33a). To a stirred suspension of AlCl₃ (3.40 g, 25.5 mmol) in DCM (100 mL) at 0 °C was added fluorobenzene (2.00 mL, 21.2 mmol) drop-wise. After 30 minutes, 3-chloropropionyl chloride (2.81 mL, 25.5 mmol) was added drop-wise. The reaction was brought to room temperature and stirred for a further 6 hours, poured out on ice and extracted with DCM (2 x 30 mL). The organic fractions were collected and washed with sat. aqueous NaHCO₃ and H₂O, dried (Na₂SO₄), filtered, and the solvent removed *in vacuo*. The residue was purified by FCC (eluent, 99:1 PE/EtOAc) to afford 3.68 g of beige crystals (93%). LCMS (m/z): 187.3 [M+H]⁺, t_R 2.75 min. ¹H NMR (CDCl₃) δ 8.07 – 7.90 (m, 2H), 7.19 – 7.09 (m, 2H), 3.91 (t, J = 6.8 Hz, 2H),

3.43 (t, $J = 6.8$ Hz, 2H). ¹³C NMR (CDCl₃) δ 195.2, 166.1 (d, $J = 255.6$ Hz), 132.9 (d, $J = 3.1$ Hz), 130.9 (d, $J = 9.4$ Hz), 116.0 (d, $J = 21.9$ Hz), 41.3, 38.7.

5-Chloro-1-(4-fluorophenyl)pentan-1-one (33c). To a stirred suspension of AlCl₃ (2.12 g, 15.9 mmol) in DCM (75 mL) at 0 °C was added fluorobenzene (1.25 mL, 13.3 mmol) drop-wise. After 30 minutes, 5-chloropentanoyl chloride (2.06 mL, 15.9 mmol) was added drop-wise. The reaction was brought to room temperature and stirred overnight, poured out on ice and extracted with DCM (2 x 30 mL). The organic fractions were collected and washed with sat. aqueous NaHCO₃ and H₂O, dried (Na₂SO₄), filtered, and the solvent removed *in vacuo*. The residue was purified by FCC (eluent, 1:99 PE/EtOAc) to afford 2.55 g of a light brown oil (90%). LCMS (m/z): 215.3 [M+H]⁺, t_R 2.91 min. ¹H NMR (CDCl₃) δ 8.01 – 7.92 (m, 2H), 7.12 (t, $J = 8.6$ Hz, 2H), 3.57 (t, $J = 6.0$ Hz, 2H), 2.98 (t, $J = 6.5$ Hz, 2H), 1.91 – 1.79 (m, 4H). ¹³C NMR (CDCl₃) δ 198.0, 165.8 (d, $J = 254.7$ Hz), 133.4 (d, $J = 3.1$ Hz), 130.7 (d, $J = 9.4$ Hz), 115.8 (d, $J = 21.9$ Hz), 44.8, 37.6, 32.1, 21.6.

3-(4-(4-Chlorophenyl)-4-hydroxypiperidin-1-yl)-1-(4-fluorophenyl)propan-1-one (34a).

General procedure C. Purification by FCC (20:1:0.1, EtOAc/MeOH/NH₄OH) gave 110 mg of a white solid (77%). LCMS (m/z): 362.4 [M+H]⁺, t_R 3.42 min. HRMS (m/z): C₂₀H₂₁ClFNO₂: requires 362.1245 [M+H]⁺; found 362.1357. ¹H NMR (CDCl₃) δ 8.01 – 7.95 (m, 2H), 7.46 – 7.39 (m, 2H), 7.34 – 7.26 (m, 2H), 7.13 (t, $J = 8.6$ Hz, 2H), 3.18 (dd, $J = 7.9, 6.7$ Hz, 2H), 2.89 (dd, $J = 8.0, 6.7$ Hz, 2H), 2.82 (dt, $J = 11.6, 3.2$ Hz, 2H), 2.54 (td, $J = 12.0, 2.5$ Hz, 2H), 2.09 (td, $J = 13.2, 4.5$ Hz, 2H), 1.89 – 1.83 (s, 1H), 1.73 (dt, $J = 14.0, 2.8$ Hz, 2H). ¹³C NMR (CDCl₃) δ 197.7, 165.9 (d, $J = 254.8$ Hz), 146.9, 133.5 (d, $J = 3.0$ Hz), 132.9, 130.8 (d, $J = 9.2$ Hz), 128.6, 126.2, 115.9 (d, $J = 21.9$ Hz), 70.9, 53.3, 49.6, 38.5, 36.4.

5-(4-(4-Chlorophenyl)-4-hydroxypiperidin-1-yl)-1-(4-fluorophenyl)pentan-1-one (34c).

General procedure C. Purification by FCC (20:1:0.1, EtOAc/MeOH/NH₄OH) gave 115 mg of a white solid (75%). LCMS (m/z): 390.3 [M+H]⁺, t_R 3.42 min. HRMS (m/z): C₂₂H₂₅ClFNO₂: requires 390.1558 [M+H]⁺; found 390.1640. ¹H NMR (CDCl₃) δ 8.02 – 7.92 (m, 2H), 7.45 – 7.37 (m, 2H), 7.31 – 7.24 (m, 2H), 7.11 (t, $J = 8.6$ Hz, 2H), 2.96 (t, $J = 7.2$ Hz, 2H), 2.79 (dt, $J = 11.9, 3.0$ Hz, 2H), 2.50 – 2.35 (m, 4H), 2.26 (s, 1H), 2.08 (td, $J = 13.1, 4.4$ Hz, 2H), 1.80 – 1.65 (m, 4H), 1.66 – 1.53 (m, 2H). ¹³C NMR (CDCl₃) δ 198.6, 165.8 (d, $J = 254.6$ Hz), 147.1, 133.5 (d, $J = 3.0$ Hz), 132.8, 130.8 (d, $J = 9.3$ Hz), 128.5, 126.2, 115.8 (d, $J = 21.8$ Hz), 71.1, 58.5, 49.5, 38.5, 38.4, 26.6, 22.4.

1-(3-Chloropropyl)-4-fluorobenzene (35a).

3-Chloro-1-(4-fluorophenyl)propan-1-one (600 mg, 3.22 mmol) was taken up in trifluoroacetic acid (5 mL) and the solution cooled to 0 °C. To this solution was added dropwise triethylsilane (1.44 mL, 9.00 mmol) and the reaction stirred at 0 °C for 5 h. The solvents were removed *in vacuo* and the crude product was purified by FCC (eluent, *n*-hexanes) to afford 437 mg of a transparent oil (79%). LCMS: t_R 3.00 min. ¹H NMR (CDCl₃) δ 7.20

– 7.12 (m, 2H), 7.03 – 6.94 (m, 2H), 3.52 (t, $J = 6.4$ Hz, 2H), 2.77 (t, $J = 7.4$ Hz, 2H), 2.13 – 2.01 (m, 2H). ¹³C NMR (CDCl₃) δ 161.6 (d, $J = 243.8$ Hz), 136.4 (d, $J = 3.1$ Hz), 130.0 (d, $J = 7.9$ Hz), 115.4 (d, $J = 21.1$ Hz), 44.2, 34.2, 32.0.

1-(4-Chlorobutyl)-4-fluorobenzene (35b). 4-Chloro-1-(4-fluorophenyl)butan-1-one (1.25 mL, 7.66 mmol) was taken up in trifluoroacetic acid (10 mL) and the solution cooled to 0 °C. To this solution was added dropwise triethylsilane (3.42 mL, 21.5 mmol) and the reaction stirred at 0 °C for 2 h. The solvents were removed *in vacuo* and the crude product was purified by FCC (eluent, *n*-hexanes) to afford 1.27 g of a transparent oil (89%). LCMS (m/z): 187.2 [M+H]⁺, t_R 3.10 min. ¹H NMR (CDCl₃) δ 7.19 – 7.09 (m, 1H), 7.03 – 6.92 (m, 1H), 3.55 (t, $J = 6.3$ Hz, 1H), 2.63 (t, $J = 7.1$ Hz, 1H), 1.87 – 1.70 (m, 2H). ¹³C NMR (CDCl₃) δ 161.4 (d, $J = 243.4$ Hz), 137.6 (d, $J = 3.1$ Hz), 129.8 (d, $J = 7.8$ Hz), 115.2 (d, $J = 21.2$ Hz), 44.9, 34.4, 32.1, 28.8.

1-(5-Chloropentyl)-4-fluorobenzene (35c). 5-Chloro-1-(4-fluorophenyl)pentan-1-one (600 mg, 2.80 mmol) was taken up in trifluoroacetic acid (5 mL) and the solution cooled to 0 °C. To this solution was added dropwise triethylsilane (1.25 mL, 7.83 mmol) and the reaction stirred at 0 °C for 5 h. The solvents were removed *in vacuo* and the crude product was purified by FCC (eluent, *n*-hexanes) to afford 472 mg of a transparent oil (84%). LCMS: t_R 3.15 min. ¹H NMR (CDCl₃) δ 7.13 (dd, $J = 8.4, 5.6$ Hz, 2H), 6.97 (t, $J = 8.7$ Hz, 2H), 3.53 (t, $J = 6.7$ Hz, 2H), 2.60 (t, $J = 7.7$ Hz, 2H), 1.81 (dd, $J = 8.0, 6.7$ Hz, 2H), 1.67 – 1.58 (m, 2H), 1.54 – 1.43 (m, 2H). ¹³C NMR (CDCl₃) δ 161.3 (d, $J = 243.0$ Hz), 138.0 (d, $J = 3.2$ Hz), 129.8 (d, $J = 7.9$ Hz), 115.1 (d, $J = 21.0$ Hz), 45.1, 35.1, 32.6, 30.9, 26.6.

4-(4-Chlorophenyl)-1-(3-(4-fluorophenyl)propyl)piperidin-4-ol (36a). General procedure C. Purification by FCC (20:0.5:0.1, EtOAc/MeOH/NH₄OH) gave 105 mg of a white solid (72 mg, 70%). LCMS (m/z): 348.3 [M+H]⁺, t_R 3.52 min. HRMS (m/z): C₂₀H₂₃ClFNO: requires 348.1452 [M+H]⁺; found 348.1532. ¹H NMR (CDCl₃) δ 7.47 – 7.40 (m, 2H), 7.35 – 7.27 (m, 2H), 7.18 – 7.10 (m, 2H), 7.01 – 6.91 (m, 2H), 2.82 (dd, $J = 9.1, 3.2$ Hz, 2H), 2.62 (t, $J = 7.7$ Hz, 2H), 2.49 – 2.37 (m, 4H), 2.13 (td, $J = 13.2, 4.5$ Hz, 3H), 1.84 (dq, $J = 9.6, 7.7$ Hz, 2H), 1.77 – 1.67 (m, 2H). ¹³C NMR (CDCl₃) δ 161.2 (d, $J = 243.1$ Hz), 146.8, 137.6 (d, $J = 3.2$ Hz), 132.8, 129.7 (d, $J = 7.8$ Hz), 128.4, 126.1, 115.1 (d, $J = 21.1$ Hz), 71.0, 57.9, 49.4, 38.4, 32.9, 28.7.

4-(4-Chlorophenyl)-1-(4-(4-fluorophenyl)butyl)piperidin-4-ol (36b). General procedure C. Purification by FCC (20:0.5:0.1, EtOAc/MeOH/NH₄OH) gave 150 of a white solid (77%). LCMS (m/z): 362.2 [M+H]⁺, t_R 3.72 min. HRMS (m/z): C₂₁H₂₅ClFNO: requires 362.1712 [M+H]⁺; found 362.1743. ¹H NMR (CDCl₃) δ 7.43 (d, $J = 8.6$ Hz, 2H), 7.30 (d, $J = 8.6$ Hz, 2H), 7.12 (dd, $J = 8.4, 5.6$ Hz, 2H), 6.95 (t, $J = 8.7$ Hz, 2H), 2.80 (dd, $J = 9.1, 3.1$ Hz, 2H), 2.61 (t, $J = 7.3$ Hz, 2H), 2.47 – 2.35 (m, 4H), 2.12 (td, $J = 13.2, 4.4$ Hz, 2H), 1.81 (s, 1H), 1.71 (dd, $J = 14.1, 2.7$ Hz, 2H), 1.58 (dtd,

$J = 23.0, 8.4, 3.3$ Hz, 4H). ¹³C NMR (CDCl₃) δ 161.3 (d, $J = 243.1$ Hz), 147.0, 138.1 (d, $J = 3.3$ Hz), 132.9, 129.8 (d, $J = 7.7$ Hz), 128.5, 126.2, 115.1 (d, $J = 21.0$ Hz), 71.2, 58.8, 49.6, 38.5, 35.1, 29.7, 26.6.

4-(4-Chlorophenyl)-1-(5-(4-fluorophenyl)pentyl)piperidin-4-ol (36c). General procedure C. Purification by FCC (20:0.5:0.1, EtOAc/MeOH/NH₄OH) gave 116 mg of a white solid (80%). LCMS (m/z): 376.3 [M+H]⁺, t_R 3.88 min. HRMS (m/z): C₂₂H₂₇ClFNO: requires 376.1765 [M+H]⁺; found 376.1846. ¹H NMR (CDCl₃) δ 7.43 (d, $J = 8.6$ Hz, 2H), 7.30 (d, $J = 8.6$ Hz, 2H), 7.12 (dd, $J = 8.4, 5.6$ Hz, 2H), 6.95 (t, $J = 8.7$ Hz, 2H), 2.82 (dt, $J = 11.6, 3.2$ Hz, 2H), 2.58 (t, $J = 7.7$ Hz, 2H), 2.45 – 2.35 (m, 4H), 2.13 (td, $J = 13.3, 4.5$ Hz, 3H), 1.76 – 1.67 (m, 2H), 1.67 – 1.57 (m, 2H), 1.55 (ddt, $J = 10.9, 7.8, 3.7$ Hz, 2H), 1.40 – 1.29 (m, 2H). ¹³C NMR (CDCl₃) δ 161.3 (d, $J = 243.0$ Hz), 147.0, 138.3 (d, $J = 3.1$ Hz), 132.9, 129.8 (d, $J = 7.7$ Hz), 128.5, 126.2, 115.1 (d, $J = 21.0$ Hz), 71.2, 58.9, 49.6, 38.5, 35.2, 31.6, 27.3, 26.9.

3-(4-Fluorophenyl)prop-2-yn-1-ol (39a). General procedure E. Purification by FCC (eluent, 1:5 EtOAc/*n*-hexanes) gave 2.45 g of a brown oil (94%). LCMS (m/z): 151.1 [M+H]⁺, t_R 2.47 min. ¹H NMR (CDCl₃) δ 7.44 – 7.37 (m, 2H), 7.03 – 6.93 (m, 2H), 4.48 (s, 2H), 2.29 (s, 1H). ¹³C NMR (CDCl₃) δ 162.7 (d, $J = 249.6$ Hz), 133.7 (d, $J = 8.4$ Hz), 118.7 (d, $J = 3.5$ Hz), 115.7 (d, $J = 22.1$ Hz), 87.1 (d, $J = 1.5$ Hz), 84.7, 51.6.

4-(4-Fluorophenyl)but-3-yn-1-ol (39b). General procedure E. Purification by FCC (eluent, 1:5 EtOAc/*n*-hexanes) gave 3.41 g of a brown oil that solidified upon standing (96%). LCMS (m/z): 165.3 [M+H]⁺, t_R 2.56 min. ¹H NMR (CDCl₃) δ 7.43 – 7.36 (m, 2H), 6.99 (t, $J = 8.7$ Hz, 2H), 3.82 (t, $J = 6.3$ Hz, 2H), 2.68 (t, $J = 6.3$ Hz, 2H), 2.14 (s, 1H). ¹³C NMR (CDCl₃) δ 162.4 (d, $J = 248.8$ Hz), 133.6 (d, $J = 8.3$ Hz), 119.5 (d, $J = 3.5$ Hz), 115.56 (d, $J = 22.0$ Hz), 86.2 (d, $J = 1.4$ Hz), 81.4, 61.2, 23.8.

5-(4-Fluorophenyl)pent-4-yn-1-ol (39c). General procedure E. Purification by FCC (eluent, 1:5 EtOAc/*n*-hexanes) gave 2.05 g of a brown oil (94%). LCMS (m/z): 179.3 [M+H]⁺, t_R 2.65 min. ¹H NMR (CDCl₃) δ 7.40 – 7.31 (m, 2H), 7.01 – 6.92 (m, 2H), 3.81 (t, $J = 6.1$ Hz, 2H), 2.52 (t, $J = 7.0$ Hz, 1H), 1.85 (p, $J = 6.6$ Hz, 2H), 1.72 (s, 1H). ¹³C NMR (CDCl₃) δ 162.2 (d, $J = 248.3$ Hz), 133.5 (d, $J = 8.3$ Hz), 119.91 (d, $J = 3.5$ Hz), 115.55 (d, $J = 22.1$ Hz), 89.1 (d, $J = 1.5$ Hz), 80.2, 61.9, 31.5, 16.1.

3-(4-Fluorophenyl)prop-2-yn-1-yl methanesulfonate (40a). General procedure G. Compound degraded after attempted FCC purification (eluent 4:1, PE/EtOAc). Therefore, the compound was used for the next reaction without purification.

1-(4-Chlorobut-1-yn-1-yl)-4-fluorobenzene (40b). General procedure D. Purification by FCC (eluent, *n*-hexanes) gave 2.56 g of a yellow oil (75%). LCMS (m/z): 183.0 [M+H]⁺, t_R 3.00 min. ¹H

NMR (CDCl₃) δ 7.44 – 7.34 (m, 1H), 7.04 – 6.93 (m, 1H), 3.67 (t, *J* = 7.2 Hz, 1H), 2.87 (t, *J* = 7.2 Hz, 1H). ¹³C NMR (CDCl₃) δ 162.5 (d, *J* = 249.1 Hz), 133.7 (d, *J* = 8.4 Hz), 119.3 (d, *J* = 3.5 Hz), 115.6 (d, *J* = 22.0 Hz), 85.5 (d, *J* = 1.5 Hz), 81.6, 42.3, 23.9.

5-(4-Fluorophenyl)pent-4-yn-1-yl methanesulfonate (40c). General procedure G. Purification by FCC (eluent 4:1, PE/EtOAc) gave 333 mg of a transparent oil (93%). LCMS (*m/z*): 257.2 [M+H]⁺, *t_R* 2.83 min. ¹H NMR (CDCl₃) δ 7.40 – 7.33 (m, 2H), 6.97 (t, *J* = 8.7 Hz, 2H), 4.40 (t, *J* = 6.1 Hz, 2H), 3.03 (s, 3H), 2.56 (t, *J* = 6.8 Hz, 2H), 2.03 (p, *J* = 6.5 Hz, 2H). ¹³C NMR (CDCl₃) δ 162.3 (d, *J* = 248.7 Hz), 133.5 (d, *J* = 8.4 Hz), 119.5 (d, *J* = 3.6 Hz), 115.6 (d, *J* = 22.1 Hz), 87.32, 80.9, 37.4, 28.2, 15.8.

4-(4-Chlorophenyl)-1-(3-(4-fluorophenyl)prop-2-yn-1-yl)piperidin-4-ol (41a). General procedure C. Purification by FCC (20:0.5:0.1, EtOAc/MeOH/NH₄OH) gave 84 mg of a yellow solid (74%). LCMS (*m/z*): 344.2 [M+H]⁺, *t_R* 3.46 min. HRMS (*m/z*): C₂₀H₁₉ClFNO: requires 344.1139 [M+H]⁺; found 344.1214. ¹H NMR (CDCl₃) δ 7.47 – 7.37 (m, 4H), 7.31 (d, *J* = 8.3 Hz, 2H), 6.98 (t, *J* = 8.5 Hz, 2H), 3.52 (s, 1H), 2.90 (dt, *J* = 11.6, 3.0 Hz, 2H), 2.71 (td, *J* = 12.0, 2.5 Hz, 2H), 2.18 (td, *J* = 13.2, 4.6 Hz, 2H), 1.84 (s, 1H), 1.77 (dd, *J* = 14.2, 2.6 Hz, 2H). ¹³C NMR (CDCl₃) δ 162.5 (d, *J* = 249.1 Hz), 146.9, 133.7 (d, *J* = 8.3 Hz), 132.9, 128.6, 126.2, 119.2 (d, *J* = 3.5 Hz), 115.6 (d, *J* = 22.1 Hz), 84.4 (d, *J* = 6.1 Hz), 70.8, 48.7, 48.0, 38.5.

4-(4-Chlorophenyl)-1-(4-(4-fluorophenyl)but-3-yn-1-yl)piperidin-4-ol (41b). General procedure C. Purification by FCC (20:0.5:0.1, EtOAc/MeOH/NH₄OH) gave 45 mg of a light brown solid (45 mg, 80%). LCMS (*m/z*): 358.2 [M+H]⁺, *t_R* 3.60 min. HRMS (*m/z*): C₂₁H₂₁ClFNO: requires 358.1400 [M+H]⁺; found 358.1440. ¹H NMR (CDCl₃) δ 7.44 (d, *J* = 8.3 Hz, 2H), 7.37 (dd, *J* = 8.4, 5.5 Hz, 2H), 7.31 (d, *J* = 8.3 Hz, 2H), 6.97 (t, *J* = 8.5 Hz, 2H), 2.89 – 2.80 (m, 2H), 2.75 (t, *J* = 7.6 Hz, 2H), 2.66 – 2.57 (m, 2H), 2.55 (d, *J* = 11.9 Hz, 2H), 2.12 (td, *J* = 13.2, 4.5 Hz, 2H), 1.81 (s, 1H), 1.79 – 1.68 (m, 2H). ¹³C NMR (CDCl₃) δ 162.3 (d, *J* = 248.5 Hz), 146.9, 133.5 (d, *J* = 8.3 Hz), 132.9, 128.6, 126.2, 119.9, 115.5 (d, *J* = 21.9 Hz), 88.1, 80.5, 71.1, 57.5, 49.2, 38.6, 17.9.

4-(4-Chlorophenyl)-1-(5-(4-fluorophenyl)pent-4-yn-1-yl)piperidin-4-ol (41c). General procedure C. Purification by FCC (20:0.5:0.1, EtOAc/MeOH/NH₄OH) gave 74 mg of a gold oil (68%). LCMS (*m/z*): 372.3 [M+H]⁺, *t_R* 3.78 min. HRMS (*m/z*): C₂₂H₂₃ClFNO: requires 372.1452 [M+H]⁺; found 372.1532. ¹H NMR (CDCl₃) δ 7.45 – 7.38 (m, 2H), 7.39 – 7.31 (m, 2H), 7.32 – 7.25 (m, 2H), 6.96 (t, *J* = 8.7 Hz, 2H), 2.80 (dt, *J* = 11.9, 3.1 Hz, 2H), 2.57 – 2.48 (m, 2H), 2.49 – 2.38 (m, 4H), 2.25 (s, 1H), 2.10 (td, *J* = 13.2, 4.5 Hz, 2H), 1.80 (p, *J* = 7.2 Hz, 2H), 1.70 (dd, *J* = 14.1, 2.7 Hz, 2H). ¹³C NMR (CDCl₃) δ 162.1 (d, *J* = 248.3 Hz), 147.1, 120.0 (d, *J* = 3.5 Hz), 115.5 (d, *J* = 22.0 Hz), 89.45 (d, *J* = 1.5 Hz), 79.9, 71.1, 57.8, 49.5, 38.5, 26.2, 17.6.

3-(4-Chlorophenyl)-8-(4-(4-fluorophenyl)-4-oxobutyl)-3-hydroxy-8-azabicyclo[3.2.1]octan-8-ium 2,2,2-trifluoroacetate (42). General procedure C. Purification by preparative HPLC (Method C) afforded 45 mg of the title compound as a white solid (68%). LCMS (*m/z*): 402.3 [M+H]⁺, *t_R* 3.58 min. HRMS (*m/z*): C₂₃H₂₅ClFNO₂: requires 402.1631 [M+H]⁺; found 402.1633. ¹H NMR (CDCl₃) δ 11.34 (s, 1H), 7.99 (dd, *J* = 8.6, 5.4 Hz, 2H), 7.52 (d, *J* = 8.3 Hz, 2H), 7.33 – 7.25 (m, 2H), 7.17 (t, *J* = 8.5 Hz, 2H), 4.71 (s, 1H), 4.00 (t, *J* = 4.1 Hz, 2H), 3.13 (t, *J* = 6.1 Hz, 2H), 3.06 (dt, *J* = 10.5, 5.8 Hz, 4H), 2.84 – 2.69 (m, 4H), 2.26 – 2.12 (m, 4H), 2.05 (d, *J* = 15.4 Hz, 2H). ¹³C NMR (CDCl₃) δ 197.1, 166.2 (d, *J* = 256.0 Hz), 145.8, 133.5, 132.7 (d, *J* = 3.0 Hz), 130.8 (d, *J* = 9.4 Hz), 128.7, 126.3, 116.1 (d, *J* = 22.0 Hz), 71.9, 61.6, 50.9, 43.6, 34.9, 24.4, 18.8.

4-(4-(4-Chlorophenyl)piperazin-1-yl)-1-(4-fluorophenyl)butan-1-one (43). General procedure C. Purification by FCC (eluent 20:0.5:0.1, EtOAc/MeOH/NH₄OH) gave 115 mg of the title compound as a white solid (69%). LCMS (*m/z*): 361.3 [M+H]⁺, *t_R* 3.41 min. HRMS (*m/z*): C₂₀H₂₂ClFN₂O: requires 361.1405 [M+H]⁺; found 361.1487. ¹H NMR (CDCl₃) δ 8.05 – 7.93 (m, 2H), 7.20 – 7.14 (m, 2H), 7.11 (t, *J* = 8.6 Hz, 2H), 6.84 – 6.79 (m, 2H), 3.09 (dd, *J* = 6.2, 3.8 Hz, 4H), 2.99 (t, *J* = 7.0 Hz, 2H), 2.57 (t, *J* = 5.0 Hz, 4H), 2.45 (t, *J* = 7.0 Hz, 2H), 1.97 (p, *J* = 7.1 Hz, 2H). ¹³C NMR (CDCl₃) δ 198.4, 165.7 (d, *J* = 254.4 Hz), 150.0, 133.7 (d, *J* = 3.0 Hz), 130.7 (d, *J* = 9.2 Hz), 128.9, 124.4, 117.2, 115.7 (d, *J* = 21.8 Hz), 57.7, 53.0, 49.1, 36.2, 21.6.

4-(4-Chlorophenyl)-1,2,3,6-tetrahydropyridine (44). To concentrated hydrochloric acid (10 mL) in a 25 mL round-bottom flask was added 4-(4-chlorophenyl)piperidin-4-ol (500 mg, 2.36 mmol), and the suspension was stirred at reflux for 5 h. The solution was allowed to cool, then slowly added to 5 M NaOH (20 mL), and extracted with DCM (3 × 20 mL). The organic extracts were dried (Na₂SO₄) and concentrated under reduced pressure to afford the 457 mg of a white solid (quantitative yield). LCMS (*m/z*): 194.3 [M+H]⁺, *t_R* 1.87 min. ¹H NMR (CDCl₃) δ 7.34 – 7.23 (m, 4H), 6.11 (dt, *J* = 3.5, 1.8 Hz, 1H), 3.51 (q, *J* = 3.0 Hz, 2H), 3.09 (t, *J* = 5.7 Hz, 2H), 2.41 (dddd, *J* = 6.9, 4.0, 2.7, 1.2 Hz, 2H), 1.65 (s, 1H). ¹³C NMR (CDCl₃) δ 139.9, 134.4, 132.7, 128.5, 126.2, 124.3, 45.7, 43.4, 27.9.

4-(4-(4-Chlorophenyl)-3,6-dihydropyridin-1(2H)-yl)-1-(4-fluorophenyl)butan-1-one (45). General procedure C. Purification by FCC (eluent 20:0.5:0.1, EtOAc/MeOH/NH₄OH) gave 49 mg of the title compound as a white solid (80%). LCMS (*m/z*): 358.2 [M+H]⁺, *t_R* 3.64 min. HRMS (*m/z*): C₂₁H₂₁ClFNO: requires 358.1296 [M+H]⁺; found 358.1379. ¹H NMR (CDCl₃) δ 8.04 – 7.94 (m, 2H), 7.33 – 7.23 (m, 4H), 7.11 (t, *J* = 8.6 Hz, 2H), 6.04 (t, *J* = 1.7 Hz, 1H), 3.14 (q, *J* = 3.0 Hz, 2H), 3.02 (t, *J* = 7.1 Hz, 2H), 2.69 (t, *J* = 5.7 Hz, 2H), 2.54 (t, *J* = 7.1 Hz, 2H), 2.49 (tt, *J* = 5.8, 2.5 Hz, 2H), 2.01 (p, *J* = 7.1 Hz, 2H). ¹³C NMR (CDCl₃) δ 198.6, 165.8 (d, *J* = 254.4 Hz), 139.4, 134.1, 133.7 (d, *J* = 3.0 Hz), 132.8, 130.8 (d, *J* = 9.3 Hz), 126.3, 122.6, 115.7 (d, *J* = 21.8 Hz), 57.5, 53.3, 50.3, 36.3, 28.1, 21.9.

4-(6-(4-Chlorophenyl)-3-azabicyclo[4.1.0]heptan-3-yl)-1-(4-fluorophenyl)butan-1-one (46). A solution of 4-(4-(4-chlorophenyl)-3,6-dihydropyridin-1(2*H*)-yl)-1-(4-fluorophenyl)butan-1-one (110 mg, 307 μ mol) in DCM (20 mL), was treated with Et₂Zn (0.9 M in hexanes; 1.71 mL, 1.54 mmol). After 10 minutes, the reaction mixture was cooled to 0 °C, and treated with a solution of CH₂I₂ (124 μ L, 1.54 mmol) in DCM (2 mL) drop-wise over and allowed to warm to ambient temperature. After 24 h, the reaction mixture was quenched slowly with sat. aqueous NH₄Cl and stirred for 10 minutes. The reaction mixture was extracted with DCM (3 x 20 mL), and the combined organic phases were washed with sat. aqueous NaHCO₃, dried (Na₂SO₄), and concentrated *in vacuo*. The resulting residue was purified by FCC (eluent, 5% MeOH/EtOAc) to yield 82 mg of the title compound as a white solid (72%). LCMS (*m/z*): 372.2 [M+H]⁺, *t_R* 3.94 min. HRMS (*m/z*): C₂₂H₂₃FNO: requires 372.1452 [M+H]⁺; found 372.1517. ¹H NMR (CDCl₃) δ 8.05 – 7.95 (m, 2H), 7.24 – 7.17 (m, 2H), 7.18 – 7.07 (m, 4H), 2.97 (t, *J* = 7.1 Hz, 2H), 2.81 (dd, *J* = 11.3, 5.8 Hz, 1H), 2.69 (dd, *J* = 11.3, 1.7 Hz, 1H), 2.36 (t, *J* = 6.9 Hz, 2H), 2.26 – 2.20 (m, 2H), 2.03 (dq, *J* = 14.0, 7.4, 6.9 Hz, 2H), 1.92 (p, *J* = 7.1 Hz, 2H), 1.37 – 1.28 (m, 1H), 0.87 (dd, *J* = 9.2, 4.2 Hz, 1H), 0.79 (dd, *J* = 5.7, 4.3 Hz, 1H). ¹³C NMR (CDCl₃) δ 196.7, 166.1 (d, *J* = 256.1 Hz), 142.7, 132.9, 132.7 (d, *J* = 3.0 Hz), 130.8 (d, *J* = 9.3 Hz), 129.9, 128.9, 116.0 (d, *J* = 22.2 Hz), 56.3, 52.7, 48.1, 34.9, 28.7, 23.6, 18.1, 17.7, 15.1.

4-Phenylpiperidine (47). Pd/C (25 mg) was added to a solution of 4-(4-chloro-phenyl)-1,2,3,6-tetrahydropyridine (300 mg, 1.55 mmol) in MeOH (20 mL). The reaction mixture was stirred for 4 h at room temperature under 1 ATM of H₂. After separation of the catalyst (Celite), the solvent was removed *in vacuo* to yield 250 mg of a beige solid (quantitative yield). LCMS (*m/z*): 162.2 [M+H]⁺, *t_R* 0.65 min. ¹H NMR (CDCl₃) δ 8.21 (s, 1H), 7.28 (t, *J* = 7.5 Hz, 2H), 7.21 (d, *J* = 7.5 Hz, 3H), 3.56 (d, *J* = 12.6 Hz, 2H), 2.98 (td, *J* = 13.0, 2.9 Hz, 2H), 2.79 – 2.66 (m, 1H), 2.17 (qd, *J* = 13.2, 3.9 Hz, 2H), 1.98 (d, *J* = 14.0 Hz, 2H). ¹³C NMR (CDCl₃) δ 143.8, 128.8, 126.9, 126.7, 44.7, 40.7, 30.2.

1-(4-Fluorophenyl)-4-(4-phenylpiperidin-1-yl)butan-1-one (48). General procedure C. Purification by FCC (eluent 20:0.5:0.1, EtOAc/MeOH/NH₄OH) gave 89 mg of the title compound as a white solid (75%). LCMS (*m/z*): 326.4 [M+H]⁺, *t_R* 3.35 min. HRMS (*m/z*): C₂₁H₂₄FNO: requires 326.1842 [M+H]⁺; found 326.1930. ¹H NMR (CDCl₃) δ 8.08 – 7.97 (m, 2H), 7.33 – 7.25 (m, 2H), 7.20 (d, *J* = 7.3 Hz, 3H), 7.14 (t, *J* = 8.6 Hz, 2H), 3.07 – 2.95 (m, 4H), 2.51 – 2.41 (m, 3H), 2.10 – 2.02 (m, 2H), 2.01 – 1.94 (m, 2H), 1.84 – 1.77 (m, 2H), 1.71 (qd, *J* = 12.4, 3.7 Hz, 2H). ¹³C NMR (CDCl₃) δ 198.6, 165.8 (d, *J* = 254.4 Hz), 146.5, 133.8 (d, *J* = 3.0 Hz), 130.8 (d, *J* = 9.2 Hz), 128.5, 126.9, 126.2, 115.7 (d, *J* = 21.8 Hz), 58.2, 54.4, 42.8, 36.5, 33.5, 22.1.

4-(4-(4-Chlorophenyl)piperidin-1-yl)-1-(4-fluorophenyl)butan-1-one (50). General procedure C. Purification by FCC (eluent 20:0.5:0.1, EtOAc/MeOH/NH₄OH) gave 59 mg of the title compound as a beige solid (68%). LCMS (*m/z*): 360.2 [M+H]⁺, *t_R* 3.72 min. HRMS (*m/z*): C₂₁H₂₃ClFNO: requires

360.1452 [M+H]⁺; found 360.1539. ¹H NMR (CDCl₃) δ 8.01 (dd, *J* = 8.7, 5.5 Hz, 2H), 7.26 – 7.22 (m, 2H), 7.16 – 7.08 (m, 4H), 3.05 – 2.94 (m, 4H), 2.52 – 2.38 (m, 3H), 2.09 – 1.90 (m, 4H), 1.76 (dq, *J* = 12.6, 2.2 Hz, 2H), 1.63 (qd, *J* = 12.4, 3.8 Hz, 2H). ¹³C NMR (CDCl₃) δ 198.5, 165.7 (d, *J* = 254.2 Hz), 144.9, 133.8 (d, *J* = 3.0 Hz), 131.8, 130.8 (d, *J* = 9.2 Hz), 128.6, 128.3, 115.7 (d, *J* = 21.7 Hz), 58.2, 54.3, 42.2, 36.4, 33.5, 22.0.

***tert*-Butyl 4-(4-chlorophenyl)-4-hydroxypiperidine-1-carboxylate (51).** To a suspension of 4-(4-chlorophenyl)piperidin-4-ol (500 mg, 2.36 mmol) and Et₃N (823 μL, 5.90 mmol) in DCM (20 mL), was added di-*tert*-butyl dicarbonate (2.06 g, 9.45 mmol) and the reaction stirred at rt for 4 h. The solvent was evaporated under reduced pressure and the residue was purified by FCC (eluent, 10:1 *n*-hexanes/EtOAc) to afford 715 mg of a clear oil (97%). LCMS (*m/z*): 312.3 [M+H]⁺, *t_R* 3.09 min. ¹H NMR (CDCl₃) δ 7.38 (d, *J* = 7.2 Hz, 2H), 7.15 (d, *J* = 7.3 Hz, 2H), 3.94 (br s, 2H), 3.18 (br s, 2H), 1.89 (br s, 2H), 1.46 (s, 11H).

***tert*-Butyl 4-(4-chlorophenyl)-4-methoxypiperidine-1-carboxylate (52).** To a stirred suspension of sodium hydride (64.7 mg, 2.69 mmol) in dry DMF (15 mL) at rt was added *tert*-butyl 4-(4-chlorophenyl)-4-hydroxypiperidine-1-carboxylate (700 mg, 2.24 mmol). After 30 minutes, methyl iodide (168 μL, 2.69 mmol) was added and the mixture was stirred overnight. The mixture was poured into an equal volume of H₂O and extracted with EtOAc (2 × 30 mL). The EtOAc extracts were collected and washed with additional H₂O (3 × 30 mL), dried (Na₂SO₄), filtered, and concentrated *in vacuo* to give an orange oil. The crude oil was purified by FCC (eluent, 10:1 *n*-hexanes/EtOAc) to afford 645 mg of a clear oil (88%). LCMS (*m/z*): 326.3 [M+H]⁺, *t_R* 3.18 min. ¹H NMR (CDCl₃) δ 8.00 (dd, *J* = 8.7, 5.5 Hz, 2H), 7.33 – 7.25 (m, 4H), 7.16 – 7.06 (m, 2H), 2.97 (t, *J* = 7.1 Hz, 2H), 2.93 (s, 3H), 2.75 – 2.65 (m, 2H), 2.45 (t, *J* = 7.2 Hz, 2H), 2.38 (td, *J* = 11.7, 2.5 Hz, 2H), 2.03 – 1.90 (m, 4H), 1.84 (dt, *J* = 13.1, 6.7 Hz, 2H). ¹³C NMR (CDCl₃) δ 198.5, 165.7 (d, *J* = 254.4 Hz), 143.6, 133.8 (d, *J* = 3.0 Hz), 133.0, 130.8 (d, *J* = 9.3 Hz), 128.6, 127.6, 115.7 (d, *J* = 21.8 Hz), 75.4, 49.2, 36.4, 34.7, 22.1.

4-(4-Chlorophenyl)-4-methoxypiperidin-1-ium chloride (53). General procedure B. Concentration *in vacuo* gave 296 mg of a white solid (95%). ¹H NMR (DMSO-*d*₆) δ 9.30 (s, 2H), 7.53 – 7.45 (m, 2H), 7.45 – 7.36 (m, 2H), 3.18 (d, *J* = 12.5 Hz, 12H), 3.11 – 2.96 (m, 2H), 2.89 (s, 3H), 2.20 – 2.08 (m, 4H). ¹³C NMR (DMSO-*d*₆) δ 141.9, 132.4, 128.6, 127.8, 73.4, 49.6, 39.3, 30.5.

4-(4-(4-Chlorophenyl)-4-methoxypiperidin-1-yl)-1-(4-fluorophenyl)butan-1-one (54). General procedure C. Purification by FCC (eluent 20:0.5:0.1, EtOAc/MeOH/NH₄OH) gave 88 mg of the title compound as a white solid (81%). LCMS (*m/z*): 390.3 [M+H]⁺, *t_R* 3.82 min. HRMS (*m/z*): C₂₂H₂₅ClFNO₂: requires 390.1558 [M+H]⁺; found 390.1639. ¹H NMR (CDCl₃) δ 8.00 (dd, *J* = 8.7, 5.5 Hz, 2H), 7.33 – 7.25 (m, 4H), 7.16 – 7.06 (m, 2H), 2.97 (t, *J* = 7.1 Hz, 2H), 2.93 (s, 3H), 2.75 –

2.65 (m, 2H), 2.45 (t, $J = 7.2$ Hz, 2H), 2.38 (td, $J = 11.7, 2.5$ Hz, 2H), 2.03 – 1.90 (m, 4H), 1.84 (dt, $J = 13.1, 6.7$ Hz, 2H). ¹³C NMR (CDCl₃) δ 198.5, 165.7 (d, $J = 254.4$ Hz), 143.6, 133.8 (d, $J = 3.0$ Hz), 133.0, 130.8 (d, $J = 9.3$ Hz), 128.6, 127.6, 115.7 (d, $J = 21.8$ Hz), 75.4, 49.2, 36.4, 34.7, 22.1.

1-(4-Chlorophenyl)-4-(4-(4-fluorophenyl)-4-hydroxypiperidin-1-yl)butan-1-one (55). General procedure C. Purification by FCC (eluent 20:0.5:0.1, EtOAc/MeOH/NH₄OH) gave 75 mg of the title compound as a light yellow solid (71%). LCMS (m/z): 376.3 [M+H]⁺, t_R 3.39 min. HRMS (m/z): C₂₁H₂₃ClFNO₂: requires 376.1401 [M+H]⁺; found 376.1488. ¹H NMR (CDCl₃) δ 7.99 – 7.88 (m, 2H), 7.48 – 7.36 (m, 4H), 7.01 (t, $J = 8.7$ Hz, 2H), 2.98 (t, $J = 7.0$ Hz, 2H), 2.76 (dd, $J = 9.1, 6.1$ Hz, 2H), 2.51 – 2.38 (m, 4H), 2.03 – 1.92 (m, 5H), 1.69 (dd, $J = 14.2, 2.6$ Hz, 2H). ¹³C NMR (CDCl₃) δ 198.9, 161.9 (d, $J = 245.2$ Hz), 144.3 (d, $J = 3.1$ Hz), 139.4, 135.7, 129.6, 128.9, 126.4 (d, $J = 7.9$ Hz), 115.0 (d, $J = 21.2$ Hz), 71.1, 57.9, 49.5, 38.6, 36.4, 22.1.

4-(4-Hydroxy-4-phenylpiperidin-1-yl)-1-phenylbutan-1-one (56). General procedure C. Purification by FCC (eluent 20:0.5:0.1, EtOAc/MeOH/NH₄OH) gave 125 mg of the title compound as a white solid (88%). LCMS (m/z): 324.3 [M+H]⁺, t_R 2.72 min. HRMS (m/z): C₂₁H₂₅NO₂: requires 324.1865 [M+H]⁺; found 324.1965. ¹H NMR (CDCl₃) δ 8.03 – 7.94 (m, 2H), 7.59 – 7.51 (m, 1H), 7.46 (dd, $J = 8.4, 6.9$ Hz, 4H), 7.33 (dd, $J = 8.4, 6.8$ Hz, 2H), 7.27 – 7.21 (m, 1H), 3.01 (t, $J = 7.0$ Hz, 2H), 2.82 (dt, $J = 11.9, 3.2$ Hz, 2H), 2.55 – 2.44 (m, 4H), 2.14 – 1.94 (m, 5H), 1.71 (dd, $J = 14.1, 2.7$ Hz, 2H). ¹³C NMR (CDCl₃) δ 200.1, 148.4, 137.3, 132.9, 128.7, 128.4, 128.2, 127.1, 124.6, 71.3, 57.9, 49.5, 38.3, 36.5, 21.9.

Pharmacological Characterisation. *Materials.* Tag-lite labeling medium (LABMED), SNAP-Lumi4-Tb, and the PPHT ((±)-2-(*N*-phenethyl-*N*-propyl)amino-5-hydroxytetralin hydrochloride;1-Naphthalenol,5,6,7,8-tetrahydro-6-[(2-phenylethyl)propylamino]) derivative labelled with a red fluorescent probe (PPHT-red) was obtained from Cisbio Bioassays (Bagnolssur-Cèze, France). Ninety-six-well polypropylene plates (Corning) were purchased from Fisher Scientific UK (Loughborough, UK) and 384-well optiplate plates were purchased from PerkinElmer (Beaconsfield, UK). GppNHp used in competition assays were obtained from Sigma-Aldrich (Poole, UK).

Cell culture. The host Chinese hamster ovary (CHO) K1 cell line was transfected with the cDNA encoding a SNAP-tagged human dopamine D_{2L} receptor (Genbank ref.: NM_000795), and a stable dilution-cloned cell line (CHO-hD_{2L}) was established by zeocin resistance encoded by the plasmid vector (pcDNA3.1zeo⁺, Invitrogen, Paisley UK). Cells were maintained in Dulbecco's modified Eagle's medium: Ham F12 (DMEM:F12) containing 2 mM glutamine (Sigma-Aldrich, Poole, UK) and supplemented with 10% fetal calf serum (Life Technologies, Paisley UK).

Terbium labelling of SNAP-tagged D_{2L} cells. Cell culture medium was removed from the t175 cm² flasks containing confluent adherent CHO–D_{2L} cells. Twelve mL of Tag-lite labelling medium containing 100 nM of SNAP-Lumi4-Tb was added to the flask and incubated for 1 h at 37 °C under 5% CO₂. Cells were washed 2× in PBS (GIBCO Carlsbad, CA) to remove the excess of SNAP-Lumi4-Tb then detached using 5 mL of GIBCO enzyme-free Hank's-based cell dissociation buffer (GIBCO, Carlsbad, CA) and collected in a vial containing 5 mL of DMEM:F12 containing 2mM glutamine (Sigma-Aldrich) and supplemented with 10% fetal calf serum. Cells were pelleted by centrifugation (5 min at 1500 rpm) and the pellets were frozen to –80 °C. To prepare membranes, homogenisation steps were conducted at 4 °C (to avoid receptor degradation). Specifically 20 mL per t175-cm² flask of wash buffer (10 mM HEPES and 10 mM EDTA, pH 7.4) was added to the pellet. This was homogenised using an electrical homogenizer Ultra-Turrax (Ika-Werk GmbH & Co. KG, Staufen, Germany) (position 6, 4 × 5-s bursts) and subsequently centrifuged at 48,000×g at 4 °C (Beckman Avanti J-251 Ultracentrifuge; Beckman Coulter, Fullerton, CA) for 30 min. The supernatant was discarded, and the pellet was re-homogenised and centrifuged as described above in wash buffer. The final pellet was suspended in ice-cold 10mM HEPES and 0.1mM EDTA, pH 7.4, at a concentration of 5–10 mg mL⁻¹. Protein concentration was determined using the bicinchoninic acid assay kit (Sigma-Aldrich), using BSA as a standard and aliquots maintained at –80 °C until required. Prior to their use, the frozen membranes were thawed and the membranes suspended in the assay buffer at a membranes concentration of 0.2 mg mL⁻¹.

Fluorescent ligand-binding assays. All fluorescent binding experiments using PPHT-red were conducted in white 384-well Optiplate plates, in assay binding buffer, 20 mM HEPES, 138 mM NaCl, 6 mM MgCl₂, 1 mM EGTA, 1 mM EDTA, and 0.02% pluronic acid pH 7.4, 100 μM GppNHp, and 0.1% ascorbic acid. GppNHp was included to remove the G protein-coupled population of receptors that can result in two distinct populations of binding sites in membrane preparations, since the Motulsky-Mahan model³¹ is only appropriate for ligands competing at a single site. In all cases, nonspecific binding was determined in the presence of 10 μM haloperidol.

Determination of PPHT-red binding kinetics. To accurately determine association rate (k_{on}) and dissociation rate (k_{off}) values, the observed rate of association (k_{ob}) was calculated using at least four different concentrations of PPHT-red (50-1.56 nM). The appropriate concentration of PPHT-red was incubated with human D_{2L} CHO cell membranes (2 μg per well) in assay binding buffer (final assay volume, 40 μL). The degree of PPHT-red bound to the receptor was assessed at multiple time points by HTRF detection to allow construction of association kinetic curves. The kinetic parameters of PPHT-red and plus those of unlabelled compounds were determined using a start time of ~1sec and an interval time of 20sec. The resulting data were globally fitted to the association kinetic model Eq.

2 to derive a single best-fit estimate for k_{on} and k_{off} as described under data analysis. The expression level of the hD_{2L}R recombinantly expressed in CHO cells was assessed, using [³H]-spiperone saturation binding and determined to be 1.13 ± 0.11 pmol mg⁻¹ protein.³⁴

Competition binding kinetics. To determine the association and dissociation rates of D₂R ligands, we used a competition kinetic binding assay recently described to profile the kinetics of a series of D₂R agonists³² and antipsychotic drugs.³⁴ This approach involves the simultaneous addition of both fluorescent ligand and competitor to the receptor preparation, so that at $t = 0$ all receptors are unoccupied. 12.5 nM PPHT-red (a concentration which avoids ligand depletion in this assay volume), was added simultaneously with the unlabelled compound of varying concentrations (at $t = \sim 1$ sec) to CHO cell membranes derived from cells stably expressing the human D_{2L}R (2 μg per well) in 40 μL of assay buffer. The degree of PPHT-red bound to the receptor was assessed at multiple time points by HTRF detection.

Non-specific binding was determined as the amount of HTRF signal detected in the presence of haloperidol (10 μM) and was subtracted from each time point, meaning that $t = 0$ was always equal to zero. Each time point was conducted on the same 384-well plate incubated at 37 °C with orbital mixing (1 s of 100 RPM per cycle). Multiple concentrations of unlabelled competitor were tested for determination of rate parameters. Data were globally fitted using Eq. 3 to simultaneously calculate k_{on} and k_{off} .

Signal detection and data analysis. Signal detection was performed on a Pherastar FS (BMG Labtech, Offenburg, Germany) using standard HTRF settings. The terbium donor was always excited with three laser flashes at a wavelength of 337 nm. A kinetic TR-FRET signal was collected at 20 s intervals both at 665 and 620 nm, when using red acceptor. HTRF ratios were obtained by dividing the acceptor signal (665 nm) by the donor signal (620 nm) and multiplying this value by 10,000. All experiments were analysed by non-linear regression using Prism 6.0 (Graphpad Software, San Diego, USA). Competition displacement data were fitted to sigmoidal (variable slope) curves using a “four parameter logistic equation”:

$$Y = \text{Bottom} + (\text{Top} - \text{Bottom}) / (1 + 10^{\log EC_{50} - X} \text{Hillcoefficient}), \quad (1)$$

IC₅₀ values obtained from the inhibition curves were converted to K_i values using the method of Cheng and Prusoff.⁶³ PPHT-red association data were fitted as follows to a global fitting model using Graphpad Prism 6.0 to simultaneously calculate k_{on} and k_{off} using the following equation, where k_{ob} equals the observed rate of association:

$$k_{ob} = [PPHT - red] \cdot k_{on} + k_{off}. \quad (2)$$

Association and dissociation rates for unlabelled compounds were calculated using the equations described by Motulsky and Mahan.³¹

$$\begin{aligned} K_A &= k_1[L] + k_2 \\ K_B &= k_2[I] + k_4 \\ S &= \sqrt{(K_A - K_B)^2 + 4 \cdot k_1 \cdot k_3 \cdot L \cdot I \cdot 10^{-18}} \\ K_F &= 0.5 \cdot (K_A + K_B + S) \\ K_S &= 0.5 \cdot (K_A + K_B - S) \\ DIFF &= K_F - K_S \\ Q &= \frac{B_{max} \cdot k_1 \cdot L \cdot 10^{-9}}{DIFF} \\ Y &= Q \times \left(\frac{k_4 \cdot DIFF}{K_F \times K_S} + \frac{k_4 - K_F}{K_F} \cdot \exp(-K_F \cdot X) - \frac{k_4 - K_S}{K_S} \cdot \exp(-K_S \cdot X) \right). \end{aligned} \quad (3)$$

Where: X = Time (min), Y = Specific binding (HTRF ratio 665 nm/620 nm $\times 10,000$), $k_1 = k_{on}$ PPHT-red, $k_2 = k_{off}$ PPHT-red, L = Concentration of PPHT-red used (nM), B_{max} = Total binding (HTRF ratio 665 nm/620 nm $\times 10,000$), I = Concentration of unlabelled antagonist (nM). Fixing the above parameters allowed the following to be calculated: k_3 = Association rate of unlabelled ligand ($M^{-1} \text{ min}^{-1}$), k_4 = Dissociation rate of unlabelled ligand (min^{-1}). Dissociation of PPHT-red was fitted to a one phase mono-exponential decay function to estimate the dissociation rate of PPHT-red directly. Specific binding was determined by subtracting the nonspecific HTRF ratio from the total HTRF ratio.

▪ ASSOCIATED CONTENT

Supporting Information. Synthetic schemes and characterisation data for literature analogues of 1. ¹H and ¹³C NMR spectra and reverse-phase analytical chromatograms for representative screening compounds. Molecular formula strings for all screening compounds.

▪ AUTHOR INFORMATION

Corresponding Authors.

*S.J.C.: phone, +44 115 8230165; e-mail, steven.charlton@nottingham.ac.uk

*S.N.M.: phone, +44 116 8467983; e-mail, shailesh.mistry@nottingham.ac.uk

▪ ACKNOWLEDGMENTS

This research was supported by the joint University of Nottingham & Monash University Doctoral Training Centre (DTC).

▪ ABBREVIATIONS USED

D₂R, dopamine D₂ receptor; DA, dopamine; APD, antipsychotic drug; EPS, extrapyramidal symptoms; FGA, first generation antipsychotic; SGA, second generation antipsychotic; TR-FRET, time-resolved fluorescence resonance energy transfer; k_{off} , dissociation rate constant; k_{on} , association rate constant; SAR, structure-activity relationship; SKR, structure-kinetic relationship; FCC, flash column chromatography; HPLC, high-performance liquid chromatography; S_NAr, nucleophilic aromatic substitution; HBSS, Hank's balanced salt solution; FBS, foetal bovine serum.

▪ REFERENCES

1. Seeman, P.; Lee, T.; Chau-Wong, M.; Wong, K. Antipsychotic drug doses and neuroleptic/dopamine receptors. *Nature* **1976**, *261*, 717-719.
2. Battaglia, J. Pharmacological management of acute agitation. *Drugs* **2005**, *65*, 1207-1222.
3. Meltzer, H. Y. An atypical compound by any other name is still a. *Psychopharmacology* **2000**, *148*, 16-19.
4. Ginovart, N.; Kapur, S. Role of dopamine D(2) receptors for antipsychotic activity. *Handb. Exp. Pharmacol.* **2012**, *212*, 27-52.
5. Miyamoto, S.; Miyake, N.; Jarskog, L. F.; Fleischhacker, W. W.; Lieberman, J. A. Pharmacological treatment of schizophrenia: a critical review of the pharmacology and clinical effects of current and future therapeutic agents. *Mol. Psychiatr.* **2012**, *17*, 1206-1227.
6. Meltzer, H. Y. Update on typical and atypical antipsychotic drugs. *Annu. Rev. Med.* **2013**, *64*, 393-406.
7. Leucht, S.; Corves, C.; Arbter, D.; Engel, R. R.; Li, C.; Davis, J. M. Second-generation versus first-generation antipsychotic drugs for schizophrenia: a meta-analysis. *Lancet* **2009**, *373*, 31-41.
8. Farde, L.; Nordstrom, A. L.; Wiesel, F. A.; Pauli, S.; Halldin, C.; Sedvall, G. Positron emission tomographic analysis of central D1 and D2 dopamine receptor occupancy in patients treated with classical neuroleptics and clozapine. Relation to extrapyramidal side effects. *Arch. Gen. Psychiatr.* **1992**, *49*, 538-544.
9. Caron, M. G.; Beaulieu, M.; Raymond, V.; Gagne, B.; Drouin, J.; Lefkowitz, R. J.; Labrie, F. Dopaminergic receptors in the anterior pituitary gland. Correlation of [3H]dihydroergocryptine binding with the dopaminergic control of prolactin release. *J. Biol. Chem.* **1978**, *253*, 2244-2253.
10. Casey, D. E. Neuroleptic drug-induced extrapyramidal syndromes and tardive dyskinesia. *Schizophr. Res.* **1991**, *4*, 109-120.
11. Leucht, S.; Pitschel-Walz, G.; Abraham, D.; Kissling, W. Efficacy and extrapyramidal side-effects of the new antipsychotics olanzapine, quetiapine, risperidone, and sertindole compared to conventional antipsychotics and placebo. A meta-analysis of randomized controlled trials. *Schizophr. Res.* **1999**, *35*, 51-68.
12. Halbreich, U.; Kinon, B. J.; Gilmore, J. A.; Kahn, L. S. Elevated prolactin levels in patients with schizophrenia: mechanisms and related adverse effects. *Psychoneuroendocrinology* **2003**, *28*, 53-67.

13. Mauri, M. C.; Paletta, S.; Maffini, M.; Colasanti, A.; Dragogna, F.; Di Pace, C.; Altamura, A. C. Clinical pharmacology of atypical antipsychotics: an update. *EXCLI J.* **2014**, *13*, 1163-1191.
14. Kapur, S.; Remington, G. Dopamine D(2) receptors and their role in atypical antipsychotic action: still necessary and may even be sufficient. *Biol. Psychiat.* **2001**, *50*, 873-883.
15. Meltzer, H. Y.; Matsubara, S.; Lee, J. C. Classification of typical and atypical antipsychotic drugs on the basis of dopamine D-1, D-2 and serotonin₂ pKi values. *J. Pharmacol. Exp. Ther.* **1989**, *251*, 238-246.
16. Marcus, M.; Wiker, C.; Frånberg, O.; Konradsson-Geuken, A.; Langlois, X.; Jardemark, K.; Svensson, T. Adjunctive alpha(2)-adrenoceptor blockade enhances the antipsychotic-like effect of risperidone and facilitates cortical dopaminergic and glutamatergic, NMDA receptor-mediated transmission. *Int. J. Neuropsychopharmacol.* **2009**, *13*, 891-903.
17. Roth, B. L.; Sheffler, D. J.; Kroeze, W. K. Magic shotguns versus magic bullets: selectively non-selective drugs for mood disorders and schizophrenia. *Nat. Rev. Drug Discov.* **2004**, *3*, 353.
18. Raja, M. Clozapine safety, 35 years later. *Curr. Drug. Saf.* **2011**, *6*, 164-184.
19. Horacek, J.; Bubenikova-Valesova, V.; Kopecek, M.; Palenicek, T.; Dockery, C.; Mohr, P.; Hoschl, C. Mechanism of action of atypical antipsychotic drugs and the neurobiology of schizophrenia. *CNS Drugs* **2006**, *20*, 389-409.
20. Kapur, S.; Seeman, P. Does fast dissociation from the dopamine d(2) receptor explain the action of atypical antipsychotics?: A new hypothesis. *Am. J. Psychiat.* **2001**, *158*, 360-369.
21. Kapur, S.; Seeman, P. Antipsychotic agents differ in how fast they come off the dopamine D2 receptors. Implications for atypical antipsychotic action. *J. Psychiatr. Neurosci.* **2000**, *25*, 161-166.
22. Copeland, R. A.; Pompliano, D. L.; Meek, T. D. Drug-target residence time and its implications for lead optimization. *Nat. Rev. Drug Discov.* **2006**, *5*, 730-739.
23. Guo, D.; Heitman, L. H.; AP, I. J. The role of target binding kinetics in drug discovery. *ChemMedChem* **2015**, *10*, 1793-1796.
24. Doornbos, M. L. J.; Cid, J. M.; Haubrich, J.; Nunes, A.; van de Sande, J. W.; Vermond, S. C.; Mulder-Krieger, T.; Trabanco, A. A.; Ahnaou, A.; Drinkenburg, W. H.; Lavreysen, H.; Heitman, L. H.; AP, I. J.; Tresadern, G. Discovery and kinetic profiling of 7-aryl-1,2,4-triazolo[4,3-*a*]pyridines: positive allosteric modulators of the metabotropic glutamate receptor 2. *J. Med. Chem.* **2017**, *60*, 6704-6720.
25. Xia, L.; Burger, W. A. C.; van Veldhoven, J. P. D.; Kuiper, B. J.; van Duijl, T. T.; Lenselink, E. B.; Paasman, E.; Heitman, L. H.; Ijzerman, A. P. Structure–affinity relationships and structure–kinetics relationships of pyrido[2,1-*f*]purine-2,4-dione derivatives as human adenosine A₃ receptor antagonists. *J. Med. Chem.* **2017**, *60*, 7555-7568.
26. Vilums, M.; Zweemer, A. J. M.; Yu, Z.; de Vries, H.; Hillger, J. M.; Wapenaar, H.; Bollen, I. A. E.; Barmare, F.; Gross, R.; Clemens, J.; Krenitsky, P.; Brussee, J.; Stamos, D.; Saunders, J.; Heitman, L. H.; Ijzerman, A. P. Structure–kinetic relationships—An overlooked parameter in hit-to-lead optimization: a case of cyclopentylamines as chemokine receptor 2 antagonists. *J. Med. Chem.* **2013**, *56*, 7706-7714.
27. Tautermann, C. S. Impact, determination and prediction of drug–receptor residence times for GPCRs. *Curr. Opin. Pharmacol.* **2016**, *30*, 22-26.
28. de Witte, W. E. A.; Danhof, M.; van der Graaf, P. H.; de Lange, E. C. M. In vivo target residence time and kinetic selectivity: The association rate constant as determinant. *Trends Pharmacol. Sci.* **2016**, *37*, 831-842.
29. Schuetz, D. A.; de Witte, W. E. A.; Wong, Y. C.; Knasmueller, B.; Richter, L.; Kokh, D. B.; Sadiq, S. K.; Bosma, R.; Nederpelt, I.; Heitman, L. H.; Segala, E.; Amaral, M.; Guo, D.; Andres, D.; Georgi, V.; Stoddart, L. A.; Hill, S.; Cooke, R. M.; De Graaf, C.; Leurs, R.; Frech, M.; Wade, R. C.; de Lange, E. C. M.; AP, I. J.; Muller-Fahrnow, A.; Ecker, G. F. Kinetics for drug discovery: an industry-driven effort to target drug residence time. *Drug. Discov. Today* **2017**, *22*, 896-911.
30. Seeman, P.; Talerico, T. Rapid release of antipsychotic drugs from dopamine D2 receptors: an explanation for low receptor occupancy and early clinical relapse upon withdrawal of clozapine or quetiapine. *Am. J. Psychiat.* **1999**, *156*, 876-884.

31. Motulsky, H. J.; Mahan, L. C. The kinetics of competitive radioligand binding predicted by the law of mass action. *Mol. Pharmacol.* **1984**, *25*, 1-9.
32. Klein Herenbrink, C.; Sykes, D. A.; Donthamsetti, P.; Canals, M.; Coudrat, T.; Shonberg, J.; Scammells, P. J.; Capuano, B.; Sexton, P. M.; Charlton, S. J.; Javitch, J. A.; Christopoulos, A.; Lane, J. R. The role of kinetic context in apparent biased agonism at GPCRs. *Nat. Commun.* **2016**, *7*, 10842.
33. Albizu, L.; Cottet, M.; Kralikova, M.; Stoev, S.; Seyer, R.; Brabet, I.; Roux, T.; Bazin, H.; Bourrier, E.; Lamarque, L.; Breton, C.; Rives, M.-L.; Newman, A.; Javitch, J.; Trinquet, E.; Manning, M.; Pin, J.-P.; Mouillac, B.; Durroux, T. Time-resolved FRET between GPCR ligands reveals oligomers in native tissues. *Nat. Chem. Biol.* **2010**, *6*, 587-594.
34. Sykes, D. A.; Moore, H.; Stott, L.; Holliday, N.; Javitch, J. A.; Lane, J. R.; Charlton, S. J. Extrapyramidal side effects of antipsychotics are linked to their association kinetics at dopamine D₂ receptors. *Nat. Commun.* **2017**, *8*, 763.
35. Sikazwe, D. M.; Li, S.; Mardenborough, L.; Cody, V.; Roth, B. L.; Ablordeppey, S. Y. Haloperidol: towards further understanding of the structural contributions of its pharmacophoric elements at D₂-like receptors. *Bioorg. Med. Chem. Lett.* **2004**, *14*, 5739-5742.
36. Ablordeppey, S. Y.; Altundas, R.; Bricker, B.; Zhu, X. Y.; Eyunni, S. E. V. K.; Jackson, T.; Khan, A.; Roth, B. L. Identification of a butyrophenone analog as a potential atypical antipsychotic agent: 4-[4-(4-chlorophenyl)-1,4-diazepan-1-yl]-1-(4-fluorophenyl)butan-1-one. *Bioorg. Med. Chem.* **2008**, *16*, 7291-7301.
37. Sikazwe, D. M.; Nkansah, N. T.; Altundas, R.; Zhu, X. Y.; Roth, B. L.; Setola, V.; Ablordeppey, S. Y. Synthesis and evaluation of ligands for D₂-like receptors: the role of common pharmacophoric groups. *Bioorg. Med. Chem.* **2009**, *17*, 1716-1723.
38. Sampson, D.; Bricker, B.; Zhu, X. Y.; Peprah, K.; Lamango, N. S.; Setola, V.; Roth, B. L.; Ablordeppey, S. Y. Further evaluation of the tropane analogs of haloperidol. *Bioorg. Med. Chem. Lett.* **2014**, *24*, 4294-4297.
39. Lyles-Eggleston, M.; Altundas, R.; Xia, J.; Sikazwe, D. M.; Fan, P.; Yang, Q.; Li, S.; Zhang, W.; Zhu, X.; Schmidt, A. W.; Vanase-Frawley, M.; Shrihkande, A.; Villalobos, A.; Borne, R. F.; Ablordeppey, S. Y. Design, synthesis, and evaluation of metabolism-based analogues of haloperidol incapable of forming MPP⁺-like species. *J. Med. Chem.* **2004**, *47*, 497-508.
40. Ravina, E.; Casariego, I.; Masaguer, C. F.; Fontenla, J. A.; Montenegro, G. Y.; Rivas, M. E.; Loza, M. I.; Enguix, M. J.; Villazon, M.; Cadavid, M. I.; Demontis, G. C. Conformationally constrained butyrophenones with affinity for dopamine (D₁, D₂, D₄) and serotonin (5-HT_{2A}, 5-HT_{2B}, 5-HT_{2C}) receptors: synthesis of aminomethylbenzo[*b*]furanones and their evaluation as antipsychotics. *J. Med. Chem.* **2000**, *43*, 4678-4693.
41. Leyva-Pérez, A.; Cabrero-Antonino, J. R.; Rubio-Marqués, P.; Al-Resayes, S. I.; Corma, A. Synthesis of the ortho/meta/para isomers of relevant pharmaceutical compounds by coupling a sonogashira reaction with a regioselective hydration. *ACS Catal.* **2014**, *4*, 722-731.
42. Liu, W.; Wang, H.; Li, C.-J. Metal-free Markovnikov-type alkyne hydration under mild conditions. *Org. Lett.* **2016**, *18*, 2184-2187.
43. Peprah, K.; Zhu, X. Y.; Eyunni, S. V. K.; Setola, V.; Roth, B. L.; Ablordeppey, S. Y. Multi-receptor drug design: Haloperidol as a scaffold for the design and synthesis of atypical antipsychotic agents. *Bioorg. Med. Chem.* **2012**, *20*, 1291-1297.
44. Olivieri, M.; Amata, E.; Vinciguerra, S.; Fiorito, J.; Giurandella, G.; Drago, F.; Caporarello, N.; Prezzavento, O.; Arena, E.; Salerno, L.; Rescifina, A.; Lupo, G.; Anfuso, C. D.; Marrazzo, A. Antiangiogenic effect of (±)-haloperidol metabolite II valproate ester [(±)-MRJF22] in human microvascular retinal endothelial cells. *J. Med. Chem.* **2016**, *59*, 9960-9966.
45. Iversen, L. L.; Rogawski, M. A.; Miller, R. J. Comparison of the effects of neuroleptic drugs on pre- and postsynaptic dopaminergic mechanisms in the rat striatum. *Mol. Pharmacol.* **1976**, *12*, 251-262.
46. Janssen, P. A. J.; Van De Westeringh, C.; Jageneau, A. H. M.; Demoen, P. J. A.; Hermans, B. K. F.; Van Daele, G. H. P.; Schellekens, K. H. L.; Van Der Eycken, C. A. M.; Niemegeers, C. J. E. Chemistry and pharmacology of CNS depressants related to 4-(4-Hydroxy-4-

- phenylpiperidino)butyrophenone. Part I--Synthesis and screening data in mice. *J. Med. Pharm. Chem.* **1959**, *1*, 281-297.
47. Simmons, H. E.; Smith, R. D. A new synthesis of cyclopropanes from olefins. *J. Am. Chem. Soc.* **1958**, *80*, 5323-5324.
48. Jumreang, T.; Somsak, R.; Poonsakdi, P. A convergent general strategy for the functionalized 2-aryl cycloalkyl-fused chromans: intramolecular hetero-Diels–Alder reactions of *ortho*-quinone methides. *Chem. Eur. J.* **2010**, *16*, 1445-1448.
49. Thomas, T.; Fang, Y.; Yuriev, E.; Chalmers, D. K. Ligand binding pathways of clozapine and haloperidol in the dopamine D₂ and D₃ receptors. *J. Chem. Inf. Model.* **2016**, *56*, 308-321.
50. Kalani, M. Y.; Vaidehi, N.; Hall, S. E.; Trabanino, R. J.; Freddolino, P. L.; Kalani, M. A.; Floriano, W. B.; Kam, V. W.; Goddard, W. A., 3rd. The predicted 3D structure of the human D₂ dopamine receptor and the binding site and binding affinities for agonists and antagonists. *Proc. Natl. Acad. Sci.* **2004**, *101*, 3815-3820.
51. Luedtke, R. R.; Mishra, Y.; Wang, Q.; Griffin, S. A.; Bell-Horner, C.; Taylor, M.; Vangveravong, S.; Dillon, G. H.; Huang, R.-Q.; Reichert, D. E.; Mach, R. H. Comparison of the binding and functional properties of two structurally different D₂ dopamine receptor subtype selective compounds. *ACS Chem. Neurosci.* **2012**, *3*, 1050-1062.
52. Wang, Q.; Mach, R. H.; Luedtke, R. R.; Reichert, D. E. Subtype selectivity of dopamine receptor ligands: insights from structure and ligand-based methods. *J. Chem. Inf. Model.* **2010**, *50*, 1970-1985.
53. Farrokhzad, S.; Diksic, M. The syntheses of no-carrier-added and carrier-added ¹⁸F-labelled haloperidol. *J. Labelled Compd. Rad.* **1985**, *22*, 721-733.
54. Seeman, P. Clozapine, a fast-off-D₂ antipsychotic. *ACS Chem. Neurosci.* **2014**, *5*, 24-29.
55. Ballesteros, J. A.; Weinstein, H. Integrated methods for the construction of three-dimensional models and computational probing of structure-function relations in G protein-coupled receptors. In *Methods Neurosci.*, Sealfon, S. C., Ed. Academic Press: 1995; Vol. 25, pp 366-428.
56. Sykes, D. A.; Dowling, M. R.; Charlton, S. J. Exploring the mechanism of agonist efficacy: a relationship between efficacy and agonist dissociation rate at the muscarinic M₃ receptor. *Mol. Pharmacol.* **2009**, *76*, 543-551.
57. Deyrup, M. D.; Nowicki, S. T.; Richards, N. G.; Otero, D. H.; Harrison, J. K.; Baker, S. P. Structure-affinity profile of 8-hydroxycarbostryl-based agonists that dissociate slowly from the beta₂-adrenoceptor. *Naunyn-Schmiedeberg's Arch. Pharmacol.* **1999**, *359*, 168-177.
58. Guo, D.; Mulder-Krieger, T.; Ijzerman, A. P.; Heitman, L. H. Functional efficacy of adenosine A(2A) receptor agonists is positively correlated to their receptor residence time. *Br. J. Pharmacol.* **2012**, *166*, 1846-1859.
59. Mould, R.; Brown, J.; Marshall, F. H.; Langmead, C. J. Binding kinetics differentiates functional antagonism of orexin-2 receptor ligands. *Br. J. Pharmacol.* **2014**, *171*, 351-363.
60. Sykes, D. A.; Charlton, S. J. Slow receptor dissociation is not a key factor in the duration of action of inhaled long-acting beta₂-adrenoceptor agonists. *Br. J. Pharmacol.* **2012**, *165*, 2672-2683.
61. Tresadern, G.; Bartolome, J. M.; Macdonald, G. J.; Langlois, X. Molecular properties affecting fast dissociation from the D₂ receptor. *Bioorg. Med. Chem.* **2011**, *19*, 2231-2241.
62. Vauquelin, G. Cell membranes... and how long drugs may exert beneficial pharmacological activity in vivo. *Br. J. Clin. Pharmacol.* **2016**, *82*, 673-682.
63. Cheng, Y.; Prusoff, W. H. Relationship between the inhibition constant (K₁) and the concentration of inhibitor which causes 50 per cent inhibition (I₅₀) of an enzymatic reaction. *Biochem. Pharmacol.* **1973**, *22*, 3099-3108.

Supplementary Information

Structure-Kinetic Profiling of Haloperidol Analogues at the Human Dopamine D₂ Receptor

Tim J. Fyfe,^{†,‡,§} J. Robert Lane,[‡] Barrie Kellam,[‡] David Sykes,[‡] Ben Capuano,[†] Peter J. Scammells,[†] Steven J. Charlton,^{‡,*} and Shailesh N. Mistry^{‡,*}

[†]Medicinal Chemistry, and [§]Drug Discovery Biology, Monash Institute of Pharmaceutical Sciences, Monash University, Parkville, Victoria 3052, Australia.

[‡]School of Pharmacy, Centre for Biomolecular Sciences, University of Nottingham, Nottingham NG7 2RD, U.K.

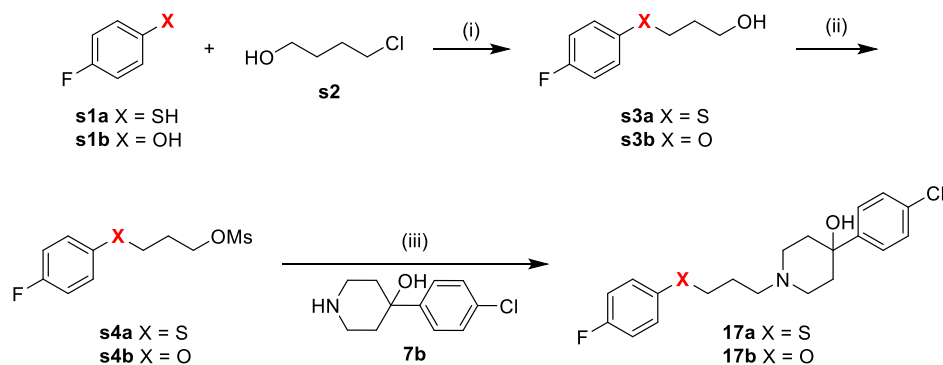
[‡]School of Life Sciences, Queen's Medical Centre, University of Nottingham, Nottingham NG7 2UH, U.K.

Table of Contents

Schemes	Supplementary schemes 1-6.....	284-286
Experimental for intermediates (da-b, f, h-i, l, 13k)	286-288
Figure 1	Determination of PPHT-red equilibrium and kinetic binding parameters.....	289
Figure 2	Plot of observed association rate (k_{on}) with calculated topological polar surface area.....	290
Figures 3-22	¹ H & ¹³ C NMR spectra for representative compounds 8e, 8f, 8i, 14c, 23, 30b, 34c, 36a, 45, 56.....	291-300
Figures 3-22	HPLC/MS traces for representative compounds 8e, 8f, 8i, 14c, 23, 30b, 34c, 36a, 45, 56.....	301-310
References	311

Supplementary Scheme 1. Commercially available 4-chlorobutan-1-ol (**s2**) was subjected to nucleophilic displacement with either 4-fluorobenzenethiol (**s1a**) or 4-fluorophenol (**s1b**) to give primary alcohols **s3a-b** respectively. These compounds were subsequently activated using methanesulfonyl chloride in the presence of Et₃N in DCM at room temperature, affording mesylates **s4a-b**. This was followed by nucleophilic displacement with **7b** using conditions outlined previously, furnishing target analogues **17a-b**.¹

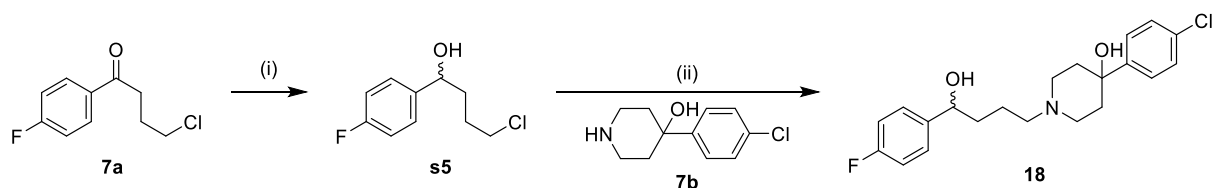
Supplementary Scheme 1. Synthesis of oxygen and sulphur analogues of 1^a



^aReagents and conditions: (i) KI, K₂CO₃, *i*-PrOH, reflux, 3-4 h, 68-83%; (ii) MsCl, Et₃N, DCM, rt, 12 h, 72-81%; (iii) NaHCO₃, KI, toluene, reflux, 24 h, 77-80%.

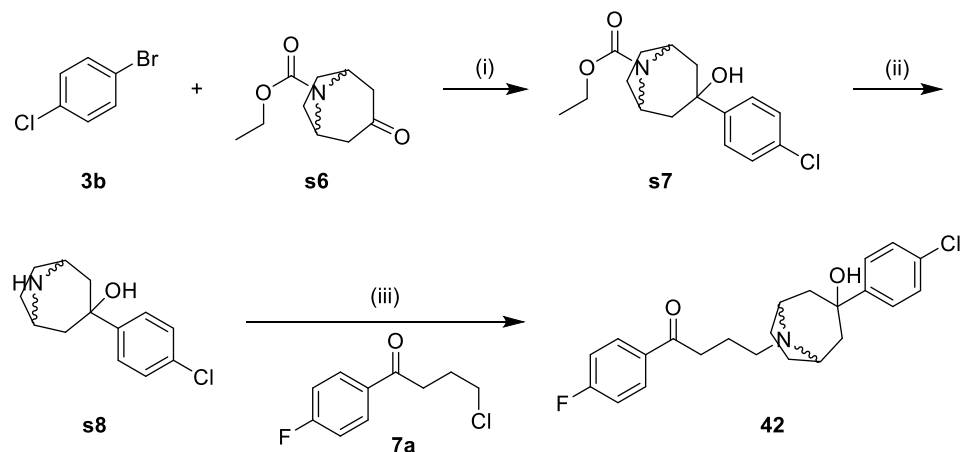
Supplementary Scheme 2. Key intermediate **7a** was treated with sodium borohydride in MeOH to afford 4-chloro-1-(4-fluorophenyl)butan-1-ol (**s5**) in excellent yield. Lastly, *N*-alkylation of **7b** with **s5** using standard conditions afforded final compound **18**.

Supplementary Scheme 2. Synthesis of racemic alcohol analogue of 1^a



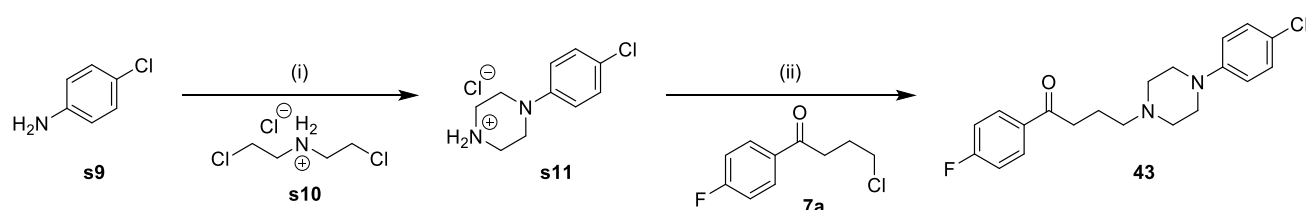
Reagents and conditions: (i) NaBH₄, EtOH, 0 °C – rt, 90%; (ii) NaHCO₃, KI, toluene, reflux, 24 h, 67%.

Supplementary Scheme 3. 4-Bromobenzene (**3b**) was subjected to *n*-butyl lithium-halogen exchange in THF followed by treatment with commercially available *N*-carbethoxy-4-tropinone (**s6**), producing tertiary alcohol (**s7**). Decarbamylation was achieved by heating **s7** in the presence of KOH in ethylene glycol, furnishing the secondary amine (**s8**) after trituration with CH₃Cl₃, followed by *N*-alkylation with **7a** to furnish the desired analogue **42** after preparative chromatography.

Supplementary Scheme 3. Synthesis of bridged analogue of 1^a

^aReagents and conditions: (i) *n*-butyl lithium, THF, -78 °C – rt, 7 h, 54%; (ii) KOH, ethylene glycol, 150 °C, 6 h, 70%; (iii) NaHCO₃, KI, toluene, reflux, 24 h, 65%.

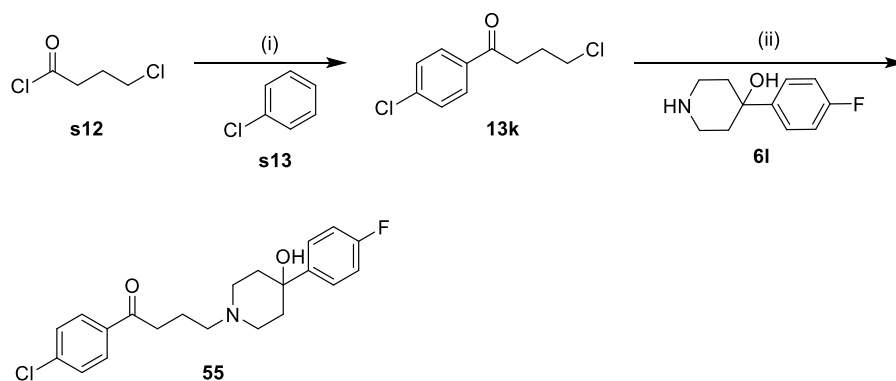
Supplementary Scheme 4. Commercially available 4-chloroaniline (**s9**) was subjected to an intermolecular cyclisation reaction with bis-(2-chloroethylamine)hydrochloride (**s10**) in the presence of catalytic *p*-TsOH in refluxing xylenes, affording the corresponding 4-chlorophenyl piperazine hydrochloride (**s11**) in excellent yield. *N*-alkylation of **s11** with key intermediate **7a** using standard conditions furnished piperazine analogue **43**.

Supplementary Scheme 4. Synthesis of piperazine analogue of 1^a

^aReagents and conditions: (i), *p*-TsOH, xylenes, reflux 16 h, 90%; alkyl halide, NaHCO₃, KI, toluene, reflux, 24 h, 69%.

Supplementary Scheme 5. Friedel Crafts acylation of chlorobenzene (**s13**) with 4-chlorobutanoyl chloride (**s12**) using conditions outlined previously, afforded the 4-chloro-1-(4-chlorophenyl)butan-1-one intermediate (**13k**). Next, *N*-alkylation of **6i** with **7a** using conditions outlined previously afforded **55**.²

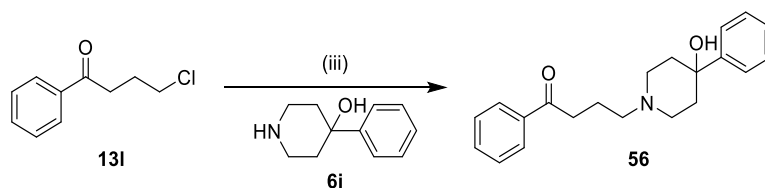
Supplementary Scheme 5. Synthesis of “reverse” analogue of 1^a



^aReagents and conditions: (i) AlCl₃, DCM, 0 °C – rt, 14 h, 91%; (ii) NaHCO₃, KI, toluene, reflux, 24 h, 71-80%; (iii) NaHCO₃, KI, toluene, reflux, 24 h, 74%.

Supplementary Scheme 6. *N*-alkylation of **6i** using the commercially available 4-chloro-1-phenylbutan-1-one (**13l**) using previously outlined conditions, afforded the *des*-halo analogue **56** in good yield.³

Supplementary Scheme 6. Synthesis of *des*-halo analogue of 1^a



^aReagents and conditions: (i) NaHCO₃, KI, toluene, reflux, 24 h, 88%.

Experimental

3-((4-Fluorophenyl)thio)propan-1-ol (s3a). A mixture of 4-fluorothiophenol (1.37 mL, 12.9 mmol), 3-chloropropanol (1.61 mL, 19.3 mmol), KI (107 mg, 644 μmol), K₂CO₃ (3.56 g, 25.8 mmol) in *i*-PrOH (25 mL) was refluxed under N₂ for 1 h. The mixture was diluted with EtOAc (50 mL), and washed with water (100 mL) and brine (50 mL). The organic layer was dried with Na₂SO₄, and filtered. The filtrate was concentrated in vacuo, and the residue was chromatographed on silica eluting with 5:1 petroleum ether/EtOAc to give the desired product as a clear oil (2.10 g, 83%). LCMS (*m/z*):

187.0 [M+H]⁺, *t*_R 2.61 min. ¹H NMR (CDCl₃) δ 7.39 – 7.29 (m, 2H), 7.02 – 6.95 (m, 2H), 3.74 (t, *J* = 6.1 Hz, 2H), 2.97 (t, *J* = 7.1 Hz, 2H), 1.87 (s, 1H), 1.83 (tt, *J* = 7.1, 6.0 Hz, 2H). ¹³C NMR (CDCl₃) δ 161.9 (d, *J* = 246.1 Hz), 132.4 (d, *J* = 8.0 Hz), 131.1 (d, *J* = 3.2 Hz), 116.1 (d, *J* = 21.8 Hz), 61.4, 31.8, 31.7.

3-(4-Fluorophenoxy)propan-1-ol (s3b). A mixture of 4-fluorophenol (3.00 g, 26.8 mmol), 3-chloropropanol (3.36 mL, 40.1 mmol), KI (222 mg, 1.34 mmol), K₂CO₃ (7.40 g, 53.5 mmol) in *i*-PrOH was refluxed under N₂ for 4 h. The mixture was diluted with EtOAc, and washed with water (200 mL) and brine (50 mL). The organic layer was dried with Na₂SO₄, and filtered. The filtrate was concentrated in vacuo, and the residue was chromatographed on silica eluting with 5:1 petroleum ether/EtOAc to give the desired product as a pink oil (3.10 g, 68%). LCMS (*m/z*): 171.1 [M + H]⁺, *t*_R 2.73 min. ¹H NMR (CDCl₃) δ 7.02 – 6.90 (m, 2H), 6.89 – 6.78 (m, 2H), 4.06 (t, *J* = 6.0 Hz, 2H), 3.84 (t, *J* = 5.9 Hz, 2H), 2.07 (s, 1H), 2.02 (p, *J* = 5.9 Hz, 2H). ¹³C NMR (CDCl₃) δ 157.4 (d, *J* = 238.4 Hz), 155.0 (d, *J* = 2.2 Hz), 115.9 (d, *J* = 23.1 Hz), 115.6 (d, *J* = 7.9 Hz), 66.4, 60.4, 32.1.

3-((4-Fluorophenyl)thio)propyl methanesulfonate (s4a). General procedure G. Purification by FCC (eluent 10:1, PE/EtOAc) gave 2.56 g of a yellow oil (72%). LCMS (*m/z*): 265.1 [M+H]⁺, *t*_R 2.81 min. ¹H NMR (CDCl₃) δ 7.02 – 6.91 (m, 2H), 6.88 – 6.78 (m, 2H), 4.43 (t, *J* = 6.1 Hz, 2H), 4.04 (t, *J* = 5.9 Hz, 2H), 2.99 (s, 3H), 2.21 (p, *J* = 6.0 Hz, 2H). ¹³C NMR (CDCl₃) δ 154.5 (d, *J* = 238.7 Hz), 151.7 (d, *J* = 2.1 Hz), 113.0 (d, *J* = 23.1 Hz), 112.6 (d, *J* = 8.0 Hz), 63.8, 60.9, 34.4, 26.3.

3-(4-Fluorophenoxy)propyl methanesulfonate (s4b). General procedure G. Purification by FCC (eluent 10:1, PE/EtOAc) gave 2.35 g of a pink oil (81%). LCMS (*m/z*): 249.1 [M+H]⁺, *t*_R 2.73 min. ¹H NMR (CDCl₃) δ 7.39 – 7.32 (m, 2H), 7.04 – 6.96 (m, 2H), 4.34 (t, *J* = 6.0 Hz, 2H), 3.00 (s, 3H), 2.97 (t, *J* = 7.0 Hz, 2H), 2.01 (tt, *J* = 7.0, 6.0 Hz, 2H). ¹³C NMR (CDCl₃) δ 162.2 (d, *J* = 247.1 Hz), 133.0 (d, *J* = 8.1 Hz), 130.2 (d, *J* = 3.4 Hz), 116.3 (d, *J* = 21.9 Hz), 68.0, 37.5, 31.2, 28.7.

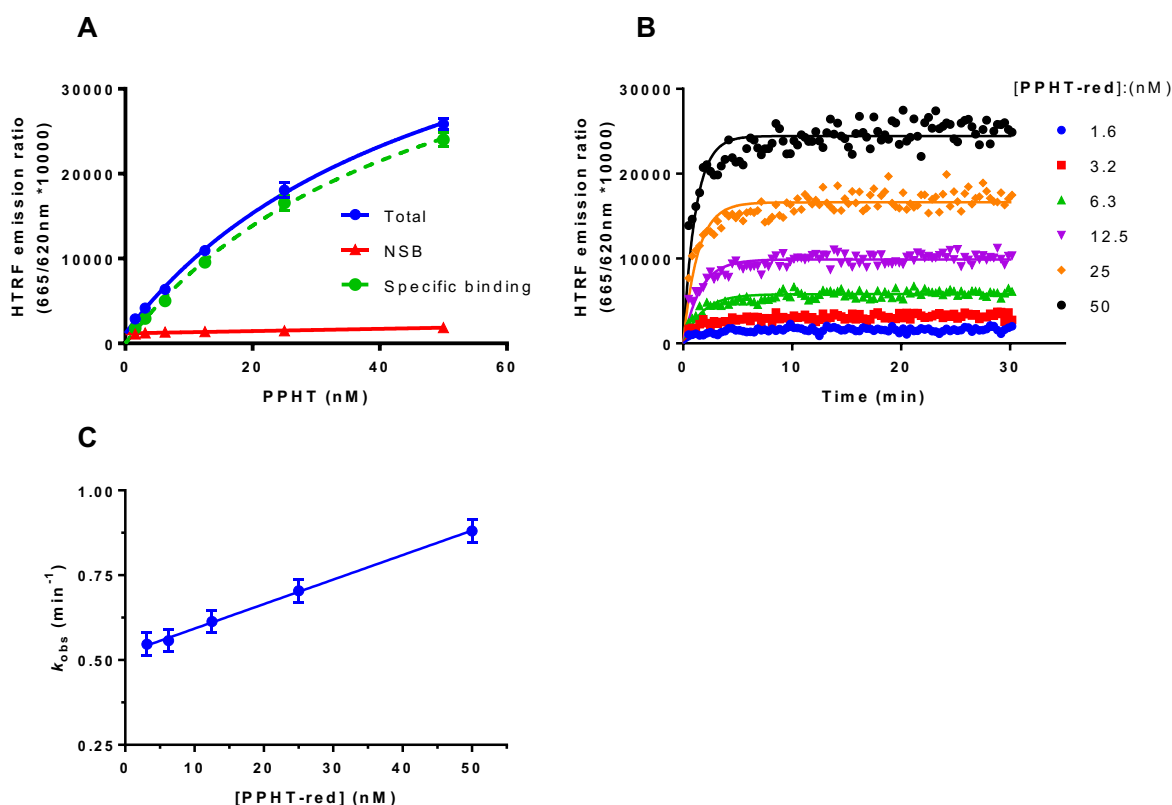
4-Chloro-1-(4-fluorophenyl)butan-1-ol (s5). NaBH₄ (245 mg, 6.48 mmol) was added to a solution of 4-chloro-1-(4-fluorophenyl)butan-1-one (1.00 g, 4.98 mmol) in EtOH (20 mL) at 0 °C. The mixture was stirred at room temperature for 3 h. The mixture was quenched with H₂O (5 mL) and evaporated to remove the organic portion. The residue was diluted with saturated aqueous NaHCO₃ solution and extracted with DCM (3 × 20 mL). The DCM extracts were washed with brine (20 mL), and evaporated to dryness to afford 947 mg of a yellow oil (94%). LCMS (*m/z*): 203.1 [M+H]⁺, *t*_R 3.62 min. ¹H NMR (CDCl₃) δ 7.34 – 7.25 (m, 2H), 7.03 (t, *J* = 8.7 Hz, 2H), 4.68 (t, *J* = 6.1 Hz, 1H), 3.54 (td, *J* = 6.0, 2.2 Hz, 2H), 2.14 (d, *J* = 2.9 Hz, 1H), 1.96 – 1.69 (m, 4H). ¹³C NMR (CDCl₃) δ 162.3 (d, *J* = 245.7 Hz), 140.2 (d, *J* = 3.1 Hz), 127.6 (d, *J* = 8.1 Hz), 115.5 (d, *J* = 21.4 Hz), 73.3, 45.0, 36.4, 28.9.

Ethyl 3-(4-chlorophenoxy)-8-azabicyclo[3.2.1]octane-8-carboxylate (s7). General procedure A. Purification by FCC (eluent, 1:5 EtOAc/PE) gave 750 mg of a transparent oil (65%). LCMS (*m/z*): 310.1 [M+H]⁺, *t_R* 2.85 min. ¹H NMR (CDCl₃) δ 7.33-7.26 (m, 4H), 4.38 (s, 2H), 4.17 (q, *J* = 6.8 Hz, 2H), 2.30-1.73 (m, 8H), 1.27 (t, *J* = 7.2 Hz, 3H). ¹³C NMR (CDCl₃) δ 154.2, 148.3, 132.8, 128.5, 126.1, 73.4, 61.2, 53.4, 45.0, 28.3, 14.9.

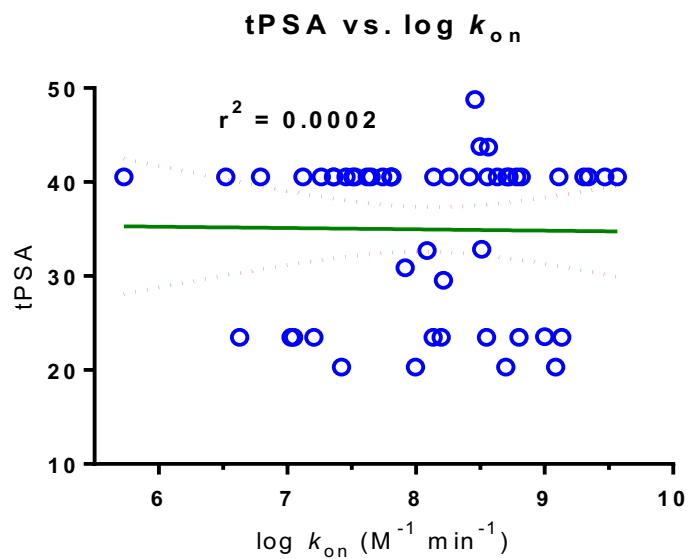
3-(4-Chlorophenyl)-8-azabicyclo[3.2.1]octan-3-ol (s8). A mixture of KOH (870 mg, 15.5 mmol) in ethylene glycol (5 mL) was added to a solution of ethyl 3-(4-chlorophenyl)-3-hydroxy-8-azabicyclo[3.2.1]octane-8-carboxylate (600 mg, 1.94 mmol) in MeOH (5 mL) and the resulting mixture was heated at 150 °C, with constant stirring, for 4 h and then allowed to cool to room temperature. H₂O (50 mL) was added, and the mixture was extracted with EtOAc (3 × 30 mL). The organic phases were combined, washed with H₂O (100 mL), brine (50 mL) and dried (Na₂SO₄). The organic phase was filtered, and the filtrate was concentrated in vacuo and the residue was purified by FCC (eluent, 4:2 CH₂Cl₂/MeOH) to give 310 mg of white-yellow crystals (310 mg, 67%). LCMS (*m/z*): 238.0 [M+H]⁺, *t_R* 1.00 min. ¹H NMR (Methanol-*d*₄) δ 7.50 – 7.46 (m, 2H), 7.29 – 7.25 (m, 2H), 3.59 – 3.53 (m, 2H), 2.37 – 2.29 (m, 2H), 2.18 (d, *J* = 3.8 Hz, 1H), 2.15 (d, *J* = 3.8 Hz, 1H), 1.85 – 1.76 (m, 4H). ¹³C NMR (Methanol-*d*₄) δ 151.1, 133.0, 128.8, 127.7, 73.8, 55.4, 46.4, 29.6.

4-(4-Chlorophenyl)piperazin-1-ium chloride (s11). The mixture of 4-chloroaniline (1.10 g, 8.62 mmol), bis-(2-chloroethylamine)hydrochloride (1.47 g, 8.21 mmol) and *para*-toluenesulphonic acid (PTSA) (70.7 mg, 411 μmol) in xylene (15 mL) were heated to reflux for 16 h. The mixture was cooled to room temperature to crystallise. The crystals were collected under vacuum filtration and washed with hot acetone to afford 1.72 g of a white solid (90%). LCMS (*m/z*): 197.2 [M+H]⁺, *t_R* 1.13 min. ¹H NMR (DMSO-*d*₆) δ 9.47 (s, 2H), 7.27 (d, *J* = 8.9 Hz, 2H), 7.02 – 6.95 (m, 2H), 3.37 (t, *J* = 5.1 Hz, 4H), 3.17 (t, *J* = 5.1 Hz, 4H). ¹³C NMR (DMSO-*d*₆) δ 148.9, 128.8, 123.5, 117.5, 45.2, 42.3, 35.9, 25.2, 17.2.

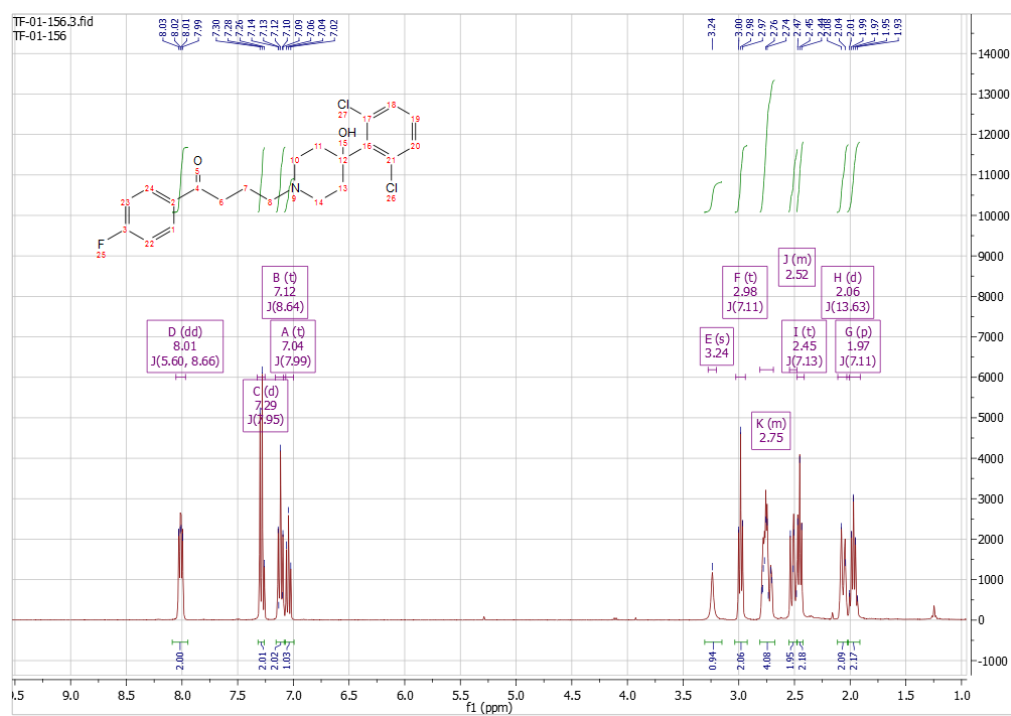
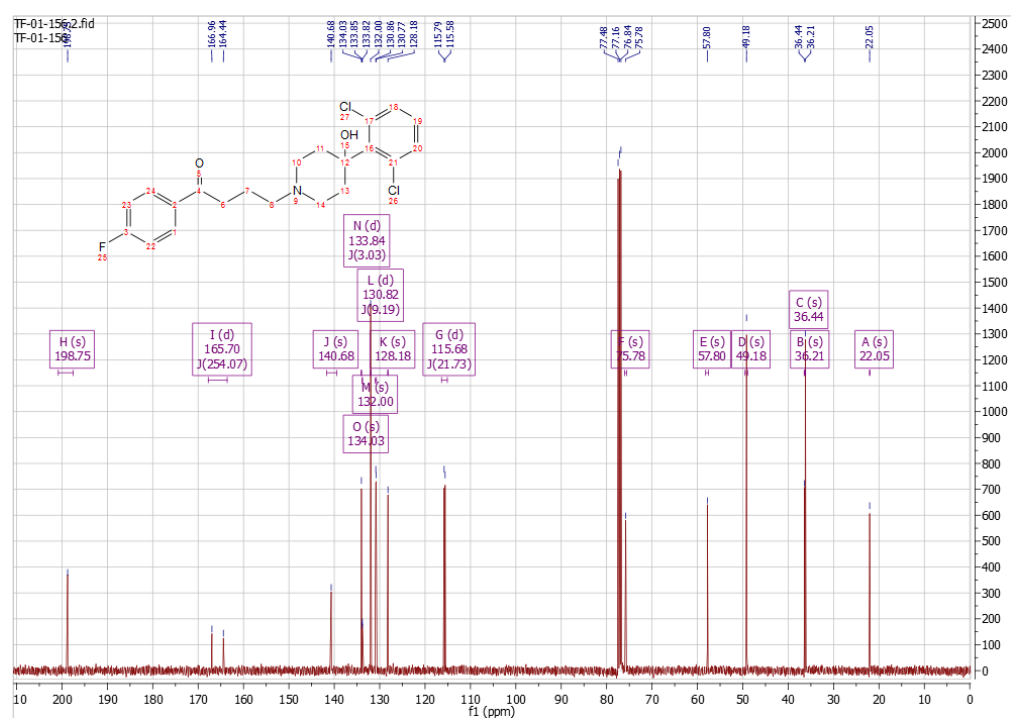
4-Chloro-1-(4-chlorophenyl)butan-1-one (13k). To a stirred suspension of AlCl₃ (3.16 g, 23.7 mmol) in DCM (75 mL) at 0 °C was added chlorobenzene (2.00 mL, 19.7 mmol) drop-wise. After 30 minutes, 4-chlorobutanoyl chloride (2.65 mL, 23.7 mmol) was added drop-wise. The reaction was brought to room temperature and stirred overnight, poured out on ice and extracted with DCM (2 × 40 mL). The organic fractions were collected and washed with sat. aqueous NaHCO₃, H₂O, dried (Na₂SO₄), filtered, and the solvent removed in vacuo. The residue was purified by FCC (eluent, 1:99 PE/EtOAc) to afford 3.90 g of a light brown oil (91%). LCMS (*m/z*): 218.3 [M+H]⁺, *t_R* 2.91 min. ¹H NMR (CDCl₃) δ 7.90 (d, *J* = 8.6 Hz, 2H), 7.43 (d, *J* = 8.6 Hz, 2H), 3.66 (t, *J* = 6.2 Hz, 2H), 3.14 (t, *J* = 7.0 Hz, 2H), 2.21 (p, *J* = 6.8 Hz, 2H). ¹³C NMR (CDCl₃) δ 197.8, 139.7, 135.1, 129.5, 129.1, 44.7, 35.4, 26.7.

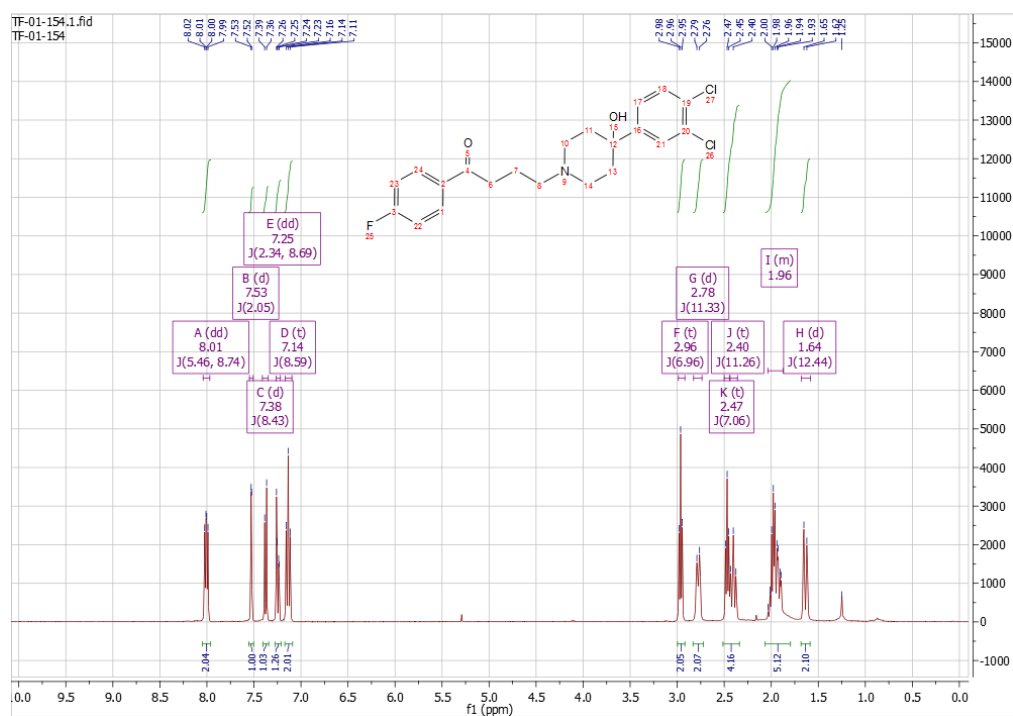
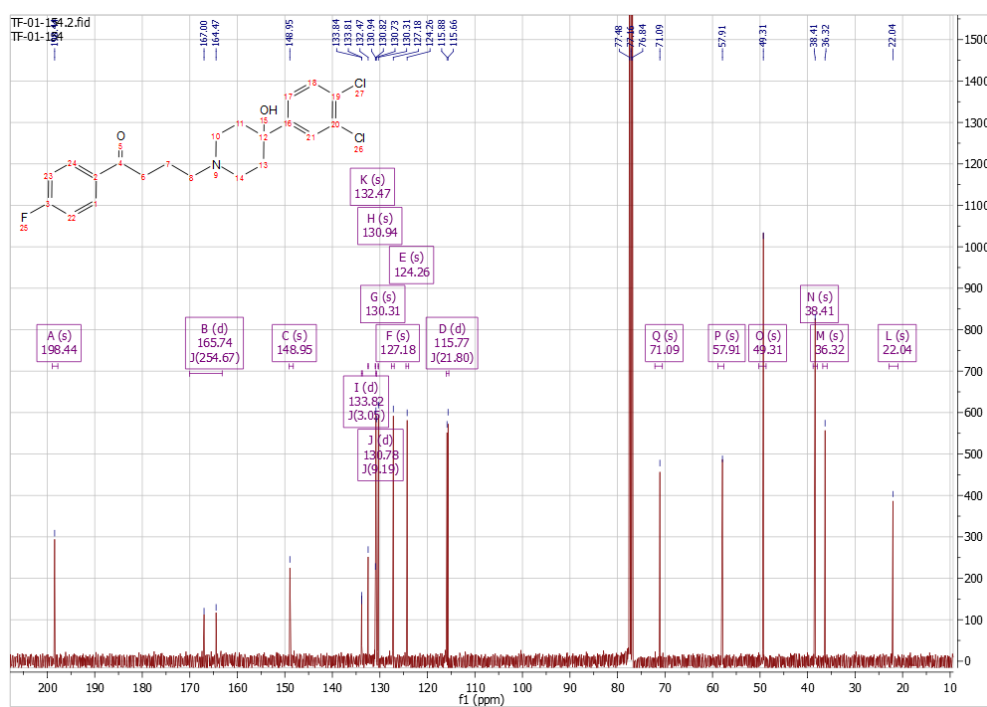


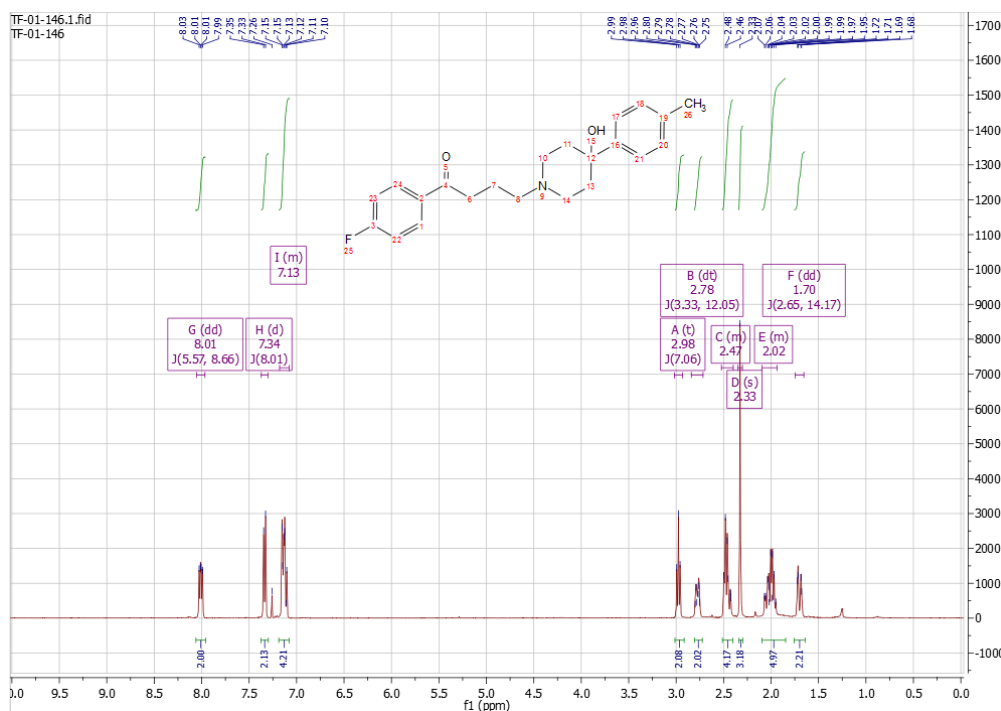
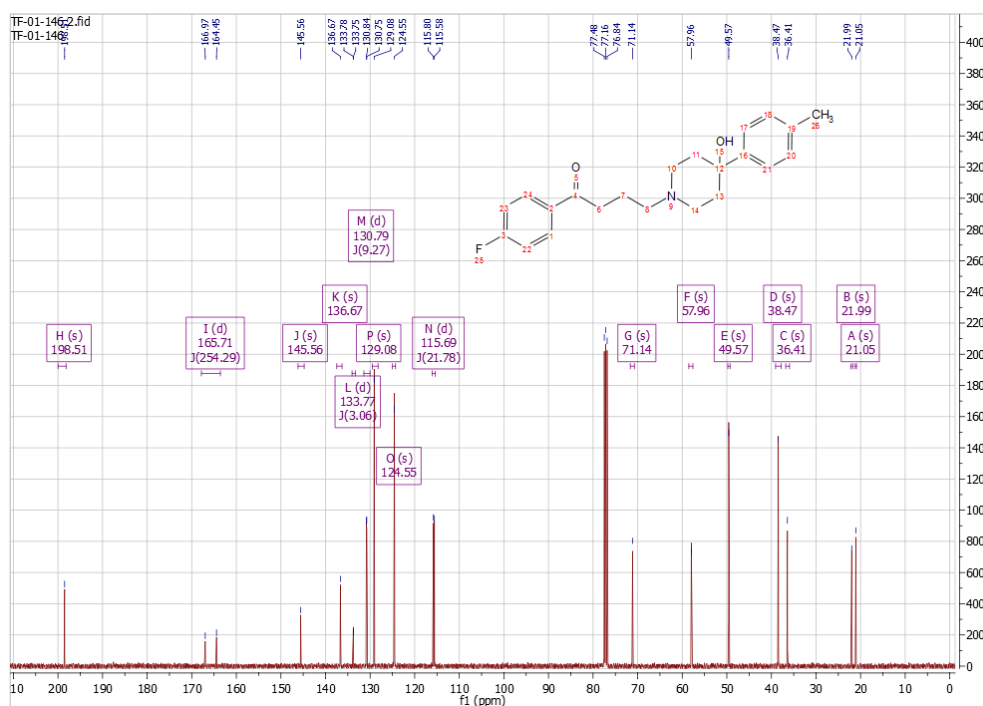
Supplementary Figure 1. Determination of PPHT-red equilibrium and kinetic binding parameters. (A) Saturation analysis showing the binding of PPHT-red to the human dopamine D₂R. CHO-hD₂L_R cell membranes (2 μ g per well) were incubated for 30 min with increasing concentrations of PPHT-red. Data are presented in singlet form from a representative of four experiments. (B) Observed association of PPHT-red binding to the hD₂L_R. Data are presented in singlet form from a representative of four experiments. (C) Plot of PPHT-red concentration vs. k_{obs} . Binding followed a simple law of mass action model, k_{obs} increasing in a linear manner with fluorescent ligand concentration. Data are presented as mean \pm S.E.M. from a total of four experiments. All binding reactions were performed in the presence of GppNHp (100 μ M with non-specific binding levels determined by inclusion of haloperidol (10 μ M)).

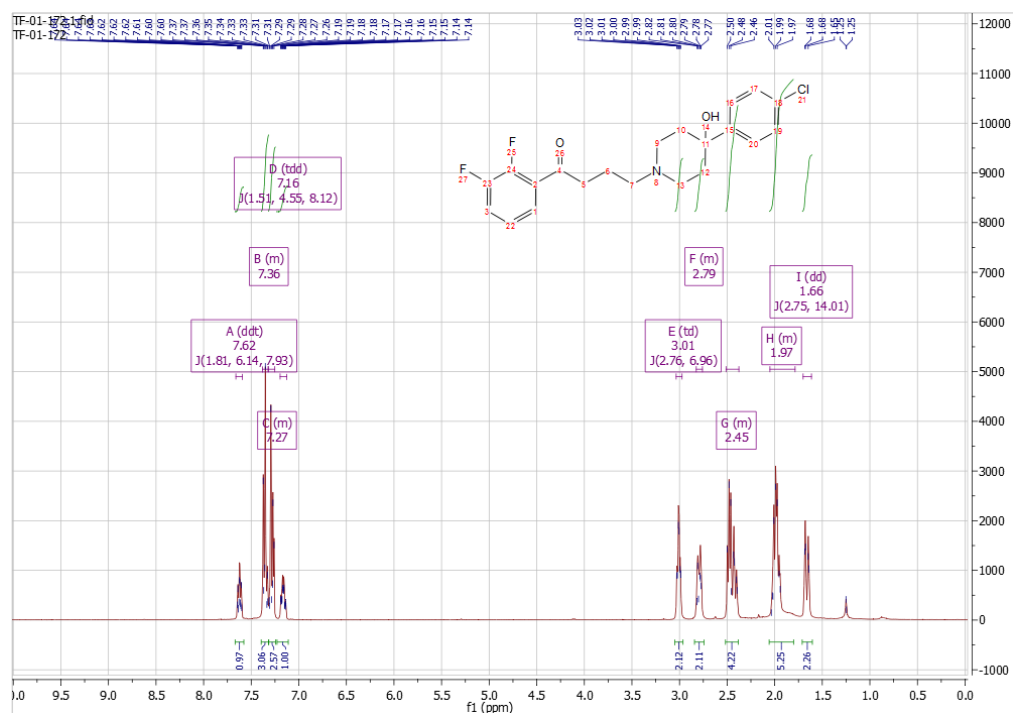
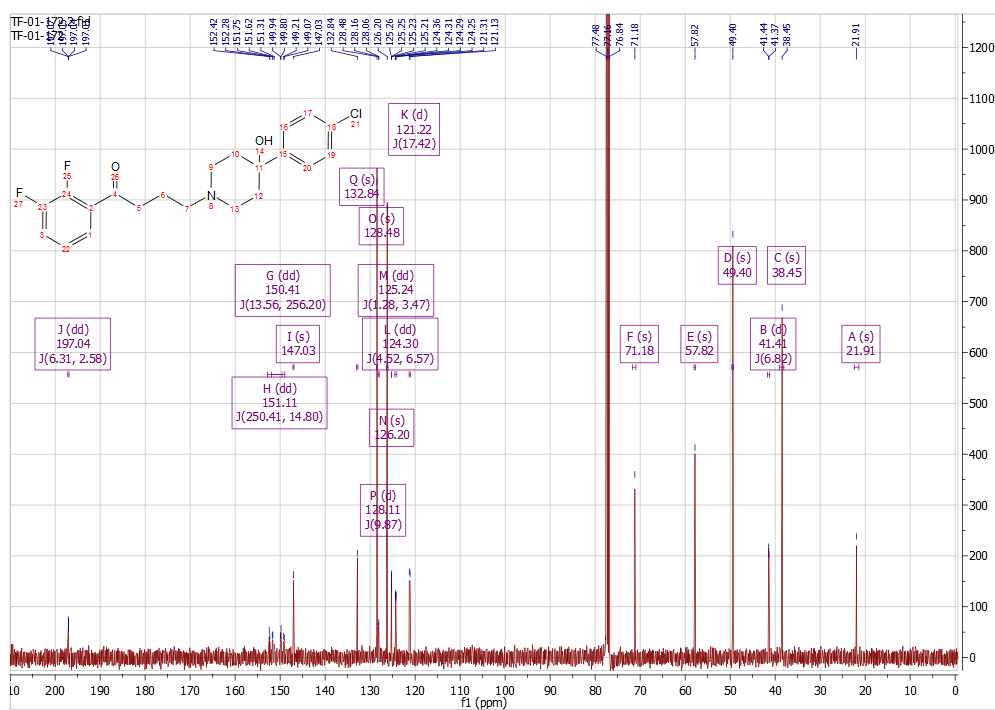


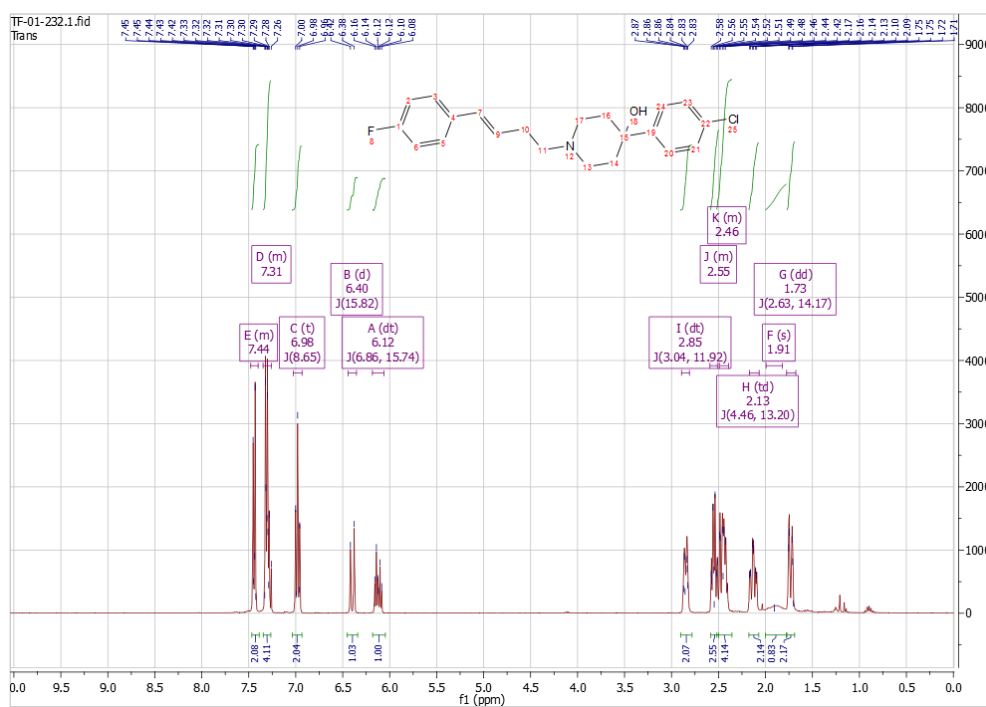
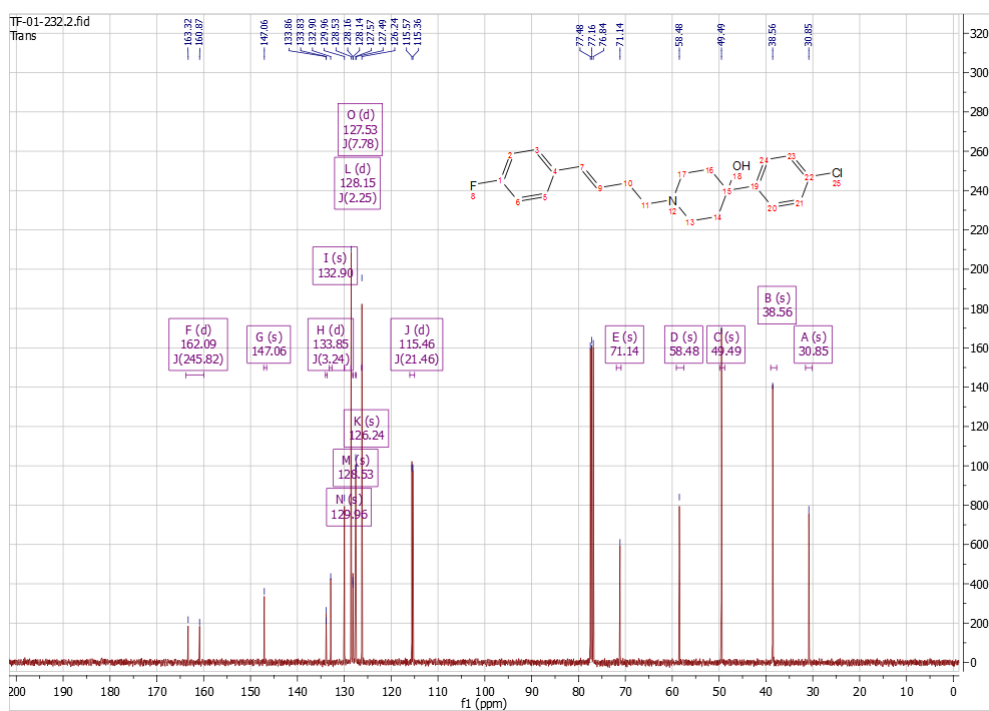
Supplementary Figure 2. Correlating the observed association rate ($\log k_{on}$) and topological polar surface area.

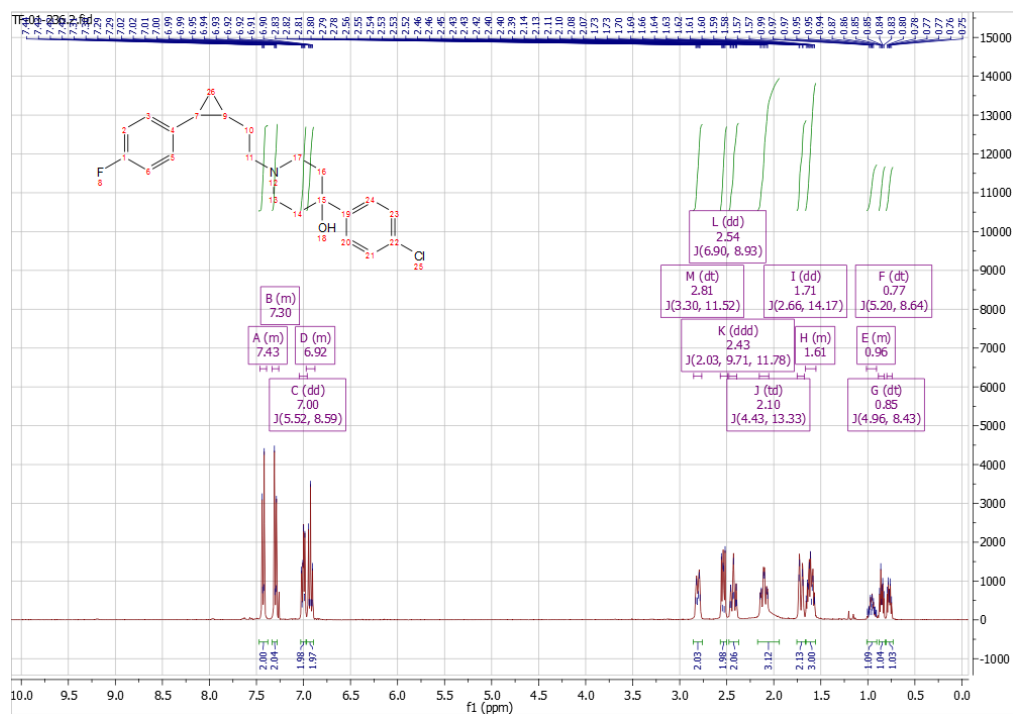
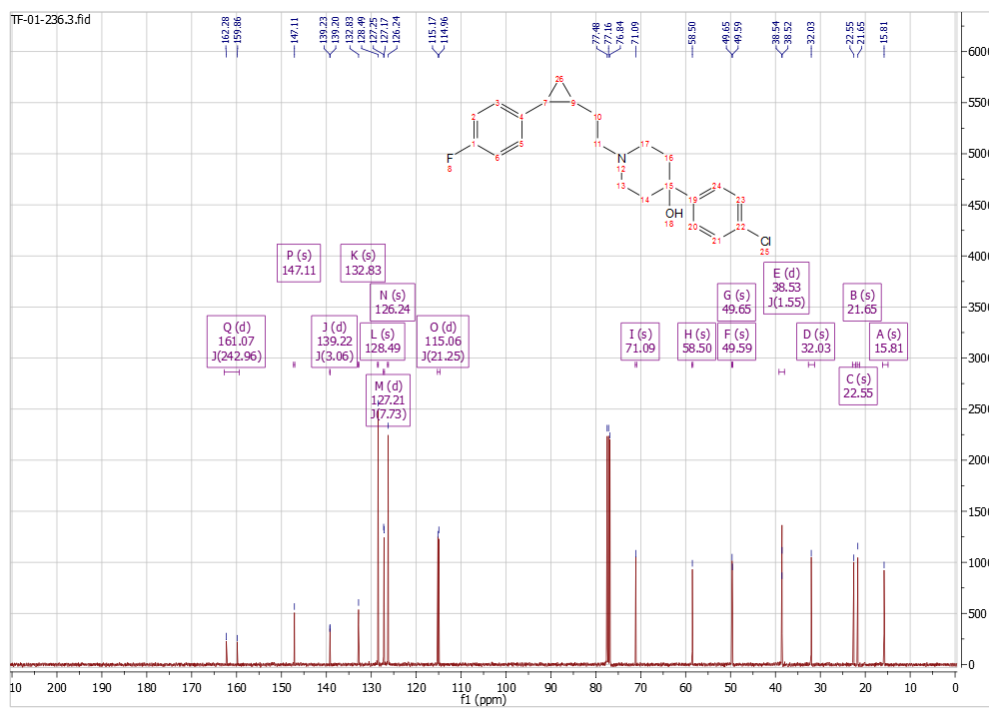
Supplemental Figure 3. ¹H NMR spectrum for compound 8e.Supplemental Figure 4. ¹³C NMR spectrum for compound 8e.

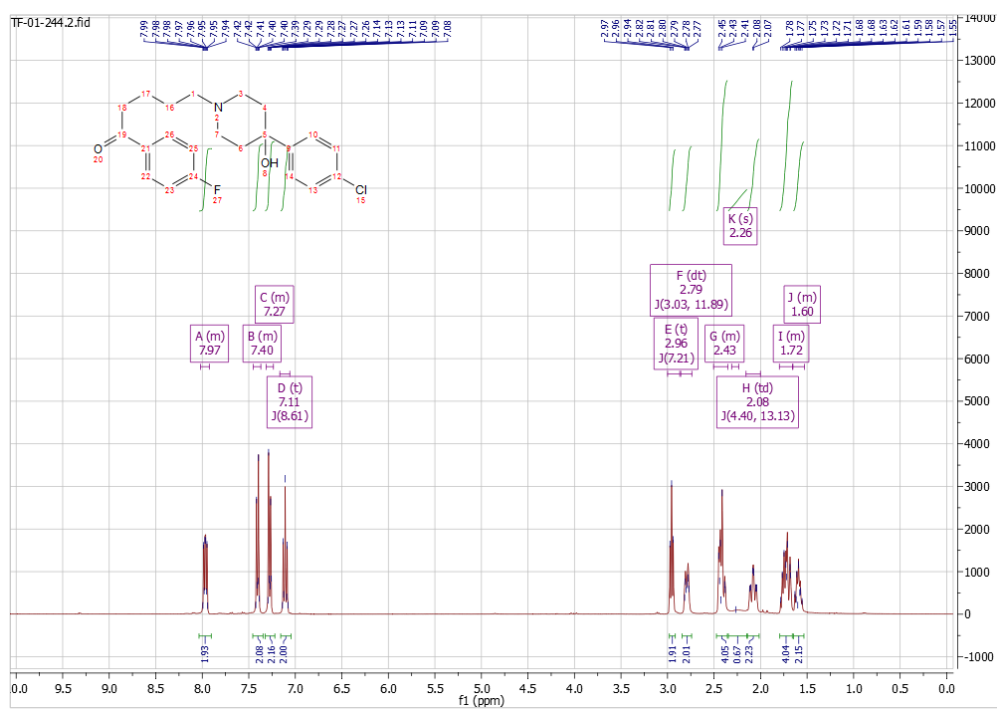
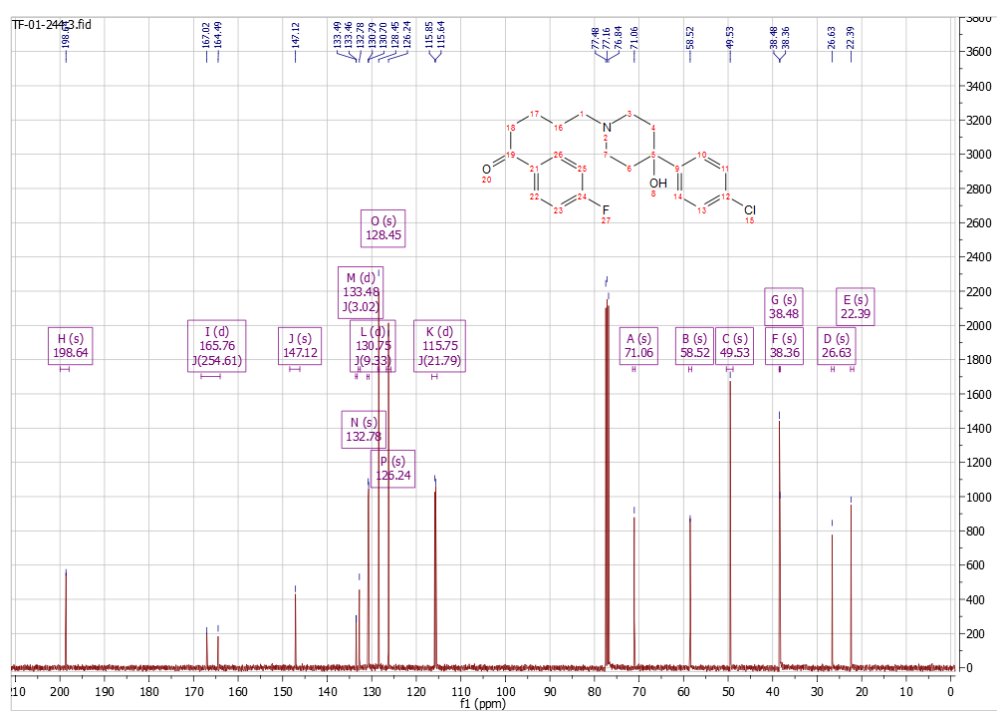
Supplemental Figure 5. ¹H NMR spectrum for compound 8f.Supplemental Figure 6. ¹³C NMR spectrum for compound 8f.

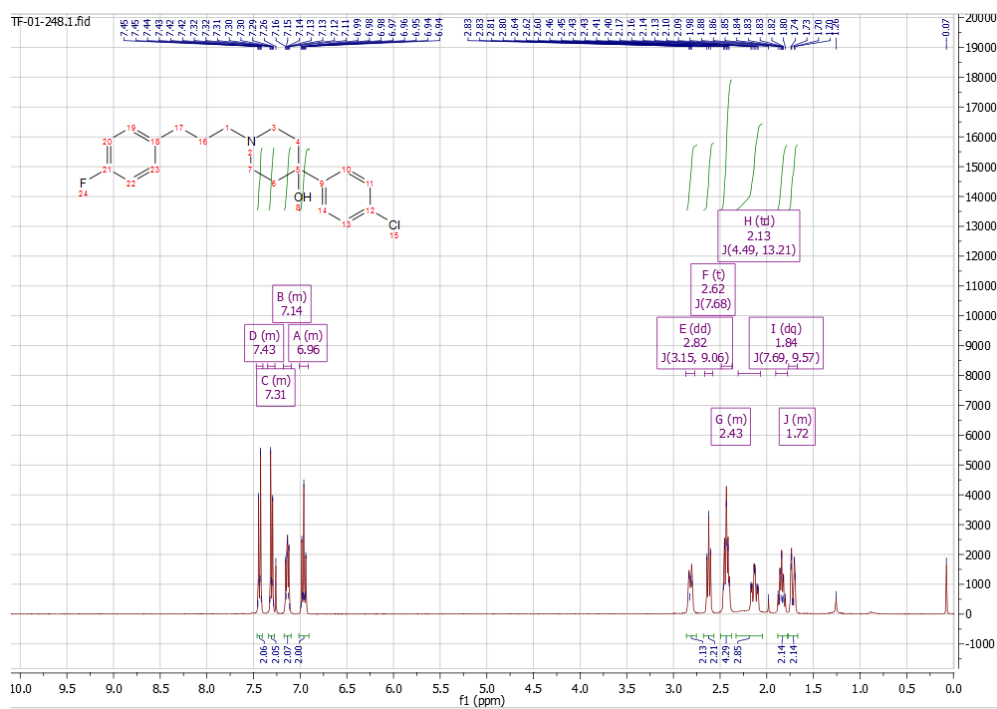
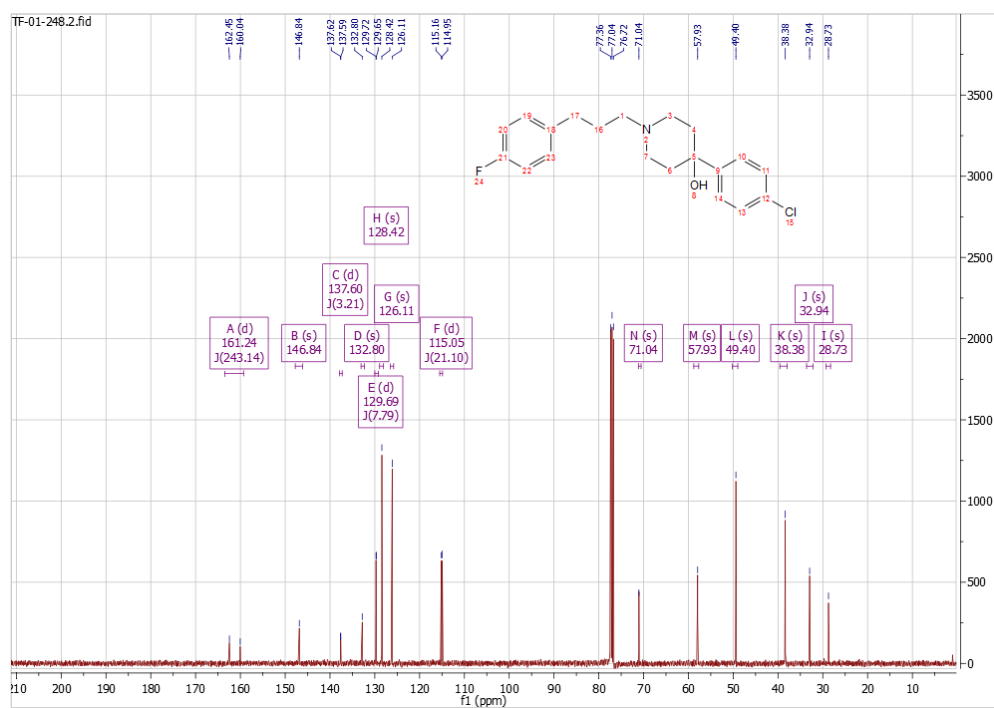
Supplemental Figure 7. ¹H NMR spectrum for compound 8i.Supplemental Figure 8. ¹³C NMR spectrum for compound 8i.

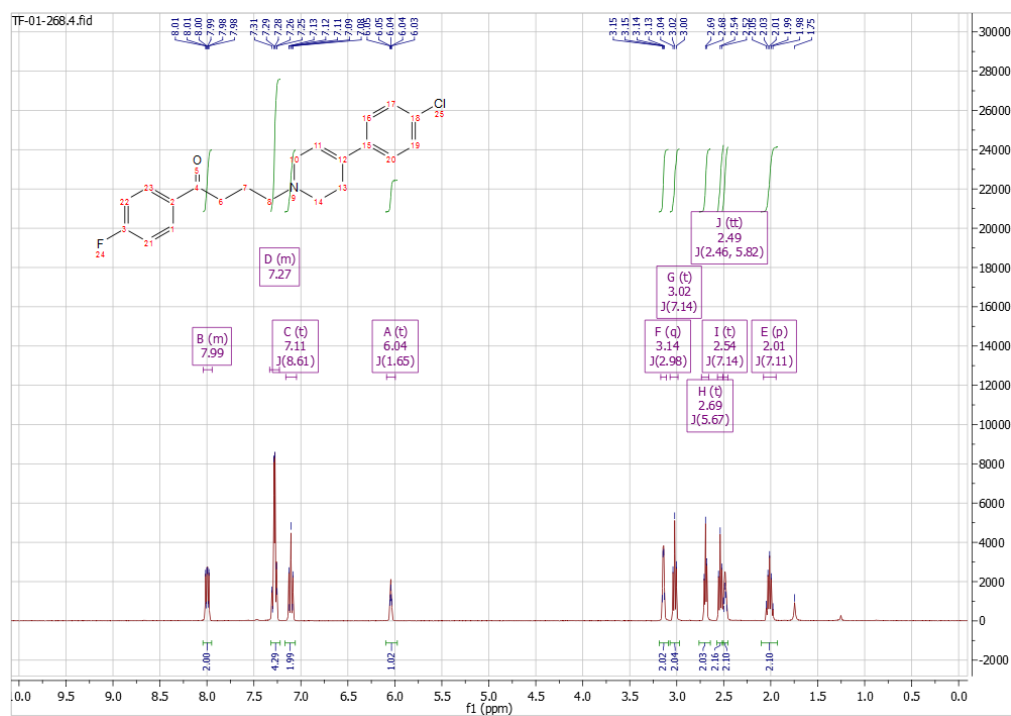
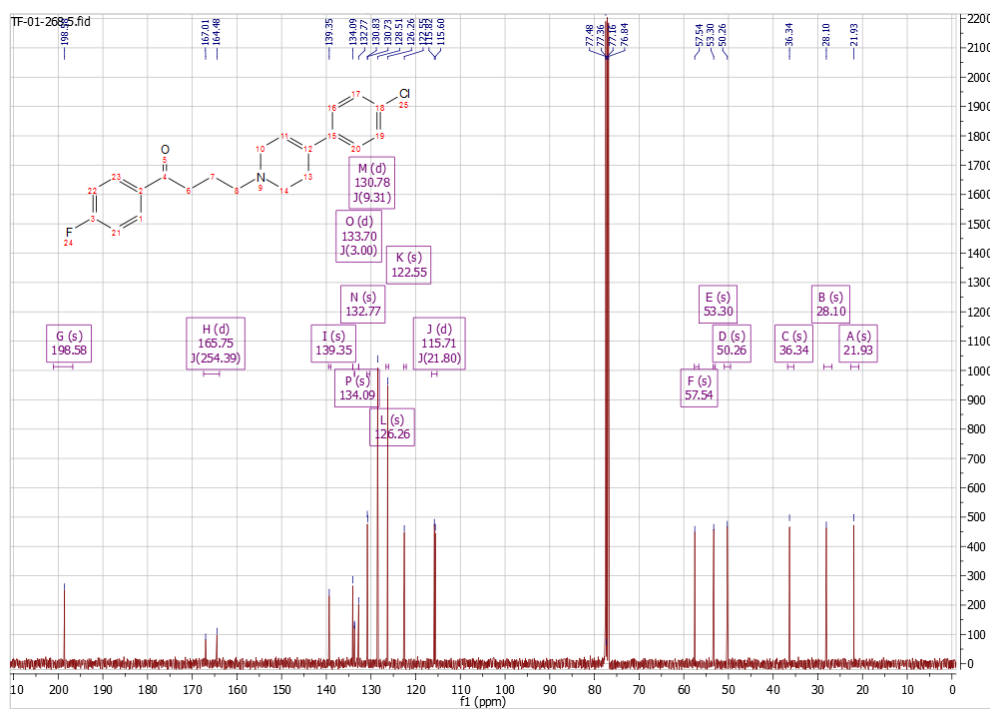
Supplemental Figure 9. ¹H NMR spectrum for compound 14c.Supplemental Figure 10. ¹³C NMR spectrum for compound 14c.

Supplemental Figure -11. ¹H NMR spectrum for compound 23.Supplemental Figure 12. ¹H NMR spectrum for compound 23.

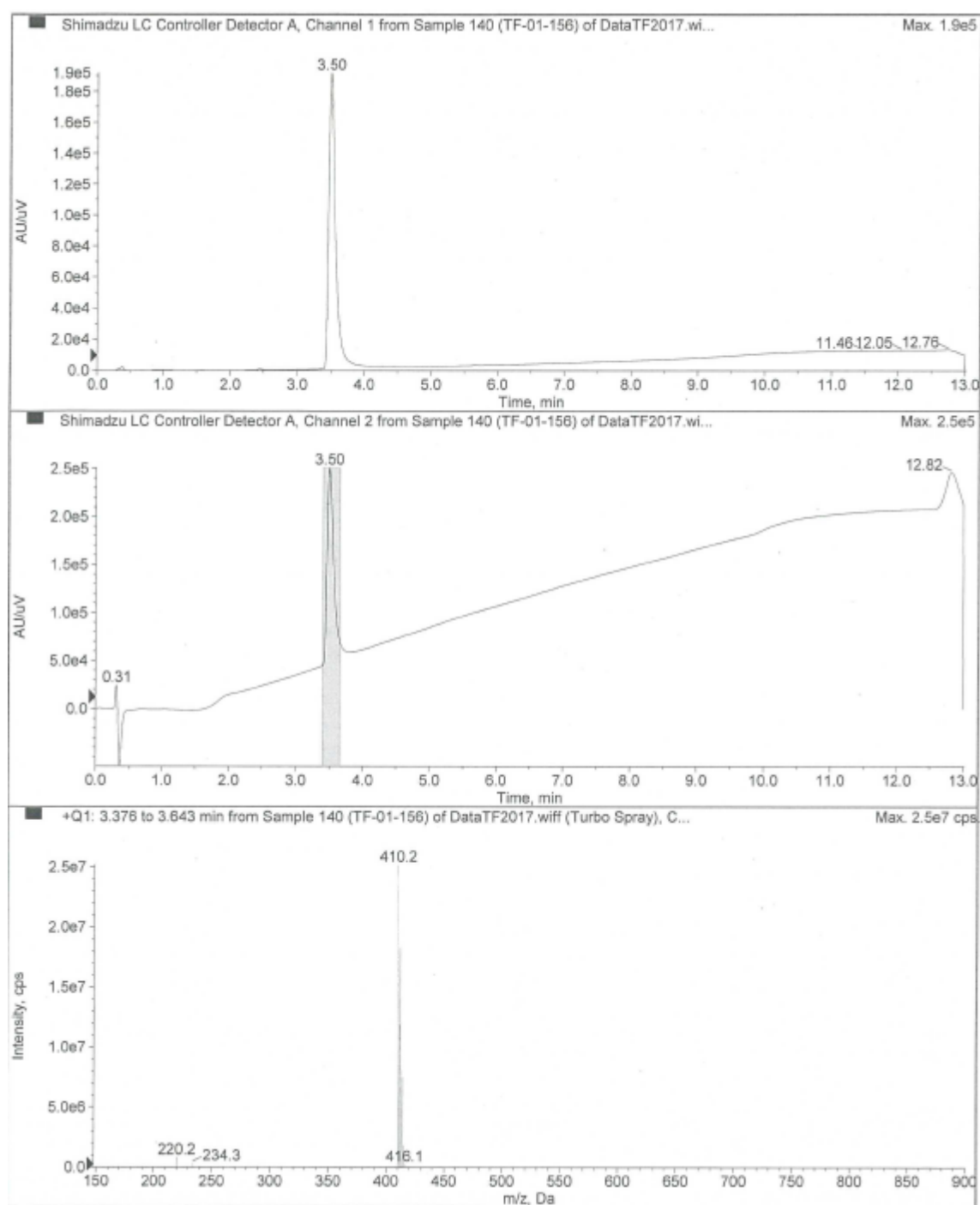
Supplemental Figure 13. ¹H NMR spectrum for compound 30b.Supplemental Figure 14. ¹³C NMR spectrum for compound 30b.

Supplemental Figure 15. ¹H NMR spectrum for compound 34c.Supplemental Figure 16. ¹³C NMR spectrum for compound 34c.

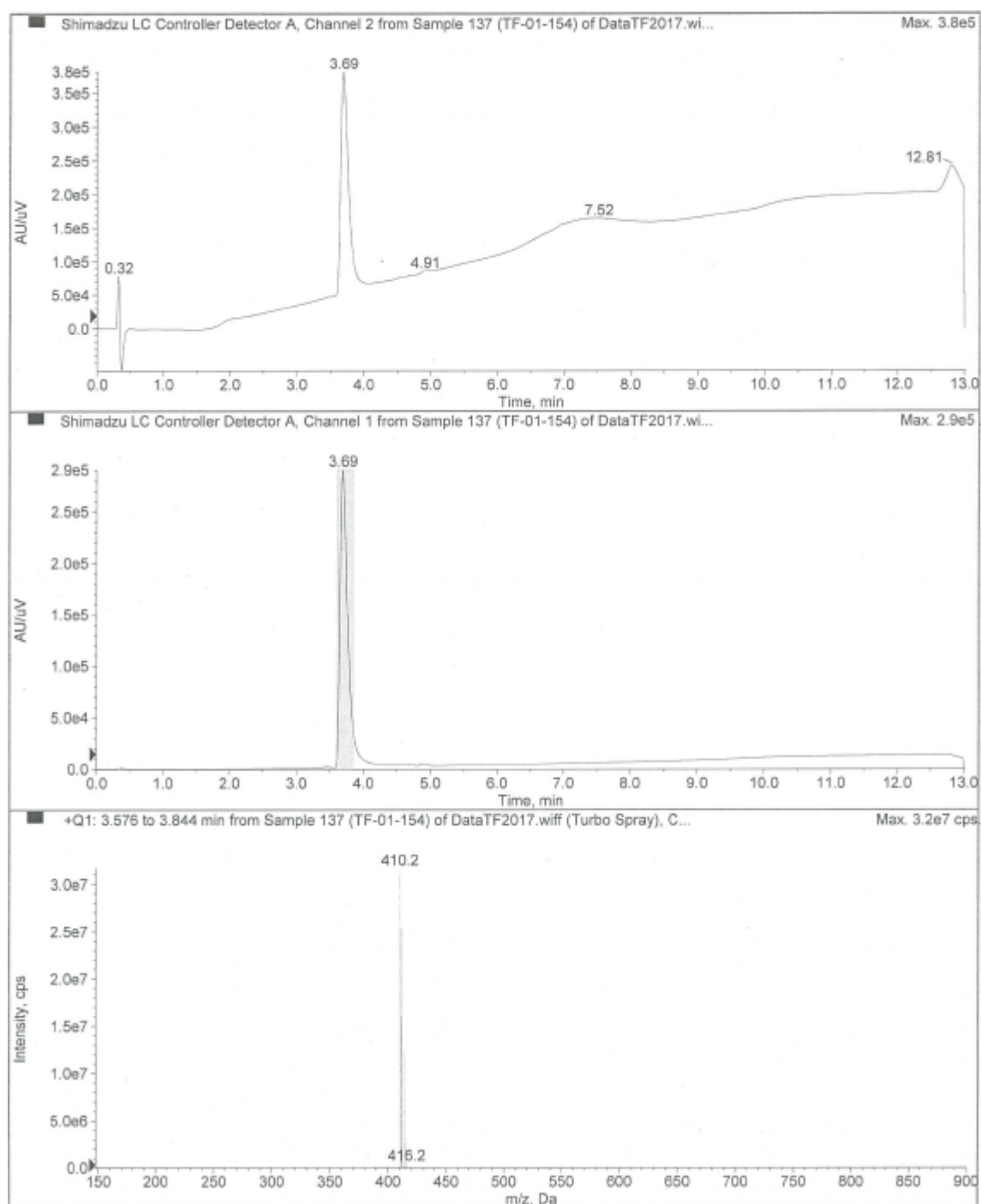
Supplemental Figure 17. ¹H NMR spectrum for compound 36a.Supplemental Figure 18. ¹³C NMR spectrum for compound 34c.

Supplemental Figure 19. ¹H NMR spectrum for compound 45.Supplemental Figure 20. ¹³C NMR spectrum for compound 45.

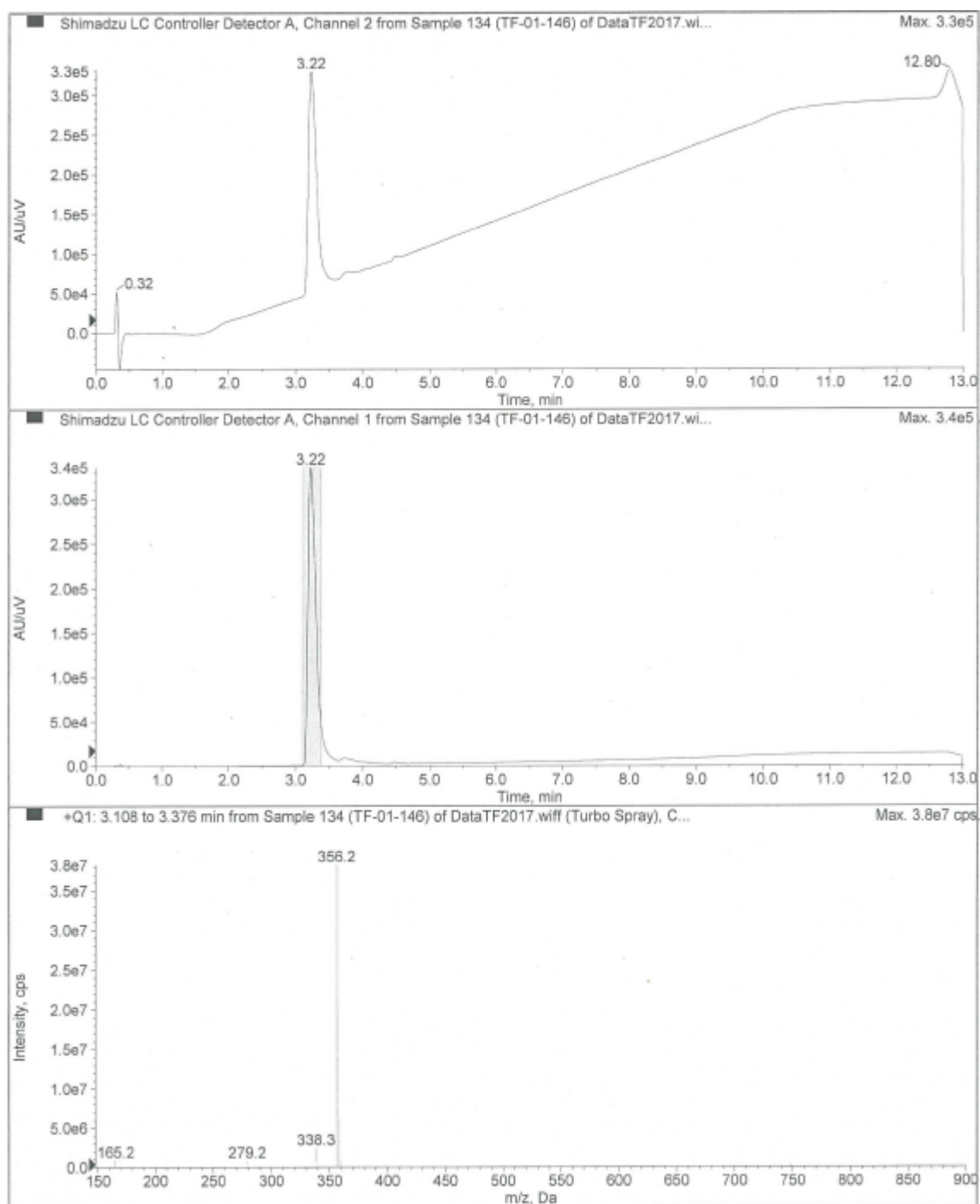
Supplemental Figure 23. Analytical HPLC/MS trace for compound 8e.



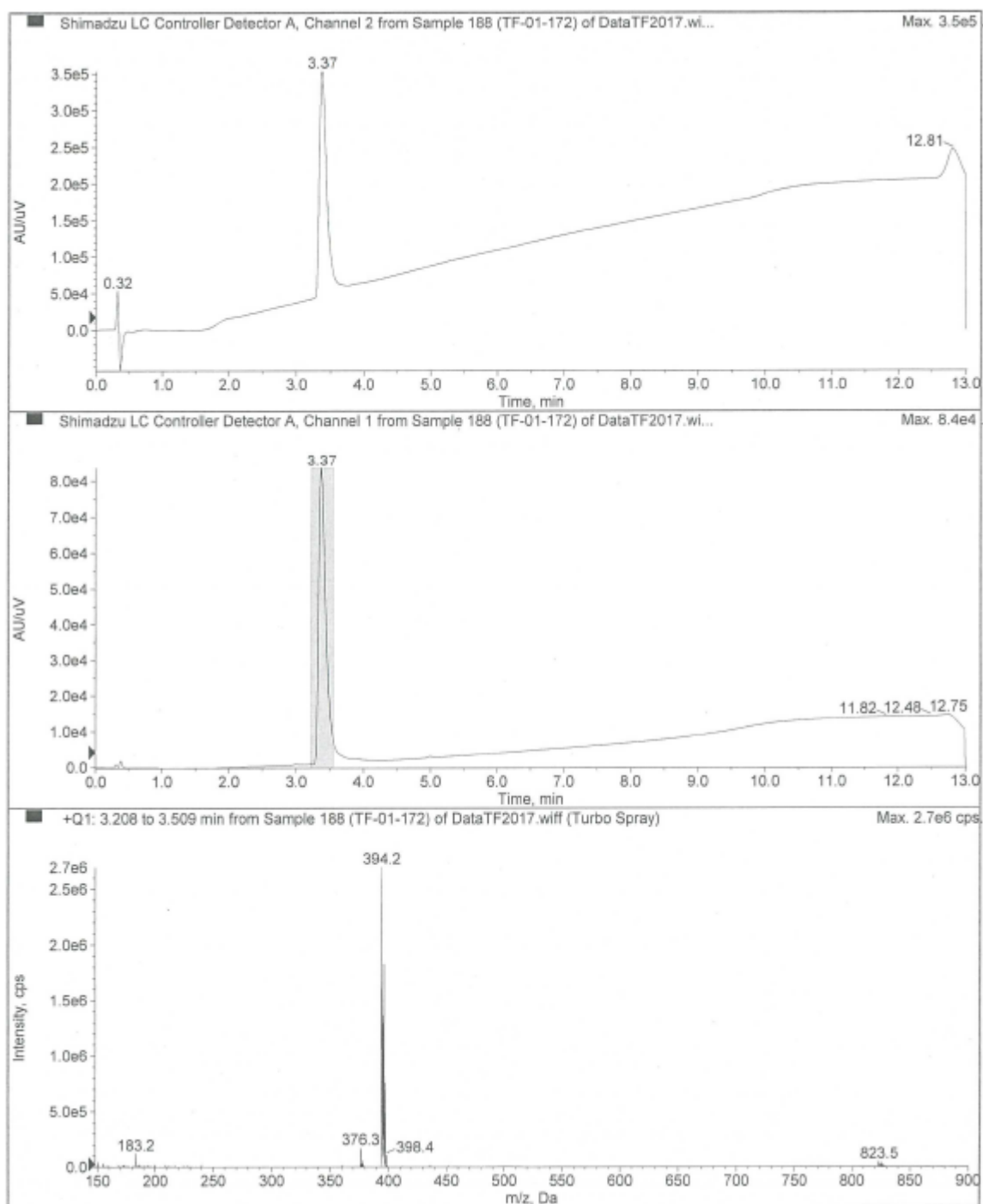
Supplemental Figure 24. Analytical HPLC/MS trace for compound 8f.



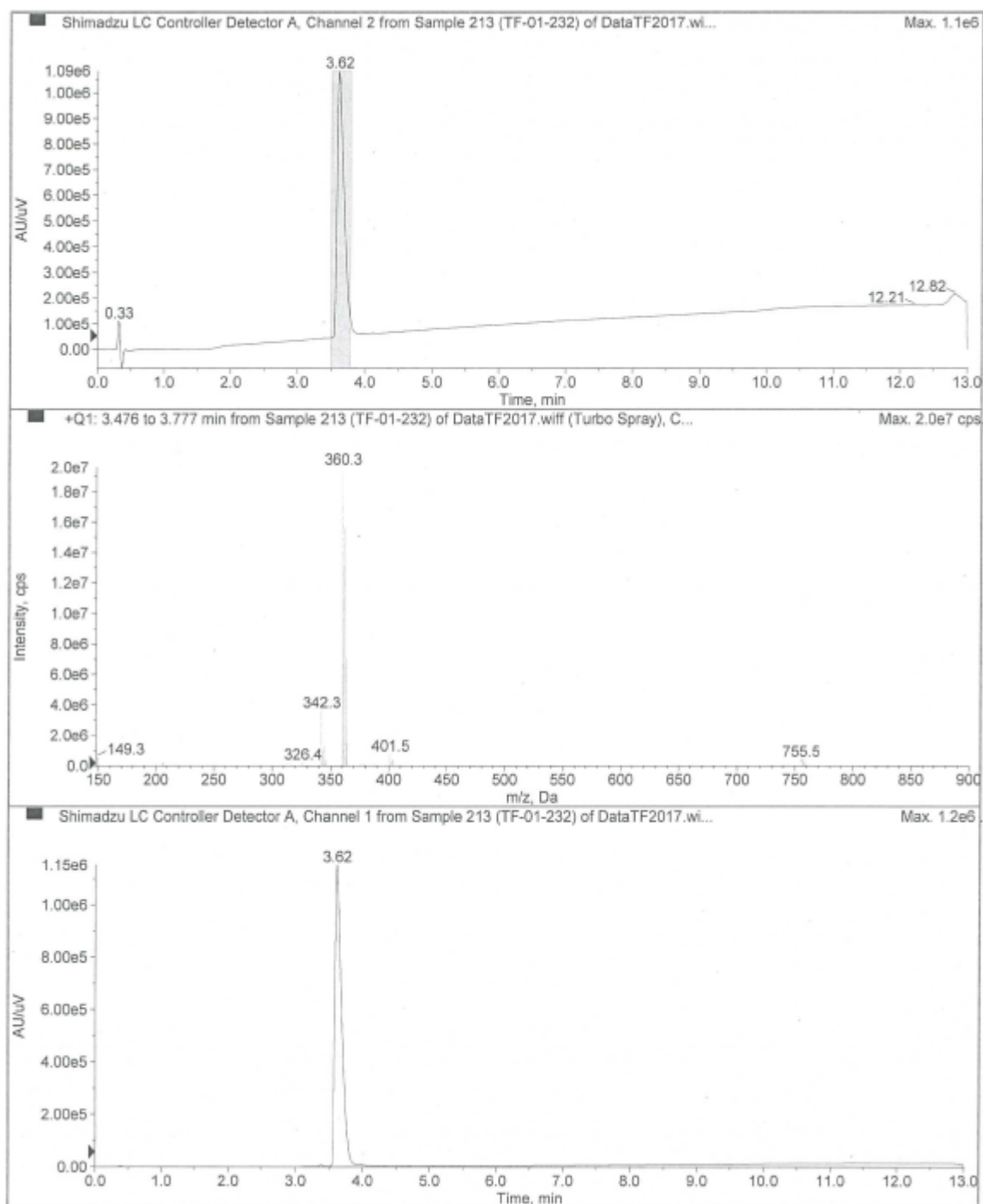
Supplemental Figure 25. Analytical HPLC/MS trace for compound 8i.



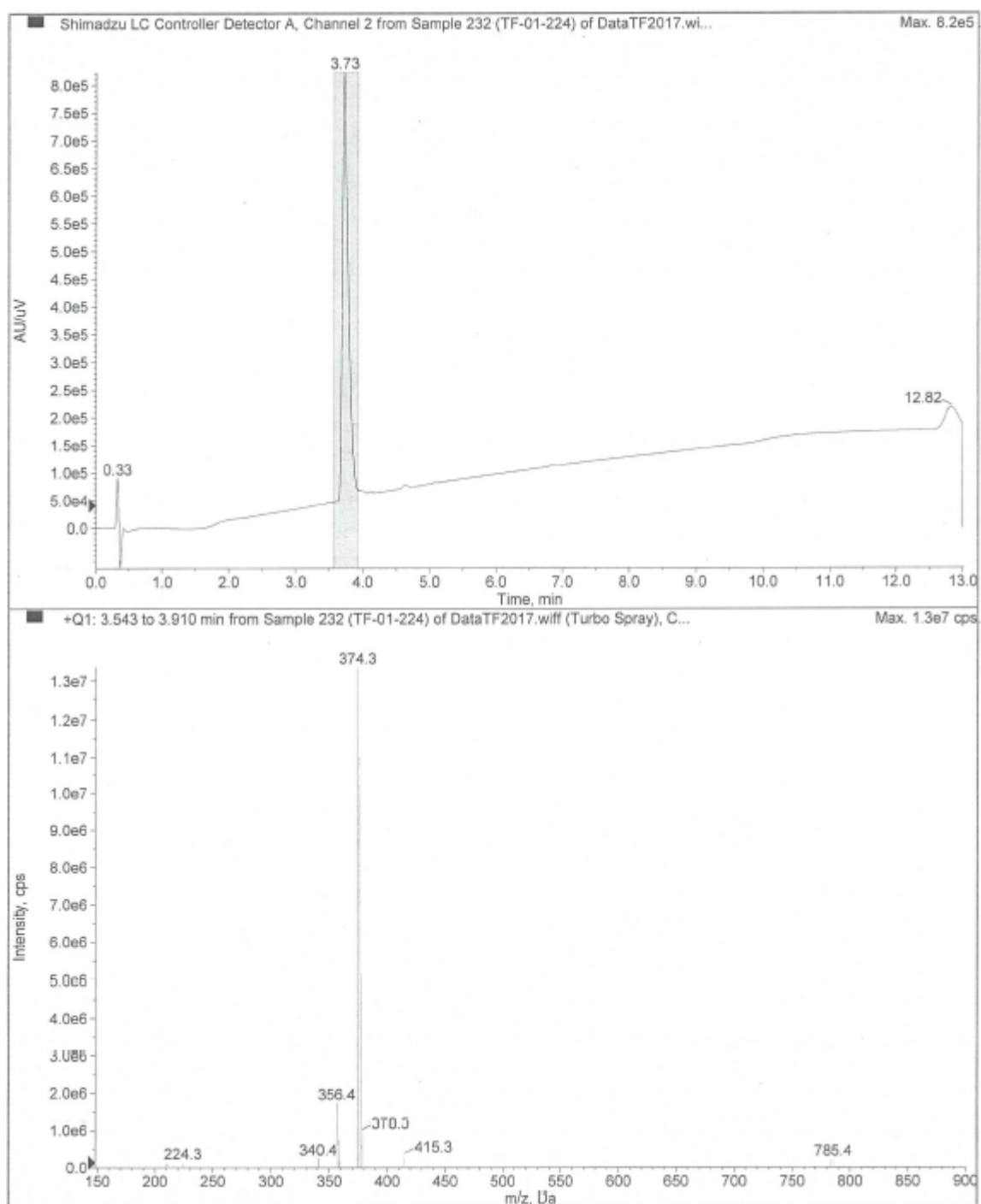
Supplemental Figure 26. Analytical HPLC/MS trace for compound 14c.



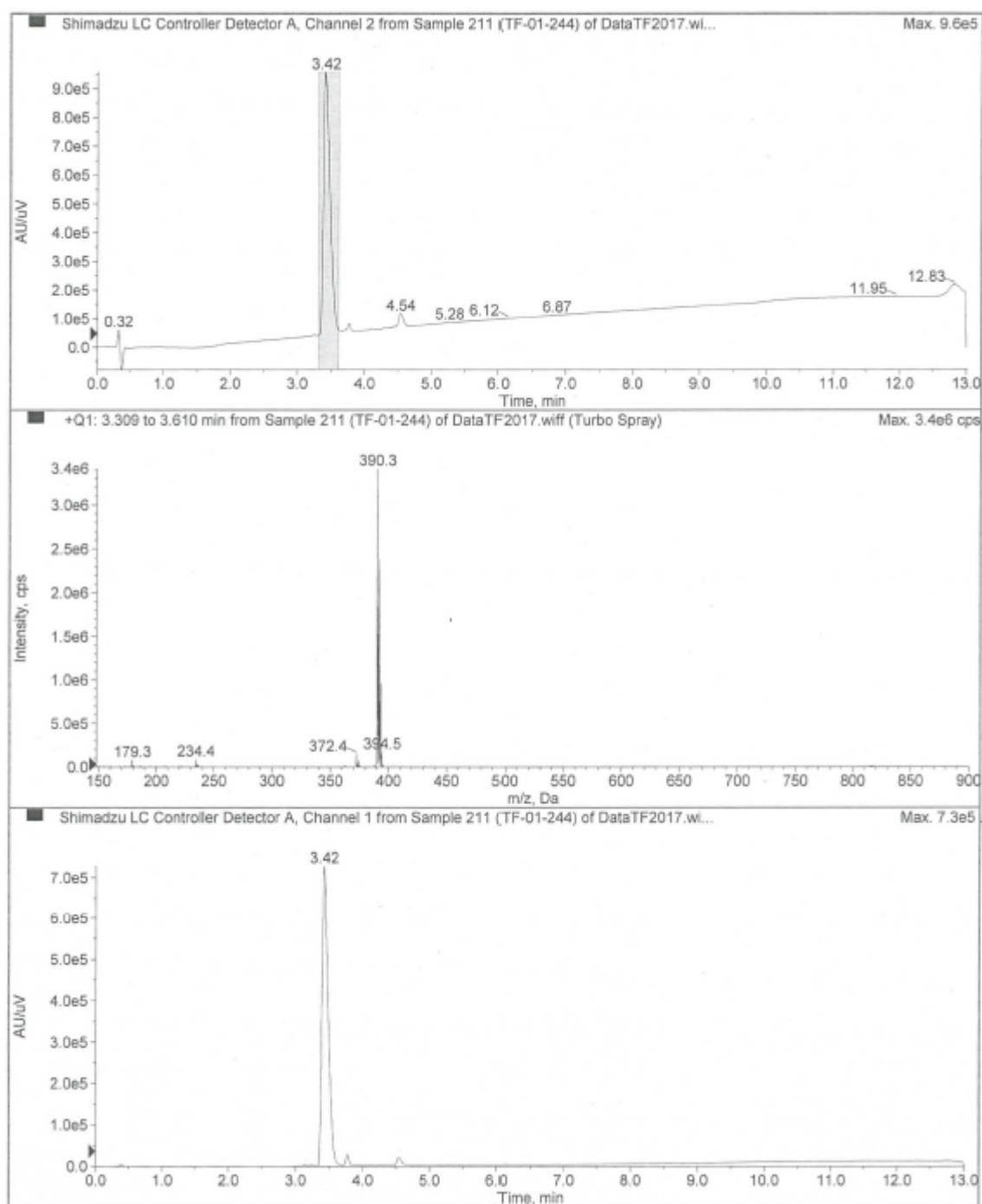
Supplemental Figure 27. Analytical HPLC/MS trace for compound 23.



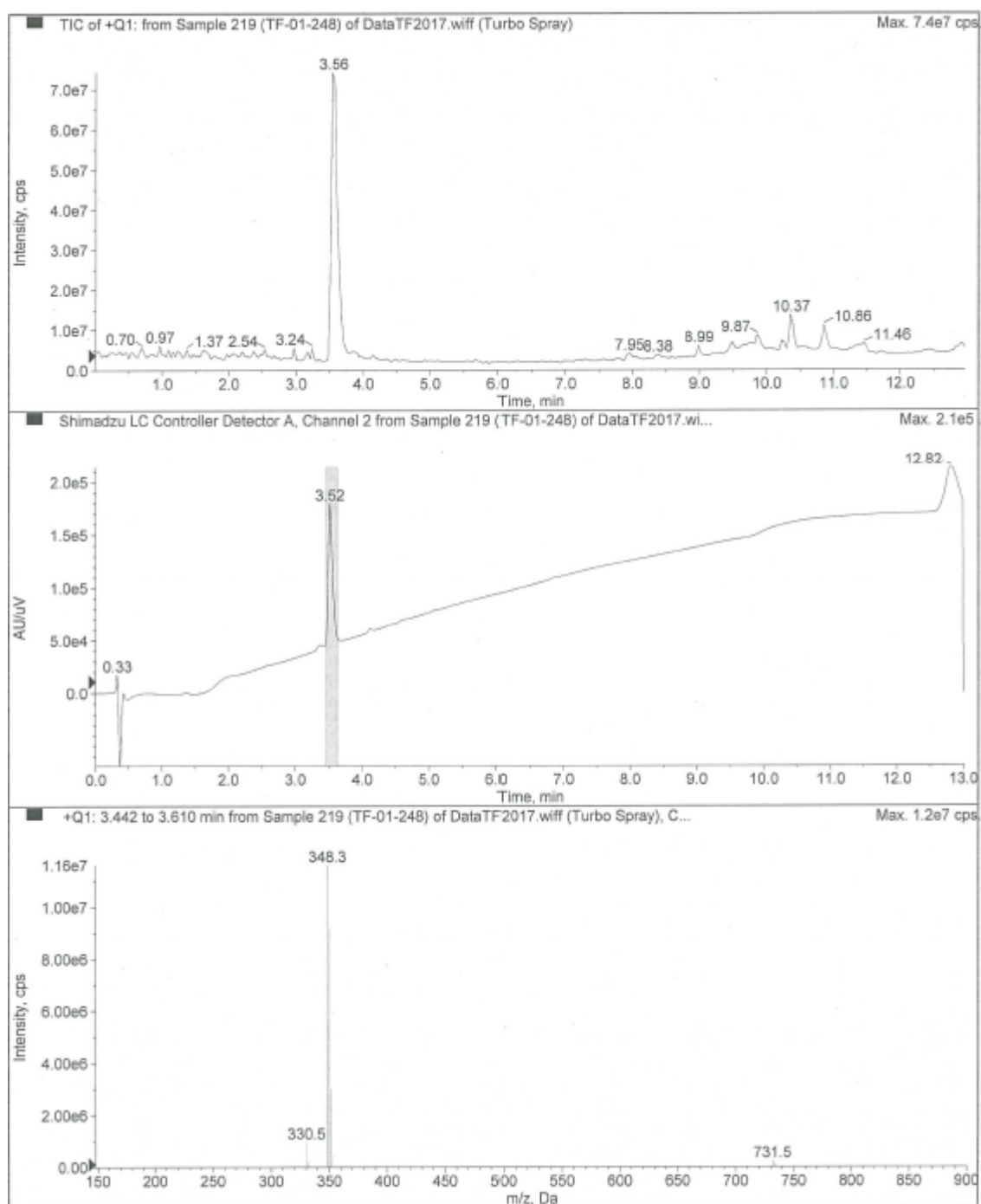
Supplemental Figure 28. Analytical HPLC/MS trace for compound 30b.



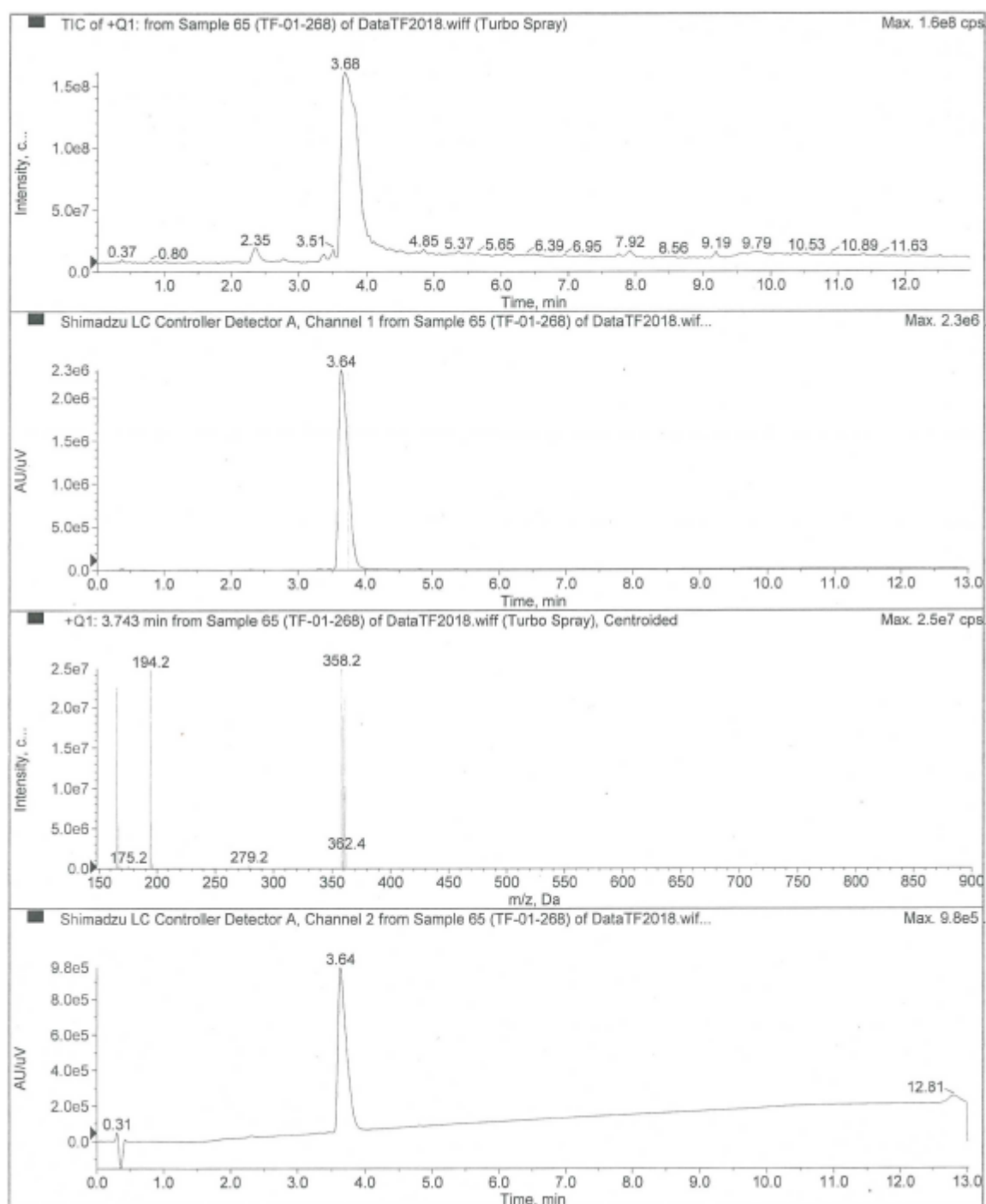
Supplemental Figure 29. Analytical HPLC/MS trace for compound 34c.



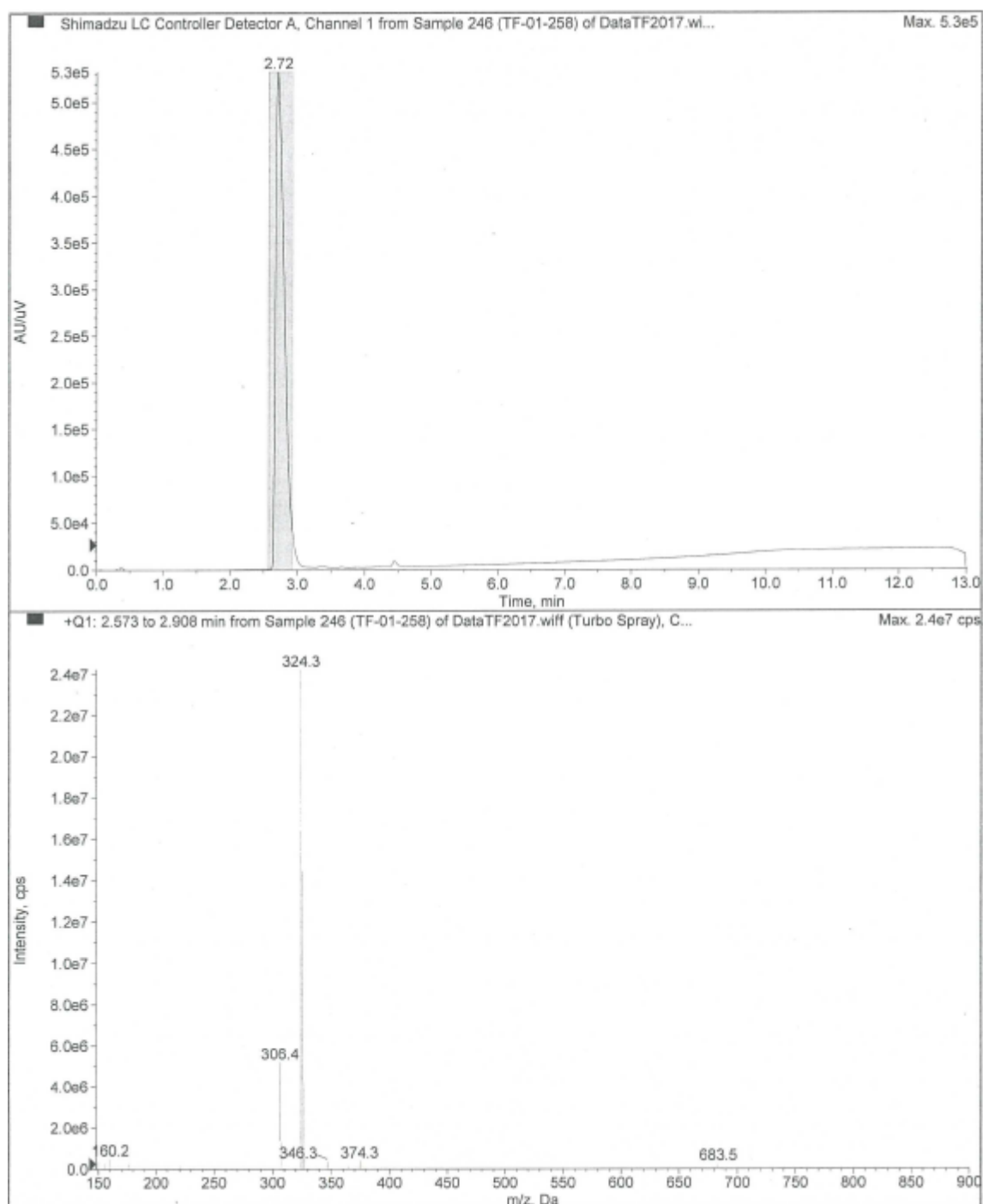
Supplemental Figure 30. Analytical HPLC/MS trace for compound 36a.



Supplemental Figure 31. Analytical HPLC/MS trace for compound 45.



Supplemental Figure 32. Analytical HPLC/MS trace for compound 56.



References

1. Peprah, K.; Zhu, X. Y.; Eyunni, S. V. K.; Setola, V.; Roth, B. L.; Ablordeppey, S. Y. Multi-receptor drug design: Haloperidol as a scaffold for the design and synthesis of atypical antipsychotic agents. *Bioorg. Med. Chem.* **2012**, *20*, 1291-1297.
2. Farrokhzad, S.; Diksic, M. The syntheses of no - carrier - added and carrier - added 18F - labelled haloperidol. *J. Labelled Compd. Rad.* **1985**, *22*, 721-733.
3. Janssen, P. A. J.; Van De Westeringh, C.; Jageneau, A. H. M.; Demoen, P. J. A.; Hermans, B. K. F.; Van Daele, G. H. P.; Schellekens, K. H. L.; Van Der Eycken, C. A. M.; Niemegeers, C. J. E. Chemistry and pharmacology of CNS depressants related to 4-(4-Hydroxy-4-phenylpiperidino)butyrophenone. Part I--Synthesis and screening data in mice. *J. Med. Pharm. Chem.* **1959**, *1*, 281-297.

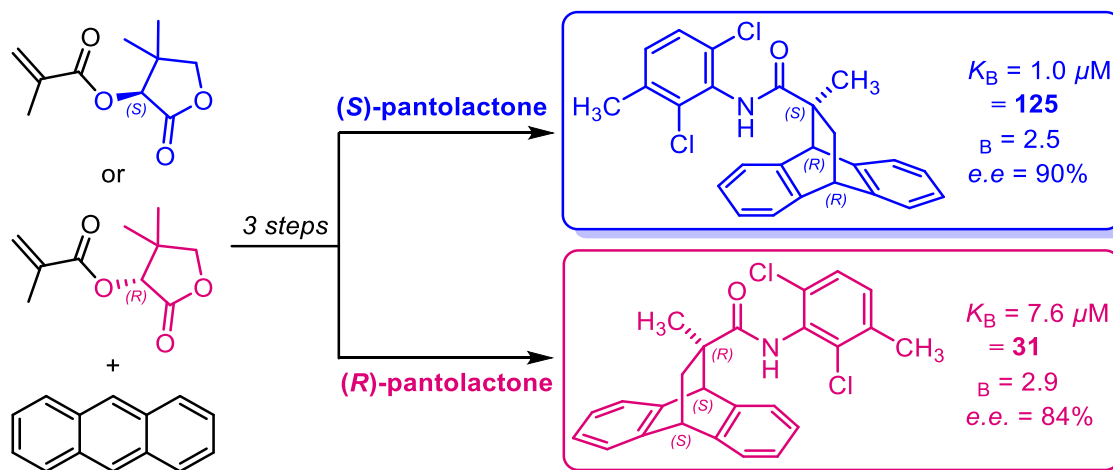
**Chapter 6 – Enantioenriched Positive
Allosteric Modulators Displays Distinct
Pharmacology at the Dopamine D₁ Receptor**

Enantioenriched Positive Allosteric Modulators Display Distinct Pharmacology at the Dopamine D₁ Receptor

Tim J. Fyfe,^{†,§} Peter J. Scammells,[†] J. Robert Lane,^{* ≠} Ben Capuano^{*†}

[†]Medicinal Chemistry, and [§]Drug Discovery Biology, Monash Institute of Pharmaceutical Sciences, Monash University

[≠]School of Life Sciences, Queen's Medical Centre, University of Nottingham, Nottingham NG7 2UH, U.K.



Abstract. Recently, two first-in-class racemic dopamine D₁ receptor (D₁R) positive allosteric modulator (PAM) chemotypes were identified from a high-throughput screen (**1** and **2**). In particular, due to its selectivity for the D₁R and reported lack of intrinsic activity, compound **2** shows promise as a starting point toward the development of small molecule allosteric modulators to ameliorate the cognitive deficits associated with some neuropsychiatric disease states. Herein, we describe the enantioenrichment of optical isomers of **2** using chiral auxiliaries derived from (R)- and (S)-3-hydroxy-4,4-dimethyldihydrofuran-2(3H)-one (D- and L-pantolactone, respectively). We confirm both the racemate and enantiomers of **2** are active and selective for the D₁R, but that the respective stereoisomers show a significant difference in their affinity and magnitude of positive allosteric cooperativity with dopamine. These data warrant further investigation of asymmetric syntheses of optically pure analogues of **2** for the discovery of D₁R PAMs with superior allosteric properties.

Introduction. Schizophrenia (SCZ) is a debilitating neuropsychiatric illness characterised by three distinct symptoms domains.^{1,2} Positive symptoms describe manifestations of psychosis such as delusions, whereas negative symptoms are defined as alterations in drive and volition.³ Cognitive deficits are a central feature of SCZ, and include deficits in working memory, attention, learning, and executive functioning.⁴ Numerous studies have demonstrated an association between the severity of cognitive impairment and functional, social, and occupational outcomes in SCZ. Thus, the development of therapeutics that address this symptom domain are desirable.⁵ Unfortunately, current clinical antipsychotic drugs (APDs) fail to address these cognitive symptoms.^{6,7}

Hypodopaminergic function in the dorsolateral prefrontal cortex (dlPFC), an area associated with cognitive control and executive functions including working memory and selective attention,⁸ is thought to be related to negative symptoms and cognitive deficits.^{9,10} Indeed, both dopamine receptor (DR) antagonists and dopamine (DA) depletion in the dlPFC impair cognitive function.¹¹⁻¹³ There is mounting evidence to suggest that D₁R agonists can reverse these deficits,^{14,15} although excessive D₁R stimulation may also impede cognitive function.^{16,17} Many orthosteric D₁R agonists display a lack of subtype selectivity (relative to other DRs) as well as poor pharmacokinetic properties. The benzazepine class of D₁R agonists have poor bioavailability¹⁸ and has the propensity to lower seizure thresholds.¹⁹ Similarly, the D₁R agonist dihydrexidine displays poor oral bioavailability and is rapidly metabolised *in vivo*.²⁰ Orthosteric D₁R agonists have also been shown to increase incidence of drug-induced hypotension, potentially mediated by D₁Rs expressed in the periphery,²¹ as well as a rapid acquisition of tolerance.^{22,23} There is clearly an unmet need for the development of selective, bioavailable small molecule D₁R ligands to further interrogate their potential utility to treat cognitive deficits associated with SCZ.

There is growing interest in the search for novel D₁R positive allosteric modulators (PAMs).²⁴⁻²⁶ PAMs represent an alternative approach to targeting the D₁R and act to modulate the affinity and/or efficacy of DA from a topographically distinct but conformationally linked binding site. The engagement of a less conserved allosteric binding site may confer greater subtype selectivity than orthosteric D₁R agonists. A D₁R PAM that displays positive allosteric cooperativity but lacks intrinsic efficacy in its own right might maintain the temporal and spatial patterns of DA neurotransmission.^{27,28} Lewis *et al.* recently identified two racemic D₁R PAM chemotypes (Compound A, **1**) and Compound B, (*rac*-**2**), Figure 1).²⁹ **1** was shown to be a D₁R PAM but also acted as an agonist at the D₂R and thus was not investigated further. As D₂R agonism is known to exacerbate the positive symptoms of SCZ, achieving selectivity for the D₁R versus the D₂R is paramount for the development of efficacious cognitive-enhancing therapeutics. *rac*-**2** was shown to have superior potency compared to **1** whilst being selective for the human D₁R. To our knowledge

there is no reported synthesis or biological characterisation of enantiomers of **2**. Herein, we report the synthesis and pharmacological characterisation of (*rac*)-**2**, and enantioenriched optical isomers of **2** (herein denoted as (*S*)-**2** and (*R*)-**2**). These enantioenriched samples were accessed by employing various chiral auxiliaries in an asymmetric Diels-Alder (ADA) cycloaddition reaction.

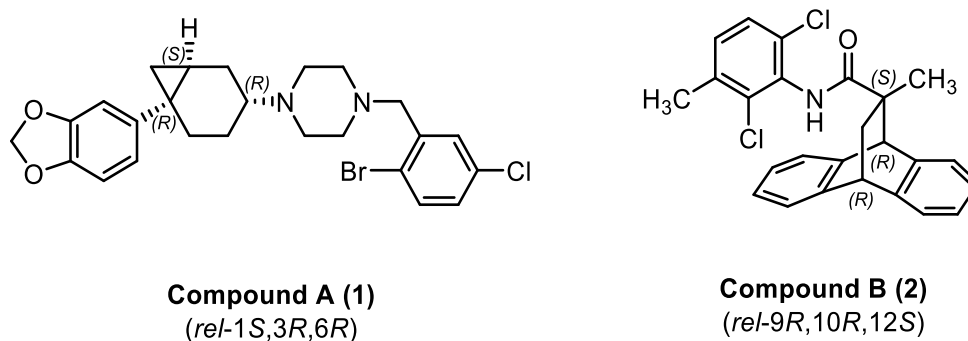
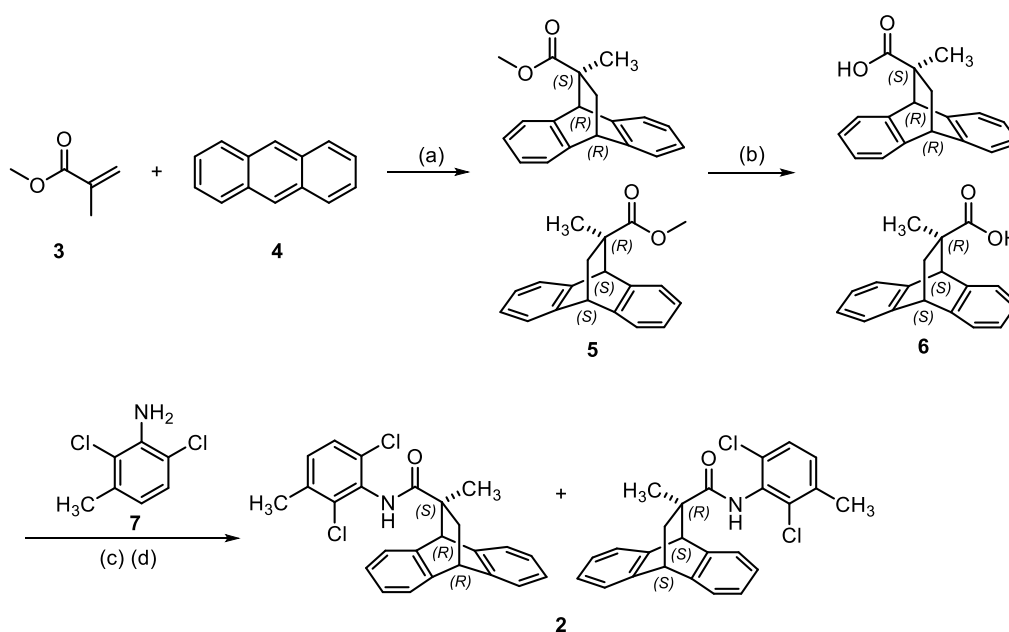


Figure 1. High-throughput racemic screening hits **Compound A (1)** and **Compound B (rac-2)** reported by Lewis *et al.*²⁹

To characterise their pharmacology, we applied analytical pharmacological methods to determine allosteric ligand affinity for the unoccupied receptor, the strength of modulatory effects upon DA activity as well as the magnitude of allosteric agonism.³⁰ We demonstrate that enantiomers of **2** can be accessed in moderate enantiopurity in four synthetic steps. Importantly we reveal that these enantiomers display different affinities for the D₁R as well as different levels of positive cooperativity with DA. The degree of allosteric cooperativity required for a ‘clinical’ D₁R PAM is currently unknown. These data illustrate the importance of characterising optically pure analogues for future structure-activity relationship studies around **2**.

Chemistry. Compound *rac*-**2** was resynthesised in three steps according to **Scheme 1**.³¹ Firstly, AlCl₃-catalysed Diels-Alder [4+2]cycloaddition of anthracene **4** with methyl methacrylate **3** afforded the 9,10-bridged esters **5** as a racemate. Ester saponification was achieved under forcing conditions with NaOH in THF/H₂O at reflux, affording acids **6**. Subsequent treatment with thionyl chloride and DMF, followed by DMAP-catalysed nucleophilic substitution with commercially available 2,6-dichloro-3-methylaniline (**7**) afforded *rac*-**2**. High-performance liquid chromatography (HPLC) using an amylose chiral stationary phase (CSP) verified the presence of two enantiomers.

Scheme 1. Chemical Synthesis of *rac*-**2**^a

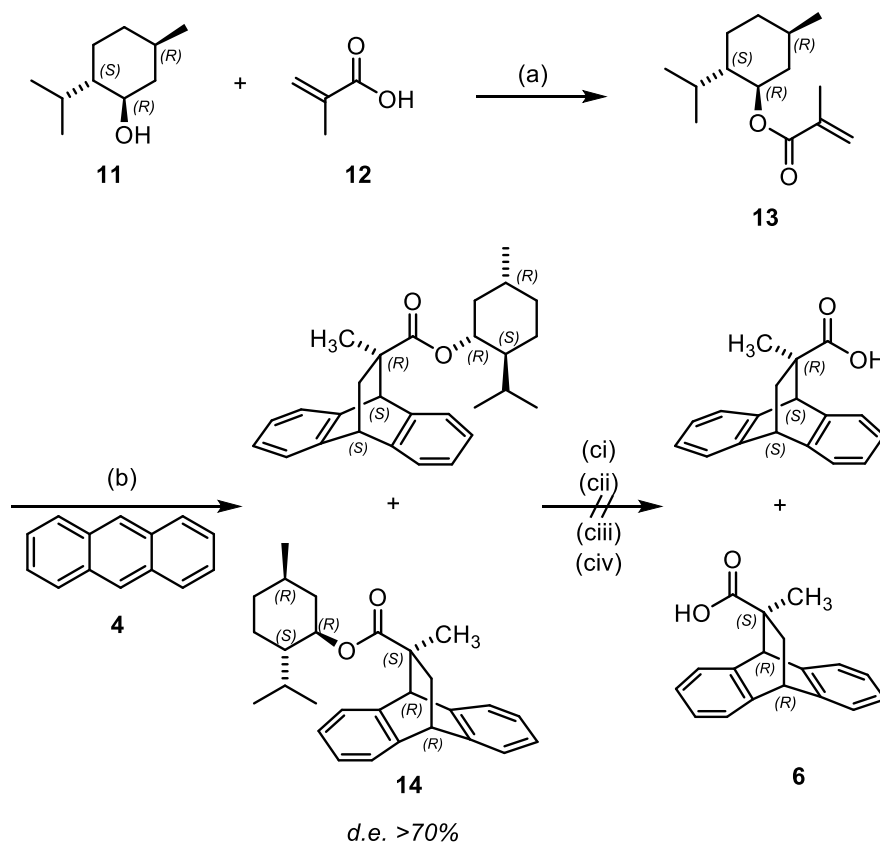
^aReagents and conditions: (a) AlCl₃, CH₂Cl₂, r.t. 72 h, 63%; (b) NaOH, 1:1 THF/H₂O, reflux 7 days, 98%; (c) SOCl₂, DMF_(cat.), reflux, 24 h; (d) DMAP_(cat.) DIPEA, MeCN, reflux, 24 h, 25%.

It is not clear from the current literature regarding the newly identified D₁R PAM scaffold whether a single enantiomer or racemate is responsible for the quoted *in vitro* activity. This led us to investigate methods to generate optically pure stereoisomers of compound **2**. Numerous attempts at chiral resolution of **5** (semi-preparative chiral HPLC) and the chromatographic resolution of derivatives of **5** (diastereomeric amides/esters, diastereomeric salts) using various resolving ligands, e.g. (*R*)-1-phenylethan-1-amine, (*S*)-2-amino-2-phenylethan-1-ol and (1*R*,2*S*,5*R*)-2-isopropyl-5-methylcyclohexan-1-ol ((-)-menthol)), all failed. Therefore, to access enantiopure synthetic precursors, it was necessary to develop and explore the use of chiral auxiliaries in an ADA reaction. The Diels-Alder reaction arises from high regio- and stereoselectivity which also entails the use of various functionalised dienes and dienophiles, and much work has been done in the last three decades to develop ADA reactions, based on both enantiopure dienes and enantiopure dienophiles.³² Accordingly, the area has been extensively reviewed.³³⁻³⁵

(-)-Menthol **11**, a chiral molecule with three stereocentres, was initially selected as a practical chiral auxiliary to probe the diastereoselectivity of the Diels-Alder cycloaddition. A derivative of **11**, (-)-8-phenylmenthol, has previously been shown to induce ADA reactions with high distereoselectivity under AlCl₃ catalysis.³⁶ As outlined in **Scheme 2**, DMAP-catalysed, EDC-mediated Steglich-type³⁷ esterification of methacrylic acid **12** with **11** furnished the corresponding auxiliary **13**. This dienophile was subjected to a TiCl₄-catalysed [4+2]cycloaddition, affording cycloadduct(s) **14**. ¹H

NMR analysis confirmed that the (1*R*,2*S*,5*R*)-menthol-acrylate chiral auxiliary conferred moderate diastereoselectivity in the cycloaddition as one diastereomer could be identified as the major product (>70% *d.e.*). Unfortunately, hydrolytic ester cleavage of **14** using LiOH or NaOH in refluxing THF/H₂O failed to furnish the acid **6** as no reaction was evident *via* LC/MS analysis. Alternative conditions for hydrolysis were sourced from work completed by Myers *et al.*, who reported the use of various synthetic examples and reagents to hydrolyse amides and esters.³⁸ Such additional methods were explored, including stirring **14** at reflux in the presence H₂SO₄ and 1,4-dioxane, stirring **14** at reflux in a 2:1:1 solution of H₂O, MeOH and *tert*-butanol in the presence of NaOH, as well as at reflux in a 4:1 solution of H₂O/1,4-dioxane in the presence of the Lewis acid iron(III) chloride hexahydrate. These chemistries all failed to provide the target acid **6**.

Scheme 2. Synthesis of Menthol Derived Diastereomers using ADA Chemistry^a

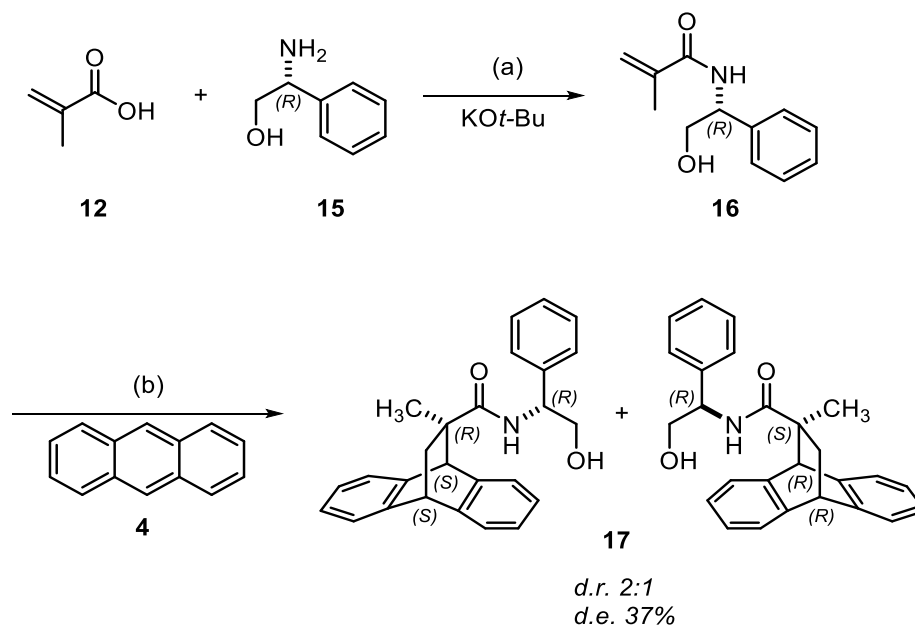


^aReagents and conditions: (i) EDCI, DMAP (cat.), anhydrous CH₂Cl₂, r.t. 48 h, 55%; (ii) TiCl₄, dry CH₂Cl₂, r.t. 15 h, 25%; (ci) NaOH, THF/H₂O, reflux 7 d; (cii) H₂SO₄ (conc.), 1,4-dioxane, reflux, 3 h; (ciii) NaOH, 2:1:1 H₂O, MeOH, *t*-butanol, reflux 72 h; (civ) FeCl₃·6H₂O, 1:4 1,4-dioxane/H₂O, reflux.

An additional auxiliary, (*R*)-2-amino-2-phenylethan-1-ol **15**, was investigated for its potential in ADA chemistry. According to **Scheme 3**, methacrylic acid **12** was subjected to a potassium *tert*-

butoxide-mediated direct amidation³⁹ using **15**, yielding the corresponding acrylamide **16**. Again, the newly formed acrylamide was directly utilised in a TiCl₄-catalysed [4+2]cycloaddition to furnish the desired ethanoanthracene derivative **17**. HPLC analysis of the purified material indicated the presence of two diastereomers in an approximate ratio of 3:1, and this was further confirmed with ¹H NMR spectroscopy (~50% *d.e.*).

Scheme 3 – Synthesis of 2-Phenylglycinol Ethanoanthracene Diastereomers^a



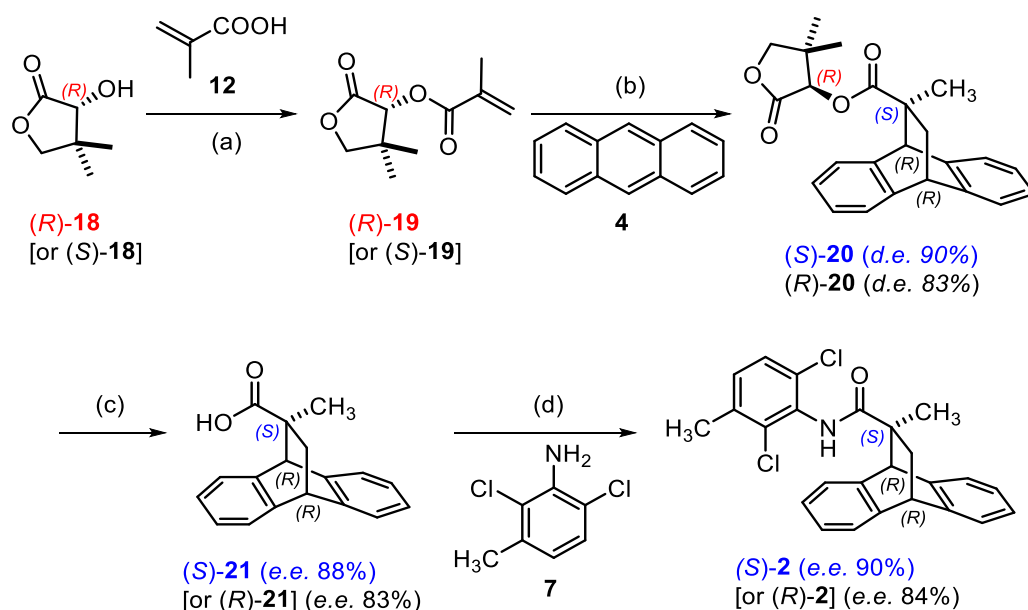
^aReagents and conditions: (a) dry THF, r.t., 2.5 h, 91%; (b) TiCl₄, dry DCM, r.t. 7 days, 75%.

The study of ADA induction involving esters derived from achiral acrylic and methacrylic acids, and the chiral auxiliaries (*R*)- and (*S*)-3-hydroxy-4,4-dimethyl-1-phenyl-2-pyrrolidinone with different dienes including anthracene (which was of particular interest), catalysed by TiCl₄ has been described.³² These studies reported adducts derived from anthracene and the (*R*)-pantolactam-acrylate ester could be obtained with high *facial*-diastereoselectivity, and subsequent saponification afforded the corresponding acid in high optical purity. In addition, the acrylates of (*R*)-pantolactone have also been extensively studied for their asymmetric capacity to direct cycloadditions with high *facial*-diastereoselectivity for a number of diene scaffolds under TiCl₄ catalysis, including anthracene.^{40,41,42} Pantolactones and their use as chiral auxiliaries in ADA chemistry has been extensively reviewed,⁴³ as well as mechanistic models proposed to explain the sense of asymmetric induction in TiCl₄-catalysed ADA reactions of pantolactone-acrylate derivatives.⁴⁴

Following an adapted procedure from Camps *et al.*,³² and as outlined in Scheme 4, commercially available D-pantolactone ((*R*)-**18**) was reacted with methacrylic acid **12** under modified Steglich esterification³⁷ conditions to give the corresponding auxiliary (*R*)-**19** in moderate yield. Subsequent

[4+2]cycloaddition with anthracene **4** as the diene in the presence of TiCl₄ as catalyst, followed by chromatographic purification and recrystallization from EtOH, afforded (*S*)-**20** as a pale white crystalline solid. ¹H NMR spectroscopic analysis confirmed high diastereoselectivity (>90% *d.e.*) for the asymmetric induction. Saponification using a large excess of NaOH in refluxing THF/H₂O was achieved to eventually yield carboxylic acid (*S*)-**21**. Although the synthesis of ((*S*)-**21**) has been reported in the literature using (*R*)-3-hydroxy-4,4-dimethyl-1-phenyl-2-pyrrolidinone as a chiral auxiliary³² our synthesis was performed to examine the asymmetric induction potential of pantolactone chiral auxiliaries. Moreover, ((*S*)-**21**) was subsequently required to form the corresponding amide (*S*)-**2**, so as it could be evaluated for its *in vitro* allosteric ligand parameters. The enantiopurity of (*S*)-**21** was characterised using polarimetry [α]_D²⁵ = -24.9° (*c* 1.0, CHCl₃) which was in accordance with literature values.³² Based on approximations from the preceding ¹H NMR spectrum of (*S*)-**20**, an enantiomeric excess (*e.e.*) of >90% was likely. Indeed, chiral HPLC confirmed the presence of predominantly a single enantiomer, supporting the high *facial*-diastereoselectivity of the pantolactone chiral auxiliary in [4+2]cycloadditions, with *e.e.* calculated to be ~88%. The enantioenriched mixture was successively activated with thionyl chloride and subjected to nucleophilic substitution employing conditions outlined previously, yielding enantioenriched (*S*)-**2**. CHPLC analysis of (*S*)-**2** determined the *e.e.* to be ~90%.

Interestingly, Camps *et al.* reported that an acrylate derived from a racemic *N*-phenyl pantolactam chiral auxiliary was unable to react with anthracene under AlCl₃ catalysis.³² In addition, the authors did not report on the effectiveness of TiCl₄ as catalyst for the cycloaddition reaction between anthracene and their (*S*)-*N*-phenyl pantolactam chiral auxiliary, nor its racemic counterpart. Thus, the asymmetric induction potential of using the enantiomeric (*S*)-pantolactone acrylate ester as an alternative chiral auxiliary to access the previously unreported (*R*)-**20** was unknown. Based on our encouraging results, though, we applied this chemistry to to L-pantolactone ((*S*)-**18**) (Scheme 4). Steglich esterification³⁷ of **12** with (*S*)-**18** using conditions outlined previously, afforded (*S*)-**19**. Subsequent cycloaddition of the auxiliary (*S*)-**19** with diene **4** gave cycloadduct (*R*)-**20** in good yield, with ¹H NMR indicating a slightly lower diastereoselectivity (*d.e.* ~90%). This apparent reduced asymmetric induction may have arisen from a failure for (*R*)-**20** to recrystallize, or is mechanistically inherent in the cycloaddition of (*S*)-**19**. Hydrolytic cleavage of the auxiliary was achieved using forcing alkaline conditions, eventually affording the free carboxylic acid (*R*)-**21**. An assessment of the enantiopurity was again made using polarimetry ([α]_D²⁵ = +24.1° (*c* 1.0, CHCl₃)), and subsequent chiral HPLC analysis determined the *e.e.* to be ~82%. Acyl halide formation and nucleophilic displacement with **7** using conditions outlined previously furnished the corresponding enantioenriched (*R*)-**2**. CHPLC analysis of (*R*)-**2** determined the *e.e.* to be ~84%.

Scheme 4 – Enantioenrichment of Optical Isomers of 2 using Chiral Auxiliaries derived from Pantolactone^a


^aReagents and conditions: (a) EDCI, DMAP, dry CH₂Cl₂, r.t. 10 h, 69-87% ((*R*)-19, (*S*)-19); (b) TiCl₄, dry CH₂Cl₂, r.t. 15 h, 80-85% ((*S*)-20, (*R*)-20); (c) NaOH, THF/H₂O, reflux, 72 h, 85-98% ((*S*)-21, (*R*)-21); (d) SOCl₂(neat), DMF_(cat.) reflux, 24 h, then acyl halide, DMAP_(cat.) DIPEA, MeCN, reflux, 24 h, 19-25% ((*S*)-2, (*R*)-2).

Pharmacology. Previous work by Lewis *et al.*²⁹ reported *rac*-2 as a PAM at the D₁R with superior potency (EC₅₀ = 43 nM) and no agonist activity. We tested *rac*-2 in an assay measuring accumulation of cyclic adenosine monophosphate (cAMP) through activation of the hD₁R stably expressed in FlpIn CHO cells using a BRET biosensor.⁴⁵ Concentration-response curves of DA were generated in the presence of increasing concentrations of test compound. An operational model of allostery was applied to these data, allowing us to determine estimates of functional affinity for the unoccupied receptor (K_B), a composite measure of allosteric cooperativity ($\alpha\beta$) that combines cooperativity with DA affinity (α) and modulatory effect upon DA efficacy (β), as well as the intrinsic efficacy (τ_B) of the allosteric ligand. Values of $\alpha\beta > 1$ indicate a positive modulatory effect. Functional assessment of *rac*-2 in our hands showed it exhibited modest affinity for the D₁R ($K_B = 1.6 \mu\text{M}$, Figure 2A, Table 1), acting to potentiate the potency of DA 100-fold ($\alpha\beta = 100$) as well as display allosteric agonism ($\tau_B = 2.1$, Table 1). Lewis and colleagues observed that *rac*-2 did not display agonism. This difference likely reflects a difference in the cell background (CHO versus HEK293) and/or a higher level of D₁R expression in our cell line and/or a greater sensitivity of our cAMP assay.²⁹ Indeed such effects have been observed for a PAM of the muscarinic M₁ acetylcholine receptor and such observations are consistent with a two-state model of allostery.⁴⁶ Consistent with the above differences, the potency of dopamine in our assay is also greater than that observed by Lewis and coworkers in their

experiments. Note that Lewis *et al.* also determined the value of potency for *rac-2* as 43 nM. This value was determined by the measuring the potency with which *rac-2* causes a shift in dopamine potency and cannot be directly compared with the value of K_B determined in our analysis that reflects the affinity of the PAM for the unoccupied receptor.

Unsurprisingly, the optical isomers of *rac-2* ((*S*)-**2**, (*R*)-**2**) displayed significant differences both in their affinity for the D₁R and their degree of positive allosteric cooperativity with DA. The enantioenriched (*S*)-**2** was determined to have comparable functional affinity, efficacy and cooperativity as compared to *rac-2* ($K_B = 1 \mu\text{M}$, $\alpha\beta = 125$, $\tau_B = 2.5$) (Figure 2B, Table 1). Conversely, the enantioenriched (*R*)-**2** displayed 4.8-fold and 7.4-fold lower functional affinity ($K_B = 7.4 \mu\text{M}$ $\alpha\beta = 31$) and 3-fold and 4-fold lower cooperativity with DA, relative to *rac-2* and (*S*)-**2**, respectively (Figure 2C, Table 1). It is interesting to note that the pharmacology of *rac-2* is not significantly different from (*S*)-**2**. This can be reconciled by the lower levels of affinity and cooperativity with dopamine that (*R*)-**2** displays. These two factors combined mean that (*S*)-**2** would effectively display a 30-fold greater affinity for the dopamine occupied receptor as compared to (*R*)-**2** even though their affinities for the unoccupied are a more modest 7-fold different. In the racemate, therefore, (*S*)-**2** would be expected to dominate meaning that the pharmacology of the racemate reflects this enantiomer. We extended our functional characterisation of these compounds to an assay measuring inhibition of forskolin-stimulated cAMP accumulation in hD₂₁R-expressing FlpIN CHO cells. *rac-2* and its respective enantiomers ((*R*)-**2**, (*S*)-**2**) displayed no activity at the D₂R up to a measured concentration of 30 μM . None of the above compounds displayed any detectable off-target response in FlpIn CHO cells transfected with the BRET biosensor, but not expressing either the D₁R or the D₂R (Figure 2D). Together our data indicate that the distinct structural configuration of the two enantiomers of **2** confer differences in their ability to potentiate DA at the D₁R.

Table 1. Functional Parameters for PAMs Derived from cAMP BRET Assay at the hD₁R

CPD	<i>e.e.</i> (%)	$\text{p}K_B (K_B, \mu\text{M})^a$	$\text{Log}\tau_B (\tau_B)^b$	$\text{Log}\alpha\beta (\alpha\beta)^c$
<i>rac-2</i>	0	5.80 ± 0.10 (1.6)	0.32 ± 0.06 (2.1)	2.00 ± 0.12 (100)
(<i>S</i>)- 2	90	5.99 ± 0.09 (1.0)	0.40 ± 0.06 (2.5)	2.10 ± 0.25 (125)
(<i>R</i>)- 2	84	5.12 ± 0.06 (7.6)* [^]	0.46 ± 0.08 (2.9)	1.51 ± 0.14 (31)* [^]

^aEstimate of the negative logarithm of the equilibrium dissociation constant determined in an cAMP functional assay.

^bEstimate of the intrinsic efficacy of the modulator. ^cEstimate of the logarithm of the net cooperativity factor between the modulator and DA. Values represent mean \pm S.D. from at least four independent experiments performed in duplicate. Significant differences parameter between (*R*)-**2** and *rac-2** or (*S*)-**2**[^], $P < 0.05$, one-way ANOVA with Tukey's Post-hoc test (GraphPad Prism Version 7).

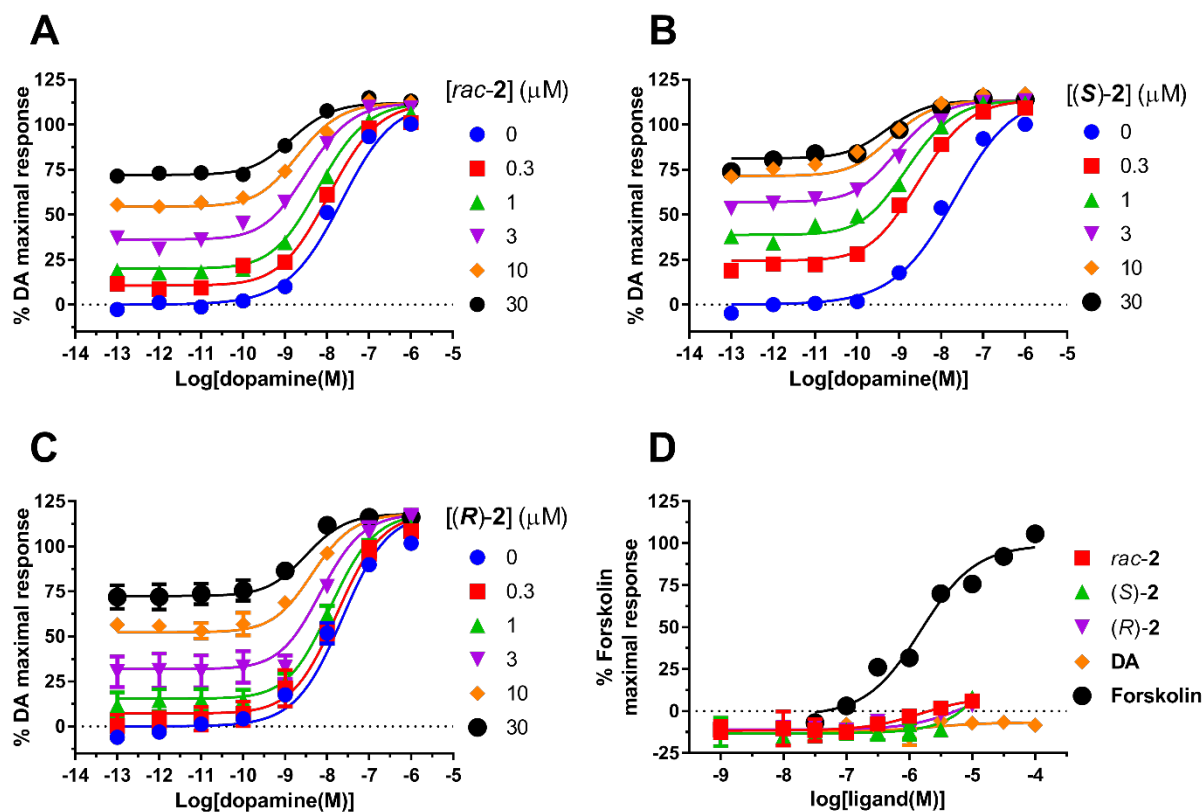


Figure 2. All compounds display allosteric pharmacology at the D₁R in an assay measuring cAMP production using a BRET biosensor. *rac*-2 (A), the enantioenriched *S*-isomer ((*S*)-2, B), and the enantioenriched *R*-isomer ((*R*)-2, C) act as an ago-PAMs, potentiating DA potency and exerting allosteric agonism. These data were fitted to an operational model of agonism to derive values of affinity, cooperativity with dopamine and intrinsic efficacy (see Table 1). Data are presented as mean \pm S.D. from at least four separate experiments. (D) All compounds were assessed for their activity at non-hD₁R/hD₂R expressing FlpIn CHO-cells transfected with the BRET biosensor, demonstrating that compound activity is mediated through the D₁/D₂Rs. Data are presented as mean \pm S.D. from at least four separate experiments.

Conclusions. In this study, we describe the first reported enantioenrichment of optical isomers of *rac*-2 using chiral auxiliaries derived from enantiomers of 3-hydroxy-4,4-dimethyldihydrofuran-2(3*H*)-one and their pharmacological characterisation. Interestingly, (*R*)-2 was shown to display 4-fold lower positive cooperativity with DA as compared to (*S*)-2 and a 7-fold lower affinity for the D₁R. Our findings illustrate the importance of further investigation into asymmetric syntheses of analogues of **2** and/or isolation of optically pure analogues as part of future SAR efforts aimed at developing enhanced D₁R PAMs based on this scaffold.

ASSOCIATED CONTENT

Supporting Information

Synthetic procedures, spectral characterisation, and pharmacological methods are provided in the supporting information. RP-HPLC and chiral HPLC chromatograms, together with ¹H & ¹³C NMR spectra are included for compounds *rac*-**2**, (*S*)-**2** and (*R*)-**2** in Supporting Information. Chiral HPLC chromatograms for compounds **5**, (*S*)-**21** and (*R*)-**21** are also included. Molecular formula strings (CSV) have been included in Supporting Information.

AUTHOUR INFORMATION

Corresponding Authors

***B.C.**: phone, +61 9903 9556; e-mail, ben.capuano@monash.edu

***J.R.L.**: phone, +44 (0)115 846 7554; e-mail, rob.lane@nottingham.ac.uk

Author Contributions

Notes The authors declare no competing financial interest.

ACKNOWLEDGEMENTS

This research was supported by a National Health and Medical Research Council (NHMRC) Project Grant Number APP1049564.

REFERENCES

1. Ibrahim, H. M.; Tamminga, C. A. Schizophrenia: treatment targets beyond monoamine systems. *Annu. Rev. Pharmacol. Toxicol.* **2011**, *51*, 189-209.
2. van Os, J.; Kapur, S. Schizophrenia. *Lancet* **2009**, *374*, 635-645.
3. Rosen, W. G.; Mohs, R. C.; Johns, C. A.; Small, N. S.; Kendler, K. S.; Horvath, T. B.; Davis, K. L. Positive and negative symptoms in schizophrenia. *Psychiatry. Res.* **1984**, *13*, 277-284.
4. Bowie, C. R.; Harvey, P. D. Cognitive deficits and functional outcome in schizophrenia. *Neuropsychiatr. Dis. Treatment* **2006**, *2*, 531-536.
5. O'Tuathaigh, C. M. P.; Moran, P. M.; Zhen, X. C.; Waddington, J. L. Translating advances in the molecular basis of schizophrenia into novel cognitive treatment strategies. *Br. J. Pharmacol.* **2017**, *174*, 3173-3190.
6. Leucht, S.; Corves, C.; Arbter, D.; Engel, R. R.; Li, C.; Davis, J. M. Second-generation versus first-generation antipsychotic drugs for schizophrenia: a meta-analysis. *Lancet* **2009**, *373*, 31-41.

7. Koster, L. S.; Carbon, M.; Correll, C. U. Emerging drugs for schizophrenia: an update. *Expert Opin. Emerg. Drugs* **2014**, *19*, 511-531.
8. Curtis, C. E.; D'Esposito, M. Persistent activity in the prefrontal cortex during working memory. *Trends. Cogn. Sci.* **2003**, *7*, 415-423.
9. Davis, K. L.; Kahn, R. S.; Ko, G.; Davidson, M. Dopamine in schizophrenia: a review and reconceptualization. *Am. J. Psychiatry* **1991**, *148*, 1474-1486.
10. Weinberger, D. R. Implications of normal brain development for the pathogenesis of schizophrenia. *Arch. Gen. Psychiatry* **1987**, *44*, 660-669.
11. Brozoski, T. J.; Brown, R. M.; Rosvold, H. E.; Goldman, P. S. Cognitive deficit caused by regional depletion of dopamine in prefrontal cortex of rhesus monkey. *Science* **1979**, *205*, 929-932.
12. Sawaguchi, T.; Goldman-Rakic, P. S. The role of D1-dopamine receptor in working memory: local injections of dopamine antagonists into the prefrontal cortex of rhesus monkeys performing an oculomotor delayed-response task. *J. Neurophysiol.* **1994**, *71*, 515-528.
13. Sawaguchi, T.; Goldman-Rakic, P. S. D1 dopamine receptors in prefrontal cortex: involvement in working memory. *Science* **1991**, *251*, 947-950.
14. Arnsten, A. F.; Cai, J. X.; Murphy, B. L.; Goldman-Rakic, P. S. Dopamine D1 receptor mechanisms in the cognitive performance of young adult and aged monkeys. *Psychopharmacology* **1994**, *116*, 143-151.
15. Locke, T. M.; Soden, M. E.; Miller, S. M.; Hunker, A.; Knakal, C.; Licholai, J. A.; Dhillon, K. S.; Keene, C. D.; Zweifel, L. S.; Carlson, E. S. Dopamine D1 receptor-Positive neurons in the lateral nucleus of the cerebellum contribute to cognitive behavior. *Biol. Psychiatry* **2018**.
16. Abi-Dargham, A.; Moore, H. Prefrontal DA transmission at D1 receptors and the pathology of schizophrenia. *Neuroscientist* **2003**, *9*, 404-416.
17. Vijayraghavan, S.; Wang, M.; Birnbaum, S. G.; Williams, G. V.; Arnsten, A. F. Inverted-U dopamine D1 receptor actions on prefrontal neurons engaged in working memory. *Nat. Neurosci.* **2007**, *10*, 376-384.
18. Mailman, R.; Huang, X.; Nichols, D. E. Parkinson's disease and D1 dopamine receptors. *Curr. Opin. Investig. Drugs* **2001**, *2*, 1582-1591.
19. Starr, M. S.; Starr, B. S. Seizure promotion by D1 agonists does not correlate with other dopaminergic properties. *J. Neural. Transm. Park Dis. Dement. Sect.* **1993**, *6*, 27-34.
20. Arnsten, A. F.; Girgis, R. R.; Gray, D. L.; Mailman, R. B. Novel Dopamine Therapeutics for Cognitive Deficits in Schizophrenia. *Biol. Psychiatry* **2017**, *81*, 67-77.
21. Amenta, F.; Ferrante, F.; Ricci, A. Pharmacological Characterisation and Autoradiographic Localisation of Dopamine Receptor Subtypes in the Cardiovascular System and in the Kidney. *Hypertens. Res.* **1995**, *18*, S23-S27.
22. Ryman-Rasmussen, J. P.; Griffith, A.; Oloff, S.; Vaidehi, N.; Brown, J. T.; Goddard, W. A., 3rd; Mailman, R. B. Functional selectivity of dopamine D1 receptor agonists in regulating the fate of internalized receptors. *Neuropharmacology* **2007**, *52*, 562-575.
23. Gulwadi, A. G.; Korpinen, C. D.; Mailman, R. B.; Nichols, D. E.; Sit, S. Y.; Taber, M. T. Dinapsoline: characterization of a D1 dopamine receptor agonist in a rat model of Parkinson's disease. *J. Pharmacol Exp. Ther.* **2001**, *296*, 338-344.
24. Bruns, R. F.; Mitchell, S. N.; Wafford, K. A.; Harper, A. J.; Shanks, E. A.; Carter, G.; O'Neill, M. J.; Murray, T. K.; Eastwood, B. J.; Schaus, J. M.; Beck, J. P.; Hao, J.; Witkin, J. M.; Li, X.; Chernet, E.; Katner, J. S.; Wang, H.; Ryder, J. W.; Masquelin, M. E.; Thompson, L. K.; Love, P. L.; Maren, D. L.; Falcone, J. F.; Menezes, M. M.; Zhang, L.; Yang, C. R.; Svensson, K. A. Preclinical profile of a dopamine D1 potentiator suggests therapeutic utility in neurological and psychiatric disorders. *Neuropharmacology* **2018**, *128*, 351-365.
25. Svensson, K. A.; Heinz, B. A.; Schaus, J. M.; Beck, J. P.; Hao, J.; Krushinski, J. H.; Reinhard, M. R.; Cohen, M. P.; Hellman, S. L.; Getman, B. G.; Wang, X.; Menezes, M. M.; Maren, D. L.; Falcone, J. F.; Anderson, W. H.; Wright, R. A.; Morin, S. M.; Knopp, K. L.; Adams, B. L.; Rogovoy, B.; Okun, I.; Suter, T. M.; Statnick, M. A.; Gehlert, D. R.; Nelson, D. L.; Lucaites, V. L.; Emkey, R.; DeLapp, N. W.; Wiernicki, T. R.; Cramer, J. W.; Yang, C. R.; Bruns, R. F. An allosteric potentiator

- of the dopamine D1 receptor increases locomotor activity in human D1 knock-in mice without causing stereotypy or tachyphylaxis. *J. Pharmacol. Exp. Ther.* **2017**, *360*, 117-128.
26. Luderman, K. D.; Conroy, J. L.; Free, R. B.; Southall, N.; Ferrer, M.; Sanchez-Soto, M.; Moritz, A. E.; Willette, B. K. A.; Fyfe, T. J.; Jain, P.; Titus, S.; Hazelwood, L. A.; Aube, J.; Lane, J. R.; Frankowski, K. J.; Sibley, D. R. Identification of positive allosteric modulators of the D1 dopamine receptor that act at diverse binding sites. *Mol. Pharmacol.* **2018**.
27. Christopoulos, A.; Kenakin, T. G protein-coupled receptor allosterism and complexing. *Pharmacol. Rev.* **2002**, *54*, 323-374.
28. Wootten, D.; Christopoulos, A.; Sexton, P. M. Emerging paradigms in GPCR allostery: implications for drug discovery. *Nat. Rev. Drug Discov.* **2013**, *12*, 630-644.
29. Lewis, M. A.; Hunihan, L.; Watson, J.; Gentles, R. G.; Hu, S.; Huang, Y.; Bronson, J.; Macor, J. E.; Beno, B. R.; Ferrante, M.; Hendricson, A.; Knox, R. J.; Molski, T. F.; Kong, Y.; Cvijic, M. E.; Rockwell, K. L.; Weed, M. R.; Cacace, A. M.; Westphal, R. S.; Alt, A.; Brown, J. M. Discovery of D1 dopamine receptor positive allosteric modulators: characterization of pharmacology and identification of residues that regulate species selectivity. *J. Pharmacol. Exp. Ther.* **2015**, *354*, 340-349.
30. Leach, K.; Sexton, P. M.; Christopoulos, A. Allosteric GPCR modulators: taking advantage of permissive receptor pharmacology. *Trends Pharmacol. Sci.* **2007**, *28*, 382-389.
31. Cabellero, A. G.; Croft, A. K.; Nalli, S. M. Remote aromatic stabilization in radical reactions. *Tetrahedron Lett.* **2008**, *49*, 3613-3615.
32. Camps, P.; Font-Bardia, M.; Giménez, S. I.; Pérez, F.; Solans, X.; Soldevilla, N. (R)- and (S)-3-Hydroxy-4,4-dimethyl-1-phenyl-2-pyrrolidinone as chiral auxiliaries in Diels–Alder reactions. *Tetrahedron: Asymmetry* **1999**, *10*, 3123-3138.
33. Brocksom, T. J.; Nakamura, J.; Ferreira, M. L.; Brocksom, U. The Diels-Alder reaction: an update. *J. Braz. Chem. Soc.* **2001**, *12*, 597-622.
34. Kagan, H. B.; Riant, O. Catalytic asymmetric Diels Alder reactions. *Chem. Rev.* **1992**, *92*, 1007-1019.
35. Nicolaou, K. C.; Snyder, S. A.; Montagnon, T.; Vassilikogiannakis, G. The Diels–Alder reaction in total synthesis. *Angew. Chem.* **2002**, *41*, 1668-1698.
36. Corey, E. J.; Ensley, H. E. Preparation of an optically active prostaglandin intermediate via asymmetric induction. *J. Am. Chem. Soc.* **1975**, *97*, 6908-6909.
37. Neises, B.; Steglich, W. Simple method for the esterification of carboxylic acids. *Angew. Chem. Int. Ed. Engl.* **1978**, *17*, 522-524.
38. Myers, A. G.; Yang, B. H.; Chen, H.; McKinstry, L.; Kopecky, D. J.; Gleason, J. L. Pseudoephedrine as a practical chiral auxiliary for the synthesis of highly enantiomerically enriched carboxylic acids, alcohols, aldehydes, and ketones. *J. Am. Chem. Soc.* **1997**, *119*, 6496-6511.
39. Kim, B. R.; Lee, H.-G.; Kang, S.-B.; Sung, G. H.; Kim, J.-J.; Park, J. K.; Lee, S.-G.; Yoon, Y.-J. *tert*-Butoxide-assisted amidation of esters under green conditions. *Synthesis* **2012**, *44*, 42-50.
40. Poll, T.; Sobczak, A.; Hartmann, H.; Helmchen, G. Diastereoface-discriminative metal coordination in asymmetric synthesis: D-pantolactone as practical chiral auxiliary for Lewis acid catalyzed Diels-Alder reactions. *Tetrahedron Lett.* **1985**, *26*, 3095-3098.
41. Miyaji, K.; Ohara, Y.; Takahashi, Y.; Tsuruda, T.; Arai, K. Synthesis of corey lactone via highly stereoselective asymmetric diels-alder reaction. *Tetrahedron Lett.* **1991**, *32*, 4557-4560.
42. Helmchen, G.; Ihrig, K.; Schindler, H. EPC-syntheses via asymmetric diels-alder reactions/retro diels-alder reactions I: (R)- and (S)-matsutake alcohol. (R)- and (S)-sarcomycin methyl ester. *Tetrahedron Lett.* **1987**, *28*, 183-186.
43. Pelayo, C.; Diego, M.-T. Synthesis and applications of (R)- and (S)-pantolactone as chiral auxiliaries. *Curr. Org. Chem* **2004**, *8*, 1339-1380.
44. Manickam, G.; Sundararajan, G. Asymmetric Diels–Alder and ene reactions promoted by a Ti(IV) complex bearing a C₂-symmetric tridentate ligand. *Tetrahedron: Asymmetry* **1999**, *10*, 2913-2925.
45. Jiang, L. I.; Collins, J.; Davis, R.; Lin, K. M.; DeCamp, D.; Roach, T.; Hsueh, R.; Rebres, R. A.; Ross, E. M.; Taussig, R.; Fraser, I.; Sternweis, P. C. Use of a cAMP BRET sensor to characterize

a novel regulation of cAMP by the sphingosine 1-phosphate/G13 pathway. *J. Biol. Chem.* **2007**, *282*, 10576-10584.

46. Canals, M.; Lane, J. R.; Wen, A.; Scammells, P. J.; Sexton, P. M.; Christopoulos, A. A Monod-Wyman-Changeux mechanism can explain G protein-coupled receptor (GPCR) allosteric modulation. *J. Biol. Chem.* **2012**, *287*, 650-659.

Supplementary Information

Enantioenriched Positive Allosteric Modulators Display Distinct Pharmacology at the Dopamine D₁ Receptor

Tim J. Fyfe,^{†,§} Peter J. Scammells,[†] J. Robert Lane,^{* †} Ben Capuano^{*†}

[†]Medicinal Chemistry, and [§]Drug Discovery Biology, Monash Institute of Pharmaceutical Sciences, Monash University

[‡]School of Life Sciences, Queen's Medical Centre, University of Nottingham, Nottingham NG7 2UH, U.K.

Table of Contents

Chemistry experimental	327-335
Pharmacology experimental	335-337
Figure 1A Chiral HPLC chromatogram for compound 5	337
Figure 2A Chiral HPLC chromatogram for compound (<i>S</i>)- 21	338
Figure 3A Chiral HPLC chromatogram for compound (<i>R</i>)- 21	338
Figures 4A-D HPLC & chiral HPLC chromatograms, ¹ H & ¹³ C NMR spectra for compound 2	339-340
Figure 5 HPLC chromatogram (MeOH blank).....	341
Figure 6A-D HPLC & chiral HPLC chromatograms, ¹ H & ¹³ C NMR spectra for compound (<i>S</i>)- 2	341-343
Figure 7A-D HPLC & chiral HPLC chromatograms, ¹ H & ¹³ C NMR spectra for compound (<i>R</i>)- 2	343-345
References	345

EXPERIMENTAL SECTION

Chemistry: General Information and Synthetic Procedures. Chemicals and solvents were purchased from standard suppliers and used without further purification. Davisil silica gel (40–63 μm) for flash column chromatography was supplied by Grace Davison Discovery Sciences (Victoria, Australia), and deuterated solvents were purchased from Cambridge Isotope Laboratories, Inc. (USA, distributed by Novachem Pty. Ltd., Victoria, Australia). Reactions were monitored by thin layer chromatography on commercially available precoated aluminum-backed plates (Merck Kieselgel 60 F₂₅₄). Visualization was by examination under UV light (254 and 366 nm). A solution of ninhydrin (in ethanol) was used to visualize primary and secondary amines. All organic extracts collected after aqueous workup procedures were dried over anhydrous Na₂SO₄ before gravity/vacuum filtering and evaporation to dryness. Organic solvents were evaporated *in vacuo* at ≤ 40 °C (water bath temperature). ¹H NMR and ¹³C NMR spectra were recorded on a Bruker Avance Nanobay III 400 MHz Ultrashield Plus spectrometer at 400.13 and 100.62 MHz, respectively. Chemical shifts (δ) are recorded in parts per million (ppm) with reference to the chemical shift of the deuterated solvent. Coupling constants (*J*) are recorded in Hz, and the significant multiplicities described by singlet (s), doublet (d), triplet (t), quadruplet (q), broad (br), multiplet (m), doublet of doublets (dd), and doublet of triplets (dt). Spectra were assigned using appropriate COSY, distortionless enhanced polarization transfer (DEPT), HSQC, and HMBC sequences. All NMR experiments were performed in CDCl₃ to permit comparison of the spectra of the various analogues. Experiments were performed in acetone-*d*₆, DMSO-*d*₆, or MeOH-*d*₄ where selected analogues lacked solubility in CDCl₃. LCMS experiments were run using one of two systems to verify reaction outcome. System A was the default unless otherwise stated. System A consisted of the following: an Agilent 6100 series single quad coupled to an Agilent 1200 series HPLC instrument using the following buffers: buffer A, 0.1% formic acid in H₂O; buffer B, 0.1% formic acid in MeCN. The following gradient was used with a Phenomenex Luna 3 μm C8(2) 15 mm \times 4.6 mm column and a flow rate of 0.5 mL/min and total run time of 12 min: 0–4 min 95% buffer A and 5% buffer B, 4–7 min 0% buffer A and 100% buffer B, 7–12 min 95% buffer A and 5% buffer B. Mass spectra were acquired in positive and negative ion modes with a scan range of 0–1000 *m/z* at 5 V. UV detection was carried out at 254 nm. System B consisted of the following: an Agilent 6120 series single quad coupled to an Agilent 1260 series HPLC instrument. The following buffers were used; buffer A, 0.1% formic acid in H₂O; buffer B, 0.1% formic acid in MeCN. The following gradient was used with a Poroshell 120 EC-C18 50 mm \times 3.0 mm, 2.7 μm column and a flow rate of 0.5 mL/min and total run time of 5 min: 0–1 min 95% buffer A and 5% buffer B, from 1 to 2.5 min up to 0% buffer A and 100% buffer B, held at this composition until 3.8 min, 3.8–4 min 95% buffer A and 5% buffer B, held until 5 min at this composition. Mass spectra were acquired in positive and negative ion modes with a scan range of 100–1000 *m/z*. UV detection was carried out at 214 and 254

nm. All retention times (t_R) are quoted in minutes. System C: To verify purity, analytical reverse-phase HPLC was performed on a Waters HPLC system coupled directly to a photodiode array detector and fitted with a Phenomenex Luna C8 (2) 100 Å column (150 mm × 4.6 mm, 5 μm) using a binary solvent system: solvent A, 0.1% TFA/H₂O; solvent B, 0.1% TFA/80% CH₃CN/H₂O. Gradient elution was achieved using 100% solvent A to 100% solvent B over 12 min at a flow rate of 1 mL/min. All compounds subjected to biological testing were found to be >95% pure by HPLC at two wavelengths (λ of 254 and 214 nm). Analytical chiral-HPLC were conducted on an Agilent Infinity 1260 system fitted with either one of (a) Lux 5 μm Amylose-2 150 × 4.60 mm, or (b) Lux 5 μm Cellulose-1 150 × 4.60 mm. A binary solvent system was used (solvent A: ethanol; solvent B: petroleum spirits), with UV detection at 254 nm. The method used isocratic elution of 1-20% solvent A and 99-80% solvent B, with a flow rate of 1 mL/min. Mass spectra were acquired in positive and negative ion mode with a scan range of 100–1000 m/z . UV detection was carried out at 214 and 254 nm. All retention times (t_R) are quoted in minutes. All screening compounds were of >95% purity unless specified in the individual monologue.

General Procedure A for Steglich Esterification. A mixture of methacrylic acid (1.0 equiv.) alcohol (1.0 equiv), EDC (1.1 equiv.) and DMAP (5 mol%) in dry DCM was stirred at rt until complete consumption of the starting acid or alcohol. The reaction mixture was washed with sat. aqueous citric acid (3 × 50 mL) and sat. aqueous NaHCO₃ (3 × 50 mL), dried (Na₂SO₄) and concentrated *in vacuo*. The residue was purified by flash column chromatography (FCC) with an appropriate eluent as indicated.

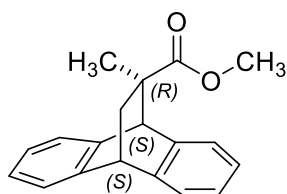
General Procedure B for TiCl₄-catalysed Diels Alder Cycloaddition. A solution of TiCl₄ (2.0 equiv.) in anhydrous DCM (20 mL) was added to a solution of the appropriate chiral auxiliary/dienophile (1.0 equiv.) in anhydrous DCM (30 mL), and the mixture stirred at rt for 15 min. Then, a solution of the anthracene (1.0 equiv.) in dry CH₂Cl₂ (20 mL) was added and the mixture stirred at r.t. for 15 h. A small amount of H₂O was added to destroy the TiCl₄ complexes, the mixture was filtered and the filtrate was dried with anhydrous Na₂SO₄. The filtrate was concentrated *in vacuo* and the residue was purified by FCC using an appropriate eluent as indicated.

General Procedure C for Alkaline Ester Hydrolysis. To a solution of ester (1.0 equiv.) in a 1:1 mixture of THF/H₂O was added NaOH (3 equiv.), and the mixture stirred at reflux temperature until complete consumption of the starting material was evident. The THF was removed *in vacuo* and the remaining aqueous phase was washed with Et₂O. The aqueous phase was then acidified (pH = 1), and any precipitated carboxylic acid was collected via vacuum filtration and recrystallised from EtOAc/PE. Similarly, the aqueous phase could be extracted with DCM and the organic extracts dried (Na₂SO₄) to afford the desired carboxylic acid to maximise the yield.

General Procedure D for Acyl Halide Formation and Nucleophilic Substitution. The carboxylic acid (1 equiv.) was taken up in thionyl chloride (5 mL) followed by three drops of DMF and the reaction was stirred at reflux temperature until complete consumption of the starting material. The solvent was removed *in vacuo* and the residue was taken up in dry MeCN (25 mL). To this solution was added 2,6-dichloro-3-methylaniline (1.1 equiv.), DMAP (0.5 equiv.), DIPEA (2.0 equiv.) and stirred at reflux temperature until complete consumption of the acyl halide was evident. The solvent was evaporated under reduced pressure and the residue was taken up in EtOAc, washed with 1M aqueous NaOH, H₂O, 1M aqueous HCl, brine, and the organic layer dried (NaSO₄). The solvent was concentrated *in vacuo* and the residue purified by FCC with an appropriate eluent as indicated.

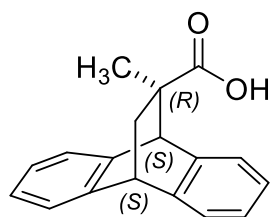
Methyl (*rel*-9*S*,10*S*,12*R*)-12-methyl-9,10-dihydro-9,10-ethanoanthracene-12-carboxylate¹ (5).

Methyl methacrylate (3.29 mL, 30.9 mmol, 1.1 eq.) was added to a suspension of AlCl₃ (3.74 g, 28.1 mmol, 1.0 eq.) in dry DCM (100 mL), in a three-necked round-bottom flask under a positive pressure of N₂. After 1 h of stirring, anthracene (5.00 g, 28.1 mmol, 1.0 eq.) was added portion-wise. The resulting mixture was stirred at room temperature for 72 h or until complete consumption of the anthracene was evident. The mixture was then poured over ice, the organic layer separated, washed with water (40 mL), dried (Na₂SO₄), and the solvent evaporated. The resulting residue was dissolved in DCM, absorbed onto silica gel and purified by FCC (eluent, 9:1 PE/Et₂O) to afford the title compound as a transparent oil which solidified under high vacuum to give a white solid (5.67 g, 72%). LCMS (*m/z*): 301.1 [M+Na]⁺. System C HPLC: *t_R* 8.389 min, >95% purity (214 & 254 nm). ¹H NMR (CDCl₃) δ 7.32 – 7.28 (m, 1H), 7.26 – 7.22 (m, 2H), 7.19 (dd, *J* = 6.9, 1.6 Hz, 1H), 7.13 – 7.08 (m, 2H), 7.08 – 7.01 (m, 2H), 4.40 (s, 1H), 4.25 (t, *J* = 2.7 Hz, 1H), 3.53 (s, 3H) 2.71 (dd, *J* = 12.7, 3.0 Hz, 1H), 1.39 (dd, *J* = 12.7, 2.5 Hz, 1H), 1.05 (s, 3H). ¹³C NMR (CDCl₃) δ 177.2, 143.8, 143.2, 141.6, 140.5, 126.4, 126.2, 126.2, 125.7, 125.6, 124.7, 123.6, 123.2, 52.9, 52.1, 44.5, 38.9, 26.7.



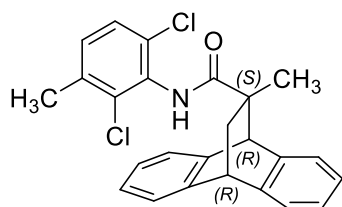
***rel*-(9*S*,10*S*,12*R*)-12-methyl-9,10-dihydro-9,10-ethanoanthracene-12-carboxylic acid (6).**

Synthesised according to general procedure C using LiOH.H₂O (2.15 g, 89.8 mmol). After acidification, the precipitated solids were washed with water and recrystallised from EtOAc/PE, affording the compound as white needles (4.75 g, quantitative). LCMS (*m/z*): 263.1 [M-H]⁺. System C HPLC: *t_R* 7.181 min, >95% purity (214 & 254 nm). ¹H NMR (CDCl₃) δ 7.31 – 7.28 (m, 1H), 7.27 – 7.23 (m, 3H), 7.23 – 7.19 (m, 1H), 7.12 (ddd, *J* = 6.1, 5.6, 3.7 Hz, 2H), 7.08 (dd, *J* = 7.2, 1.5 Hz, 1H), 7.06 – 7.01 (m, 1H), 4.37 (s, 1H), 4.26 (t, *J* = 2.7 Hz, 1H), 2.62 (dd, *J* = 12.7, 3.0 Hz, 1H), 1.40 (dd, *J* = 12.7, 2.5 Hz, 1H), 1.07 (s, 3H). ¹³C NMR (CDCl₃) δ 181.7, 143.6, 143.3, 141.3, 140.5,



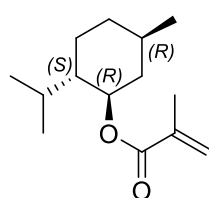
126.5, 126.3, 126.2, 125.8, 125.7, 125.2, 123.5, 123.3, 52.6, 48.5, 44.5, 38.7, 26.9. Analytical data including ¹H NMR and ¹³C NMR spectra are in accordance with those published.^{2,3}

***rel*-(9*R*,10*R*,12*S*)-*N*-(2,6-dichloro-3-methylphenyl)-12-methyl-9,10-dihydro-9,10-ethanoanthracene-12-carboxamide (*rac*-2).**

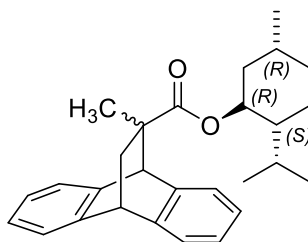


Synthesised according to general procedure D using oxalyl chloride (243 μ L, 2.84 mmol), *rel*-(9*S*,10*S*,12*R*)-12-methyl-9,10-dihydro-9,10-ethanoanthracene-12-carboxylic acid (**6**) (375 mg, 1.42 mmol), DMAP (4.32 mg, 35.4 μ mol), DIPEA (120 μ L, 707 μ mol) and 2,6-dichloro-3-methylaniline (65.4 mg, 371 μ mol). Purification by FCC (eluent, 10:1 PE/EtOAc) afforded the racemic compound as a white solid (75 mg, 50%). LCMS (m/z): 446.1 [M+Na]⁺, 423.1 [M+H]⁺. System C HPLC: t_R 8.496 min, >95% purity (214 & 254 nm). HRMS (m/z): C₂₅H₂₁Cl₂NO: requires 422.1083 [M+H]⁺; found 422.1073. ¹H NMR (CDCl₃) δ 7.40 – 7.37 (m, 1H), 7.34 – 7.31 (m, 1H), 7.30 – 7.25 (m, 2H), 7.18 – 7.11 (m, 3H), 7.08 – 7.01 (m, 3H), 6.89 (s, 1H), 4.52 (s, 1H), 4.34 (t, J = 2.6 Hz, 1H), 2.64 (dd, J = 12.5, 2.8 Hz, 1H), 2.29 (s, 3H), 1.66 (dd, J = 12.4, 2.7 Hz, 1H), 1.18 (s, 3H). ¹³C NMR (CDCl₃) δ 174.7, 143.3, 143.2, 141.5, 141.4, 136.1, 133.8, 132.2, 130.8, 129.6, 127.4, 126.5, 126.4, 126.2, 125.9, 125.9, 125.7, 123.5, 123.2, 52.7, 49.2, 44.7, 40.3, 28.3, 20.5. Analytical data including ¹H NMR and ¹³C NMR spectra are in accordance with those published.³

(1*R*,2*S*,5*R*)-2-Isopropyl-5-methylcyclohexyl methacrylate (13**).**

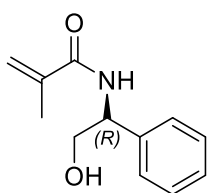


Synthesised according to general procedure A using methacrylic acid (1.62 mL, 19.2 mmol), (1*R*,2*S*,5*R*)-2-isopropyl-5-methylcyclohexan-1-ol (3.00 g, 19.2 mmol), EDC (4.05 g, 21.2 mmol) and DMAP (117 mg, 960 μ mol). Purification by FCC (eluent, DCM) gave the title compound as a transparent oil (3.20 g, 74%). LCMS (m/z): 225.2 [M+H]⁺. System C HPLC: t_R 9.042 min, >95% purity (214 & 254 nm). ¹H NMR (CDCl₃) δ 6.23 – 6.20 (m, 1H), 5.81 (dd, J = 2.0, 1.2 Hz, 1H), 3.39 (td, J = 10.4, 4.3 Hz, 1H), 2.16 (dtd, J = 14.0, 7.0, 2.7 Hz, 1H), 1.99 (dt, J = 1.5, 0.9 Hz, 3H), 1.95 – 1.91 (m, 1H), 1.61 (ddd, J = 16.1, 14.6, 7.9 Hz, 2H), 1.45 – 1.37 (m, 2H), 1.14 – 1.05 (m, 1H), 0.96 (dd, J = 12.1, 4.1 Hz, 1H), 0.94 – 0.88 (m, 6H), 0.80 (dd, J = 7.0, 0.9 Hz, 3H). ¹³C NMR (CDCl₃) δ 163.2, 135.9, 129.1, 71.7, 50.3, 45.2, 34.7, 31.8, 25.9, 23.3, 22.3, 21.1, 16.2. Analytical data in accordance with those published.⁴

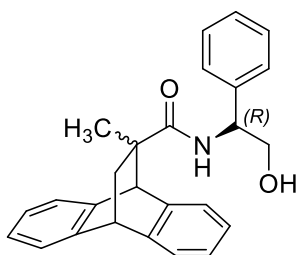
(1*R*,2*S*,5*R*)-2-Isopropyl-5-methylcyclohexyl-12-methyl-9,10-dihydro-9,10-ethanoanthracene-12-carboxylate (14).

Synthesised according to general procedure B using TiCl₄ (4.38 μ L, 3.93 mmol), (1*R*,2*S*,5*R*)-2-isopropyl-5-methylcyclohexyl methacrylate (**13**) (440 mg, 1.96 mmol) and anthracene (350 mg, 1.96 mmol). Purification by FCC (eluent, 10:1 PE/EtOAc] gave the anthracene ester derivative as a light yellow oil (400 mg, 51%, *d.e.* >70%). LCMS (*m/z*): 401.1 [M-H]⁻.

System C HPLC: *t_R* 2.204 min, >95% purity (214 & 254 nm). ¹H NMR (CDCl₃) δ 7.30 – 7.27 (m, 1H), 7.25 – 7.18 (m, 3H), 7.11 – 7.07 (m, 2H), 7.07 – 6.98 (m, 2H, H3), 4.48 (td, *J* = 10.8, 4.3 Hz, 1H), 4.38 (s, 1H), 4.23 (t, *J* = 2.6 Hz, 1H), 2.70 (dd, *J* = 12.7, 3.0 Hz, 1H), 1.86 (tt, *J* = 11.3, 3.5 Hz, 1H), 1.67 – 1.57 (m, 3H), 1.41 – 1.36 (m, 2H), 1.36 – 1.32 (m, 1H), 1.02 (s, 3H), 0.98 (dd, *J* = 13.1, 3.2 Hz, 1H), 0.91 (d, *J* = 7.0 Hz, 3H), 0.88 – 0.85 (m, 2H), 0.82 (d, *J* = 6.5 Hz, 3H), 0.68 (d, *J* = 6.9 Hz, 3H). ¹³C NMR (CDCl₃) δ 176.3, 143.9, 143.4, 141.5, 141.0, 126.3, 126.1, 126.0, 125.5, 125.5, 125.2, 123.4, 123.2, 74.7, 52.9, 47.1, 44.6, 40.6, 38.8, 34.3, 31.4, 27.3, 26.0, 23.2, 22.1, 21.1, 16.1.

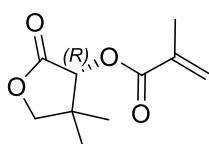
(*R*)-*N*-(2-hydroxy-1-phenylethyl)methacrylamide⁵ (16).

KO*t*-Bu (3.27 g, 29.2 mmol) was dissolved in THF (100 mL; technical grade, containing ca. 0.2% H₂O) with stirring in air at rt for 1 min. Methyl methacrylate (1.55 mL, 14.6 mmol) and (*R*)-2-amino-2-phenylethan-1-ol (2.00 g, 14.6 mmol) were added immediately and the mixture was stirred at rt for 1 h. After evaporating the THF under reduced pressure, H₂O (75 mL) and DCM (75 mL) were added and the organic layer was separated and dried (Na₂SO₄). The solvent was evaporated under reduced pressure and residue was purified by FCC (eluent, 1:10 DCM/MeOH) to give the corresponding amide as a yellow/orange solid (2.45 g, 89%). LCMS (*m/z*): 206.1 [M+H]⁺. System C HPLC: *t_R* 4.465 min, >95% purity (214 & 254 nm). ¹H NMR (CDCl₃) δ 7.38 – 7.33 (m, 2H), 7.32 – 7.28 (m, 3H), 6.57 (d, *J* = 5.6 Hz, 1H), 5.75 (s, 1H), 5.37 – 5.36 (m, 1H), 5.10 (dt, *J* = 7.0, 5.0 Hz, 1H), 3.89 (d, *J* = 4.9 Hz, 2H), 2.96 (s, 1H), 1.98 – 1.97 (m, 3H). ¹³C NMR (CDCl₃) δ 168.9, 139.8, 139.2, 129.0, 128.0, 126.8, 120.3, 66.6, 56.1, 18.8. Analytical data in accordance with those published.⁵

***N*-((*R*)-2-Hydroxy-1-phenylethyl)-11-methyl-9,10-dihydro-9,10-ethanoanthracene-11-carboxamide (17).**

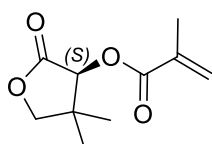
Synthesised according to general procedure B using TiCl₄ (1.45 mL, 13.0 mmol), (*R*)-*N*-(2-hydroxy-1-phenylethyl)methacrylamide (1.34 g, 6.51 mmol) (**16**) and anthracene (1.16 g, 6.51 mmol). Residue chromatographed with 5:1 PE/EtOAc to afford a pair of diastereomers (2:1 ratio) as a transparent oil (2.00 g, 80%). LCMS (*m/z*): 384.2 [M+H]⁺.

System C HPLC: *t_R* 7.254min, >95% purity (214 & 254 nm). ¹H NMR (401 MHz, CDCl₃) δ 7.36 – 7.25 (m, 12H), 7.20 – 7.11 (m, 6H), 7.08 – 6.99 (m, 4H), 6.04 (s, 0.5H), 5.75 (s, 1H), 4.86 (dt, *J* = 12.5, 5.8 Hz, 1.7H), 4.34 (d, *J* = 2.2 Hz, 3H), 3.80 (dd, *J* = 4.6, 2.4 Hz, 1H), 3.68 (dd, *J* = 11.3, 5.6 Hz, 1H), 3.59 (dd, *J* = 11.3, 3.9 Hz, 1H), 2.58 (dd, *J* = 12.8, 3.0 Hz, 0.7H), 2.38 (dd, *J* = 13.1, 3.0 Hz, 1H), 1.59 (dd, *J* = 13.2, 2.5 Hz, 1H), 1.55 (dd, *J* = 13.4, 3.0 Hz, 0.6H), 1.10 (s, *J* = 2.6 Hz, 1.4H), 1.09 (s, 3H).

(*R*)-4,4-Dimethyl-2-oxotetrahydrofuran-3-yl methacrylate ((*R*)-19).

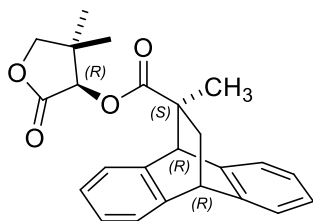
Synthesised according to general procedure A using methacrylic acid (1.49 g, 17.3 mmol), (*R*)-3-hydroxy-4,4-dimethyldihydrofuran-2(3*H*)-one (2.25 g, 17.3 mmol), EDC (3.31 g, 17.3 mmol) and DMAP (106 mg, 864 μmol). Purification by FCC (eluent, DCM) gave the title compound as a transparent oil (3.55 g, 67%). LCMS

(*m/z*): 221.1 [M+Na]⁺. System C HPLC: *t_R* 6.010 min, >95% purity (214 & 254 nm). ¹H NMR (CDCl₃) δ 6.26 – 6.15 (m, 1H), 5.68 (dd, *J* = 2.6, 1.2 Hz, 1H), 5.41 (d, *J* = 0.8 Hz, 1H), 4.09 – 4.01 (m, 2H), 1.98 (dd, *J* = 1.7, 0.8 Hz, 3H), 1.21 (s, 3H), 1.13 (s, 3H). ¹³C NMR (CDCl₃) δ 172.4, 165.9, 135.1, 127.5, 76.2, 75.2, 23.1, 19.9, 18.2.

(*S*)-4,4-Dimethyl-2-oxotetrahydrofuran-3-yl methacrylate ((*S*)-19).

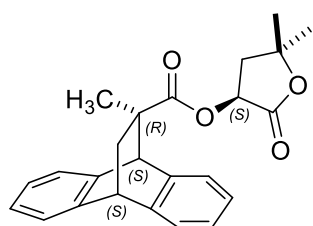
Synthesised according to general procedure A using methacrylic acid (2.32 g, 26.9 mmol), (*S*)-3-hydroxy-4,4-dimethyldihydrofuran-2(3*H*)-one (3.50 g, 26.9 mmol), EDC (5.16 g, 26.9 mmol) and DMAP (164 mg, 1.34 mmol). Purification by FCC (eluent, DCM) gave the title compound as a transparent oil (1.05 g, 69%).

LCMS (*m/z*): 221.1 [M+Na]⁺. System C HPLC: *t_R* 6.010 min, >95% purity (214 & 254 nm). ¹H NMR (CDCl₃) δ 6.26 – 6.15 (m, 1H), 5.68 (dd, *J* = 2.6, 1.2 Hz, 1H), 5.41 (d, *J* = 0.8 Hz, 1H), 4.09 – 4.01 (m, 2H), 1.98 (dd, *J* = 1.7, 0.8 Hz, 3H), 1.21 (s, 3H), 1.13 (s, 3H). ¹³C NMR (CDCl₃) δ 172.4, 165.9, 135.1, 127.5, 76.2, 75.2, 23.1, 19.9, 18.2.

(R)-4,4-Dimethyl-2-oxotetrahydrofuran-3-yl-(S)-12-methyl-9,10-dihydro-9,10-ethanoanthracene-12-carboxylate ((S)-20).

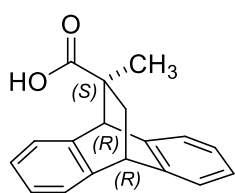
Synthesised according to general procedure B using TiCl₄ (2.39 mL, 21.8 mmol), (R)-4,4-dimethyl-2-oxotetrahydrofuran-3-yl methacrylate ((R)-19) (2.06 g, 10.4 mmol) and anthracene (1.85 g, 10.4 mmol). Purification by FCC (eluent, DCM) afforded the title compound as a brown solid. Recrystallization from EtOH gave white crystals (3.25 g, 83%, *d.e.* ~90%).

LCMS (*m/z*): 399.1 [M+Na]⁺. System C HPLC: *t_R* 8.320 min, >95% purity (214 & 254 nm). ¹H NMR (401 MHz, CDCl₃) δ 7.33 (dt, *J* = 5.4, 3.3 Hz, 1H), 7.30 – 7.26 (m, 2H), 7.24 – 7.21 (m, 1H), 7.16 – 7.10 (m, 2H), 7.10 – 7.02 (m, 2H), 5.18 (s, 1H), 4.40 (s, 1H), 4.30 (t, *J* = 2.7 Hz, 1H), 4.04 (d, *J* = 9.0 Hz, 1H), 3.97 (d, *J* = 9.0 Hz, 1H), 2.76 (dd, *J* = 12.8, 3.0 Hz, 1H), 1.50 (dd, *J* = 12.8, 2.6 Hz, 1H), 1.25 (s, 3H), 1.18 (s, 3H), 1.17 (s, 3H). ¹³C NMR (CDCl₃) δ 175.6, 172.1, 143.7, 143.5, 141.2, 140.4, 126.6, 126.6, 125.7, 125.5, 124.8, 123.9, 123.4, 76.2, 75.5, 52.6, 49.0, 44.4, 39.2, 27.2, 23.0, 20.3.

(S)-4,4-Dimethyl-2-oxotetrahydrofuran-3-yl-(R)-12-methyl-9,10-dihydro-9,10-ethanoanthracene-12-carboxylate ((R)-20).

Synthesised according to general procedure B using TiCl₄ (1.61 mL, 14.7 mmol), (S)-4,4-dimethyl-2-oxotetrahydrofuran-3-yl methacrylate ((S)-19) (1.39 g, 7.01 mmol) and anthracene (1.25 g, 7.01 mmol). Purification by FCC (eluent, DCM) afforded the title compound as a beige solid (2.15 g, 82%, *d.e.* ~83%) LCMS (*m/z*): 399.1 [M+Na]⁺. System C HPLC: *t_R* 8.320

min, >95% purity (214 & 254 nm). ¹H NMR (CDCl₃) δ 7.33 (dt, *J* = 5.4, 3.3 Hz, 1H), 7.30 – 7.26 (m, 2H), 7.24 – 7.21 (m, 1H), 7.16 – 7.10 (m, 2H), 7.10 – 7.02 (m, 2H), 5.18 (s, 1H), 4.40 (s, 1H), 4.30 (t, *J* = 2.7 Hz, 1H), 4.04 (d, *J* = 9.0 Hz, 1H), 3.97 (d, *J* = 9.0 Hz, 1H), 2.76 (dd, *J* = 12.8, 3.0 Hz, 1H), 1.50 (dd, *J* = 12.8, 2.6 Hz, 1H), 1.25 (s, 3H), 1.18 (s, 3H), 1.17 (s, 3H). ¹³C NMR (CDCl₃) δ 175.6, 172.1, 143.7, 143.5, 141.2, 140.4, 126.6, 126.6, 125.7, 125.5, 124.8, 123.9, 123.4, 76.2, 75.5, 52.6, 49.0, 44.4, 39.2, 27.2, 23.0, 20.3.

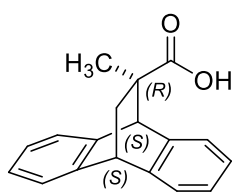
(S)-12-Methyl-9,10-dihydro-9,10-ethanoanthracene-12-carboxylic acid ((S)-21).

Synthesised according to general procedure C using (R)-4,4-Dimethyl-2-oxotetrahydrofuran-3-yl-(S)-12-methyl-9,10-dihydro-9,10-ethanoanthracene-12-carboxylate ((S)-20) (3.00 g, 7.97 mmol) and NaOH (956 mg, 23.9 mmol).

The aqueous phase was extracted with DCM, and the organic extracts were dried (Na₂SO₄) and evaporated to dryness to afford the desired acid as a white foam (2.05 g, 95%, *e.e.* ~88%). [α]_D²⁵ = -24.9° (*c* 1.0, CHCl₃), ^{lit}[α]_D²⁰ = -26.7° (*c* 1.08, CHCl₃),² LCMS (*m/z*): 263.1 [M-H]⁻.

System C HPLC: t_R 7.181 min, >95% purity (214 & 254 nm). Analytical data including ¹H NMR and ¹³C NMR spectra are in accordance with those reported by Camps *et al.*²

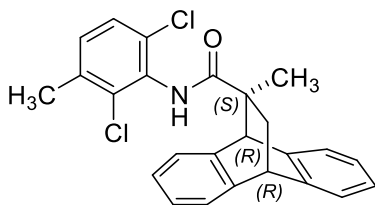
(R)-12-Methyl-9,10-dihydro-9,10-ethanoanthracene-12-carboxylic acid ((R)-21).



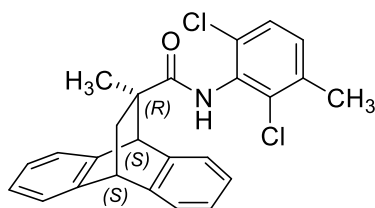
Synthesised according to general procedure C using (*S*)-4,4-Dimethyl-2-oxotetrahydrofuran-3-yl-(*S*)-12-methyl-9,10-dihydro-9,10-ethanoanthracene-12-carboxylate ((*R*)-20) (1.40 g, 3.72 mmol) and NaOH (446 mg, 11.2 mmol).

The aqueous phase was extracted with DCM, and the organic extracts were dried (Na₂SO₄) and evaporated to dryness to afford the desired acid as a white solid (956 mg, 98%, *e.e.* ~83%). [α]_D²⁵ = +24.1° (*c* 1.0, CHCl₃), LCMS (*m/z*): 263.1 [M-H]⁻. System C HPLC: t_R 7.181 min, >95% purity (214 & 254 nm). ¹H NMR (CDCl₃) δ 7.31 – 7.28 (m, 1H), 7.27 – 7.23 (m, 3H), 7.23 – 7.19 (m, 1H), 7.12 (ddd, *J* = 6.1, 5.6, 3.7 Hz, 2H), 7.08 (dd, *J* = 7.2, 1.5 Hz, 1H) 7.06 – 7.01 (m, 1H), 4.37 (s, 1H), 4.26 (t, *J* = 2.7 Hz, 1H), 2.62 (dd, *J* = 12.7, 3.0 Hz, 1H), 1.40 (dd, *J* = 12.7, 2.5 Hz, 1H), 1.07 (s, 3H). ¹³C NMR (CDCl₃) δ 181.7, 143.6, 143.3, 141.3, 140.5, 126.5, 126.3, 126.2, 125.8, 125.7, 125.2, 123.5, 123.3, 52.6, 48.5, 44.5, 38.7, 26.9.

(9*S*,10*R*,12*R*)-*N*-(2,6-Dichloro-3-methylphenyl)-12-methyl-9,10-dihydro-9,10-ethanoanthracene-12-carboxamide ((*S*)-2).



Synthesised according to general procedure D using (*S*)-12-methyl-9,10-dihydro-9,10-ethanoanthracene-11-carbonyl chloride ((*S*)-21) (260 mg, 919 μ mol), 2,6-dichloro-3-methylaniline (162 mg, 920 μ mol), and DMAP (56.2 mg, 460 μ mol). Purification by FCC (eluent, 1:10 EtOAc/PE) afforded the title compound as a white solid (75 mg, 19%, *e.e.* 90%). LCMS (*m/z*): 446.1 [M+Na]⁺, 423.1 [M+H]⁺. System C HPLC: t_R 8.496 min, >95% purity (214 & 254 nm). HRMS (*m/z*): C₂₅H₂₁Cl₂NO: requires 422.1083 [M+H]⁺; found 422.1073. ¹H NMR (CDCl₃) δ 7.40 – 7.37 (m, 1H), 7.34 – 7.31 (m, 1H), 7.30 – 7.25 (m, 2H), 7.18 – 7.11 (m, 3H), 7.08 – 7.01 (m, 3H), 6.89 (s, 1H), 4.52 (s, 1H), 4.34 (t, *J* = 2.6 Hz, 1H), 2.64 (dd, *J* = 12.5, 2.8 Hz, 1H), 2.29 (s, 3H), 1.66 (dd, *J* = 12.4, 2.7 Hz, 1H), 1.18 (s, 3H). ¹³C NMR (CDCl₃) δ 174.7, 143.3, 143.2, 141.5, 141.4, 136.1, 133.8, 132.2, 130.8, 129.6, 127.4, 126.5, 126.4, 126.2, 125.9, 125.9, 125.7, 123.5, 123.2, 52.7, 49.2, 44.7, 40.3, 28.3, 20.5.

(9R,10S,12S)-N-(2,6-Dichloro-3-methylphenyl)-12-methyl-9,10-dihydro-9,10-ethanoanthracene-12-carboxamide ((R)-2).

Synthesised according to general procedure D using (*R*)-12-methyl-9,10-dihydro-9,10-ethanoanthracene-11-carbonyl chloride ((*R*)-**21**) (135 mg, 477 μ mol), 2,6-dichloro-3-methylaniline (84.1 mg, 477 μ mol), and DMAP (29.1 mg, 239 μ mol). Purification by FCC (eluent, 1:10 EtOAc/PE) afforded the title compound as a white solid (50 mg, 25%, *e.e.* 84%). LCMS (*m/z*): 446.1 [M+Na]⁺, 423.1 [M+H]⁺. System C HPLC: *t_R* 8.496 min, >95% purity (214 & 254 nm). HRMS (*m/z*): C₂₅H₂₁C₁₂NO: requires 422.1083 [M+H]⁺; found 422.1073. ¹H NMR (CDCl₃) δ 7.40 – 7.37 (m, 1H), 7.34 – 7.31 (m, 1H), 7.30 – 7.25 (m, 2H), 7.18 – 7.11 (m, 3H), 7.08 – 7.01 (m, 3H), 6.89 (s, 1H), 4.52 (s, 1H), 4.34 (t, *J* = 2.6 Hz, 1H), 2.64 (dd, *J* = 12.5, 2.8 Hz, 1H), 2.29 (s, 3H), 1.66 (dd, *J* = 12.4, 2.7 Hz, 1H), 1.18 (s, 3H). ¹³C NMR (CDCl₃) δ 174.7, 143.3, 143.2, 141.5, 141.4, 136.1, 133.8, 132.2, 130.8, 129.6, 127.4, 126.5, 126.4, 126.2, 125.9, 125.9, 125.7, 123.5, 123.2, 52.7, 49.2, 44.7, 40.3, 28.3, 20.5.

Pharmacological Characterisation. *Materials.* Dulbecco's modified Eagle's medium, Flp-In CHO cells, and hygromycin B were purchased from Invitrogen (Carlsbad, CA). Fetal bovine serum (FBS) was purchased from ThermoTrace (Melbourne, VIC, Australia). All other reagents were purchased from Sigma Aldrich (St. Louis, MO).

Cell culture. FlpIn Chinese Hamster Ovary (CHO) cells (Invitrogen, Carlsbad, CA, USA) were grown in DMEM supplemented with 10% fetal bovine serum and maintained at 37 °C in a humidified incubator containing 5% CO₂. The Flp-In-CHO cells were transfected with the pOG44 vector encoding Flp recombinase and the pDEST vector encoding the D_{2L}R or the hD₁R at a ratio of 9:1 using polyethylenimine as the transfection reagent. Twenty-four hours after transfection, the cells were subcultured and the medium was supplemented with 700 mg.ml⁻¹ HygroGold (Invivogen) as selection agent, to obtain cells stably expressing the D_{2L}R or D₁R. FlpIn Chinese Hamster Ovary CHO cells stably expressing the hD_{2L}R or hD₁R were grown and maintained in Dulbecco's modified Eagle's medium (DMEM) supplemented with 10% fetal bovine serum (FBS), and 200 μ g/mL of Hygromycin-B, and maintained at 37 °C in a humidified incubator containing 5% CO₂.

Cell culture and transfection for cAMP assay: FlpIn CHO cells stably expressing the human dopamine D₁ receptor were maintained in DMEM supplemented with 5% foetal calf serum (FBS) and 0.2 mg/mL hygromycin at 37 °C in a humidified incubator supplied with 5% CO₂. For transfection, the cells were grown in 10 cm culture dishes until 60 % confluent. A mixture of 4 μ g

plasmid DNA containing BRET-based cAMP (CAMYEL) biosensor construct⁶ and 25 µg 20 kDa linear polyethylene imine (PEI) in 500 µL 150 mM NaCl was added into a dish of cells.

cAMP measurement: The cellular cAMP levels were measured with the CAMYEL BRET-based biosensor for cAMP.⁶ One day after transfection, cells were trypsinised and seeded in white 96-well microplates. The cells were then cultured for an additional day, rinsed twice with Hank's Balanced Salt Solution (HBSS) and were then incubated in fresh HBSS. For the D₁R functional assay, the cells were stimulated with dopamine together with addition of the modulators. The BRET signals were measured using a BMG Lumistar counter 30 min after stimulation. For the D₂R functional assay, the cells were stimulated with dopamine in the presence of 10 µM forskolin (final concentration). Dopamine and the modulators were added 15 min prior to stimulation and the BRET signals were measured using a BMG Lumistar counter 30 min after stimulation. The BRET signal (BRET ratio) was detected at 445-505 and 505-565 nm using a LUMIstar Omega instrument (BMG LabTech, Offenburg, Germany), and determined by calculating the ratio of the light emitted at 535 ± 30 nm (YFP) to the light emitted at 475 ± 30 nm (RLuc).

Data analysis. Computerized nonlinear regression, statistical analyses and simulations were performed using Prism 6.0 (GraphPad Prism 6.0b Software, San Diego, CA).

Analysis of functional data. All concentration-response data were fitted to the following modified four-parameter Hill equation to derive potency estimates.⁷

$$E = Basal + \frac{(E_{max}-Basal) \cdot [A]^{nH}}{[A]^{nH} + EC_{50}^{nH}} \quad (1)$$

where E is the effect of the system, nH is the Hill slope and EC₅₀ is the concentration of agonist [A] that gives the midpoint response between basal and maximal effect of dopamine or other agonists (E_{max}), which are the lower and upper asymptotes of the response, respectively.

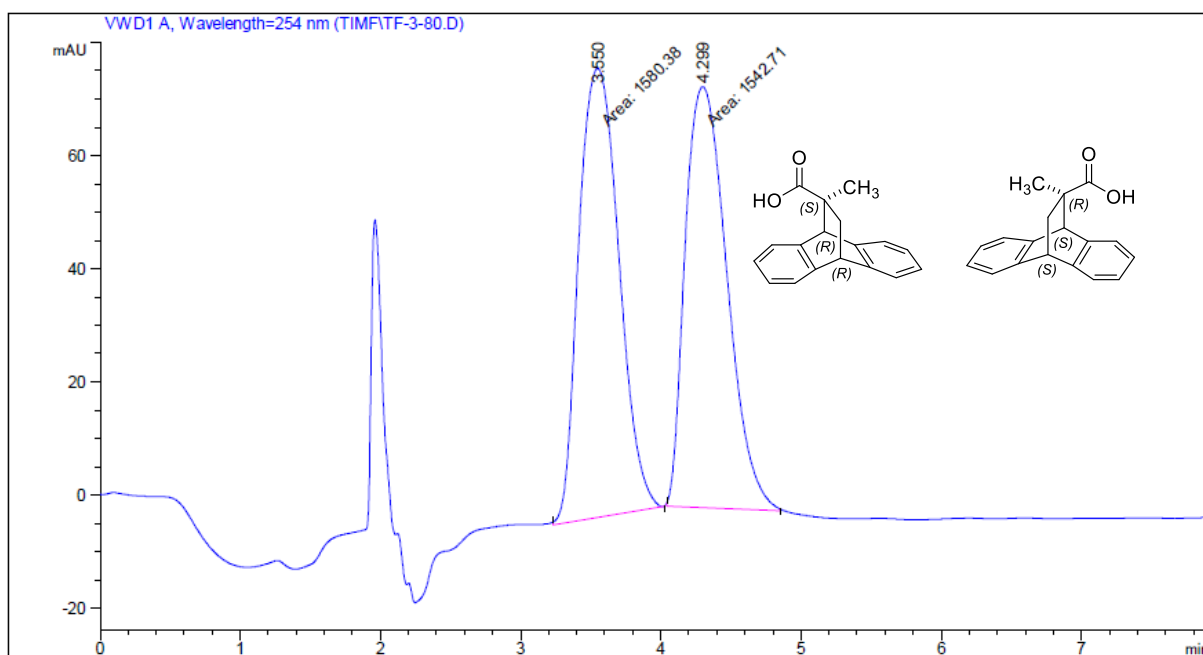
To determine the mode of interaction of compounds **2**, and optical isomers of **2** at the D₁R in relation to the agonist dopamine, all data were analyzed using a complete operational model of allosterism and agonism according to equation 2:⁸

$$E = \frac{E_m(\tau_A[A](K_B + \alpha\beta[B]) + \tau_B[B]K_A)^{nH}}{([A]K_B + K_A K_B + K_A[B] + \alpha[A][B])^{nH} + (\tau_A[A](K_B + \alpha\beta[B]) + \tau_B[B]K_A)^{nH}} \quad (2)$$

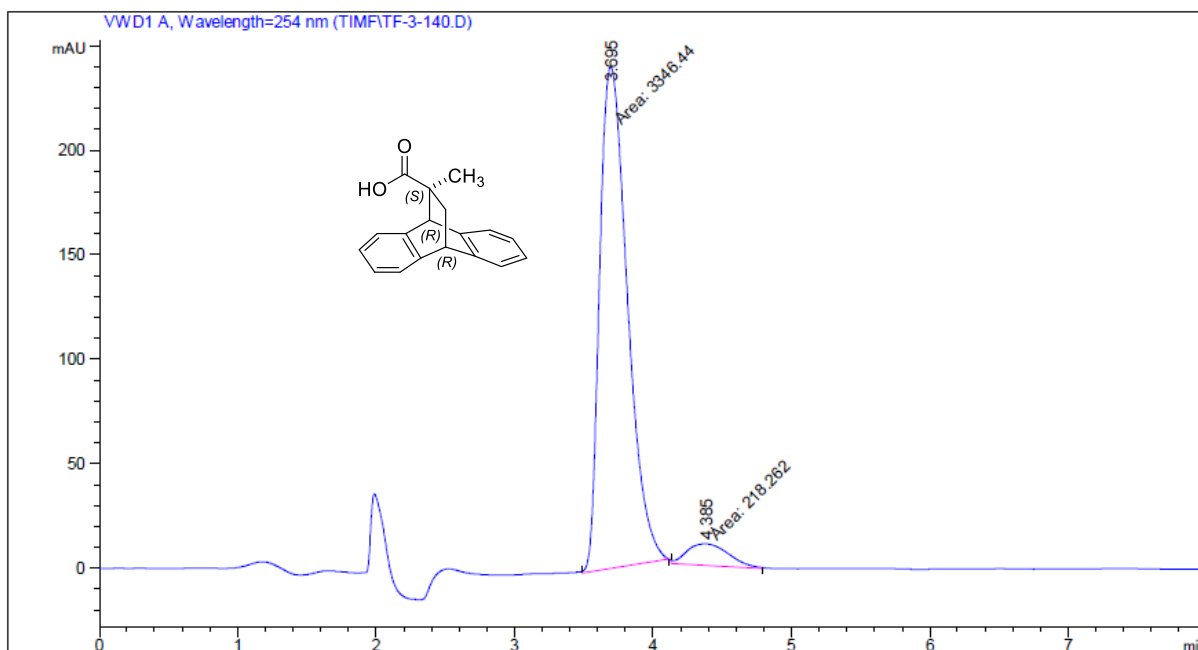
Where E_m is the maximum possible cellular response, [A] and [B] are the concentrations of orthosteric and allosteric ligands, respectively, K_A and K_B are the equilibrium dissociation constant of the orthosteric and allosteric ligands, respectively, τ_A and τ_B are operational measures of orthosteric and allosteric ligand efficacy (which incorporate both signal efficiency and receptor density), respectively, α is the binding cooperativity parameter between the orthosteric and allosteric ligand, and β denotes

the magnitude of the allosteric effect of the modulator on the efficacy of the orthosteric agonist. The K_A for dopamine was determined through receptor depletion by phenoxybenzamine alkylation as the proportional relationship of R_T to measured τ , K_A is invariant with receptor depletion. Thus, unique estimates of K_A could be obtained by direct operational model fitting of the family of concentration-response curve for dopamine.^{9,10} A series of cAMP inhibition assays were conducted in cells which were pre-treated with phenoxybenzamine (an alkylating agent which is used to inhibit high affinity orthosteric interactions at the D₂R).¹¹ The data for DA evaluated in the presence of the alkylating agent were then fit to an operational model of receptor depletion in order to determine values of K_A and τ_A ($\log K_A = -5.78 \pm 0.16$, $\log \tau_A = 1.84 \pm 0.16$). These data were used to constrain values of K_A and τ_A when we fitted the operational model of allostery (equation 2) to functional data. The value of the Hill slope (nH) was fixed to unity. The logarithms of affinity and cooperativity values are normally distributed, whereas the absolute values (antilogarithms) are not, and therefore all statistical analyses were performed on the logarithmic values. However for ease of interpretation, allosteric parameter antilogarithms are highlighted in the main text.¹²

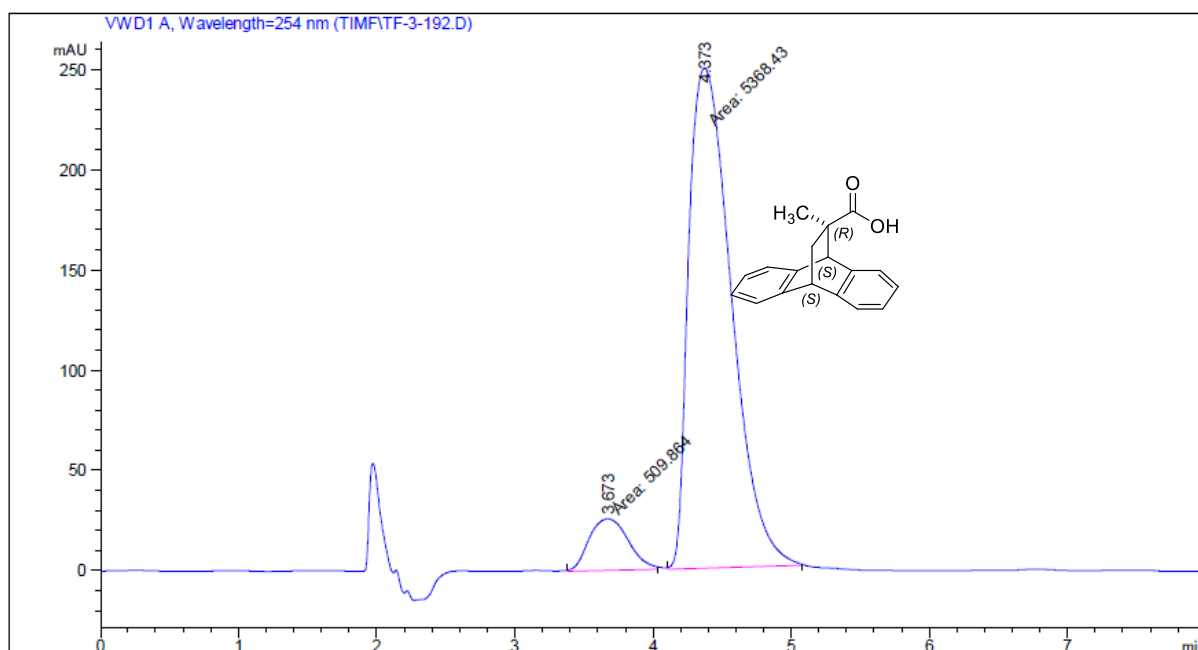
Supplemental Figure 1A. Chiral HPLC trace for Compound 5 (racemic carboxylic acid), obtained using ‘Column A’ as outlined in general information.



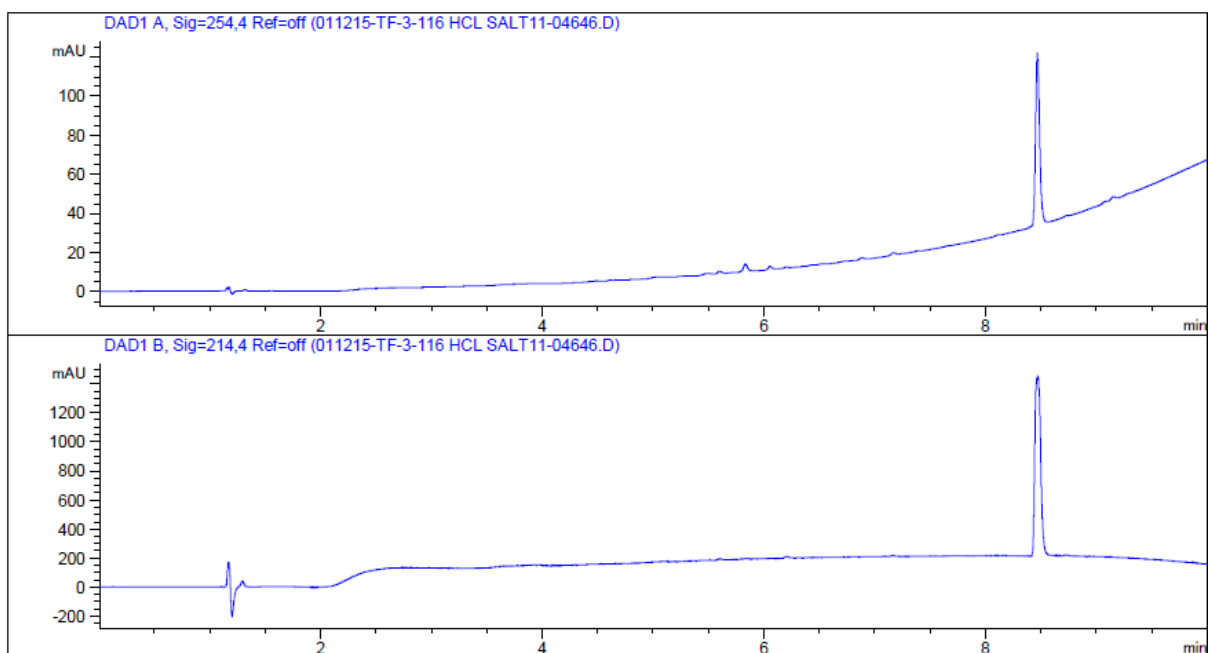
Supplemental Figure 2A. Chiral HPLC trace for Compound (S)-21 (carboxylic acid), obtained using ‘Column A’ as outlined in general information.



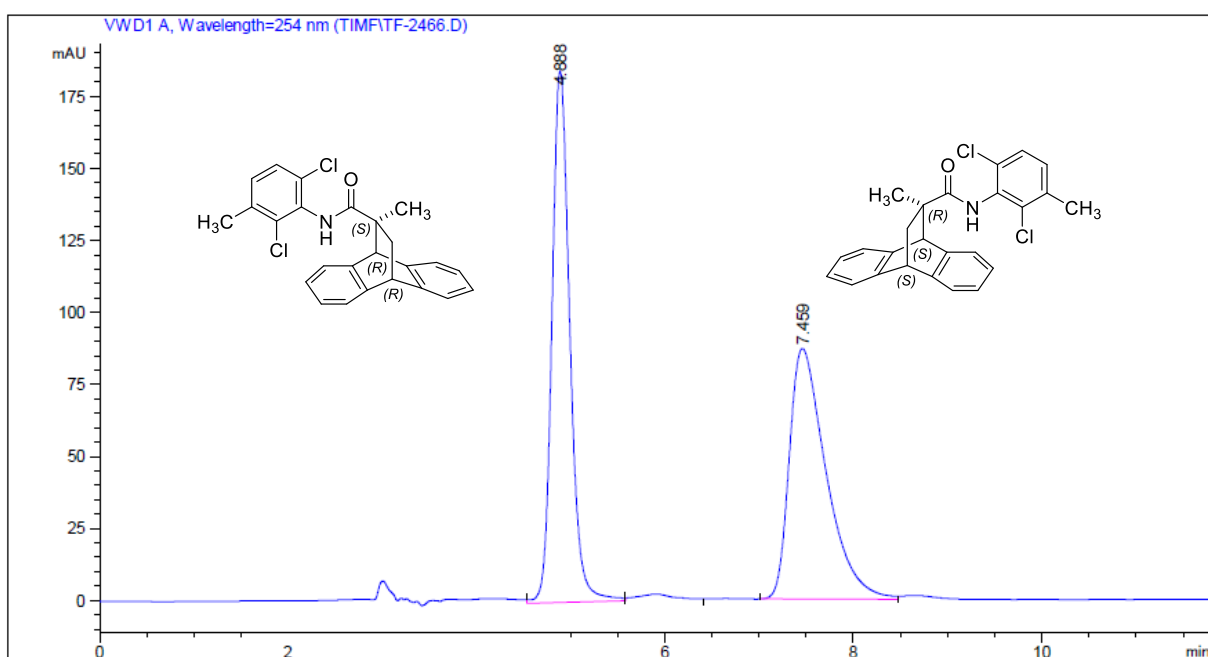
Supplemental Figure 3A. Chiral HPLC trace for Compound (R)-21 (carboxylic acid), obtained using ‘Column A’ as outlined in general information.

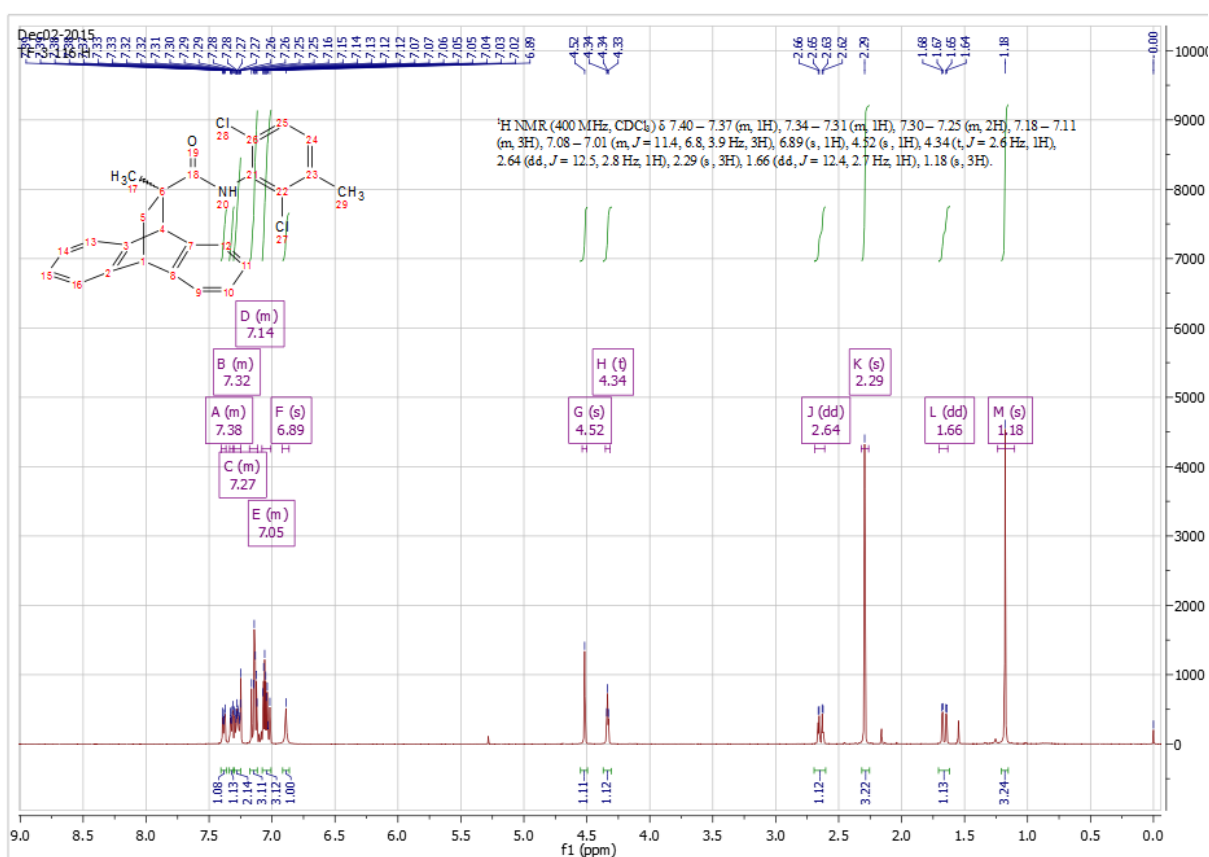
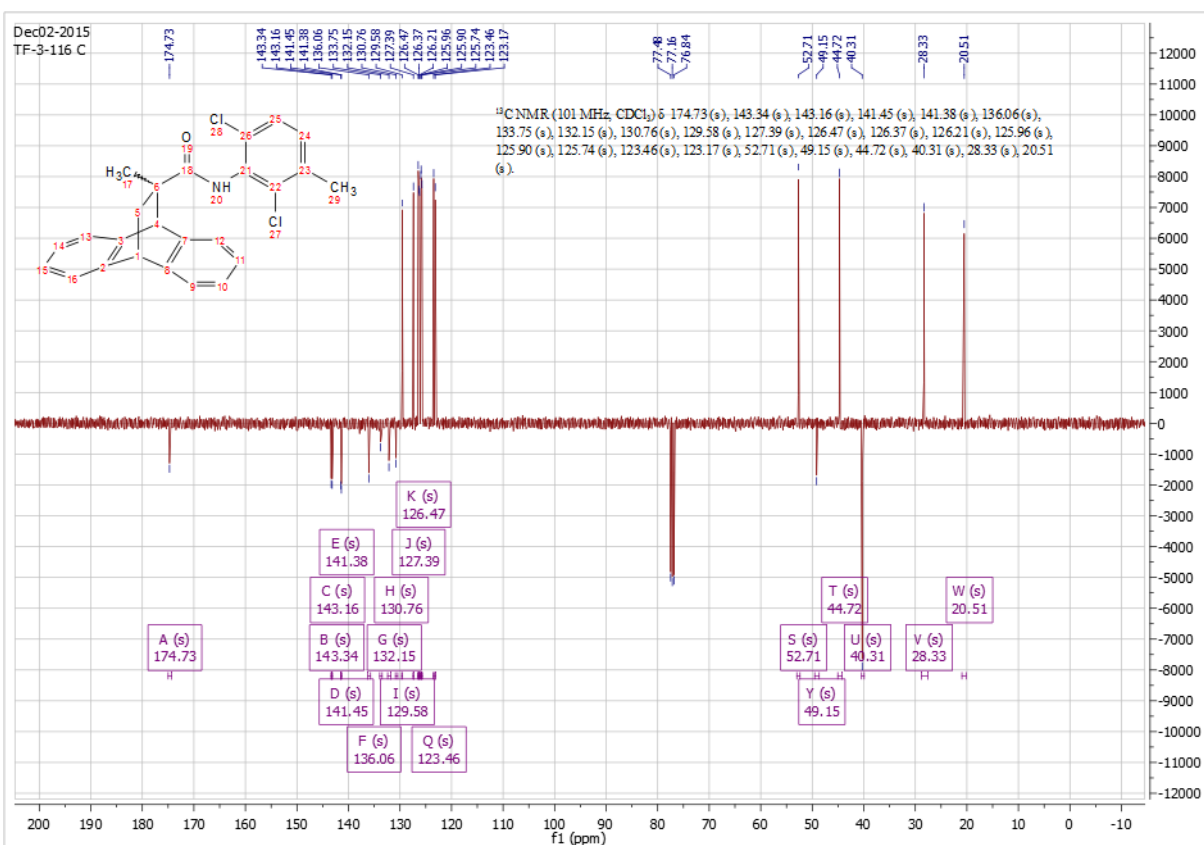


Supplemental Figure 4A. Analytical HPLC trace for Compound (*rac*-2).

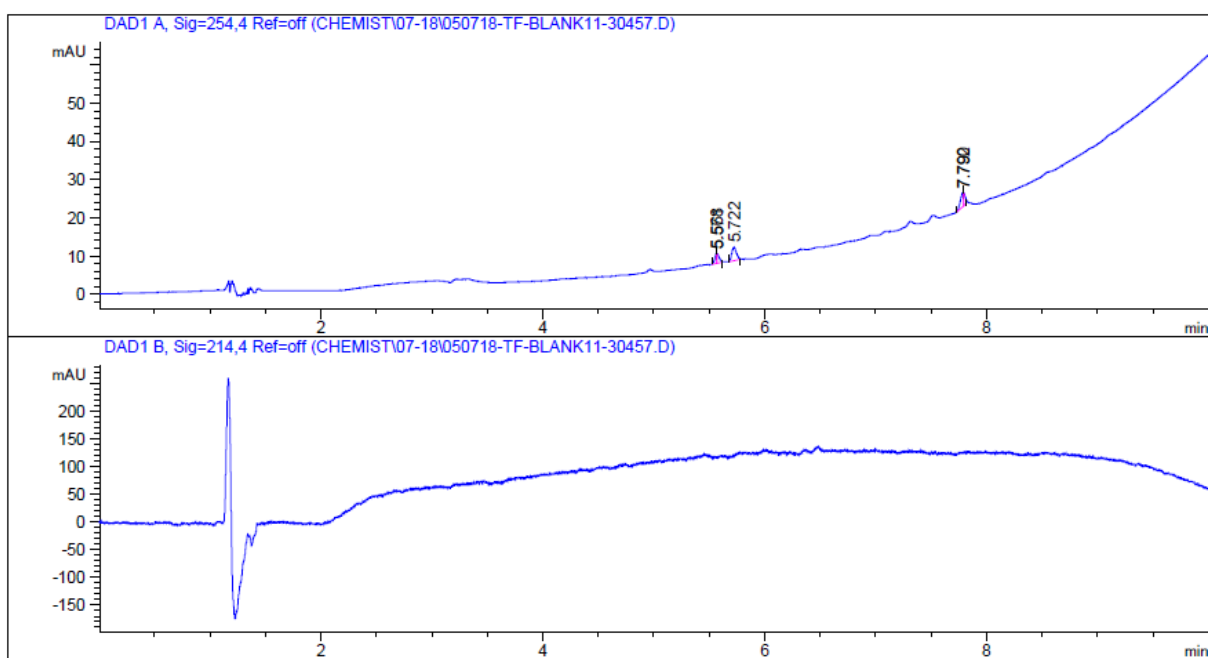


Supplemental Figure 4B. Chiral HPLC trace for Compound (*rac*-2), obtained using 'Column B' as outlined in general information.

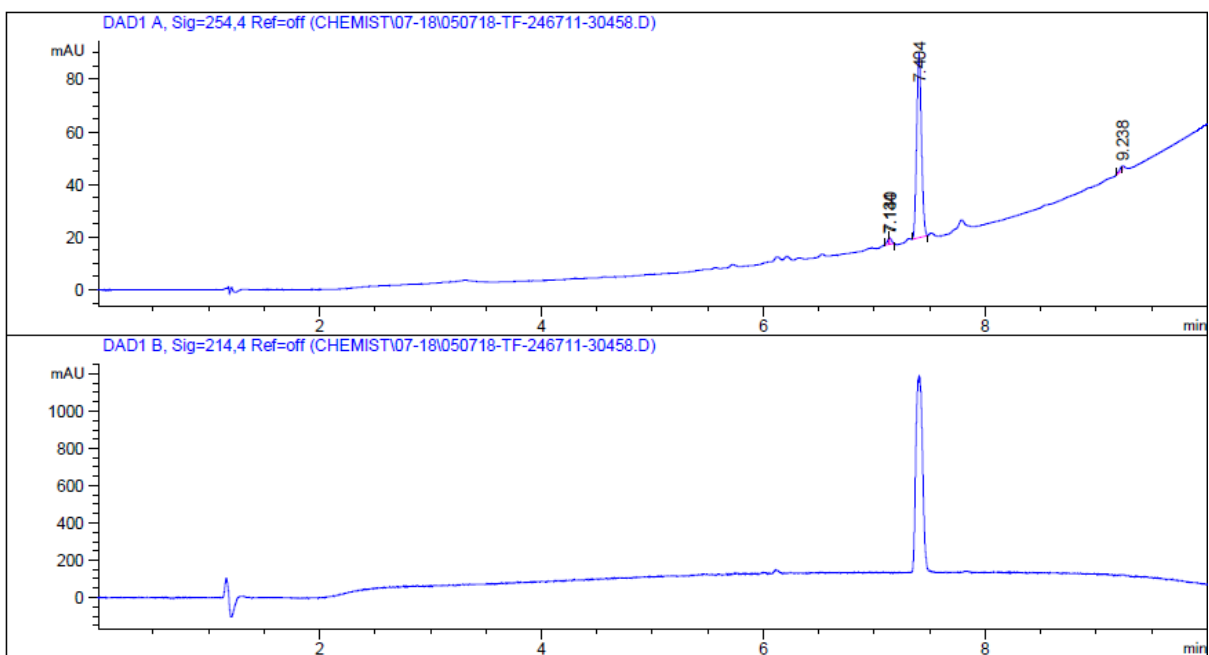


Supplemental Figure 4C. ¹H NMR spectrum for Compound (*rac*-2).Supplemental Figure 4D. ¹³C NMR spectrum for Compound (*rel*-2).

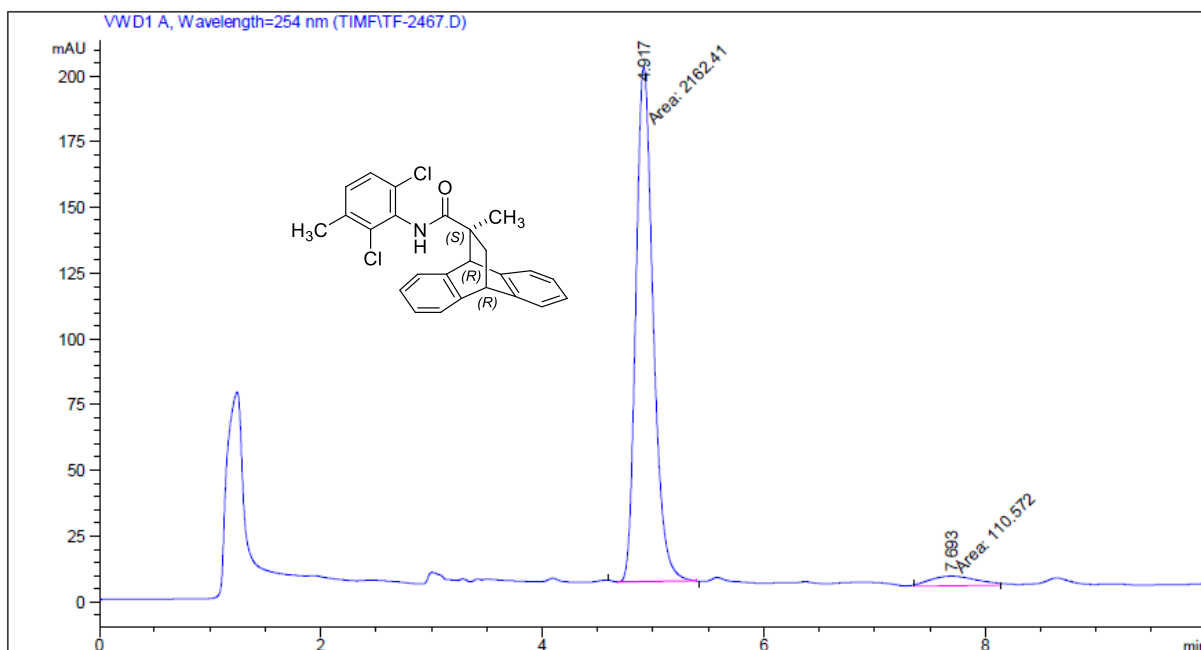
Supplemental Figure 5. Analytical HPLC trace (MeOH BLANK).



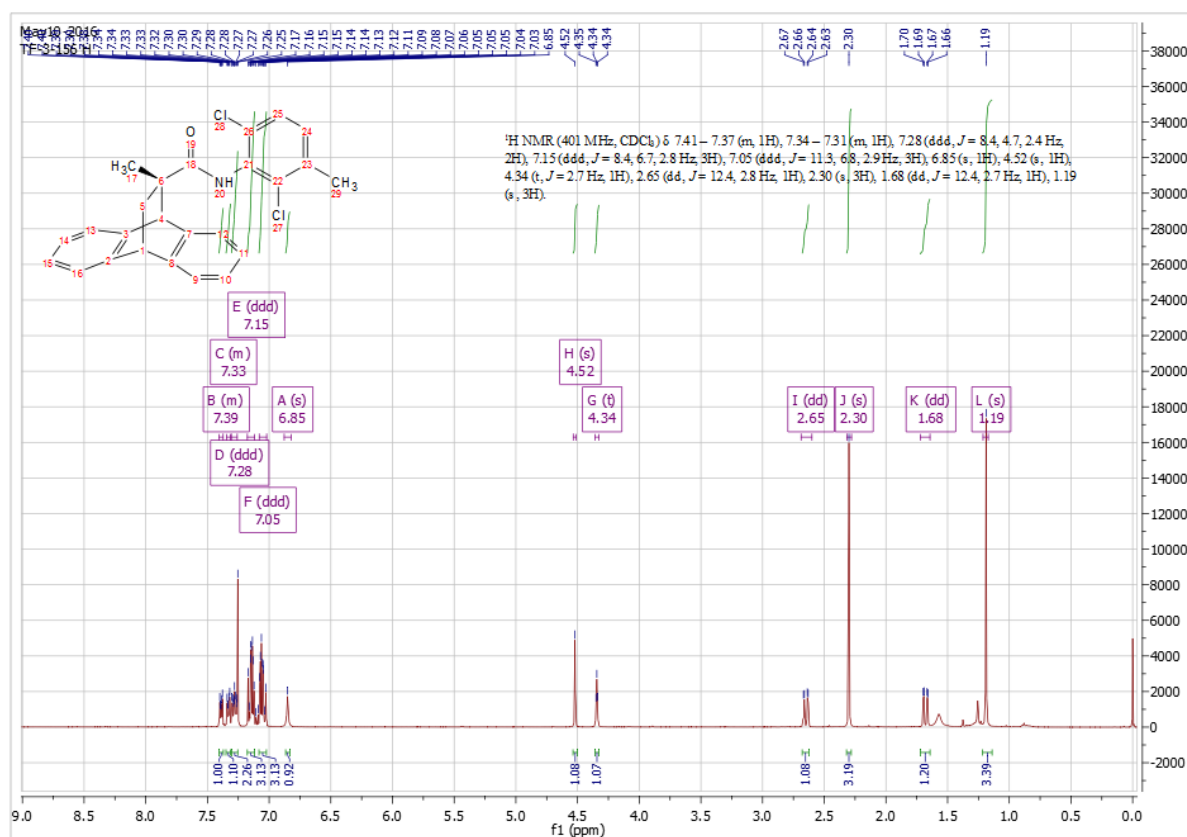
Supplemental Figure 6A. Analytical HPLC Trace for Compound (S)-2.

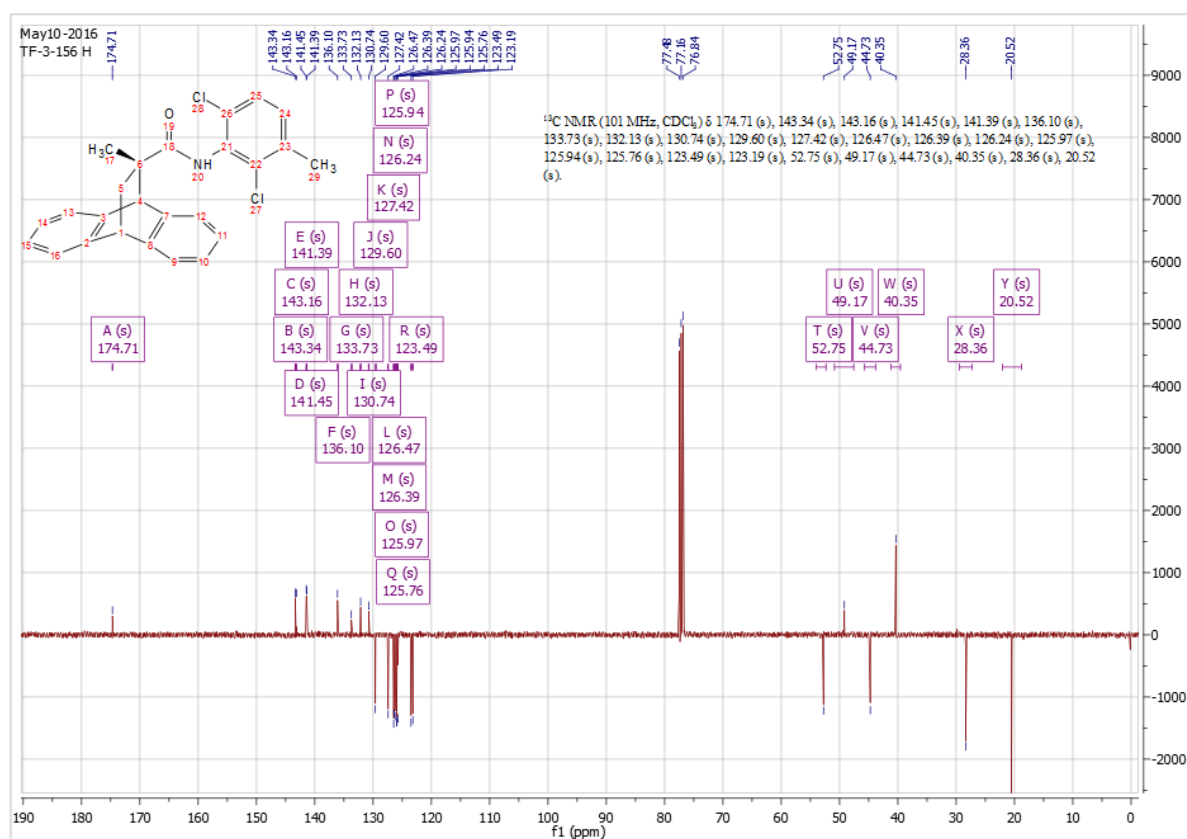


Supplemental Figure 6B. Chiral HPLC Trace for Compound (S)-2, obtained using ‘Column B’ as outlined in general information.

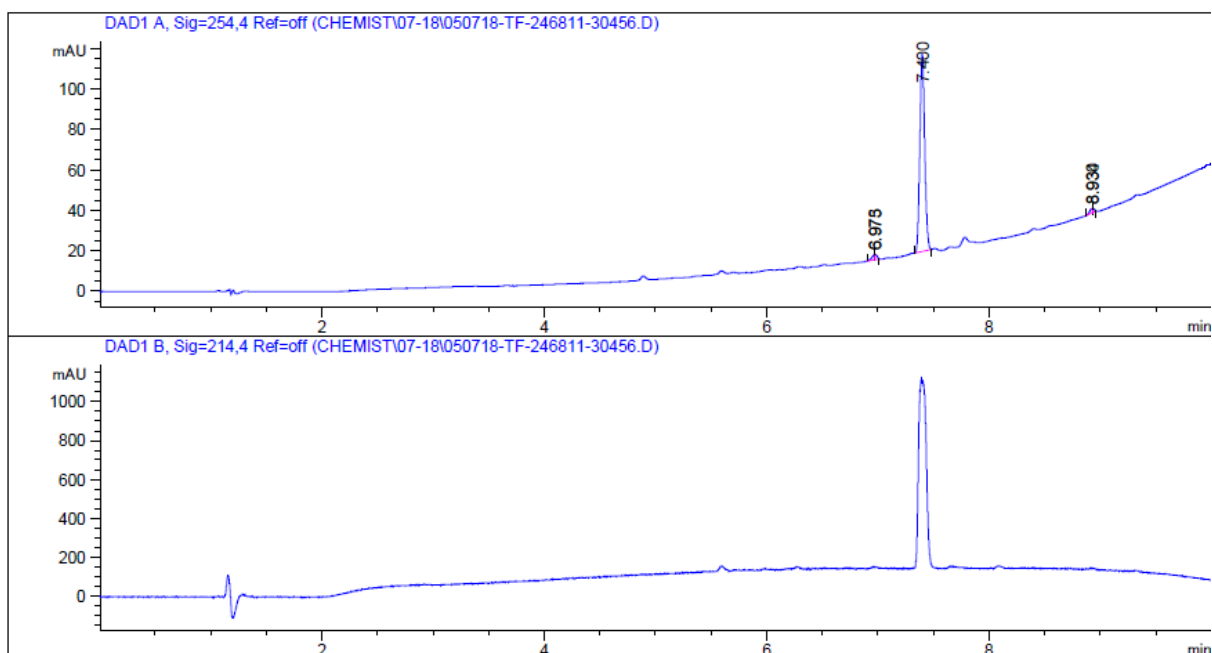


Supplemental Figure 6C. ¹H NMR spectrum for Compound (S)-2.

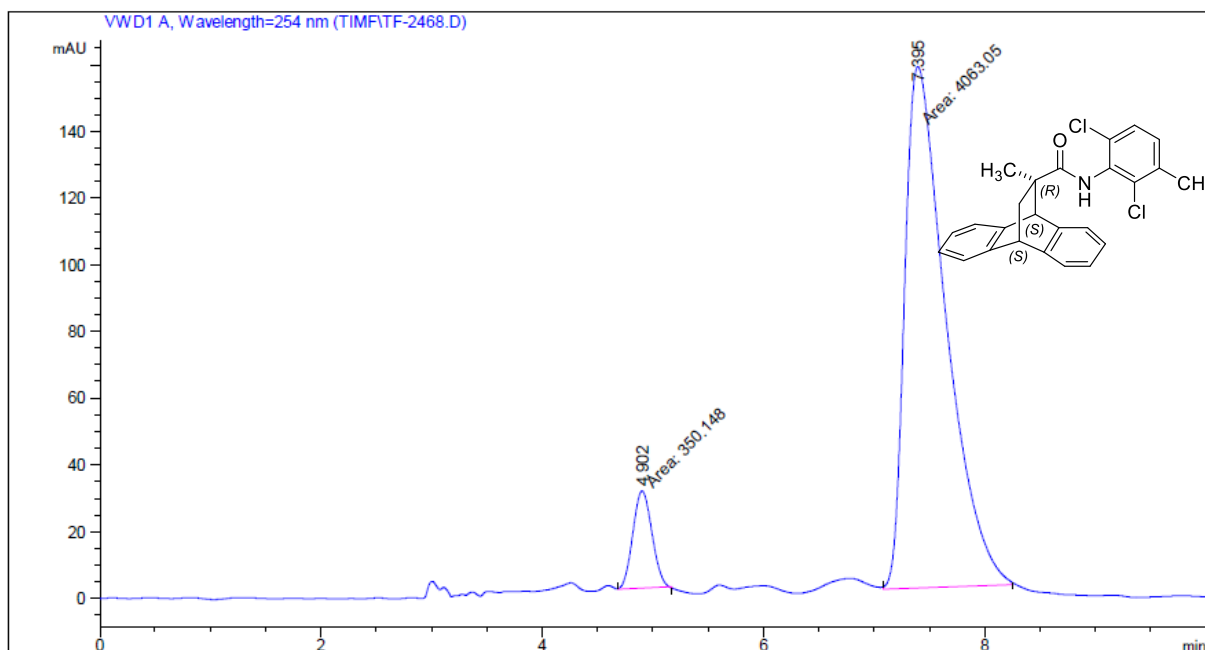


Supplemental Figure 6D. ¹³C NMR spectrum for Compound (S)-2.

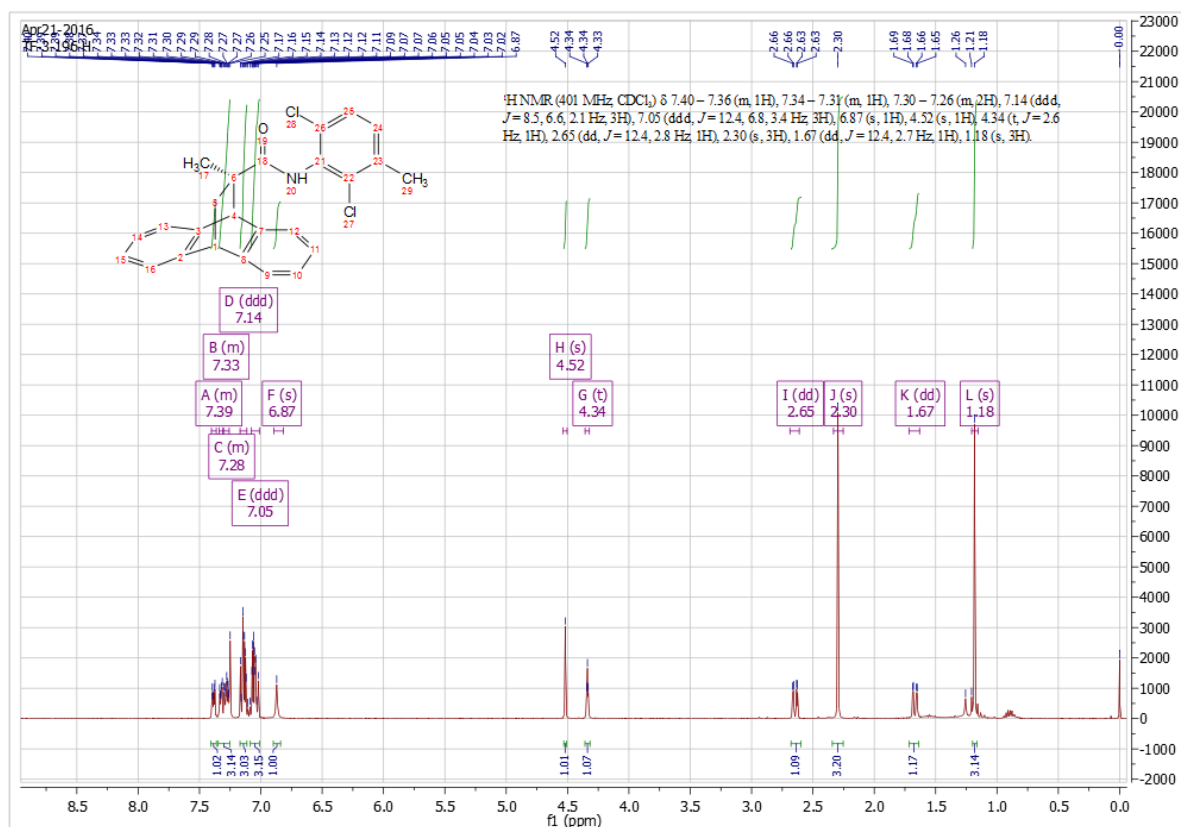
Supplemental Figure 7A. Analytical HPLC trace for Compound (R)-2.

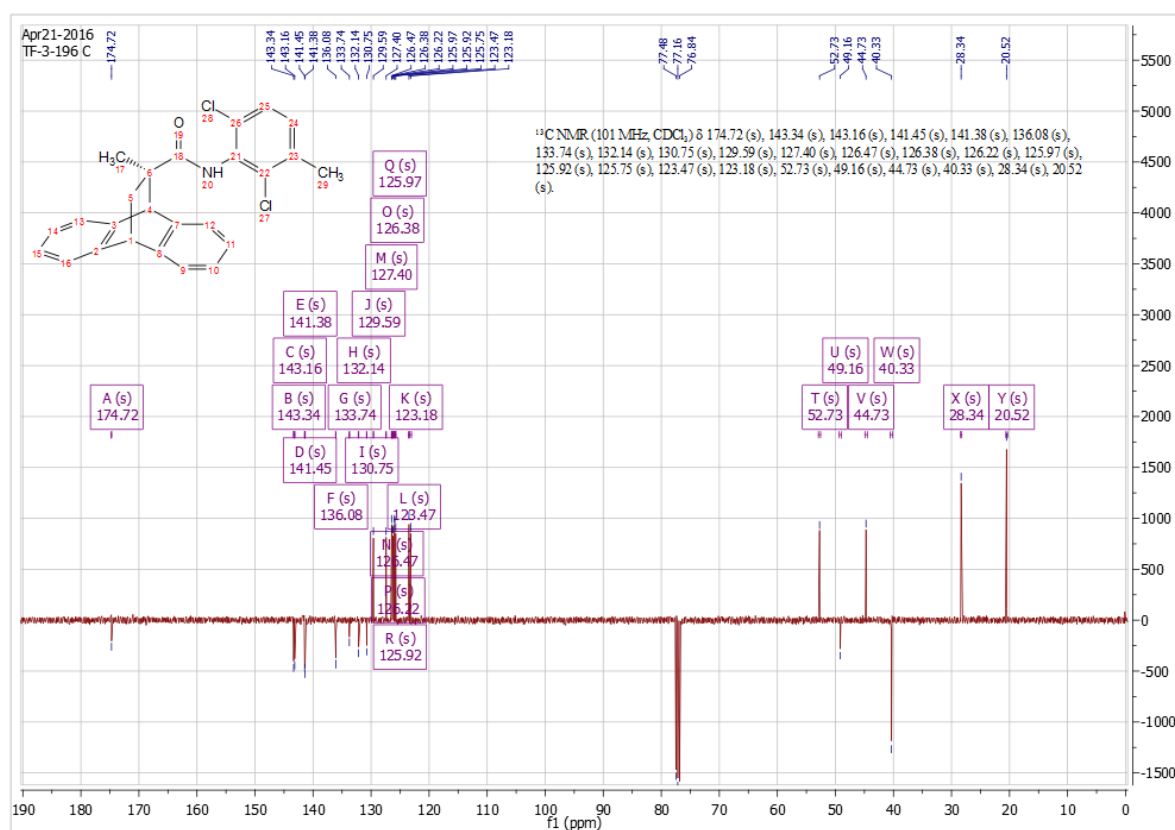


Supplemental Figure 7B. Chiral HPLC trace for Compound (R)-2, obtained using ‘Column B’ as outlined in general information.



Supplemental Figure 7C. ¹H NMR spectrum for Compound (R)-2.



Supplemental Figure 7D. ¹³C NMR spectrum for Compound (R)-2.

References

1. Cabellero, A. G.; Croft, A. K.; Nalli, S. M. Remote aromatic stabilization in radical reactions. *Tetrahedron Lett.* **2008**, *49*, 3613-3615.
2. Camps, P.; Font-Bardia, M.; Giménez, S. I.; Pérez, F.; Solans, X.; Soldevilla, N. (R)- and (S)-3-Hydroxy-4,4-dimethyl-1-phenyl-2-pyrrolidinone as chiral auxiliaries in Diels–Alder reactions. *Tetrahedron: Asymmetry* **1999**, *10*, 3123-3138.
3. Luderman, K. D.; Conroy, J. L.; Free, R. B.; Southall, N.; Ferrer, M.; Sanchez-Soto, M.; Moritz, A. E.; Willette, B. K. A.; Fyfe, T. J.; Jain, P.; Titus, S.; Hazelwood, L. A.; Aube, J.; Lane, J. R.; Frankowski, K. J.; Sibley, D. R. Identification of positive allosteric modulators of the D1 dopamine receptor that act at diverse binding sites. *Mol. Pharmacol.* **2018**.
4. Rodríguez, J. B.; Markey, S. P.; Ziffer, H. Preparation of 2(R) and 2(S) methyl-2-methylglycerates. *Tetrahedron: Asymmetry* **1993**, *4*, 101-108.
5. Xu, X.; Feng, S.; Zhu, Y.; Li, H.; Shen, X.; Zhang, C.; Bai, J.; Zhang, L. Stereospecific radical polymerization of optically active (*S*)-*N*-(2-hydroxy-1-phenylethyl) methacrylamide catalyzed by Lewis acids. *Eur. Polym. J.* **2013**, *49*, 3673-3680.
6. Jiang, L. I.; Collins, J.; Davis, R.; Lin, K. M.; DeCamp, D.; Roach, T.; Hsueh, R.; Rebres, R. A.; Ross, E. M.; Taussig, R.; Fraser, I.; Sternweis, P. C. Use of a cAMP BRET sensor to characterize a novel regulation of cAMP by the sphingosine 1-phosphate/G13 pathway. *J. Biol. Chem.* **2007**, *282*, 10576-10584.
7. Motulsky, H. J. C. Fitting models to biological data using linear and nonlinear regression: a practical guide to curve fitting. In Graphpad Software Inc., San Diego CA.: 2003.

8. Christopoulos, A.; Kenakin, T. G protein-coupled receptor allosterism and complexing. *Pharmacol. Rev.* **2002**, *54*, 323-374.
9. Keov, P.; López, L.; Devine, S. M.; Valant, C.; Lane, J. R.; Scammells, P. J.; Sexton, P. M.; Christopoulos, A. Molecular mechanisms of bitopic ligand engagement with the M(1) muscarinic acetylcholine receptor. *J. Biol. Chem.* **2014**, *289*, 23817-23837.
10. Black, J. W.; Leff, P.; Shankley, N. P.; Wood, J. An operational model of pharmacological agonism: the effect of E/[A] curve shape on agonist dissociation constant estimation. *Br. J. Pharmacol.* **1985**, *84*, 561-571.
11. Sibley, D. R.; Creese, I. Regulation of ligand binding to pituitary D-2 dopaminergic receptors. Effects of divalent cations and functional group modification. *J. Biol. Chem.* **1983**, *258*, 4957-4965.
12. Christopoulos, A. Assessing the distribution of parameters in models of ligand-receptor interaction: to log or not to log. *Trends Pharmacol. Sci.* **1998**, *19*, 351-357.

Chapter 7 – Thesis Outcomes & Future Prospects

Thesis Outcomes & Future Prospects

The principal aim of this thesis was the design, synthesis and *in vitro* pharmacological characterisation of small molecule allosteric modulators of the D₁/D₂Rs. Specifically, it details the evaluation of numerous series of compounds that either act at:

- (i) the D₂R as NAMs toward the further understanding of allosterity and their prospective development as APDs with novel mechanisms of action;
- (ii) the D₂R as PAMs towards understanding their structure-activity-relationships to aid in their development as biochemical tool compounds which may facilitate an understanding of their novel binding modes to potentially enable rational structure-based design;
- (iii) the D₁R towards furthering our understanding of the structural features governing D₁R PAM allosterity and their prospective utility in ameliorating the cognitive deficits associated with SCZ.

In addition, this thesis explored the chemical synthesis of an extensive library of structural analogues of the prototypical antipsychotic drug haloperidol, and detailed the *in vitro* kinetic profiling of these ligands at the D₂R toward further understanding the kinetic basis of on-target antipsychotic drug toxicities. These data may be utilised to facilitate the rational design of novel antipsychotic drugs with a reduced propensity to elicit debilitating EPS and hyperprolactinemia liabilities.

Chapter 1 provided an overview GPCRs, in particular the dopamine receptors, and their implication in the disease states schizophrenia and Parkinson's disease, in addition to a review of all research that has been conducted in the area of dopamine receptor allosteric modulation. All currently identified small molecule allosteric chemotypes for the D₁R and D₂R were summarised in detail, encompassing known structure-activity-relationships as well as any interesting biochemical and preclinical data.

Chapter 2, which is published in the *Journal of Medicinal Chemistry*, centred on the chemical synthesis and validation of a small molecule thieno[2,3-*d*]pyrimidine hit arising from a virtual ligand screen. Its allosteric mode of action at the D₂R was validated through equilibrium and dissociation kinetic radioligand binding assays together with functional interaction assays measuring its effect on the second messenger cAMP. Its activity was profiled using an operational model of allosterity to determine estimates of functional affinity (K_B), cooperativity on dopamine binding (α) and function (β), and intrinsic agonism (τ_B). In addition to this, a focused library of structural analogues were designed and synthesised to understand the molecular determinants of allosterity at the D₂R. Moreover, and in collaboration, molecular docking studies using the D₂R crystal structure were conducted on all compounds in an attempt to rationalise structure-activity-relationships to further supplement the design and synthesis of improved D₂R modulators. Key findings were the identification of analogues

that display differential modulatory effects upon dopamine affinity and efficacy. Finally, we showed the scaffold can be structurally simplified to reveal a low molecular weight fragment-like core that retains negative modulatory properties with very high lipophilic ligand efficiency, and can be elaborated on through multiple vectors.

Chapter 3, which is published in the *European Journal of Medicinal Chemistry*, reported the further structural exploration of this thieno[2,3-*d*]pyrimidine scaffold based on a key analogue identified in chapter 2. The initial area of focus observed the effect of introducing different amines to the 4-position of the scaffold (series 1). Subsequent functional pharmacological evaluation of these analogues inspired the design and synthesis of a secondary chemical series observing the effect of various substituents at the 5-/6-positions (e.g., aromatic/aliphatic carbocycles) in the presence of interesting 4-amino substituents. All compounds were functionally profiled, and an operational model of allosterism was applied to the data to determine estimates of functional affinity (K_B), cooperativity on dopamine binding (α) and function (β), and intrinsic agonism (τ_B). Key findings include the identification of two of the highest affinity analogues to arise from a thieno[2,3-*d*]pyrimidine derivative, as well as the identification of agonists of similar chemical nature. This study demonstrates that allosteric modulators of the D₂R based on this scaffold provide flat SAR, and may be challenging to optimise into high affinity ligands that retain their modulatory profiles.

Understanding structural changes that drive increases in D₂R functional affinity and negative allosteric cooperativity are of great interest. Future prospects for the previous two chapters include the further synthesis and evaluation of novel thieno[2,3-*d*]pyrimidine analogues, interrogating previously unexplored vectors to expand our understanding of D₂R allosterism. Proposed modifications include incorporating fused aromatic and heteroaromatic moieties, heteroatom replacement (S to CH₂, O or N), together with analogues bearing *N*-substituents at the 3-position (Figure 1).

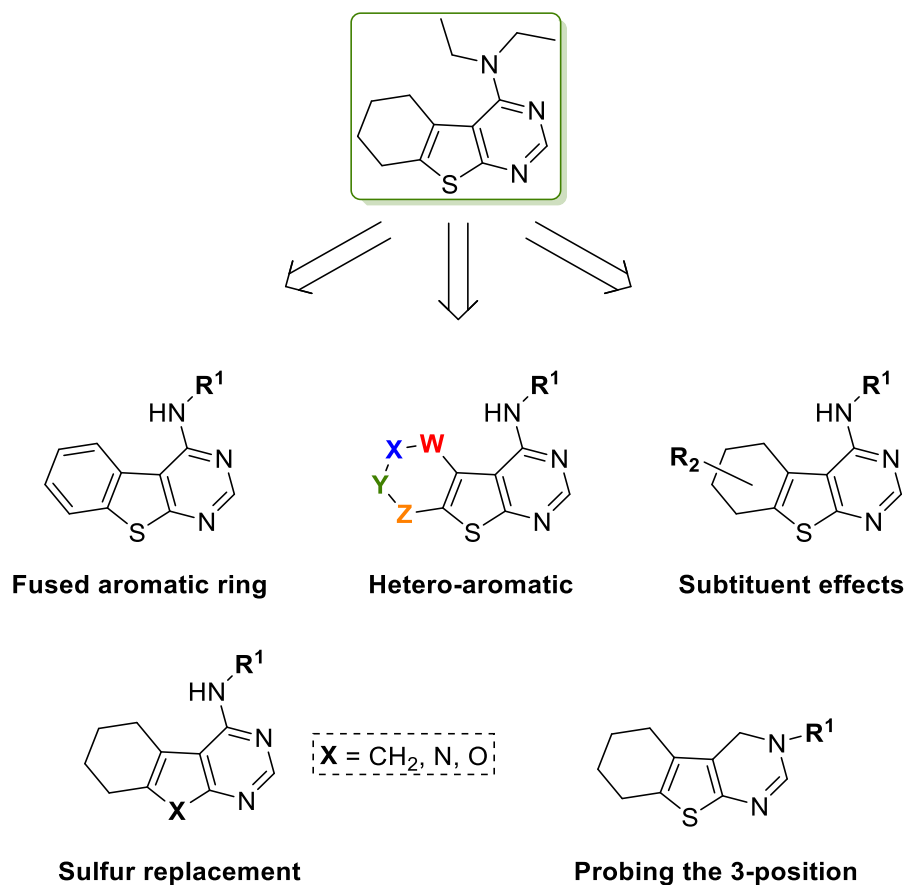


Figure 1. Potential thieno[2,3-*d*]pyrimidine derivatives to further probe uncharted chemical space.

Chapter 4 explored the chemical synthesis and SAR of a novel D₂R PAM chemotype towards its potential for the development of fluorescent and irreversible biochemical tool derivatives. We described a more efficient synthesis to access structural analogues of this PAM in fewer steps compared to literature, and detailed its functional characterisation at the D₂R together with 14 structural analogues, highlighting the first reported SAR information. We show that essentially all chemical modifications to the core scaffold abolishes PAM activity, and demonstrate removal of the aryl methyl ether substituent abolishes positive allosteric cooperativity and confers a ~25-fold increase in allosteric agonism whilst having no impact on the functional binding affinity.

Our initial SAR findings demonstrate that development of fluorescent analogues based on this scaffold are currently not feasible. However, future prospects for this work include the chemical synthesis and pharmacological profiling of a series of azido variants for their potential utility as photoactivatable irreversible probes (Figure 2). To be useful biochemical tools, these molecules must maintain their modulatory properties which will ensure they still engage a topographically distinct binding domain to that of the orthosteric site. The majority of these compounds will arise from a starting aryl amine, which may be converted to the corresponding aryl azide upon treatment with *tert*-

butyl nitrite and trimethylsilyl azide in acetonitrile (Figure 3). Alternatively, an alkyl azide functionality may be installed via a starting bromomethyl intermediate upon treatment with sodium azide in DMSO (Figure 3). These probes may potentially aid in elucidating a novel D₂R binding mode.

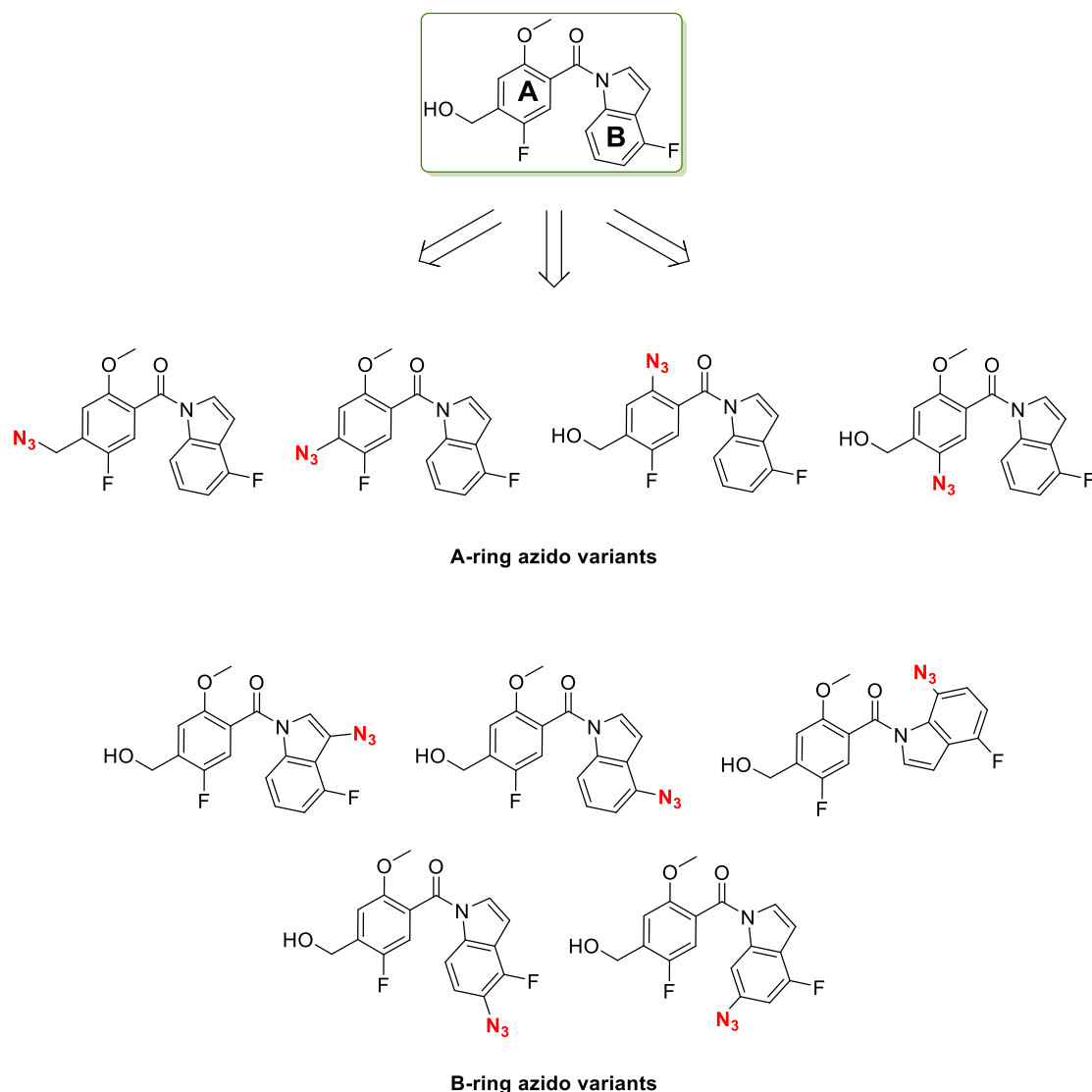


Figure 2. Potential structural azido-analogues of **36** toward the development of photoactivatable irreversible probes that retain D₂R allostery.

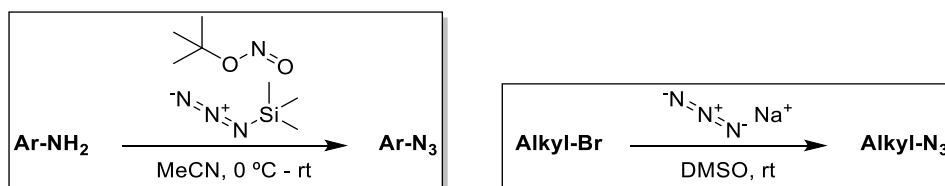


Figure 3. Synthetic chemical methodology to generate aryl (left) and alkyl (right) azido substituents.

Chapter 5, which is formatted for submission for *The Journal of Medicinal Chemistry*, detailed the chemical synthesis and kinetic profiling of an extensive library of analogues of the typical antipsychotic drug haloperidol. Synthetic emphasis was placed on all four of haloperidol's structural moieties to permit in depth analyses of the effect of subtle structural modification on kinetic rate-constants. To determine ligand association and dissociation rate-constants, all compounds were profiled using a TR-FRET competition association kinetic binding assay. These experiments revealed that even subtle modifications to the core scaffold can have dramatic influences on kinetic rate constants, affording compounds with structural similarity to haloperidol, whilst possessing a clozapine-like kinetic profile. These data will advance our understanding of the kinetic hypothesis and may permit the fine tuning of these parameters to generate APD's devoid of EPS and hyperprolactinemia propensities.

As a direct follow up to work presented in this chapter, selected kinetically clozapine-like butyrophenones should be assessed for their aminergic receptor binding and functional profiles, and if deemed satisfactory, progressed on to *in vivo* models of psychosis, and monitored for their propensity to elicit on-target toxicities, namely EPS and hyperprolactinemia. In addition, structural moieties that resulted in favourable changes in both association and dissociation rate constants, namely a 2,3-difluorophenyl, *cis*-cycloalkane, and a 5-carbon linker, may be further explored via their concurrent incorporation into novel structural analogues of haloperidol (Figure 4). This will further our understanding in regards to how these moieties influence the corresponding kinetic rate constants of D₂R orthosteric antagonists.

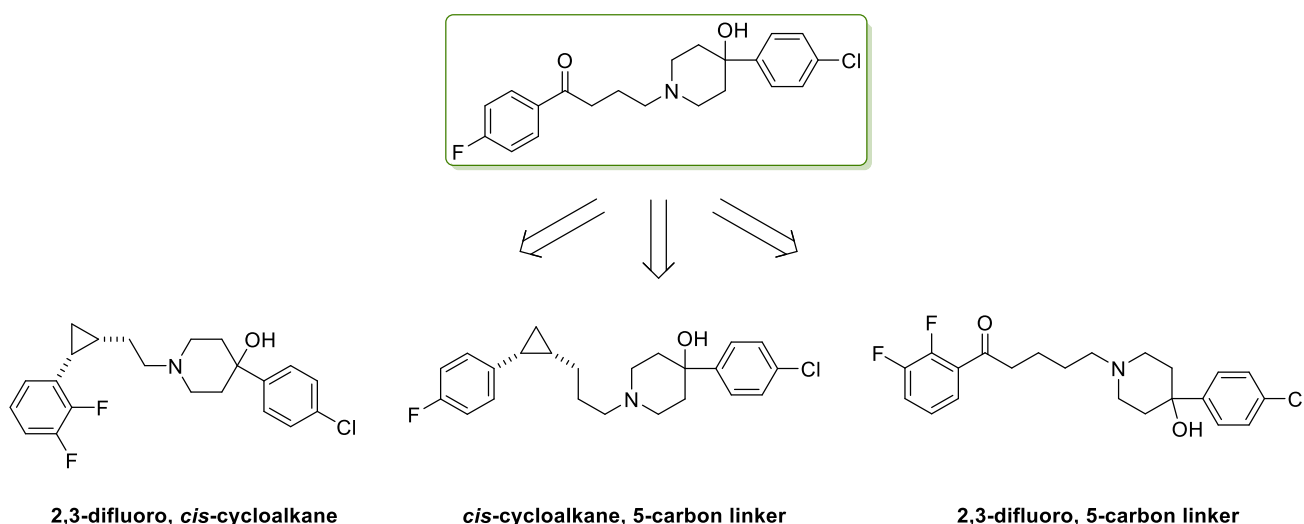


Figure 4. Potential structural analogues of haloperidol to assess the kinetic effects of concurrently incorporating favourable modifications.

Chapter 6, which is formatted for submission to the journal *MedChemComm*, explored the symmetrical and asymmetrical chemical syntheses of two novel D₁R PAM chemo types (compound A and B) due to their potential as starting points for the development of novel drugs to ameliorate the cognitive deficits association with SCZ. Various chiral resolving techniques were initially explored to in an attempt to isolate optically pure stereoisomers of compound B, including semi-preparative chiral chromatography and diastereomer formation. Following on from this, several optically pure amines and alcohols were selected as chiral auxiliaries and profiled for their effectiveness in an asymmetric Diels-Alder cycloaddition reaction. Chiral auxiliaries derived from (*R*)- and (*S*)-3-hydroxy-4,4-dimethyldihydrofuran-2(3*H*)-one (D and L-pantolactone, respectively) were determined to confer high diastereoselectivity, eventually yielding enantioenriched stereoisomers of compound B ((*S*)-**2** and (*R*)-**2**). Using a functional interaction assay measuring the second messenger cAMP, the pharmacology of all compounds was assessed at both the D₁R and D₂Rs, and an operational model of allostery was applied to the data to determine estimates of functional affinity (K_B), cooperativity on dopamine binding (α) and function (β), and intrinsic agonism (τ_B). “Compound A” was shown to be an ago-PAM of the D₁R and a competitive partial agonist of the D₂R. Racemic “compound B” and isomers (*S*)-B and (*R*)-B were shown to be D₁R/D₂R-selective. The functional affinities of these compounds spanned 7-fold, of which the modulatory properties for respective enantiomers were also shown to differ significantly in magnitude. (*R*)-**2** was shown to display 4-fold lower positive cooperativity with DA as compared to (*S*)-**2** and a 7-fold lower affinity for the D₁R.

The results presented in this chapter are the first to describe the enantioenrichment of D₁R PAMs, subsequently demonstrating these stereoisomers to display differential levels of positive allosteric cooperativity *in vitro*. These data warrant the further assessment of alternative practical chiral auxiliaries that will provide enhanced diastereoselectivity, and in turn, generate optically pure carboxylic acids that can be utilised for the synthesis of optically pure analogues of compound B. This will permit the identification of comparable hit compounds from ensuing SAR studies to be followed up with the asymmetric synthesis of the selected target. Future SAR studies will examine key components of compound B to determine what aspects of the molecule are responsible for its allosteric pharmacology (Figure 5). Specifically, this will include observation of: the effect of various substituents and their substitution pattern on the aniline moiety; the role of the amide carbonyl and the subsequent effect of an ionisable nitrogen; the importance of the chiral methyl substituent; the effect of introducing a methylene spacer bridging the amide and the adjacent phenyl ring; and finally, modification to the anthracene core through a variety of bridged- and non-bridged variants.

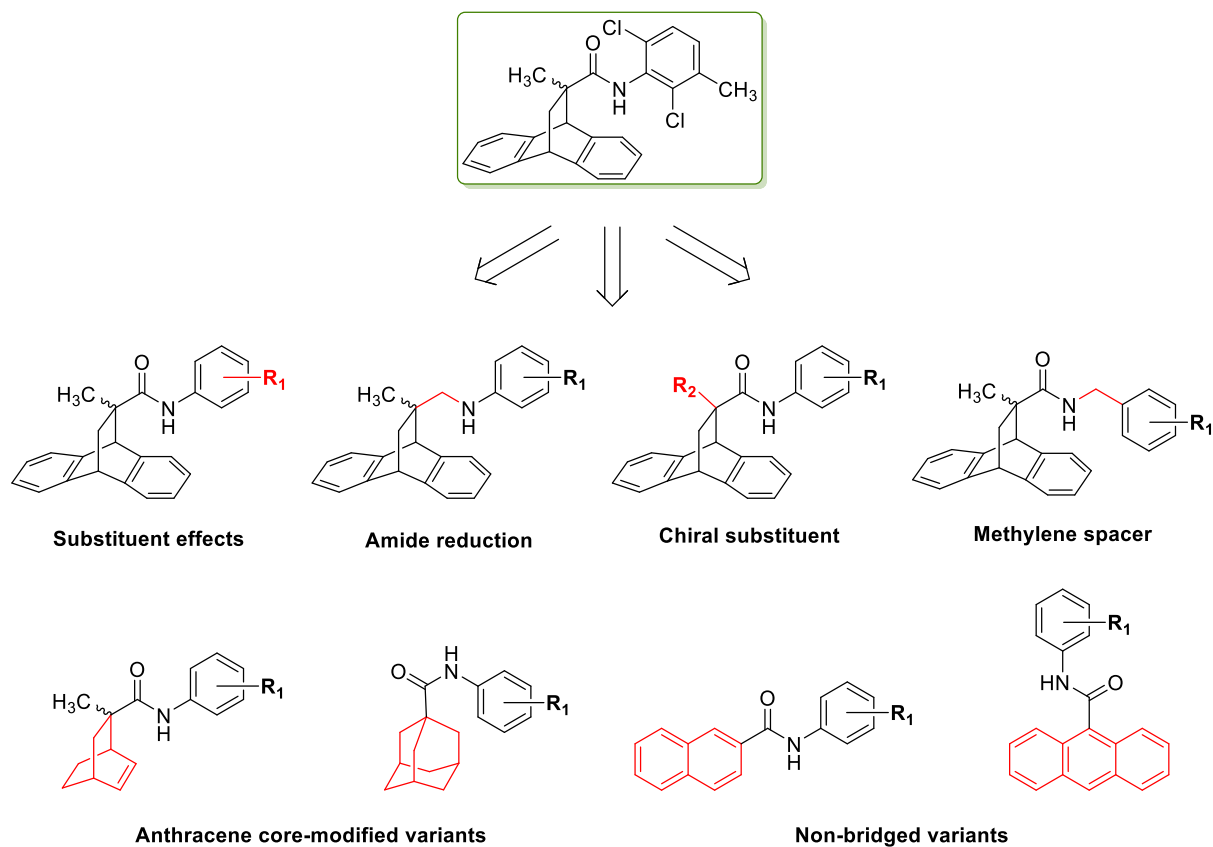
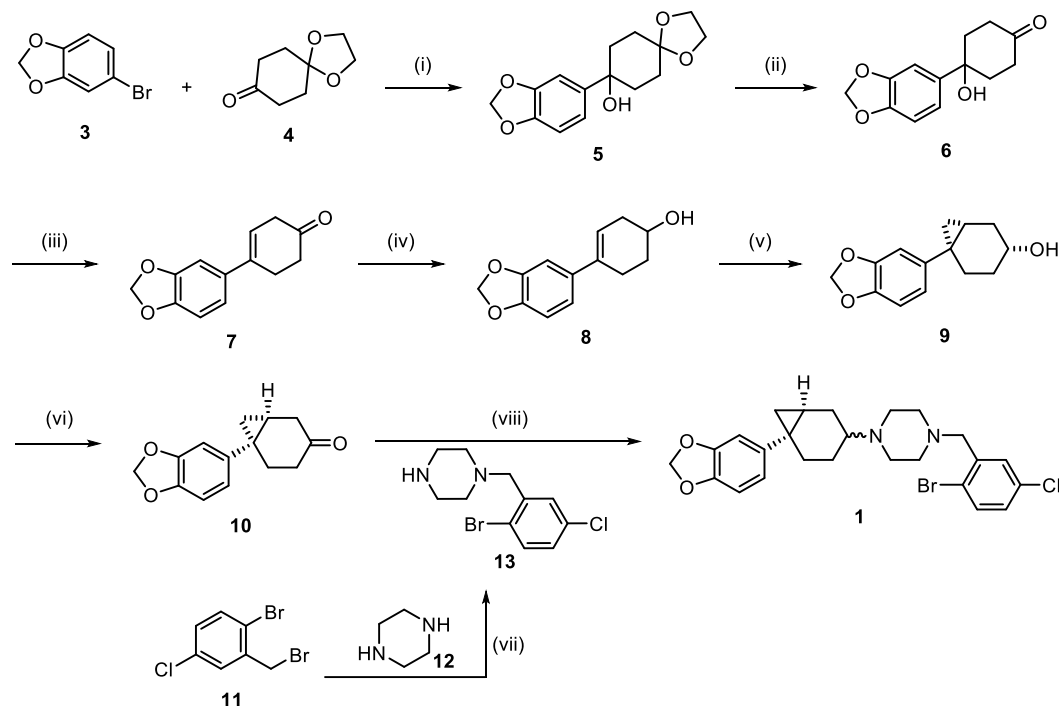


Figure 5. Potential structural analogues of compound B (19) for initial SAR investigation into D₁R allostery.

Appendices

Appendix 1 – Chapter 6 synthesis and pharmacological characterisation data for “compound A” (1).

Chemistry. As indicated in chapter 6, Lewis *et al.*¹ identified compound **1** from an HTS campaign and reported it to be a PAM at the D₁R (EC₅₀ = 230 nM) but with agonist activity at the D₂R. This compound represents a distinct chemotype and is one of the first reported D₁R PAMs, providing initial steps toward the development of drugs for the potential treatment of cognitive dysfunction associated with neuropsychiatric disorders, such as SCZ. In order to validate the pharmacological activity of **1** at both the D₁R and D₂R, it was accessed using a seven step synthesis (Scheme 1). To begin, 5-bromobenzo[*d*] [1,3]dioxole (**3**) was subjected to lithium-halogen exchange using *n*-BuLi, followed by treatment with 1,4-dioxo-spiro[4.5]decan-8-one (**4**) to provide the corresponding tertiary alcohol **5**. Acid-catalysed hydrolysis of the hemiketal gave hydroxycyclohexanone intermediate (**6**), followed by dehydration with aqueous HCl to afford the corresponding cyclohexenone (**7**). To access the alcohol whilst circumventing reduction of the olefin, selective Lúche ketone reduction was facilitated by sodium borohydride in the presence of the lanthanide cerium(III) chloride heptahydrate, affording homoallylic alcohol (**8**).² Treatment of the olefin with diethyl zinc and diiodomethane using Simmons-Smith³ [2+1]cyclopropanation conditions gave fused cycloalkane (**9**), followed by oxidation with Dess-Martin periodinane to give ketone (**10**). 1-(2-Bromo-5-chlorobenzyl)piperazine (**13**) was constructed by alkylating commercially available 1-bromo-2-(bromomethyl)-4-chlorobenzene (**11**) with a molar excess of piperazine (**12**) in refluxing toluene. Lastly, reductive alkylation of ketone (**10**) with (**13**) in the presence of sodium triacetoxyborohydride and catalytic trifluoroacetic acid was achieved to furnish the target compound **1** in moderate yield.

Scheme 1 – Chemical Synthesis of Racemic **1**^a

^aReagents and conditions: (i) *n*-BuLi, THF, -78°C , 2.5 h, 71%; (ii) 1 M HCl_(aq), acetone, r.t. 4 h, 90%; 6 M HCl_(aq), N_{2(g)}, r.t. 4 h, 67%; (iii) NaBH₄, CeCl₃·7H₂O, 0°C – r.t. 12 h, 79%; (iv) Et₂Zn (1 M in hexanes), CH₂I₂, CH₂Cl₂, r.t. 14 h, 60%; (v) Dess-Martin periodinane, pyridine, CH₂Cl₂, r.t. 12 h, 75%; (vi) toluene, reflux 2 h, 60%; (vii) NaBH(OAc)₃, TFA, CH₂Cl₂, r.t. 48 h, 25%.

Pharmacology. In our functional assay as described in chapter 6, compound **1** exhibited modest affinity for the D₁R ($K_B = 55.2 \mu\text{M}$), acted to potentiate the potency of DA by 19-fold ($\alpha\beta = 18.6$) and displayed allosteric agonism ($\tau_B = 1.90$, Figure 1A, Table 1). Functional characterisation of this compound was extended to an assay measuring inhibition of forskolin-stimulated cAMP accumulation in hD₂₁R-expressing CHO-cells. At the D₂R, **1** caused a limitless dextral shift of the DA concentration-response curve along with an increase in the basal signal (Figure 1B). These data are consistent with the action of **1** as a competitive partial agonist ($\log EC_{50} = -7.08 \pm 0.08$, 83.2 nM). Thus **1** displays an apparently different mode of action between DR subtypes. **1** contains a piperazinyl moiety bearing an ionisable nitrogen, a feature demonstrated to be critical for all orthosteric monoaminergic receptor ligands.^{4,5} Therefore, while its orthosteric mode of action at the D₂R might be anticipated from its structure, its apparently allosteric mode of action at the D₁R is more surprising. Whilst informative, though, these measures can be of limited use since receptor expression levels, and the efficiency with which the pathway is coupled to the receptor may influence the maximum effect and potency of a compound.⁶ To mitigate this system dependence, a series of cAMP inhibition assays were conducted in cells which were pre-treated with phenoxybenzamine (an alkylating agent which is used to inhibit high affinity orthosteric interactions at the D₂R).⁷ The data for DA evaluated

in the presence of the alkylating agent were then fit to an operational model of receptor depletion in order to determine values of K_A and τ_A ($\log K_A = -5.78 \pm 0.16$, $\log \tau_A = 1.84 \pm 0.16$). Accordingly, these data were integrated into an operational model of allostery to supplement our functional data.

Table 1. Functional Parameters for 1 Derived from cAMP BRET Assay at the hD₁R^a

CPD	<i>e.e.</i> (%)	$pK_B (K_B, \mu M)^a$	$\text{Log } \tau_B (\tau_B)^b$	$\text{Log } \alpha\beta (\alpha\beta)^c$
1	0	4.26 ± 0.11 (55.2)	0.28 ± 0.07 (1.90)	1.27 ± 0.13 (18.6)

Estimate of the negative logarithm of the equilibrium dissociation constant determined in an cAMP functional assay.

^bEstimate of the intrinsic efficacy of the modulator. ^cEstimate of the logarithm of the net cooperativity factor between the modulator and dopamine. ^dEstimate of the logarithm of the modulatory effect upon efficacy factor induced by the allosteric modulator. Values represent mean \pm S.E.M. from at least three independent experiments performed in duplicate

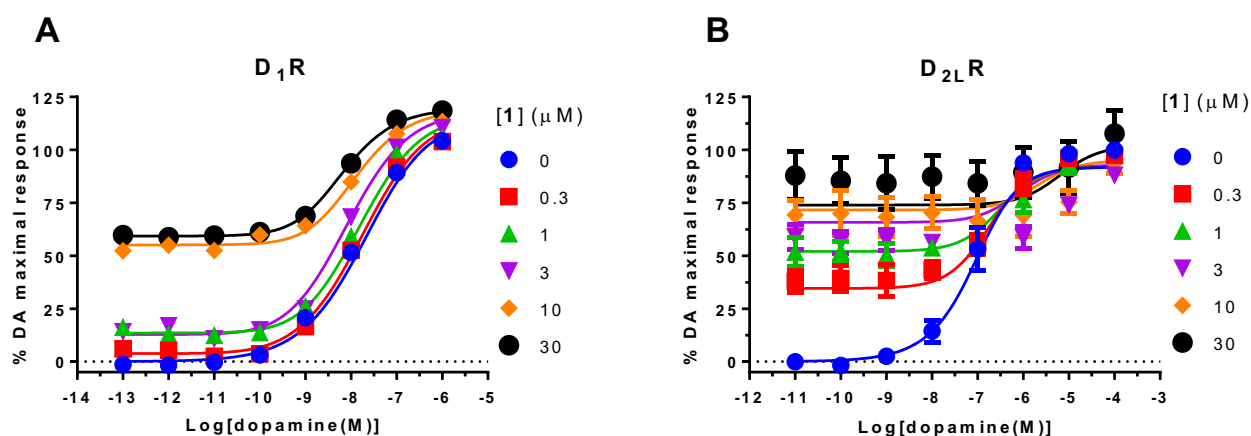
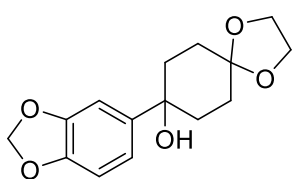
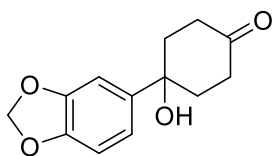


Figure. (A) In an assay measuring inhibition of forskolin-stimulated cAMP production using a BRET biosensor at the hD₁R, **1** was shown to display μM functional affinity at the D₁R and acted as an ago-PAM, both potentiating the action of DA and exhibiting efficacy in its own right. (B) At the D₂R, **1** displayed pharmacology consistent with the action of a competitive partial agonist, eliciting a response at a concentration of 0.3 μM .

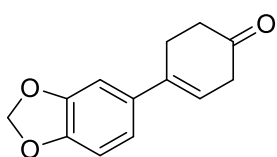
Chemistry Experimental.



8-(Benzo[*d*][1,3]dioxol-5-yl)-1,4-dioxaspiro[4.5]decan-8-ol (5). A solution of *n*-BuLi (2.5 M in hexanes) (11.9 mL, 29.9 mmol) was dropped slowly into a solution of 5-bromobenzo[*d*][1,3]dioxole (2.99 mL, 24.9 mmol) in dry THF (100 mL) at -78 °C over 10 min. The reaction was stirred for an additional 20 min at -78 °C. A solution of 1,4-dioxaspiro[4.5]decan-8-one (4.27 g, 27.4 mmol) in dry THF (25 mL) was slowly dropped into the reaction. After addition, the reaction was stirred for additional 2 hours at -78 °C. The reaction was then quenched with diluted aqueous NH₄Cl solution and warmed to room temperature. The solvent was removed *in vacuo* and the residue was partitioned between EtOAc (25 mL) and H₂O (25 mL). The organic layer was washed with brine, dried over anhydrous Na₂SO₄, filtered and concentrated *in vacuo* to give a yellow solid, which was then purified by FCC (eluent, 50:50 EtOAc, *n*-hexanes) to afford the title compound as a transparent oil that solidified as a white solid upon standing (5.11 g, 74%). LCMS (*m/z*): 301.1 [M + Na]⁺. (*m/z*): 261.1 [M - OH]⁺. HPLC: *t*_R 5.452min, >95% purity (214 & 254 nm). ¹H NMR (CDCl₃) δ 7.04 (d, *J* = 1.8 Hz, 1H), 6.98 (dd, *J* = 8.2, 1.9 Hz, 1H), 6.77 (d, *J* = 8.1 Hz, 1H), 5.94 (s, 1H), 3.98 (dd, *J* = 5.0, 3.4 Hz, 4H), 2.13 – 2.06 (m, 4H), 1.83 – 1.77 (m, 2H), 1.71 – 1.65 (m, 2H), 1.53 (s, 1H). ¹³C NMR (CDCl₃) δ 147.8, 146.5, 142.9, 117.7, 108.5, 107.9, 105.9, 101.1, 72.5, 64.5, 64.4, 36.9, 30.9.

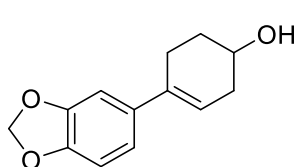


4-(Benzo[*d*][1,3]dioxol-5-yl)-4-hydroxycyclohexan-1-one (6). A solution of 8-benzo[1,3]dioxol-5-yl-1,4-dioxaspiro[4.5]decan-8-ol (5.50 g, 19.8 mmol) in acetone (50 mL) was treated with aqueous 1 M HCl (~15 mL) at rt for 5 h. The white precipitate was filtered, washed with cold acetone and dried to afford the title compound as a white solid which required no further purification (4.22 g, 90%). LCMS (*m/z*): 217.1 [M - OH]⁺. HPLC: *t*_R 4.849 min, >95% purity (214 & 254 nm). ¹H NMR (CDCl₃) δ 7.03 (dd, *J* = 1.9, 0.4 Hz, 1H), 6.97 (dd, *J* = 8.2, 1.9 Hz, 1H), 6.80 (dd, *J* = 8.1, 0.4 Hz, 1H), 5.96 (s, 2H), 2.89 (ddd, *J* = 14.0, 13.0, 6.8 Hz, 2H), 2.34 (ddt, *J* = 14.7, 4.7, 2.1 Hz, 2H), 2.24 (td, *J* = 13.4, 4.5 Hz, 2H), 2.16 (ddt, *J* = 11.7, 6.7, 2.9 Hz, 2H), 1.90 (t, *J* = 0.8 Hz, 1H). ¹³C NMR (CDCl₃) δ 148.0, 146.9, 141.4, 117.6, 108.2, 105.7, 101.3, 72.1, 38.9, 37.5.

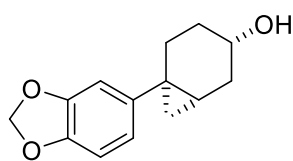


4-(Benzo[*d*][1,3]dioxol-5-yl)cyclohex-3-en-1-one (7). A solution of 4-(benzo[*d*][1,3]dioxol-5-yl)-4-hydroxycyclohexan-1-one (4.02 g, 17.1 mmol) in THF (20 mL) was treated with aqueous 6 M HCl (7 mL) overnight under a N₂ atmosphere at rt. The resulting solution was quenched with 1 M NaOH to neutralize the reaction. The solvent was removed and the residue was partitioned between DCM (25 mL) and H₂O (25 mL). The organic layer was collected and washed with brine, then dried over anhydrous Na₂SO₄, filtered and concentrated to give a yellow oil, which was then purified by FCC (eluent, 2:10, *n*-

hexanes/EtOAc) to afford the title compound as a white solid (2.75 g, 75%). LCMS (m/z): 217.1 $[M+H]^+$. HPLC: t_R 6.369 min, >95% purity (214 & 254 nm). 1H NMR ($CDCl_3$) δ 6.90 (d, $J = 1.7$ Hz, 1H), 6.86 (dd, $J = 8.1, 1.8$ Hz, 1H), 6.78 (d, $J = 8.0$ Hz, 1H), 5.98 (ddd, $J = 5.2, 2.5, 1.2$ Hz, 1H), 5.96 (s, 1H), 3.04 (dt, $J = 3.7, 1.8$ Hz, 2H), 2.84 (ddd, $J = 6.8, 2.4, 1.4$ Hz, 2H), 2.62 (t, $J = 6.9$ Hz, 2H). ^{13}C NMR ($CDCl_3$) δ 210.2, 147.9, 147.1, 137.4, 135.3, 120.1, 118.8, 108.2, 105.9, 101.2, 40.0, 38.8, 28.3.

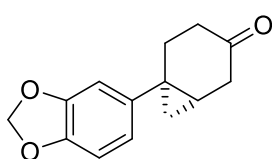


4-(Benzo[*d*][1,3]dioxol-5-yl)cyclohex-3-en-1-ol² (8). A solution of 4-(benzo[*d*][1,3]dioxol-5-yl)cyclohex-3-en-1-one (1.55 g, 7.17 mmol) in methanol (20 mL) at 0 °C was treated with cerium(III) chloride heptahydrate (3.47 g, 9.32 mmol) followed by portion wise addition of sodium borohydride (352 mg, 9.32 mmol). The reaction was warmed to ambient temperature over 14 h, quenched with sat. aqueous NH_4Cl and concentrated to remove MeOH. The concentrate was diluted with H_2O and extracted with EtOAc (3×25 mL). The combined organic extracts were washed with sat. aqueous $NaHCO_3$, brine, dried (Na_2SO_4) and concentrated *in vacuo*. The resulting white solid was subsequently used without further purification (1.24 g, 79%). LCMS (m/z): 201.0 $[M - OH]^+$. HPLC: t_R 6.008 min, >95% purity (214 & 254 nm). 1H NMR ($CDCl_3$) δ 6.89 (d, $J = 1.7$ Hz, 1H), 6.84 (dd, $J = 8.1, 1.8$ Hz, 1H), 6.75 (d, $J = 8.1$ Hz, 1H), 5.93 (s, 2H), 5.88 (ddd, $J = 6.5, 3.2, 1.3$ Hz, 1H), 4.04 (tdd, $J = 8.3, 5.1, 3.2$ Hz, 1H), 2.59 – 2.55 (m, 1H), 2.54 – 2.50 (m, 1H), 2.50 – 2.40 (m, 1H), 2.19 (dtd, $J = 9.4, 5.3, 2.2$ Hz, 1H), 2.03 – 1.95 (m, 1H), 1.86 – 1.75 (m, 1H), 1.69 (s, 1H). ^{13}C NMR ($CDCl_3$) δ 147.8, 146.6, 136.2, 135.9, 120.5, 118.5, 108.1, 105.9, 101.1, 66.7, 34.9, 31.3, 25.9.



6-(Benzo[*d*][1,3]dioxol-5-yl)bicyclo[4.1.0]heptan-3-ol⁸ (9). A solution of 4-(benzo[*d*][1,3]dioxol-5-yl)cyclohex-3-en-1-ol (1.00 g, 4.58 mmol) in DCM (75 mL) was treated with Et_2Zn (1.0 M in hexanes; 23.8 mL, 23.8 mmol). After 10 min, the reaction mixture was cooled to 0 °C, treated with a solution of CH_2I_2 (1.92 mL, 23.8 mmol) in DCM (20 mL) drop-wise over 10 minutes and allowed to warm to ambient temperature. After 48 h, the reaction mixture was quenched slowly with sat. aqueous NH_4Cl and stirred for 10 min. The reaction mixture was extracted with DCM (2×30 mL), and the combined organic phases were washed with aqueous sat. $NaHCO_3$, dried (Na_2SO_4) and concentrated *in vacuo*. Purification by FCC (eluent, 2:5 EtOAc/PE) gave the title compound as a transparent oil (854 mg, 80%). LCMS (m/z): 215.1 $[M - OH]^+$. HPLC: t_R 6.259 min, >95% purity (214 & 254 nm). 1H NMR ($CDCl_3$) δ 6.74 (t, $J = 1.1$ Hz, 1H), 6.71 (d, $J = 1.1$ Hz, 2H), 5.90 (s, 2H), 3.70 (dddd, $J = 11.3, 10.1, 6.6, 3.4$ Hz, 1H), 2.48 (dddd, $J = 13.5, 8.8, 6.6, 2.0$ Hz, 1H), 2.21 (dddd, $J = 13.7, 4.1, 3.1, 0.6$ Hz, 1H), 1.96 (m, $J = 1H$), 1.75 – 1.68 (m, 1H), 1.45 (ddd, $J = 13.4, 10.3, 1.7$ Hz, 2H), 1.26 – 1.17 (m, 1H), 1.17 – 1.11 (m, 1H), 0.94 (ddd, $J = 9.3, 4.6, 0.7$ Hz, 1H), 0.67 (app t, J

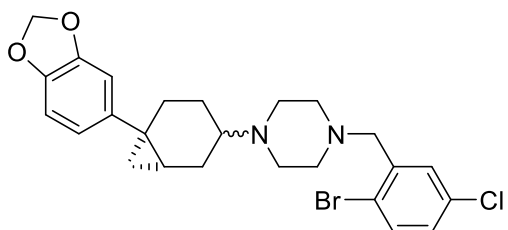
= 5.0 Hz, 1H) ^{13}C NMR (CDCl_3) δ 147.5, 145.6, 142.5, 120.8, 108.7, 108.1, 100.9, 68.8, 34.3, 31.4, 30.4, 18.7, 17.6.



6-(Benzo[*d*][1,3]dioxol-5-yl)bicyclo[4.1.0]heptan-3-one (10). A solution of 6-(benzo[*d*][1,3]dioxol-5-yl)bicyclo[4.1.0]heptan-3-ol (350 mg, 1.51 mmol) in DCM (20 mL) at 0 °C was treated with pyridine (267 μL , 3.31 mmol) followed by Dess-Martin periodinane (1.28 g, 3.01 mmol) and warmed to ambient temperature. After 3 h, 3 drops of H_2O were added. After a further 30 min, the reaction was quenched with sat. aqueous NaHCO_3 and sat. aqueous Na_2SO_3 , and extracted with DCM (3×20 mL). The combined organic phases were dried (Na_2SO_4) and concentrated *in vacuo*. FCC (eluent, 1:4 EtOAc/PE) afforded the title compound as a white solid (310 mg, 89%). ^1H NMR (CDCl_3) δ 6.80 (dd, $J = 1.7, 0.4$ Hz, 1H), 6.78 (dd, $J = 8.0, 1.7$ Hz, 1H), 6.74 (dd, $J = 7.9, 0.4$ Hz, 1H), 5.93 (s, 2H), 2.84 (dd, $J = 18.5, 5.0$ Hz, 1H), 2.66 (dd, $J = 18.5, 2.5$ Hz, 1H), 2.45 – 2.32 (m, 2H), 2.26 – 2.14 (m, 2H), 1.43 (dddd, $J = 9.8, 7.6, 5.1, 2.5$ Hz, 1H), 1.01 (dd, $J = 9.0, 5.7$ Hz, 1H), 0.94 (app t, $J = 5.5$ Hz, 1H). ^{13}C NMR (CDCl_3) δ 211.0, 147.8, 146.1, 140.3, 120.8, 108.5, 108.3, 101.1, 39.2, 36.8, 28.9, 17.2, 15.2.

1-(2-Bromo-5-chlorobenzyl)piperazine (13). Piperazine (1.82 g, 21.1 mmol) and 1-bromo-2-(bromomethyl)-4-chlorobenzene (1.00 g, 3.52 mmol) were taken up in toluene (25 mL) and stirred at reflux temperature for 2 h. The reaction mixture was filtered directly and the solids washed with DCM. The filtrate was acidified with 1 M aqueous KHSO_4 solution and extracted with further DCM, and the organic extracts were discarded. The aqueous phase was then adjusted to pH 12 with 1 M NaOH and extracted with DCM (3×25 mL). The organic extracts were washed with water, brine, and dried (Na_2SO_4). The solution was concentrated *in vacuo* to yield the compound as a transparent oil which was utilised without further purification (895 mg, 87%). LCMS (m/z): 289.1 [$\text{M} + \text{H}$] $^+$. HPLC: t_{R} 4.401 min, >95% purity (214 & 254 nm). ^1H NMR (CDCl_3) δ 7.48 (d, $J = 2.6$ Hz, 1H), 7.42 (d, $J = 8.5$ Hz, 1H), 7.06 (dd, $J = 8.5, 2.6$ Hz, 1H), 3.50 (s, 2H), 2.92 – 2.86 (m, 4H), 2.46 (s, 4H), 1.53 (s, 1H). ^{13}C NMR (CDCl_3) δ 139.7, 133.7, 133.5, 130.4, 128.4, 122.2, 62.2, 54.7, 46.3.

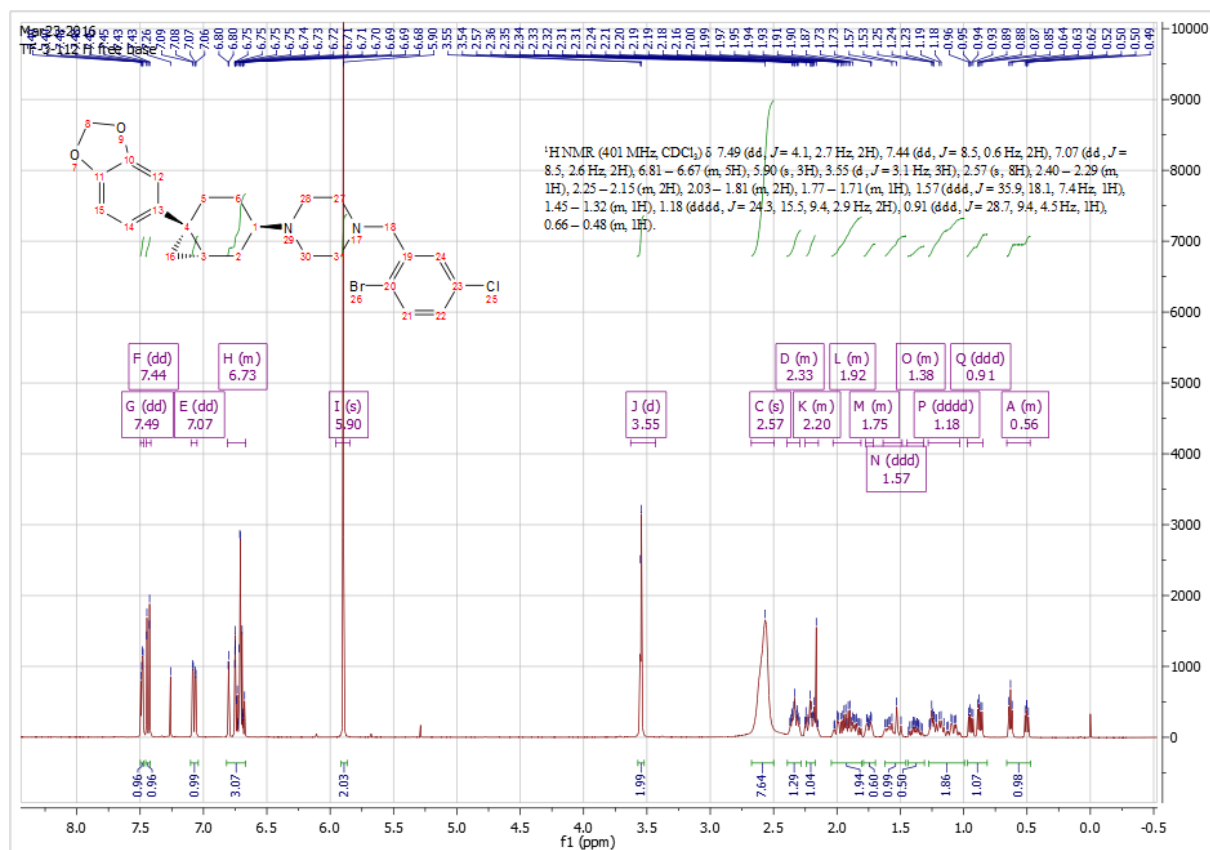
1-((*rel*-1*S*,6*R*)-6-(Benzo[*d*][1,3]dioxol-5-yl)bicyclo[4.1.0]heptan-3-yl)-4-(2-bromo-5-chlorobenzyl)piperazine (1). 1-(2-Bromo-5-chlorobenzyl)piperazine (126 mg, 434 μmol) and 6-(benzo[*d*][1,3]dioxol-5-yl)bicyclo[4.1.0]heptan-3-one (100 mg, 434 μmol) were taken up in 1,2-

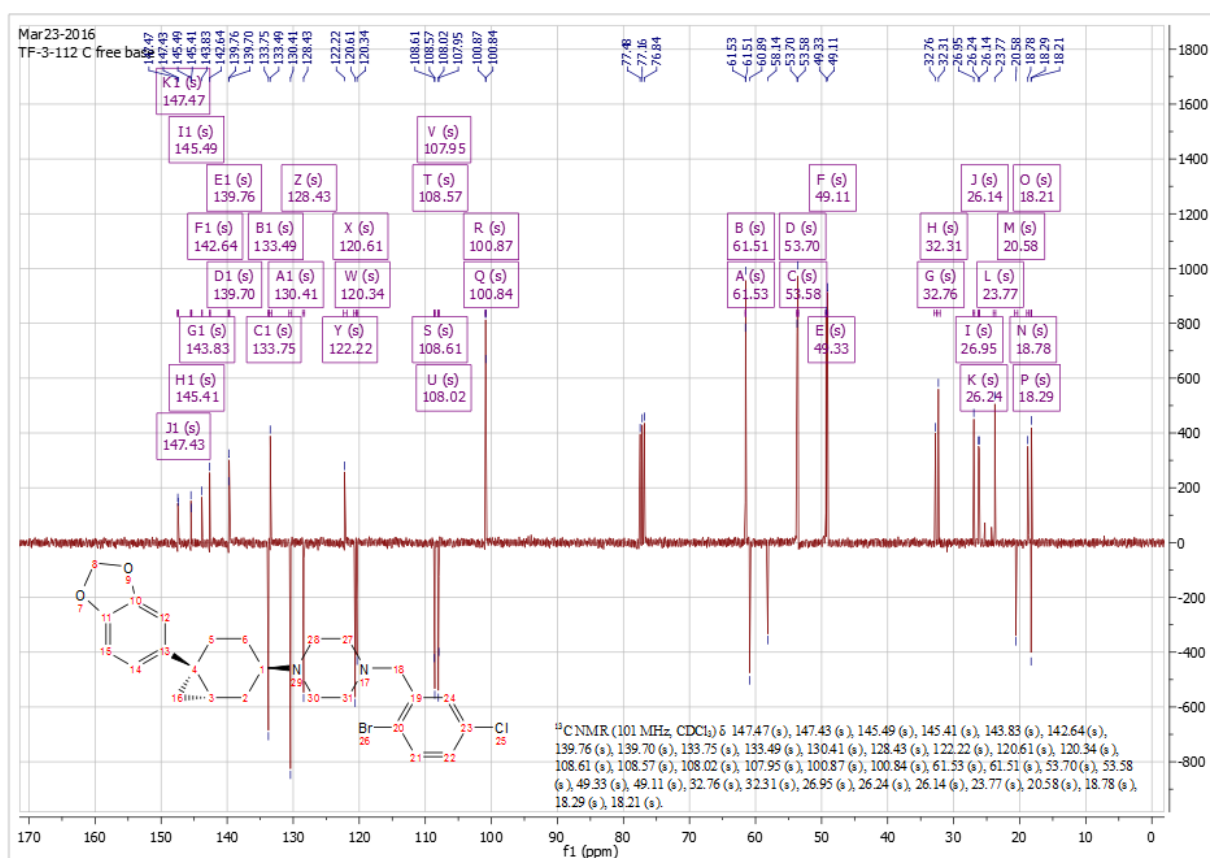


dichloroethane (25 mL) and then treated with sodium triacetoxyborohydride (138 mg, 651 μmol) and AcOH (24.9 μL , 434 μmol). The mixture was stirred at room temperature under a N_2 atmosphere for 24 h until the

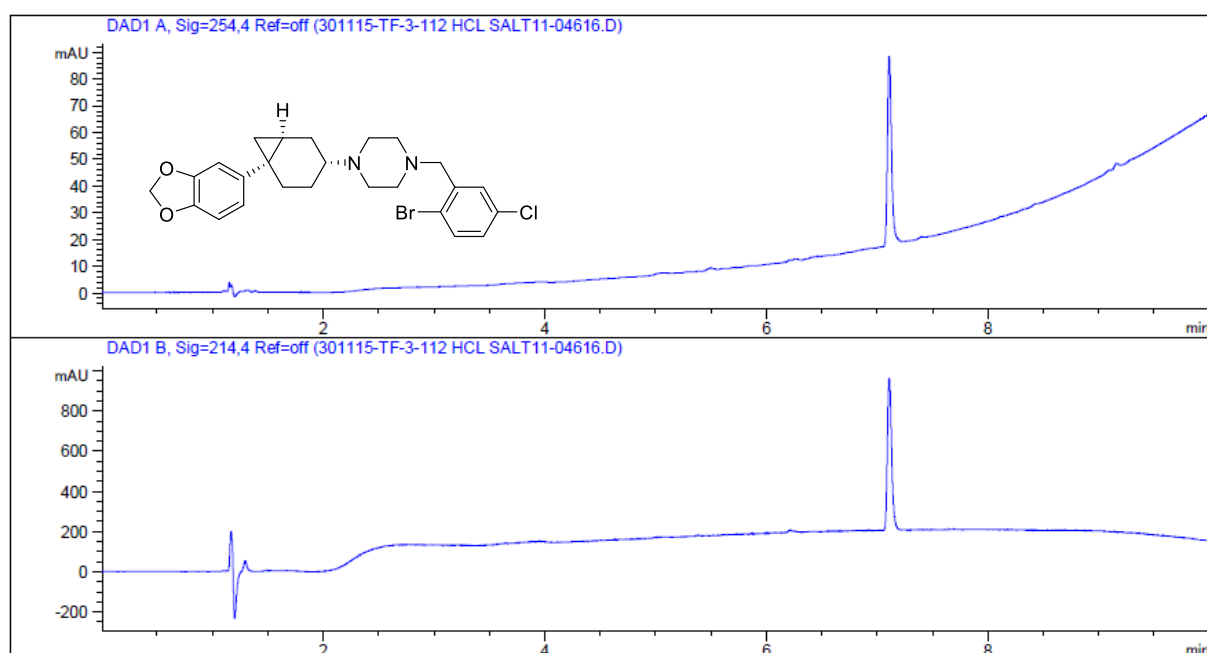
reactants were consumed as determined by LC/MS analysis. The reaction mixture was quenched by adding 1 M NaOH, and the product was extracted with Et₂O (3 × 30 mL). The ether extracts were washed with brine (30 mL) and dried (Na₂SO₄). The solvent was evaporated to give the crude residue which was purified by FCC (eluent, 1:5 EtOAc/PE) to give a semi-pure product as a transparent oil. The crude oil treated with ethereal HCl to give the corresponding hydrochloride salt as a white solid (65 mg, 30 %). LCMS (*m/z*): 503.1 [M + H]⁺. HPLC: *t*_R 7.093 min, >95% purity (214 & 254 nm). HRMS (*m/z*): C₂₅H₂₈BrClN₂O₂: requires 503.1109 [M+H]⁺; found 503.1095. ¹H NMR (CDCl₃) δ 7.49 (dd, *J* = 4.1, 2.7 Hz, 1H), 7.44 (dd, *J* = 8.5, 0.6 Hz, 1H), 7.07 (dd, *J* = 8.5, 2.6 Hz, 1H), 6.81 – 6.67 (m, 3H), 5.90 (s, 2H), 3.55 (d, *J* = 3.1 Hz, 2H), 2.57 (s, 8H), 2.40 – 2.29 (m, 1H), 2.25 – 2.15 (m, 1H), 2.03 – 1.81 (m, 2H), 1.77 – 1.71 (m, 1H), 1.65 – 1.47 (m, 1H), 1.21 (ddd, *J* = 23.1, 10.9, 6.3 Hz, 1H), 1.08 (qd, *J* = 12.9, 4.1 Hz, 1H), 0.91 (ddd, *J* = 28.7, 9.4, 4.5 Hz, 1H), 0.66 – 0.48 (m, 1H). ¹³C NMR (CDCl₃) δ 147.5, 147.4, 145.5, 145.4, 143.8, 142.6, 139.8, 139.7, 133.6, 133.5, 130.4, 128.4, 122.2, 120.6, 120.3, 108.6, 108.6, 108.0, 107.9, 100.9, 100.8, 61.5, 61.5, 53.7, 53.6, 49.3, 49.1, 32.8, 32.3, 26.9, 26.2, 26.1, 23.8, 20.6, 18.8, 18.3, 18.2.

Supplemental Figure 1A. ¹H NMR spectrum for Compound 1.



Supplemental Figure 1C. ^{13}C NMR spectrum of Compound 1.

Supplemental Figure 1A. HPLC trace for Compound 1.



References

1. Lewis, M. A.; Hunihan, L.; Watson, J.; Gentles, R. G.; Hu, S.; Huang, Y.; Bronson, J.; Macor, J. E.; Beno, B. R.; Ferrante, M.; Hendricson, A.; Knox, R. J.; Molski, T. F.; Kong, Y.; Cvijic, M. E.; Rockwell, K. L.; Weed, M. R.; Cacace, A. M.; Westphal, R. S.; Alt, A.; Brown, J. M. Discovery of D1 dopamine receptor positive allosteric modulators: characterization of pharmacology and identification of residues that regulate species selectivity. *J. Pharmacol. Exp. Ther.* **2015**, *354*, 340-349.
2. Gemal, A. L.; Luche, J. L. Lanthanoids in organic synthesis. Reduction of alpha-enones by sodium borohydride in the presence of lanthanoid chlorides: synthetic and mechanistic aspects. *J. Am. Chem. Soc.* **1981**, *103*, 5454-5459.
3. Simmons, H. E.; Smith, R. D. A new synthesis of cyclopropanes from olefins. *J. Am. Chem. Soc.* **1958**, *80*, 5323-5324.
4. Michino, M.; Beuming, T.; Donthamsetti, P.; Newman, A. H.; Javitch, J. A.; Shi, L. What can crystal structures of aminergic receptors tell us about designing subtype-selective ligands? *Pharmacol. Rev.* **2015**, *67*, 198-213.
5. Vaidehi, N.; Bhattacharya, S.; Larsen, A. B. Structure and dynamics of G-protein coupled receptors. *Adv. Exp. Med. Biol.* **2014**, *796*, 37-54.
6. Shonberg, J.; Lopez, L.; Scammells, P. J.; Christopoulos, A.; Capuano, B.; Lane, J. R. Biased agonism at G protein-coupled receptors: the promise and the challenges--a medicinal chemistry perspective. *Med. Res. Rev.* **2014**, *34*, 1286-1330.
7. Sibley, D. R.; Creese, I. Regulation of ligand binding to pituitary D-2 dopaminergic receptors. Effects of divalent cations and functional group modification. *J. Biol. Chem.* **1983**, *258*, 4957-4965.
8. Clader, J. W.; Mc, B. M. D.; Palani, A.; Su, J.; Tang, H.; Xu, R. N-aryl-n'-arylcycloalkyl-urea derivatives as mch antagonists for the treatment of obesity. In Google Patents: 2003.

Appendix 2

List of Publications

- **Fyfe, T. J.**; Zarzycka, B.; Lim, H. D.; Kellam, B.; Mistry, S. N.; Katritch, V.; Scammells, P. J.; Lane, J. R.; Capuano, B. A thieno[2,3-*d*]pyrimidine scaffold is a novel negative allosteric modulator of the dopamine D₂ receptor. *J. Med. Chem.* **2018**, *62*, 371-377. DOI: 10.1021/acs.jmedchem.7b01565
- Luderman, K. D.; Conroy, J. L.; Free, B.; Southall, N.; Ferrer, M.; Sanchez-Soto, M.; Moritz, A. E.; Willet, B. K. A.; **Fyfe, T. J.**; Jain, P.; Titus, S.; Hazelwood, L. A.; Aube, J.; Lane, J. R.; Frankowski, K. J.; Sibley, D. R. Identification of positive allosteric modulators of the D₁ dopamine receptor that act at diverse binding sites. *Mol. Pharmacol.* **2018**, *94*, 1197-1209
- **Fyfe, T. J.**; Kellam, B.; Mistry, S. N.; Scammells, P. J.; Lane, J. R.; Capuano, B. Subtle modification to a thieno[2,3-*d*]pyrimidine scaffold yields negative allosteric modulators and agonists of the dopamine D₂ receptor. *Eur. J. Med. Chem.* **2019**, DOI: 10.1016/j.ejmech.2019.01.061.

Awards

- February 2019 Postgraduate Publication Award
- January 2014 Monash Honours Jubilee Scholarship

Conference Presentations

Fyfe, T. J., et al. *Kinetic Profiling of Analogues of the Butyrophenone Antipsychotic Drug Haloperidol at the Human Dopamine D₂ Receptor*

- The RACI Medicinal Chemistry and Chemical Biology Conference, Brisbane, Australia, 18th – 21st November 2018. (Oral Presentation)

Fyfe, T. J., et al. *A Thieno[2,3-*d*]pyrimidine Scaffold is a Novel Negative Allosteric Modulator of the Dopamine D₂ Receptor*

- Symposium on Medicinal Chemistry, Manchester, United Kingdom. 28th August – 1st September 2016. (Poster Presentation)